

**METALLOGENIC, TECTONIC AND GEOCHEMICAL  
EVOLUTION OF THE CAPE RAY FAULT ZONE  
WITH EMPHASIS ON ELECTRUM MINERALIZATION**

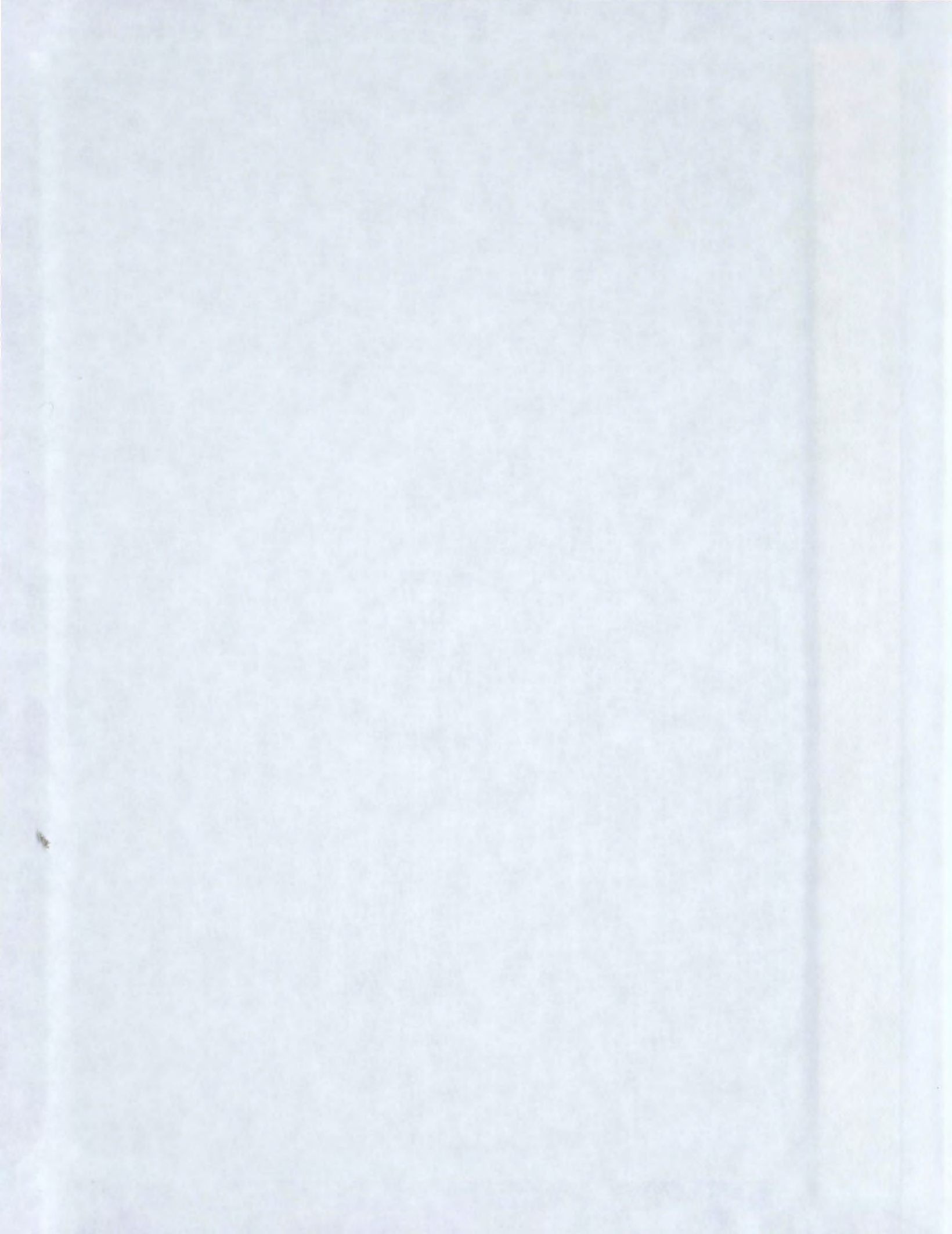
**CENTRE FOR NEWFOUNDLAND STUDIES**

**TOTAL OF 10 PAGES ONLY  
MAY BE XEROXED**

**(Without Author's Permission)**

**VOL. 1**

**DEREK HAROLD CLEMENT WILTON**





## CANADIAN THESES ON MICROFICHE

I.S.B.N.

## THESES CANADIENNES SUR MICROFICHE



National Library of Canada  
Collections Development Branch

Canadian Theses on  
Microfiche Service

Ottawa, Canada  
K1A 0N4

Bibliothèque nationale du Canada  
Direction du développement des collections

Service des thèses canadiennes  
sur microfiche

### NOTICE

The quality of this microfiche is heavily dependent upon the quality of the original thesis submitted for microfilming. Every effort has been made to ensure the highest quality of reproduction possible.

If pages are missing, contact the university which granted the degree.

Some pages may have indistinct print especially if the original pages were typed with a poor typewriter ribbon or if the university sent us a poor photocopy.

Previously copyrighted materials (journal articles, published tests, etc.) are not filmed.

Reproduction in full or in part of this film is governed by the Canadian Copyright Act, R.S.C. 1970, c. C-30. Please read the authorization forms which accompany this thesis.

THIS DISSERTATION  
HAS BEEN MICROFILMED  
EXACTLY AS RECEIVED

### AVIS

La qualité de cette microfiche dépend grandement de la qualité de la thèse soumise au microfilmage. Nous avons tout fait pour assurer une qualité supérieure de reproduction.

S'il manque des pages, veuillez communiquer avec l'université qui a conféré le grade.

La qualité d'impression de certaines pages peut laisser à désirer, surtout si les pages originales ont été dactylographiées à l'aide d'un ruban usé ou si l'université nous a fait parvenir une photocopie de mauvaise qualité.

Les documents qui font déjà l'objet d'un droit d'auteur (articles de revue, examens publiés, etc.) ne sont pas microfilmés.

La reproduction, même partielle, de ce microfilm est soumise à la Loi canadienne sur le droit d'auteur, SRC 1970, c. C-30. Veuillez prendre connaissance des formules d'autorisation qui accompagnent cette thèse.

LA THÈSE A ÉTÉ  
MICROFILMÉE TELLE QUE  
NOUS L'AVONS REÇUE

Metallogenic, Tectonic and Geochemical Evolution  
of the Cape Ray Fault Zone  
with emphasis on  
Electrum Mineralization

by

© Derek Harold Clement Wilton, BSc., MSc.

A thesis submitted to the School of Graduate  
Studies in partial fulfillment of the  
requirements for the degree of

Doctor of Philosophy

Department of Earth Sciences  
Memorial University of Newfoundland

October 1983

St. John's

Newfoundland



Frontispiece.

Upper - View looking southeast along the Trans-Canada Highway near Cape Ray. The southern end of the Long Range Mountains ( "Cape Ray high lands") is visible just to the northeast (ie. left) of the highway. These uplands are underlain by tonalitic Cape Ray Granite and the hill to the southwest is underlain by megacrystic Cape Ray Granite.

Lower - Electrum (bright yellow) intergrown with euhedral pyrite cube (dull yellow) and quartz gangue (black) in mineralized vein from the Windowglass Hill Showing. An example of the "treasures laid open to the mineralogist". This section is about 0.4 mm across.



"The high lands of Cape Ray lie several miles inland, north-east of the Cape, and consist of a group of granite mountains seemingly nearly two thousand feet in height. The scenery among them is sublime; the steep sides of the wedge-shaped valleys appear smooth and striped at a distance, owing to the crumbled rocks and blocks detached by frost being hurled from the very summits to the bottom, where they lay in heaps of ruins. I had reluctantly to behold only the treasures laid open to the mineralogist."

W.E. Cormack, Esq., 1823

from "Narrative of a journey across the island  
of Newfoundland in 1822"



ABSTRACT

The Cape Ray Fault Zone is host to two electrum/base metal sulphide-bearing quartz vein deposits. The deposits occur within an alaskitic granite (the Windowglass Hill Granite) and an intermixed graphite/chlorite/sericite schist unit (part of the Windsor Point Group). This study was initiated to determine the origin of these two deposits, but the metallogensis could not be ascertained until the tectonic and lithogeochemical framework of the entire region was understood.

The Cape Ray Fault cuts through an area of tectonic complexity in southwestern Newfoundland. The fault occurs within the Windsor Point Group, a northeasterly-striking, intermixed sequence of felsic and mafic pyroclastic/volcaniclastic and associated sedimentary rocks, which is centrally located between a tonalitic terrane to the northwest (the Cape Ray Granite) and an amphibolite facies gneiss unit, with synkinematic granite, to the southeast (the Port aux Basques Complex). The tonalite contains isolated metagabbroic remnants of an ophiolite sequence (the Long Range Mafic/Ultramafic Complex). The Windsor Point Group contains tonalitic fragments in the ignimbritic rhyolite at its base, and is in tectonic contact with the gneiss unit, wherein the gneiss is extensively retrogressed. The Windowglass Hill



v

Granite intrude the Windsor Point Group in the northeastern part of the zone. Both sides of the fault zone were intruded by post-tectonic granites (the Strawberry Granite on the northwestern side and Isle aux Morts Brook Granite on the southeast).

Geochronological determinations indicate that the tonalitic terrane is Ordovician in age, the Windsor Point Group and Windowglass Hill Granite are late Devonian, and the Strawberry/Isle aux Morts Brook Granites are early Carboniferous.

Isograds defined in the Windsor Point Group indicate that metamorphic grade increases from lower to upper greenschist facies towards the SE, and that pressures are rather low. Within the Port aux Basques Complex metamorphic isograds record amphibolite facies parageneses, and pressures are estimated to be  $>2$  kb higher.

Except for the post-tectonic granites, all units in the fault zone were subjected to a three-phase deformational event of Acadian age which overprinted earlier fabrics in the gneiss complex, and produced D1 schistosity axial planar to F1 isoclinal folds with axes parallel to L1 mineral elongation lineations. D2 effected crenulation cleavages and asymmetrical, open to tight, F2 folds. D3 resulted in conjugate kink folding. D1 also produced mylonites within the Windsor Point Group.

Geochemical evidence suggests that a) the tonalite and associated phases were derived as partial melts of the

ophiolitic material with some continental crust involvement, b) the felsic volcanism in the Windsor Point Group, and the Windowglass Hill, Strawberry and Isle aux Morts Brook. Granites formed from partial melts of underlying continental crust, and c) the Port aux Basques Complex was derived from felsic volcanic rocks with a probable island arc affinity (though continental crust is also implicated in their origin). The entire Cape Ray Fault Zone region appears to be a completely allochthonous terrane, from tonalite/ophiolite in the northwest to a meta-felsic eruptive igneous complex to the southeast, which was emplaced on Grenvillian basement.

Wall rocks to the electrum-bearing quartz veins experienced a potassic alteration with LREE-depletion and minor elevations in chalcophile element concentrations. Background Au and Ag abundances are typically low, but there are elevations in those units in the immediate vicinity of the Windowglass Hill Granite.

Ore metals in the showings are Au, Ag, Cu, Pb and Zn, and distributions resemble those seen in auriferous massive sulphide deposits. The minerals present are galena, sphalerite, chalcopyrite, pyrite and electrum with rare arsenopyrite; all of which are extensively intergrown. Temperatures of ore formation (from arsenopyrite and equilibrium sulphide mineral intergrowths) appear to be around 300° C.

Sulphur isotope ratios indicate sulphur in the showings is of magmatic origin. Pb isotope ratios in galenas from the showings and felsic volcanic members of the Windsor Point Group are similar and have an oceanic crust/mantle isotopic signature.

The precious/base metal-bearing quartz veins were deposited by hydrothermal fluids evolved as a vapour phase from the Windowglass Hill Granite. The ultimate origin of the magma was from partial melting of underlying Grenvillian crust. This same crustal material is implicated in the origins of the other granites.



### ACKNOWLEDGEMENTS

Due to the duration, size and scope of this project, numerous individuals have yielded invaluable assistance and made incalculable contributions to its final form. I just hope I remember them all.

My supervisor, Dr. D.F. Strong, and supervisory committee, Dr's. T.J. Calon and B.J. Fryer, are owed the greatest acknowledgements. Dr. Strong cheerfully provided knowledge, encouragement, inspiration, time and patience. He gave me an opportunity where many wouldn't have. I hope the result lives up to his expectations and high standards. Dr. Calon taught me structural geology from basics to detailed kinematics and greatly improved the structural portion of this work. Dr. Fryer instructed me in the ways and means of geochronology, trace gold/silver analysis and REE determination, and provided helpful repartee and criticism. All three provided cohesive supervision.

Mr D.E. Press assisted in most of the geochemical analysis and data reduction. His mastery of the X-Ray Fluorescence spectrometer and wizardry with the mini- and main frame computer systems were invaluable. He went out of his way to help me. Mrs. G. Andrews did the major element analyses, standard preparation for background Au and Ag determinations, instructed the author in laboratory techniques and showed how an efficient lab works. Dr. H.

Longerich taught me how to use the microprobe and provided assistance with computing. Ms. P. Davis assisted in Rb/Sr and REE sample preparation. Mr. E. Gellately permitted and instructed my use of the Varian Carbon Rod Analyser in the Water Analysis Facility in the Chemistry Department at Memorial University. Dr. C.L. Godwin, of the University of British Columbia, quite kindly did the Pb isotope analysis gratis.

Mr. D. Dingwell provided interesting discussion and samples of the Port aux Basques Granite. My fellow graduate students, especially G.R. Dunning, J.D. Greenough, R.S. Hildebrand, and A. Kay, and Dr's N. Higgins, and R. P. Taylor are thanked for stimulating geo-conversations. Ms L. Chorlton, then of the Nfld. Dept. of Mines and Energy, introduced me to the complexities of the Cape Ray Fault Zone and provided continual intriguing discussions of southwestern Newfoundland geology.

Excellent draughting for various stages of this project was supplied by Ms. J. Burry and Mr's. M. McIntyre and W. Howell. Mr. W. Marsh did superb photographic work and also instructed the author in techniques. Mr's. F. Thornhill, L. Warford and G. Ford produced excellent thin, polished and polished-thin sections. Ms. J. Hiscock typed the bibliography, and Mr. P. Browne looked after finances and travel arrangements

during this project.

Personnel of Riocanex Ltd. openly took me into their confidence and granted me access to all their proprietary material. The company also graciously provided assistants, salaries, lodging, transportation and equipment for the two summers spent doing field work. Mr's. P. Kavangh, W. Marsh and H. Hall are to be thanked for overseeing and permitting my studies, and also for helpful discussions. Mr's. W. Bucknell, J. Harris and C. McKenzie introduced me to the area and its deposits, worked with me, provided constructive observations and criticisms, and spent many a fine evening at the Port Club.

Finally, to my two ladies, Sue and Felicie, must go the greatest appreciation for enduring and understanding my pre-occupation with this project during the last four years.



## TABLE OF CONTENTS

	Page
TITLE.....	1
FRONTISPIECE CAPTION.....	ii
FRONTISPIECE.....	iii
ABSTRACT.....	iv
ACKNOWLEDGEMENTS.....	viii
TABLE OF CONTENTS.....	xi
LIST OF TABLES.....	xx
LIST OF FIGURES.....	xxiii
LIST OF PLATES.....	xxx

## CHAPTER 1

## INTRODUCTION

1.1 Location and Access.....	1
1.2 Physiography.....	3
1.3 History of Exploration and Development.....	5
1.4 Previous Geological Work.....	8
1.5 Purpose, Scope and Methods of the Present Study....	12

## CHAPTER 2

## THE GEOLOGY OF THE CAPE RAY FAULT ZONE

2.1 Introduction.....	14
2.2 The Long Range Mafic/Ultramafic Complex (Map unit 1).....	18
2.3 The Port aux Basques Complex (Map unit 2).....	19

2.3.1 The Port aux Basques Gneiss.....	20
2.3.1.1 Amphibolitic (or Melanocratic) Bands...	20
2.3.1.2 Gneiss (or Leucocratic) Bands.....	21
2.3.1.3 Other Interbands.....	22
2.3.1.4 Retrograde rocks along the Windsor Point Group Contact.....	23
2.3.2 Port aux Basques Granite.....	28
2.4 The Cape Ray Granite (Map unit 3).....	30
2.4.1 The Tonalite.....	31
2.4.2 The Megacrystic Phase.....	35
2.4.3 The Xenoliths.....	36
2.5 The Red Rock's Granite (Map unit 4).....	37
2.6 Basaltic Dykes (Map unit 5).....	38
2.7 Gabbro (Map unit 6).....	39
2.8 The Windsor Point Group (Map unit 7).....	41
2.8.1 The Little Barachois Formation (Map units 7a, b and c).....	41
2.8.2 Chlorite/Sericite Schist (Map unit 7d).....	47
2.8.2.1 Chlorite Schist.....	48
2.8.2.2 Sericite Schist.....	48
2.8.2.3 Limestone Interbeds.....	49
2.8.2.4 Gabbro.....	49
2.8.2.5 Graphite Schist.....	50
2.8.2.6 Chert (quartzite).....	51
2.8.2.7 Sandy Tuff/Ignimbrite.....	51
2.8.3 Limestone (Map unit 7e).....	54

2.8.4 Felsic Tuff (Map unit 7f).....	54
2.8.5 Conglomerate (Map unit 7g).....	55
2.8.6 Feldspar Porphyry Dykes (Map unit 8).....	56
2.8.7 Summary of the Windsor Point Group.....	56
2.9 The Windowglass Hill Granite (Map unit 9).....	59
2.10 Mylonite (Map unit 10).....	62
2.10.1 Mylonite at Windsor Point.....	65
2.10.2 Mylonite in the Isle aux Morts Brook.....	66
2.10.3 Mylonite at the Red Rocks/Cape Ray Granite Contact.....	70
2.11 Strawberry and Isle aux Morts Brook Granites, and Aplites (Map units 11a, 11b, 11c and 12).....	70
2.11.1 Strawberry Granite (Map unit 11a).....	71
2.11.2 Isle aux Morts Brook Granite (Map unit 11b) and breccia (Map unit 11c).....	73
2.11.3 Aplite Dykes (Map unit 12).....	76
2.12 Lithic Breccia (Map unit 13).....	77
2.13 Regional Correlations and Location with respect to the rest of the northeastern Appalachians.....	78
2.13.1 Location of SW Newfoundland with respect to Appalachian Tectonic Zones (or Terranes).....	80
2.13.2.1 Eastern Correlations.....	86
2.13.2.2 Northern Correlations.....	91
2.13.3 Summary.....	94



## CHAPTER 3

## GEOCHRONOLOGY

3.1 Introduction.....	97
3.2 The Port aux Basques Granite.....	97
3.3 The Cape Ray Granite.....	103
3.4 The Red Rocks Granite.....	106
3.5 The Windsor Point Group Ignimbrite.....	107
3.6 The Windowglass Hill Granite.....	110
3.7 The Strawberry and Isle aux Morts Brook Granites..	112
3.8 Areal Isochrons.....	115

## CHAPTER 4

## METAMORPHIC HISTORY

4.1 Metamorphic Mineral Assemblages.....	121
4.1.1 The Granites.....	121
4.1.2 The Long Range Mafic/Ultramafic Complex.....	123
4.1.3 Port aux Basques Gneiss.....	124
4.1.4 Gabbros.....	128
4.1.5 Windsor Point Group.....	129
4.1.6 Mylonites and Breccias.....	131
4.2 Garnet Compositions.....	132
4.3 Isograds.....	144
4.4 P-T Conditions and Path of Metamorphism.....	152
4.4.1 The Windsor Point Group.....	152
4.4.2 The Port aux Basques Complex.....	157
4.4.3 Contact Metamorphism.....	164

4.5 Conclusions.....	164
----------------------	-----

## CHAPTER 5

### STRUCTURAL HISTORY

5.1 Introduction.....	166
5.2 Detail of Structural Development in Each Unit.....	178
5.2.1 Long Range Mafic/Ultramafic Complex.....	178
5.2.2 The Port aux Basques Complex.....	178
5.2.3 The Cape Ray and Red Rocks Granites.....	181
5.2.4 Gabbros.....	182
5.2.5 The Windsor Point Group.....	184
5.2.6 The Windowglass Hill Granite.....	187
5.2.7 The Mylonites.....	189
5.3 Interpretation of Fabrics.....	190
5.4 Relationship between Structural and Metamorphic History.....	195
5.5 Principal Stress Orientations.....	196
5.6 Discussion.....	205
5.7 The New Interpretation.....	209
5.8 Conclusions.....	212

## CHAPTER 6

### GEOCHEMISTRY

6.1 Introduction.....	214
6.2 The Windsor Point Group.....	215
6.2.1 The Ignimbrite/Felsic Tuff (WPGIG),.....	221

6.2.1.1 Rare Earth Elements in the Little Barachois Formation.....	224
6.2.2 Graphite Schist (GAST).....	229
6.2.2.1 Rare Earth Elements in Windsor Point Group Schists.....	233
6.3 Port aux Basques Gneiss (PAB/GN).....	236
6.3.1 Rare Earth Elements in the Port aux Basques Gneiss.....	237
6.3.2 Origin of the Gneiss.....	239
6.3.3 Comparison with other Port aux Basques and Bay du Nord Analyses.....	240
6.3.4 Contact Zone Windsor Point Group (WPGQ) and Port aux Basques Gneiss (PABQ).....	242
6.4 Wall Rock to the Main Shear Mineralization (WAL/RX).....	243
6.4.1 Volume/Density Relationships.....	244
6.4.2 Rare Earth Elements in Wall Rock Samples....	248
6.5 Comparison with the Data of Others.....	253
6.6 Variation and Discrimination Diagrams.....	260
6.6.1 Summary of Geochemical Data.....	275
6.7 Intermediate to Mafic Intrusives.....	276
6.7.1 Variation and Discrimination Diagrams.....	277
6.7.2 Rare Earth Elements.....	288
6.8 Granitoids.....	289
6.8.1 Petrogenesis of the Granitoids.....	312
6.8.1.1 The Port aux Basques Granite.....	315

6.8.1.2 The Cape Ray and Red Rocks Granites.....	318
6.8.1.2a The Tonalite.....	318
6.8.1.2b The Megacrystic Phase.....	328
6.8.1.2c The Red Rocks Granite.....	329
6.8.1.2d Conclusions regarding the Cape Ray and Red Rocks Granites.....	331
6.8.1.3 Windowglass Hill Granite.....	335
6.8.1.4 Strawberry and Isle aux Morts Brook Granites.....	342

## CHAPTER 7

### THE ORE DEPOSITS

7.1 Sulphide Mineral Occurrences.....	348
7.1.1 Windowglass Hill Showings.....	348
7.1.1.1 The H and I Brook Showings.....	351
7.1.2 The Main Shear.....	353
7.1.2.1 The Four Zone.....	356
7.1.2.2 The Trench Showing.....	359
7.2 Assay Data.....	366
7.2.1 Introduction.....	366
7.2.2 Conclusions on Assay Data.....	370
7.2.3 Discriminant Function Analyses.....	373
7.3 Ore and Trace Element Concentrations in the Showings.....	374
7.3.1 Means and Distributions.....	374
7.3.2 Correlation Coefficients and Factor	

Analyses.....	379
7.3.3 Relative Enrichment Factors.....	387
7.3.4 Au/Ag Ratios.....	396
7.4 Background Au-Ag Abundances in the Regional Lithologic Units.....	400
7.4.1 Windsor Point Group Schists.....	401
7.4.2 The Port aux Basques Gneiss, WPCQ and PABQ samples.....	404
7.4.3 Windsor Point Group Ignimbrites.....	405
7.4.4 The Mafic Units.....	406
7.4.5 The Granites.....	407
7.4.6 Comparison of Background Au and Ag Contents with Other Reports.....	409
7.4.6.1 Au Abundances.....	409
7.4.6.2 Ag Abundances.....	425
7.5 Ore Petrography and Microprobe Analyses.....	427
7.5.1 Pyrite.....	428
7.5.2 Chalcopyrite.....	430
7.5.3 Sphalerite.....	430
7.5.4 Galena.....	438
7.5.5 Arsenopyrite.....	439
7.5.6 Gold/Silver (Electrum).....	445
7.5.7 Other Minerals.....	456
7.6 Significance of Intergrowth Textures and Compositions.....	456
7.7 Sulphur Isotopes.....	462

7.7.1 Temperatures.....	469
7.8 Lead Isotopes.....	474
7.9 Conclusions.....	483

## CHAPTER 8

### CONCLUSIONS AND TECTONIC/METALLOGENIC MODELS

8.1 Metallogeny of the Fault Zone.....	486
8.1.1 Metallogenic Conclusions.....	495
8.2 Tectonic Models.....	496
8.3 Prospecting Implications.....	508
ENDISPIECE.....	510
BIBLIOGRAPHY.....	511
APPENDIX I Microprobe Techniques.....	533
APPENDIX II Rb/Sr Geochronological Techniques.....	534
APPENDIX III Geochemical Methods.....	535
III.1 Sample Preparation.....	535
III.2 Major Element Analyses.....	536
III.3 Trace Element Analyses.....	537
III.4 Precious Metals Analyses.....	539
III.5 Rare Earth Element Analyses.....	542
APPENDIX IV.....	543
IV.1 Major and Trace Elements, S, CO <sub>2</sub> and Precious Metals.....	544
IV.2 Rare Earth Elements.....	614
REFERENCES CITED IN THE APPENDICES.....	617

## LIST OF TABLES

	Page
I Petrography of lithologies in the Cape Ray Fault Zone.....	15
II Garnet composition in the Strawberry Granite.....	74
III Rb-Sr regression results for whole rocks in the Cape Ray Fault Zone.....	98
IV Rb and Sr contents and isotopic compositions for units in the Cape Ray Fault Zone.....	99
V Averaged isochron data used to construct areal isochrons.....	116
VI Metamorphic mineral assemblages.....	122
VII Garnet compositions from microprobe analyses.....	133
VIII Clinopyroxene compositions in sample 79-132.....	139
IXa Average chemical compositions of schists.....	217
IXb Average chemical compositions of mafic rocks.....	218
IXc Average chemical compositions of granitoids.....	219
X Average chemical data from Taylor (1970) and Chorlton (1980b).....	241
XI Samples and specific gravities for volume/density calculations.....	247
XII Average chemical data from other authors.....	254
XIII Enrichment values (from Vine and Tourtelot, 1969).....	258
XIV Samples and specific gravities for volume/density calculations.....	339



XV Other mineral occurrences in the Fault Zone.....	349
XVI Data for cross-section through the number four zone.....	358
XVII Mean assay values.....	362
XVIII Correlation coefficients for assay data.....	369
XIX Varimax rotated factors in assay data.....	371
XX Mean trace element contents.....	377
XXI Element distributions in ore samples.....	378
XXII Correlation coefficient matrix for trace elements in samples from the Main Shear Showing.....	380
XXIII Varimax rotated factor matrix for samples from the Main Shear Showing.....	383
XXIV Correlations of Au and Ag with other elements....	403
XXVa Background gold abundances in mafic rocks.....	413
XXVb Background gold abundances in felsic rocks.....	414
XXVc Background gold abundances in metamorphic rocks..	415
XXVI Varimax rotated factor matrix for samples from the Windowglass Hill Granite.....	421
XXVII Varimax rotated factor matrix for trace elements in samples from the Windowglass Hill Granite.....	424
XXVIII Background silver contents in common terrestrial rocks.....	426
XXIX Pyrite compositions.....	429
XXX Chalcopyrite compositions.....	433
XXXI Sphalerite compositions.....	437
XXXII Galena compositions.....	442

XXXIII Arsenopyrite compositions.....	443
XXXIV Electrum compositions.....	448
XXXV 34S data.....	464
XXXVI Lead isotope data.....	477 •

## LIST OF FIGURES

	page
1 - Geology and location of the Cape Ray Fault Zone...	2
2 - Outcrop form of the Port aux Basques Granite.....	29
3 - Lithic breccia in the Gulch region.....	79
4 - Tectonic zones of Newfoundland.....	81
5 - Regional tectonic and stratigraphic correlations in southwestern Newfoundland.....	87
6a - Rb/Sr whole rock isochron for the Port aux Basques Granite.....	101
6b - Rb/Sr whole rock isochron for four samples of the Port aux Basques Granite.....	101
7a - Rb/Sr whole rock isochron and mineral separate isochron for the megacrystic Cape Ray Granite.....	105
7b - Rb/Sr whole rock isochron for five samples of the megacrystic Cape Ray Granite.....	105
8 - Rb/Sr whole rock isochron for the Red Rocks Granite.....	108
9 - Rb/Sr whole rock isochron for the basal ignimbrite member of the Windsor Point Group.....	109
10 - Rb/Sr whole rock isochron for the Windowglass Hill Granite.....	111
11a - Rb/Sr whole rock isochron for the Strawberry Granite.....	114
11b - Rb/Sr whole rock isochron for the Isle aux Morts	

Brook Granite.....	114
11c - Combined whole rock isochron for the Strawberry and Isle aux Morts Brook Granite.....	114
12a - Areal isochron for all units analysed in the Cape Ray Fault Zone.....	119
12b - Areal isochron for all units analysed in the Cape Ray Fault Zone except the Port aux Basques Granite.....	119
12c - Areal isochron for all units analysed in the Cape Ray Fault Zone except the Port aux Basques, Red Rocks and Cape Ray Granites.....	119
12d - Areal isochron for the Cape Ray and Red Rocks Granites.....	119
13 - Location and form of Brown's (1975) metamorphic mineral zones in the Port aux Basques Complex.....	125
14 - Garnet composition diagram.....	137
15 - Metamorphic mineral isograd map.....	147
16 - Paths of progressive metamorphic mineral development in the Port aux Basques and Windsor Point Group...	154
17 - Schematic illustration of the deformational history of the Cape Ray Fault Zone.....	167
18 - Equal area stereographic projection of poles to schistosity for lithological units in the Cape Ray Fault Zone.....	170
19 - Equal area stereographic projection for D1 mineral elongation lineations.....	173
20 - Equal area stereographic projection of F2 fold axes	

directions.....	175
21 - Equal area stereographic projection of poles to F2 axial planes.....	177
22 - Schematic illustration of the deformational history of the Port aux Basques Complex.....	179
23 - Equal area stereographic projection of poles to shear fractures/faults in the Red Rocks Granite...	183
24 - Equal area stereographic projection of D2 crenulation directions in the Windsor Point Group.	188
25 - Equal area stereographic projection of poles to shear fractures in the Cape Ray Granite and Windsor Point and Cape Ray Granite.....	198
26 - Stereographic projection of the intersections between great circle maxima for shear/fractures in the Windsor Point Group and Cape Ray Granite.....	200
27 - Equal area stereographic projection of poles to tension gashes in the Windsor Point Group.....	204
28 - Equal area stereographic projection of poles to quartz veins in the Isle aux Morts Brook Granite..	206
29 - K2O vs. SiO2 diagram for the Windsor Point Group ignimbritic rhyolite.....	223
30 - Chondrite-normalized REE patterns for the Windsor Point Group ignimbritic rhyolites.....	225
31 - Gas chromatogram for sample 80-611.....	230
32 - REE patterns for the Windsor Point Group schists..	234
33 - REE patterns for the Port aux Basques Complex.....	238

34 - REE patterns for wall rocks to Main Shear Showing.	249
35 - REE patterns for wall rocks ratioed to NASC values.	251
36 - Total alkalies <u>vs.</u> SiO <sub>2</sub> diagram for Windsor	
Point Group and Port aux Basques Gneiss.....	262
37 - K <sub>2</sub> O <u>vs.</u> Na <sub>2</sub> O diagram.....	264
38 - Rb <u>vs.</u> Sr diagram.....	265
39a - Na <sub>2</sub> O/Al <sub>2</sub> O <sub>3</sub> <u>vs.</u> K <sub>2</sub> O/Al <sub>2</sub> O <sub>3</sub> diagram for Windsor	
Point Group and Port aux Basques Complex averages..	267
39b - Na <sub>2</sub> O/Al <sub>2</sub> O <sub>3</sub> <u>vs.</u> K <sub>2</sub> O/Al <sub>2</sub> O <sub>3</sub> diagrams for the Windsor	
Point Group and Port aux Basques Complex.....	269
40a - Log (SiO <sub>2</sub> /Al <sub>2</sub> O <sub>3</sub> ) <u>vs.</u> log ((CaO+Na <sub>2</sub> O)/K <sub>2</sub> O) for	
Windsor Point Group and Port aux Basques Complex	
averages.....	271
40b - Log (SiO <sub>2</sub> /Al <sub>2</sub> O <sub>3</sub> ) <u>vs.</u> log ((CaO+Na <sub>2</sub> O)/K <sub>2</sub> O) for	
the Windsor Point Group and Port aux Basques	
Complex.....	273
41 - Total alkalies <u>vs.</u> SiO <sub>2</sub> diagram for the mafic	
volcanic/plutonic rocks of the Cape Ray Fault Zone.	278
42 - AFM diagram.....	279
43a - Na <sub>2</sub> O <u>vs.</u> K <sub>2</sub> O diagram.....	282
43b - Rb <u>vs.</u> Sr diagram.....	282
44a - Ti/Zr/Y diagram.....	284
44b - Log (Zr/Y) <u>vs.</u> log (Zr) diagram.....	284
45a - TiO <sub>2</sub> <u>vs.</u> Zr diagram.....	286
45b - Cr <u>vs.</u> Y diagram.....	286
46 - Al/(CNK) <u>vs.</u> SiO <sub>2</sub> diagrams for granitoids in the	

Cape Ray Fault Zone.....	291
47 - Normative Ab-An-Or diagrams.....	292
48 - Na <sub>2</sub> O <u>vs.</u> K <sub>2</sub> O diagrams.....	295
49 - Rb <u>vs.</u> Sr diagrams.....	298
50 - K/Rb <u>vs.</u> Rb/Sr diagrams.....	300
51 - K <u>vs.</u> Rb diagrams.....	303
52 - AFM diagrams.....	305
53 - CNK diagrams.....	308
54a - Normative Qz-Ab-Or diagram for the Red Rocks, Port aux Basques, megacrystic and tonalitic Cape Ray Granites.....	310
54b - Normative Ab-An-Or diagram.....	310
54c - Normative Qz-Ab-Or diagram for the Windowglass Hill Strawberry and Isle aux Morts Brook Granites.....	310
55 - Chondrite-normalized REE patterns for the Port aux Basques Granite.....	316
56 - Yb <u>vs.</u> Al <sub>2</sub> O <sub>3</sub> diagrams.....	320
57 - K <sub>2</sub> O <u>vs.</u> SiO <sub>2</sub> diagrams.....	322
58a - Chondrite-normalized REE patterns for the tonalitic Cape Ray Granite.....	324
58b - REE patterns for the megacrystic Cape Ray Granite.....	324
58c - REE patterns for the Red Rocks Granite.....	324
59 - REE patterns for the Windowglass Hill Granite.....	337
60a - REE patterns for the Strawberry Granite.....	345
60b - REE patterns for the Isle aux Morts Brook Granite.....	345
61 - Location of the Main Shear ore zones.....	354



62 - Cross-sectional view of the number four zone.....	357
63 - Map of veins in the Trench Showing.....	360
64 - Histogram of the canonical discriminant function for assay data.....	375
65 - Plots of varimax rotated factors in the Main Shear samples.....	386
66a - Enrichment/depletion factors for elements in the Main Shear Showing.....	389
66b - Enrichment/depletion factors for elements in the Windowglass Hill Showing.....	390
66c - Enrichment/depletion factors for the Main Shear samples <u>vs.</u> background Windowglass Hill Granite.....	391
67 -Au enrichment <u>vs.</u> Cu+Zn enrichment diagram for the Windowglass Hill and Main Shear Showings.....	395
68a - Histogram of Au/Ag ratios in Windowglass Hill and Main Shear Showings.....	398
68b - Histogram of Au/Ag ratios in the assay samples...	399
69a - Plot of Au <u>vs.</u> Na2O in the Windowglass Hill Granite.....	420
69b - Plot of La/Y <u>vs.</u> Au.....	420
69c - Plot of Au <u>vs.</u> S.....	420
70 - Plot of the varimax rotated factors in the Windowglass Hill Granite.....	423
71 - Detailed map of the Fe-As-S system.....	444
72 - Log aS2 <u>vs.</u> temperature diagram for the Fe-As-S	

system.....	447
73 - Log $a_{S_2}$ <u>vs.</u> temperature grid for sulphide phases relevant to the Main Shear mineralization.....	461
74 - Range of $^{34}S$ (‰) ratios for sulphide separates..	465
75 - Comparison of $^{34}S$ values in the Cape Ray Showings with those of porphyry copper and volcanogenic massive sulphide deposits.....	468
76 - Histogram of temperature determinations based on sulphur isotope fractionations.....	471
77 - Pyrite-sphalerite-galena sulphur isotope geothermometer for sample PB63-5.....	473
78 - Pb isotope growth curves and the Cape Ray sample data.....	480
79 - Schematic diagram showing the tectonic evolution of the Cape Ray Fault Zone.....	504

## LIST OF PLATES

	page
PLATE 2-1A Staurolite porphyroblast.....	33
2-1B Phyllonite.....	33
2-1C Tonalitic Cape Ray Granite.....	33
2-1D Agmatitic tonalite.....	33
2-1E Reaction rims on xenoliths.....	33
2-1F Flattened xenoliths.....	33
PLATE 2-2A Megacrystic Cape Ray Granite.....	44
2-2B Crystal layering of megacrysts.....	44
2-2C Biotite schleiren and clots.....	44
2-2D Mylonite along contact.....	44
2-2E Ignimbritic rhyolite.....	44
2-2F Autobrecciated rhyolite.....	44
PLATE 2-3A Volcaniclastic conglomerate.....	53
2-3B Tonalitic Cape Ray Granite clast.....	53
2-3C Isoclinally folded limestone interbed.....	53
2-3D Chert interbed.....	53
2-3E Conglomerate.....	53
2-3F Graphic intergrowths of quartz and feldspar in the Windowglass Hill Granite.....	53
PLATE 2-4A.....	69
2-4B Twisted/folded clast in conglomerate.....	69
2-4C Augen mylonite.....	69
2-4D Quartz porphyroclast.....	69
2-4E Porphyritic Strawberry Granite.....	69

2-4F Orbicular gas breccia.....	69
2-4G Granite contact.....	69
PLATE 5-1A D1 fabric.....	186
5-1B D2 crenulation.....	186
5-1C Boudinaged amphibolite.....	186
5-1D D3 conjugate kinks.....	186
5-1E F1 isoclinal fold.....	186
5-1F Flattened clasts.....	186
PLATE 5-2A D2 crenulation cutting D1 fabric.....	194
5-2B D1 mineral elongation lineation in the Windowglass Hill Granite.....	194
5-2C F2 fold in the Windowglass Hill Granite.....	194
5-2D D1 simple shear "pull apart" structure.....	194
5-2E Rotational component to D1.....	194
5-2F Feldspar augen.....	194
PLATE 5-3A Pressure shadows.....	203
5-3B Spessartine garnet.....	203
5-3C Quartz-filled tension gashes.....	203
PLATE 7-1A Knots of galena in H Brook.....	363
7-1B Boudinaged quartz veins in Trench Showing...	363
7-1C Sheared quartz veins in Trench Showing.....	363
7-1D Folded graphite schist in Trench Showing.....	363
PLATE 7-2A Elongate pyrite.....	432
7-2B Intergrown galena, quartz and chalcopryrite..	432
PLATE 7-3A Massive sphalerite with galena and chalcopryrite	

inclusions.....	436
7-3B Sphalerite with non-coherent chalcopyrite exsolution.....	436
PLATE 7-4A Galena with quartz gangue and sphalerite....	441
7-4B Massive arsenopyrite cut by chalcopyrite fracture-fillings.....	441
PLATE 7-5A Electrum intergrown with pyrite.....	451
7-5B Electrum intergrown with chalcopyrite.....	451
PLATE 7-6A Electrum intergrown with and included in galena.....	453
7-6B Electrum intergrown with sphalerite.....	453
PLATE 7-7A Electrum intergrown with galena and sphalerite.....	455
7-7B Solitary electrum grain.....	455

## CHAPTER 1

### INTRODUCTION

#### 1.1 Location and Access

This study is focused on a 5 km wide zone, extending in a northeasterly direction for approximately 33 km inland from the coastal community of Cape Ray, along the Cape Ray Fault in southwestern Newfoundland (see Figure 1). Mapping also encompassed a 13 km wide portion of the coast, yielding a total mapped area of about 200 km<sup>2</sup>. The area is roughly rectangular in shape, bounded by latitudes 47° 41' and 47° 36', and longitudes 59° 14' and 59° 19' on its southwestern edge, and latitudes 47° 45' and 47° 46', and longitude 58° 54' on the northeastern edge (see Map 1 - in pocket).

The major emphasis of this study was examination of two gold-silver /base metal sulphide-bearing occurrences in the northeastern end of the map region on either side of the Isle aux Morts Brook. These two occurrences are herein called the Main Shear Showing (on the eastern side of the Isle aux Morts Brook) and the Windowglass Hill Showing.

The southwestern corner of the map area is crossed by the Trans-Canada Highway and by a paved secondary road leading to Cape Ray. Gravel roads lead to Red Rocks Point

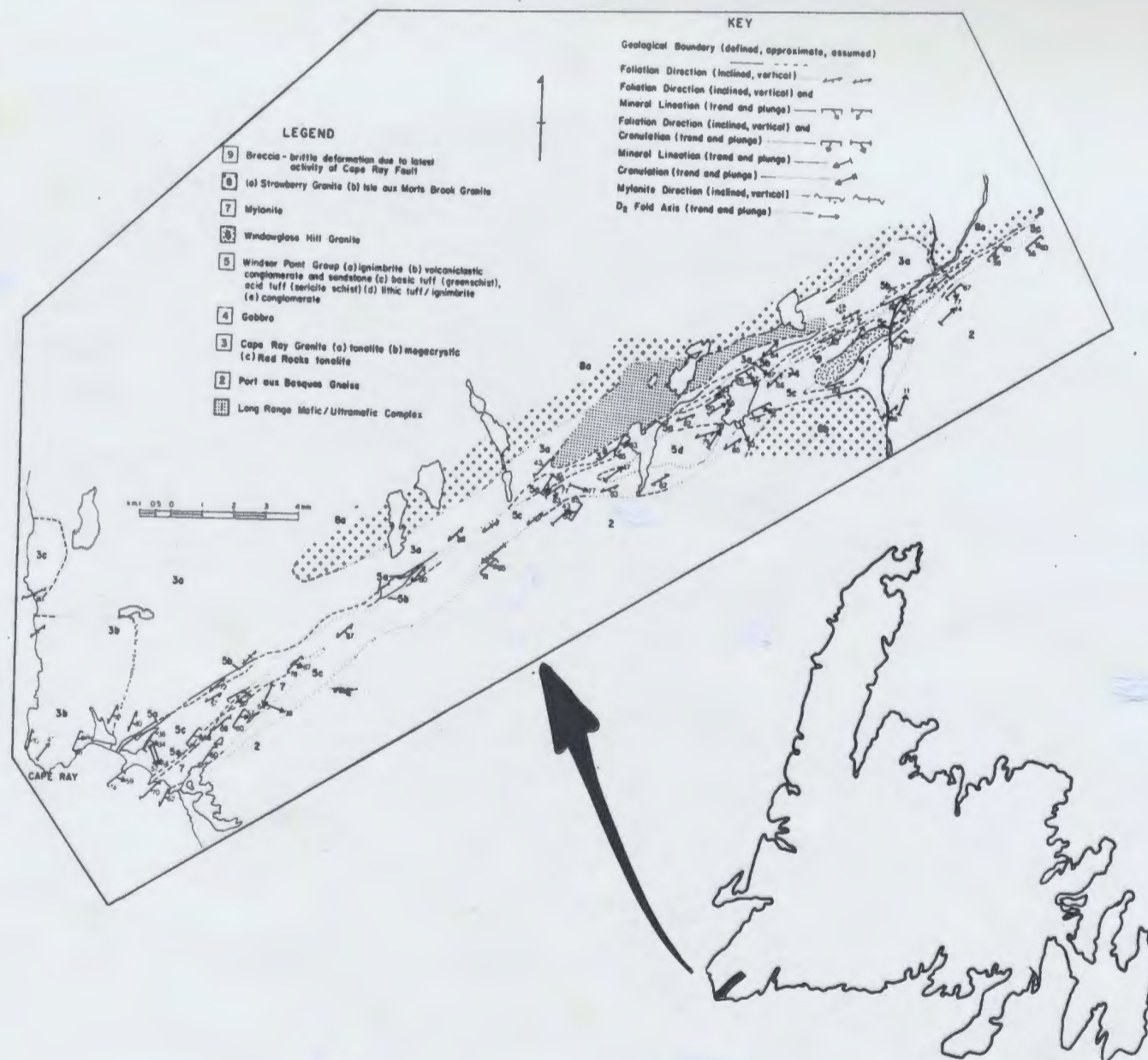


Figure 1 Geology (with generalized structural elements) and location of the Cape Ray Fault Zone. Inset shows location of map area with respect to the island of Newfoundland.

and through Cheeseman Provincial Park, which surrounds the Little Barachois. Numerous all-terrain vehicle trails cut through marshy areas away from the Trans-Canada Highway, and one extends all the way into Dog Pond (see Map 1 in pocket).

Access to the gold showings is difficult, but they can be reached by a very rough, tracked-vehicle trail which starts just west of the town of Isle aux Morts at the Port aux Basques-Rose Blanche highway and extends inland for over 16 km. Otherwise use of a helicopter is necessary for access, as there are no ponds near the properties large enough to accomodate a float plane.

### 1.2 Physiography

Just to the north of Billy's Pond, the southern end of the Long Range Mountain upland plateau rears up to a height of 375 m with a maximum vertical relief of 300 m (see frontispiece). This upland encompasses all of the fault zone except for a 1 km wide coastal fringe, and the area on either side of the Little Barachois Brook, which rises gradually into the upland 1 km west of Little Barachois Pond.

The Windowglass Hill Granite forms a prominent ridge on the western side of the Isle aux Morts Brook, with a maximum elevation of 375 m. The Main Shear occurs in a



marshy area, at an elevation of about 320 m, that slopes into the southwestern bank of the Isle aux Morts Brook.

The upland within the map area contains numerous ponds, streams and marshes, and is in general poorly drained. The only appreciable timber occurs within river valleys, and aside from occasional thickets of tuckermore in the slightly more protected hollows, the vegetative cover consists of tundra and marsh grasses. Outcrop is abundant throughout the zone (eg. the Windowglass Hill Granite is barren outcrop), but till cover is locally extensive, as at the Main Shear Showing, where trenches had to be dug to a depth of 5 m to reach bedrock.

The geomorphological features are products of both early and late Wisconsinian glaciations, which have affected the entire area except for a small southeastern portion of the Long Range Mountains, to the north of Billy's Pond, which Brookes (1977) claims was never covered by ice during these glaciations. Along with the locally abundant till, the glaciers produced a south/southeasterly drainage pattern as exemplified by the three major streams that dissect the area (viz. the Grand Bay River, Eastern Brook and the Isle aux Morts Brook). However pre-glacier structural trends within the region of the northeasterly-striking Cape Ray Fault have exerted a strong influence on the glacial features. For instance ridges of outcrop trend in a southwesterly direction (eg. the

Windowglass Hill Granite) reflecting the structural grain of the formations that were sculpted by the glaciers. Also all of the rivers show a pronounced southwesterly deflection in their courses when the fault zone is encountered, and the Little Barachois Brook, which occurs solely in the fault zone, flows only to the southwest.

One other geomorphological feature of note is the pronounced level outcrop surface of the megacrystic granite at Cape Ray. According to Brookes(1977), this outcrop pattern represents a wave cut platform of "pre-last glaciation" (ie. pre-Wisconsinian) indicating sea level erosion during the Sangamonian.

### 1.3 History of exploration and development

Except for the coastal strip from Cape Ray to Red Rocks Point, the whole map area is enclosed within a mineral lands concession granted to Brinex Ltd. by the Newfoundland government in 1953. In 1968 Brinex completed a regional geochemical survey for U, Zn, Ba, Cu, Pb, Ni, Mn and Mo in stream sediments through the concession and did follow-up mapping on some anomalies as defined in the survey. (See Taylor (1970) for a detailed description of an anomalous U area).

Phillips Management optioned the concession from Brinex in 1975, and did some mapping, silt sampling and an

EM survey in the general vicinity of the Main Shear showings. George Bailey, a prospector employed by Phillips, discovered sulphide-bearing quartz veins in fault gouge within the Gulch (ie. a narrow valley at the northeastern end of the map area).

AMAX Ltd. optioned the concession in 1976. George Bailey, then employed by AMAX, found galena-filled quartz veins cutting mylonitized granite in the H and I Brooks near the Main Shear showings (see Map 1). AMAX drilled three diamond drill holes in an attempt to delineate these H and I Brook Showings.

In 1977 Riocanex Ltd. optioned the concession, but concentrated exploration work near the H and I Brook showings. A grid system for diamond drilling and geochemical sampling was established over these showings. The drilling outlined the subsurface trace of the mylonitized granite and also encountered gold-silver /base metal sulphide-bearing quartz veins in graphitic and chloritic schist. This schist horizon, which was called the Main Shear Showing, does not crop out. Following its discovery, exploration work for the remainder of 1977 was concentrated on this Main Shear horizon.

Geologists with Riocanex Ltd. mapped the entire concession area, with special reference to the Main Shear area, in the summer of 1978. During this mapping project, Jim Harris discovered gold/sulphide-bearing quartz veins in

7

the Windowglass Hill Granite. These veins were drilled and trenched to determine their grade, size and form. Drilling was continued along the Main Shear and outlined three main mineralized zones, named the Numbers 4, 41 and 51 zones. A geochemical survey of the area and a VLF-EM survey of the Main Shear were also completed during 1978.

During 1979 a grid was laid out over the Windowglass Hill Granite along which soil and humus samples were collected for geochemical analyses and an IP survey conducted. An IP survey was also done on the Main Shear grid. Drilling continued along the Main Shear and along extensions of the Cape Ray Fault to the northeast. A lake sediment geochemical survey was also completed through the whole concession area in 1979.

In 1980 trenches were dug to bedrock over particularly promising vein zones, as delineated by drilling, in the Main Shear. Extensive systematic sampling for geochemical studies were carried out in these trenches. Active developmental work ceased at the end of 1980, when a total of 170 drill holes had been drilled by Riocanex.

This author mapped the concession/fault zone region from the Main Shear showing(s) to the coast during the summers of 1979 and 1980 while in the employ of Riocanex Ltd.. This mapping forms the basis for the present work.

#### 1.4 Previous geological work

The first report on the geology of southwestern Newfoundland was by Jukes (1843) based on examination of coastal exposures during a reconnaissance survey of the coast of Newfoundland between 1839 and 1840. Jukes said that rocks in the area from Dead Islands (now known as Isle aux Morts) round Cape Ray and up the coast were interstratified gneiss and mica slate. He said these rocks had a consistent east-northeast strike and southeasterly dip from Port aux Basques past Cape Ray. He also noted that "beds of peculiar character were interstratified with the gneiss and mica slate. They were not more than a foot or two thick, but were finegrained black, heavy and crystalline, consisting almost entirely of small crystals of hornblende" (Jukes, 1843, p108.). He was referring to interbands of amphibolite within the Port aux Basques Gneiss which will be described below.

Murray (1868) defined the gneisses around the Cape Ray area as part of the Laurentian system of gneisses which he said extended from the Great Northern Peninsula through the west coast of Newfoundland. These Laurentian gneisses on the Great Northern Peninsula are now known as Grenvillian gneisses (eg. Williams et.al., 1973).

Phair (1949) mapped an area from southeast of Cape Ray to north of Red Rocks Point and inland to Grand Bay Brook. However, he described the region southeast of Little Barachois Brook in very little detail, concentrating

instead on the western portion, where he described mafic to ultramafic rocks that were intrusive into gneissic metasediments and marble hosts. He disagreed with Murray's Precambrian age assignment of these gneisses and referred to them as Early Palaeozoic. According to Phair, these Devonian mafic/ultramafic rocks were intruded by a series of granitic rocks ranging from biotite quartz diorite to granodiorite, also of Devonian age. South of the Cape Barachois, Phair mapped shear zones in what he called the Cape Ray Schists, a biotite and biotite-garnet schist unit which graded southwards into migmatites and gneisses. However he did not recognize the Cape Ray Fault in the schistose zone.

Gillis (1972) defined the Cape Ray Fault as a prominent lineament that separated a mainly granitic terrane (with associated metasediments, gabbros and ultramafics), to the northwest, from a gneiss and schist terrane to the southeast. According to Gillis, the age of the gneiss and schist unit was somewhere between Ordovician and Devonian, while that of the granitic terrane could have been anywhere from Precambrian to Ordovician. Gillis mapped the fault as extending from the head of the Little Barachois, parallel to the trace of the Little Barachois Brook inland along the northern shore of Big Pond and through the Main Shear area on the southern side of the Isle aux Morts Brook. Gillis also noted the presence of a

younger (Devonian ?) undeformed granite intruding the gneiss unit south of Big Pond.

As a result of mapping along the coast inland to the Trans-Canada Highway from Red Rocks Point past the Big Barachois, Brown (1973) redefined the geographical trace of the Cape Ray Fault and assigned formational names to the relevant lithological units. Rocks to the northwest of Little Barachois, Brown called the Cape Ray Complex, consisting of; a) the Long Range Gneiss (which he correlated with Grenvillian gneisses elsewhere in western Newfoundland), b) the Cape Ray Granite, a foliated megacrystic granite of Paleozoic age, and c) the Red Rocks Granite, an undeformed granite that occurs at Red Rocks Point.

As defined by Brown (1973), the Windsor Point Group extends from the western side of Little Barachois to approximately 0.25 km southeast of Windsor Point where mylonites (developed in the Cape Ray Fault) separate it from the Port aux Basques Complex. This complex consists of the Port aux Basques Gneiss, a banded biotite-gneiss and amphibolite sequence, and the synkinematic, migmatitic Port aux Basques Granite. According to Brown, the Windsor Point Group was deposited on the Cape Ray Fault and was deformed by later reactivations of this fault. The fault was thus defined as separating two gneissic terranes.

Brown (1973b) described the Cape Ray Fault as a

cryptic suture separating the opposed margins of the Lower Paleozoic Iapetus Ocean. The Long Range Gneiss as such represented the continental basement of proto-North America, and the Port aux Basques Gneiss was thought to be representative of the continental basement to proto-Europe/North Africa.

Brown (1975) extended his mapping of southwestern Newfoundland along the south coast to Garia Bay, over 50 km east of Cape Ray, and inland from Windsor Point to near Dilly's Pond. Brown indicated that in this extension, the Cape Ray Fault was marked by a one km wide mylonite zone between the Long Range and Port aux Basques Gneisses, and that the Windsor Point Group thinned and disappeared completely by Little Barachois Pond.

Brown (1976a) further enlarged his work in southwestern Newfoundland to complete the geological mapping of the Rose Blanche Map Area (NTS 110/10). In this study he described the Devonian(?) post-tectonic granite of Gillis (1972) as Carboniferous(?) and he also noted the impressive interference-type outcrop pattern of the synkinematic Port aux Basques Granite. Brown (1976b) identified the large mafic/ultramafic masses, defined by Phair (1949) as intrusives, as ophiolites and called them the Long Range Mafic/Ultramafic Complex.

Brown (1977) finished his work in this area by extending his geological framework through the Port aux



Basques Map Area (NTS 110/11). He found that the Windsor Point Group reappeared overlying the fault zone near Dog Pond and continued past the end of the map sheet. Brown also reported more extensive exposures of the Long Range Mafic-Ultramafic Complex and assigned a Devonian or earlier age to the complex (probably Ordovician).

Chorlton (1980a and 1982), and Chorlton and Dingwell (1981) correlated Brown's lithological subdivisions to the northwest, including the area of the Main Shear showings. Dingwell (1980) mapped, and conducted a geophysical survey and geochemical study of the Port aux Basques Granite, and concluded that the granite was of local derivation from in situ partial melting of the Port aux Basques Gneiss.

#### 1.5 Purpose, scope and methods of the present study

This study was initiated to determine the physical and geochemical parameters, and origin of the Windowglass Hill and the Main Shear Showings. In order to conduct and complete such a study the tectonic setting and regional lithologic framework had to be understood. However, ideas from previous studies proved to be somewhat outdated and erroneous, and the whole fault zone had to be re-interpreted. This new study has determined important structural and metamorphic relations, and coupled with geochronological studies, a new tectonic synthesis of this

corner of SW Newfoundland has been achieved. Granites play an important role in formation of the ore deposits, and thus all granitoid bodies in the area were studied in detail with a view to understanding their petrogenesis. In studying the actual ore deposits a number of analytical techniques and methods were used to determine sources for the ore minerals, modes of transport, and geochemical conditions attendant at precipitation. Among these methods were: general geochemical analyses, background gold and silver analyses, rare earth element analyses, general petrography, detailed metamorphic and ore petrology, microprobe analyses of garnets and ore minerals, structural analysis etc.. Pb isotope analyses were completed in the Department of Geological Sciences at the University of British Columbia by Dr. C. I. Godwin. S isotope analyses were done, for a fee, at the University of Waterloo.

## CHAPTER 2

### The Geology of the Cape Ray Fault Zone

#### 2.1 Introduction

The Cape Ray Fault is a regional lineament extending from the southwestern corner of Newfoundland northeastward for more than 35 km (Figure 1) separating two contrasting geological terranes. To the northwest is the dominantly tonalitic Cape Ray Granite with isolated ophiolitic remnants of the Long Range Mafic/Ultramafic Complex. To the southeast is the Port aux Basques Complex, comprising a staurolite/kyanite-grade gneiss and amphibolite unit (the Port aux Basques Gneiss) and a migmatitic synkinematic granite (the Port aux Basques Granite) (Brown, (1977), Dingwell (1980)). The fault has its strongest expression within the Windsor Point Group, an intermixed ignimbrite and mafic tuff sequence, with associated sediments, that lies between the two previously defined terranes. Both sides of the fault zone were intruded by post-tectonic granites (the Isle aux Morts Brook and Strawberry Granites).

Petrographical descriptions of each unit in the fault zone as mapped for this thesis are presented in Table I.

<u>UNIT</u>	<u>ROCK TYPE</u>	<u>TEXTURE</u>	<u>DEFINING MINERALOGY</u>	<u>COMMENTS</u>
Long Range Mafic Ultramafic Complex	metagabbro	allotriomorphic- to hypidiomorphic-granular	plag(25-60%; 3-10 mm in len.), hb(25-70%), mag, ap. Near Cape Ray Granite contains qtz (up to 10%), py(0-5%) and bio (0-5%)	hb pseudomorphic after px
Port aux Basques Gneiss	(a) amphibolite interbands	matrix of granoblastic-polygonal qtz/fspar to poikiloblastic hornblende and garnet	hb(40-80%), plag and qtz(10-30%; 0.15 mm in dia.), gar(2-25%; 2-3 mm in dia.) bio(0-10%), chl(3-5%), ep(3-5%), mag (1-5%), py(0-5%), sphene (1-2%), zir	hb is acicular to rhombohedral with inclusions of qtz, fspar and/or bio
	(b) leucocratic interbands	granoblastic-polygonal	qtz, plag, kspar, bio, musc, gar, staurolite, mag, py, chl, zir, sphene, hb, allanite (+ act, and, tour)	micaceous minerals range from intergranular to discrete layers - microcline, gar are poikiloblastic - qtz sometimes as porphyroclasts
Port aux Basques Granite	granite to granodiorite	allotriomorphic-granular to gneissose	qtz(up to 7x4 mm), plag(up to 4x2 mm), microcline, ortho, bio, mag(up to 5%), allanite(up to 0.07x0.12 mm), ap, zir, musc, hb(av. 0.4x0.5 mm), ep, sphene	in places could be called two-mica leucogranite
Cape Ray Granite	(a) tonalite (to granodiorite)	coarse-grained equigranular	plag, qtz, bio, ortho, mag, sphene, zir, ap, tour (0.75x0.4 mm), py	plagioclase totally replaced by sericite, chlorite and epidote
	(b) microcline-biotite granite	megacrystic	perthitic microcline, plag(up to 5x7 mm), qtz, bio, sphene, zir, ap, mag	abundant plag inclusions in microcline - sphene as euhedral rhombs
Red Rocks Granite	granite	allotriomorphic- to	qtz, kspar (up to 4-5 mm in dia.),	most muscovite is secondary

TABLE I Petrography of lithologies in the Cape Ray Fault Zone

		hypidiomorphic-granular	plag, bio, musc, allanite, ap, zir, mag and rutile	but some may be primary - allanites as zoned crystals
Gabbro	titaniferous hornblende gabbro	hypidiomorphic-granular to schistose	plag, hb, act, chl, ep, bio, sphene	typically mylonitized feldspathic groundmass ( $\leq 0.01$ mm in dia. per grain) with intergrown acicular to fibrous amphibole
Windsor Point Group	(a) ignimbrite	welded pyroclastic with euhedral fspar and qtz crystals	ortho, microcline, plag, qtz, with spherulites	typical pyroclastic with rare shards and flame
	(b) volcaniclastic conglomerate	clast-supported conglomerate	clasts of felsic volcanic rocks, glass spherulites, qtz, fspar	matrices strongly replaced by sericite
	(c) volcaniclastic sandstone	medium to well-sorted sandstone, equigranular	fspar, qtz and volcanic rock fragments	matrices replaced by sericite carbonate, chlorite and bio.
schist member	(i) chlorite schist	metasediment	clastic plag, kspar, qtz, felsic volcanic rock clasts	all clasts are slightly rounded indicating some transport modification, but are also fresh, indicating close-to-source derivation
	(ii) sericite schist	metafelsic tuff	clastic kspar, plag, qtz	strongly overgrown by sericite layers
	(iii) gabbro	panidiomorphic-granular	plag, hb, sphene, mag, py	sphene can account for up to 20% of rock

TABLE I (cont.)

	(iv) graphite schist	metasediment	clastic fspar and qtz with graphite, ser, chl	graphite as amorphous material, ranging from isolated specks to laminae
	(d) rhyolite	quartz-feldspar porphyry	plag(up to 30%), ortho(up to 10%), qtz(up to 10%)	
	(f) conglomerate	mylonitic	qtz and fspar (0.06 mm in dia.), ser, chl, ep, mag, tour	recrystallized qtz/fspar layers with schistose interlayers (up to 1-2 mm thick) of dense ser/chl
	(g) feldspar porphyry dykes	quartz-feldspar porphyry	qtz(av. 2 mm in dia.), plag(up to 1x1 mm), ortho(av. 2x3 mm, but up to 6x2 mm), mag, bio, ap, zir, sphene	qtz and fspar grains are idiomorphic crystals set in qtz/fspar groundmass (av. grain size $\leq$ 0.04 mm in dia.)
Windowglass Hill Granite	granophyric granite	graphic intergrowths of qtz and fspar	ortho, alb, microcline, qtz(30-40%), bio(<2%), py( $\leq$ 3%)	spectacular graphic intergrowths of fspar and qtz - groundmass is allotriomorphic-granular to fspar phenocrysts - mafic-poor
Mylonite	mylonite	recrystallized with porphyroclasts	plag, ortho, microcline (all up to 1.25 mm <sup>2</sup> ), qtz, ser, carb, ep, bio, chl	porphyroclasts in recrystallized matrix (grain sizes $\leq$ 0.01 mm in dia.) with intergranular mica flakes
Strawberry/Isle aux Morts Brook Granites	granite to quartz monzonite	allotriomorphic-granular to porphyritic	perthitic microcline (av. 6x4 mm, up to 1.5x2 cm), ortho, plag (25-30%; av. 1.25x1.25 mm), qtz, bio(2-5%), zir, ap, py, molybdenite	microclines are poikilolitic with crystallographically orientated plag and ortho inclusions

Abbreviations: act= actinolite; alb= albite; and= andalusite; ap= apatite; bio= biotite; carb= carbonate; chl= chlorite; ep= epidote; fspar= feldspar; gar= garnet; hb= hornblende; kspar= alkali feldspar; mag= magnetite; musc= muscovite; plag= plagioclase; py= pyrite; ortho= orthoclase; qtz= quartz; ser= sericite; tour= tourmaline; zir= zircon; av. = average; dia. = diameter

## 2.2 The Long Range Mafic/Ultramafic Complex (Map Unit 1)

In this study area, the Long Range Mafic/Ultramafic Complex is represented by a single body (see Map 1 in pocket), approximately 2x9 km, extending from just north of Dog Pond to south of Deer Pond, and two smaller bodies east and southeast of Deer Pond. Due to the extensive intermingling of this unit with the Cape Ray Granite, delineation of its areal extent is quite difficult and the boundaries on the map are mostly inferred.

This complex was identified as ophiolitic remnants by Brown (1976b and 1977) on the basis of the much larger bodies that occur to the northwest of this map area. There is a well-developed layered sequence in the largest body with a lowermost dunite grading upwards through banded troctolites, olivine gabbros and norites. Thus it exhibits the central portion of a classic ophiolitic sequence (eg. Malpas and Stevens, 1977), missing the mantle (or non-cumulate) ultramafics from the base and sheeted dykes plus pillow lavas from the top.

In the vicinity of the Cape Ray Fault, however, the representatives of this complex are solely metagabbro and metapyroxenite. The smallest body, southeast of Deer Pond, is metagabbro, and the two larger bodies are intermixed metagabbro and metapyroxenite.

The Cape Ray Granite is intrusive into the gabbros but

the contacts are transitional as quartz is locally significant, forming up to 10% in the bordering gabbros. Biotite also occurs in the gabbro in these contact zones. Towards the gabbro bodies, the granite (tonalite) becomes progressively enriched in metagabbro xenoliths.

Tonalitic Cape Ray Granite, Strawberry Granite and aplite dykes commonly cut the metagabbros. There are also rare patches and dykes of plagioclase-rich material, containing less than 10% mafics and/or quartz, that invade the metagabbros. These appear to be plagiogranite (cf. Coleman and Peterman, 1975) dykes.

### 2.3 The Port aux Basques Complex (Map Unit 2)

This complex consists of two units, viz.; the Port aux Basques Gneiss and the Port aux Basques Granite, both of which were originally defined by Brown (1973). The Port aux Basques Granite does not occur to any great extent within the Cape Ray Fault Zone but is present as a zone of outcrops that parallel the length of the map area, 3 km to the southeast.



### 2.3.1 The Port aux Basques Gneiss

This unit has been described in extensive detail by Brown (1973, 1975). The portion mapped in this study represents only a small fraction of the total outcrop area of this unit, so that all the features described by Brown (1973, 1975) are not present.

This unit (see Map 1 - in pocket), as mapped by the present author, is a banded leucocratic/melanocratic sequence with intense retrogression towards its contact with the Windsor Point Group. The melanocratic and leucocratic bands occur on all scales from 2-3 cm to 4 m, averaging about 0.5 m in width. Banding within individual amphibolite or gneiss bands is visible down to a scale of 0.5 mm. As a crude approximation the ratio of leucocratic:melanocratic bands is about 4:1.

#### 2.3.1.1 Amphibolitic (or Melanocratic) Bands

Most of these bands consist of 50-80% fine-grained ( $\leq 1.2 \times 0.5$  mm, up to  $2.3 \times 1$  cm), acicular, green hornblende crystals with intergranular, leucocratic feldspar (+ quartz), but there are bands, with  $< 25\%$  hornblende, that appear to be transitional between gneiss and amphibolite. Generally the hornblende forms are massive intergrowths, but occasionally single, large acicular crystals (up to 10

mm long, but averaging 1 mm long) overgrow the massive amphibolite on cleavage surfaces.

Garnets are fairly common in the amphibolites, averaging 2-3 mm in diameter and accounting for 5-10 % of the rock. However, there are some bands that contain up to 30% red garnets, on the order of 1-2 cm in diameter, giving the amphibolite a "plum pudding" appearance.

#### 2.3.1.2 Gneiss (or Leucocratic) Bands

Lithologies of this type run the gamut from massive quartz-feldspar rocks with < 10% mafics to micaceous layers with < 10% leucocratic material. Essentially the mafic minerals are biotite and/or hornblende (layers < 1 mm thick) and the leucocratic minerals are quartz and feldspar (layers average 2-3 mm thick).

Garnets are typically present and are usually 2-3 mm in diameter, though some leucocratic layers are massive pink rocks that contain up to 30-40% garnets of 0.1-0.15 mm in diameter. Very large garnets (up to 2 cm in diameter) occur in the gneiss near the northeastern edge of the map area, along with large staurolite crystals, up to 1.5x5 cm (Plate 2-1A).

Disseminated pyrite cubes are common and can account for 10% of the gneiss and the gneiss layers locally have rusty stains due to oxidation and breakdown of both pyrite

and biotite.

The Al<sub>2</sub>O<sub>3</sub> polymorphs are usually absent in the gneiss unit (as mapped during this project), however, just to the south of Big Pond (see Map 1), by its contact with the Isle aux Morts Brook Granite, crystals of andalusite, up to 1.5x0.5 cm, are concentrated in the gneiss proximal to quartz veins. As a result of alteration post-dating the main prograde event, these andalusite porphyroblasts are extensively rimmed and replaced by sericite.

#### 2.3.1.3 Other Interbands

A single outcrop (approximately 125 m wide) of a massive, dense, green rock occurs in Bailey's Brook which contrasts with the surrounding gneisses in both colour and complete lack of fabric. The rock consists of 80% granoblastic, subhedral epidote grains (average 0.8 mm in diameter) with intergranular actinolite (5%). Magnetite (5%) occurs as inclusions within the epidote and there are 1-3% anhedral, intergranular patches of sphene and 7% patches of anhedral garnet surrounding the smaller epidote grains. This rock is apparently of the type called calc-silicate by Brown (1973), later called epidosite (Brown, 1975; 1976a).

Also in Bailey's Brook there is a 1-2 m thick garnetiferous amphibolite band that contains up to 25%

pyrrhotite. The rock consists of 30% rounded garnet patches (average 1 mm in diameter, but up to 3-4 mm) intergranular to relict poikiloblastic hornblende grains that are themselves extensively altered to limonite-chlorite-carbonate. Secondary lath-like actinolite crystals have rosette-forms in places. The pyrrhotite occurs as amorphous, rounded grains about 1 mm in diameter. In very schistose portions of this band, garnet is absent and pyrrhotite layers (accounting for up to 60% of the rock) are interfolded with sericitized-epidotized amphibole.

#### 2.3.1.4 Retrograde Rocks along the Windsor Point Group Contact

The contact between the Port aux Basques Gneiss and the Windsor Point Group was not observed within the map area and probably would be obscured by the structural and metamorphic complexity of this boundary, aside from the lack of outcrop due to glacial overburden. Prograde metamorphic overprinting of the Windsor Point Group and retrograde metamorphism of the Port aux Basques Gneiss, coupled with a structural history involving at least three deformational events, have so effectively modified and masked the contact that its location can only be approximated.

Brown (1973, 1975, 1976a and 1977) described the Cape Ray Fault as a tectonised-mylonitized zone between the Long Range Gneiss/Cape Ray Granite and the Port aux Basques Gneiss. He described the Windsor Point Group as a mixed sedimentary-volcanic unit that was deposited upon the mylonite. Brown (1976a and 1977) showed that the mylonite zone separated the Port aux Basques Gneiss and the Windsor Point Group except in the region of Big Pond where the two groups are in geologic contact. Although this contact was not described by Brown, according to his formational definitions, it would have to be an unconformable relationship with Windsor Point Group 'cover' resting on Port aux Basques Gneiss 'basement'.

As is described in greater detail below, most of the mylonites in the Cape Ray Fault Zone defined by Brown (1973, 1975, 1976a and 1977) have been reinterpreted as Windsor Point Group material. Hence the problem is to delineate a geological contact in a zone of combined structural and metamorphic complexity.

In order to differentiate between the two units near their contact, recognizable and distinctive features in each unit must be defined. The Port aux Basques Gneiss consists of interbanded gneiss units, with a typical granoblastic-polygonal texture, and amphibolites, with abundant poikiloblastic hornblende grains overgrowing a polygonal groundmass. The lowest retrograde metamorphism in this

unit is upper greenschist facies (eg. Miyashiro, 1973) as indicated by intergrowths of biotite-chlorite-garnet.

The Windsor Point Group, near the contact, consists of metatuffaceous sediments with recognizable clastic quartz and feldspar grains in a sandy to silty matrix. These rocks are also upper greenschist facies containing chlorite-biotite intergrowths.

Both units were deformed during a three-phase deformational sequence that was intense enough to have produced mylonites within the Windsor Point Group. The Port aux Basques Gneiss had been previously deformed and these later events retrogressed the gneiss/amphibolites to lower metamorphic grades.

The main discriminating features are:

- 1) relict sedimentary textures in the Windsor Point Group vs. recrystallized polygonal intergrowths in the gneiss,
- 2) lack of amphibolite grade metamorphism in the Windsor Point Group, and
- 3) greater structural complexity in the gneiss.

These differences form the basis for defining the contact as it appears on the geological map (see Map 1 in pocket for the following geographical locales of this contact).

To the south of Dog Pond, a rock type, best termed phyllonite, occurs that is massive, dark grey and micaceous with a lustrous sheen and 5% garnet porphyroblasts (average

2 mm in diameter) (Plate 2-1B). The rock consists of dense muscovite layers overgrowing a quartzo-feldspathic groundmass, which consists of minute (average  $0.05 \times 0.02$  mm), ovoid to rectangular, strain-free granoblastic grains. The garnets are fractured and many are replaced by chlorite and sericite. Rare tourmaline grains are visible in the groundmass.

Phyllonites, as first described by Knopf (1931) and elaborated upon by Higgins (1971), are products of retrogressive metamorphism coupled with intense recrystallization, due to low temperature mylonitization (Spry, 1969), to finer grain sizes. Phyllonites have a phyllitic appearance, but may be derived from coarser-grained granular or gneissic rocks (Higgins, 1971), thus the protolith of this phyllonite could have been either amphibolite or gneiss of the Port aux Basques Complex.

Sericite schists occur just to the northeast of the phyllonite and the petrography of these schists indicates that they were derived from felsic tuffs and thus they are inferred to have been derived from the Windsor Point Group. Recognizable lithic felsic (lapilli) tuff also occurs further to the northeast. The contact in this area is therefore marked by retrogression and deformation of the Port aux Basques Complex.

Definitive garnet-biotite-muscovite gneiss (with

andalusite) of the Port aux Basques Complex occurs southeast of Big Pond. However to the north, this gneiss passes through a poorly defined zone of massive sericite/muscovite schist. These schists are somewhat phyllonitic, with broken, altered garnets. North of the phyllonitic schist, biotite-chlorite-sericite schist occurs that somewhat resembles metatuff.

The contact as it appears eastwards from the Isle aux Morts Brook, through I and H Brooks to the Gulch, and including the Main Shear mineralization area is relatively well-defined (Map 1). Interbanded biotite gneiss and garnetiferous amphibolite gradually become more tectonized and retrogressed to the north, and near the contact the last recognizable unit with Port aux Basques affinity is a silvery-grey muscovite schist which has a strongly folded, "wavey" aspect. These pyritiferous schists consist of massive muscovite layers, with chlorite, overgrowing a granular (relict granoblastic) quartzo-feldspathic groundmass, which, along with rare relict hornblende and biotite, indicate these schists are retrogressed gneiss. There was strong shearing parallel to the muscovite layers. It would seem that the previously described phyllonites are simply more extreme examples of the same retrogressive processes which produced these schists. The Windsor Point Group, north of the contact, is mainly chlorite-sericite schist (after metatuff) with visible sedimentary bedding



and clasts.

### 2.3.2 Port aux Basques Granite

Figure 2 shows the outcrop pattern of the granite in relation to this map area. The only occurrences of this unit within the map area are restricted to thin folded interbands (~0.1 m wide) within the Port aux Basques Gneiss south of Big Pond.

Brown (1973, 1975, 1976a) described the granite as a synkinematic intrusion produced during the same D2 deformation that resulted in folding of the Port aux Basques Gneiss. Subsequently a third folding event, D3, overprinted the gneiss and granite, yielding an interference-type pattern (type 2 as modelled by Ramsay, 1967). This deformation also produced the strong planar fabric present in the granite (Brown, 1975) defined by alignment of biotite.

Dingwell (1980, using Streckeisen's (1976) modal classification scheme), described the southwestern intrusion as ranging from granite to granodiorite in composition, with rare quartz monzonite. According to both Dingwell (1980) and Brown (1975), this granite had no thermal metamorphic effects upon the host gneiss.

In coastal exposures to the southeast of the map area, migmatites occur within the Port aux Basques Gneiss. Brown

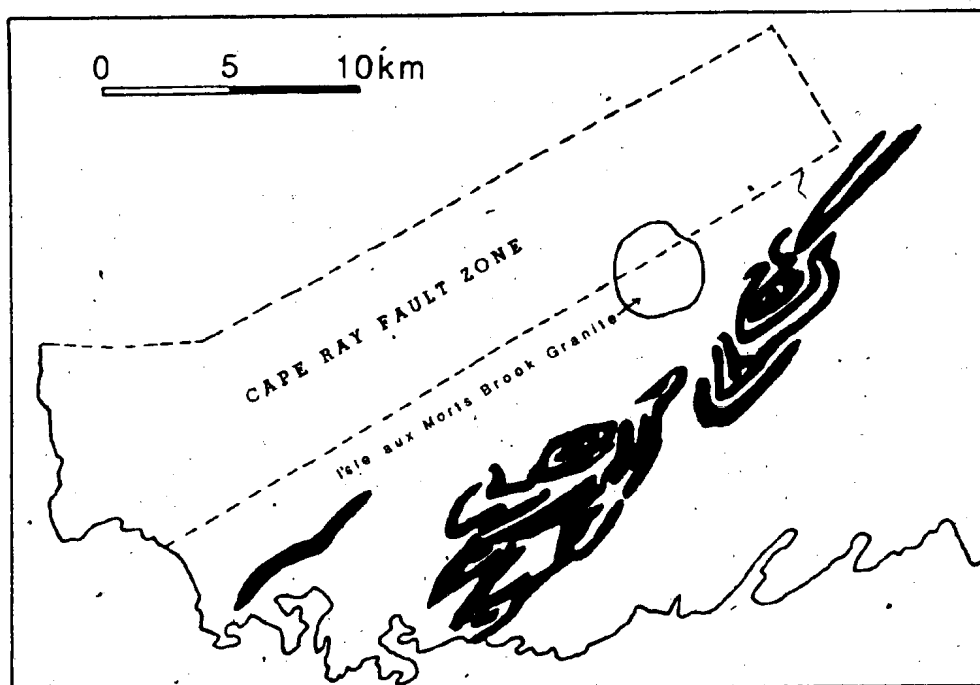


Figure 2 Outcrop form of the Port aux Basques Granite (after Brown, 1975) and location with respect to the Cape Ray Fault Zone. The granite is outlined in black.

(1975) suggested that these migmatites and the Port aux Basques Granite were transitional, and therefore the migmatites probably represent a root zone (or generation zone) for the granitic magmas (ie. the granite was derived from partial melting of the gneiss).

A gravity survey over the southwestern "bull's eye" by Dingwell (1980), indicated that the granite was present as a series of thin sheets of shallow depths, and his modelling of aeromagnetic data indicated that the granite was probably present to a depth of less than 750 m. This geophysical evidence, coupled with geochemical constraints, led Dingwell (1980) to support Brown's suggestion that the granite was derived by partial melting of a nearby source, probably the Port aux Basques Gneiss.

#### 2.4 The Cape Ray Granite (Map unit 3)

This unit consists of two phases, a tonalite (unit 3a) and a megacrystic granite (unit 3b) (see Map 1). The tonalite is the more extensive phase and occurs along (and as) the northwestern edge of the map area. The megacrystic phase is restricted to the headland at Cape Ray and inland to Billy's Pond to the northwest.

#### 2.4.1 The Tonalite

This medium- to coarse-grained equigranular intrusive contains up to 30% chloritized biotite and approximately equal amounts of quartz and feldspar (Plate 2-1C). Grain sizes ranges up to 2x2 cm, but generally average 1 cm. This granitoid is generally a homogeneous tonalite but grades into granodioritic or megacrystic phases with the appearance of potassium feldspar. There are also some transitional phases, produced by metasomatic effects, where the tonalite is in contact with the later Strawberry Granite.

Amphibolite xenoliths are ubiquitous through the entire outcrop area of the tonalite (Plate 2-1C) and increase in size and quantity as the contacts with the Long Range Mafic/Ultramafic Complex are approached to the point that rocks at the contact are transitional between tonalite and gabbro. Elsewhere xenoliths can be so abundant that the tonalite is better called an agmatite (Plate 2-1D).

Smaller xenoliths have variably developed reaction rims with the enclosing tonalite (Plate 2-1E). These reaction rims probably reflect differential removal of plagioclase from the xenolith due to contrasting plagioclase compositions between tonalite and xenolith. Alternatively, the dykelets of tonalite cut larger xenoliths with little chemical reaction and occasionally xenoliths contain pink potassium feldspar porphyroblasts.

These xenoliths fit Didier's (1973) criteria for

PLATE 2-1 A) Large staurolite porphyroblasts in garnet-biotite gneiss of the Port aux Basques Complex. Single staurolite crystals are up to 3x1.5 cm.

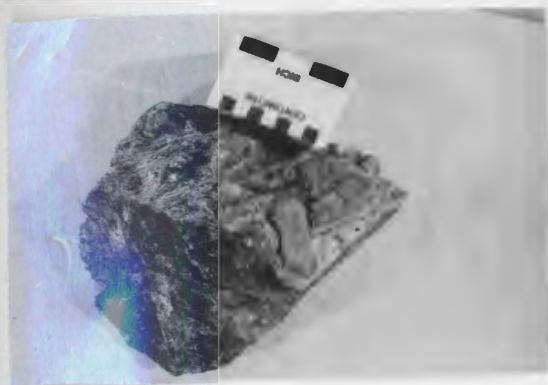
B) Port aux Basques Complex phyllonite from contact with the Windsor Point Group.

C) Tonalitic Cape Ray Granite. Consists of coarse-grained feldspar/quartz intergrowths (note penny for scale) and amphibolite xenoliths.

D) Agmatitic textures in tonalitic Cape Ray Granite.

E) Reaction rims between amphibolite xenoliths and enclosing tonalitic Cape Ray Granite.

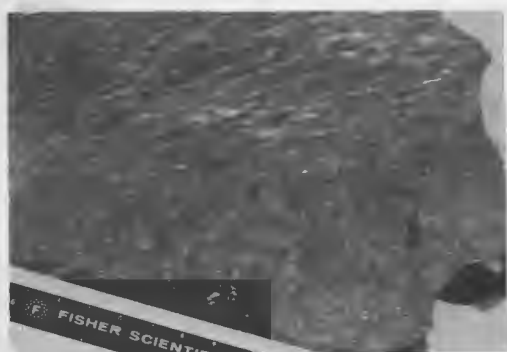
F) Flattened xenoliths in tonalite Cape Ray Granite. The flattening plane is parallel to the long axis of the plate, this vein is about 1 m across.



A



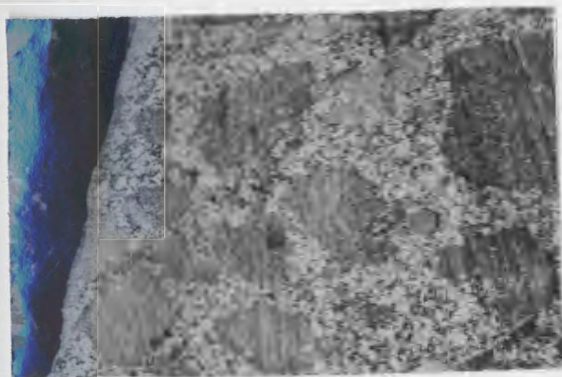
D



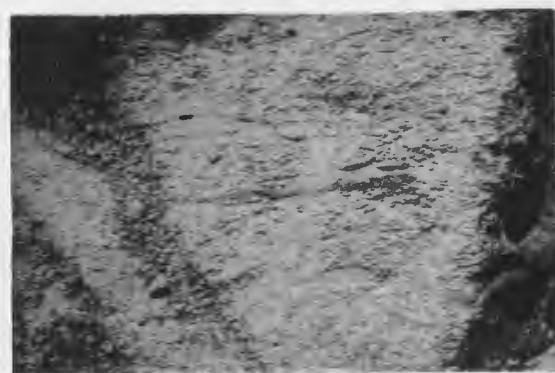
B



E



C



F

congeneric igneous xenoliths. These criteria include: presence throughout the tonalite (not concentrated near contacts); round shape with diffuse contacts (not angular with sharp contacts); equivalent structural fabric (no earlier fabric); and the presence of feldspar porphyroblasts within the xenolith. Paraphrasing Didier (1973), congeneric igneous xenoliths are genetically linked to an enclosing host as either first-formed phases of a magmatic suite, or as parents to partial melting. Since the xenoliths seem to be fragments of the Long Range Mafic/Ultramafic Complex, the tonalite phase of the Cape Ray Granite is interpreted to be a partial melt of these ophiolitic remnants.

Towards the contact with the Windsor Point Group the tonalite becomes increasingly deformed and is characterized by well developed S. and L. fabrics, which are also displayed by the shapes of amphibolite xenoliths (Plate 2-1F). The tonalite however does not have a gneissic aspect. This latter observation contradicts those of Brown (1973, 1973b, 1975, 1976a, 1976b and 1977), who called all of this unit the Long Range Gneiss and correlated it with Grenvillian (900-1100 Ma) basement gneisses that underlie the Great Northern Peninsula.

Brown (1975, 1976b and 1977) stated that the contact between the "Long Range Gneiss" and the Long Range Mafic/Ultramafic Complex ophiolites was tectonic, as the ophiolites were thrust upon the older gneiss. This study concurs with Phair (1949) in that the tonalitic terrane is

(re)defined as intruding the ultramafics, (although Phair (1949) thought the ophiolites were themselves intrusive into pre-existing early Paleozoic gneisses and that the tonalite represented the final phases of this intrusive sequence).

#### 2.4.2 The Megacrystic Phase

This phase is best called a megacrystic microcline-biotite granite because it consists of abundant (30-40% of the rock), large, pink (average 2x1 cm), euhedral microcline crystals set in groundmasses of plagioclase, quartz and biotite (Plate 2-2A). The relatively fresh biotite occurs as clots up to 0.5 cm in diameter while plagioclase is euhedral, with grain sizes averaging 0.75x0.3 mm. Often the plagioclase is greenish, and when contrasted with the large pink megacrysts and black biotite patches, produces a stunningly colourful rock. Meta-amphibolite xenoliths, similar to those in the tonalite, occur throughout this granite.

Occasionally, primary rhythmic layering of the megacrysts (and also xenoliths) is visible (Plate 2-2B) which appears to be a gravity-settling feature, in which denser xenoliths and microcline crystals settled through a magmatic fluid. Closer examination reveals that the megacrysts are concentrated in biotite-rich layers (biotite



up to 30% of the rock), with intervening megacryst- and biotite-poor layers, thus biotite may be an early crystallized phase. Such layering indicates that the megacrysts are primary and not a product of later metasomatism. The euhedral nature of the megacrysts, the concentrically aligned inclusions and smaller grain size of included plagioclase vs. plagioclase in the groundmass, are also indicative of a primary magmatic origin for these megacrysts (after Higgins and Kawachi, 1977).

This granite occurs only within the tonalite and their contacts are transitional, with fewer megacrysts in the megacrystic phase, and scattered microcline megacrysts in the tonalite at their contact. The transitional contacts, similar mineralogy, and type of xenoliths, indicate that these two granitoids are separate phases of the same suite. Elsewhere in the tonalite, there are areas where megacrysts of alkali feldspar occur but these are never large enough to map separately.

#### 2.4.3 Xenoliths

The xenoliths are green and are usually more readily weathered (recessive) with respect to their hosts. Close to the Long Range Mafic/Ultramafic Complex, the xenoliths are often recognizable gabbro with intergranular quartz but away from these ophiolitic fragments, the xenoliths are

smaller and are strongly chloritized.

In thin section relict hornblende crystals are very poorly preserved as they are replaced by green biotite (early; due to the tonalite), or combinations of chlorite, sphene and epidote (late). Small quartz patches are ubiquitous (due to silicification from the enclosing tonalite).

#### 2.5 The Red Rocks Granite (Map Unit 4)

This granitoid occurs inland from Red Rocks Point where it has limited areal extent (~ 2.25 km<sup>2</sup>) and the best exposures are in the walls of a gravel pit in its centre (see Map 1 in pocket). There are numerous phases present but the rock is mainly an equigranular, fine- to medium-grained, white to pink granite with granodioritic phases, and pegmatite and aplite dykes. The thickest aplite dykes (up to 2 m wide) contain pegmatite cores.

Biotite generally occurs as fine (2-3 mm) flakes but there are large biotitic clots (up to 10 cm in diameter) and abundant biotite schlieren (Plate 2-2C). These schlieren probably represent xenolithic remnants (as outlined by Didier, 1973).

The only visible contact of this granite is at its southwestern boundary with the Cape Ray Granite tonalite. This contact is marked by an intense tectonised zone in

which mylonite was produced (Plate 2-2D).

Basal biotite sections quite commonly have crystallographically orientated rutile needle (0.15x0.015 mm) inclusions. These intergrowths of rutile and biotite are called sagenitic textures and have been reported by Collerson and Bridgewater (1979) in biotites of the Uivak Gneisses of Labrador. They described the intergrowths (p. 229) as rutile exsolution from titaniferous biotite due to "volatile fluxing (diffusion) synchronously with the addition of potassium (and other LIL elements) to lithologies previously depleted in these elements".

Brown (1973 and 1975) defined the Cape Ray Granite as consisting of only the megacrystic phase, and the Red Rocks Granite as a post-tectonic granite. He later (Brown, 1977) dropped the Red Rocks Granite as a separate geologic unit and included it in a revised Cape Ray Granite which also included the Strawberry Granite (described below) and the megacrystic phase, all supposedly Devonian or earlier in age.

#### 2.6 Basaltic Dykes (Map unit 5)

Two dykes, up to 5 m wide, cut the Red Rocks Granite just north of Red Rocks Point and deformed dykes cut the megacrystic Cape Ray Granite near Billy's Pond (see Map 1). These are the only basic dykes seen in the area by the

author. Their age is unknown except they are post-Cape Ray and Red Rocks Granites

The dyke in the Red Rocks Granite has relict epidote-filled <sup>64</sup>amygdules, large euhedral plagioclase phenocrysts (up to 12x5 mm) and granitic xenoliths. The dykes are typical diabases, though altered, with subophitic to intergranular textures.

#### 2.7 Gabbro (Map unit 6)

The largest outcrop of this unit occurs along the southern contact of the Windowglass Hill Granite. Smaller outcrops are found south of Dog Pond, near the northeast edge of Big Pond and southeast of the Gulch (ie. the northeastern edge of the map area). (There are also abundant interbands of gabbro through the Windsor Point Group but they are too small to be mapped independently, and so are described as members of that group).

The gabbro south of Windowglass Hill is so extensively deformed that relict granular textures are only rarely visible. In general the gabbro is a dense green, schistose and folded rock usually with attenuated green and white banding where the white layers are extremely stretched feldspar concentrations. Small dykelets of Windowglass Hill Granite cut through the gabbro and closest to the granite, there appears to have been a slight hornfelsing of

the gabbro, since this rock becomes black and aphanitic. Epidote veins and pods are common, as are quartz veins. Pyrite is often disseminated through the gabbros and minor pyrrhotite is present also.

In the stream flowing south from Dog Pond, gabbro forms a continuous outcrop. The gabbro has various degrees of deformation through its length, but is generally fresh, consisting of 80% subhedral plagioclase (up to 1.5x3 mm), and lesser perthite, with a hypidiomorphic-granular texture. Intergranular to the plagioclase are chlorite laths (after mafics) and light brown biotite.

Gabbro occurs in a small stream flowing into the Gulch. This gabbro contains single phenocrysts and glomeroporphyritic masses of plagioclase in a sheared groundmass replaced by chlorite and epidote. There is also biotite and pyrite in the groundmass.

These latter two gabbroic bodies occur within the contact region between the Port aux Basques Gneiss and the Windsor Point Group, but contact and age relations of the gabbros with these units are indeterminate. They are somewhat unusual, almost lamprophyric, due to the presence of primary biotite and absence of hornblende, and are thus distinct from the gabbro south of the Windowglass Hill Granite.

## 2.8 The Windsor Point Group (Map unit 7)

The group is divisible into seven mappable units of which the dominant unit, a chlorite/sericite schist, contains numerous small interbeds of other lithologies. A basal ignimbrite unit unconformably overlies the tonalitic Cape Ray Granite, and feeder dykes intrude the tonalite. This ignimbrite passes progressively upwards through a volcaniclastic conglomerate/sandstone into the main chlorite/sericite schist unit which is in tectonised contact with the Port aux Basques Complex.

### 2.8.1 The Little Barachois Formation (Map units 7a, b and c)

The Little Barachois Formation is an informal name for those lower portions of the Windsor Point Group comprising ignimbrite/rhyolite (unit 7a), volcaniclastic conglomerate (unit 7b), and intermixed conglomerate and sandstone (unit 7c). All three extensively intercalated members are genetically linked and they occur along the northwestern fringe of the Windsor Point Group throughout the Cape Ray Fault Zone, in thin (<600 m wide) discontinuous bands between the tonalitic Cape Ray Granite and the chlorite/sericite schist subunit of the Windsor Point Group. The base of the Little Barachois Formation in all exposures comprises a combination of ignimbrite and rhyolite rock types.

Along the northeast shore of Little Barachois, the ignimbrite ranges from a dark purple to reddish, massive rock with minute ( $<3 \times 3$  mm), equant feldspar and quartz grains in an aphanitic matrix cut by jasperoid veins. Lithic ignimbritic clasts (Plate 2-2E) are locally visible, indicating the pyroclastic nature of the rock. Generally, however, due to strong welding, the rock does not contain visible fiamme or pumice.

Towards the southeast, the outcrop progressively changes from massive ignimbrite to ignimbrite with sericitized volcanic clasts (up to 0.3 m in diameter), and finally to a sedimentary sequence consisting of interbedded mudstones (metatuffs), sandstones and conglomerates. Clasts in the conglomerates are of aphanitic felsic volcanics (*ie.* the underlying ignimbrite), and some of the conglomerates appear to be laharic, with felsic volcanic clasts (up to 0.5 m in diameter) in a muddy matrix.

In its most extreme form, alteration of volcanic clasts within the conglomerates yields clasts that are totally replaced by sericite with tourmaline needles. This style and degree of alteration is very reminiscent of that seen in eruptive volcanic piles (*cf.* Williams and McBirney, 1979) wherein hot boron-rich volcanic gases rise through the pile selectively altering portions.

To the NE, the next outcrop of ignimbrite occurs as a small inlier on either end of Dilly's Pond, where the rock

PLATE 2-2 A) Megacrystic Cape Ray Granite. The megacrysts are euhedral microcline crystals.

B) Crystal layering in megacrystic Cape Ray Granite. Megacrysts and biotite are concentrated in the melanocratic layers, and plagioclase and quartz are concentrated in the leucocratic layers.

C) Biotite schlieren and clots in the Red Rocks Granite.

D) Mylonite along the contact between the Red Rocks and tonalitic Cape Ray Granites.

E) Ignimbritic rhyolite at the base of the Windsor Point Group (Little Barachois Formation): Note the ignimbritic clast by the lens cover.

F) Autobrecciated rhyolite of the Little Barachois Formation. The autobreccia consists of aphanitic rhyolite set in an aphanitic, magnetite-bearing matrix of rhyolite. Note hand lens scale to right.

5





A



D



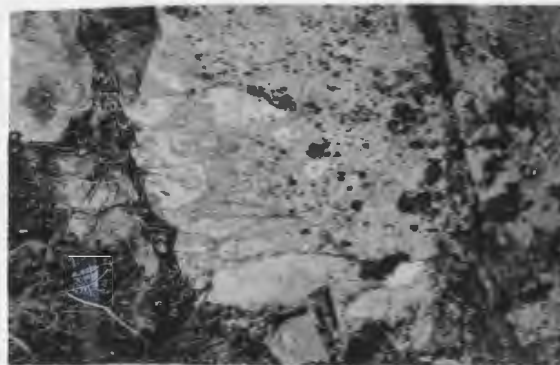
B



E



C



F

looks like an autobrecciated rhyolite. It consists of flesh-coloured aphanitic material hosting reddish to flesh coloured fragments of aphanitic rhyolite/ignimbrite (Plate 2-2F). Both matrix and clasts have small (~ 1 mm in diameter) euhedral quartz phenocrysts and rare, minute  $\leq$  1 mm) pyrite cubes.

In the western-most stream flowing into Dog Pond, the contact with the underlying tonalite is visible. At the contact, the tonalite contains large (up to 1 cm in diameter) round quartz patches in a sericitized groundmass of chlorite/biotite. The aphanitic and silicified ignimbrite/rhyolite contains screens and xenoliths of tonalite near the contact. Approximately 50 m from the contact, the rock is massive with 1 mm in diameter quartz and feldspar crystals set in a pink aphanitic groundmass.

The clast-supported volcanoclastic conglomerates (unit 7b) extend for a distance of about 10 km from near the mouth of the Little Barachois Brook to the Grand Bay River, but are never wider than 200 m. The vast majority of clasts are red, purple and black ignimbritic and rhyolitic volcanics, derived from the underlying ignimbrite/rhyolite, with minor mudstone (Plate 2-3A). The clasts are generally flattened and stretched. There are rare clasts that resemble both tonalitic Cape Ray Granite (Plate 2-3B) and Red Rocks Granite. The matrices generally range from black mud to medium/coarse-grained sand but in places the

4

Conglomerates resemble rhyolitic autobreccias. Abundant disseminated magnetite grains ( $\leq 1-2$  mm in diameter) occur in both matrices and clasts. The conglomerate grades into black mudstones and siltstones, with occasional felsic volcanic clasts, to the southeast.

The mixed volcanoclastic sandstone and conglomerate unit (map unit 7c) occurs in a narrow 7 km long band from the northern edge of Long Pond and as a small outcrop just above the Isle aux Morts Brook along strike from the main outcrop. The rock type ranges from mudstone to coarse-grained sandstone containing felsic volcanic grains. Generally all lithologies are schistose and often are so deformed that clasts are barely distinguishable from sericitized matrices. Rare beds of purple rhyolite/ignimbrite, from 1 to 3 m thick, are scattered through the sediments. The massive nature of these interbeds contrasts with the schistosity of the sediments.

5

In one location, north of the Windowglass Hill Granite, a relict sedimentary sequence is visible in this unit. A 6 m thick conglomerate bed is conformably overlain by a 12 m thick bed of sandy, lithic felsic tuff. This tuff is in turn overlain by a 0.6 m thick, schistose, basal portion to an ignimbrite that is itself 6 m thick. The schistose basal layer probably represents the chilled margin at the bottom of a pyroclastic eruptive sequence.

The Little Barachois Formation is an example of what

Self (1982) defined as a pyroclastic flow (vs. a pyroclastic surge or fall deposit). According to Self (p.23), these deposits are produced by "lateral movement of pyroclastic material as a gravity-controlled, hot, high concentration gas/solid dispersion". A typical feature of these deposits is small-scale fumarolic activity (Self, 1982). The distinctive sericitized tourmaline-bearing patches in the ignimbrites, near Little Barachois, are probable examples of this type of hydrothermal activity (ie. fumarolic).

#### 2.8.2 Chlorite/Sericite Schist (Map unit 7d)

The Main Shear showings occur within this unit which forms the bulk of the Windsor Point Group, accounting for > 65% of the group. The dominant lithology is intermixed chlorite and sericite schist, but distinctive (though not differentiable at this scale of mapping) interbeds abound through this unit. To describe the schist unit in detail, reference must be made to each distinctive subunit or interbed within it.

The contact between the Little Barachois Formation and these schists is gradational and may be more a case of lateral facies changes than a direct superpositional feature. The contact with the Port aux Basques Gneiss is complex as discussed above.

#### 2.8.2.1 Chlorite Schist

This rock type is predominantly a fine-grained (grain size  $\leq 1$  mm in diameter), granular metatuffaceous sediment, but interbeds can range from phyllite through metasandstone to metaconglomerate. Scattered through interlayers of all grain sizes (excluding the conglomerates) are rare clasts of felsic volcanic rocks. Schistosity is variably developed, such that the rock ranges from a more or less massive greenstone with original sedimentary textures visible, to an intensely flattened schist, but in general the schistose nature becomes more pronounced towards the Port aux Basques Complex.

Chlorite schists are gradational with both sericitic and graphitic schist interlayers, and often the chlorite schist contains thin interlaminae of either graphite or yellowish, massive sericite. Epidote layers, augen, and grains are also common in the chlorite schists and there are occasional pyritiferous layers (up to 10 cm thick).

#### 2.8.2.2 Sericite Schist

These schists are extensively interlayered with chlorite and graphite schists. In field aspects these schists resemble the chlorite schists except grain sizes range from medium sand ( $\leq 2$  mm in diameter) to aphanitic,

and euhedral equant feldspar and quartz grains are common. The sericite schists, which range from a massive aphanitic siliceous rock to a granular sandy rock with sericite interlaminae, grade into layers, or even subunits, of definite ignimbrite/rhyolite. In contrast, the sericite schists developed as a retrogressive feature in the Port aux Basques Gneiss is a dense grey-black rock with scattered quartzitic eyes.

#### 2.8.2.3 Limestone Interbeds

Carbonate interbeds are quite common throughout the chloritic schists. In their most common form these interbeds are laminated rocks with thin brown to white carbonate and green chlorite schist or phyllite interlayers, that are usually 3-5 mm thick.

There are also distinctive interbeds of limestones, ranging from 2-3 cm (Plate 2-3C) to 20 cm thick within the chlorite schists. In general these limestones are somewhat silicified and strongly infolded within the chlorite schists.

#### 2.8.2.4 Gabbro

Gabbroic interlayers occur irregularly through the schist unit. A small body of granular gabbro that crops

out at the southeastern corner of Little Barachois contains white plagioclase, green hornblende and disseminated pyrite, with grain sizes on the order of 2-4 mm in diameter. This gabbro is massive and contact relations with the surrounding Windsor Point Group are not visible.

All other interbeds of gabbro are so strongly schistose and altered to chlorite that they resemble their enclosing chlorite schists except they contain relict subhedral hornblende and/or plagioclase grains (identification as a gabbroic rock often awaits petrographic analyses).

These gabbroic interlayers represent a titaniferous (as shown by their sphene contents) mafic volcanic phase within the Windsor Point Group. In general they appear to have been some sort of dyke-like intrusions consanguinous with the enclosing tuffaceous material.

#### 2.8.2.5 Graphite Schist

The best exposures of these schists are on the eastern side of Little Barachois, in the Little Barachois Brook, and in the small stream flowing out of the Windowglass Hill Granite into the Isle aux Morts Brook. The graphitic schists that host the Main Shear showing do not crop out, but drilling has revealed that these and other graphitic schist interbands are quite common through the entire

chlorite schist horizon between the northeastern Windowglass Hill Granite extension and the Port aux Basques Gneiss (ie. southeast of the Isle aux Morts Brook). It is reasonable to assume that graphite schist interbeds are extensive elsewhere through the schist member, but due to their easily eroded nature, may be present only in the subsurface.

#### 2.8.2.6 Chert (quartzite)

Chert beds, though not common, are best developed within the chlorite schists at Jerret Point. Here they are an average of 0.3 m thick, but they bulge up to 0.6 m wide (Plate 2-3D). They are an aphanitic silicious rock with variegated colours of green, red and buff.

#### 2.8.2.7 Sandy Tuff/Ignimbrite

These small interbands within the chlorite schists contain quartz and feldspar crystals (average 2x4 mm) in an aphanitic groundmass, and are also best developed at Jerret Point. Petrographically these interbands consist of bedded plagioclase, quartz and alkali feldspar grains in cryptocrystalline quartz-rich groundmass. The crystals are generally slightly broken indicating possible air fall or transport degradation. In general these interbands appear



PLATE 2-3 A) Volcaniclastic conglomerate in the Little Barachois Formation. In this clast-supported conglomerate, the fragments are of the underlying felsic volcanics.

B) Tonalitic Cape Ray Granite clast in the Little Barachois Formation volcaniclastic conglomerate. The clast is to the right of the scale.

C) Isoclinally folded limestone interbed in the Windsor Point Group schist unit.

D) Chert interbed in the Windsor Point Group schist unit.

E) Conglomerate unit at Windsor Point. Clasts are mainly of felsic volcanics.

F) Graphic intergrowths of quartz and feldspar in the Windowglass Hill Granite. The isolated feldspar grains are in optical continuity. This section is about 2 mm across.



A



D



B



E



C



F

to represent small felsic tuffaceous layers.

#### 2.8.3 Limestone (Map unit 7e)

The solitary outcrop of this member occurs within the chlorite/sericite schist unit as a road cut on the Trans-Canada Highway. The rock consists of 2.5-3 cm thick grey limestone layers with 0.5-1 cm thick interlayers of grey mudstone. The mudstone bands have abundant quartz vein tension gashes (indicative of ductility contrasts with the mudstone) containing pyrite. This limestone unit is actually a large scale version of the laminated limey tuff interbeds that occur in the schist unit.

Examination of this limestone, and also of the various limestone interbands within the schist unit, for conodonts, by standard techniques (L.E. Fahraeus, 1981, pers. comm.), proved fruitless as no fossils were found.

#### 2.8.4 Felsic Tuff (Map unit 7f)

This unit occurs within the schist unit (unit 7d) between Big Pond and Dog Pond. In field aspect, the rocks of this unit are porphyritic with 1-4 mm in diameter phenocrysts of quartz and feldspar in silicious aphanitic groundmasses. The colour of the groundmasses ranges from buff to pink. The rhyolite usually has a planar fabric

defined by sericite-coated partings, and it grades into sericite schist. This unit is a relatively unmetamorphosed felsic volcanic interbed within the Windsor Point Group.

#### 2.8.5 Conglomerate (Map unit 7g)

In contrast with the conglomerates in the Little Barachois Formation, this conglomerate is extremely deformed. It is least deformed at Windsor Point where phyllites, with isolated clasts, grade into a conglomerate containing stretched clasts in a muddy matrix (Plate 2-3E). The clasts are predominantly felsic volcanics (with feldspar phenocrysts), granites, mudstones and epidosite (?). Inland near the highway, the conglomerate is so deformed that relict clasts (epidote and felsic volcanic) are visible only on plan surfaces. On surfaces perpendicular to the schistosity, the conglomerate consists of grey sericitic/chloritic interlayers with layers (3-5 mm thick) of pink silicious aphanitic material (meta-clasts). The sericite layers have a strong mica sheen developed on parting planes.

Epidotitic clasts in the undeformed conglomerate consist of 60-70% epidote grains with intergranular quartz and magnetite (up to 5%). The protolithology of these grains is problematical because they could represent

fragments of epidosite as occurs within the Port aux Basques Gneiss, but there is no garnet present, or they might represent silicified xenoliths of Long Range Mafic/Ultramafic Complex material as occur within the Cape Ray Granite, or they could be clasts of the enclosing chlorite schist.

#### 2.8.6 Feldspar Porphyry Dykes (Map unit 8)

These dykes intrude the Red Rocks and Cape Ray Granites along the coast at the western edge of the map area (near Red Rocks Point) and are up to 5 m wide. They contain euhedral phenocrysts of plagioclase, quartz and alkali feldspar in an aphanitic buff groundmass. One 1.5 m wide dyke has a 0.5 m wide schistose mafic border, indicating a bimodality to the intrusive suite.

The similar settings and petrologies of these dykes when compared to the basal ignimbrites of the Windsor Point Group tend to suggest that the dykes represent feeder dykes of the acid volcanism. Geochemical and geochronological evidence (described below) support this correlation.

#### 2.8.7 Summary of the Windsor Point Group

The Windsor point Group is fundamentally a volcanic sequence with associated sediments. According to Williams

and McBirney (1979) the presence of rhyolitic feeder dykes, strong welding in ignimbrites, and hydrothermal alteration ("fumarolic pipes"), are indicative of the central to proximal facies of a volcanic centre, while reworked volcanic material and interlayered sedimentary horizons are typical of more distal facies. Rather than representing a superpositional sequence (ie. vertical geochronological variations), the various members of the Windsor Point Group exhibit those lateral facies changes typical of explosively eruptive volcanic centres (cf. Williams and McBirney, 1979).

The demonstrably intrusive contact with the Cape Ray Granite, screens of tonalitic inclusions, plus the presence of ignimbritic/rhyolitic fragments in the rest of the Little Barachois Formation (and the Windsor Point Group) indicate the ignimbrite member was the locus for Windsor Point Group volcanism (ie. the source). The thin, attenuated, elongate outcrop pattern of the ignimbrite, shows that the volcanism occurred as a fissure-type eruption, rather than the "classical" cone-type.

The ignimbrite/rhyolite member exhibits no evidence of marine or lacustrine re-working and appears to be a subaerial deposit. Similarly the conglomerate/autobreccia member of the Little Barachois Formation, apparently reflects syn-eruptional re-working of the ignimbrite/rhyolite as is typically found in eruptive

terrane (eg. Self, 1982; LaJoie, 1980; Williams and McBirney, 1979).

Fragments of the Cape Ray and Red Rocks Granites within the conglomerates of the Little Barachois Formation (and possibly elsewhere in the Windsor Point Group), indicate that the granitic terrane to the northwest was topographically elevated relative to the Windsor Point Group during its deposition. The lack of definitive clasts of the Port aux Basques Complex within the Windsor Point Group suggests that the two units were topographically equivalent such that all the clastic input was derived solely from the northwest (ie. the volcanic locus).

As shown by their transitional relations, the sericite schists appear to be altered felsic tuffs. The chlorite schists on the other hand, contain greater amounts of mafic components (eg. plagioclase) and therefore are metabasic tuffs. These mafic tuffs imply a bimodal nature to the Windsor Point group volcanism. The supposed northeastern equivalent to the Windsor Point Group, the Billiards Brook Group (Chorlton, 1980b), contains mafic lava flows.

The relative freshness of lithic and crystal fragments in the Windsor Point Group schists is indicative of a low energy depositional environment that was near the source of the volcanic detritus. The extensive limestone interbeds are characteristic of shallow water environments and their interlaminar textures with tuffaceous material shows the

cyclic nature of the volcanism and sedimentation. The graphitic schists were derived from organic-rich muds, that were probably deposited in a lagoonal-type sulphur-rich environment. The reduced nature of the depositional area is further substantiated by the presence of magnetite and absence of hematite.

In summary, the sedimentary portions of the Windsor Point Group were deposited under shallow water, low energy conditions in a restricted basin (ie. thin and linear). The northwestern edge of the basin was topographically elevated. The proximal (or basal) felsic volcanic portions were deposited, at least in part, under subaerial conditions.

#### 2.9 The Windowglass Hill Granite (map unit 9)

This granite occurs in the northeastern edge of the map area. The granite has an elongate elliptical form, approximately 2.7x0.6 km, on the western side of the Isle aux Morts Brook, and a thin, attenuated outcrop, less than 100 m wide and 3.4 km long, on the eastern side of the brook. In the main (ie. western) outcrop, the granite ranges from a dominantly pink, aphanitic, silicious rock to one that looks somewhat rhyolitic with minute ( $\leq 1-2$  mm in diameter) quartz and/or alkali feldspar phenocrysts in a pink aphanitic groundmass with less than 1-2 % biotite.



Disseminated pyrite is concentrated in specific zones, especially as diffuse haloes surrounding sulphide-bearing quartz veins where the granite often has a rusty limonite-weathering surface. Magnetite octahedra account for less than 2 % of the rock.

The granite is so strongly jointed in one direction, that it is often broken into thin (1-2 cm to 5-10 cm thick) sheets that resemble "panes of windowglass". There is also a set of quartz veins which pinch and swell, from 3-4 mm to 3-5 m in width, over their lengths, that constitutes the Windowglass Hill Granite Showing.

Along its southern contact, dykes of the granite intrude gabbroic rocks, but the actual contact between granite and gabbro is sheared and faulted, and, nearest the contact, there is some tectonic breccia composed of granitic fragments in a silicious matrix. The northern contact is similarly sheared and faulted, such that the granite is mylonitized and consists of pink granitic augen set in massive aphanitic black chlorite/sericite matrix. In the Isle aux Morts Brook, the granite has a strong linear fabric at its contact with mylonitized chlorite schist. In drill hole PB133 the granite grades outwards, to the south, into a pyritiferous diorite.

Granite in the northeastern extension crops out in only the H and I Brooks, and the outcrop pattern as mapped (see Map 1 - in pocket) is outlined from drill core and

trench intersections. The granite in this area is very heavily mylonitized with strong linear fabrics, is altered to a light buff colour and has silky sericite partings. Galena-bearing quartz veins are quite abundant in the granite here, and constitute the H and I Brook Showings. These veins are apparently post-deformational and reflect deformation-induced remobilization.

In undeformed portions of the granite, the dominant texture is graphic intergrowths of albitized feldspar phenocrysts (up to 4 mm in length) and quartz (Plate 2-3F). Using Streckeisen's (1976) classification scheme, the Windowglass Hill Granite is an alaskite (or mafic-poor alkali feldspar granite).

Barker (1970) called graphic intergrowths, such as those in this granite, granophyric textures, and defined them as epizonal (*ie.* upper crustal) phenomena. According to Barker, such textures indicate rapid simultaneous growth of quartz and feldspar. The rapid crystallization of the silicate phases probably causes the evolution of an aqueous phase which produces the typical deuteric alteration present in granitoids with these textures. The Windowglass Hill Granite, with its sericite dustings and albitized feldspars, appears to have undergone some deuteric alteration. This is borne out in the geochemical studies below which indicate that a deuteric sodic metasomatism altered the granite.

In its most mylonitized portions, the granite consists of fine-grained recrystallized quartz and feldspar, on the order of 0.01-0.03 mm in diameter (Plate 2-4A), with occasional porphyroclasts of quartz and alkali feldspar, and strong sericitic overgrowths. There is actually a continuum between the most and least deformed granite samples as nearly all the samples show some evidence of deformation-induced recrystallization. Relict graphic textures are present in all samples, except the most completely deformed, and they constitute an identifying characteristic for the granite.

Brown (1976b) mapped this granite as Port aux Basques Granite.

#### 2.10 Mylonite (Map unit 10)

There are three significant mylonite zones within the map area. The smallest occurs along the southern contact between the Red Rocks and Cape Ray Granites, near Red Rocks Point. The other two zones are much larger and occur near Windsor Point and inland, within the Windsor Point Group, and in the Isle aux Morts Brook along the contact between the Cape Ray Granite and the Windsor Point Group.

Before describing these mylonites in detail, some consideration has to be given as to what a mylonite actually is, how it formed, and how it differs from other

rock types, or its protoliths. The term mylonite was defined first by Lapworth (1885). He described "mechanical metamorphism" in gneisses that were cut by a thrust fault. As a result of this "metamorphism", the gneisses were "crushed, dragged, and ground out into a finely-laminated schist (Mylonite, Gr., mylon, a mill) composed of shattered fragments of the original crystals of rock set in a cement of secondary quartz, the lamination being defined by minute inosculating lines (fluxion lines) of kaolin or chloritic material and secondary mica" (ibid., p. 559).

Mylonites were thus defined as cataclastic rocks derived by fracture and breakage of a parental rock (ie. brittle processes). This classical interpretation of mylonite and mylonite formation persisted in geological literature until, and probably reached its zenith with, Higgins (1971). Higgins (1971) developed a classification scheme for cataclastic rocks based on grain size and/or proportion of porphyroclasts (a remnant coarse-grained crystal or aggregate, also called phenoclasts (eg. Berthe et al., 1979)). Higgins also stated that cataclasis was most important in formation of mylonites, and neomineralization (recrystallization) was of secondary importance.

Bell and Etheridge (1973) disagreed with these hypotheses and showed that mylonites formed as a result of ductile deformation in which there is strong to extreme

grain size reduction due to recrystallization. Accordingly they redefined mylonite as a "foliated rock, commonly lineated and containing megacrysts, which occurs in narrow, planar zones of intense deformation.. It is often finer grained than the surrounding rocks, 'into which it grades" (*ibid.*, p.347). Numerous authors, for example White (1976), Bell (1978), Berthe *et al.* (1979) and Vauchez (1980), have subsequently substantiated that mylonites are derived from ductile deformation-induced recrystallization.

As described above, most of the rock types in the map area have undergone at least minor recrystallization and subgrain development. Some units, for example the northeastern extension of the Windowglass Hill Granite, have undergone such intense recrystallization that they are totally recrystallized into finer grains with no remnants of the protolith. Therefore, based on Bell and Etheridge's (1973) definition, most rock types exhibit some evidence of mylonitization.

The mylonites described below and mapped as separate units were differentiated from surrounding rocks on the basis of aphanitic (with occasional porphyroclasts) textures, due to intense recrystallization, that made normal petrological classification impossible.

### 2.10.1 Mylonite at Windsor Point

The conglomerate member (Map unit 7g) of the Windsor Point Group becomes progressively deformed towards its southeastern margin. Fragments in the conglomerate become progressively flattened and twisted (Plate 2-4B) until they are so extenuated they resemble tongues. The conglomerate then passes into pink to buff mylonite.

Brown (1973, 1975 and 1977) described this mylonite as the thin southwestern extension of a much larger mylonite zone that separates the Cape Ray Granite and Port aux Basques Complex. He also described a thin rhyolite unit overlying the conglomerate at Windsor Point, which grades into the mylonite, just before the mylonite grades out into Port aux Basques Gneiss.

This mylonite is a banded, aphanitic, siliceous rock. The colour ranges from pink to buff with some green chloritic interlayers. Occasional minute feldspar porphyroclasts are present, as are thin (2-4 mm thick), buff sericite interlaminae. Quartz veins are common but are usually boudinaged in the same general planar sense as the mylonite fabric. Some interbands are pyrite-rich and in the mylonite outcrop on the Trans-Canada Highway, minute, < 1 mm, galena grains are disseminated.

Overall the mylonite resembles deformed rhyolite or acid tuff in mineralogy and texture, and indeed on its southeastern margin the mylonite grades into meta-felsic tuffs. Higgins (1971) noted that acidic rocks more readily

deformed into mylonites than basic rocks, because quartz readily recrystallizes, while feldspars alter. Thus it would be reasonable to define the protoliths of the mylonite as Windsor Point Group felsic tuff/rhyolite.

#### 2.10.2 Mylonite in the Isle aux Morts Brook

This mylonite is a banded, aphanitic silicious rock in which the interbands range from massive monochromatic bands to 1-5 cm wide bands. Colour in the various bands ranges from pink to black. North of the Windowglass Hill Granite, the mylonite grades into a sandstone/conglomerate and/or chlorite schist of the Windsor Point Group along its northeastern edge, and into lithic breccia along its southeastern margin.

Northwest of the Isle aux Morts Brook, bands of mylonite, up to 3 m thick, are interlayered with schistose Cape Ray Granite tonalite. In outcrop along the banks of the Isle aux Morts Brook, the mylonite consists of typical pink to buff, aphanitic bands, and black aphanitic interbeds which contain large (up to 2x3 cm) pink augen (Plate 2-4C), which in hand specimen can be identified as granular quartz-feldspar intergrowths. There are also numerous dykes of Strawberry Granite cutting the mylonite here.

The augen mylonites contain two types of groundmass. One type consists of fine-grained ( $\leq 0.03$  mm in diameter)

PLATE 2-4 A) Mylonitized Windowglass Hill Granite. Note the bands of finer recrystallized grains cutting across the larger feldspar grain. This section is about 0.5 mm across.

B) Twisted and folded clast in the second conglomerate of the Windsor Point Group. The protolith of this clast is indeterminate.

C) Augen mylonite from the Isle aux Morts Brook. The large quartz and feldspar augen indicate this mylonite was derived from the Cape Ray Granite.

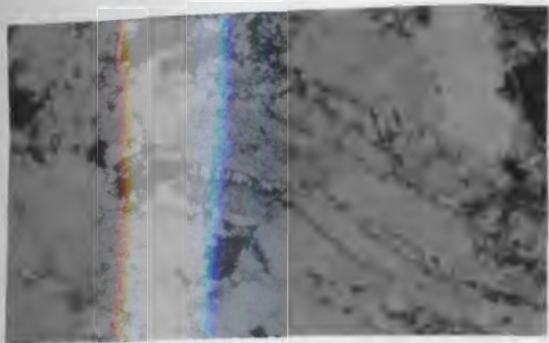
D) Quartz porphyroclast (augen) in mylonitic groundmass of recrystallized quartz and feldspar. Note development of subgrains in central portions of the porphyroclast and also recrystallized grains along the margins. This section is about 2 mm across.

E) Porphyritic Strawberry Granite. The phenocrysts are perthitic microcline.

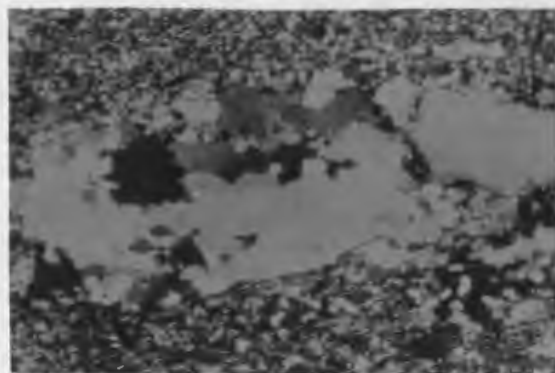
F) Orbicular gas breccia in the Strawberry Granite. Note the miarolitic cavities.

G) Contact between the Isle aux Morts Brook Granite (light) and the Port aux Basques Gneiss (dark). The granite is intruded along, and melts out, layers in the gneiss.

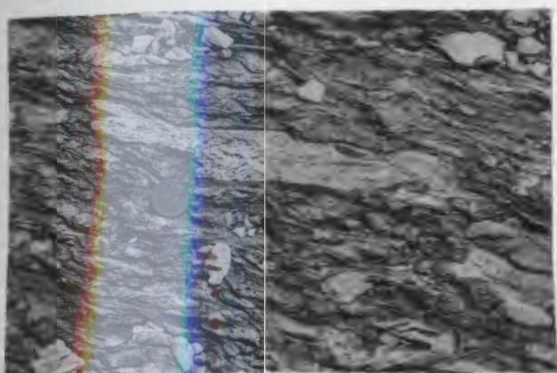




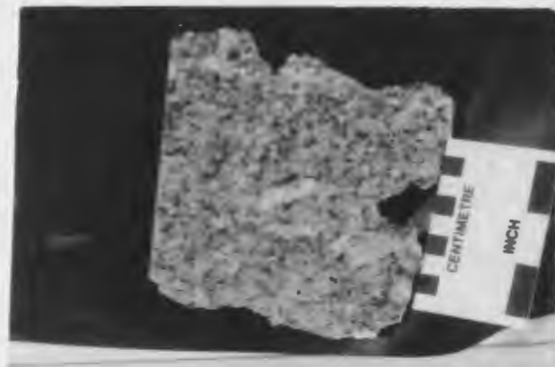
A



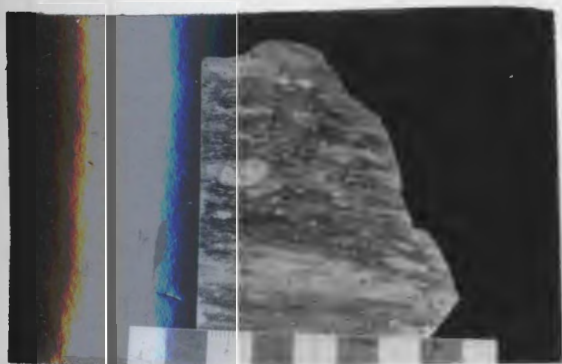
D



B



E



C



F




G

recrystallized quartz and feldspar with sericite and magnetite. The second type, which has a grain size of 0.05 mm in diameter, is polygonal recrystallized quartz-feldspathic material, and contains the augen. The larger augen are porphyroclasts of orthoclase and/or microcline (+ plagioclase) (Plate 2-4D). There are also smaller porphyroclasts (up to 5 mm in diameter) of quartz that are strongly deformed into subgrains. There are pressure shadows along the ends of the porphyroclasts.

In general the mylonites appear to be the same as those on the coast, and they similarly grade into the Windsor Point Group meta-volcanic sedimentary rocks. It is therefore reasonable to assume that the protolith of these mylonites was the Windsor Point Group also. The augen mylonites, on the other hand, are unique to the area where the Windsor Point Group is in close proximity to the Cape Ray Granite. This granite is noticeably more schistose and deformed as the contact is approached and the augen themselves are remnants of a former coarse-grained (probably granular) texture, unlike any visible in the Windsor Point Group. These facts indicate the protolith of the augen mylonites was the Cape Ray Granite.

### 2.10.3 Mylonite at the Red Rocks/Cape Ray Granite Contact

This mylonite has a small areal extent near the Red Rocks Point, but is important for relative geochronological differentiation between times of intrusion for the two granitoids and time of deformation. The mylonite is a layered rock consisting of buff, aphanitic, silicious layers, white quartz layers, massive green chloritic layers, and boudinaged/flattened aplite dykes (Plate 2-2D). The protolith of this mylonite could be Red Rocks Granite.  this granite grades into the mylonite but the presence of such large amounts of chloritic material indicates the protolith contained a large mafic component. The Cape Ray Granite is the only one of the two that contains a significant mafic content (ie. the xenoliths).

### 2.11 Strawberry and Isle aux Morts Brook Granites, and Aplites (Map units 11a,b,c and 12)

The Strawberry and Isle aux Morts Brook Granites are classified together as they are lithologically similar and are both post-tectonic granites (ie. without the planar fabrics as developed in other units in the fault zone). They intrude opposite sides of the fault zone and are never seen together, though, as shown below, they are temporally equivalent.

Aplite dykes (Map unit 12) are found throughout the map area in most lithologic units. Their descriptions are

included with those of the post-tectonic granitoids, as aplite phases are significant components of these granitoids. This is not to suggest that all the aplites are phases of these later granitoids, but that the aplites represent final phases of each of the granite systems.

#### 2.11.1 Strawberry Granite (Map unit 11a)

Outcrop of this granite extends from 3 km southwest of Little Barachois Pond to the northeastern edge of the map area, and as such runs along almost the entire northwestern edge of the area. The granite is a typically red (hematite-stained feldspars), coarse-grained (crystals up to 2 cm in length) to porphyritic intergrowth of potassium feldspar, plagioclase, quartz and biotite (Plate 2-4E). Pyrite is irregularly disseminated and there is rare disseminated molybdenite.

Contacts with the Long Range Mafic/Ultramafic Complex are quite sharp, and near Caribou Pond are sheared. The Long Range metagabbros near the contact often are cut by dykes of Strawberry Granite and/or aplite and at the northeastern edge of the map area, there is a large solitary xenolith of Long Range Mafic/Ultramafic meta-gabbro within the granite.

The tonalitic Cape Ray Granite is intruded by dykes of Strawberry Granite near their contacts, but in other places

the contact is somewhat nebulous and there appears to have been some assimilation of the tonalite. These assimilated phases are tonalite with visible potassium feldspar, or are a lighter-coloured version of the Strawberry Granite (due to more plagioclase than normal).

The Strawberry Granite is not seen in contact with the Windsor Point Group, but aplite and pegmatite dykes of probable Strawberry Granite affinity intrude the mylonites within the Isle aux Morts Brook. Along the northern edge of the Gulch, the Strawberry Granite becomes brecciated with silicified granite fragments cemented by quartz and chalcedony (see descriptions of lithic breccia below). However in the Isle aux Morts Brook, just to the north of the gulch, the granite exhibits orbicular textures (Plate 2-4F) in which rounded, fresh granite fragments are cemented by vuggy quartz. The presence of minor fluorite as cement and fracture-fillings within the orbicular granite, indicate that it is a gas breccia (ie. indicative of the high-level nature of this granite).

A pegmatite dyke in the Isle aux Morts Brook has very large microcline crystals (up to 10 cm) with quartz prisms (40x5 mm) that are arranged in 'herring-bone' type intergrowths. Barker (1971) suggests that such pegmatitic textures, which he termed graphic granite, represent simultaneous crystallization of quartz and alkali feldspar from a vapour phase or fluid. This is consistent with the

dyke being a late stage offshoot of the Strawberry Granite.

One aplitic dyke in Isle aux Morts Brook has phenocrysts of plagioclase and microcline and also contains euhedral garnets up to 3 mm in diameter). This garnet, for which microprobe analyses are given in Table II (and methods are given in Appendix I) is spessartine-rich. According to the data of Miller and Stoddard (1981), such compositions are typical of garnets in peraluminous granites. Using the experimental, pressure-dependant curve derived by Green (1977) for CaO contents in granitic melts, the garnet in sample 79-162 crystallized at near surface conditions (a not unexpected result since the granite in all other features is epizonal).

Brown (1977) defined most of this granite as the quartz monzonite phase of his Cape Ray Granite (ie. the quartz monzonite was older than the Long Range Mafic/Ultramafic Complex).

#### 2.11.2 Isle aux Morts Brook Granite (Map unit 11b) and Breccia (Map unit 11c)

This granitoid intrudes the Port aux Basques Gneiss and the Windsor Point Group south of the Windowglass Hill, as a circular plug approximately 5 km in diameter. It strongly resembles the Strawberry Granite, in that it is a coarse-grained to porphyritic granite with red feldspars,

TABLE II GARNET COMPOSITION IN THE STRAWBERRY GRANITE

SAMPLE 79-162

ANALYSIS	Mg	Al	Si	Ca	Mn	Fe	Total
1 (wt %)	0.25	20.67	35.88	0.71	24.67	17.05	99.23
(At. prop.)*	0.029	2.021	2.975	0.061	1.733	1.183	8.001
2 (wt %)	0.36	20.91	36.71	0.82	23.91	18.06	100.77
(At. prop.)	0.043	2.008	2.990	0.071	1.649	1.229	7.990
3 (wt %)	0.27	21.04	37.10	0.64	24.79	16.87	100.71
(At. prop.)	0.031	2.014	3.012	0.55	1.704	1.144	7.958

\*At. prop. = atomic proportion \

quartz and biotite (up to 5 %). A subtle zoning is visible in larger alkali feldspar phenocrysts (up to 1.5x1 cm).

There are scattered aplite dykes up to 1 m thick, and also a prominent set of southeast-striking, pyritiferous (some cubes up to 2 cm in width), quartz veins ranging from 0.3-1 m thick. Along the margins of some of these veins, the host rock is visibly altered with secondary muscovite flakes overgrowing the granite.

Contacts between the granite and enclosing schists are quite sharp. In the Isle aux Morts Brook, interbeds of the Port aux Basques Gneiss are at first intruded by granite dykes and thereafter at the contact, the main mass of the granite selectively replaces ('eats out') interlayers within the gneiss (Plate 2-4G). Along its northern boundary, the granite is in 'knife-sharp' contact with the schists, though alkali feldspar and quartz porphyroblasts are often developed within the schists.

The most spectacular contact occurs in the small stream flowing out of Big Pond into Eastern Brook (see Map 1). The stream has eroded down through the gneiss to reveal granite underlying the gneiss (ie. the gneiss is a roof pendant to the granite). The granite at the contact is mafic-poor and is often slightly brecciated with fragments of pink granitic material set in silicious matrices. This probably indicates the ponding of a vapour phase in the upper reaches of the pluton.



There are scattered aplite dykes, with minute flakes of molybdenite, intruding the gneiss between this contact and Big Pond, indicative of underlying granite. The underlying granite also thermally metamorphosed the gneiss, as shown by the previously described development of andalusite.

The breccia (Map unit 11c) occurs within the felsic tuff member of the Windsor Point Group, and consists of altered and silicified fragments (up to 7 mm in diameter) of granitic-looking material enclosed in massive vuggy quartz. It would appear this breccia represents a vapour/gas pipe upwelling from underlying granite. The presence of gas breccias in the Isle aux Morts Brook Granite supports the supposition that the orbicular breccias within the Strawberry Granite are likewise gas-derived (ie. rather than tectonic).

In the contact zone south of Big Pond, one granite sample contained a single, broken, (1.25 mm in diameter) garnet. It was not possible to analyse this garnet.

### 2.11.3 Aplite Dykes (Map unit 12)

The aplites intrude the Red Rocks Granite, Cape Ray Granite and mylonite of the Windsor Point Group, and unlike previously described aplite phases in the Red Rocks, Strawberry and Isle aux Morts Brook Granites, they have no

definitive association with any granitoid phase.

### 2.12 Lithic Breccia (Map unit 13)

This breccia unit, composed of country rock fragments, occurs as two thin bands, less than 100 m wide, along the northern edge of Gulch and to the north of Windowglass Hill (see Map 1). Both bands are what Higgins (1971) would classify as fault breccia, as they are without primary cohesion, though they are cemented by secondary quartz. The breccias represent definite cataclastic (brittle) deformation and, as described below in the structure chapter, are the final episode in the structural history of the fault zone.

The breccia layer north of the Windowglass Hill Granite is composed of silicified and hematitized schist and meta-granite fragments cemented by amorphous white silica. The fragments are poorly sorted and range in size from <2 mm in diameter to >10 cm. In thin section the fragments are generally too silicified and recrystallized to determine a protolith, but some appear to be sericite schist (ie. the brecciation post-dates the fabric of the enclosed fragments). There is no planar (or otherwise) fabric developed within the breccias.

The breccias north of the Gulch appears to have formed from Strawberry Granite, Windsor Point Group and mylonite

rocks. Alteration (to clay minerals and sericite) and quartz veining increases in the granite as the breccia is approached until highly altered (silicified and hematitized) granite fragments occur in jasper/chalcedony/quartz cement. There are also fragments of schistose material (meta-Windsor Point Group ?) and mylonite intermixed with the granitic fragments. The granite fragments decrease in size and quantity towards the south and it seems the breccia occurs along the contact between the granite and Windsor Point Group.

Figure 3 shows the general cataclasis that is visible in all rocks in the Gulch. In this particular section, isolated, rootless, folded portions of more strain-resistant pink aphanitic mylonite are enclosed in fractured chlorite schist gouge. This sort of texture is a common expression of the shearing and cataclasis which produced the breccia. In the general region of these breccias, all rock types exhibit some minor brecciation and shearing.

### 2.13 Regional Correlation and Location with respect to the rest of the northeastern Appalachians

The island of Newfoundland represents the northeastern termination of the Appalachian orogenic belt and is a cross-section through this complex Paleozoic tectonic

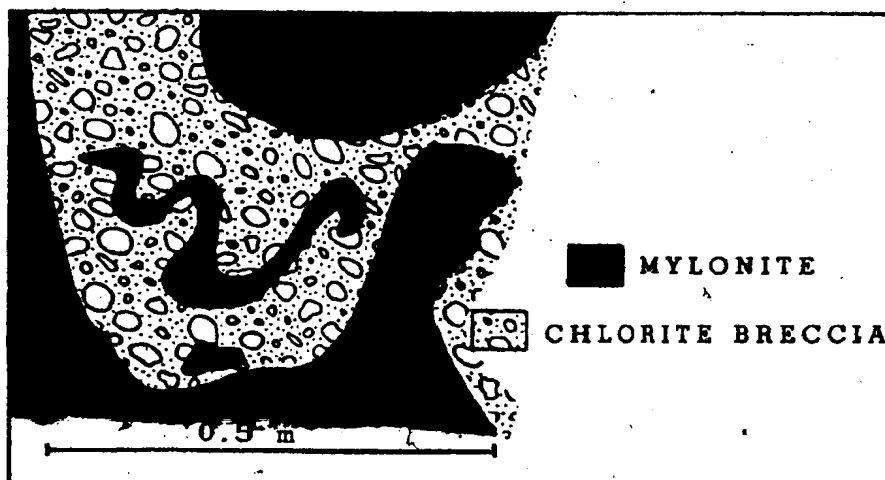


Figure 3 Lithic breccia in the Gulch region. Derived by cataclasis of interbedded silicious mylonite and chlorite schist.

system (see Figure 4). Williams (1978 and 1979) subdivided the Appalachian orogen in Newfoundland into four zones, which represented simplified versions of the zonation described by Williams *et al.* (1973, 1974). These new zones were the Humber Zone (the former Lomond and Hampden Zones), the Dunnage Zone (*ie.* the Fleur de Lys, Notre Dame, Exploits and Botwood Zones), the Gander Zone and the Avalon Zone.

The exact location and correlation of units in the Cape Ray Ray Fault Zone, in terms of the various tectonic models developed for Newfoundland, were poorly understood at first. They were subsequently used to define a cryptic suture between two opposed continental margins (*ie.* Brown, 1973), and recently have been the subjects of major re-interpretation and revision (eg. Wilton, 1981; Chorlton, 1982). (This thesis represents a part of this revision).

#### 2.13.1 Location of SW Newfoundland with respect to Appalachian Tectonic Zones (or Terranes)

Brown (1973b), having mapped the area around the Cape Ray Fault (Brown, 1973a), defined the tonalitic Cape Ray Granite as Grenvillian basement gneiss of the Western Platform (Humber Zone on Figure 4), and the Port aux Basques Complex as part of the Eastern Marginal Metamorphic

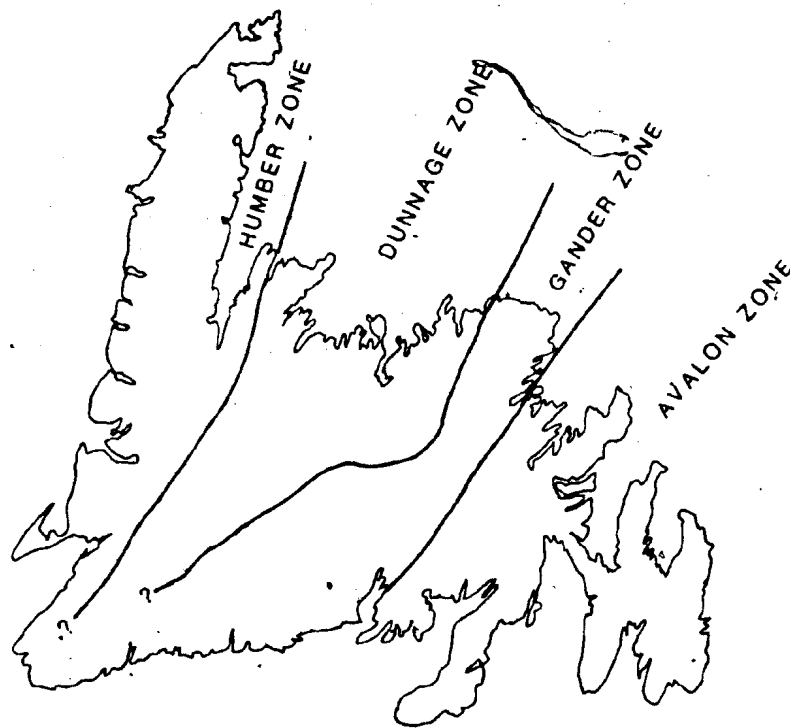


Figure 4 Tectonic zones of Newfoundland (after Williams, 1979). The position of southwestern Newfoundland with respect to these zones is controversial.

Belt (basement rocks in the Avalon Zone, Figure 4). In this model (Brown, 1973b), the Cape Ray Fault represented a cryptic suture between the opposed margins of the proto-Atlantic, and the Central Mobile Belt was defined as disappearing in southwestern Newfoundland. The actual point of juxtaposition was marked by mylonite zones that were supposedly subsequently overlain by the Windsor Point Group (ibid.).

Williams et al. (1974) concurred with Brown's (1973b) correlations of the Cape Ray Granite with Grenville gneiss and the Port aux Basques Complex with the Gander Zone, and his definition of the Cape Ray Fault as a cryptic suture. Williams and Stevens (1974) also described the Cape Ray Fault as a cryptic suture juxtaposing two ancient continental margins.

Based on further mapping and discovery of more extensive (than seen by Phair, (1949)) exposures of gabbroic to ultramafic rocks of the Long Range Mafic/ultramafic Complex (Brown 1975), Brown (1976b) defined rocks in this complex as ophiolites. As such he correlated them with the more extensive ophiolites that occur in western and northwestern Newfoundland (ie. the Bay of Islands and White Hills Complexes, described by Stevens (1970); Williams (1975); and Malpas and Stevens (1977)). Brown (1976b and 1977) defined the contact between the Long Range Mafic/Ultramafic Complex and the underlying

Grenvillian gneisses of his Long Range Gneiss (read tonalitic Cape Ray Granite) as a thrust fault. He (Brown, 1976b) used this contact as further evidence for correlation with other western Newfoundland ophiolites

(eg. Williams, 1975), which were obducted unto the Western Platform (ie. allocthonous). The biggest difference between the ophiolitic terranes is that the Long Range Mafic/Ultramafic Complex thrust slabs are missing the typical sedimentary package that underlies the other allocthonous ophiolitic slabs (ie. the Long Range ophiolites were thrust directly unto Grenvillian basement).

Brown (1976b) interpreted the presence of these ophiolites as further evidence of his cryptic suture idea for the Cape Ray Fault. In his view the ophiolites were remnants of proto-Atlantic ocean floor material such as that present in the Central Mobile Belt (Dunnage Zone in Figure 4). However Brown (1976b) also stated that the absence of the voluminous island arc volcanic rocks as occur to the northeast in Central Mobile Belt (eg. Strong, 1977, Kean et al., 1981), indicated that Western Platform crystalline material was subducted beneath continental crust (ie. the Port aux Basques Complex, or Kennedy's (1975) Eastern Crystalline Belt - basement to the Avalon Zone) rather than ocean floor as in the north.

Brown and Coleman-Sadd (1976) re-interpret the



Eastern Crystalline Belt as having a much larger areal extent to the northwest, encompassing portions of what had previously been called the Central Mobile Belt. Their ideas supported those of Brown (1976b) in stating that the ocean floor material had effectively disappeared in southwestern Newfoundland and, in its stead, crystalline belts representing opposed margins of the Proto-Atlantic Ocean were juxtaposed along the Cape Ray Fault.

Susequent work in the Eastern Crystalline Belt (or Gander Zone) by Blackwood (1978) indicated that the previously described basement/cover relationships (eg. Kennedy, 1975; Blackwood and Kennedy, 1975) were actually a conformable sequence between higher grade migmatitic gneisses (the Hare Bay Gneiss) and overlying metasediments (the Gander Group). Thus one of main foundations for describing the Port aux Basques Complex as Precambrian basement was removed.

Notwithstanding Blackwood's (1978) redefinition of the Gander Zone, Williams (1978, 1979) implied the Port aux Basques Complex represented metamorphosed basement and cover rocks correlative through the Gander Zone. The Cape Ray Granite was similarly defined (ibid.) as Grenville basement (or the ancient continental margin of North America).

Chorlton (1980b) raised objections re' equivalents of the Port aux Basques Complex (the Bay du Nord Group) having

a basement/cover relationship typical of the Eastern Crystalline Belt. According to her, the cover rocks (ie. the Billiards Brook Group, equivalents of the Windsor Point Group) were Devonian (not pre-Silurian), while the so-called basement rocks yield Ordovician ages (Anon, 1980). Chorlton (1980b) interpreted the metamorphic sequence southeast of the Cape Ray Fault (ie. the Port aux Basques Complex) as an Ordovician to Silurian island arc sequence with associated marine sediments.

As a result of preliminary mapping for this thesis, this author (Wilton, 1981) described the Grenvillian Long Range Gneiss as a Paleozoic tonalite terrane and the Cape Ray Fault as a portion of a ductile deformation history which affected all three main lithologic units (viz. the tonalitic Cape Ray Granite, the Windsor Point Group and the Port aux Basques Complex), and not as a cryptic suture.

The Cape Ray Suture was defined as the extension of the Baie Verte-Brompton Line through southwestern Newfoundland by Williams and St. Julien (1982). They showed this line as marking the eastward extent of Grenville basement (ie. the Cape Ray Granite outcrop area) and as such represents the "structural junction between deformed rocks of an ancient continental margin and bordering ocean" (ibid., p.177- the underlining is mine).

### 2.13.2.1 Eastern Correlations

In a series of reports, Chorlton (1978a, 1978b, 1979, 1980a, 1980b, 1980c and 1982) and Chorlton and Dingwell (1981) redefined the stratigraphy and nomenclature of the entire region from Cape Ray through to the Blue Hills of Couteau (*ie.* the eastern edge of Gillis' (1972) mapping). Within the La Poile River Map area, Chorlton (1980b) re-assigned most of the schistose rocks lying between the Cape Ray Fault to the north and the Bay d'Est Fault to the south, to the Bay du Nord Group (Figure 5). She assigned the fossiliferous meta-sediments in the Billiards Brook-Cape Ray Fault Zone region to a newly named unit, the Billiards Brook Group, and not as part of the Bay du Nord Group as defined by Cooper (1954). The main results of these sub-divisions is that the Bay du Nord Group is now thought to be Ordovician, while the Billiards Brook is late early Devonian (based on fossil identification, Chorlton, 1980b).

Chorlton (1980b) showed the Cape Ray Fault bifurcating near the western edge of the La Poile River map area. One fork continues in the same easterly direction as that of the main fault zone and is present 15 km east (or 105 km east of this map area), where it is called the Gun Flap Hills Fault (O'Brien, 1982). The second fork continues to the northeast extending into the King George IV Lake map area (Kean and Jayasinghe, 1981). Kean and Jayasinghe (1981) didn't recognize the fault zone, but there are a

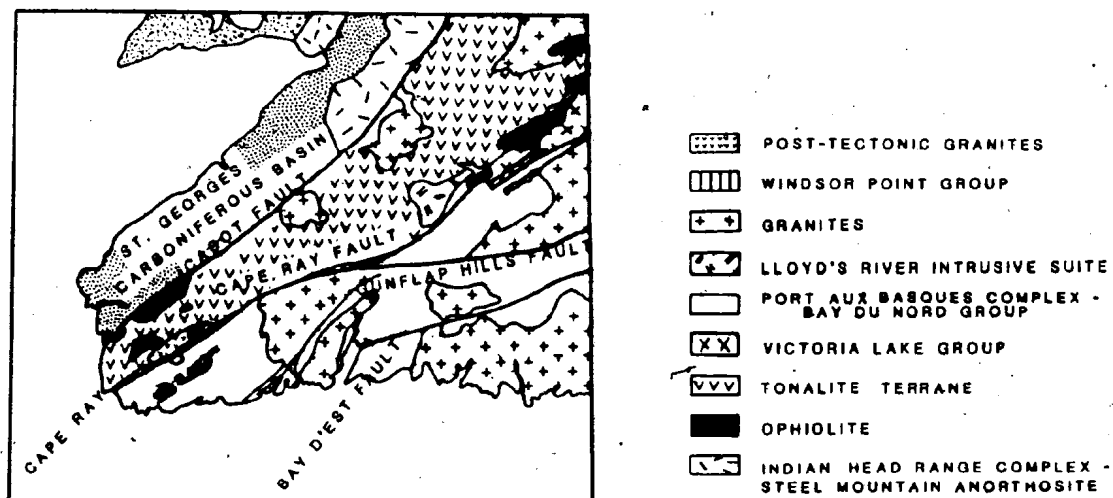


Figure 5 Regional tectonic and stratigraphic correlations in southwestern Newfoundland (after Kean and Herd, 1982). The post-tectonic Strawberry and Isle aux Morts Brook Granites as mapped in this study are outlined as "post-tectonic granites".

series of small faults in their area parallel to the northeastern trend as shown by Chorlton (1980b).

As redefined by Chorlton (1980b) the Bay du Nord Group consists of garnetiferous amphibolites, metasediments, metatuffs, conglomerates and felsic volcanic rocks which include the felsic pyroclastic Dolman Formation (the Dolman Gneiss of Cooper (1954)) that both overlies and underlies the Bay du Nord Group in different areas, and the Baggs Hill Granite. This Bay du Nord Group is separated from the La Poile Group by the Bay d'Est Fault, but Chorlton (1980b) suggests the two groups are "time-stratigraphic equivalent(s)" (*ibid.*, p.23). The new La Poile Group consists mainly of felsic pyroclastic rocks with associated sedimentary rocks and mafic flows. Chorlton thought both the La Poile and Bay du Nord Groups are metamorphosed representatives of island arc volcanism.

The Devonian Billiards Brook Group, which was correlated by Chorlton (1980b) as a direct analogue of the Windsor Point Group (Brown 1976a, 1977), contains felsic pyroclastics, chlorite and sericite schists, conglomerates and mafic flows. The Nitty Gritty Brook Granite occurs near the Cape Ray Fault Zone (Chorlton, 1980b) and this alaskitic granitoid has been tentatively correlated with the Windowglass Hill Granite (C.B. McKenzie, 1981, pers. comm.). Though the Billiards Brook Group and the Nitty Gritty Brook Granite are not in contact, Chorlton (1980b)

described the granite as at least partially older since similar-looking granitic clasts occur in conglomerates of the Billiards Brook Group.

Various radiometric dates have been determined (Anon, 1980) for the units in the La Poile River map area. U/Pb zircon determinations indicate an age of  $449 \pm 20$  Ma for the Dolman Formation of the Bay du Nord Group,  $410 \pm 20$  Ma for the La Poile Group and  $377 \pm 20$  Ma for the Chetwynd Granite.  $^{40}\text{Ar}/^{39}\text{Ar}$  cooling ages for biotite and hornblende, respectively, are  $350 \pm 5$  Ma and  $361 \pm 5$  Ma for the Chetwynd Granite,  $360 \pm 5$  Ma and  $380 \pm 5$  Ma for the La Poile Batholith,  $377 \pm 5$  Ma and  $388 \pm 5$  Ma for amphibolite in the Bay du Nord Group.

Chorlton and Dingwell (1981) and Chorlton (1982) continued the La Poile River mapping westwards into the Grandy's Lake mapsheet which adjoins the northern part of Brown's (1976a) area. Chorlton (1982) described the ophiolites of the Long Range Mafic/Ultramafic Complex as the oldest units in the entire area from the Port aux Basques mapsheet (Brown, 1977) to the eastern edge of the La Poile mapsheet. She correlated the ophiolites with scattered mafic plutonic rocks in the Blue Hills of Couteau (Chorlton, 1980b). The second oldest (Ordovician or older) unit described by Chorlton (1982) is a metasedimentary unit (paragneiss) that occurs north of the Cape Ray Fault (northeast of the area mapped in this thesis). These

metasedimentary rocks pre-dated the "modified" Bay du Nord Group into which Chorlton (1982) included the Port aux Basques Gneiss. The eastern extension of this modified Bay du Nord Group is abruptly truncated by the Rose Blanche Granite (ibid.), which is described as a synkinematic migmatitic granite correlative with the Port aux Basques Granite (Chorlton and Dingwell, 1981). The Rose Blanche Granite is termed Silurian (Chorlton, 1982).

North of the Cape Ray Fault, Chorlton (1982) described tonalites and granodiorites (ie. the tonalitic Cape Ray Granite herein) that were intruded into the ophiolites and metasediments, and also a Silurian megacrystic quartz monzonite, which she says was intruded into the tonalites (the megacrystic Cape Ray Granite herein?).

Chorlton's (1982) map locations and lithological descriptions of the Windsor Point Group concur with those of this thesis. She describes the northeast extension of the Strawberry Granite (as herein) as Devonian or younger pink, biotite-perthite leucogranite. She also found some small plugs of pink, two feldspar leucogranite (Isle aux Morts Brook Granite?) south of the Cape Ray Fault intruding the Rose Blanche Granite, which she mapped as a separate granitoid sequence from the former leucogranite.

Nomenclature problems still persist for southwestern Newfoundland because of the chronological order in definition of names etc., so to resolve these problems,

Chorlton (in prep., and pers. comm. 1982) has renamed all of the "modified" Bay du Nord Group from Cape Ray east, the La Poile River Group, and that section of the group formerly called the Port aux Basques Gneiss (+ Granite) is to be called the Bunker Hill Brook Group.

O'Brien (1982), working to the east of the La Poile River mapsheet, states the area is part of the Dunnage Zone and agrees with Chorlton's (1980c) geological framework with minor revisions.

Swinden (1981) suggests that the Ordovician sequence represented by the Bay du Nord Group might extend across the south coast of Newfoundland and connect with the Baie D'Espoir Group (Coleman-Sadd, 1980).

#### 2.13.2.2 Northern Correlations

The southwestern edge of the Annieopsquotch ophiolite belt (Dunning, 1981) occurs approximately 100 km northeast of the end of this map area and extends for a further 100 km in the same northeasterly direction. This belt consists of the Annieopsquotch Igneous Complex (Herd and Dunning, 1979, Dunning and Herd, 1980, and Dunning, 1981), the Star Lake ophiolite (Dunning, 1981, Dunning, et al., 1982), the Shanadithit ophiolite (Dunning, 1981), and the King George IV Lake ophiolite (Kean and Jayasinghe, 1981, Dunning, 1981). The age of the Annieopsquotch ophiolite, based on



U/Pb zircon dating, is  $483 \pm 3$  Ma, or Lower Ordovician (age quoted in Dunning et al., 1982). Dunning and Herd (1980) and Dunning (1980) have directly correlated this ophiolite belt with the Long Range Mafic/Ultramafic Complex of this present map area. The Star Lake ophiolite, the northernmost of the belt, is intruded and engulfed to the west by what Dunning et al. (1982) call an Ordovician tonalite. The other ophiolites have younger (Devonian (?)) granitoids along their western margins. The mafic to intermediate volcanics of the Victoria Lake Group (Kean, 1977) occur to the east all of the ophiolites.

Kean and Jayasinghe (1981) mapped the King George IV map area which adjoins the northern boundaries of Chorlton's (1980b, 1980c) map areas. The oldest units in the map are the paragneisses and amphibolites of the Cormacks Lake Complex which Herd and Dunning (1979) assumed were Grenvillian. The ophiolite terrain is separated from these gneisses by intrusions of diorite and coarse-grained megacrystic hornblende-biotite granite.

In the northwestern half of the map area these same authors describe a sedimentary sequence that contains Lower Devonian plant fossils. The basal member of this sequence is a grey conglomerate with various clast types ranging from felsic pyroclastics, to mafic volcanics and occasional sedimentary and gneissic clasts. These sedimentary rocks are overlain by an intermixed reddish sequence of

rhyolites, rhyolite breccias and associated sediments. This felsic member is in fault contact all along its southeastern margin with the meta-sedimentary terrane, the ophiolite in the centre and a late intrusive to the north.

Correlating Chorlton's (1980b and 1980c) map area with the King George IV map area, Kean and Jayasinghe's meta-sedimentary terrane is the Bay du Nord Group, and the sedimentary sequence (conglomerate/pillow lava/felsic tuff) is the Billiards Group. The Windsor Point/Billiards Brook Group can thus be traced inland from Cape Ray in a northeasterly direction for over 150 km (though not continuously).

The rocks at the northeastern end of these Windsor Point Group equivalents were described as Silurian (?) red beds, correlative with the Springdale Group, by Herd and Dunning (1979) and Dunning and Herd (1980). These red beds were described (*ibid.*) as overlying (and terminating against) the Annieopsquotch ophiolite. To the west the sediments are truncated by a granitic terrane (Herd and Dunning, 1979) that contains various granitoids ranging from Ordovician tonalite to post-tectonic granite (Dunning, 1982, pers. comm.).

The correlation problem between Kean and Jayasinghe (1981) and Dunning and Herd (1980) with regard to the Siluro-Devonian sediments was resolved by Chandler (1982) who recognized that the grey conglomerate and red rhyolitic

members described by Kean and Jayasinghe are two different sedimentary sequences. The red rhyolitic member is the same as Herd and Dunning's red bed horizon, and as such Chandler (1982) says may be correlative with the Silurian (but maybe Devonian) Springdale Group. Chandler and Dunning (1983) report a U/Pb zircon date for this underlying rhyolite of  $431 \pm 5$  Ma thus proving its Silurian age. The grey conglomerates, on the other hand, are part of a Lower Devonian (fossiliferous) fluvial sequence.

### 2.13.3 Summary

For the remainder of this report, the gneissic terrane south of the Cape Ray Fault is referred to as the Port aux Basques Complex, the central sedimentary terrane will be called the Windsor Point Group, and the tonalitic terrane to the north will be identified as the Cape Ray Granite.

The Port aux Basques Complex is part of a large metamorphic terrane that extends both east and northeastwards. The protoliths for the metamorphic rocks were predominantly felsic pyroclastic and volcanic rocks and associated sedimentary rocks, with abundant amphibolite interbands developed from intrusive/extrusive mafic volcanic rocks. It is currently assumed (Chorlton, 1982) that this whole sequence represents island-arc type volcanism, with a minor ophiolitic component.

The absence of the typical intermediate andesitic-type volcanic rocks (or their metamorphic equivalents) in the sequence, suggests such an interpretation requires modification, as does isotopic and, geochemical data as described below.

The Windsor Point Group is a mixed felsic and mafic pyroclastic assemblage with associated sediments that forms the southwestern end of a narrow Devonian sequence that extends for over 150 km to the northeast. Missing from the Windsor Point Group (sensu stricto, Brown, 1977) are the mafic volcanic rocks so typical of the Billiards Brook Group. Due to deformation and metamorphism, the Windsor Point Group appears to grade into the Port aux Basques Complex. Indeed most of the Windsor Point Group herein defined (ie. the chlorite-sericite schists and second conglomerate), and especially those portions at Windsor Point, have lithological similarities with portions of the Bay du Nord Group or La Poile Group as described elsewhere (Chorlton, 1980b, O'Brien, 1982). The only truly distinctive portion of the Windsor Point Group is the Little Barachois Formation and in some future subdivision etc. this uniqueness may form the basis for a new nomenclature. Chorlton (1980, pers. comm.) stated that the Windsor Point Group along the coast strongly resembled the Billiards Brook Group, yet she has also mapped (Chorlton 1980a, 1982) portions of the inland exposures of the Windsor Point Group

as Bay du Nord Group, even though these inland exposures correlate with the coastal ones.

The tonalitic Cape Ray Granite is part of a large terrane that intrudes and engulfs ophiolitic fragments all the way up to and including the Annieopsquotch Ophiolite Belt (cf. Dunning and Chorlton, 1983). This terrane is always to the north/northwest of the sediments belonging to the Windsor Point Group equivalents.

## CHAPTER 3

### GEOCHRONOLGY

#### 3.1 Introduction

The purpose of this chapter is to describe the results and significance of the various Rb/Sr age determinations carried out on igneous rocks within the Cape Ray Fault Zone. The complete results are listed in Table III. Descriptions of the basic principles and assumptions used in Rb/Sr geochronology are beyond the scope of this thesis, but reference can be made to the review papers of Faure (1977) and Jager (1979). Radioactive decay constants and isotopic ratios used throughout are those of Steiger and Jager (1977) and the methodology used in the radiometric determinations is described in Appendix II.

#### 3.2 The Port aux Basques Granite

Six samples of this granite were analysed and their isotopic and elemental compositions are given in Table IV. As seen from the Isochron diagram (Figure 6a), these data yield an errorchron date of  $436 \pm 214$  Ma. The true measure

TABLE III  
RB-SR REGRESSION RESULTS FOR WHOLE ROCKS IN THE CAPE RAY FAULT ZONE

UNIT	NO. OF SAMPLES	AGE $\pm 2\sigma$ (Ma)	INITIAL RATIO $\pm 2\sigma$	MSWD
Port aux Basques Granite	6	435.5 $\pm$ 214.1	0.70822 $\pm$ 0.0032	1155.94
Port aux Basques Granite	4	452.6 $\pm$ 70.9	0.70800 $\pm$ 0.0017	114.98
Megacrystic Cape Ray Granite	9	241.7 $\pm$ 297.7	0.70960 $\pm$ 0.0018	107.54
Megacrystic Cape Ray Granite	5	438.8 $\pm$ 81.5	0.70883 $\pm$ 0.00048	5.77
Red Rocks Granite	8	494.8 $\pm$ 57.1	0.70844 $\pm$ 0.00057	45.5
Windsor Point Group	8	377.3 $\pm$ 21	0.70870 $\pm$ 0.0015	29.51
Windowglass Hill Granite	9	368.8 $\pm$ 12	0.70993 $\pm$ 0.00022	4.63
Strawberry Granite	7	362 $\pm$ 26.5	0.70650 $\pm$ 0.0017	5.39
Isle aux Morts Brook Granite	4	352 $\pm$ 5.6	0.70842 $\pm$ 0.00056	0.49
Combined Strawberry and Isle aux Morts Brook Granites	11	362 $\pm$ 15.5	0.70680 $\pm$ 0.0012	6.29

TABLE IV

Rb AND Sr CONTENTS AND ISOTOPIC COMPOSITIONS FOR UNITS IN THE CAPE HAT FAULT ZONE

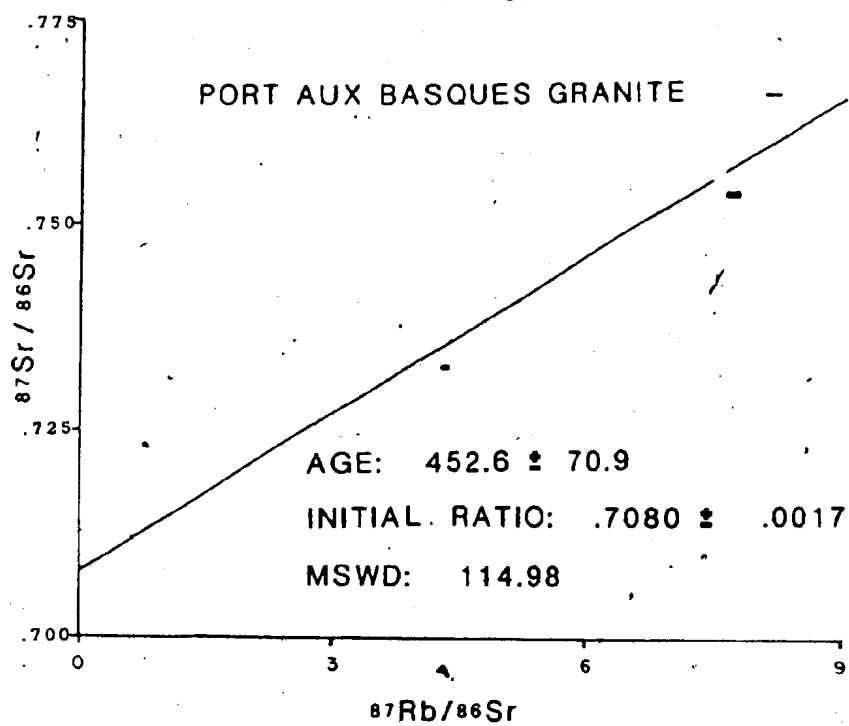
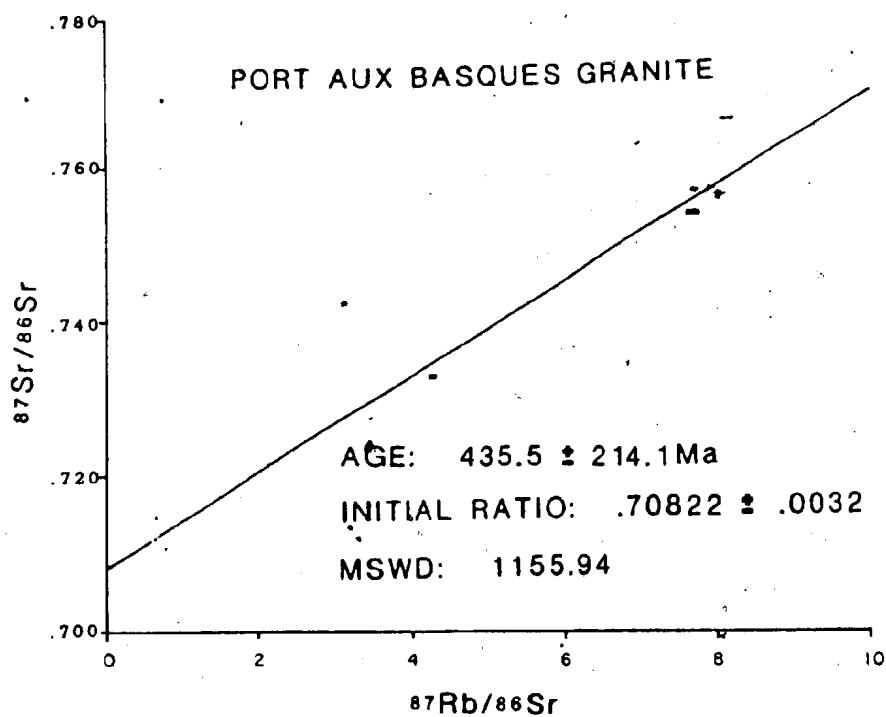
Errors are  $\pm 1\%$  for Rb, Sr and  $^{87}\text{Rb}/^{86}\text{Sr}$ . The  $^{87}\text{Sr}/^{86}\text{Sr}$  ratios are normalized to  $^{87}\text{Sr}/^{86}\text{Sr} = 0.1194$  and corresponding errors (95% confidence interval) are quoted in terms of  $10^{-3}$ .

SAMPLE	Rb(ppm)	Sr(ppm)	Rb/Sr	$^{87}\text{Rb}/^{86}\text{Sr}$	$^{87}\text{Sr}/^{86}\text{Sr}$	SAMPLE	Rb(ppm)	Sr(ppm)	Rb/Sr	$^{87}\text{Rb}/^{86}\text{Sr}$	$^{87}\text{Sr}/^{86}\text{Sr}$
<u>Port aux Basques Granite</u>						<u>Windsor Point Group</u>					
A-1	126.6	85.7	1.477	4.286	$0.732908 \pm 19.4$	WPG-1	180.2	57.7	3.123	9.082	$0.757169 \pm 4.9$
A-2	45.1	207.9	0.217	0.629	$0.714784 \pm 3.8$	WPG-2	167.8	90.5	1.853	5.381	$0.740457 \pm 3.8$
A-3	105.8	37.9	2.797	8.143	$0.766466 \pm 5.3$	WPG-3	157.7	28.6	5.520	16.113	$0.794554 \pm 10.8$
A-4	35.5	168.0	0.211	0.611	$0.711957 \pm 5.7$	WPG-4	188.6	17.9	10.523	30.931	$0.865022 \pm 11.8$
A-5	55.0	208.9	0.264	0.763	$0.910688 \pm 2.2$	79-15	107.7	328.1	0.328	0.950	$0.713040 \pm 13.9$
A-6	181.7	68.6	2.649	7.703	$0.754158 \pm 27.6$	79-19	97.0	106.3	0.912	2.645	$0.723210 \pm 11.8$
<u>Megacrystic Cape Bay Granite</u>						79-28	192.3	41.1	4.684	13.659	$0.783215 \pm 5.8$
CRG-1	188.0	664.5	0.283	0.819	$0.713920 \pm 11.5$	79-32	92.4	22.5	4.109	11.967	$0.770581 \pm 10.5$
CRG-1P	154.0	1241.6	0.124	0.359	$0.711621 \pm 7.5$	<u>Windowless Hill Granite</u>					
CRG-2	91.9	686.1	0.134	0.388	$0.711396 \pm 7.8$	WGH-1	21.0	66.0	0.318	0.920	$0.714529 \pm 5.6$
CRG-2P	22.3	842.0	0.027	0.077	$0.711738 \pm 69.0$	WGH-2	10.7	85.5	0.125	0.361	$0.711666 \pm 8.8$
CRG-3A	89.1	631.4	0.141	0.408	$0.711288 \pm 16.7$	WGH-3	54.2	70.0	0.775	2.214	$0.722051 \pm 36.3$
CRG-3AP	49.9	390.6	0.128	0.370	$0.710864 \pm 8.4$	WGH-4	38.7	86.5	0.448	1.297	$0.716938 \pm 8.8$
CRG-4SA	94.4	1436.9	0.066	0.190	$0.710624 \pm 19.1$	79-112	107.6	46.4	2.321	6.472	$0.745880 \pm 14.8$
CRG-5B	117.5	1355.8	0.009	0.251	$0.710267 \pm 6.4$	79-112A	9.1	37.5	0.242	0.700	$0.711733 \pm 4.5$
CRG-6	37.2	194.5	0.191	0.554	$0.709946 \pm 7.3$	79-112B	6.0	86.9	0.069	0.199	$0.711311 \pm 21.3$
<u>Red Rocks Granite</u>						79-126	153.8	38.1	4.039	11.765	$0.771728 \pm 49.4$
RRG-1	72.4	656.3	0.110	0.319	$0.710900 \pm 4.6$	79-140	106.1	34.2	3.102	9.022	$0.755540 \pm 52.8$
RRG-2	106.7	740.7	0.144	0.417	$0.711029 \pm 2.4$	<u>Strawberry Granite</u>					
RRG-2A	107.0	740.5	0.145	0.419	$0.711613 \pm 26.7$	STG-1	241.6	167.0	1.447	4.196	$0.728142 \pm 5.1$
RRG-3	98.2	438.7	0.224	0.648	$0.713646 \pm 6.8$	STG-1B	227.0	158.0	1.437	4.166	$0.727336 \pm 10.5$
RRG-4	114.6	322.3	0.356	1.030	$0.716356 \pm 3.5$	STG-2	289.6	181.3	1.597	4.634	$0.729739 \pm 21.4$
RRG-5	124.3	136.2	0.913	2.646	$0.726689 \pm 6.2$	STG-3	242.6	182.8	1.327	3.848	$0.726007 \pm 45.4$
RRG-6	133.5	138.0	0.968	2.807	$0.726728 \pm 15.3$	STG-3	189.1	53.5	3.538	10.292	$0.760332 \pm 15.2$
RRG-7	101.7	208.1	0.489	1.416	$0.718857 \pm 28.4$	79-94	156.4	118.0	1.325	3.842	$0.727195 \pm 22.2$
						79-102	12.7	103.7	0.123	0.356	$0.709896 \pm 74.5$
						<u>Isle aux Morts Brook Granite</u>					
						IAM-1(CO 286.5	136.5	2.098	6.091		$0.738695 \pm 8.6$
						IAM-2	260.9	124.4	2.098	6.091	$0.739124 \pm 9.7$
						IAM-3	265.2	129.7	2.045	5.936	$0.738223 \pm 9.0$
						79-108	365.0	22.1	16.502	48.922	$0.953567 \pm 11.0$



Figure 6a Rb/Sr whole rock isochron for the Port aux Basques Granite. See Table IV for the isotopic data used to construct this diagram.

Figure 6b Rb/Sr whole rock isochron for four samples of the Port aux Basques Granite. Constructed without data of samples A-2 and A-5 (see Table IV).



of the unacceptable nature of this age is given by the Mean Square of Weighted Deviates (MSWD), which is 1156. The MSWD is a statistical function which evaluates the contribution of analytical (machine) error vs. geological error to the age determination (i.e. it reflects whether the error is due to the samples or the actual analyses), the higher the MSWD, the greater the geological error (or intra-sample variation). Brooks et al. (1972) suggest that MSWD's of  $> 2.5$  are from 'errorochrons' rather than true isochrons. MSWD's of 1156 are totally unacceptable and in the case of the Port aux Basques Granite indicate extreme sampling error.

With two samples (A-2 and A-5) omitted because of their deviation from the general trend (an acceptable screening process according to Brooks (1980)), the revised isochron (Figure 6b) showed the age as  $453 \pm 71$  Ma. The age is mid-Ordovician but the age of the Port aux Basques Complex has been postulated as Silurian (Chorlton, 1982). Also the reported age of the Rose Blanche Granite, a supposed equivalent of the Port aux Basques Granite (Chorlton, 1982), is  $392 \pm 10$  Ma (Anon, 1980). Therefore this determination should be rejected (the MSWD of 115 is also too high).

Although the sample size available for this granite was limited to only six samples, the main reason for problems in defining an Rb/Sr isochron lie in metasomatism

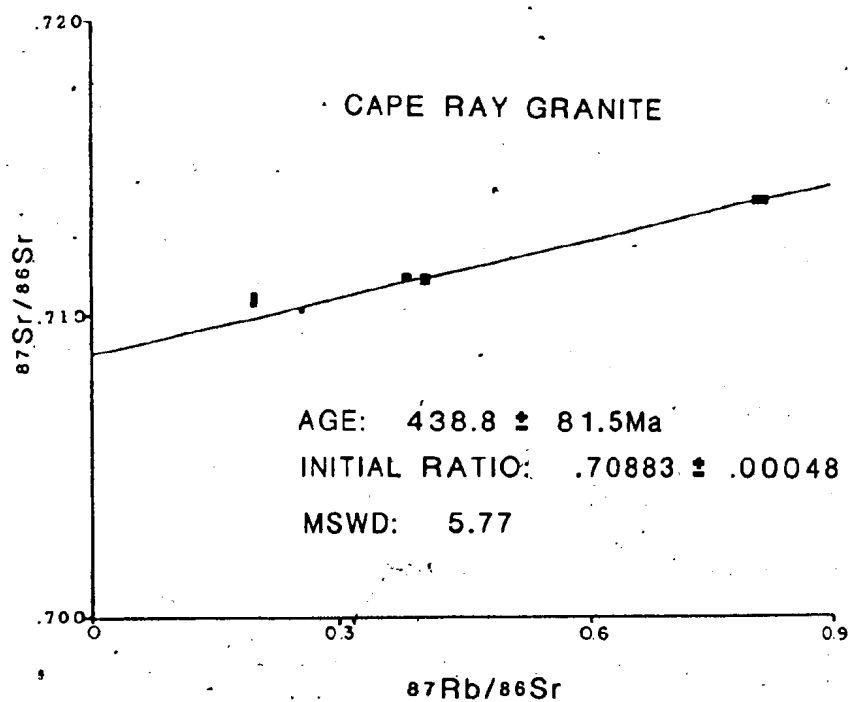
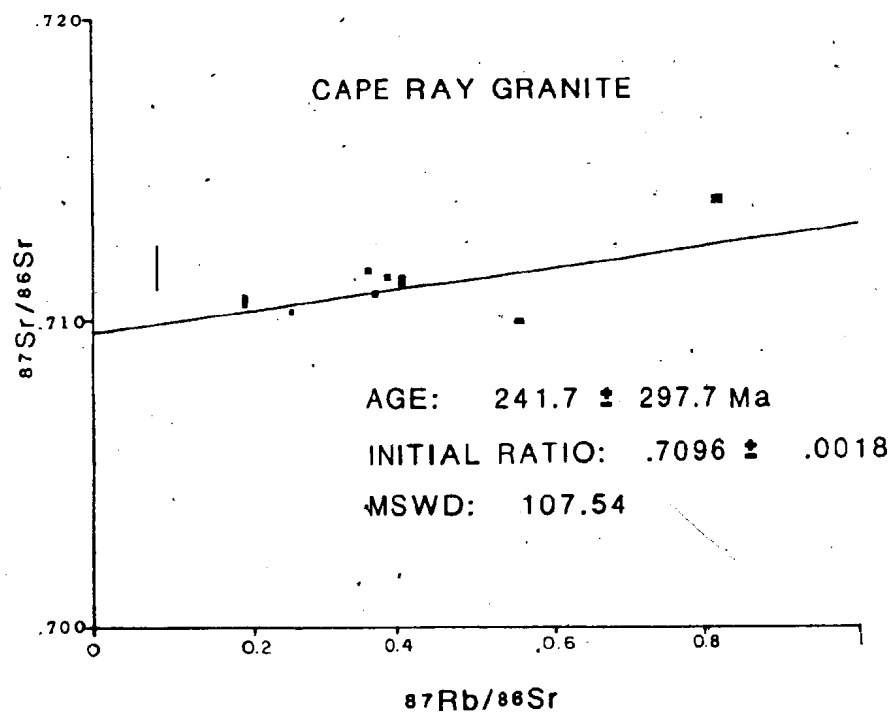
of the granite. According to Brown (1975) the granite was affected by two major deformational events which produced the interference type of outcrop pattern. Dingwell (1980) supported this interpretation, and further showed that the granite underwent extensive metasomatism and alkali redistribution in which Rb and Sr concentrations were affected such that either or both of the elements can be added or subtracted. Mobility of Rb and Sr makes the initial and most fundamental assumption of radiometric dating, the existence of a closed system since magma generation, invalid.

### 3.3 The Cape Ray Granite

Trace element and isotopic data for nine samples from the megacrystic phase of this granite are given in Table IV. Three samples (CRG-1F, CRG-2F and CRG-3AF) are microcline megacryst separates from whole rock samples (CRG-1, CRG-2 and CRG-3A respectively). Figure 7a shows the errorchron derived from these data with an age of  $242 \pm 298$  Ma. Removal of the feldspar splits and CRG-6 samples from consideration, yields a Silurian age of  $439 \pm 82$  Ma (Figure 7b). The U/Pb zircon age of trondhjemitic granites in the Annieopsquotch area is 477-481 Ma (Dyning and Krogh, 1983), and these granites are correlative with the Cape Ray Granite. Therefore the Silurian age for the

Figure 7a Rb/Sr whole rock and mineral separate isochron for the megacrystic Cape Ray Granite. See Table IV for isotopic data used to construct this diagram.

Figure 7b Rb/Sr whole rock isochron for five samples of the megacrystic Cape Ray Granite. Constructed without the data of samples CRG-1F, CRG-2F, CRG-3AF (feldspar megacrysts) and CRG-6 (see Table IV).



megacrystic phase is too young. There are also large errors in the date relative to the restricted  $87\text{Rb}/86\text{Sr}$  values.

Brooks (1980) suggested that samples with volatile contents of  $>1.2$  wt % should be rejected from geochronological determinations because of the probability of isotopic resetting. The high contents of LOI's (volatiles) in these analysed samples is indicative of the strong alteration that these samples have undergone. As described in Chapters 2 and 4, feldspars are heavily sericitized and chloritized, and biotite is strongly chloritized (*ie.* these minerals underwent hydration). Therefore the Sr and Rb isotopic ratios were probably reset during hydration (*ie.* rendering the Rb/Sr radiometric system useless in the case of this granitoid).

No attempt was made to date the tonalitic phase of Cape Ray Granite as this phase underwent even more extensive, alteration (hence trace element mobility) than the megacrystic phase.

### 3.4 The Red Rocks Granite

Table IV lists the elemental and isotopic concentrations for eight samples from the Red Rocks Granite. The Sr contents, as outlined in Table IV are high for a normal granitic rock. All samples were collected

from within the gravel pit at Red Rocks Point and thus represent a localized selection of values. The errorchron derived from this data set (Figure 8) indicates an age of  $495 \pm 57$  Ma for this pluton. As will be shown in Chapter 6 below, this granite seems to be a more felsic phase of the tonalitic granite system. This date, though older than the  $350 \pm 50$  Ma age for correlative tonalite in the Annieopsquotch area (Dunning, pers. comm., 1983), indicates an Ordovician (Odin, 1982) age for the plutonic Cape Ray Granite system which is associated with an Ordovician ophiolite. The MSWD of 46, however, indicates this age determination should be treated with caution as there are obviously problems with the data.

### 3.5 The Windsor Point Group Ignimbrite

Eight samples, from the ignimbritic member of the Little Barachois Formation, listed in Table IV, were used to construct the isochron diagram of Figure 9. Two of these samples, 79-15 and 79-19, are of feldspar porphyry dykes that intrude the Cape Ray Granite (i.e. distal feeder dykes of the Windsor Point Group volcanism) and one, WPG-4, is from a large ignimbritic clast in the autobreccia associated with the ignimbrite.

The age defined is  $377 \pm 21$  Ma, or the Givetian stage of the Late Devonian (Odin, 1982). This is in good agreement with the Devonian fossil age for the Billiards



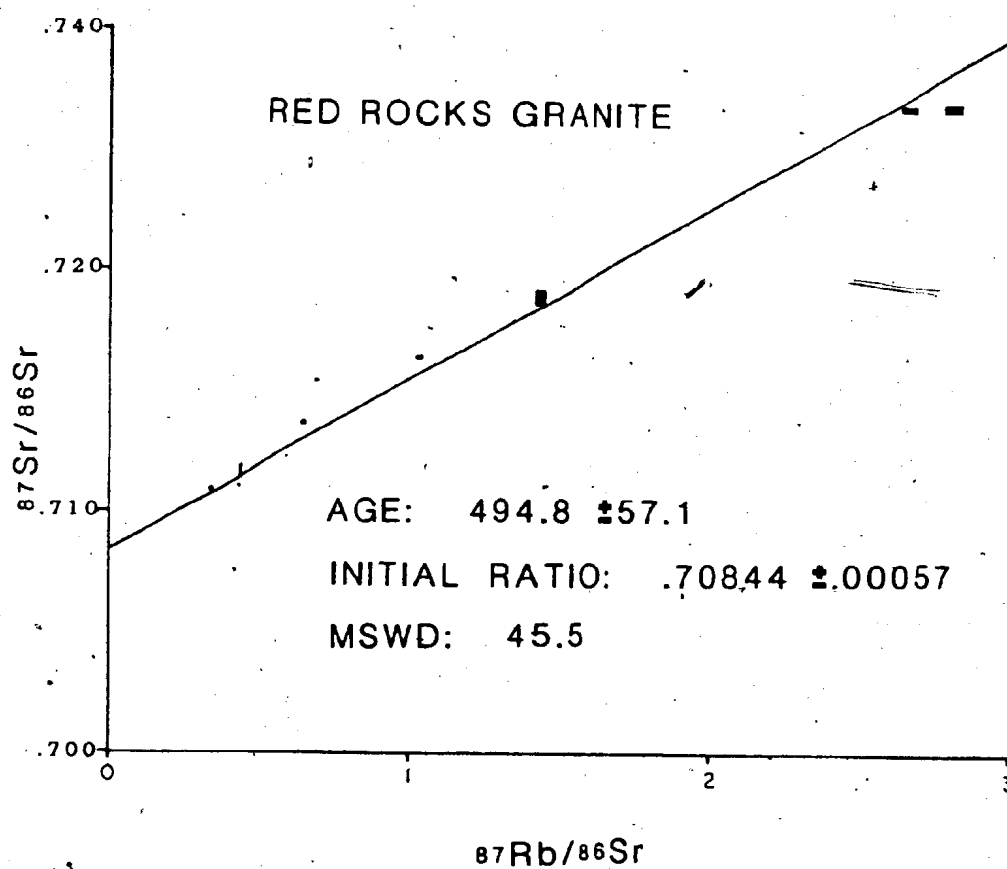


Figure 8 Rb/Sr whole rock isochron for the Red Rocks Granite. See Table IV for the isotopic data used to construct this diagram.

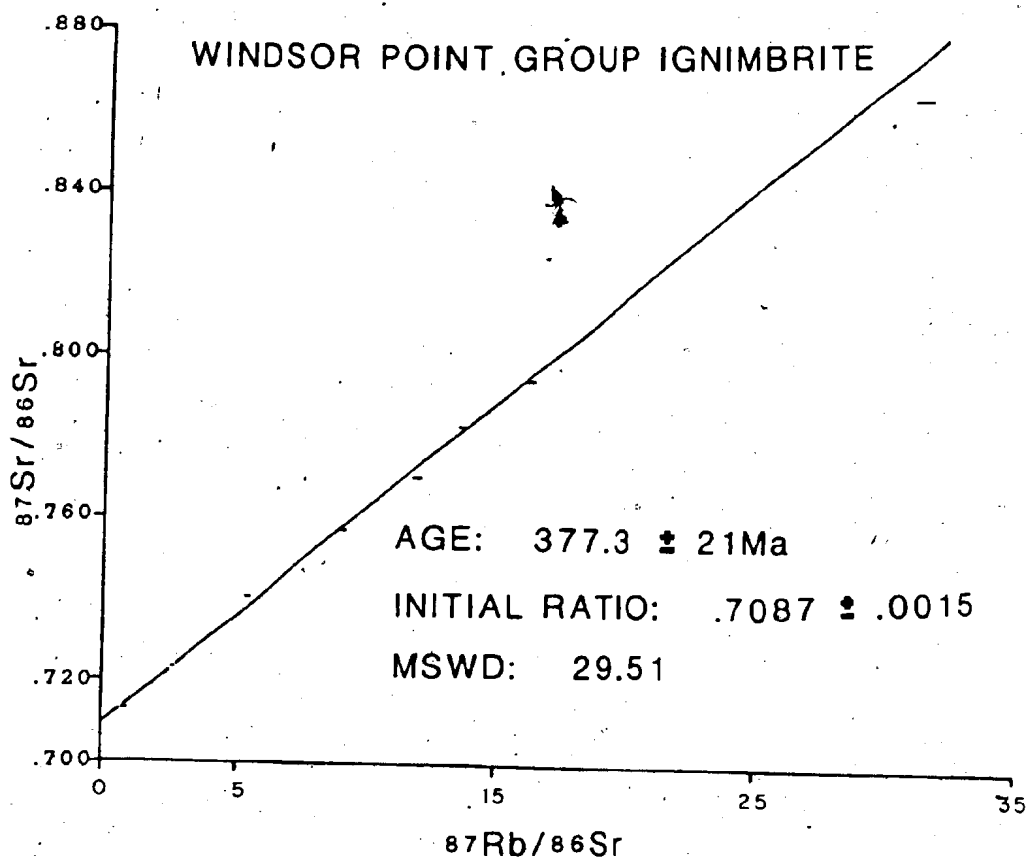


Figure 9 Rb/Sr whole rock isochron for the basal ignimbrite member of the Windsor Point Group. See Table IV for the isotopic data used to construct this diagram.

Brook Group, which is correlative (Chorlton, 1980b) with the Windsor Point Group, and also the Lower Devonian fossil age from equivalents in the King George IV Lake area (Kean and Jayasinghe, 1981).

The MSWD is 29.51 of this determination reflects some problems with geological sampling. The strong deformation that overprints portions of this unit along its strike may have affected element distributions, but in general the date is consistent with the known geological constraints.

### 3.6 The Windowglass Hill Granite

An isochron for the Windowglass Hill Granite (Figure 10) is based upon nine samples (Table IV) from throughout the pluton and includes one mylonitized sample (79-140) from its margin. The age of  $369 \pm 12$  Ma derived from this isochron has an MSWD of 4.63. The good fit is unexpected because the granite has undergone sodic enrichment and thus presumably some Rb/Sr redistribution. However, as will be described below, this metasomatic event was deuteritic (i.e. was produced by magmatic fluids). These same deuteritic fluids are implicated in the ore-forming system for the Windowglass Hill and Main Shear Showings.

The similar ages and initial Sr ratios for this granite and the Windsor Point Group support the interpretation that the granite was a subvolcanic

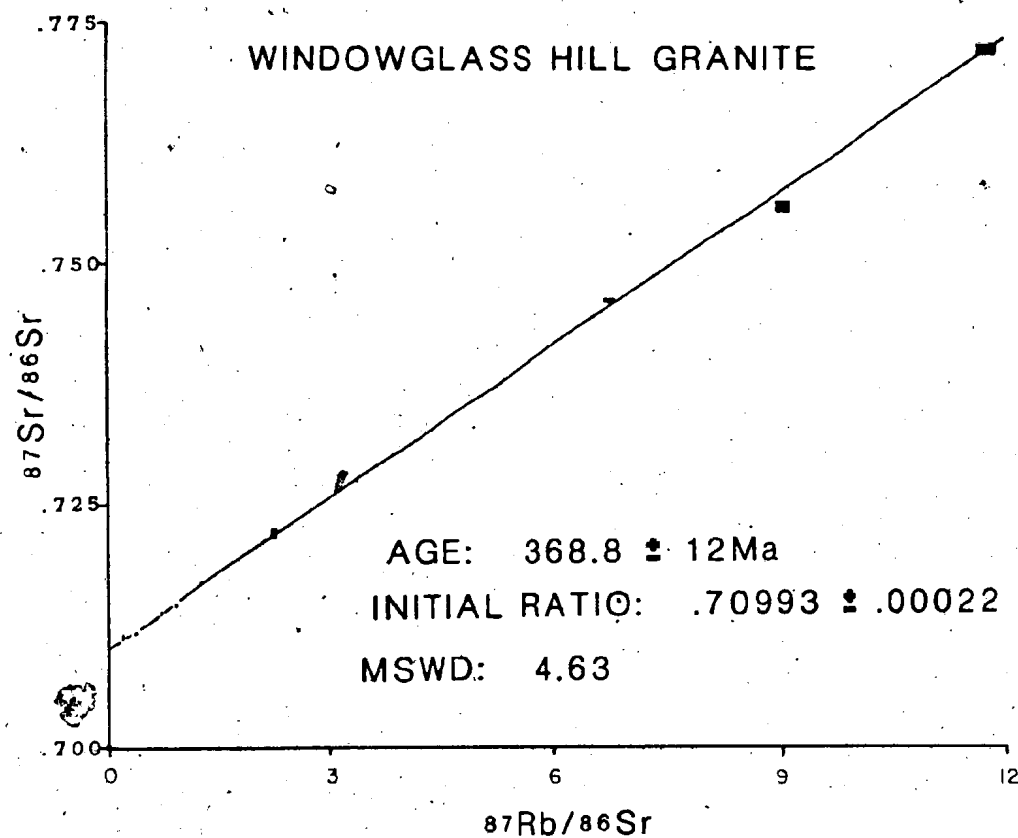


Figure 10 Rb/Sr whole rock isochron for the Windowglass Hill Granite. See Table IV for the isotopic data used to construct this diagram.

equivalent of the felsic volcanism.

### 3.7 The Strawberry and Isle aux Morts Brook Granites

The data for the seven samples of the Strawberry Granite used to construct the isochron (Figure 11a) are given in Table IV. The radiometric date obtained for this granite is  $362 \pm 27$  Ma with an MWSD of 5.39.

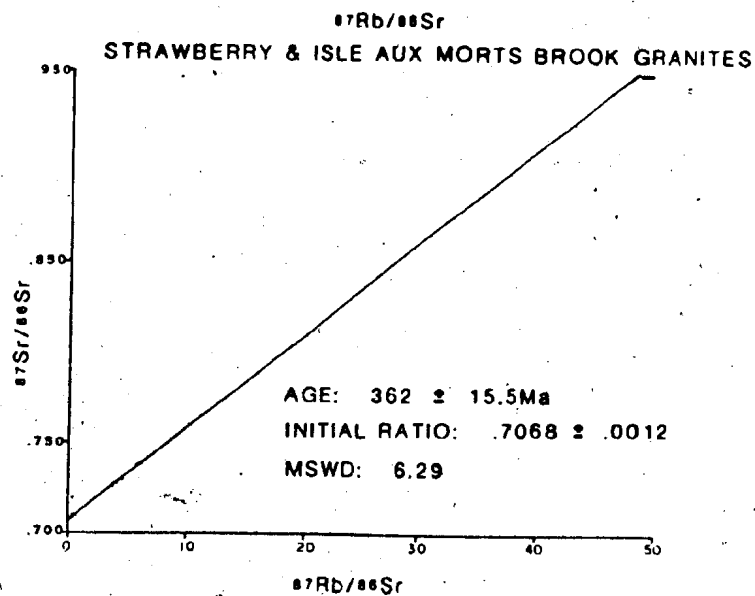
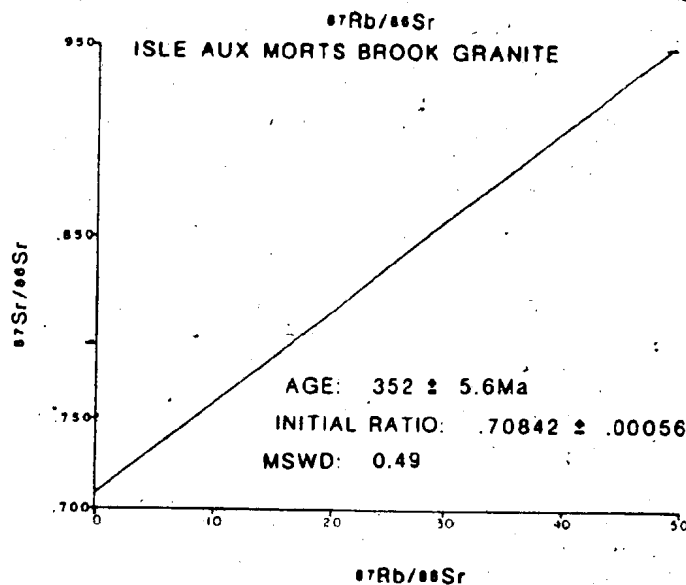
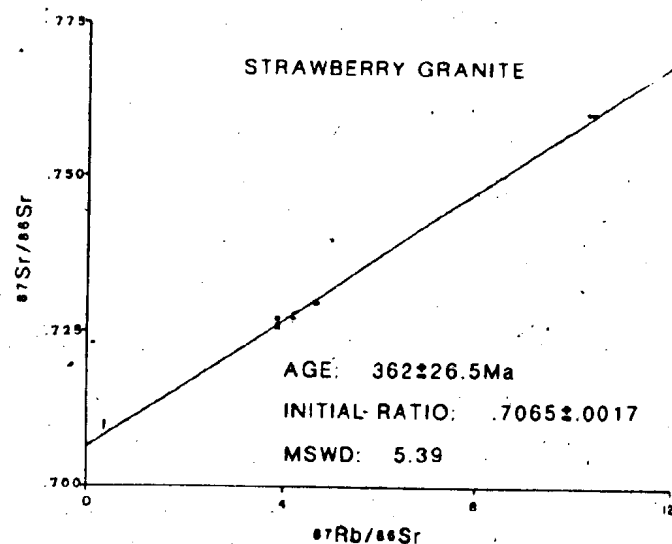
The Rb/Sr date for the Isle aux Morts Brook Granite is  $352 \pm 6$  Ma (Figure 11b) based on only four samples (Table IV). Three of these samples cluster so closely together to almost constitute a single point. The reason for this clustering is the homogeneous nature of this small pluton. The unique point on the isochron is contributed by an aplite sample (79-108). The MSWD of this isochron is 0.49 and it also shows the homogeneity of the samples. This is the youngest age (Carboniferous) yet defined for any unit in southwestern Newfoundland.

Since both post-tectonic granites are chemically, and temporally similar, and since the available spectrum of  $^{87}\text{Rb}/^{86}\text{Sr}$  and  $^{87}\text{Sr}/^{86}\text{Sr}$  isotopic values for the Isle aux Morts Brook Granite is limited, the isotopic data of both were combined to construct an isochron for the post-tectonic granites (Figure 11c). The combined age is  $362 \pm 16$  Ma with an MSWD of 6.29. The initial  $^{87}\text{Sr}/^{86}\text{Sr}$  ratio of  $0.707 \pm 0.001$  matches that of the Strawberry

Figure 11a Rb/Sr whole rock isochron for the Strawberry Granite.  
(Data in Table IV).

Figure 11b Rb/Sr whole rock isochron for the Isle aux Morts Brook  
Granite. (Data in Table IV).

Figure 11c Combined whole rock isochron for the Strawberry/Isle, aux  
Morts Brook Granites. (Data in table IV).



Granite ( $0.707 \pm 0.002$ ) rather than that of the Isle aux Morts Brook Granite ( $0.708 \pm 0.0005$ ), but the relative difference is minor.

The Late Devonian to Early Carboniferous age of these post-tectonic granites is in agreement with other post-tectonic granites in Newfoundland (eg. the St. Lawrence Granite dated at  $355 \pm 11$  Ma, B. J. Fryer, 1983, pers. comm.).

### 3.8 Areal Isochrons

Haack et al. (1982) averaged the  $^{87}\text{Rb}/^{86}\text{Sr}$  and  $^{87}\text{Sr}/^{86}\text{Sr}$  ratios in each of a series of granites from Namibia, with an age range of 459-553 Ma, and re-plotted these average values on a  $^{87}\text{Sr}/^{86}\text{Sr}$  vs.  $^{87}\text{Rb}/^{86}\text{Sr}$  diagram. They found that the points defined new "isochrons", which they termed "areal isochrons". These areal isochrons indicate the existence of a continuity of isotopic equilibrium between the various granites, and therefore the sources of the granites were probably the same (with defineable ages of metamorphic re-setting).

Following this approach, the isotopic data for all granitoids and the ignimbrite in the Cape Ray Fault Zone were averaged and plotted (see Table V for details) in an attempt to discern the presence of areal isochrons (or common sources). (The Strawberry and Isle aux Morts Brook



TABLE V AVERAGED ISOCHRON DATA USED TO CONSTRUCT AREAL ISOCHRONS  
(Errors -1% for  $^{87}\text{Rb}/^{86}\text{Sr}$ , errors in  $^{87}\text{Sr}/^{86}\text{Sr}$  quotes in terms of  $10^{-5}$ ).

<u>UNIT</u>	<u><math>^{87}\text{Rb}/^{86}\text{Sr}</math></u>	<u><math>^{87}\text{Sr}/^{86}\text{Sr}</math></u>
Port. aux Basques Granite	5.186	$0.741372 \pm 14.5$
Cape Ray Granite (megacrystic)	0.411	$0.711499 \pm 12.3$
Red Rocks Granite	1.213	$0.716977 \pm 14.5$
Windsor Point Group	11.341	$0.768406 \pm 9.2$
Windowglass Hill Granite	3.695	$0.729264 \pm 22.5$
Strawberry Granite	4.476	$0.729807 \pm 27.8$
Isle aux Morts Brook Granite	16.760	$0.792404 \pm 9.6$

Granites have already been combined with the assumption of a common origin). Figure 12a shows the "isochron" for all units. The MSWD of 74 shows that this is a poorly-fitted, determination, suggesting non-common sources for all the units. This is not surprising in view of the different pre-defined sources of the Port aux Basques and Cape Ray Granites.

Figure 12b shows the "isochron" with the Port aux Basques Granite data removed. The high MSWD (34) and large error on the "age" ( $> 7\%$ ) indicates non-communality of the data (i.e. different sources). Figure 12c, the "isochron" with the Red Rocks, Cape Ray and Port aux Basques Granites removed, has an even poorer fit than the previous one (Figure 12b).

The average data for the Red Rocks and Cape Ray Granites, supposed phases of the same granitic sequence, define a two-point isochron with an age of 480 Ma (Figure 12d). Since the Cape Ray Granite is thought to have been a partial melt of the Long Range Mafic/Ultramafic Complex ophiolite, and the Red Rocks Granite, a probable more felsic phase of this same I-type melt, it is worthy of note that Dunning *et al.* (1982) report an age of  $483 \pm 3$  Ma for the correlative Annieopsquotch ophiolite (determined by U/Pb methods).

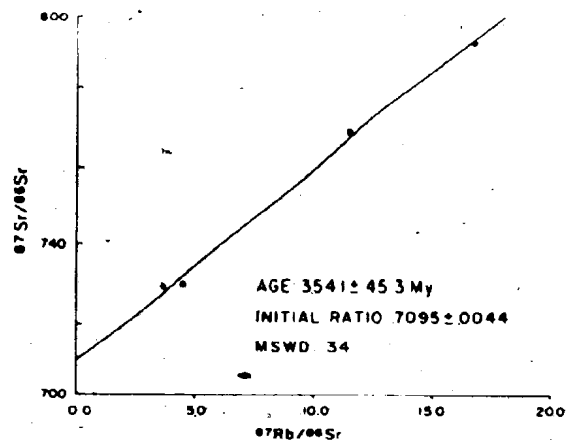
In summary, the data from southwestern Newfoundland do not define areal isochrons with better than two-point fits.

Figure 12a Areal isochron for all units analysed in the Cape Ray Fault Zone. Data points based on the isotopic averages from each unit. Data used for this and the following diagrams are listed in Table V.

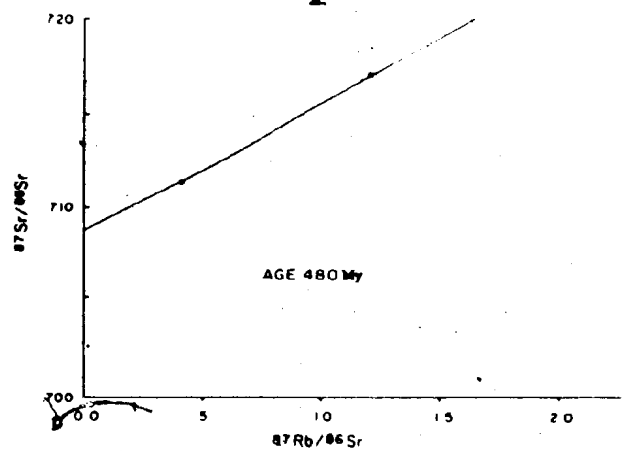
Figure 12b Areal isochron for all units analysed except the Port aux Basques Granite.

Figure 12c Areal isochron for all units analysed except the Port aux Basques, Red Rocks and Cape Ray Granites.

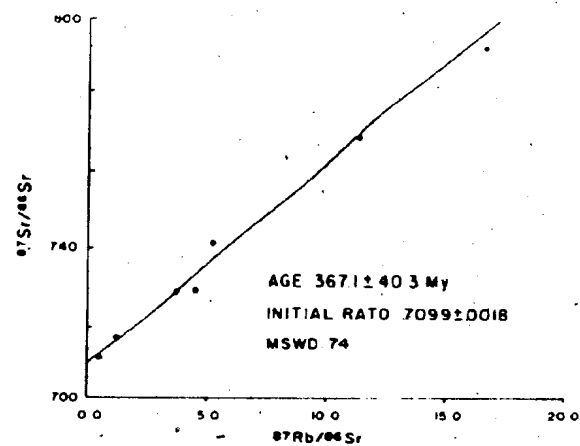
Figure 12d Areal isochron for the Cape Ray and Red Rocks Granites.



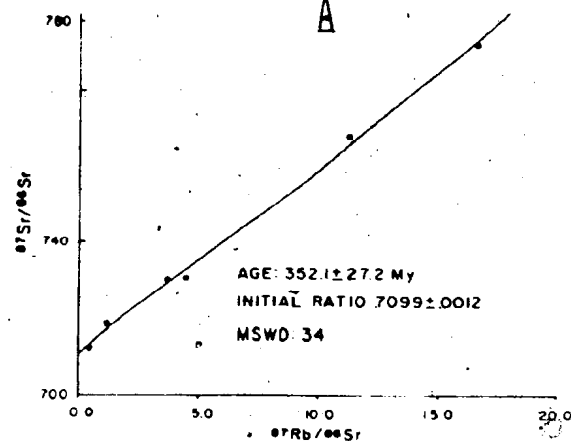
C



D



A



B

However combinations of the data do reveal the noncommunitality of sources for all the units and also distinct groupings of units with similiar sources: viz. the Strawberry and Isle aux Morts Brook Granites; the Cape Ray and Red Rocks Granites; the Windowglass Hill Granite and the Windsor Point Group ignimbrite; and the Port aux Basques Granite.

## CHAPTER 4

### METAMORPHIC HISTORY

#### 4.1 Metamorphic Mineral Assemblages

Coexisting metamorphic mineral assemblages found in each of the main geological units in the Cape Ray Fault Zone are illustrated in Table VI. The number of observations of each assemblage is also recorded in order to give some idea of its relative abundance. Stability in these assemblages is defined as those metamorphic minerals in direct contact with each other with no visible replacement textures.

All assemblages are assumed to be in equilibrium with quartz and feldspar. In the granites (except for the Cape Ray Granite), biotite is incipiently replaced and as such has not been included as a member of the given metamorphic assemblage. In other special cases, as noted, primary prograde hornblende and staurolite are retrogressed by lower grade assemblages.

##### 4.1.1 The Granites

The Red Rocks, Strawberry and Isle aux Morts Brook Granites do not have prominent fabrics, and most stable metamorphic mineral assemblages suggest a deuteric, or late

TABLE VI Metamorphic Mineral Assemblages

LOW RANGE NAPIC/ULTRAMAFIC COMPLEX

SPH	CAR	CHL	EP1	SPH	BIO	ACT	CAR	HRB	STA	AND	TOL	CPE	(#)
X													1
X													2
X													3
X													4
X													5
X													6
X													7
X													8
X													9
X													10

CAPE RAY GRANITE (TORNALITES)

SPH	CAR	CHL	EP1	SPH	BIO	ACT	CAR	HRB	STA	AND	TOL	CPE	(#)
X													1
X													2
X													3
X													4
X													5
X													6
X													7
X													8
X													9
X													10

(MIGACITIC)

SPH	CAR	CHL	EP1	SPH	BIO	ACT	CAR	HRB	STA	AND	TOL	CPE	(#)
X													1
X													2
X													3
X													4
X													5
X													6
X													7
X													8
X													9
X													10

RED ROCKS GRANITE

SPH	CAR	CHL	EP1	SPH	BIO	ACT	CAR	HRB	STA	AND	TOL	CPE	(#)
X													1
X													2
X													3
X													4
X													5
X													6
X													7
X													8
X													9
X													10

WINDOGLASS HILL GRANITE

SPH	CAR	CHL	EP1	SPH	BIO	ACT	CAR	HRB	STA	AND	TOL	CPE	(#)
X													1
X													2
X													3
X													4
X													5
X													6
X													7
X													8
X													9
X													10

STREAMBURY GRANITE

SPH	CAR	CHL	EP1	SPH	BIO	ACT	CAR	HRB	STA	AND	TOL	CPE	(#)
X													1
X													2
X													3
X													4
X													5
X													6
X													7
X													8
X													9
X													10

ISLE AUX PORTS BROOK GRANITE

SPH	CAR	CHL	EP1	SPH	BIO	ACT	CAR	HRB	STA	AND	TOL	CPE	(#)
X													1
X													2
X													3
X													4
X													5
X													6
X													7
X													8
X													9
X													10

PORT AUX BASQUES COMPLEX

SPH	CAR	CHL	EP1	SPH	BIO	ACT	CAR	HRB	STA	AND	TOL	CPE	(#)
X													1
X													2
X													3
X													4
X													5
X													6
X													7
X													8
X													9
X													10

PORT AUX BASQUES COMPLEX NEAR WINDSOR POINT GROUP CONTACT

SPH	CAR	CHL	EP1	SPH	BIO	ACT	CAR	HRB	STA	AND	TOL	CPE	(#)
X													1
X													2
X													3
X													4
X													5
X													6
X													7
X													8
X													9
X													10

CABRIO

SPH	CAR	CHL	EP1	SPH	BIO	ACT	CAR	HRB	STA	AND	TOL	CPE	(#)
X													1
X													2
X													3
X													4
X													5
X													6
X													7
X													8
X													9
X													10

CABRIO (SOUTH OF WINDOGLASS HILL)

SPH	CAR	CHL	EP1	SPH	BIO	ACT	CAR	HRB	STA	AND	TOL	CPE	(#)
X													1
X													2
X													3
X													4
X													5
X													6
X													7
X													8
X													9
X													10

WINDSOR POINT GROUP (LOWHILLITE)

SPH	CAR	CHL	EP1	SPH	BIO	ACT	CAR	HRB	STA	AND	TOL	CPE	(#)
X													1
X													2
X													3
X													4
X													5
X													6
X													7
X													8
X													9
X													10

(CONGLOMERATE)

SPH	CAR	CHL	EP1	SPH	BIO	ACT	CAR	HRB	STA	AND	TOL	CPE	(#)
X													1
X													2
X													3
X													4
X													5
X													6
X													7
X													8
X													9
X													10

(SANDSTONE)

SPH	CAR	CHL	EP1	SPH	BIO	ACT	CAR	HRB	STA	AND	TOL	CPE	(#)
X													1
X													2
X													3
X													4
X													5
X													6
X													7
X													8
X													9
X													10

(FELSIC TUFF)

SPH	CAR	CHL	EP1	SPH	BIO	ACT	CAR	HRB	STA	AND	TOL	CPE	(#)
X													1
X													2
X													3
X													4
X													5
X													6
X													7
X													8
X													9
X													10

(1<sup>st</sup> CONGLO

magmatic, origin for the alteration minerals. In general the Red Rocks Granite has stable assemblages of sericite-chlorite-epidote  $\pm$  sphene  $\pm$  carbonate. The assemblage sericite-chlorite  $\pm$  epidote  $\pm$  sphene is representative of the Isle aux Morts brook Granite. The Strawberry Granite typically has intergrown sericite-chlorite-epidote-sphene.

The Cape Ray and Windowglass Hill Granites have been tectonized and the alteration minerals appear to represent a regional metamorphic effect (especially in the Cape Ray Granites). The megacrystic Cape Ray Granite has some combination of sericite-chlorite-epidote as stable assemblages while in the tonalitic phase, epidote is more abundant and occurs with sericite-chlorite-sphene  $\pm$  carbonate. The Windowglass Hill Granite is generally altered to chlorite-sericite  $\pm$  epidote assemblages.

The typical chlorite-epidote (-muscovite) assemblages of these granites are indicative of greenschist facies metamorphism (Miyashiro, 1973), or low grade metamorphism (Winkler, 1979).

#### 4.1.2 The Long Range Mafic/Ultramafic Complex

The normal assemblage in this unit is sericite-chlorite-epidote-actinolite  $\pm$  biotite (the sericite alters plagioclase), or low grade greenschist



facies.

#### 4.1.3 Port aux Basques Complex

Brown (1973 and 1975) was able to define four zones of prograde metamorphic mineral assemblages within the Port aux Basques Complex. These zones, defined for a small coastal area near Port aux Basques (see Figure 13), trend northeasterly (ie. parallel to the structural fabric in the Port aux Basques Complex). Type metamorphic mineral assemblages within each zone, grading from lowest to highest grade, as defined by Brown, are garnet, garnet-staurolite-kyanite, kyanite-garnet, and sillimanite-garnet. Biotite is present as a stable component in each assemblage. The highest grade of metamorphism would have taken place even further to the southeast, where P-T conditions were sufficient to induce partial melting and migmatite formation.

The limited examination of the Port aux Basques Complex (ie. only the northwestern edge of this unit) in this study, suggests that Brown's metamorphic mineral assemblage zonation is applicable inland to, and including, the Main Shear Showing region. In this area most gneiss outcrops have garnet-biotite assemblages as their highest prograde development. However, staurolite-biotite-garnet occur to the southeast of the Gulch, grading outwards from

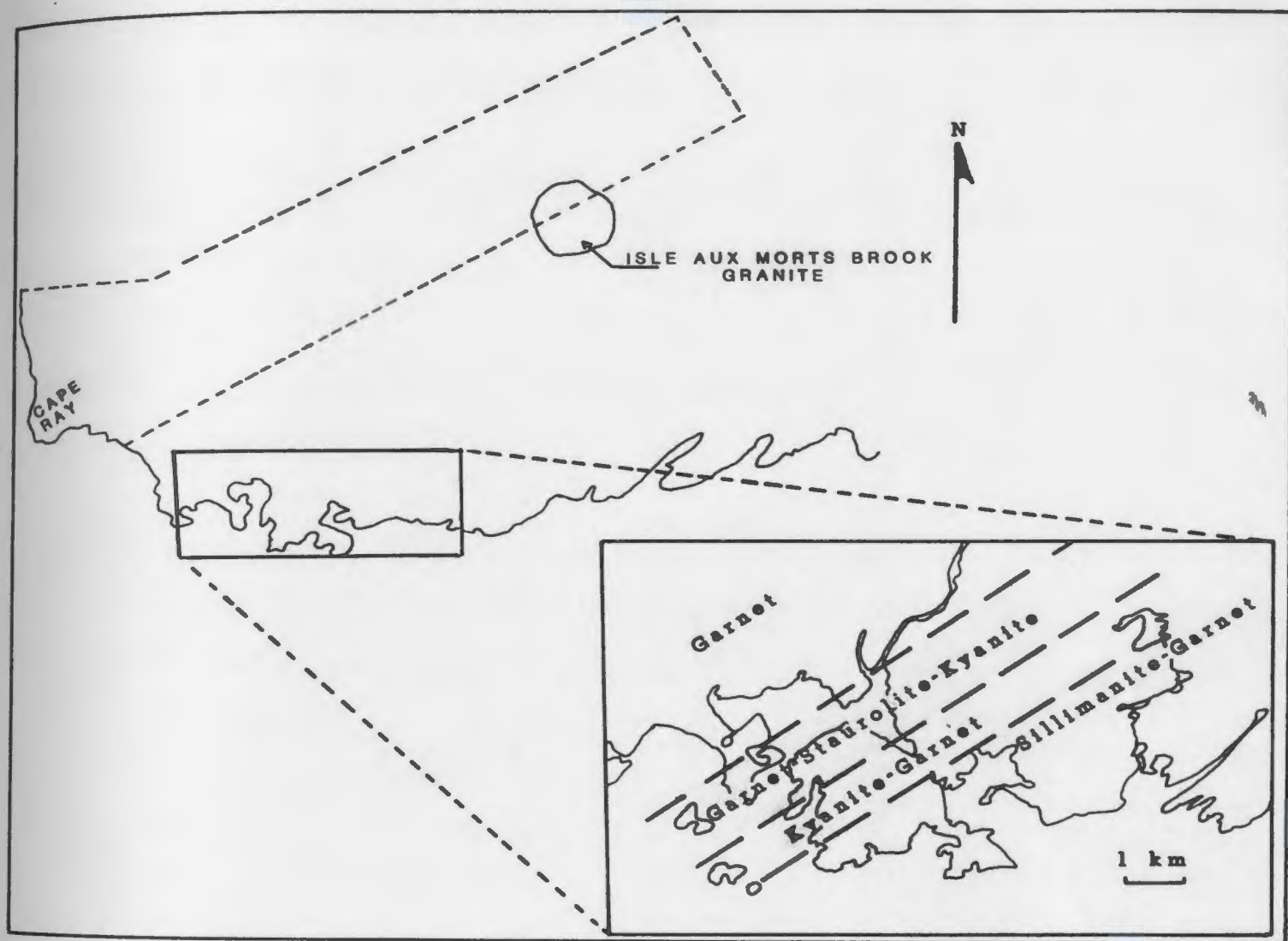


Figure 13 Location and form of Brown's (1975) metamorphic mineral zones in the southwestern portion of the Port aux Basques Complex. The general position of the Cape Ray Fault Zone map area is also indicated.

biotite-garnet zones (see Plate 2-1A). Kyanite and sillimanite were not found in this study but by extrapolation should occur further to the southeast.

Chlorite is also a significant component in the metamorphic mineral assemblages represented in this unit. Some of this chlorite, especially in the rocks closest to the Windsor Point Group contact, is produced by retrograde replacement of higher grade metamorphic assemblages, but chlorite is also a prograde mineral in equilibrium with the other minerals. This is especially true in the staurolite-bearing assemblage where the gneiss is not retrogressed. XRD identification indicates that the chlorites in the Port aux Basques Complex are Fe-rich.

Miyashiro (1973) would call the metamorphic grade of this gneiss unit, upper greenschist to lower amphibolite facies. Winkler (1979), on the other hand, rejects useage of the terms amphibolite and greenschist facies on the grounds that they bestow an unwarranted mineralogical connotation to metamorphic subdivisions. He prefers the use of the terms very-low -grade, low-grade, medium-grade and high-grade metamorphism. Rocks containing chlorite-muscovite-biotite would be classified as low-grade in this scheme. Using the experimental data of Hoschek (1969), which indicated the permissible reaction:  
$$\text{chlorite} + \text{muscovite} = \text{staurolite} + \text{biotite} + \text{quartz} + \text{H}_2\text{O},$$
Winkler (1979) defined the boundary between the low- and

medium-grade metamorphism as the point where staurolite first occurs due to breakdown of Fe-rich chlorite.

The decrease in chlorite content as the staurolite zone is approached and the original Fe-rich nature of the chlorite indicates this reaction is quite plausible for the Port aux Basques Complex. Thus, the gneiss unit in the region of the Main Shear Showing grades from low-grade to medium-grade metamorphism. The common low-grade nature of both the Windsor Point Group and Port aux Basques Complex is therefore one more obscuring factor in delineating their contact.

The low pressure  $Al_2SiO_5$  polymorph, andalusite, occurs in the Port aux Basques Complex (as mapped herein -see Map 1) only near its contact with the Isl  aux Morts Brook Granite. The andalusite appears to be the result of granite-induced contact metamorphism that has overprinted the prograde regional metamorphism. Andalusite is a common contact metamorphic mineral, so much so that Winkler (1979) lists a metamorphic mineral assemblage seen in contact metamorphosed low-grade rocks as:

white mica (i.e. sericite) + biotite

+ chlorite + quartz + andalusite,

which is exactly what is seen in the gneisses in the contact zone. If the gneisses were of medium-grade, then staurolite and cordierite could have been diagnostic contact metamorphic minerals.

There has also been extensive retrogressive metamorphism of the gneiss. This retrogression is most extreme where the gneisses are in tectonized contact with the Windsor Point Group, as phyllonites are developed. Minor retrogression is visible in both the Port aux Basques Gneiss and Granite, wherein chlorite replaced biotite, oxidation of pyrite and biotite produced limonite, and carbonate, quartz and/or limonite-filled fractures and shears cut the rocks.

This retrogression is reflected in the metamorphic mineral assemblages, as shown for gneiss samples near this contact (Table VI), where chlorite-sericite + carbonate have become significant, ubiquitous components in the assemblages. They are the products of alteration of biotite and/or hornblende. In garnet grains, carbonate-chlorite often fill fractures. The rare presence of actinolite helps place the grade of retrogression as low-grade or greenschist facies.

#### 4.1.4 Gabbros

Metamorphic mineral assemblages in the gabbros (unit 6) south of the Windowglass Hill Granite are relatively high grade consisting predominantly of chlorite-epidote-sphene-hornblende + biotite + sericite + actinolite and rare clinopyroxene. There is some primary

hornblende replaced by chlorite-actinolite, but generally the hornblende seems to be a primary prograde development. These gabbros straddle the greenschist and epidote-amphibolite facies boundary (Miyashiro, 1973), but are more amphibolitic. Winkler (1979) would call these gabbros, low grade amphibolites. Clinopyroxene and clinopyroxene-garnet intergrowths occur in carbonaceous zones that were contact metamorphosed by the Isle aux Morts Brook Granite.

The other gabbro bodies scattered through the map area have a lower grade (greenschist facies) metamorphic assemblages. The predominant mineralogy is sericite-carbonate-chlorite-epidote-biotite  $\pm$  actinolite. The biotite, however, is a primary magmatic phase and not a metamorphic mineral. The only presence of hornblende is as a relict mineral.

#### 4.1.5 Windsor Point Group

Metamorphic mineral assemblage data for the Windsor Point Group can be broken down into groups because of significantly different assemblages present in different members. In the ignimbrite of the Little Barachois Formation, the dominant alteration mineral is sericite which usually occurs by itself, though rarely with chlorite-carbonate  $\pm$  biotite. This mono-mineralic

alteration is low grade, and in fact is probably not a dynamothermal effect, but a deuteric one (even fumarolic - witness the presence of sericite-tourmaline intergrowths in portions of the rhyolite/autobreccia). The conglomerate and mixed conglomerate-sandstone members of this formation are similarly low grade/deuteric, but there is some metamorphic biotite.

There are a large number of stable metamorphic mineral assemblages present in the various and sundry units which make up the schist member. Significantly however, the majority are simply sericite-carbonate-chlorite intergrowths. Epidote, sphene and biotite are common, but biotite generally occurs to the southeast. Garnet occurs only in the graphitic schists near the Port aux Basques Complex contact. Primary hornblende occurs within gabbroic interbeds. Tourmaline in these schists, unlike that in the Little Barachois Formation, is probably a clastic mineral. The great preponderance of sericite-carbonate-chlorite assemblages shows that the interlayered chlorite-sericite schist nature of this unit persists down to a microscopic level and therefore this member is greenschist (or low-grade) facies.

The inland felsic tuff/rhyolite has definitively higher-grade assemblages than the basal ignimbrite, as the assemblages are basically sericite-chlorite with some biotite and sphene. The second conglomerate (unit 7g)

consists of similar sericite-carbonate-chlorite-epidote assemblages. Both are low/grade (or greenschist) facies.

Windsor Point Group wall rocks enclosing the Main Shear mineralization have the same predominance of sericite-carbonate-chlorite assemblages as seen in the schist member (of which they are a part). Highest grade metamorphism in the Windsor Point Group occurs in those nebulous schists near the gneiss contact, where the rocks contain sericite-carbonate-chlorite-epidote-sphene-biotite assemblages.

In summary metamorphic grade in the Windsor Point Group ranges from almost nil in the northwest through progressively increasing grade to the southeast where upper greenschist facies assemblages are developed. This range in metamorphic gradation further emphasizes the problems in defining the Windsor Point Group, as again the Little Barachois Formation is distinct from the remainder of the group.

#### 4.1.6 Mylonites and Breccias

The mylonite unit on the coast has a slightly lower grade metamorphic mineral assemblages than the inland unit. This latter mylonite has a strong biotite component with sericite-chlorite-epidote (ie. upper greenschist facies).



The coastal mylonite is basically sericite-carbonate-chlorite-epidote + biotite (greenschist to upper greenschist facies).

Metamorphic grade in the breccias (unit 13) is low grade, mainly sericite.

#### 4.2 Garnet Compositions

The presence of garnets in graphitic schists of the Windsor Point Group presents an interpretative problem as the appearance of almandine garnet in a progressive metamorphic sequence can usually be mapped as a distinctive reaction, or isograd, (eg. Zen, 1981, Holdaway *et al.*, 1982, Ferry, 1981), and is often taken to represent the onset of the amphibolite facies. (Miyashiro, 1973).

In order to evaluate whether the garnets in the graphite schist and those of the Port aux Basques Complex are similar, and also to determine compositions of those in the garnet-clinopyroxene intergrowths of gabbro skarns, several garnet samples were probed (analytical specifications given in Appendix I).

The resultant data are presented in Table VII and graphically illustrated on Figure 14. Garnets from sample

TABLE VII Garnet Compositions from Microprobe Analyses

## GARNET COMPOSITIONS IN GABBRO (Sample 79-132)

ANALYSIS	Mg	Al	Si	Ca	Ti	Mn	Fe	Total	COMMENTS
1 (wt %)	0.06	12.19	37.60	36.25	1.20	0.22	13.83	101.36	
(at. prop.)*	0.004	1.154	3.023	3.122	0.070	0.014	0.930	8.317	
2 (wt %)	0.06	13.05	36.52	37.00	1.68	0.24	12.36	100.93	
(at. prop.)	0.007	1.238	2.940	3.193	0.102	0.014	0.832	8.327	
3 (wt %)	0.07	12.52	37.44	36.80	1.84	0.27	12.88	101.83	
(at. prop.)	0.007	1.175	2.987	3.146	0.110	0.016	0.859	8.301	
4 (wt %)	0.06	11.38	37.30	36.64	1.15	0.28	14.80	101.61	
(at. prop.)	0.004	1.083	3.013	3.170	0.068	0.019	0.998	8.356	
5 (wt %)	0.06	12.66	37.20	36.73	1.81	0.23	12.61	101.30	
(at. prop.)	0.007	1.194	2.979	3.152	0.108	0.014	0.844	8.298	

## GARNET COMPOSITION IN PYRRHOTITE-BEARING AMPHIBOLITE OF THE PORT AUX BASQUES COMPLEX (Sample 80-59)

1 (wt %)	0.98	21.02	37.84	13.07	0.08	7.28	22.25	102.52	Garnets were difficult to probe due to contrasting hardnesses of constituent minerals.
(at. prop.)	0.115	1.939	2.962	1.096	0.004	0.482	1.457	8.055	
2 (wt %)	0.91	20.95	37.73	10.97	0.07	8.34	23.20	102.17	
(at. prop.)	0.106	1.945	2.971	0.925	0.002	0.555	1.528	8.032	

## GARNET COMPOSITIONS IN GARNETIFEROUS EPIDOTITE (Sample 80-55)

1 (wt %)	2.70	20.70	38.30	11.45	0.03	10.07	18.12	101.36	
(at. prop.)	0.313	1.910	3.000	0.958	--	0.667	1.186	8.033	
2 (wt %)	2.62	21.32	37.67	11.33	0.02	9.90	18.38	101.23	
(at. prop.)	0.304	1.972	2.958	0.951	--	0.656	1.205	8.046	
3 (wt %)	2.71	21.26	37.20	11.52	0.02	10.28	18.30	101.29	
(at. prop.)	0.316	1.971	2.928	0.970	--	0.684	1.204	8.072	
4 (wt %)	2.66	21.01	37.46	11.89	0.05	9.55	17.84	100.45	
(at. prop.)	0.311	1.957	2.958	1.006	0.002	0.637	1.178	8.052	
5 (wt %)	2.45	20.56	37.76	11.60	0.03	9.96	18.58	100.93	
(at. prop.)	0.287	1.911	2.980	0.979	--	0.665	1.225	8.047	
6 (wt %)	2.48	21.39	37.21	11.23	0.03	11.00	18.16	101.49	
(at. prop.)	0.288	1.983	2.927	0.946	--	0.731	1.193	8.069	

## GARNET COMPOSITIONS IN AMPHIBOLITE INTERBANDS OF THE PORT AUX BASQUES COMPLEX

## (Sample 80-52)

1 (wt %)	3.88	21.73	38.04	5.90	0.05	6.41	25.93	101.95	
(at. prop.)	0.498	1.996	2.964	0.492	0.002	0.423	1.690	8.017	
2 (wt %)	4.03	22.13	37.36	6.07	0.03	6.36	26.60	102.58	
(at. prop.)	0.466	2.028	2.908	0.504	--	0.418	1.731	8.056	
3 (wt %)	3.78	21.94	37.84	5.50	0.07	8.35	24.49	101.99	Core of large garnet.
(at. prop.)	0.437	2.016	2.949	0.459	0.002	0.551	1.597	8.012	
4 (wt %)	4.02	21.82	38.10	5.68	0.06	7.84	25.18	102.70	Towards rim in garnet in analysis 3.
(at. prop.)	0.464	1.993	2.954	0.471	0.002	0.514	1.631	8.031	

## (Sample 80-57)

1 (wt %)	4.66	21.86	37.04	4.74	0.01	0.56	32.49	101.35	Garnet in contact with biotite - all following are in contact with hornblende.
(at. prop.)	0.545	2.026	2.916	0.399	--	0.037	2.140	8.063	
2 (wt %)	3.68	21.84	37.51	4.72	0.06	1.77	32.02	101.59	Core of large garnet.
(at. prop.)	0.429	2.024	2.950	0.397	0.002	0.118	2.105	8.024	
3 (wt %)	4.18	22.09	38.10	5.05	0.04	1.34	31.51	102.21	Rim of garnet in analysis 2.
(at. prop.)	0.483	2.023	2.961	0.419	--	0.086	2.048	8.022	
4 (wt %)	4.07	22.01	38.02	4.83	0.04	2.04	31.51	102.50	Core of large garnet.
(at. prop.)	0.470	2.017	2.954	0.401	0.002	0.132	2.048	8.024	
5 (wt %)	4.38	22.26	37.34	4.96	--	1.21	32.16	102.34	Rim of garnet in analysis 4.
(at. prop.)	0.508	2.047	2.913	0.415	--	0.078	2.098	8.059	
6 (wt %)	4.24	21.86	37.78	5.32	0.07	1.18	30.86	101.31	
(at. prop.)	0.494	2.016	2.958	0.446	0.002	0.078	2.020	8.014	

TABLE VII (cont.)

ANALYSIS	Fe	Al	Si	Ca	Ti	Mn	Pb	Total	COMMENTS
7 (wt %)	3.72	21.94	37.37	5.15	0.13	2.33	30.57	101.21	
(at. prop.)	0.436	2.034	2.939	0.434	0.007	0.154	2.011	8.015	
8 (wt %)	3.99	22.28	35.54	5.08	0.04	1.42	31.31	99.65	
(at. prop.)	0.476	2.10	2.855	0.436	0.002	0.094	2.103	8.075	
9 (wt %)	4.43	21.78	37.89	5.04	0.05	0.62	31.91	101.70	
(at. prop.)	0.515	2.002	2.958	0.421	0.002	0.039	2.083	8.020	

## GARNET COMPOSITIONS IN LEUCOCRATIC (GNEISS) BANDS OF THE PORT AUX BASQUES COMPLEX

## (Sample 79-170)

1 (wt %)	3.47	22.03	36.36	2.45	--	4.96	32.08	101.35	Rim of large garnet.
(at. prop.)	0.411	2.068	2.895	0.208	--	0.334	2.136	8.051	
2 (wt %)	4.02	21.54	37.66	2.71	--	4.31	32.51	102.74	Core of garnet in analysis 1.
(at. prop.)	0.468	1.987	2.947	0.227	--	0.285	2.127	8.042	
3 (wt %)	3.20	21.92	37.49	2.35	--	5.01	32.47	102.44	Opposite rim of garnet in analysis 1.
(at. prop.)	0.374	2.033	2.950	0.196	--	0.333	2.137	8.022	
4 (wt %)	3.29	21.93	37.32	2.17	0.02	4.82	32.96	102.51	
(at. prop.)	0.386	2.034	2.939	0.182	--	0.321	2.170	8.032	

## (Sample 80-47G)

1 (wt %)	1.48	21.18	36.82	1.96	--	4.26	34.89	100.59	Near core of large garnet.
(at. prop.)	0.178	2.020	2.980	0.168	--	0.292	2.362	8.001	
2 (wt %)	3.03	21.91	37.46	1.27	0.02	1.92	37.12	102.72	Towards rim of garnet in analysis 1.
(at. prop.)	0.356	2.035	2.951	0.106	--	0.127	2.445	8.020	
3 (wt %)	3.85	21.39	37.08	0.52	--	0.42	38.50	101.77	Rim of garnet in analysis 1.
(at. prop.)	0.455	2.004	2.947	0.042	--	0.028	2.367	8.036	

## (Sample 79-150)

1 (wt %)	1.50	20.93	37.05	5.21	0.21	13.86	22.68	101.45	
(at. prop.)	0.178	1.973	2.964	0.446	0.012	0.939	1.518	8.031	
2 (wt %)	1.66	21.38	36.66	5.15	0.09	12.74	24.05	101.74	
(at. prop.)	0.197	2.012	2.929	0.440	0.004	0.860	1.606	8.048	
3 (wt %)	1.80	21.31	36.78	5.05	0.07	12.49	23.25	100.75	
(at. prop.)	0.214	2.016	2.950	0.433	0.002	0.848	1.559	8.021	
4 (wt %)	1.85	20.82	36.68	4.56	0.08	11.75	24.52	100.27	
(at. prop.)	0.220	1.983	2.965	0.394	0.004	0.804	1.658	8.029	
5 (wt %)	1.77	21.32	37.14	4.05	0.02	12.38	24.22	100.88	
(at. prop.)	0.209	2.013	2.975	0.348	--	0.839	1.623	8.007	

## (Sample 80-200)

1 (wt %)	0.33	22.03	36.73	7.80	0.07	9.44	25.45	101.85	
(at. prop.)	0.037	2.067	2.922	0.663	0.002	0.635	1.693	8.020	
2 (wt %)	0.29	21.58	37.50	6.82	0.08	13.70	22.86	102.83	
(at. prop.)	0.032	2.010	2.967	0.576	0.004	0.917	1.511	8.018	
3 (wt %)	0.21	20.81	37.05	7.31	0.14	14.90	20.29	100.70	
(at. prop.)	0.023	1.979	2.987	0.629	0.007	1.018	1.368	8.010	
4 (wt %)	0.33	21.27	37.07	7.09	0.07	10.18	25.85	102.76	
(at. prop.)	0.037	1.989	2.942	0.678	0.002	0.682	1.714	8.044	

## GARNET COMPOSITIONS IN RETROGRESSION PORT AUX BASQUES COMPLEX ROCKS

## (Sample 80-131)

1 (wt %)	0.56	21.82	36.65	4.90	0.08	13.21	25.36	102.57	Core of large garnet.
(at. prop.)	0.065	2.050	2.922	0.417	0.004	0.891	1.689	8.039	
2 (wt %)	0.62	21.47	36.92	4.889	0.13	12.48	25.73	102.24	Towards rim of garnet in analysis 1.
(at. prop.)	0.072	2.020	2.948	0.417	0.007	0.843	1.717	8.024	
3 (wt %)	0.88	21.77	36.23	5.32	0.08	5.92	31.91	102.10	Rim of garnet in analysis 1.
(at. prop.)	0.103	2.056	2.903	0.456	0.004	0.400	2.138	8.060	
4 (wt %)	1.09	21.64	36.93	6.14	0.07	2.51	34.46	102.83	Rim of large garnet.
(at. prop.)	0.128	2.021	2.926	0.521	0.002	0.167	2.284	8.048	

TABLE VII (cont.)

ANALYSIS	Mg	Al	Si	Ca	Ti	Mn	Fe	Total	COMMENTS
5 (wt %)	0.67	20.77	37.00	4.91	0.09	12.27	26.18	101.89	Towards core of garnet in analysis 4.
(at. prop.)	0.078	1.964	2.970	0.421	0.004	0.833	1.757	8.029	
6 (wt %)	0.59	21.17	36.47	4.32	0.05	16.52	22.54	101.67	Closer to core of garnet in analysis 4.
(at. prop.)	0.068	2.010	2.940	0.371	0.002	1.7125	1.519	8.036	
7 (wt %)	0.39	21.41	36.99	4.65	0.07	15.83	22.22	101.47	Fast core towards outer rim of garnet of analysis 4.
(at. prop.)	0.044	2.027	2.963	0.398	0.002	1.075	1.492	8.002	

## (Sample 79-71)

1 (wt %)	2.46	21.55	36.77	3.28	0.07	13.10	25.15	102.39	
(at. prop.)	0.291	2.015	2.919	0.277	0.002	0.880	1.668	8.052	
2 (wt %)	2.24	21.59	36.24	3.35	0.05	14.55	23.23	101.25	
(at. prop.)	0.266	2.041	2.907	0.287	0.002	0.988	1.558	8.049	
3 (wt %)	2.40	21.77	37.52	3.13	0.02	12.14	24.63	101.61	
(at. prop.)	0.281	2.033	2.975	0.265	--	0.814	1.630	7.998	
4 (wt %)	2.27	21.26	38.75	3.52	0.08	12.91	24.30	101.90	
(at. prop.)	0.271	2.008	2.947	0.301	0.004	0.875	1.629	8.036	
5 (wt %)	2.26	21.34	35.45	3.80	0.05	13.46	23.57	101.03	
(at. prop.)	0.268	2.018	2.931	0.325	0.002	0.913	1.580	8.036	

## (Sample 80-105)

1 (wt %)	1.41	21.68	36.14	0.77	0.05	8.74	33.34	102.13	
(at. prop.)	0.167	2.057	2.913	0.063	0.002	0.596	2.246	8.045	
2 (wt %)	1.30	21.19	36.71	0.88	0.08	9.82	32.73	102.72	
(at. prop.)	0.153	2.002	2.943	0.750	0.004	0.666	2.193	8.036	
3 (wt %)	1.27	21.06	36.27	0.64	--	9.19	33.70	102.14	
(at. prop.)	0.152	2.008	2.934	0.054	--	0.629	2.279	8.056	

## GARNET COMPOSITIONS IN THE WINDSOR POINT GROUP

## (Sample 80-38)

1 (wt %)	0.29	20.75	36.88	4.55	0.24	24.50	12.91	100.11	
(at. prop.)	0.033	1.985	2.996	0.396	0.014	1.685	0.875	7.982	
2 (wt %)	0.39	22.00	37.05	3.67	0.08	23.24	15.64	102.08	
(at. prop.)	0.046	2.066	2.955	0.311	0.004	1.567	1.041	7.991	
3 (wt %)	0.29	20.97	37.11	5.09	0.26	23.46	12.79	99.98	
(at. prop.)	0.033	2.000	3.005	0.441	0.014	1.608	0.865	7.968	
4 (wt %)	0.31	21.42	37.22	4.26	0.14	24.64	12.50	100.49	
(at. prop.)	0.035	2.034	2.999	0.366	0.007	1.681	0.842	7.963	
5 (wt %)	0.18	21.42	36.11	5.03	0.30	24.72	11.16	98.92	
(at. prop.)	0.021	2.067	2.952	0.439	0.017	1.714	0.762	7.977	

## (Sample 79-106)

1 (wt %)	1.59	21.24	37.04	3.24	0.27	25.67	11.59	100.64	
(at. prop.)	0.188	2.010	2.975	0.278	0.016	1.747	0.778	7.992	
2 (wt %)	1.66	21.42	37.89	2.57	0.11	23.99	13.47	101.12	
(at. prop.)	0.196	2.009	3.017	0.219	0.004	1.617	0.897	7.959	
3 (wt %)	1.19	21.45	35.81	5.50	0.30	24.20	10.75	99.21	
(at. prop.)	0.143	2.059	2.918	0.480	0.017	1.669	0.731	8.020	
4 (wt %)	1.49	21.48	37.40	4.43	0.16	23.75	12.14	100.86	
(at. prop.)	0.175	2.020	2.985	0.377	0.009	1.605	0.811	7.981	
5 (wt %)	0.88	20.54	36.25	7.17	0.44	24.76	8.97	99.01	
(at. prop.)	0.105	1.976	2.957	0.625	0.026	1.709	0.610	8.008	

## (Sample 79-116)

1 (wt %)	0.57	21.39	37.68	10.33	0.13	15.00	16.57	101.68	
(at. prop.)	0.067	1.990	2.974	0.873	0.007	1.003	10.93	8.007	
2 (wt %)	0.48	22.52	37.91	12.40	0.16	12.64	15.41	101.52	
(at. prop.)	0.055	2.075	2.965	1.037	0.009	0.835	1.007	7.985	
3 (wt %)	0.48	21.88	38.28	9.81	0.20	16.04	16.01	102.70	
(at. prop.)	0.055	2.012	2.985	0.819	0.011	1.060	1.043	7.985	

ANALYSIS	Mg	Al	Si	Ca	Ti	Mn	Fe	Total	COMMENTS
4 (wt %)	0.57	22.49	35.99	10.09	0.20	14.61	16.33	100.28	
(at. prop.)	0.068	2.122	2.881	0.865	0.012	0.989	1.093	8.029	
5 (wt %)	0.54	21.26	37.23	10.58	0.13	13.68	17.06	100.48	
(at. prop.)	0.063	2.001	2.972	0.952	0.007	0.923	1.139	8.029	
(Sample 79-133)									
1 (wt %)	0.71	21.16	36.89	7.39	0.07	14.34	20.03	100.59	
(at. prop.)	0.084	2.005	2.965	0.634	0.002	0.977	1.344	8.013	
2 (wt %)	0.37	20.52	37.45	7.96	0.07	15.41	20.71	102.49	
(at. prop.)	0.042	1.925	2.981	0.284	0.002	1.037	1.378	8.042	
3 (wt %)	0.84	20.60	36.47	2.85	0.21	29.36	20.27	100.60	
(at. prop.)	0.100	1.975	2.969	0.284	0.012	1.333	1.378	8.014	
4 (wt %)	1.20	21.09	37.00	4.73	0.09	15.74	21.32	101.17	
(at. prop.)	0.141	1.994	2.969	0.405	0.004	1.069	1.429	8.012	
(Sample 80-106)									
1 (wt %)	0.57	19.97	35.26	1.63	2.55	15.13	27.70	102.81	
(at. prop.)	0.066	1.904	2.852	0.140	0.154	1.035	1.874	8.025	
2 (wt %)	0.69	21.33	35.82	2.43	0.16	13.23	28.41	101.78	
(at. prop.)	0.081	2.040	2.907	0.189	0.009	0.910	1.927	8.057	
3 (wt %)	0.72	20.88	36.18	1.32	0.18	12.04	29.50	100.81	
(at. prop.)	0.086	2.009	2.956	0.115	0.009	0.832	2.014	8.020	

TABLE VII (cont.)

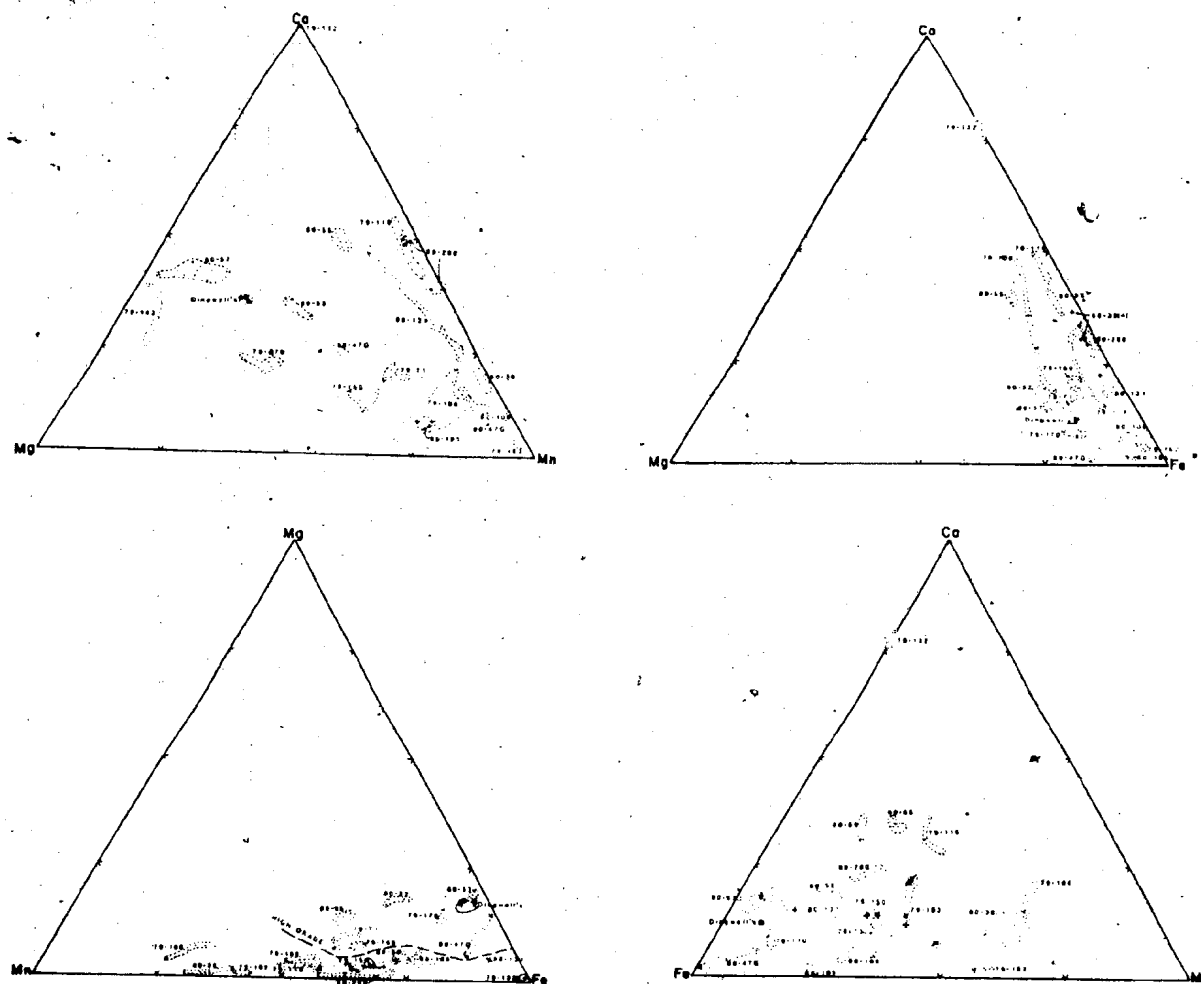


Figure 14 Garnet composition diagram. Individual garnet compositions and sample ranges are indicated, as are the compositions of the Port aux Basques Complex garnets analysed by Dingwell (1980). Higher grade Port aux Basques Complex are separated from Windsor Point Group garnets on the Mn-Mg-Fe diagram.

79-132 (average composition  $\text{Py} < 1\text{Gr}78\text{Sp} < 1\text{Al}22$ ) are the most calcic and they come from the diopside/garnet skarn in the gabbros of unit 6. As would be expected, due to their metasomatic origin (Miyashiro, 1973), these garnets are very grossularitic (or Ca-rich), with very little Mn and Mg. The five analyses are from different garnets in direct contact with diopside. Seven microprobe analyses of coexisting diopside are given in Table VIII.

Geothermometers have been developed using the partition coefficients of Fe, Mg, Ca and Mn between coexisting garnet and clinopyroxene (Saxena, 1979; Raheim and Green, 1974). By setting up a matrix of the five garnet and seven clinopyroxene analyses, the maximum series of Fe/Mg distribution concentrations between garnet and clinopyroxene in sample 79-132 could be determined. These values were then entered into the two different geothermometer equations to yield the maximum possible range of formation temperatures. Saxena's (1979) relatively pressure-independant geothermometer yields average temperatures for sample 79-132 at 500 bars, 1, 3 and 6 kb of 292, 293, 298 and 305° C respectively. Raheim and Green's (1974) geothermometer is pressure-dependant, but if the pressure is assumed to have been less than 3.4 kb (ie. andalusite-stable), then the permissible temperatures range from 242-307° C ~~with~~ with a mean of 260° C (ie. KD's for their equations are 141, 77 and 114

TABLE VIII CLINOPYROXENE COMPOSITIONS IN SAMPLE 79-132

Analysis	Na	Mg	Al	Si	Ca	Mn	Fe	Total
1 (wt %)	0.12	8.50	0.43	52.39	22.05	0.38	15.08	98.95
(At. prop.)*	0.009	0.489	0.019	2.027	0.914	0.012	0.487	3.957
2 (wt %)	0.20	8.20	0.30	51.91	23.02	0.39	15.25	99.28
(At. prop.)	0.015	0.474	0.013	2.015	0.957	0.012	0.494	3.979
3 (wt %)	0.13	8.60	0.42	51.01	22.89	0.19	14.85	98.09
(At. prop.)	0.009	0.502	0.018	2.001	0.963	0.005	0.487	3.986
4 (wt %)	0.29	7.11	0.70	51.06	22.59	0.28	16.69	98.72
(At. prop.)	0.021	0.415	0.032	2.005	0.951	0.009	0.547	3.980
5 (wt %)	0.22	8.45	0.35	51.40	23.23	0.38	14.35	98.38
(At. prop.)	0.016	0.492	0.015	2.008	0.972	0.011	0.469	3.982
6 (wt %)	0.14	8.11	0.43	51.04	23.28	0.32	15.15	98.47
(At. prop.)	0.010	0.472	0.020	2.000	0.977	0.100	0.495	3.984
7 (wt %)	0.20	8.33	0.30	51.82	22.57	0.32	14.89	98.42
(At. prop.)	0.014	0.484	0.014	2.022	0.944	0.100	0.485	3.974

\*At. prop. = atomic proportion



respectively). Even if the pressure is assumed to be 10 kb, the determined temperatures are always  $< 320^{\circ}$  C.

Though there are problems with extending these geothermometers to such low pressures (they were designed primarily for granulite facies rocks), they indicate that the metasomatism which produced the garnet/diopside pockets was of a low temperature (ie.  $< 300^{\circ}$  C).

Garnets in sample 80-59 (average  $\text{Py}_{4}\text{Gr}_{32}\text{Sp}_{17}\text{Al}_{47}$ ) are composed of almost equal amounts of almandine and grossular with minor spessartine. This rock is the pyrrhotite-garnet-amphibole rock in Bailey's Brook. The high Ca content of the garnets distinguish them from most others in the Port aux Basques Complex. In the case of sample 80-59, lack of available Mg may have precluded the uptake of Ca.

Similarly in sample 80-55 (average  $\text{Py}_{10}\text{Gr}_{31}\text{Sp}_{22}\text{Al}_{37}$ ), a sample of garnetiferous-epidotite, the high Ca component distinguishes these garnets. The anomalous amount of Ca in these garnets probably reflects the original Ca-rich nature of the protolith (ie. in view of the abundant epidote).

Samples 80-52 and 80-57 are of amphibolitic interbands within the Port aux Basques Complex. Garnets in 80-52 (average  $\text{Py}_{15}\text{Gr}_{16}\text{Sp}_{15}\text{Al}_{54}$ ) and 80-57 (average  $\text{Py}_{16}\text{Gr}_{13}\text{Sp}_{4}\text{Al}_{67}$ ), though almanditic, are amongst the most Mg-rich (ie. pyrope) of all samples. Element zonation of increasing Mg, Fe and Ca, and decreasing Mn from core to

rim, is well-developed in these samples. In some garnets, Mn almost disappears as a component towards the rim. This type of zonation is a normal feature of 'prograde' metamorphic rocks (Atherton, 1968; Zen, 1981), and apparently reflects the increase in metamorphic grade (ie. P and T) with garnet growth (see also Black, 1973), ie., the uptake of Mn occurs at lower grades (Hsu, 1968), but with increasing grade the partition coefficient of Mn between a growing garnet and its host rock decreases (Atherton, 1968).

In sample 80-57 there is a biotite layer that also contains garnets. These garnets generally have the same compositions as those in the hornblende-rich layers, except there is slightly more Mg, with correspondingly less Ca, Mn and Fe. Garnets in sample 80-57 also have the lowest Mn component of all examined (probably indicative of the mafic, Mn-poor, protolith of the amphibolite).

Garnets in the gneiss samples from the Port aux Basques Complex (samples 79-150, 79-170, 80-47G and 80-200) are typically almandines, but they also show relative differences in composition with variations in metamorphic grade. Sample 79-170 (average  $\text{Py}_{13}\text{Gr}_{7}\text{Spl}_{10}\text{Al}_{70}$ ) is from the garnet zone of Brown (1975) at a distance of 8 km east from Cape Ray (ie. outside the map area). Garnets in this sample have higher Mg (pyrope) contents than the garnets of other gneiss samples. Since the uptake of Mg is enhanced at

higher pressures and temperatures (eg. Hsu, 1968, Miyashiro, 1973), this correlates with the higher metamorphic grade exhibited by the gneiss in the sample area. Dingwell's (1980) analyses of garnet (see Figure 14) in the sillimanite-garnet zone of the Port aux Basques Complex similarly exhibits an enriched Mg component.

Sample 80-47G is from the staurolite zone of the gneiss. Garnets in this sample (average  $\text{Py}_{11}\text{Gr}_{3}\text{Sp}_{5}\text{Al}_{81}$ ) have higher Fe than those in the other gneiss samples (79-150, average  $\text{Py}_{7}\text{Gr}_{13}\text{Sp}_{28}\text{Al}_{52}$ , and 80-200, average  $\text{Py}_{1}\text{Gr}_{21}\text{Sp}_{27}\text{Al}_{51}$ ) that are closer to the Windsor Point Group contact. These latter samples have a strong Mn (or low temperature) component. Thus garnets in the gneiss show a progressive decrease in Mn and increase in Mg from northwest to southeast (ie. a reflection of the metamorphic gradients).

Garnets in sample 80-47G exhibit normal zoning. Dingwell's (1980) garnets had no zonation developed. Garnets in sample 79-170, on the other hand, exhibit reverse zoning in that Mg decreases and Mn increases from core to rim. This may reflect the waning of metamorphism as the garnets grew (ie. the more Mg-rich cores started to grow at the peak of metamorphism and with waning P-T conditions Mn-rich garnet became stable - this would be indicative of the high grade nature of the metamorphism, in that P-T conditions, even though dropping, would still

provide the activation energy for the deposition of an Mn phase).

Three garnetiferous gneiss samples (79-71, 80-105 and 80-131) were collected near the Windsor Point Group contact. 80-131 is a phyllonite from along the 'fault/contact'. Garnets (average  $\text{Py}_{3}\text{Gr}_{14}\text{Sp}_{23}\text{Al}_{60}$ ) in this sample exhibit extreme variations in compositions from core to rim. The cores have high Mn concentrations (almost equal to Fe) which decrease rapidly and significantly towards the rims. Garnets in 79-71 (av.  $\text{Py}_{9}\text{Gr}_{9}\text{Sp}_{29}\text{Al}_{53}$ ) and 80-105 (av.  $\text{Py}_{5}\text{Gr}_{2}\text{Sp}_{20}\text{Al}_{73}$ ) are relatively enriched in Mn. All of these garnets are almandines of a lower grade (indicated by the spessartine contents) than the other gneisses. Except for 79-71, there is also a linear inverse relationship between Ca and Mn. 80-105 is an andalusite-bearing contact metamorphosed gneiss, but its garnet compositions do not appear to have been affected by the metasomatism.

The five remaining garnet-bearing samples (79-106, 79-116, 79-133, 80-38 and 80-106) are from the Windsor Point Group. One of them (80-38) is a sample of graphite schist. The garnets (av.  $\text{Py}_{1}\text{Gr}_{13}\text{Sp}_{56}\text{Al}_{30}$ ) in this sample are spessartines with a lesser almandine component (*ie.* Mn content is usually  $> 2\times$  that of Fe). These garnets are the lowest grade found in this study (they also have the lowest relative pyrope content). 79-106 contains similar

spessartines (av. Py5Gr13Sp56Al26). The garnets in 79-116 (av. Py2Gr30Sp32Al36), 79-133 (av. Py3Gr16Sp36Al45) and 80-106 (av. Py3Gr4Sp30Al63) are almandines but they have elevated Mn contents.

When all the garnet compositions are viewed in the Mn-Mg-Fe diagram (Figure 14) the Windsor Point Group spessartines seem to form a linear, low Mg trend that grades into those Port aux Basques gneiss samples that occur near their common contact. The other gneiss and amphibolites samples are readily distinguishable by their elevated Mg contents.

The most important conclusions to be drawn from the garnet compositions are :

- 1) regional prograde metamorphism increases to the southeast, paralleled by garnet compositions grading from spessartine to almandine
- 2) the garnet compositions of the Windsor Point Group and the Port aux Basques Complex are transitional
- 3) delineation of the contact between these two units is further complicated.

#### 4.3 Isograds

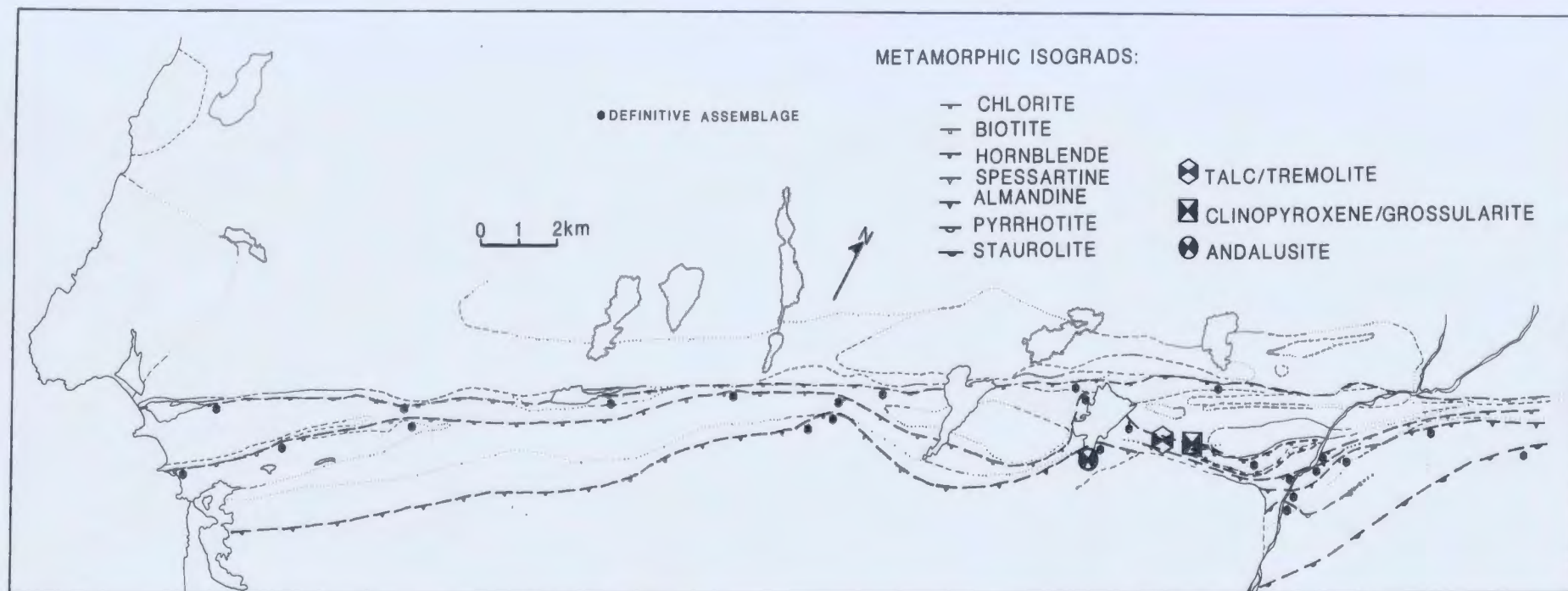
Based on the foregoing analyses of metamorphic mineral

assemblages and compositions, it is possible to derive mineral reaction boundaries (or isograds) through the map area (Figure 15). (The isograds are defined for the northeastern edge of the map area, where sampling and study were concentrated, due to the presence of the gold showings, and are tentatively extended through the map area). The tonalitic Cape Ray Granite terrain along the northwestern edge of the map area is greenschist facies and contains metamorphic minerals distinctive of that facies. This zone is bounded to the southeast by the Little Barachois Formation which effectively defines a metamorphic zone in which the single most important diagnostic mineral is sericite (+ carbonate).

Chlorite appears at the southern boundary of this formation after which the stable metamorphic assemblages are sericite-chlorite-carbonate (+ epidote, + actinolite). The chlorite was produced by alteration of primary ferromagnesian minerals as are the other metamorphic/alteration minerals.

Rather than representing an isograd, talc-tremolite assemblages are shown as a point on Figure 15, because they occur in a single outcrop. This assemblage is consistent with the greenschist facies designation of the enclosing schist member of the Windsor Point Group. Talc probably formed as:

Figure 15. Metamorphic mineral isograd map. Each isograd is based on the presence of definite equilibrium assemblages. The solitary locations of andalusite, clinopyroxene-grossularite and talc/tremolite intergrowths are also indicated. The outlined geology and contacts are the same as in Figure 1 and Map 1. The 'teeth' in each isograd point towards the higher grade side.





3 dolomite + 4 quartz + H<sub>2</sub>O = 3 talc + 6 CO<sub>2</sub> + 2H<sub>2</sub>O,  
 with higher temperature tremolite would form as:  
 5 talc + 6 calcite + 4 quartz = 3 tremolite + 6 CO<sub>2</sub> + 2 H<sub>2</sub>O.  
 after Miyashiro (1973).

The next significant reaction takes place when biotite appears. As illustrated in Figure 15, this isograd is poorly defined, and there are isolated points where biotite occurs within the dominant chlorite zone.

Formation of biotite in low grade meta-pelitic rocks, according to Winkler (1979), occurs as:

phengite (*ie.* sericite) + chlorite =

biotite + Al-rich chlorite + quartz

or,

phengite + chlorite + microcline =

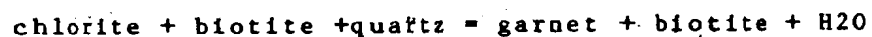
biotite + quartz + phengite (with less Mg, Fe)

in meta-greywackes. Both reactions are applicable to the appearance of biotite in this area. Sericite is not as prevalent in biotite-bearing assemblages, and microcline is common as clastic volcanic grains in the meta-tuffs.

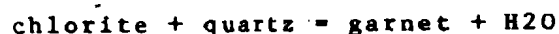
A hornblende isograd can be drawn around gabbro south of the Windowglass Hill Granite (*ie.* unit 6). This isograd reflects differences in primary composition (rather than higher grade) between the gabbros and surrounding metatuffs (*ie.* metabasic *vs.* metapelitic). The common intergrowths with chlorite, indicate these amphibolites are low-grade (Winkler, 1979) rather than retrograde.

The next regional isograd is defined by the appearance of spessartine garnet in graphitic meta-sediments of the Windsor Point Group. This isograd is defineable only in the northeastern edge of the map area (Figure 15). This garnet isograd is quickly followed by the appearance of almandine (they grade into each other, but there is a definite zone of Mn > Fe garnets). Hsu (1968) showed that Mn garnets form at temperatures 100-200° C lower than Fe garnets, and that Mn garnets form from the reaction of quartz, Mn-bearing chlorite and fluid. Atherton (1968) found that rare, high-Mn garnets occur in rocks just prior to the almandine isograd (but he couldn't define a spessartine isograd as herein). Loomis and Nimick (1982) thought that "tiny grains" of spessartine probably occur (but have usually been overlooked), in front of almandine isograds in regional metamorphic sequences, as a reaction product of Mn-chlorite.

Winkler (1979) suggested that almandine forms from some combination of the reactions:



either of which are directly applicable to rocks in this study. Miyashiro (1973) thought almandine formed simply as:



In all three reactions chlorite is involved as a

reactant, just as it would be in the formation of spessartine. The difference in garnet composition reflects the lowering of the partition coefficients between chlorite and garnet (as suggested by Atherton, 1968) and not differences in the chlorite compositions (ie. the chlorites in all cases probably have the same Mn contents).

The almandine isograd is not defined to the southwest of the map area, it is inferred, as the sampling was not as extensive and no garnet-bearing samples (except 79-170 from outside the map area) were found. The almandine isograd is defined for those garnets that have an Fe content of  $> 55$  wt.%. Winkler, (1979) thinks that an almandine isograd should only be defined with garnets containing  $\geq 90\%$  Fe, however if this was done with the garnets in this study, none would define such an isograd.

The SE-most regional isograd is defined by staurolite, whose reaction equation has been previously described. This isograd is commonly taken to indicate the onset of amphibolite facies metamorphism (eg. Ermanovics and Froese, 1978). According to Brown's (1975) isograds, extrapolated inland from the coast (Figure 13), this staurolite isograd lies in his garnet mineral zone, which changes into the garnet-staurolite-kyanite zone ~ 2 km to the southeast. These zones (Brown, 1975) pass out into kyanite-garnet and sillimanite-garnet zones. The mapping completed for this project did not extend far enough to the

southeast to check these isograds, but if the prograde assemblages continue to increase in grade towards the southeast, then transition into sillimanite-stable assemblages would be expected (cf. Guidotti, 1974).

A pyrrhotite isograd (ie. marking the replacement of pyrite by pyrrhotite) can be delineated in the Port aux Basques Complex in the extreme northeast of this map area (Figure 15). Disseminated pyrite is common in gneiss samples beyond this isograd, but massive sulphide layers in amphibolites are composed solely of pyrrhotite. This isograd occurs well within the biotite zone and is unlike that of Carpenter (1974) which occurred in the chlorite zone prior to the appearance of biotite (almost in contact with the biotite isograd). The appearance of pyrrhotite is complex and is not entirely dependant on P-T conditions but also on the local oxidation state. Ferry (1981) states that the pyrite-pyrrhotite transition is produced by the introduction and concomittant reaction of an externally-derived fluid containing low total sulphur contents with the host rock. There is abundant evidence for fluid mobilization in these schists.

The only remaining assemblages on the metamorphic map are the andalusites in the Port aux Basques Gneiss and the garnet-clinopyroxene intergrowths in the gabbro induced by contact metamorphism of the Isle aux Morts Brook Granite.

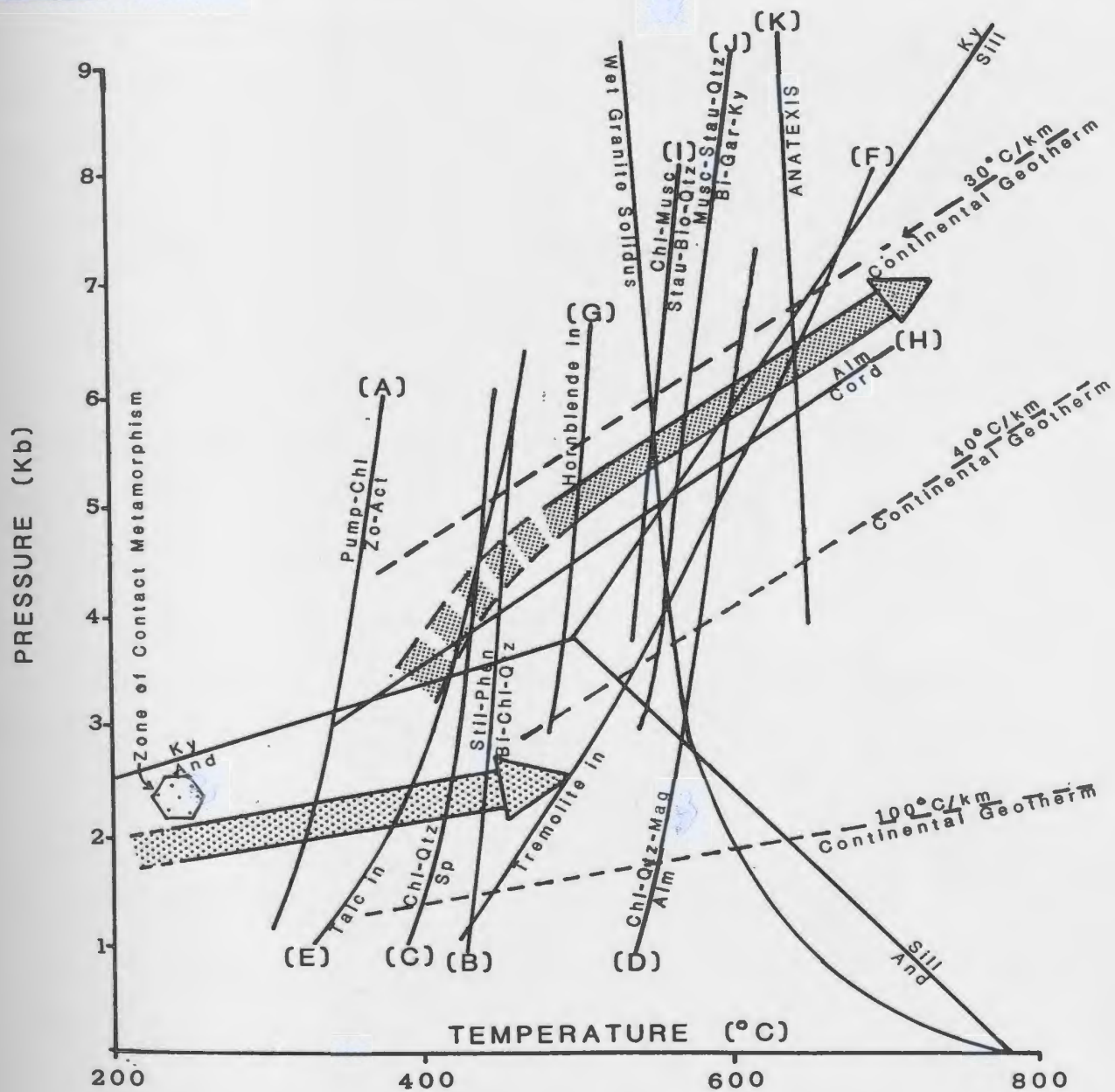
#### 4.4 P-T Conditions and Path of Metamorphism

##### 4.4.1 The Windsor Point Group

The metamorphic mineral assemblages in this and Brown's (1975) map areas grade into each other in a classic Barrovian-type sequence (cf. Miyashiro, 1973; Winkler, 1979; Turner, 1980) and the mineral zonation implies increasing P-T conditions towards the southeast. The proposed paths of progressive regional metamorphism in the Windsor Point Group and Port aux Basques Complex are illustrated on Figure 16 along with the relevant experimentally-derived P-T curves for mineral equilibria.

Determination of the pressure conditions during the metamorphism is hindered by the lack of  $Al_2SiO_5$  polymorphs in the map area. Andalusite occurs in the Port aux Basques Gneiss, but is developed as a result of contact metamorphism by the Isle aux Morts Brook Granite. Its presence indicates that when the granite intruded the gneiss, the lithostatic pressure in the gneiss was less than 3.5 kb (after Holdaway's (1971) triple point determination). The granite is post-tectonic but was intruded relatively quickly after the deposition of the Late Devonian Windsor Point Group (as indicated by Rb/Sr age dates). Between deposition and intrusion of the Isle aux Morts Brook Granite, this group was regionally

Figure 16 Paths of progressive metamorphic mineral development in the Port aux Basques Complex and the Windsor Point Group. The lower temperature end of the path in the Port aux Basques Complex is broken to indicate the realm of retrogression superimposed on this unit near its contact with the Windsor point Group. Full explanations of each curve are given in the text. The curves are: (a) pumpellyite + chlorite = zoisite + actinolite (Nitsch, 1971); (b) stilpnomelane + phengite = biotite + chlorite + quartz + H<sub>2</sub>O (Nitsch, 1970); (c) Mn-chlorite + quartz + H<sub>2</sub>O = spessartine (Hsu, 1968); (d) Fe-chlorite + quartz + magnetite + H<sub>2</sub>O = almandine (Hsu, 1968); (e) dolomite + quartz + H<sub>2</sub>O = talc + calcite + CO<sub>2</sub>;  $x_{CO_2}^{gas}$  is internally buffered (Turner, 1980); (f) talc + calcite + quartz = tremolite + H<sub>2</sub>O;  $x_{CO_2}^{gas}$  is internally buffered (Turner, 1980); (g) hornblende + almandine in (Winkler, 1979); (h) almandine = cordierite (Hirschburg and Winkler, 1968); (i) chlorite + muscovite = staurolite + biotite + quartz (Hoschek, 1969); (j) muscovite + staurolite + quartz = biotite + Al<sub>2</sub>O<sub>3</sub> + H<sub>2</sub>O (Price and MacKasey, 1978); (k) anatexis curve of Winkler (1979).



# PATH OF METAMORPHISM:



IN THE WINDSOR POINT GROUP



IN THE PORT AUX BASQUES COMPLEX

metamorphosed along with the gneiss unit. Since there is no evidence for a large degree of post-metamorphic uplift in the area, the pressure conditions at the time of metamorphism were probably close to that of the contact metamorphism (ie.  $< 3.5$  kb).

The lower end of P-T conditions for the Windsor Point Group are difficult to define in this area due to the lack of assemblages that are specifically pre-greenschist (ie. they don't persist to higher grade, eg. zeolites). The first relevant mineral stability (curve a on Figure 16) encountered in the metamorphic path is:

pumpellyite + chlorite =

zoisite + actinolite (after Nitsch, 1971)

This reaction has a rather limited temperature range of 300-350° C. The presence of epidote and actinolite in more mafic schists of the Windsor Point Group indicates metamorphism in most of the chlorite zone occurred at temperatures  $> 350^{\circ}$  C.

The appearance of biotite constitutes the next higher grade stability field. As discussed by Winkler (1979), the reactions leading to the formation of biotite are only poorly understood but the reaction:

stilpnomelane + phengite = biotite + chlorite + quartz + H<sub>2</sub>O

(or stilpnomelane and muscovite out - biotite and chlorite in)

(after Nitsch, 1970, as reproduced in Winkler, 1979) is commonly taken as the lower stability limit for biotite.

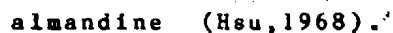
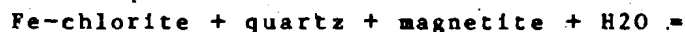


The P-T curve (curve b, Figure 16) has a restricted temperature range of 400-450° C, thus the metamorphic temperatures in the biotite zone were at least > 400° C.

The growth of spessartine is governed by a reaction similar to:



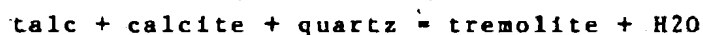
The reaction curve (curve c, Figure 16) for this reaction has a rather limited temperature range around 400° C. Almandine forms just after the formation of spessartine probably as:



The reaction curve (curve d on Figure 16) governing the appearance of almandine has a temperature range of 500-550° C. As described in the previous section, the garnets in the Windsor Point Group are not pure end members but are part of a spessartine-almandine solid solution (ie. appreciable quantities of each end member occur in all garnets with varying ratios). Similarly the reactant chlorite would be some sort of solid solution between Fe and Mn end members. Therefore the first appearance of garnet (eg. sample 80-38;  $\text{Py}1\text{Gr}13\text{Sp}56\text{Al}30$ ) occurs above 400° C and the almandine isograd occurs at a temperature somewhat less than 500° C.

Talc-tremolite occurs in a metalimestone in the biotite-spessartine zone. The talc probably developed as:

dolomite + quartz + H<sub>2</sub>O = talc + calcite + CO<sub>2</sub>  
 (after Turner, 1980), while the tremolite formed at a higher temperature from the breakdown of talc as:



and,  $\text{talc} + \text{calcite} = \text{tremolite} + \text{dolomite} + \text{CO}_2 + \text{H}_2\text{O}$   
 (after Turner, 1980). At higher grades diopside would develop from the tremolite and talc would have disappeared. Curves e and f on Figure 16 (from Turner, 1980, derived from the experimental data of Slaughter *et al.*, 1975) indicate the general regime of metamorphism in these limestones. Assuming a temperature of > 400° C yet < 450° C (as shown by the biotite-spessartine assemblages), the pressure of metamorphism was < 2 kb (consistent with the < 3.5 kb estimate from the presence of andalusite).

#### 4.4.2 The Port aux Basques Complex

The path of prograde regional metamorphism in the Port aux Basques Complex is illustrated on Figure 16. The low grade end of this path is obscured by the intense upper greenschist facies grade retrogression of the gneisses, and the upper end is extrapolated from the regional work of Brown (1975) and Dingwell (1980). No prograde aluminosilicates occur in this map area but the andalusite in the granite contact zone is taken to indicate a minimum pressure for the start of this path (*i.e.* < 3.5 kb).

In its lowest grade portions that have been unaffected by retrograde reactions, the Port aux Basques Gneiss consists of interbanded biotite gneiss and garnetiferous amphibolite. Curve g on Figure 16 represents the hornblende (+ almandine)-in reaction from Winkler (1979). As stated by Winkler, the appearance of hornblende (with almandine) cannot be precisely defined thus the curve is at best an approximation. The curve indicates a temperature of around 500° C for the lower stability of hornblende.

Though a hornblende isograd is defined around the gabbros south of Windowglass Hill, the occurrence of hornblende in these gabbros does not reflect a metamorphic temperature of over 500° C since; 1) there is no almandine present, and 2) the gabbros were originally hornblende gabbros, thus the activation temperature for prograde metamorphic hornblende would be lessened.

Hirschberg and Winkler (1968) and Winkler (1979) inferred from experimental work that almandine-hornblende intergrowths (ie. such as the garnetiferous amphibolite interbands in the Port aux Basques Gneiss) only occur at temperatures > 500° C and pressures > 4 kb (intersection of curves H and G, Figure 16); unless the garnet has a significant spessartine component. For garnets with up to 13 mole % MnO, Hirschberg and Winkler (1968) state that curve h might be depressed to 3-3.5 kb at 500° C. Garnets in the two amphibolite samples (80-52 and 80-57), with spessartine

contents of 15 and 4 % respectively, indicate the lowest grade (non-retrogressed) of metamorphism in the Port aux Basques complex occurred at  $> 500^{\circ} \text{C}$  and  $> 3.5 \text{ kb}$  (kyanite or sillimanite would be expected as the  $\text{Al}_2\text{SiO}_5$  polymorph; though none were found in the area mapped).

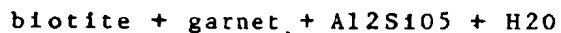
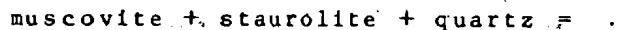
The path of metamorphism quickly passes into the staurolite stability field. The garnets in the staurolite gneiss (sample 80-47G) have spessartine and almandine contents (5 and 81%) consistent with the increasing pressure along this path (as dictated by curves h and i, Figure 16).

Garnets in sample 80-131 (meta-amphibolite) have a high average Sp content (i.e. 23%). However this high average is a result of very strong zoning (one garnet has a core of  $\text{Py}_2\text{Gr}_{14}\text{Sp}_{29}\text{Al}_{55}$  and a rim of  $\text{Py}_3\text{Gr}_{15}\text{Sp}_{13}\text{Al}_{69}$ ), and the rim concentrations are acceptable for the P-T conditions as in the other amphibolites. Tracy *et al.* (1976) report garnets with rim compositions of up to 18.2% Sp as having originated in pressures  $> 5.7 \text{ kb}$  and temperatures of  $585\text{--}655^{\circ} \text{C}$ . The assumed mobility of Mn during garnet growth (eg. Hollister, 1966) though may have had an effect on the extreme ranges of Mn content during retrogression.

Correlating this final mineral stability field in the map area with Brown's (1975) work, shows that the metamorphic pressure was in the kyanite stability field.

(since Brown found kyanite with the staurolite, thus defining his garnet-staurolite-kyanite stability zone, see Figure 13).

Brown's (1975) next zone, kyanite-garnet, occurs with the breakdown of staurolite. Since muscovite and biotite are still common constituents in these assemblages (Brown, 1975), the breakdown reaction possibly was:



(curve j, Figure 16, after Pirie and MacKasey (1978) based on the unpub. work of D.M. Carmichael). This breakdown curve represents temperatures of around 560° C and pressures of 5.5 kb.

The following metamorphic zone encountered is that of sillimanite derived from kyanite (Brown, 1975, Dingwell, 1980) (ie. the metamorphic path is in the stability field of the high pressure, high temperature Al<sub>2</sub>SiO<sub>5</sub> polymorph). This zone is also where the anatectic Port aux Basques Granite occurs (Dingwell, 1980). Based on garnet compositions, using Green's (1977) compositionally-defined stability curves, Dingwell stated the granite was intruded at pressures of > 6.5 kb, which agrees with the proposed metamorphic path.

The final metamorphic zonation in the Port aux Basques Complex is defined by migmatites (further to the southeast) which indicate partial melting. The anatexis curve (curve

k, Figure 16) of Winkler (1979) has been used to define this final P-T condition. This curve is a higher temperature melting curve than that of Tuttle and Bowen (1958) for the "wet granite solidus", but this latter curve is at too low a temperature for the stability relations as outlined for the metamorphic path. The actual partial melting curves for the Port aux Basques Complex probably lies between these two extremes.

The metamorphic path for this complex is intermediate between the 30° C/km and 40° C/km continental geotherms (Figure 17). Dingwell (1980) thought the Port aux Basques Granite was derived by partial melting of a source from along the 30° C/km geotherm. Extending the metamorphic path backwards indicates that the lower grade assemblages would all be in the kyanite stability field. However these relatively lower grade assemblages are not seen because of the intense retrogression near the Windsor Point Group contact. According to the two metamorphic paths illustrated on Figure 16, this contact also marks a large pressure jump from ~ 2 kb at the highest grade level in the Windsor Point Group to > 4.5 kb in the non-retrogressed, lowest grade Port aux Basques Complex. In other words, the Port aux Basques Complex was metamorphosed and then underwent substantial uplift before the Windsor Point Group was deposited.

The effective metamorphic grade in the Windsor Point

Group at the peak of its metamorphism also affected the Port aux Basques Complex and retrogressed the gneiss units. This retrogression so strongly overprinted the gneiss units, that they resemble the Windsor Point Group in metamorphic mineral assemblages.

The garnets in the retrogressed gneiss have significant Sp components (eg. samples 79-71 with 29% Sp and 79-150 with 28% Sp) which are significantly higher than the spessartine contents of garnets in the non-retrogressed gneiss (eg. 80-47G).

The breakdown of hornblende and staurolite indicate that the retrogression occurred at temperatures  $< 500^{\circ}$  C. and pressures of  $< 3$  kb (ie. andalusite in slightly retrogressed gneiss). These P-T conditions would place the gneiss in the spessartine stability field (ie. almandine garnet is stable at higher temperatures and pressures), suggesting that the spessartine garnets grew during the period of retrograde metamorphism.

The nucleation of spessartine-rich garnets during retrogression has not been described elsewhere, though Roper and Dunn (1973) have described garnets developed during an upper greenschist M2 metamorphism which overprinted a higher grade almandine-amphibolite M1 metamorphism (though they have no analyses to compare the two garnet compositions). What typically happens during retrogression is that the rims of almandine garnets are

resorbed and the Mn from the resorbed areas migrates inwards (Ca, Fe, Mg migrate outwards into the matrix) producing a new Mn-rich rim on the garnet (eg. Grant and Weiblen, 1971; Birk, 1973; Amit, 1976). In the Cape Ray Fault Zone however, the almandine was not stable in the lower grade portions of the gneisses during the prograde metamorphism so there were no garnets to resorb.

The growth of spessartine-rich cores (relative to spessartine-poor rims) is commonly held to result from changes in the diffusion gradients between garnet and matrix with changing P-T (Atherton, 1968), or fractionation-depletion in which Mn is fractionated into the garnet from the matrix until all the available Mn is taken up in the garnet and it has to change its composition (eg. Woodsworth, 1977). In either model the most important factor is the mobility of Mn through the matrix. The graphite schists in the Windsor Point Group are somewhat manganiferous (up to 0.74 wt. % MnO), therefore during the peak of metamorphism some Mn may have migrated from these Mn reservoirs (ie. graphite schists) into the adjoining retrogressing Port aux Basques Gneiss where P-T conditions were correct for garnet (spessartine) growth. That fluid movement was important during retrogression is shown by the intense sericitization of gneisses near the contact. The high initial Mn contents visible in garnets from retrogressed amphibolite (sample 80-131), indicate



that Mn concentrations within the gneiss units themselves may have been sufficient to form spessartine.

#### 4.4.3 Contact Metamorphism

The presumed P-T conditions of metasomatism related to intrusion of the Isle aux Morts Brook Granite are also indicated on Figure 16. Pressure conditions ( $<3.5$  kb) are defined by andalusite in the contact aureole and the temperatures ( $<300^{\circ}$  C) from the clinopyroxene-garnet intergrowths in gabbros. This pressure level is in agreement with that of  $< 2.5$  kb for the intrusion of a pegmatite offshoot of the granite derived using Green's (1977) curves for Ca content in garnets.

#### 4.5 Conclusions

Stable metamorphic mineral assemblages have been used to define mineral isograds within the Windsor Point Group and indicate a progradation of temperature conditions during metamorphism. Extrapolation from the non-retrogressed Port aux Basques Complex rocks along strike into zones defined by Brown (1975), indicate increasing P-T conditions (up to anatexis), during metamorphism, at a much higher grade (i.e.  $>3.5$  kb to  $>6$  kb and  $400^{\circ}$  C to  $>600^{\circ}$  C) than in the Windsor Point Group. The metamorphic reaction path appears

to be intermediate between the 30° and 40° C/km continental geotherms.

In the contact zone with the Windsor Point Group, gneisses and amphibolites of the Port aux Basques Complex are extensively retrogressed and have mineral assemblages consistent with those of the highest metamorphic grade achieved by the Windsor Point Group (ie. even down to the presence of spessartine).

Mineral assemblages in the contact metamorphosed regions surrounding the Isle aux Morts Brook indicate P-T conditions of at least 2 kb and 280° C for the intrusion of this granite.

The age of the amphibolite grade metamorphism in the Port aux Basques Complex cannot be precisely determined but was pre-Windsor Point Group (ie. pre-380 Ma, or late Devonian), and since the complex is supposedly Silurian in age itself (cf. Chorlton, 1980b), the age had to be Silurian to Devonian. Retrogressive metamorphism of the Port aux Basques Complex and prograde metamorphism of the Windsor Point Group had to have occurred in the late Devonian, but pre-Carboniferous (ie. the age of the post tectonic granitoids). The contact metamorphism by definition was the same age as the Isle aux Morts Brook Granite.

## CHAPTER 5

### STRUCTURAL HISTORY

#### 5.1 Introduction

In the immediate region of the Cape Ray Fault three major deformational events (schematically illustrated in Figure 17) have affected the Port aux Basques Gneiss, the Cape Ray Granite and the Windsor Point Group. Sequential development of these three events has produced the same general structural geometry in each of the lithologic units. The resulting structural geometry is, however, best displayed in the Windsor Point Group due to its primary layered nature and relatively low grade of metamorphism. The various members of this group show different degrees of deformation resulting mainly from differences in their rheological behaviour related to primary compositional differences. Strain gradients were also inhomogeneous through this group leading to development of mylonites in susceptible zones. A minor fourth deformational event locally produced breccias within the Windsor Point Group, the Strawberry Granite and the mylonite.

The first deformational event in the Cape Ray Fault Zone (D1) produced a northeasterly-striking schistosity (S<sub>1</sub>) that dips steeply to the southeast (see Figure 18). This schistosity is axial planar to small, isoclinal folds

Figure 17 Schematic illustration of the deformational history of the Cape Ray Fault Zone. Three deformations affected most units viz.; D1 - produced the dominant northeasterly-striking and southeasterly-dipping planar fabric which is axial planar to isoclinal folds with the fold axes and a mineral elongation lineation plunging steeply southeast; D2 - asymmetrical folds, verging to the northwest, with curvilinear axes, and axial planes parallel to D1; D3 - poorly developed conjugate kink folds.)

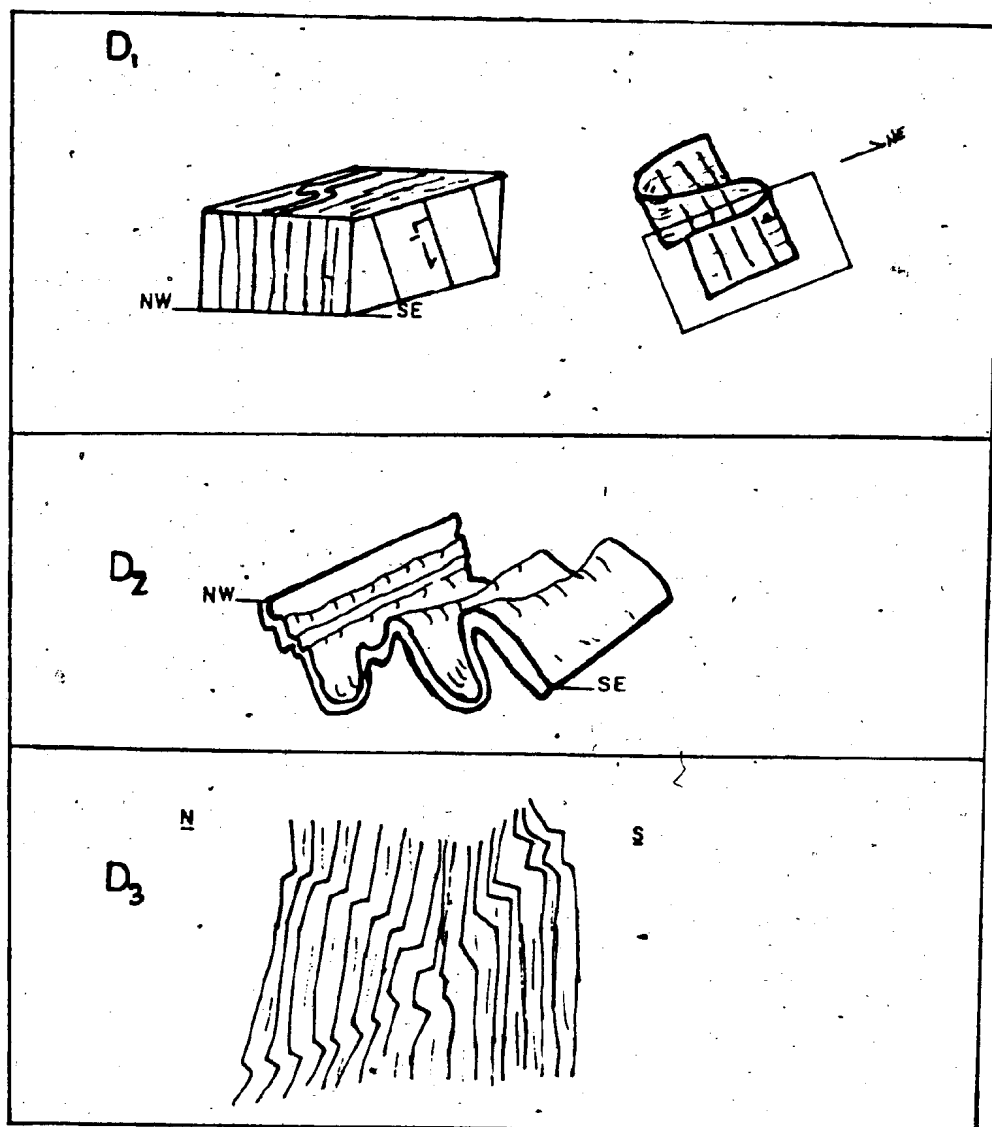
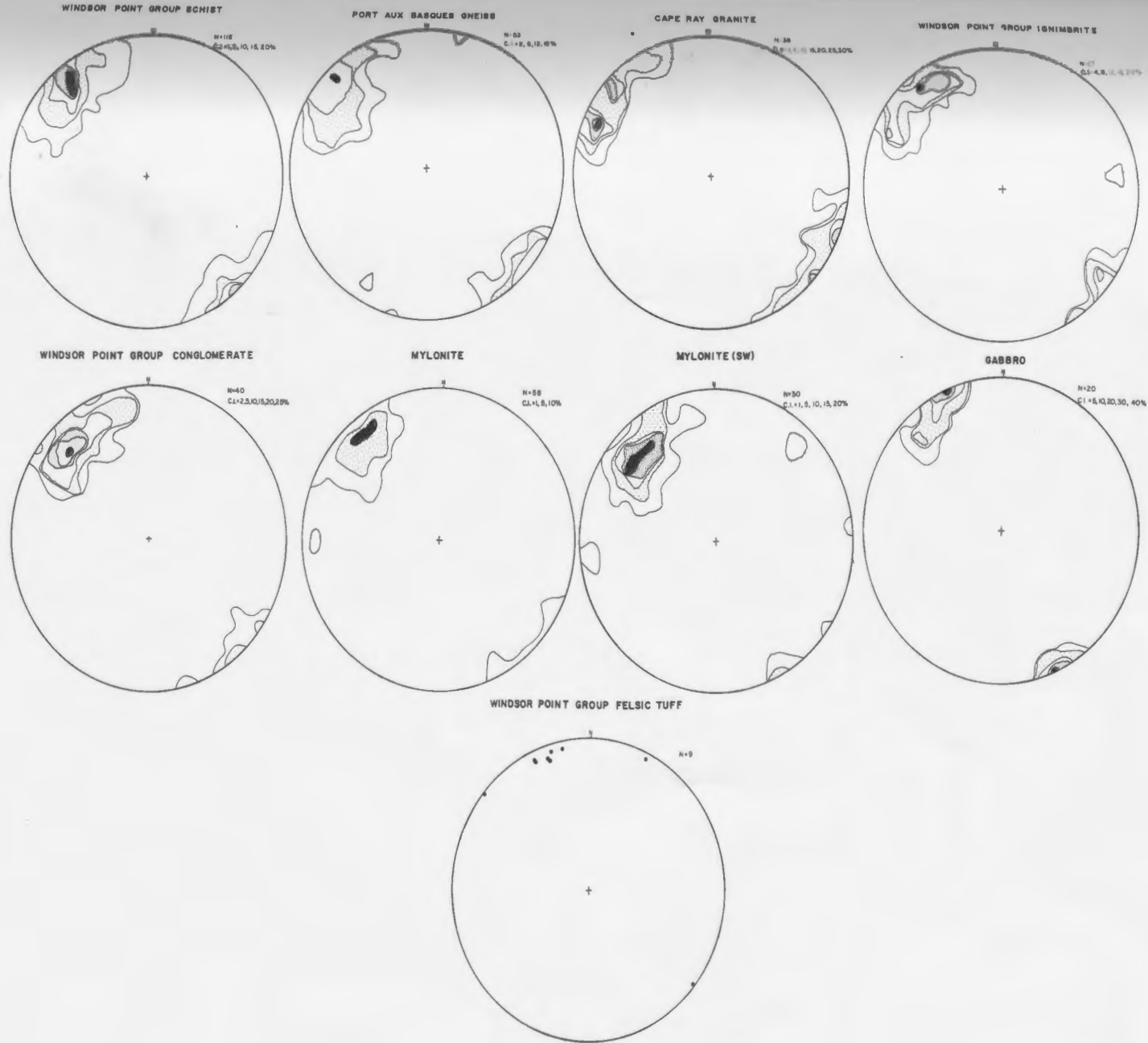


Figure 18 Equal area stereographic projections of poles to schistosity for lithological units in the Cape Ray Fault Zone. Contoured where the number of measurements warrants. These plots show that the planar fabrics in each unit have a common northeasterly strike and steep southeasterly dip. In this and all following stereonet, the stereographic projections are for an equal area net in the lower hemisphere, and contours are percentage per 1% area of the net.



(F1), in which the fold axes plunge steeply to the southeast. These folds are reclined to vertical. A mineral elongation lineation (L1), plunging steeply to the southeast (see Figure 19), apparently parallel to the isoclinal fold axes, was also produced during D1. There is also extensive boudinage of thin interbands and veins, with the long axes parallel to the S1 and the extension direction parallel to L1.

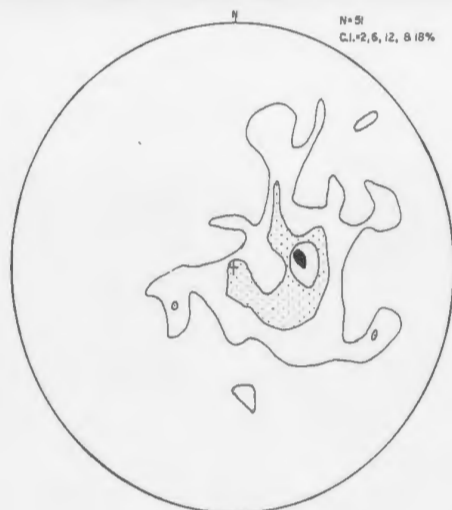
D1 fabrics overprint pre-existing fabrics in the Port aux Basques Gneiss, are developed within inhomogeneous, ductile simple shear zones (Ramsay and Graham, 1970) in the Cape Ray Granite, define the main fabric in all units of the Windsor Point Group (Plate 5-1A), and constitute the fabric in the mylonites. F1 isoclinal folds are poorly preserved, but are observed in the Windsor Point Group, the mylonites and in a shear zone in the Cape Ray Granite. Steeply plunging L1 mineral elongation lineations are visible in the same three units and the Windowglass Hill Granite.

Open to tight, asymmetrical folds (F2), with amplitudes ranging from several metres to several millimetres, were the product of the second deformational event (see Figure 20). The axial planes of these folds have a general northeasterly strike and southeasterly dip and thus are co-planar with the D1 schistosity, but there is considerable scatter in the measurements as shown in

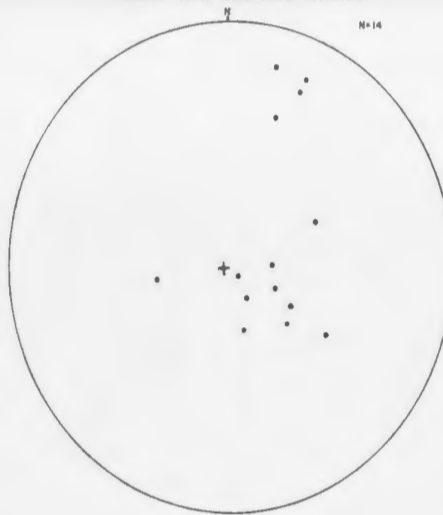


Figure 19 Equal area stereographic projections for D1 mineral elongation lineations. These plots show a common southeasterly plunge for the lineations. F1 isoclinal folds were too few, and too strongly overprinted by F2 folds to be accurately measured and statistically analysed. However, as a qualitative observation, the D1 fold axes parallel the L1 lineations.

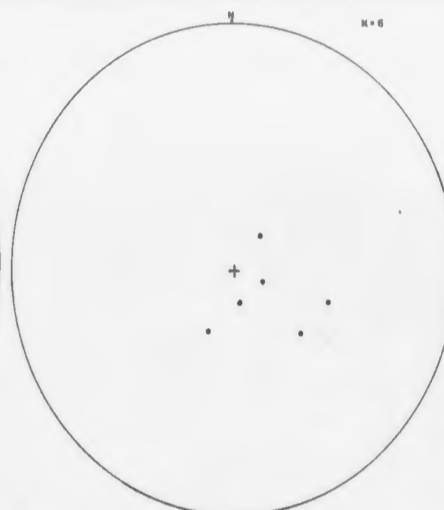
WINDSOR POINT GROUP SCHIST



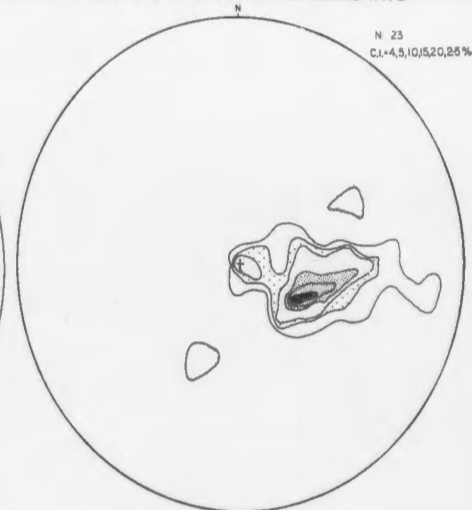
PORT AUX BASQUES GNEISS



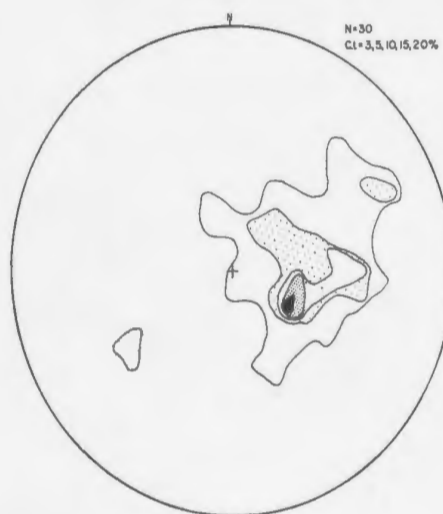
WINDSOR POINT GROUP IGIMBRITE



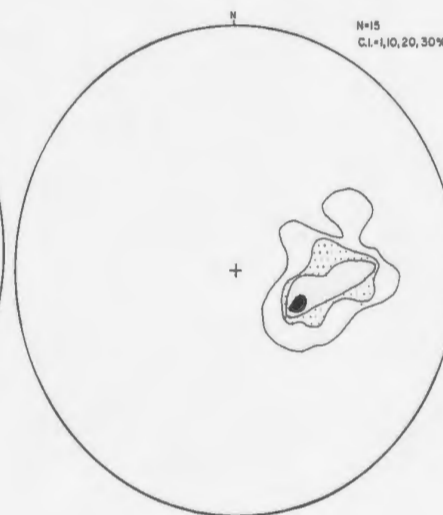
WINDSOR POINT GROUP CONGLOMERATE



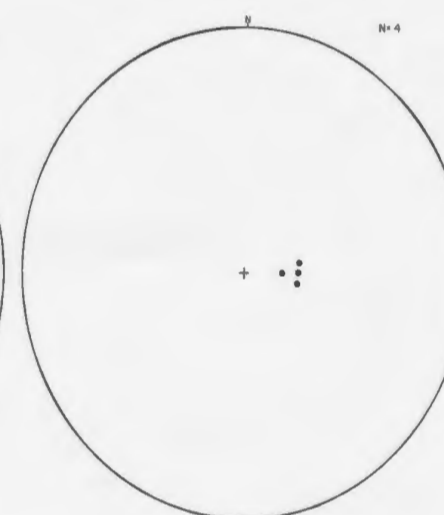
MYLONITE



MYLONITE (SW)



WINDSOR POINT GROUP FELSIC TUFF



WINDOWGLASS HILL GRANITE

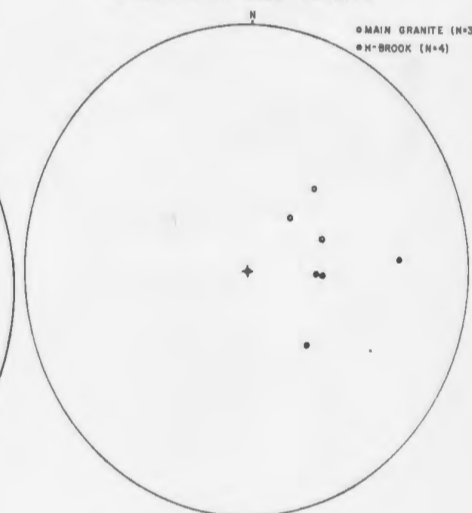
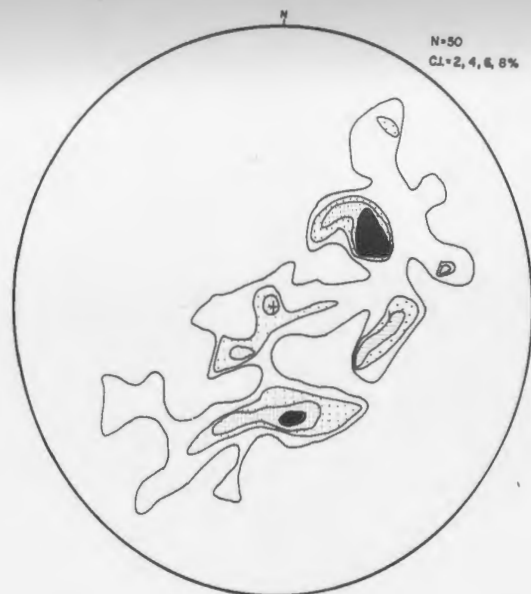


Figure 20 Equal area contoured stereographic projections of F2 fold axes directions. The axes plunge steeply to the northeast and southeast in all units, but there is also a shallow northeast-plunging set in the Port aux Basques Gneiss which is possibly a remnant of the D3 deformation which affected this unit prior to the fault zone deformations.

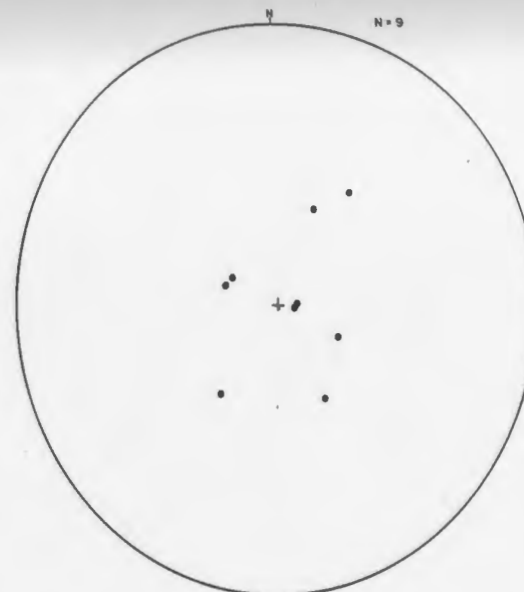
WINDSOR POINT GROUP SCHIST



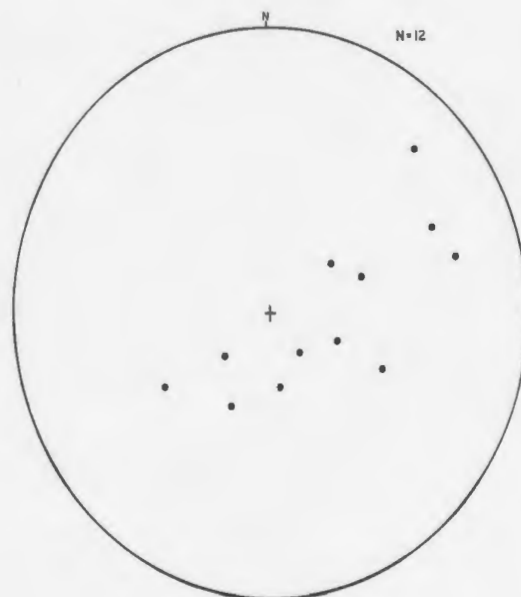
PORT AUX BASQUES GNEISS



WINDSOR POINT GROUP IGNIMBRITE



WINDSOR POINT GROUP CONGLOMERATE



MYLONITE

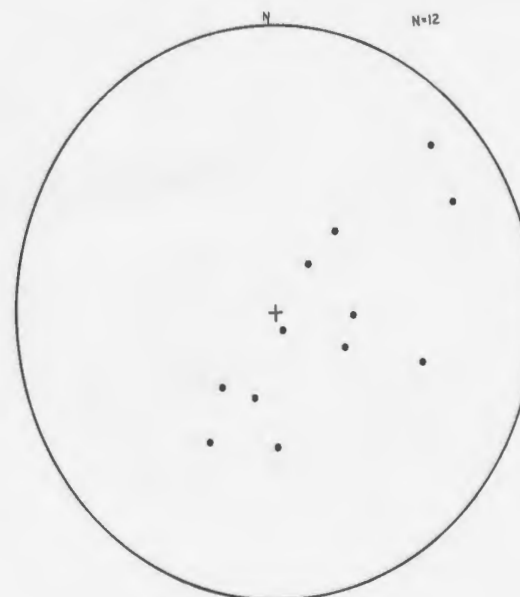


Figure 21. The vergence of the folds is towards the northwest. The limbs of the larger folds contain numerous smaller parasitic folds. Crenulation lineations are commonly developed on the limbs of large-scale F2 folds in sericitic schists (Plate 5-1B). The fold axes of these D2 folds are curvilinear within the axial planes, and plunge moderately to the northeast or southwest especially as shown for the Windsor Point Group schists in Figure 20. The D2 folds are developed in all units (except the Strawberry and Isle aux Morts Brook Granites) to varying degrees.

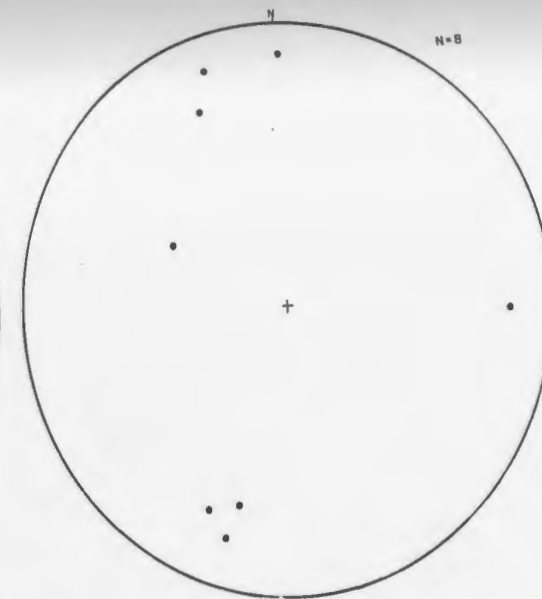
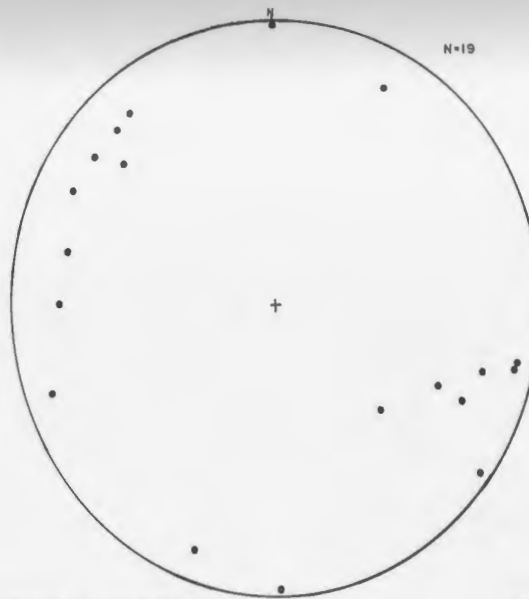
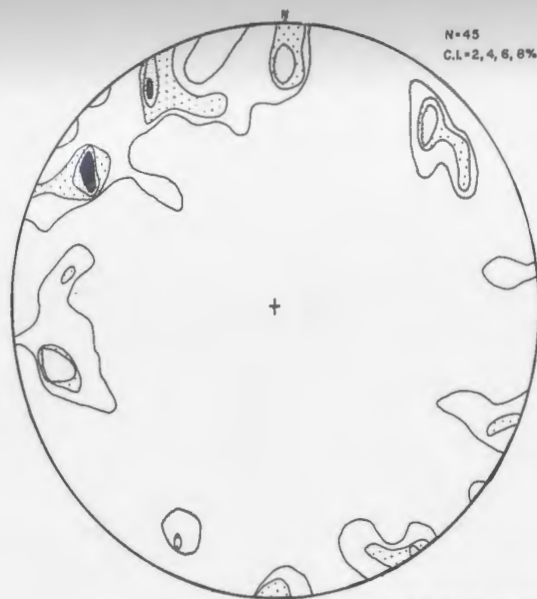
The third deformation (D3) locally produced poorly developed conjugate sets of kink folds. These kink folds are scattered through the Cape Ray Granite, Windsor Point Group, Windowglass Hill Granite, and the mylonite.

The fourth and final deformational event was localised to a narrow belt along the trace of the Cape Ray Fault itself, and produced the lithic breccias (map unit 13). The breccias occur within the mylonite, the Windsor Point Group and along the southern margin of the Strawberry Granite. Brecciation is the only deformational event to have affected this post-tectonic granite. These breccias resulted from brittle deformation, induced by reactivation of the Cape Ray Fault. The physical expression of the Cape Ray Fault was produced during this deformation, with the fault visible as escarpments occurring along the trace of

WINDSOR POINT GROUP SCHIST

PORT AUX BASQUES GNEISS

WINDSOR POINT GROUP IGNIMBRITE



WINDSOR POINT GROUP CONGLOMERATE

MYLONITE

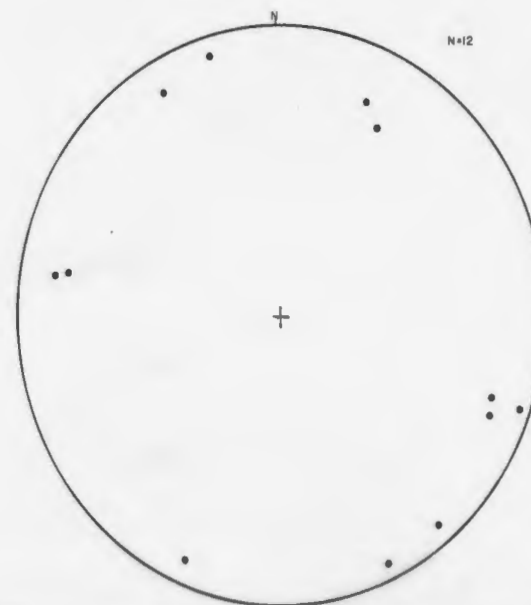
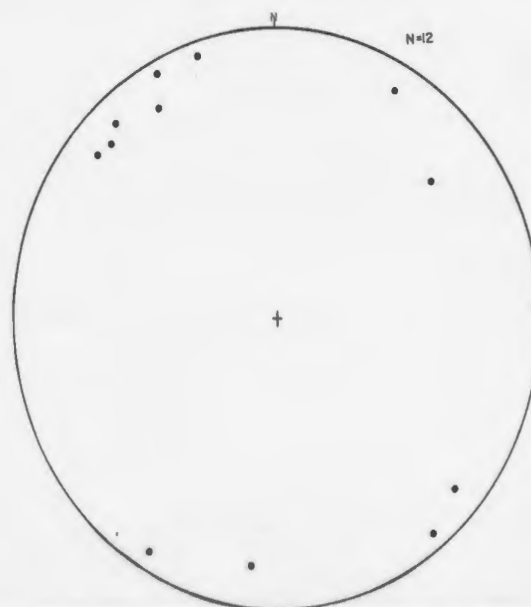


Figure 21 Equal area contoured stereographic projections of poles to  
F2 axial planes.

the western stream feeding Big Pond and along the trace of the lithic breccia in the Gulch. In the linear valley of the Gulch, the fault has an upthrown northwestern edge at least 10 m above the valley floor. In these exposures the fault appears to be a normal fault. As shown on Map 1 (in pocket) there are also a number of small offshoot faults from the main fault developed during this final deformational event.

## 5.2 Detail of Structural Development in Each Unit

### 5.2.1. Long Range Mafic/Ultramafic Complex

No consistent fabrics nor deformational sequences were found in these rocks. In one location, at the contact with the post-tectonic Strawberry Granite, a metagabbro has a strong mylonitic fabric developed that parallels the contact. This fabric is probably related to an intrusion-induced deformation.

### 5.2.2 The Port aux Basques Complex

Brown (1975) presented evidence for four deformational events having affected the Port aux Basques Complex (schematically illustrated in Figure 22). These events (after Brown, 1975) are represented as :

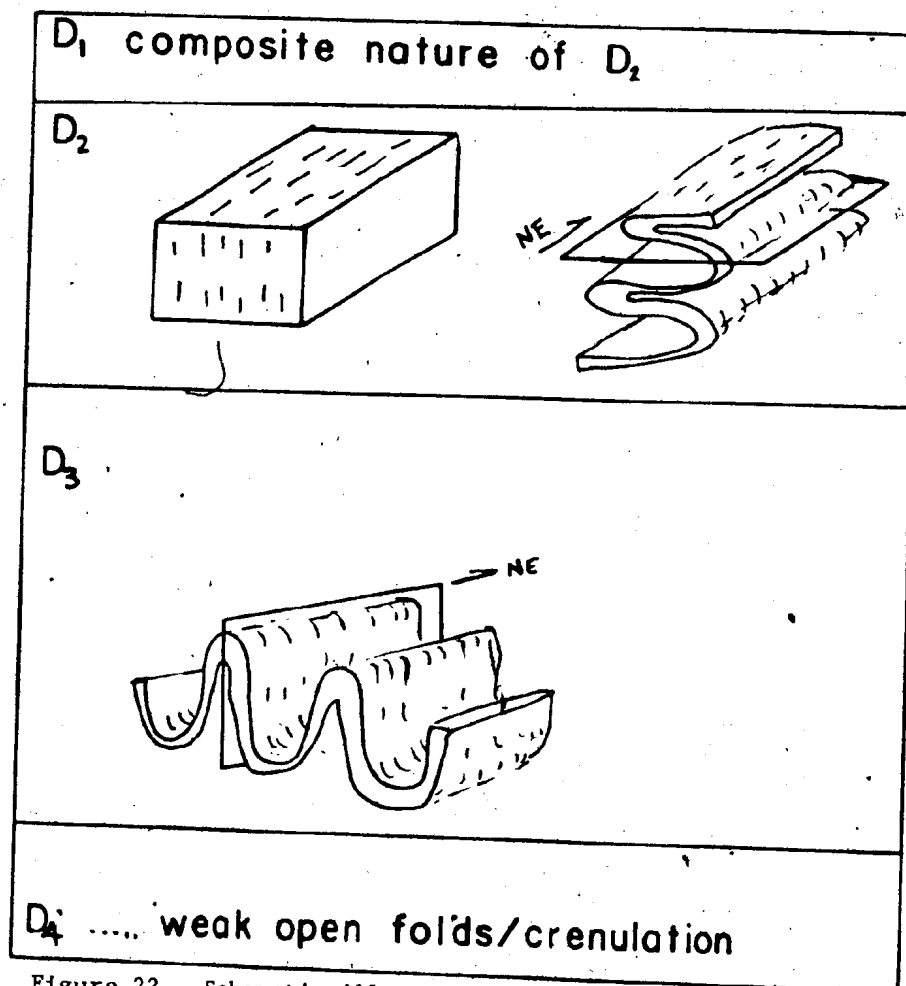


Figure 22 Schematic illustration of the deformational history of the Port aux Basques Complex (as outlined by Brown, 1975). A full explanation of these deformations is given in the text.



1) D1 - a poorly preserved biotite fabric, that can usually only be inferred from the composite nature of S2, or rarely, observed as inclusion trails in garnet and/or staurolite porphyroblasts

2) D2 - produced gneissic banding and flat-lying isoclinal folds with axial planes that strike northeast and close to the northwest

3) D3 - upright, sub- to isoclinal folds, with northeasterly-striking axial planes, which are slightly overturned to the southeast

4) D4 - a minor, sparsely developed deformation which resulted in slight crenulation of the earlier fabrics.

The Port aux Basques Granite intruded syntectonically during the D2 deformation and contains a D2 fabric of aligned biotite. Correlations between these four deformational events and the three Cape Ray Fault Zone deformations are obscure. On a regional scale, the gneissic fabric of the Port aux Basques Gneiss (as detailed by Brown, 1975, and Dingwell, 1980) is parallel to the D1 fabrics in the Cape Ray Fault Zone. However, close to the fault zone, amphibolites interlayered with the gneiss are boudinaged and the boudins were then folded (Plate 5-1C). It would thus appear that the first deformational event of the fault zone overprinted the pre-existing gneissic fabric (of the Port aux Basques Gneiss) and produced the boudins.

The boudins were then slightly folded by later folding episodes.

All traces of earlier fabrics are obliterated from, and the three fault zone deformations are superimposed on the retrogressed gneisses near the Windsor Point Group contact, such that their fabrics match those in the Windsor Point Group.

#### 5.2.3 The Cape Ray and Red Rocks Granites

The tonalitic and megacrystic phases of the Cape Ray Granite were inhomogeneously deformed during the D1 event. Northeasterly-striking/southeasterly-dipping ductile simple shear zones were produced locally. The zones have variable widths from centimetres to metres, but they increase in width, quantity, and intensity of deformation as the Cape Ray Fault is approached. The fabric of these shear zones often shows an anastomosing pattern of the foliation planes, the poles of which define two maxima at small angles to one another (see the stereoplot for this unit in Figure 18).

Xenoliths in the granites were also affected by D1 deformation. They are highly flattened in the S1 plane (Plate 2-1F). In the megacrystic phase, deformation in shear zones is often intense enough to obliterate the megacrysts by reduction of grain size due to dynamic

recrystallization.

The Red Rocks Granite is undeformed and has no fabric (neither linear nor planar) developed. Deformation here is restricted to faulting. Figure 23 is a stereographic projection of poles to shear fractures as measured in this granite. There are several scattered fault directions present, but their inter-relations could not be discerned. The faulting has produced zones of cataclastic rocks, some of which contain galena. There are also thin ( $\leq 5$  cm thick) mylonite zones where stress has resulted in ductile deformation.

L1 lineations, and F1, F2 and F3 folds were not apparent in the Cape Ray or Red Rocks Granites sensu stricto. However, in the mylonite that marks the contact between these two granitoid bodies, the mylonitic fabric is axial planar to F1 isoclinal folds; a mineral elongation lineation is parallel to the fold axes and the mylonite is overprinted by conjugate F3 kink folds (Plate 5-1D).

#### 5.2.4 Gabbros

The gabbros south of Windowglass Hill are highly schistose and have effectively lost their original igneous textures. The D1 planar fabric parallels S1 developed elsewhere in the region (Figure 18). The S1 plane in the metagabbros was extensively folded during the D2

## RED ROCKS GRANITE

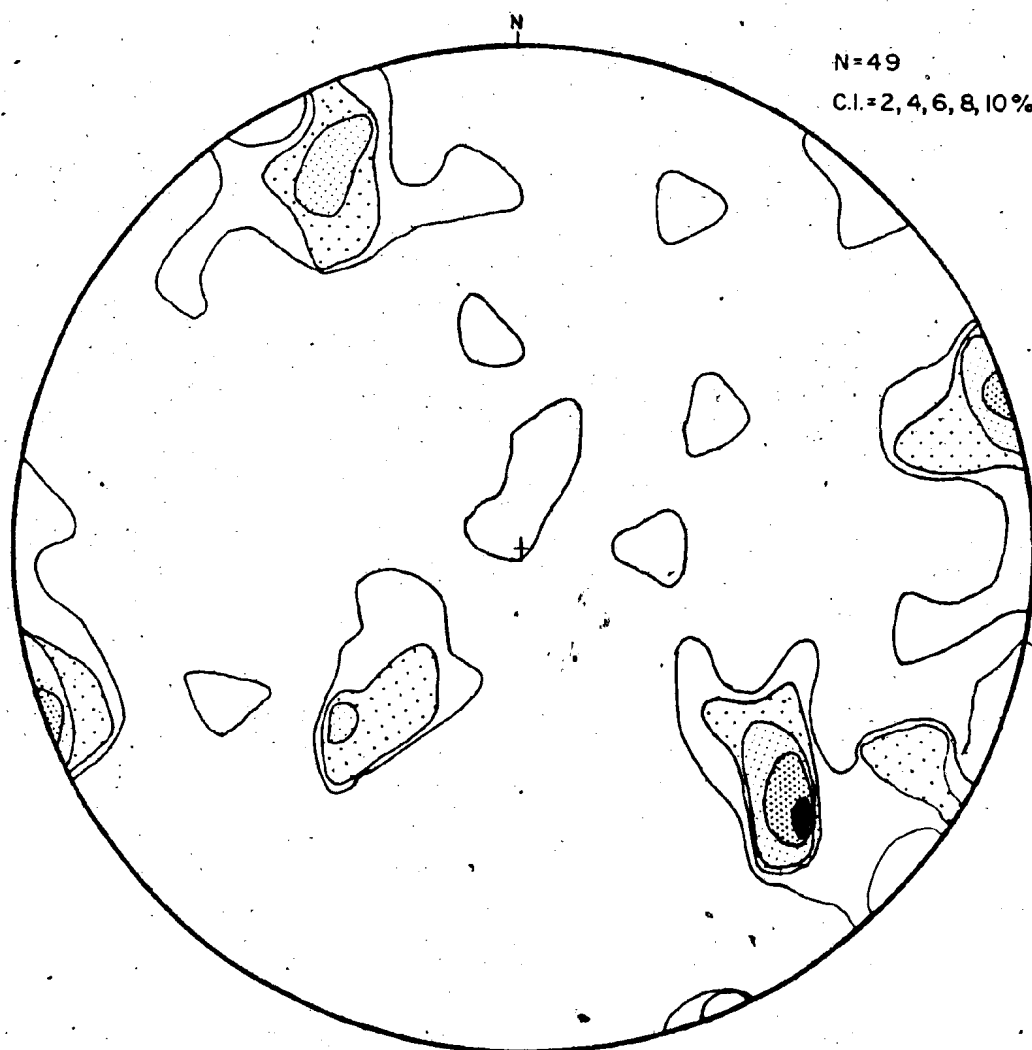


Figure 23 Equal area contoured stereographic projection of poles to shear fractures/faults in the Red Rocks Granite.

deformation event and the folds have the typical F2 asymmetry.

#### 5.2.5 The Windsor Point Group

The rocks within the Windsor Point Group show evidence for intense D1 deformation, leading to transposition of bedding parallel to the axial plane schistosity (S1) of isoclinal folds. These folds are best exhibited by thin interbeds (particularly limestone) within the schist member (Plate 5-1E).

The intensity of the D1 deformation in the Windsor Point Group increases towards the southeast (*ie.* towards the Port aux Basques Complex), and on the coast the second conglomerate passes into the mylonite horizon. The clasts in this conglomerate are strongly flattened (Plate 2-4B) parallel to S1 and elongated in the L1 direction. Clasts within the conglomerate/autobreccia of the Little Barachois Formation are much less deformed, yet are still flattened (Plate 5-1F).

A stereographic projection of F2 fold axes measurements within the Windsor Point Group schist is shown on Figure 20. It should be noted that this is the only unit in which statistically significant fold axes measurements were obtainable. The curvilinear nature of the D2 fold axes orientations is apparent from the partial

PLATE 5-1 A) D1 fabric in Windsor Point Group schist " wrapping around" a felsic volcanic clast.. D1 fabric parallels the pen in the plate.

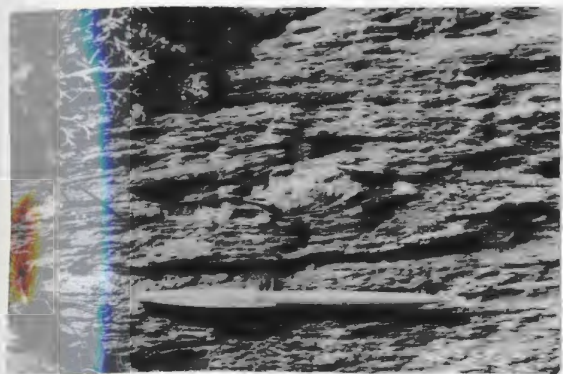
B) D2 crenulation lineations in Windsor Point Group sericitic schist. These lineations are parallel to the fold axes of F2 folds and plunges steeply to the southeast.

C) Boudinaged garnetiferous amphibolite interband in the Port aux Basques Gneiss. The ends of the boudins were subsequently slightly folded. The boudinage was produced during the D1 flattening episode in the Cape Ray Fault Zone and overprints pre-existing fabrics in the gneiss.

D) Conjugate D3 kink folds in the mylonite from along the contact between the Red Rocks and Cape Ray Granites. The scale is a twenty-five cent piece.

E) F1 isoclinal fold of thin limestone (white) interbed in Windsor Point Group chlorite schist. Overprinted by D3 kink folds.

F) Flattened clasts in Little Barachois Formation volcaniclastic conglomerate. The fabric wraps around the felsic volcanic clasts,



A



D



B



E



C



F

great circle girdle pattern, the great circle lying parallel to the mean orientation of S1 in the area (see Figure 20 with two maxima indicating two axial trends at about  $45^\circ$  from each other). A plot (Figure 24) of crenulation lineations in the same unit indicates that these axes are parallel to the F2 fold axes and could be a product of the same D2 deformation. This S2 axial planar crenulation cleavage is usually parallel to the S1 but occasionally occurs at angles of up to  $45^\circ$  to S1 (Plate 5-2A).

Figure 19 also shows that the D1 mineral lineations are not parallel to the D2 fold axes. These lineations, though occurring within the general D2 fold axes girdle are orientated at a high angle to many of the D2 fold axes.

The orientation distribution pattern of D1 and D2 elements in this unit suggests that the two deformation events may have been co-planar (XY-plane of the finite strain ellipsoid). Unfortunately the stretching direction for F2 deformation could not be established with certainty, so that it could not be demonstrated that the two deformations followed similar movement paths.

#### 5.2.6 The Windowglass Hill Granite

The undeformed western end of the Windowglass Hill Granite has an elongate elliptical outcrop appearance. To



## WINDSOR POINT GROUP SCHIST

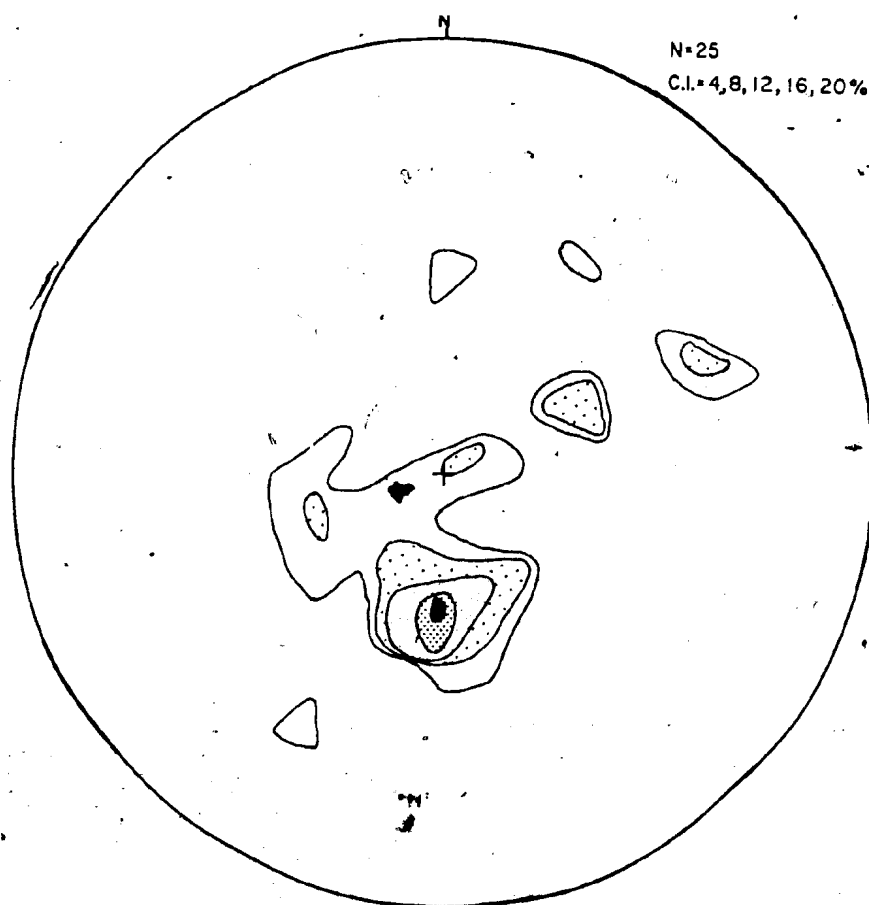


Figure 24 Equal area contoured stereographic projections of  $D_2$  crenulation directions measured in the schist unit of the Windsor Point Group. This plot indicates the crenulations were produced by  $F_2$  folding (i.e. the crenulation maximum is the same as one of the maxima for  $F_2$  folding in Figure 20).

the northeast, however, the granite has a dyke-like appearance and is mylonitized. There is no clear planar D1 mylonite fabric within the northeastern extension of the granite, but an intense L1 mineral elongation lineation is developed (Plate 5-2B). This lineation plunges steeply to the east or southeast and generally parallels the L1 lineations in the Windsor Point Group. Asymmetrical D2 folds, with amplitudes of up to 2 m, are also developed in the northeastern part of the granite (Plate 5-2C).

#### 5.2.7 The Mylonites

Poles to the mylonitic foliation in the coastal mylonite unit (Figure 18) and the combined data for both the coastal and inland mylonite units (also Figure 18) have almost identical maxima and form, suggesting that mylonites were produced at the same time by equivalent deformational mechanisms.

Some of the largest F2 folds occur within the southwestern mylonite where their axial planes, with amplitudes of over 10 m, are often dissected by streams; the hinge zones may have acted as loci of strong fracturing.

### 5.3 Interpretation of Fabrics

The F1 isoclinal fold axes were too few and frequently too strongly overprinted by F2 folds to be accurately measured and statistically analysed. However as a qualitative observation, the F1 fold axes seem to parallel the L1 mineral elongation lineations. The parallelism of elongation lineations and fold axes has been studied and discussed in some detail by several authors (eg., Bryant and Reid, 1969; Sanderson, 1973; Nicolas and Boudier, 1975; Hobbs et al., 1976; Bell, 1978). Hobbs et al. (1976) stated that such parallelism is quite common in mylonite zones and represents a major interpretative problem.

Briefly, the various hypotheses formulated to deal with such parallelism state that the fold axes and lineations either developed parallel to each other initially (for example due to some perturbation in the stress field; eg. Nicolas and Boudier, 1975), or the fold axes were originally parallel to the Y-axis of the finite strain ellipsoid, but with progressive deformation the fold axes rotated towards parallelism with the X-axis (i.e. mineral elongation lineation and kinematic stretching direction; eg. Sanderson, 1973). This last idea is probably most applicable to the Cape Ray Fault Zone F1 fold axes, as there is evidence of rotational deformation during the D1 deformation (as described below).

Stereographic projections of the poles to F2 axial

planes (Figure 21) show that there is a broad dispersal of orientations, with a maximization (especially in the Windsor Point Group) in a great circle parallel to the northeasterly striking/southeasterly dipping regional S1 fabric. The slight variations in axial planar direction explain the occasional strong transposition of S1 fabric by S2 crenulation cleavage.

The F2 fold axes generally plunge steeply southeast or northeast and plot as diffuse girdles on stereographic projections (Figure 20) except in the Port aux Basques Gneiss. In this gneiss there is a strong maximum of directions plunging north northeast at a more shallow angle than the axes in the Windsor Point Group. These axes probably represent the horizontal F3 folds defined by Brown (1975) for this unit (see Figure 22). The secondary maxima plunging steeply to the southeast (Figure 20) result from Cape Ray Fault Zone F2 folds.

According to Hansen (1971), flexural-slip folding of pre-existing lineations during later deformations produces a cone in space (corresponding to a small circle in stereographic projection) while slip folding, of pre-existing lineations describes a planar path in space (corresponding to a great circle in stereographic projection) (see also Figure 4.25 from Hobbs, Means and Williams, 1976). The L1 mineral elongation lineations in Figure 19 are strongly concentrated in maxima, but the

peripheral values define great circle projections rather than small circles. Therefore the F2 folding would be classified by Hansen (1971) as slip folding.

Slip folding involves differential movement along planes of slip while flexural-slip folding involves movement parallel to S-surfaces (Whitten, 1969). The crenulation cleavage, S2, associated with the F2 folds often offsets S1 as seen in thin section confirming that the F2 folds formed at least partially in response to simple shear (ie. are of slip nature). Sometimes the S2 surfaces (subparallel to the S1 surfaces) act as shear planes and dissect the fabric with microshears.

Macroscopic markers, which can be used to demonstrate the presence or absence of a simple shear component to the deformation, are not common in any of the lithologies in the fault zone but, in some Windsor Point Group metamudstones, solitary clasts have "pull-apart" textures in which the boudinage blocks are rotated with respect to S1 (Plate 5-2D).

The obliquity of pressure shadows to a dominant fabric is indicative of non-coaxial shear (ie. rotational shear) (Berthe et al., 1979, Burg et al., 1981, Mattauer et al., 1981). Similarly sigmoidal micas growing in between shear planes are typical of simple (rotational) shear (eg. Burg and Laurent, 1978, Mattauer et al., 1981, Burg et al., 1981). In microstructural studies of all units there is

PLATE 5-2 A) D2 crenulation cutting the main D1 fabric at ~ 30'.

The D1 fabric is best seen in the lower right hand side of the plate where it strikes towards the NE. The D2 crenulation is seen in the upper left half of the plate where it cuts through to the ENE. This section is about 2 mm across.

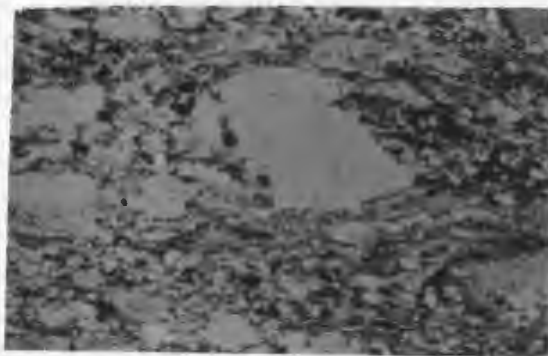
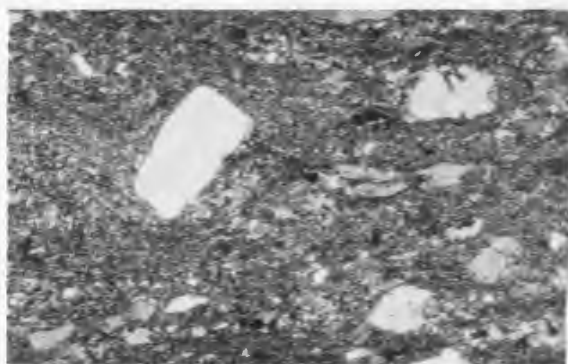
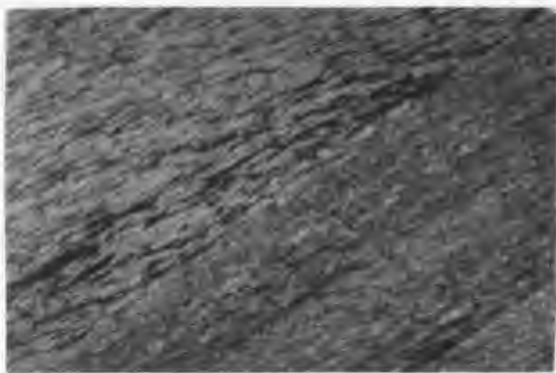
B) D1 mineral elongation lineation in the margin of the mylonitized Windowglass Hill Granite. This lineation plunges steeply to the SE.

C) F2 fold in the mylonitized Windowglass Hill Granite in I Brook. The hammer is resting on the hinge of this fold in which the asymmetry closes to the right (ie. the NW).

D) D1 simple shear "pull-apart" structure superimposed on a lithic fragment within a Windsor Point Group mudstone. The sense of displacement is sinistral.

E) Rotational component to D1 flattening in Windsor Point Group. Shown by micaceous fabric wrapping around quartz and feldspar grains. This section is 2 mm across.

F) Feldspar augen in unorientated mylonitic rock with recrystallized quartz and feldspar in obliquely orientated pressure shadows. This section is about 2 mm across.



evidence of sinistral rotations indicated by oblique pressure shadows around clastic grains within the Windsor Point Group (Plate 5-2E), porphyroclasts in the mylonites (Plate 5-2F), and garnets in the Port aux Basques Gneiss. The sense of asymmetry of sigmoidal mica layers between shear zones in all units also indicate a general sinistral rotation component to the deformation.

Furthermore, the distribution of subsidiary faults off the main Cape Ray Fault is indicative of sinistral movement on this fault.

#### 5.4 Relationship between structural and metamorphic history

The peak of metamorphism within the Windsor Point Group either slightly pre-dated or was synchronous with the D1 deformation. The S1 fabric within this unit is defined by alignment of muscovite (sericite), chlorite and biotite. Retrogression in the Port aux Basques Complex was similarly synkinematic with D1. In the non-retrogressed gneiss garnets were rotated during the D1 flattening, and their fractures filled with chlorite.

The L1 lineations are defined by trails of magnetite, recrystallized quartz and feldspar, carbonate, tourmaline needles, and by fibrous carbonate pressure shadows around pyrite cubes (Plate 5-3A).

The F2 crenulation/shearing post-dated the peak of



metamorphism. This shearing, when at angles to the S1 direction visibly displaces the S1 micaceous material. Spessartine garnets within the Windsor Point Group are pre-tectonic to this S2 shearing (Plate 5-3B), according to the strictures of Vernon (1978).

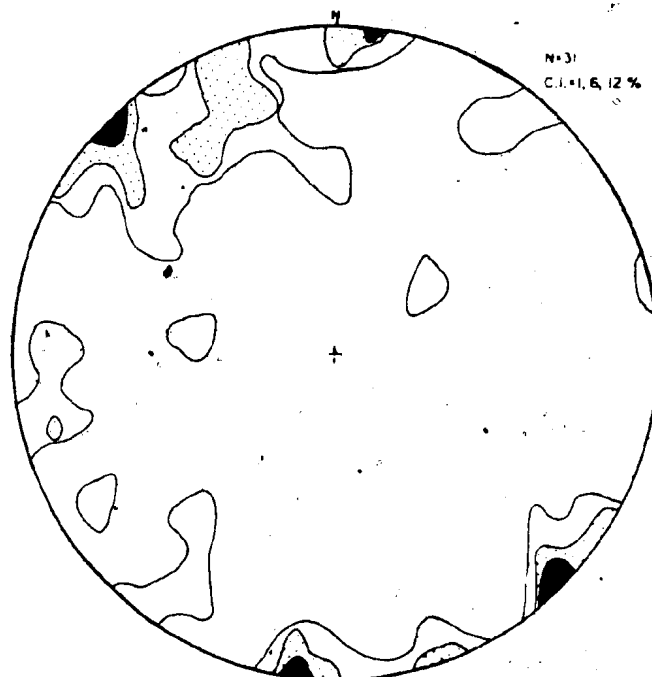
### 5.5 Principal Stress Orientations

Stereographic projections of shear/fractures within the Windsor Point Group and the Cape Ray Granite (Figure 25) indicate two dominant directions in both of these units. These fracture sets fit the criteria (ie. neither consistently offsets the other; and they have opposed senses of movement) of Hobbs *et al.* (1976) for conjugate faults. By resolving the intersections of the sets, the principal stress directions (ie.  $\sigma_1$ ,  $\sigma_2$ ,  $\sigma_3$ ) can be determined; where  $\sigma_1$  is maximum compression,  $\sigma_3$  is maximum extension and  $\sigma_2$  is the intermediate axis.

Maxima of poles to fractures in the Windsor Point Group occur at 45° with dips of 84° E and 80° W (mean 45°/88° W), and 93° with dips of 86° S and 83° N (mean 93°/89° N). In the Cape Ray Granite the maxima are; 7° with dips of 87° E and 87° W (mean 7°/vertical) and 25° with dips of 78° E and 87° W (mean 25°/86° E). The line of intersection of the two great circles of each set (Figure 26) in stereographic projection is parallel to the  $\sigma_1$  direction (Phillips, 1971,

Figure 25 Equal area contoured stereographic projections of poles to shear fractures in the Windsor Point Group and Cape Ray Granite.

## WINDSOR POINT GROUP SCHIST



## CAPE RAY GRANITE

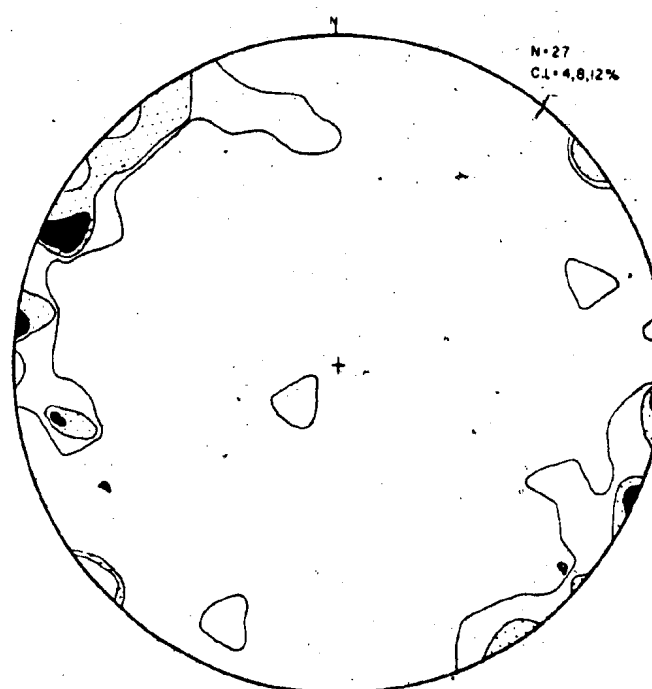
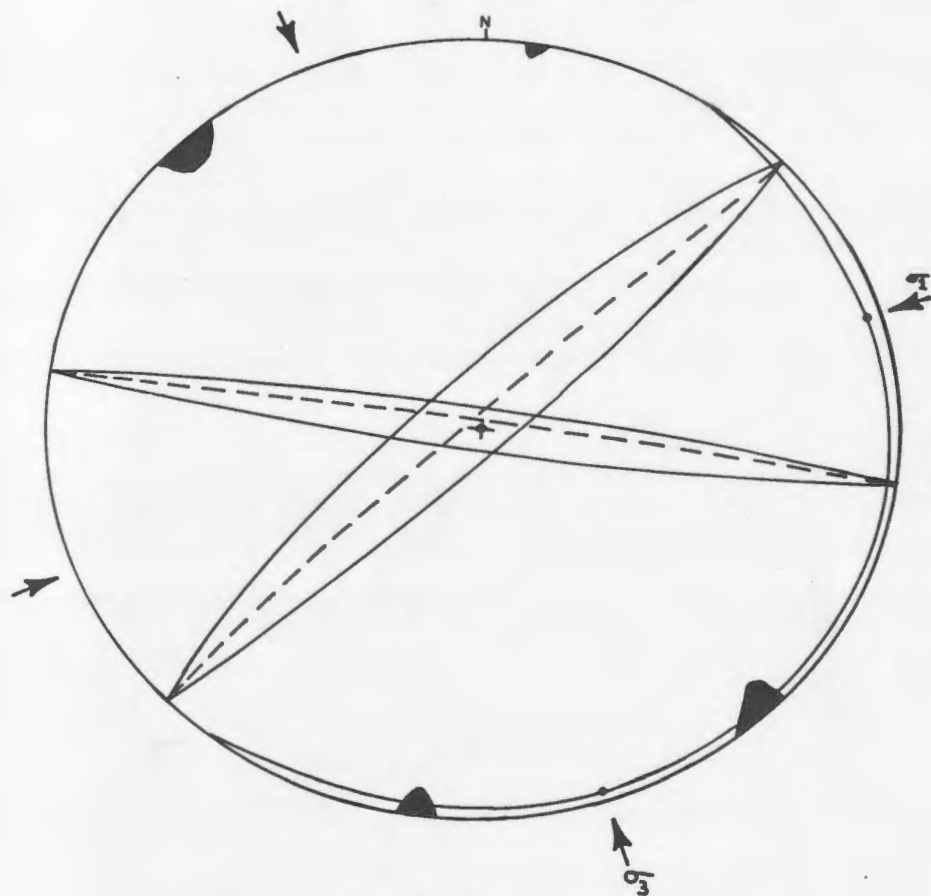
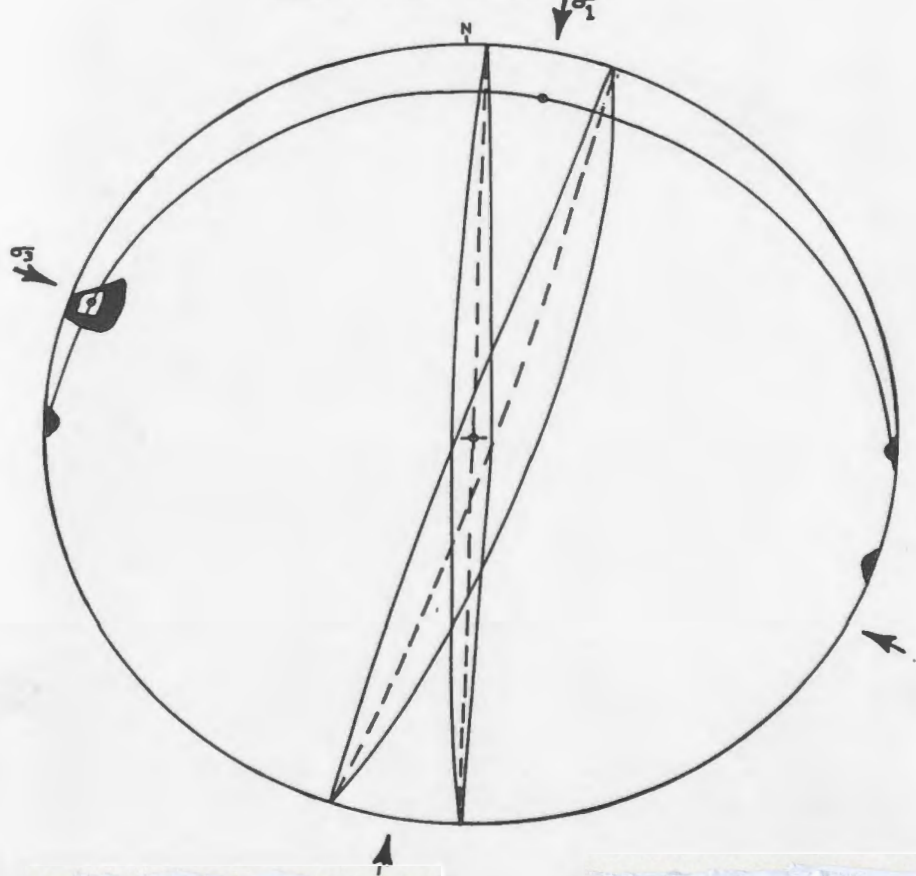


Figure 26 Stereographic projections of the intersections between the great circle maxima for shear/fractures in the Windsor Point Group and Cape Ray Granites. Each dashed great circle represents the mean value for the range in maxima as seen in Figure 25.  $\sigma_1$  is parallel to the line of intersection of these two great circle maxima and  $\sigma_3$  is at 90° to this direction in the same general plane.

## WINDSOR POINT GROUP



## CAPE RAY GRANITE



Hobbs et al., 1976) of the stress field. The  $\sigma_1$  direction (Figure 26) occurs along the great circle perpendicular to  $\sigma_2$  (line of intersection) as the bisector of the compressional angle (ibid.). The  $\sigma_3$  direction is on this same great circle  $90^\circ$  from  $\sigma_1$ .

As determined in the Windsor Point Group and Cape Ray Granite respectively these orientations of  $\sigma_1$ ,  $\sigma_2$  and  $\sigma_3$  are; T71P2, T327P88, T161P2 and T16P12, T190P79, T296P4. The direction of the maximum compressional stress in both cases was directed NE/SW and extension was NW/SE. The median stress is near vertical (especially in the Windsor Point Group). These stress directions are consistent with sinistral movement along the fault zone.

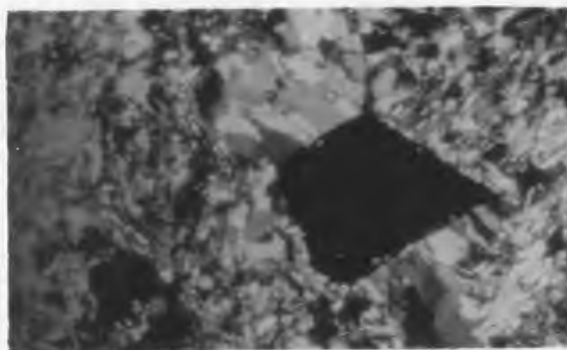
The determined stress directions in the two units are not identical, but have the same general orientation. The lack of exact parallelism may be caused by differences in mechanical behaviour of the units (ie. the granite was a massive medium, while the schists by definition are highly layered units), lack of statistically significant observations, and the problems involved with collecting directional data.

Corroboration for the inferred principal stress directions is indicated by quartz vein tension gashes in the Little Barachois Formation (Plate 5-3C). These tension gashes are perpendicular (Figure 27) to the inferred  $\sigma_3$  direction.

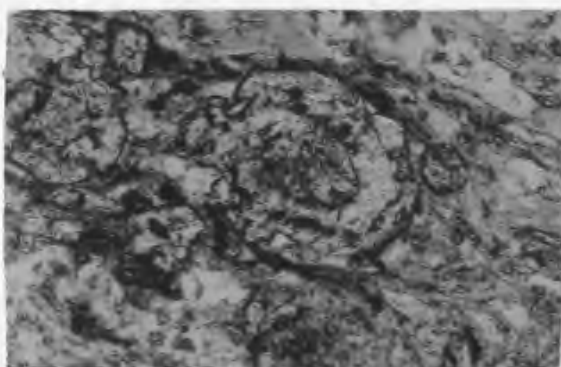
PLATE 5-3 A) Pressure shadows of fibrous carbonate around pyrite grain. This section is 1.25 mm across.

B) Spessartine garnet in graphitic schist of the Windsor Point group. The garnet is pre to syntectonic with respect to the deformation. This section is about 1.25 mm across.

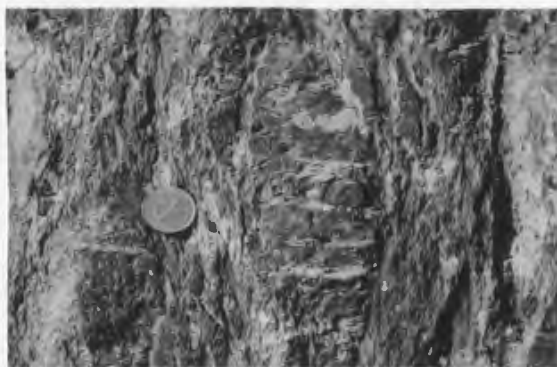
C) Quartz-filled tension gashes cutting felsic volcanic clast in the Little Barachois Formation. See Figure 21 for stereographic projections of the orientations of these veins.



A



B



C



## WINDSOR POINT GROUP IGNIMBRITE

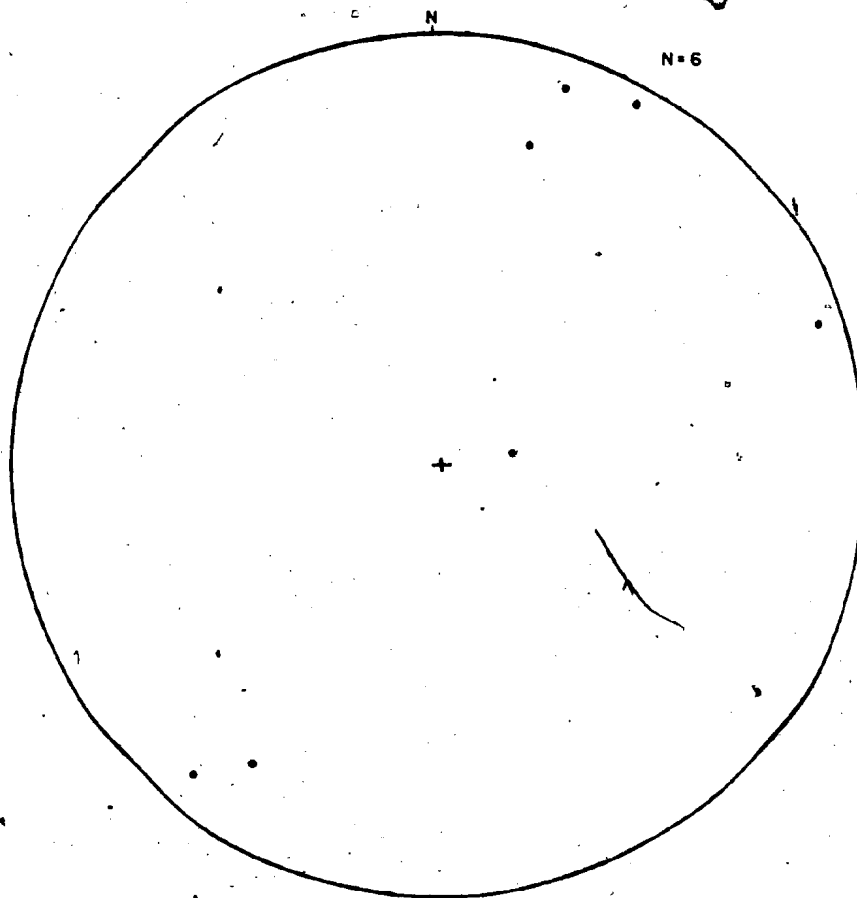


Figure 27 Equal area stereographic projections of poles to tension gashes in the ignimbritic member of the Windsor Point Group.

The shear/fractures were probably developed late in the deformational history of the fault zone (ie. they disrupt S1 and S2) and may have even post-dated the main events. However there is no evidence (or reason to assume) that the stress directions changed drastically after the initiation of the fault zone.

The planar tension-like quartz veins that cut the post-tectonic Isle aux Morts Brook Granite (Figure 28) are also orientated perpendicular to the  $\sigma_3$  direction, indicating that the stress regime existed until at least the D4 deformational event.

#### 5.6 Discussion

Brown (1973a, 1973b, 1976a, and 1977) described the Cape Ray Fault Zone as an example of an Ordovician cryptic suture between continental basement of the eastern margin of the Iapetus Ocean (ie. the Port aux Basques Complex) and the Long Range Gneiss/Cape Ray Granite. The Long Range Gneiss was correlated with the Grenvillean inlier which forms the backbone of Newfoundland's Great Northern Peninsula and was thus presumed to be continental basement to the western margin of the Iapetus.

The zone of juxtaposition of these two dominantly gneissic terranes along the Cape Ray Fault, according to Brown (1977), was partially obscured on the coast by the

## ISLE AUX MORTS BROOK GRANITE

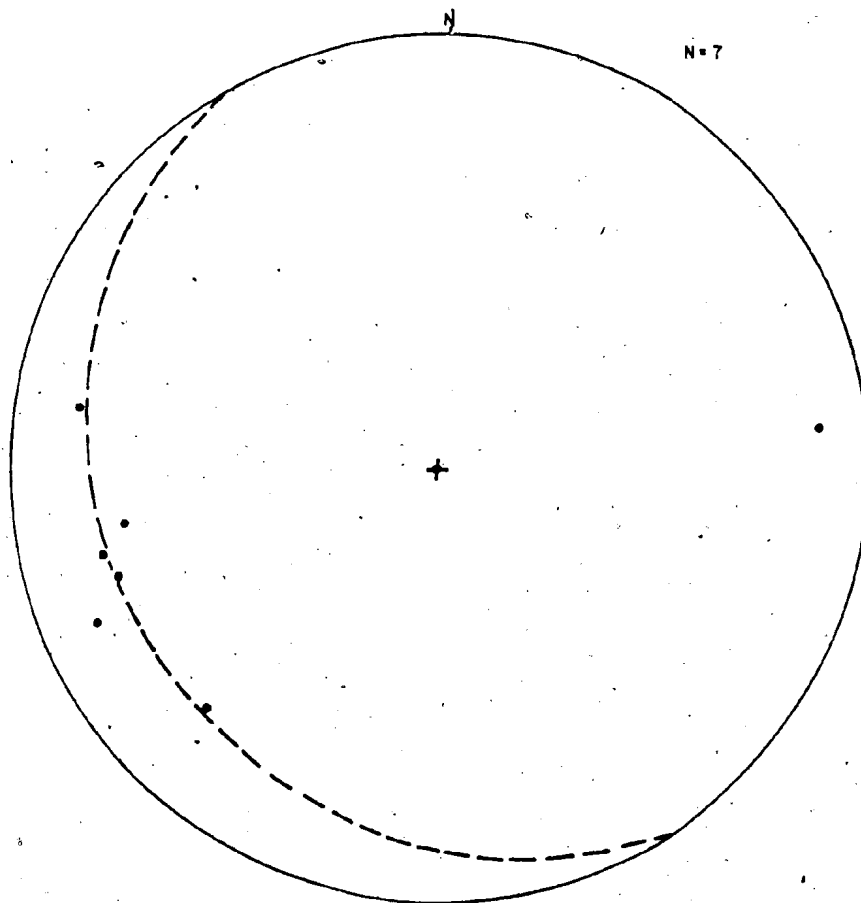


Figure 28 Equal area stereographic projections to poles to quartz veins in the Isle aux Morts Brook Granite.

Windsor Point Group. Inland, however, where he suggested that the Windsor Point Group thins, Brown described the contact between these two terranes as a "1 km wide zone of mylonitization" (Brown, 1977, p.5). He further suggested that the Windsor Point Group was deposited along the trace of the Cape Ray Fault during exhumation of the fault. The Windsor Point Group was therefore defined as post-dating and overlying the mylonite zone which marked the actual physical point of closure and juxtaposition of the opposed continental margins.

Brown (1976a and 1977) stated that the Long Range Mafic/Ultramafic Complex ophiolites were thrust onto rocks of the Long Range Gneiss, and represent remnants of the Iapetus oceanic crust which were "obducted" unto the western continental margin of this paleo-ocean.

In addition to the four deformational events which affected the Port aux Basques Complex, Brown (1975) described the evidence for three deformations in the Cape Ray Complex which pre-dated deposition of the Windsor Point Group. He did not correlate deformational events between the Port aux Basques and Cape Ray Complexes, and did not describe any structural history for the development of the mylonites other than the presence of the mylonite itself. Reactivation of the Cape Ray Fault after deposition of the Windsor Point Group supposedly produced a three-phase deformational history which affected both the Windsor Point

Group and the mylonite.

Based on the structural and geochronological data described above, concepts regarding the structural evolution and origin of the Cape Ray Fault need to be revised. A number of factors indicate that the fault does not represent a cryptic suture. These include:

1) There is no overall gneissic (or Grenvillian) fabric developed within the tonalite phase of the Cape Ray Granite. The tonalitic and megacrystic phases have the same structural history (ie. Brown's Long Range Gneiss and Cape Ray Granite have similar structural fabrics).

2) The Long Range Mafic/Ultramafic Complex ophiolites were intruded by the tonalite, and not thrust (or obducted) unto the tonalite. Assuming a Cambrian to Ordovician age for the ophiolites (the commonly accepted age of ocean floor in the Iapetus Ocean (eg. Williams, 1979)), the tonalite must be post-Ordovician, and therefore cannot represent the Grenvillian western continental margin of the Iapetus Ocean.

3) Within the Cape Ray Fault Zone three deformational events overprinted all lithological units. Since it appears that the Cape Ray Granite was deformed at the same time as the Windsor Point Group, there is no structural evidence contained within the Cape Ray Granite of a pre-Windsor Point Group collision of this complex with the Port aux Basques Complex (ie. no evidence of a

pre-Windsor Point Group mylonitization).

4) Brown (1975) stated that three deformational events overprinted the tonalitic Long Range Gneiss; of these D1, was seen as a fabric in xenoliths, and D2 and D3 overprinted both the gneiss and Brown's Cape Ray Granite. If the tonalite developed a gneissic fabric due to the Grenvillian orogeny (ie. 1100 to 900 Ma), how could the Cape Ray Granite be equivalently deformed unless it was also Grenvillian? Brown (1975), however, described the Cape Ray Granite as Devonian or earlier in age, not Precambrian. Thus there are internal contradictions in Brown's original definition of the western continental margin of the Iapetus.

#### 5.7 The New Interpretation

The geochronological evidence in this study has shown that the age of deformation in the Cape Ray Fault Zone is much younger than the postulated Ordovician age of cryptic suturing advanced by Brown (1973). Deformation of the Windowglass Hill Granite was synchronous to that which affected other units in the fault zone. Since the Windowglass Hill Granite is  $369 \pm 12$  Ma old, the deformational events which affected the fault zone are post-Middle Devonian in age. Similarly, the Windsor Point Group ignimbrite, deformed by the same events and dated at

377±21 Ma, indicates a maximum age for the deformations of Late-Middle Devonian. These ages indicate that structural developments within the Cape Ray Fault Zone occurred over a relatively short time, were successive, and took place in the Late Devonian.

Goldstein (1982) described a somewhat similar mylonite zone in New England that was previously interpreted as a result of collisional suturing between an Avalonian basement and its overlying metamorphic rocks, but which was actually a result of Acadian decollement between basement and cover along a fold surface. According to Goldstein (1982, p.1400), the mylonites "must be interpreted as having a geologically brief life with one episode of motion, rather than a history of repeated motion during several deformational events".

Rather than representing highly deformed basement rocks juxtaposed by continental collision, the Cape Ray Fault Zone mylonites were developed along incipient structural inhomogeneities and they were derived from Windsor Point Group sedimentary rocks and Cape Ray Granite. Cobbold (1977) indicated that shear zones (or band-like deformation features) are usually coincident with zones of rheological differences (or compositional layering) within the host rock. The mylonites of the Cape Ray Fault Zone fit this model as they occur along a contact or within the layered Windsor Point Group.

The mylonites and thus the fault zone can be likened to a ductile shear zone in which deformation produced an extreme degree of grain-size reduction due to recrystallization relative to the enclosing rock (cf. Bell and Etheridge, 1973). Regional fault zones or lineaments have been described as similar large shear zone environments elsewhere, such as in Brittany (eg. Berthe et al., 1979, Gapais and Le Corre, 1980) and the Iberian Peninsula (Burg et al., 1981).

Wilkinson et al. (1975) described mylonite zones within the Moine Thrust of Scotland as shear zones. By studying the effects on worm burrows, they showed that the mylonites were developed as a result of simple shear. Bell (1978) showed that the Woodroffe Thrust mylonite of Australia was formed by deformation that was at least partly simple shear in nature. Since there was a rotational component to the deformation (ie. simple shear) which produced them, as shown by the oblique pressure shadows, the Cape Ray Fault Zone mylonites are the products of similar mechanisms in a shear zone-type environment.

The strike-slip nature of the movements on the Cape Ray Fault and the pattern of subsidiary faults are reminiscent of wrench fault-type environments (eg. as described by Reading, 1980). Chorlton (1982) has also described the northeastern Cape Ray Fault as a wrench fault.



The transition from ductile to brittle deformation in the fault zone (ie. D1-D3 to D4) is typical of long-lived fault systems (eg. Watterson, 1975; Grocott 1977). Sibson (1977) developed a two-layer model for fault systems in which brittle deformation generating random fabrics, occurs at high crustal levels, while the mylonites developed in the ductile regime 10-15 km below the crustal surface. However, the metamorphic assemblages associated with various structural elements have constrained the lithostatic pressure at which deformation of the Windsor Point Group rocks occurred, to  $< 3.5$  kb; therefore the Cape Ray Fault may not really be a direct analogue of deep-seated faults as the ductile deformation occurred at somewhat higher crustal levels.

### 5.8 Conclusions

The main conclusions to be drawn from the structural study are :

- (1) There is no evidence for the presence of Grenvillian gneiss in the Cape Ray Fault Zone of southwestern Newfoundland. The unit, which was described (Brown 1973, 1975) as a direct correlative of the Grenvillian gneiss underlying the Humber Zone (Williams *et al.* 1973; Williams, 1979), is actually a post-Ordovician tonalite. The tonalite is intrusive into overlying

ophiolite; it does not represent the footwall of an overlying thrust sheet.

(2) The Cape Ray Fault and its delineating mylonites are the products of intense localised ductile deformation. The mylonites were produced during the first phase of a three phase deformational episode which occurred post-370 Ma, and may have terminated pre-360 Ma (ie. Late Devonian- Early Carboniferous). A post-360 Ma reactivation of this fault system produced the last deformation and also the present expression of the fault. Rather than representing an Ordovician intercontinental cryptic suture, the fault zone is actually a large, sinistral shear zone or wrench-fault system produced by NE/SW directed compression during upper Paleozoic times.

## CHAPTER 6

### GEOCHEMISTRY

#### 6.1 Introduction

Concentrations of up to 34 elements including major and assorted trace elements and the rare earth elements, were determined for a series of samples from the different lithological units in the Cape Ray Fault Zone. Detailed descriptions of methods, precision and accuracy for the analytical methods are given in Appendix III and the data in Appendix IV. Average compositions are listed in Table IX.

The lithological units fall into three natural and logical subdivisions viz.; a) schistose meta-tuffaceous rocks, b) mafic volcanics and intrusives, and c) granites. Accordingly each group will be described in turn with respect to this subdivision. The geochemical studies were initiated to a) classify the various lithologic units, b) compare and contrast the units with each other and with other examples described in the literature, c) to determine petrogenetic models for the units, and d) ultimately to provide clues as to the origin of gold-bearing sulphide-quartz veins in these rocks. The major results of this study were discrimination of elemental differences

between wall rocks to the ore veins and other equivalent units with no relation to mineralization, and petrogenetic models for the various granitoids.

Sampling, though covering the entire fault zone, was concentrated in the northeastern edge of the map area in the immediate vicinity of the ore deposits. Samples designated PB- are portions of drill core that are exclusively of the Main Shear region south of the Isle aux Morts Brook.

#### 6.2 The Windsor Point Group

This unit is broken down into four main chemical groups viz.; 1) the rhyolites/ignimbrites of the Little Barachois Formation, 2) schists, 3) graphitic schists, and 4) wall rocks to the Main Shear Showings. The graphite schists are separated from the other schist units because they have a sedimentary protolith (vs. metatuff for the others) and because they are the most common ore host.

When comparing and contrasting the element distributions between these different groups, the role of prograde and retrograde metamorphism must be addressed. In general other studies have demonstrated that in any given lithological sequence (except calc-silicate) which has undergone progressive regional metamorphism without the influence of a fluid from some external source (ie.

metasomatism), changes in elemental abundances are minor and are attributable to loss of volatiles. Shaw (1956), in one of the first such studies, demonstrated that in the pelitic Littleton Formation of New Hampshire, the only chemical changes from a chlorite through to a sillimanite zone, were loss of H<sub>2</sub>O, Cu and Ni, and a slight increase in CaO, Na<sub>2</sub>O, Li and Pb. Ferry (1981) observed that minor Na<sub>2</sub>O depletion had occurred during metamorphism of graphitic rocks in Maine. Tanner and Miller (1980) found that in Moian calc-silicate pods, Na<sub>2</sub>O and K<sub>2</sub>O were released during prograde metamorphism, but when the pods were included in the overall metamorphic sequence, such changes were imperceptible. Ferry (1982) also found that carbonates lose Na<sub>2</sub>O and K<sub>2</sub>O during metamorphism, but the surrounding pelitic country rocks, when examined for changes in element concentrations, showed no statistically significant differences with the grade of metamorphism. Therefore when comparing the groups, emphasis for examining differences should be placed on elements other than Na<sub>2</sub>O and K<sub>2</sub>O.

According to the listed means and standard deviations in Table IX, the only group which is distinctly different from the others on the basis of its chemistry is the Little Barachois Formation (and felsic tuff - listed as WPGIG). This unit is more siliceous (has relatively higher SiO<sub>2</sub>, K<sub>2</sub>O, Rb, La, Ce and correspondingly lower TiO<sub>2</sub>, Fe<sub>2</sub>O<sub>3</sub>, MnO,

TABLE IXa Average Chemical Compositions of Schists

	CHL/SC		SER/SC		SE/CL		CL/BIO		WPGIG		GAST		WAL/RX		PAB/GN		WPGQ		PABQ	
	MEAN	S.D.	MEAN	S.D.	MEAN	S.D.	MEAN	S.D.	MEAN	S.D.	MEAN	S.D.	MEAN	S.D.	MEAN	S.D.	MEAN	S.D.	MEAN	S.D.
	n=3	n=3	n=3	n=3	n=11	n=11	n=3	n=3	n=22	n=22	n=12	n=12	n=11	n=11	n=7	n=7	n=3	n=3	n=3	n=3
wt %																				
SiO <sub>2</sub>	58.8	51	67.7	74.5	70.3	78	66	59.5	73.7	23.9	66.5	66.6	59.2	38.1	68.7	9.3	56	10.5	59.9	9.1
TiO <sub>2</sub>	1.1	1.1	0.58	0.72	0.69	1.2	0.64	0.60	0.34	0.26	0.51	0.57	1.0	1.1	0.61	0.28	1.5	0.82	0.38	0.1
Al <sub>2</sub> O <sub>3</sub>	14.3	12.5	12.9	14.4	13.3	15.1	14.9	13.8	12.8	4.4	14.97	15.2	15.8	10.3	14.9	4.2	15.5	1.6	15.3	3.4
Fe <sub>2</sub> O <sub>3</sub>	9.7	8.9	6.3	7.4	5.5	7.3	6.97	6.8	2.7	2.1	7.4	7.6	11.0	7.8	5.9	2.98	9.9	4.3	9.4	4
MnO	0.17	0.16	0.18	0.23	0.10	0.14	0.11	0.11	0.04	0.05	0.25	0.32	0.27	0.24	0.11	0.05	0.23	0.18	0.18	0.08
MgO	4.97	4.9	1.97	2.4	2.4	3.3	2.2	2.3	0.65	1.24	2.9	3.0	3.1	2.3	2.7	1.6	5.4	2.8	6.1	3.4
CaO	6.4	5.8	5.3	6.9	2.5	4.6	3.1	3.2	1.5	3.7	3.4	4.8	4.9	4.6	2.1	2.0	6.5	4.8	2.6	1.1
Na <sub>2</sub> O	3.7	3.4	1.7	2.2	3.5	4.4	2.8	3.6	2.1	2.1	0.65	1.0	0.95	1.3	3.0	1.9	3.6	1.8	4.8	1.5
K <sub>2</sub> O	0.61	0.93	2.98	3.3	1.6	1.9	2.1	2.0	6.0	3.5	3.4	3.5	3.3	2.4	1.9	2.1	1.3	1.2	1.1	0.8
P <sub>2</sub> O <sub>5</sub>	0.18	0.20	0.21	0.28	0.13	0.20	0.14	0.16	0.12	0.16	0.24	0.32	0.42	0.44	0.15	0.09	0.19	0.05	0.05	0.05
ppm	n=12	n=12	n=12	n=12	n=12	n=12	n=12	n=12	n=12	n=12	n=12	n=12	n=12	n=12	n=12	n=12	n=12	n=12	n=12	n=12
Pb	9	5	758	1709	11	13	28	37	52	153	62	96	103	172	14	10	11	8	21	11
Th	3	4	11	5	8	5	10	6	14	9	9	7	8	8	9	8	6	6	5	8
U	2	3	4	3	3	3	12	21	4	4	8	5	8	18	1	2	5	3	2	3
Rb	16	29	93	39	51	34	55	24	132	62	108	35	93	35	66	83	42	35	31	19
Sr	211	139	119	85	106	69	131	74	59	71	89	62	96	56	165	122	144	54	168	88
Y	39	32	52	31	41	19	52	30	67	41	38	9	55	24	34	11	35	17	26	9
Zr	146	124	304	79	185	108	265	173	285	174	135	30	186	98	213	143	152	41	99	57
Nb	12	19	15	6	12	8	17	10	18	10	15	5	14	9	10	6	11	4	6	5
Zn	93	39	270	403	84	49	80	37	69	153	123	104	125	63	57	19	110	37	72	24
Cu	85	101	363	720	54	66	95	181	19	13	93	54	73	81	66	63	30	22	334	630
Ni	26	40	16	14	16	19	22	20	11	19	48	28	13	16	10	8	39	45	21	17
La	25	13	38	8	28	16	44	11	47	24	39	12	40	22	34	16	27	10	20	9
Ba	171	130	1055	1313	551	455	1899	2249	742	461	861	1193	443	221	940	561	424	474	456	327
V	256	138	78	28	198	165	149	121	40	42	320	182	505	1004	170	95	240	102	192	119
Co	48	31	63	15	58	29	81	25	87	39	69	22	70	34	68	28	52	24	38	19
Cr	69	94	63	47	46	47	47	43	16	38	78	27	46	74	48	37	118	112	133	161
Ga	17	7	29	32	16	6	15	5	15	8	19	7	23	9	18	10	19	3	15	5
Au	9	14	31	36	8	14	17	25	14	13	87	99	48	55	14	28	8	10	20	14
wt %																				
S	0.36	0.74	0.81	2.18	0.08	0.12	0.82	2.11	0.01	0.02	0.86	0.96	0.14	0.19	0.15	0.19	0.02	0.03	1.64	1.4
CO <sub>2</sub>	0.37	0.59	0.9	1.01	0.47	0.60	0.32	0.42	0.20	0.3	1.73	1.12	1.61	1.89	0.22	0.34	0.04	0.06	0.21	0.33
ppb	n=7	n=7	n=7	n=7	n=7	n=7	n=7	n=7	n=7	n=7	n=7	n=7	n=7	n=7	n=7	n=7	n=7	n=7	n=7	n=7
Au	15.8	21.8	7.9	17.8	6.8	12.4	7.5	14.4	3.1	3.1	7.1	7.7	6.1	6.5	3.7	5.3	11.5	21.1	8.9	8.3
Ag	33.3	44.6	217	497	35.4	61.9	58	109	526	1886	74.2	115	779	2297	3000	6936	38.4	44.3	55.3	63.3

Abbreviations: CHL/SC = chlorite schist; SER/SC = sericite schist; SE/CL = sericite-chlorite schist; CL/BIO = chlorite-biotite schist; WPGIG = ignimbrites, rhyolites and felsic tuffs; GAST = graphite schist; WAL/RX = wall rock to Main Shear Showing; PAB/GN = Port aux Basques Gneiss; WPGQ = problematical Windsor Point Group rocks; PABQ = problematical Port aux Basques Gneiss rocks. S.D. = Standard Deviation

\*Iron analysed as total Fe<sub>2</sub>O<sub>3</sub>.

	PABM		LRM/UM		GABB		GABMG		BSC/DK		DIOR		GRANO	
	MEAN	S.D.	MEAN	S.D.	MEAN	S.D.	MEAN	S.D.	MEAN	S.D.	MEAN	S.D.	MEAN	S.D.
wt %														
SiO <sub>2</sub>	50.0	7.1	49.3	22.1	51.7	38.4	48.6	1.5	47.9	2.2	57.3	3.7	67.9	107
TiO <sub>2</sub>	0.83	0.38	0.28	0.17	1.9	1.68	1.8	0.65	3.0	0.28	1.7	0.52	0.88	0.77
Al <sub>2</sub> O <sub>3</sub>	17.3	1.4	16.0	9.9	15.2	11.3	14.7	1.5	13.9	0.41	14.0	0.67	15.8	24.9
Fe <sub>2</sub> O <sub>3</sub>	11.8	2.6	9.0	4.7	12.8	9.9	12.7	1.9	15.3	1.3	13.0	1.9	4.2	7.2
MnO	0.35	0.13	0.17	0.10	0.20	0.16	0.21	0.03	0.24	0.04	0.18	0.05	0.10	0.17
MgO	6.7	1.4	11.6	7.3	6.2	4.9	8.3	3.4	6.2	0.84	2.7	0.75	1.2	2.0
CaO	9.8	5.3	11.6	5.7	7.0	5.7	9.8	1.5	9.3	0.56	6.2	4.3	2.6	4.2
Na <sub>2</sub> O	2.6	1.6	0.82	0.56	4.1	3.3	3.1	0.82	2.8	0.17	3.6	2.0	6.0	9.5
K <sub>2</sub> O	0.39	0.26	1.2	0.90	0.59	0.51	0.66	0.79	0.71	0.56	0.59	0.54	1.6	2.5
P <sub>2</sub> O <sub>5</sub>	0.22	0.05	0.08	0.05	0.30	0.55	0.19	0.09	0.59	0.01	0.78	0.27	0.17	0.27
ppm														
Pb	20	11	11	5	11	19	7	4	15	12	30	20	11	9
Th	1	2	2	4	2	3	3	3	2	3	5	3	6	4
U	2	3	2	4	2	3	3	4	2	3	3	3	4	3
Rb	8	6	42	25	29	29	17	14	19	16	24	22	42	20
Sr	326	194	341	264	142	65	223	57	400	74	322	309	253	143
Y	28	11	9	7	51	20	38	14	55	0.7	72	40	50	30
Zr	127	17	31	13	134	60	119	59	219	2	285	51	223	80
Nb	6	3	3	0.49	9	4	8	5	13	0	22	6	10	7
Zn	108	21	78	19	102	21	94	26	132	11	114	69	77	29
Cu	55	47	35	46	30	23	49	36	29	8	15	17	30	29
Ni	54	42	129	104	18	28	55	27	48	12	0	0	0.3	0.7
La	22	6	21	7	31	14	22	13	44	2	49	12	31	13
Ba	246	250	448	360	240	167	97	49	274	175	201	120	427	247
V	284	78	130	71	336	158	304	130	399	50	157	58	117	103
Co	46	7	23	10	60	27	38	23	94	4	107	16	68	26
Cr	158	104	284	267	84	122	166	120	34	21	2	3	5	7
Ga	18	5	12	3	19	2	15	4	20	5	26	3	20	5
As	11	10	6	9	11	16	14	11	22	4	65	61	6	7
wt %														
S	0.06	0.09	0.01	0.01	0.03	0.04	0.07	0.12	0.16	0.06	1.1	1.5	0.09	0.14
CO <sub>2</sub>	0.13	0.28	--	--	0.61	0.91	0.06	0.16	--	--	0.69	0.76	0.38	1.01
ppb														
Au	11	12.4	6	9	3.8	6.1	5.5	8.5	1.8	0.4	8.7	8.2	--	--
Ag	54	52	25	29	42	81.6	59.8	78.1	38	36.8	62.6	61.2	--	--

Abbreviations: PABM = amphibolite interbands of the Port aux Basques Gneiss; LRM/UM = Long Range Mafic/Ultramafic Complex; GABB = gabbro; GABMG = gabbro along the southern margin of the Windowless Hill Granite; BSC/DK = basaltic dykes; DIOR = diorite; GRANO = granodiorite. S.D. = Standard Deviation  
 \*Iron analysed as total Fe<sub>2</sub>O<sub>3</sub> \*\*Not Determined

TABLE IXb Average Chemical Composition of Mafic Rocks

	PABGRN		CRG-TN		CRG-MX		RD-R-G		WGMGR		STG		IAM/OR	
	MEAN	S.D.	MEAN	S.D.	MEAN	S.D.	MEAN	S.D.	MEAN	S.D.	MEAN	S.D.	MEAN	S.D.
wt %	n=7	n=7	n=11	n=11	n=7	n=7	n=7	n=7	n=11	n=11	n=11	n=11	n=7	n=7
SiO <sub>2</sub>	75.2	2.03	70.3	1.9	84.2	3.94	74.5	2.1	77.5	30.2	75.2	1.6	75.2	1.8
TiO <sub>2</sub>	0.21	0.12	0.53	0.11	0.48	0.38	0.11	0.08	0.11	0.09	0.15	0.10	0.18	0.12
Al <sub>2</sub> O <sub>3</sub>	13.4	0.97	14.3	0.51	16.4	1.01	14.2	0.82	13.1	5.5	13.8	0.73	13.7	0.60
Fe <sub>2</sub> O <sub>3</sub>	1.6	0.64	3.9	1.2	4.7	3.0	1.0	0.65	1.0	0.78	0.89	0.43	1.1	0.48
MnO	0.04	0.02	0.08	0.02	0.08	0.03	0.03	0.02	0.02	0.01	0.03	0.02	0.04	0.02
MgO	0.40	0.27	1.8	0.71	2.0	1.6	0.32	0.27	0.16	0.26	0.26	0.16	0.28	0.21
CaO	1.2	0.60	3.9	1.31	3.3	1.4	1.7	0.67	0.71	0.85	0.87	0.46	0.74	0.34
Na <sub>2</sub> O	4.4	0.88	3.1	0.61	4.0	2.4	4.1	0.59	5.6	3.1	4.3	1.1	4.9	0.21
K <sub>2</sub> O	3.6	2.04	1.9	1.4	3.8	3.1	4.0	0.84	1.7	2.1	4.5	2.1	4.7	0.35
P <sub>2</sub> O <sub>5</sub>	0.04	0.02	0.12	5.6	0.27	0.20	0.03	0.03	0.02	0.03	0.04	0.03	0.06	0.03
ppm														
Pb	15	7	12	9	23	49	37	11	452	977	38	13	44	6
Th	17	10	4	4	31	25	4		21	10	25	14	35	5
U	1	1	2	1	3	3	2	2	4	4	7	6	12	4
Rb	82	66	59	35	108	84	111	21	49	66	229	122	338	68
Sr	138	80	386	253	809	809	432	270	118	142	115	80	80	65
Y	43	28	21	20	23	14	9	2	100	53	31	25	41	13
Zr	152	83	151	67	288	177	75	45	266	91	81	55	309	40
Nb	31	24	8	6	17	13	10	2	30	33	20	15	32	14
Zn	31	12	55	11	78	86	23	9	230	825	31	12	36	9
Cu	14	8	25	11	18	13	11	1	163	419	17	6	18	8
Ni	0	0	5	6	14	11	0	0	8	10	15	16	16	30
La	45	21	27	20	78	84	25	19	38	31	23	22	31	13
Ba	741	738	836	682	1549	1382	1308	951	223	227	306	179	279	216
V	21	18	104	51	88	84	13	11	11	18	14	8	17	8
Co	78	30	49	32	123	66	45	27	76	61	51	41	58	32
Cr	15	11	12	8	10	10	8	6	3	4	6	5	9	9
Ga	20	3	15	2	13	8	16	2	25	19	16	7	24	3
As	7	7	3	4	18	10	0	0	22	22	0.4	0.8	5	5
wt %														
S	0.003	0.004	0.02	0.006	0.007	0.009	0	0	0.37	0.75	0.07	0.24	0	0
CO <sub>2</sub>	--**	--	0.16	0.23	--	--	--	--	0.29	0.51	--	--	--	--
ppb														
Au	2.9	2.9	5.4	7.9	8.1	13.8	4.1	6.9	177.2	729.4	7	8.2	3.7	2.7
Ag	141.8	170	51.2	63.2	180.2	808	541	1011	2381	5639	259	339	64	53

Abbreviations: PABGRN - Port aux Basques Granite; CRG-TN - tonalitic Cape Ray Granite; CRG-MX - megacrystic Cape Ray Granite; RD-R-G - Red Rocks Granite; WGMGR - Windoglass Hill Granite; STG - Strawberry Granite; IAM/OR - Isle-aux-Morts Brook Granite. S.D. - Standard Deviation  
 \*Iron analysed as total Fe<sub>2</sub>O<sub>3</sub> \*\* Not Determined

TABLE IXc Average Chemical Compositions of Granitoids



MgO, CaO, Cr, V, Ni and Cu concentrations) than the other units. It also contains lower S.

The other members of the Windsor Point Group have slightly different chemical compositions as would be expected from their differing micaceous mineralogies. For instance the chlorite schists (CHL/SC) have lower concentrations of the felsic/silicic elements (eg. SiO<sub>2</sub>, Rb, Th, U etc.) and higher concentrations of those elements found in mafic mineralogies (eg. CaO, Fe<sub>2</sub>O<sub>3</sub>, Al<sub>2</sub>O<sub>3</sub>, Sr etc.) when compared with the other subgroupings. The chemistry of the CHL/SC is typical of that in a basic tuff.

The SER/SC (sericite schist) and SE/CL (sericite-chlorite schist) rocks are deformed and altered tuffs (SE/CL samples have a significant mafic component also, and thus may be somewhat transitional between SER/SC and CHL/SC), but they have only minor resemblances with the WPGIG samples (the major differences being higher Ce, La, Rb, K<sub>2</sub>O; and lower Cr, V, Cu, Zn, Sr, MgO, MnO, Fe<sub>2</sub>O<sub>3</sub> and TiO<sub>2</sub> in the WPGIG samples).

The CL/BIO (chlorite-biotite schist) samples are quite different from those of the CHL/SC group (ie. lower Fe<sub>2</sub>O<sub>3</sub>, TiO<sub>2</sub>, MgO, CaO, Sr, and higher concentrations of K<sub>2</sub>O, Th, U, Zr, La, etc.) and do not represent metamorphosed equivalents. The CL/BIO samples are similar to the more felsic groups SE/CL and SER/SC.

The samples of graphitic schist (GAST) are chemically

similar to the more felsic groups except for elevated MnO, K<sub>2</sub>O and Rb contents, and lower Na<sub>2</sub>O and Zr. The GAST are also distinctive because of consistently higher CO<sub>2</sub>, S and As values (ie. the means are not influenced by a few high values, but are representative of overall higher values).

WAL/RX (schist wall rock to ore veins) samples, which are actually representatives of the other groups occurring in contact with the products of hydrothermal fluids (ie. veins), have higher Al<sub>2</sub>O<sub>3</sub>, Fe<sub>2</sub>O<sub>3</sub> and P<sub>2</sub>O<sub>5</sub>, and higher background Zn concentrations than all the other units. K<sub>2</sub>O, MnO and CO<sub>2</sub> are similar to the values in the GAST samples, and TiO<sub>2</sub> is similar to that in the CHL/SC samples (ie. higher than in the other groups). The relatively enriched concentrations of the so-called immobile elements (Al<sub>2</sub>O<sub>3</sub>, P<sub>2</sub>O<sub>5</sub>, MnO and TiO<sub>2</sub>) may result from leaching of the other elements from the rock by hydrothermal fluids, and the higher K<sub>2</sub>O contents may indicate that the fluids were potassic. In terms of the ore elements (Cu, Pb, Zn, Au, Ag, S) there are no greater average concentrations than those in rocks from the non-ore areas.

#### 6.2.1 The ignimbrite/ felsic tuff (WPGIG)

The felsic nature of these rocks is reflected in the relatively high SiO<sub>2</sub>, Zr and alkalis, and the low Fe<sub>2</sub>O<sub>3</sub>, MgO and Sr contents. In most samples from the Little

Barachois Formation some sort of potash metasomatism is indicated as  $K_2O$  is greater than combined  $CaO$  and  $Na_2O$ . The potash enrichment is illustrated in Figure 29 where the WPGIG samples are plotted according to Ewart's (1979) classification scheme for modern-day rhyolite and related volcanic rocks. In the majority of WPGIG samples, the  $K_2O$  contents are higher than most modern rhyolites (though they do plot in the high  $SiO_2$  rhyolitic portions).

Rb/Sr ratios are usually  $>1$  and there are typically low concentrations of Cu, Ni, Cr, V, Ga and As in these samples. Mean Zn and Pb concentrations (69 and 52 ppm respectively) are positively skewed by sample PB27-32 which has anomalously high values (relative to the other samples) for these elements (i.e. 774 and 765 ppm). This sample is cut by numerous quartz veins (they account for 5-10% of the sample) that contain disseminated pyrite, chalcopyrite and galena.

The range of chemical compositions in these felsic volcanic rocks most strongly parallel those of orogenic terranes, such as the Southwestern United States, as defined by Ewart's (1979) compilations. According to Ewart's classification, the ignimbrites and felsic tuffs of the Windsor Point Group are potassic rhyolites of orogenic associations, and are not typical of the calc-alkali salic magmas associated with island arcs. Correlation coefficients calculated for these samples indicate

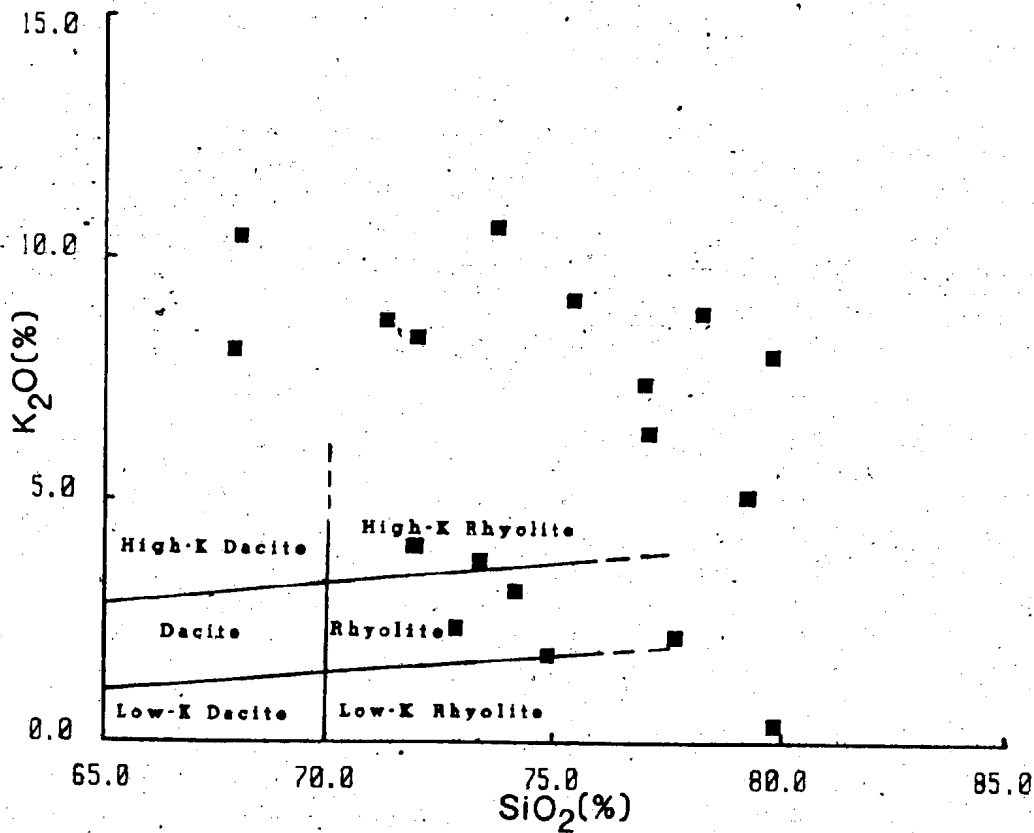


Figure 29.  $K_2O$  vs.  $SiO_2$  diagram for Windsor Point Group ignimbritic rhyolites. Ewart's (1979) fields for silicic volcanic series are superimposed to show the potassic nature of these rocks.

statistically significant (at 98% probability) positive correlations of K2O with Rb, La, Ce; Zr with Nb, La, Ce; and Nb with Ce, which are also typical of high-K silicic magmas (Ewart, 1979).

#### 6.2.1.1 Rare Earth Elements in the Little Barachois Formation

Figure 30 has the chondrite-normalized REE patterns for three samples of the Little Barachois Formation. WPG-4 and 80-135 are from the basal ignimbrite (WPG-4 on the coast, 80-135 near Dog Pond), and 79-15 is of a quartz feldspar porphyry dyke near Red Rocks Point. These three samples were pre-selected (on the basis of La/Y ratios as analysed by the routine XRF trace element methods) to provide a spectrum of REE concentrations in this unit; the maximum La/Y ratio of the WPG/IG group occurs in sample WPG-4, the median of 80-135, and the minimum in 79-15. (In all following REE analyses, see Appendix IV, a similar selection process was used).

The patterns are typical of felsic rocks (eg. Hanson, 1980) in that the most elevated chondrite-normalized ratios occur in the light rare earths (LREE's) with a gradual decrease towards the heavy rare earths (HREE's). There is no appreciable Eu anomaly in either sample and the HREE's have a slight concave upward pattern in 80-135 and WPG-4.

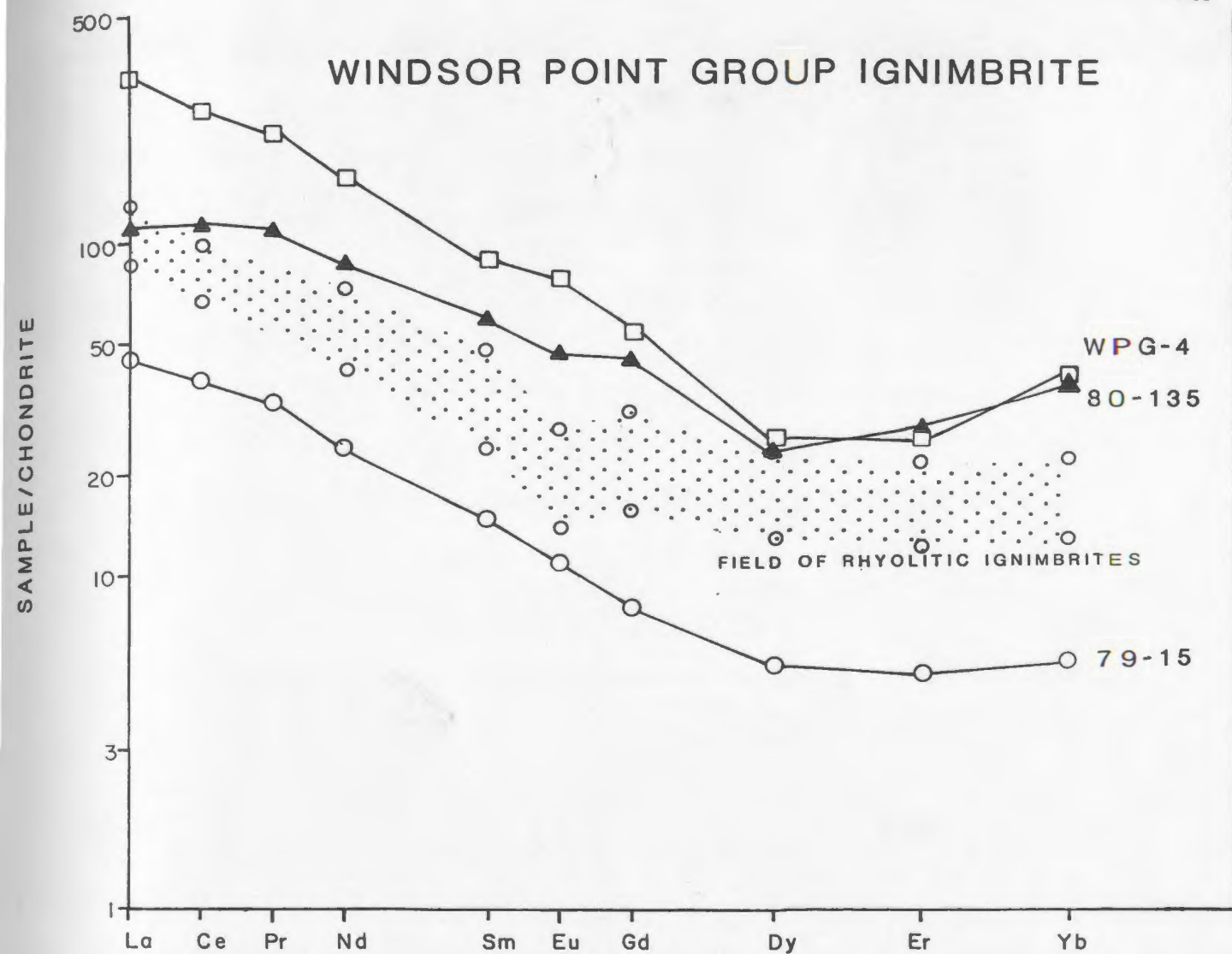


Figure 30 Chondrite-normalized REE patterns for the Windsor Point Group ignimbritic rhyolites. Normalized to chondrite values from Taylor and Gorton (1977); the field of rhyolitic ignimbrites is from Cameron and Hanson (1982).

The actual concentrations of LREE's ( $>300\times$  chondrite)\* in WPG-4 are rather elevated when compared to the REE data of Cameron and Hanson (1982) for Mexican rhyolitic-ignimbrites (plotted on Figure 30 for comparison).

Sample 79-15 differs from the others in that the REE concentrations are from  $30\times$  to  $250\times$  less abundant. 79-15 also differs in having more  $MgO$ ,  $CaO$ ,  $Na_2O$ ,  $Sr$ ,  $Pb$ ,  $Zn$  and  $Ag$ , and less  $SiO_2$ ,  $K_2O$ ,  $Rb$  and  $Zr$  than the other two samples. In other words, sample 79-15 is distinctly more mafic, which may explain its lower REE concentrations, as mafic rocks generally contain lower concentrations of REE's than more felsic rocks (eg. Hanson, 1980).

Sample 80-135 has a depleted LREE content, but similar HREE's when compared with WPG-4. The two samples are chemically alike except for slightly elevated  $SiO_2$ ,  $MgO$ ,  $Zr$  and  $Ba$ , and lesser  $CaO$  and  $Y$  in 80-135. Secondary sericite is more abundant in 80-135 and this sample is also more deformed than WPG-4. It has been suggested that LREE's are mobile during weathering processes (eg. Ludden and Thompson, 1979), and in hydrothermal meteoric fluid systems, REE's are often mobile (eg. Taylor and Fryer 1980, 1982, in press). The depletion of LREE's in 80-135 is probably a function of later superimposed alteration.

The lack of either a positive or negative Eu anomaly indicates that feldspar concentrations in these felsic volcanics do not differ greatly from their source rocks

(since residual feldspar would create a negative anomaly in a daughter melt, and total incorporation of feldspar into the melt would lead to a positive Eu anomaly). Residual apatite and/or sphene would lead to a positive Eu anomaly (or at least partial nullification of a feldspar-induced negative anomaly), but these phases would also lower the overall, and especially the middle, REE contents of the melts. Residual hornblende would yield positive Eu anomalies and  $LREE's > HREE's$  in resulting melts. However the very strong enrichment of  $LREE's$  (and also  $HREE's$ ) in these felsic volcanics cannot be accounted for by these mechanisms.

Similar upward concavities in REE patterns have been reported elsewhere by Taylor et al. (1981) in peralkaline granites, where the concavity is attributed to HREE complexing (and thus concentration) by  $CO_2$ -bearing fluids, possibly derived from the mantle. These same fluids were also implicated as the alkali carriers which produced the alkalic nature of the granites. This model is applicable to the WPGIG samples beyond just REE patterns as the felsic volcanics have undergone a definite  $R_{20}$  enrichment. The mantle origin for such alkali-bearing fluids is not demonstrable in the case of these felsic volcanics as their initial  $^{87}Sr/^{86}Sr$  ratio is 0.7087 which generally indicates melt origin in the crust (eg. Shibata and Ishihara, 1979).

Most recent work (eg. Hildreth, 1979 and Bacon et al.



1982) attribute the voluminous Tertiary to Recent acid volcanism (ignimbrites and rhyolites) of the SW United States to partial melting of pre-existing continental crust. The enriched REE patterns, high initial Sr ratios, peraluminous and silicious nature of the Windsor Point Group felsic volcanics suggest that they resulted from partial melting of continental crust. The similar geochemical compositions of these volcanics and those in the SW United States, and dissimilarity with acid volcanics formed in other environments (eg. island arcs), is a further indication of crustal melt origin.

Hildreth (1981) presented a wide-ranging model for the origin of such felsic volcanic terranes which involved the introduction of mafic melts from the mantle, or lower crust, into mid to upper levels of the crust where they caused widespread partial melting of crustal material and production of the voluminous silicic melts. According to this model, mafic melts would usually not mix with the felsic melts, yielding bimodal assemblages. The rare mafic selvages with the quartz feldspar porphyry dykes (eg. sample 79-166) may therefore represent exotic remnants of a deep seated mafic melting source (these selvages are extremely altered to carbonate).

Such an origin for the Windsor Point Group ignimbritic/rhyolitic rocks is diametrically opposed to the supposed island arc origin for the felsic volcanic rocks

within the older Bay du Nord Group (as suggested by Chorlton, 1982). In this latter case, the volcanics may be derived by either fractional crystallization from a mafic source, or partial melting of thin continental crust material (with a strong mafic overprint). Rare earth element data for the genetic evaluation of the Bay du Nord Group are unavailable at present.

#### 6.2.2 Graphite Schist (GAST)

In order to examine the graphite content of these schists, a sample was analysed by gas chromatography. Figure 31 is the chromatogram for sample (80-611), a wall rock to quartz veins in the Main Shear showing. The chromatogram shows that though there are no light hydrocarbons, there is a definite heavy hydrocarbon content. Identifiable peaks are C17, pristane, C18, phytane, C19 and C20. Powell and McKirdy (1973) state that both pristane and phytane are produced during diagenetic alteration of chlorophyll, while Tissot and Welte (1978) say these hydrocarbons occur within zooplankton also. Whatever the actual source of the hydrocarbons, their presence definitely indicates the graphite within the schists is organically-derived.

Tissot and Welte (1978) distinguish three stages of hydrocarbon development, viz.: diagenesis, catagenesis and

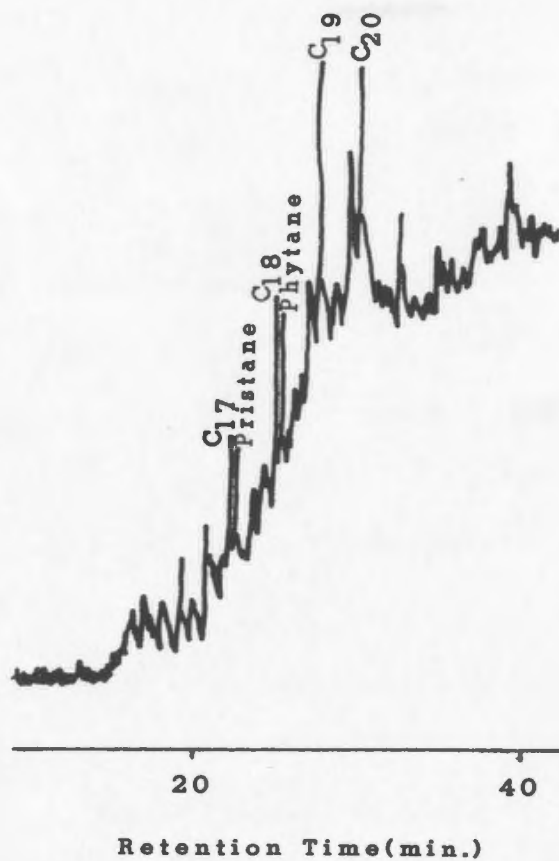


Figure 31 Gas chromatogram for sample 80-611. The peaks for C<sub>17</sub>, C<sub>18</sub>, C<sub>19</sub>, C<sub>20</sub>, phytane and pristane are defined.

metagenesis. Metagenesis is directly comparable to greenschist/amphibolite facies metamorphism, and catagenesis occurs at temperatures of 50-150°C and pressures of 0.3-1.5 kb. They also state that in strongly altered oils, pristane and phytane are important remnants of hydrocarbons, but even they disappear at higher grades of alteration. The occurrence of pristane and phytane in the graphite schists (and absence of lighter hydrocarbons) is therefore indicative of strong alteration (in terms of hydrocarbons) of up to greenschist facies.

Cannon and Cassou (1980) show that with increasing maturity (*ie.* heat and pressure), the pristane/C17 ratio of hydrocarbons decreases and that pristane/C17 ratios of < 1 are representative of mature material. Sample 80-611 has a pristane/C17 ratio of about 0.88 further indicating the altered nature of the graphitic schists.

Pristane to phytane ratios have been used by various authors (eg. Powell and McKirdy, 1973 ; Cannon and Cassou, 1980) to indicate the paleoenvironment, since ratios of < 1.5 indicate derivation from marine shale (or reducing) environments, and those of > 1.5 are indicative of terrestrial origin for hydrocarbons. Using this classification with the ratios in sample 80-611, it would seem the hydrocarbons developed in a reducing environment (*ie.* ratio of 0.8), though the state of alteration of the schists may have affected the ratios. This concurs with

the widespread presence of pyrite in the schists (ie. also indicative of a reducing environment).

Samples of this rock type (graphite schist) have moderate to high SiO<sub>2</sub> contents, averaging 66.5 wt. %, and TiO<sub>2</sub>, Al<sub>2</sub>O<sub>3</sub>, Fe<sub>2</sub>O<sub>3</sub> and CaO contents are unremarkable, if slightly higher than in the other schists. MnO, S and C have the highest concentrations in this schist type (reflected in the spessartine, pyrite and graphite mineral components). K<sub>2</sub>O generally has higher concentrations than CaO, and Na<sub>2</sub>O are much lower than these other two. The high K<sub>2</sub>O contents are due to the common presence of sericite in these schists. Rb is typically greater than Sr. U and Th contents are variable (ranging from 1-17 ppm and 0-20 ppm respectively), though the mean contents are about equal. Zr, Nb, La and Ga are low. Ba, As, Zn, Pb and Cu have some very high values (in pyritiferous samples) which distort the mean.

There is one major grouping of elements according to correlation coefficients, defined by positive inter-correlations of Al<sub>2</sub>O<sub>3</sub>, Fe<sub>2</sub>O<sub>3</sub>, K<sub>2</sub>O, Rb, Nb, Ba, Cr, Ga, La, Ce, Th. Though there are some similarities in geochemical properties between these elements, their total congregation is not explicable on these grounds alone. In detailed factor analyses of elemental distributions in Upper Viséan sedimentary rocks, Hirst and Kaye (1971) were able to define a 'clay factor' based on positive loadings

of  $TiO_2$ ,  $Al_2O_3$ ,  $Fe_2O_3$ ,  $MgO$ ,  $Na_2O$ ,  $K_2O$ ,  $H_2O$ , C, B, F, V, Cr, Ni, Cu, Rb and Ba. Similarly Cosgrove (1973) defined a clay factor in Permian red beds consisting of  $TiO_2$ ,  $Al_2O_3$ ,  $Fe_2O_3$ , LOI., V, Ga, Rb, Y, Nb, La, Nd and Th. And Stephens et al. (1975) classified a clay group of elements, Al-K-Ti-Rb-Zr in graptolitic shales of Scotland. The common correlation of these same elements in the GAST samples is therefore indicative of a clay component to the rocks and is also further evidence of the sedimentary nature of at least part of the Windsor Point Group.

In a study of Devonian black shales from the southern United States, Leventhal and Hosterman (1982) found that; a) organic C correlated with (and controls) the distribution of U and Mo, and b) both S and organic C control Hg, As, Zn and Ni. Though there is a comparable sulphide phase in graphitic schists of the Windsor Point Group, there is no significant correlation of U with anything (let alone  $CO_2$ ).

#### 6.2.2.1 Rare Earth Elements in Windsor Point Group Schists

The chondrite-normalized REE patterns for two samples of graphitic schist (samples PB38-42 and 80-38) and one sample of sericite-chlorite (79-78C) are illustrated in Figure 32. Also illustrated on this diagram are the

## WINDSOR POINT GROUP SCHIST

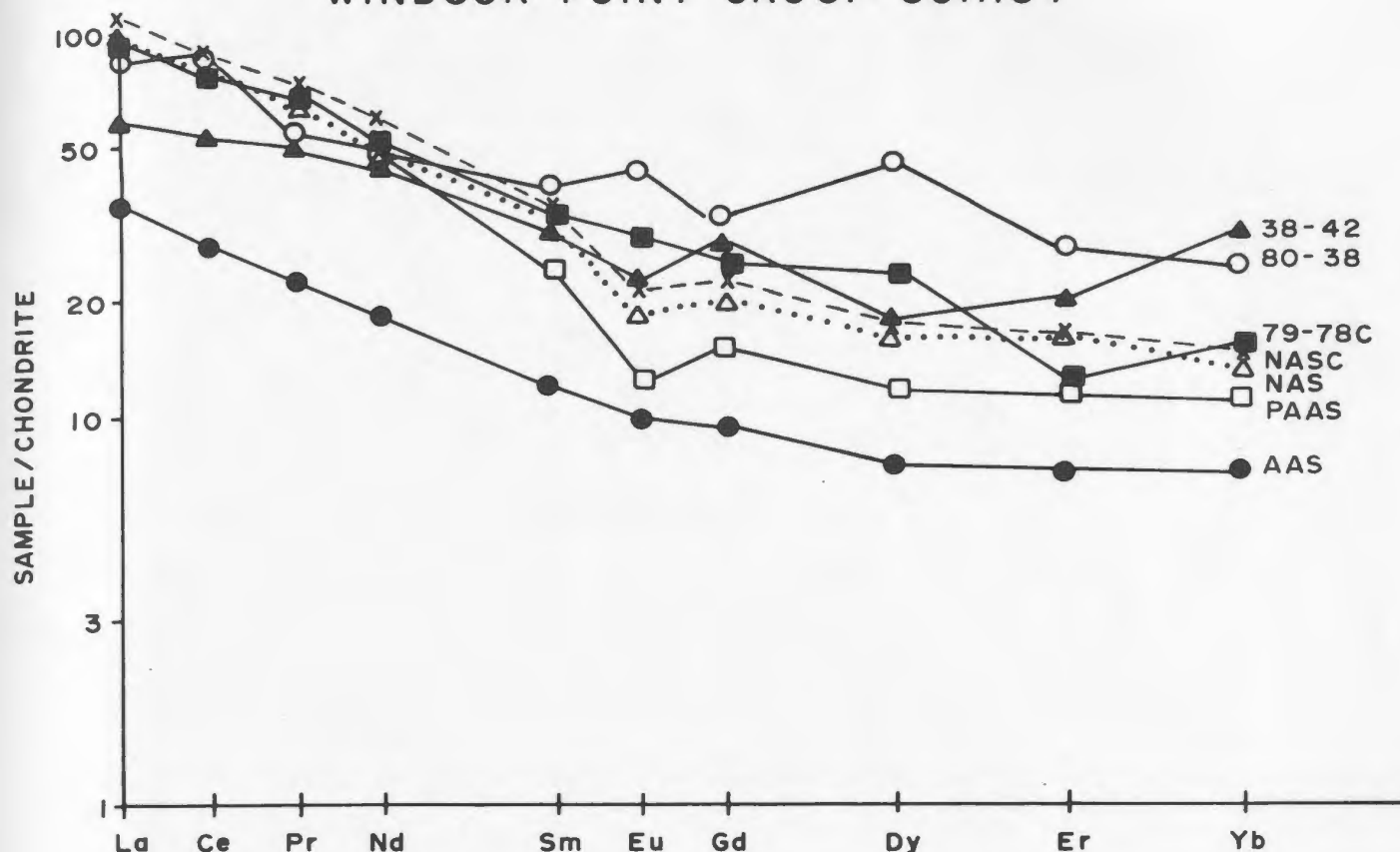


Figure 32 Chondrite-normalized REE patterns for samples of the Windsor Point Group schist. Samples 80-38 and 38-42 are of graphitic schist, and 79-78C is of sericite/chlorite schist. Average North American Shale (NAS) and North American Shale Composite (NASC) patterns as outlined, are from Haskin *et al.* (1968). Pattern of average Archean Australian sediment (AAS) is from Taylor and McLennan (1981) and the pattern of the average Post-Archean Australian sediment is from Nance and Taylor (1977). Normalized to Taylor and Gorton's (1977) chondrite values.

patterns for the average North American Shale (NAS), average North American Shale Composite (NASC), both from Haskin *et al.* (1968), average Archean sedimentary rock from Australia (AAS- from Taylor and McLennan, 1981) and average post-Archean Australian Shale (PAAS- from Nance and Taylor, 1977).

The REE pattern from the SE/CL sample (79-78C) is similar to those of NAS, NASC and PAAS. The only important difference is its lack of a negative Eu anomaly, however since this sediment is derived from volcanic debris that is apparently of close-to-source derivation, detrital feldspar grains are incorporated in the sediment without significant weathering or breakdown. Since Eu is usually enriched in feldspars (relative to the rocks), the lack of weathering preserves the whole-rock pattern without a Eu depletion. There is also a slight dip in Er concentration which is most likely a result of analytical error.

Both graphite schist samples have patterns that are roughly comparable to those of NAS, NASC and PAAS, however the LREE contents are lower, and the decrease in HREE's is not as pronounced (*ie.* the schist samples have flatter curves). PB38-42 most closely parallels the average patterns, but Yb (and Er to a lesser extent) are significantly enriched yielding the 'saucer-shaped' pattern as seen in the WPGIG samples. This increase in HREE may also be attributable to alteration by carbonate-bearing



hydrothermal fluids, since carbonate is visible both petrographically and chemically in the schists and if the HREE's are complexed by carbonate, precipitation of carbonate in the GAST samples would yield increased HREE contents. Sample 80-38 has a small positive Eu anomaly which, as in the SE/C1 sample, probably indicates the presence of fresh volcanic detritus in the protolith of the schist.

### 6.3 Port aux Basques Gneiss (PAB/GN)

The Port aux Basques Gneiss samples rank as felsic/siliceous rocks with element contents equivalent to the sericitic schist groups. When compared to the other units, PAB/GN has the lowest CaO, U, Nb, Zn, Ni and Au concentrations. The low U content (average 1 ppm) is surprising, as 15 km to the northwest, this gneiss unit contains anomalously high concentrations of U (average 9 ppm) related to biotite (Taylor, 1970).

The mean contents of SiO<sub>2</sub>, K<sub>2</sub>O, CO<sub>2</sub>, Ba, Ce and Ag (see Table IX) in this unit are somewhat elevated, those of TiO<sub>2</sub>, Fe<sub>2</sub>O<sub>3</sub>, MnO, CaO, Na<sub>2</sub>O, P<sub>2</sub>O<sub>5</sub>, Sr, Y, Zr, Zn, Cu, La, V, Cr, Ga, As and S are moderate, and MgO, Pb, Th, U, Rb, Nb, Ni, and Au are low. Generally the gneisses are albitic (Na<sub>2</sub>O > CaO > K<sub>2</sub>O), but two samples (79-77 and 80-105) are potassic (ie. K<sub>2</sub>O > Na<sub>2</sub>O > CaO). Sr is greater than Rb in the

albitized samples, but Sr is less than Rb in the potassic samples. The albitic samples are generally more silicious than the potassic ones.

#### 6.3.1 Rare Earth Elements in the Port aux Basques Gneiss

Chondrite-normalized REE patterns for samples from the Port aux Basques Gneiss are illustrated in Figure 33, along with the patterns for two average pelitic schists from Maine (after Cullers et al., 1974). Cullers et al. found that REE contents are not affected by the grade of metamorphism and in the case of their samples from Maine, the chondrite-normalized patterns resemble those of NASC (they also state that the LREE depletion in the Perry Mountain Formation samples is due to weathering and/or differential clay contents within the parental sediment prior to diagenesis - current hypotheses would include hydrothermal alteration as a possible cause).

In the Port aux Basques Gneiss samples, the negative Eu anomaly is barely perceptible. Aside from this minor difference, samples 79-170S (from the garnet zone) and 80-47G (from the beginning of the staurolite zone) are similar (and unremarkable) when compared to the Cullers et al. (1974) averages (and thus when compared to the NASC average). In general the chondrite-normalized patterns for

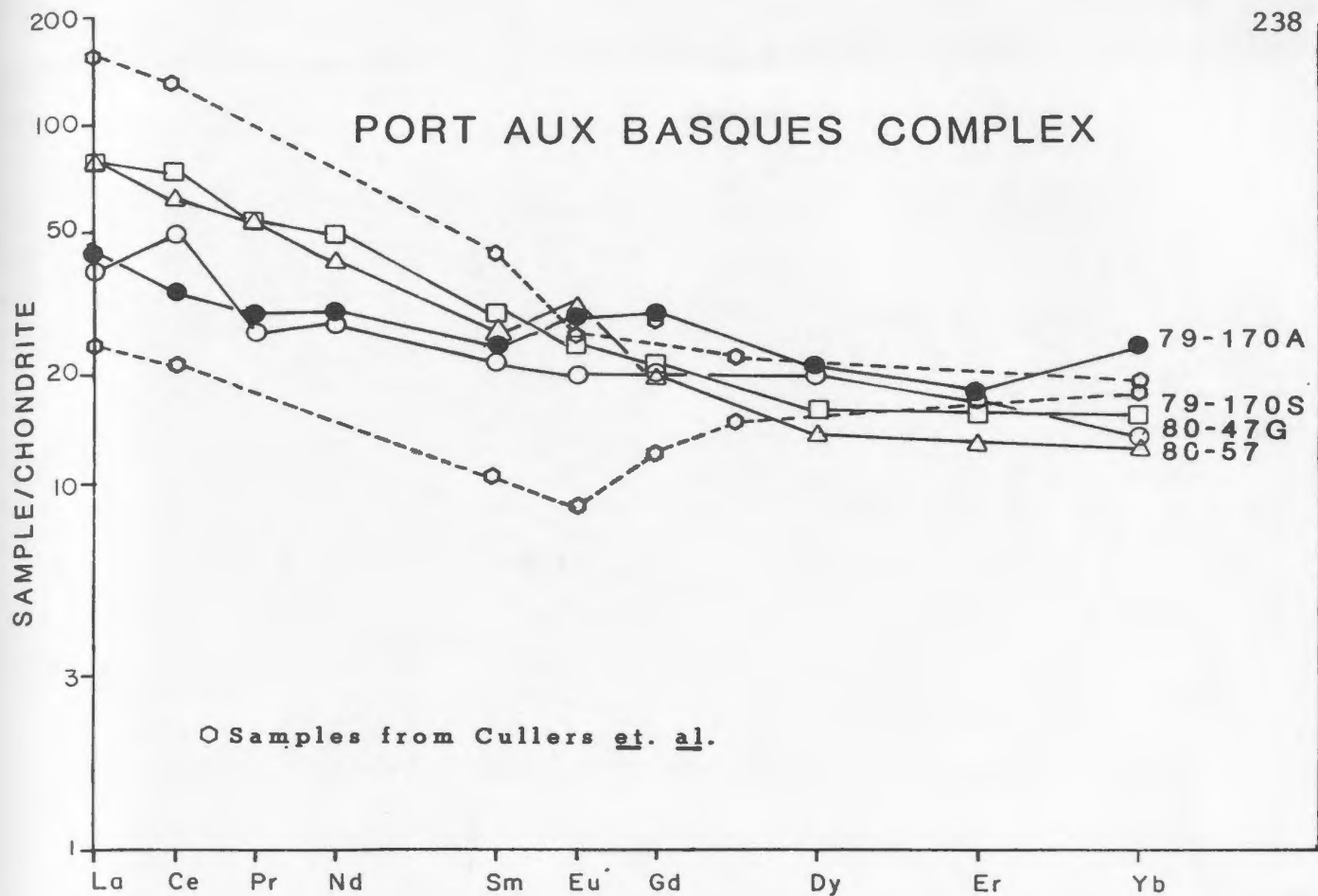


Figure 33 Chondrite-normalized REE patterns for the Port aux Basques Complex. Samples 79-170S and 80-47G are from gneiss bands, 79-170A and 80-57 are from amphibolite bands. Two patterns for pelitic schists from Maine (after Cullers *et al.*, 1974) are illustrated for comparison. Normalized to Taylor and Gorton's (1977) data.

the gneiss are similar to those in the Windsor Point Group except they don't have a positive Eu anomaly, and have lower HREE contents, yet higher or equivalent LREE contents (thus the 'hydrothermal LREE depletion' has not affected the gneiss).

### 6.3.2 Origin of the gneiss

The very aluminous nature of the gneiss, as shown by the amount and size of garnet, staurolite, kyanite and sillimanite porphyroblasts, suggests it is a para-gneiss (ie. derived from sedimentary rocks). Using Shaw's (1972) Discriminant Function 4 (ie.  $DF = -39.49 + 0.42SiO_2 + 0.3Fe_2O_3 + 0.89MgO + 1.53CaO + 0.58Na_2O + 2.07K_2O - 0.037Cr + 0.005V - 0.027Ni - 0.001Sr$ ) to distinguish between gneisses of sedimentary vs. igneous origin; four of seven (or 57 %) Port aux Basques Gneiss samples correspond to a sedimentary origin, while in the Windsor Point Group all units indicate an igneous origin, with the lowest average in the CL/BIO samples where 60 % of the samples classify as igneous. According to the same function, all the Port aux Basques Granite samples are of igneous origin and three of four PABQ samples (ie. retrogressed gneissic samples near the Windsor Point Group contact) indicate a sedimentary origin.

### 6.3.3 Comparison with other Port aux Basques and Bay du Nord Analyses

Taylor (1970) analysed the Fe<sub>2</sub>O<sub>3</sub> and trace element contents in gneiss samples from the Brinex Lake area, 15 km east of the northern edge of this map area. These gneiss samples are from small, scattered pendants within the mass of the Rose Blanche Granite. Compared with the gneiss samples from this study (see Table IX), Taylor's (Table X) rocks have much higher Fe<sub>2</sub>O<sub>3</sub> (~ 2x) and elevated Pb, U, Zn, Cu, Ni and Ba contents. The Ag content (1.25 ppm) is lower than the average of the PAB/GN samples (3 ppm), but this latter high average is influenced by a single sample, which when removed from consideration, produces a much lower mean (47 ppb). The elevation of metal concentrations in Taylor's samples may have been caused by hydrothermal fluids emanating from the enclosing granite/granodiorite.

Table X contains averages for the Billiards Brook Group, Bay du Nord Group (Piglet Brook Rhyolite, Dolman Formation, and Bay du Nord felsite bands), and La Poile Group (Hawks Nest Porphyry, Georges Brook Upper Crystal Tuff, Georges Brook felsic flows, Georges Brook fine-grained tuffs, and Georges Brook mafic flow) as reported by Chorlton (1980b). The Billiards Brook basalt flows, supposed Windsor Point Group equivalents, are distinctly different from any unit of this group. Indeed,

TABLE X Average Chemical Data from Taylor (1970) and Chorlton (1980b)

Taylor (1970)		Chorlton (1980b)								
	MEAN	(1)	(2)	(3)	(4)	(5)	(6)	(7)	(8)	(9)
wt %	MEAN	MEAN	MEAN	MEAN	MEAN	MEAN	MEAN	MEAN	MEAN	MEAN
SiO <sub>2</sub>	--*	45.97	75.83	63.98	67.20	75.85	66.28	70.10	71.80	49.47
TiO <sub>2</sub>	--	1.55	0.08	0.56	0.58	0.24	0.64	0.43	0.49	1.01
Al <sub>2</sub> O <sub>3</sub>	--	15.58	13.25	14.57	14.54	12.86	14.77	13.95	14.00	16.60
Fe <sub>2</sub> O <sub>3</sub> **	10.13	10.33	0.90	3.15	3.97	2.00	4.21	3.27	2.92	9.97
MnO	0.10	0.23	0.06	0.07	0.08	0.04	0.08	0.09	0.08	0.19
MgO	--	8.16	0.14	1.22	1.11	0.34	1.36	1.18	0.93	8.23
CaO	--	8.94	0.50	2.02	2.19	0.46	2.69	1.81	1.38	8.07
Na <sub>2</sub> O	--	2.89	3.51	3.40	3.36	3.87	3.20	3.11	3.85	2.63
K <sub>2</sub> O	--	0.87	5.08	4.57	4.38	3.11	4.25	3.71	2.79	1.32
P <sub>2</sub> O <sub>5</sub>	--	0.31	0.04	0.14	0.19	0.02	0.15	0.13	0.16	0.19
L.O.I.*	--	4.37	0.64	0.89	2.12	0.89	2.1	1.44	1.27	3.57
ppm										
Pb	57	49	37	31	20	23	20	24	15	11
Th	--	--	--	--	--	--	--	--	--	--
U	9	--	--	--	--	--	--	--	--	--
Rb	--	22	232	188	194	115	180	142	93	30
Sr	--	422	72	174	152	63	171	156	134	268
Y	--	27	36	32	50	36	35	29	27	21
Zr	--	147	109	204	226	210	234	220	190	115
Nb	--	6	19	13	13	11	13	14	11	8
Zn	109	516	34	67	71	31	72	72	90	107
Cu	169	40	6	13	16	12	12	22	8	51
Ni	43	112	9	13	11	6	12	10	15	72
La	--	15	35	44	55	--	49	40	40	20
Ba	1223	214	385	855	823	493	815	744	668	285
V	---	240	4	62	58	23	85	57	55	229
Co	--	19	69	81	96	--	90	77	80	35
Cr	--	201	3	22	22	14	29	24	26	174
Ga	--	23	17	20	19	19	19	18	19	17
Ag	1.25	--	--	--	--	--	--	--	--	--

UNITS: (1) = Billiards Brook Basalt Flows; (2) = Piglet Brook Rhyolite; (3) = Delman Formation; (4) = Hawks Nest Porphyry; (5) = Bay du Nord felsite bands; (6) = Georges Brook Upper Crystal Tuff; (7) = Georges Brook felsic flows; (8) = Georges Brook fine-grained tuffs; (9) Georges Brook mafic flows

\*Not Determined \*\*Iron reported as total Fe<sub>2</sub>O<sub>3</sub> L.O.I. = Loss on Ignition

the Bay du Nord/La Poile Groups, which Chorlton (1982) has attempted to correlate with the Port aux Basques Gneiss, have distinct chemical differences from all the groups analysed in this thesis, notwithstanding their wide range of compositions; MnO, CaO, Zn, Cu, V and Cr are depleted, and K<sub>2</sub>O, Rb and occasionally La are elevated in Chorlton's samples with respect to samples in this study.

#### 6.3.4 Contact Zone Windsor Point Group (WPGQ) and Port aux Basques Gneiss (PABQ)

These samples are those which ~~could~~ not be classified into either the Windsor Point Group or Port aux Basques Complex because of deformational and metamorphic overprinting. In terms of their chemistries they are unremarkable and could fit into most of the other lithologic units. The WPGQ samples are chemically similar to those of the CHL/SC but are the most mafic of all groups. They have a basaltic-type value for mean SiO<sub>2</sub> and correspondingly enriched TiO<sub>2</sub>, Al<sub>2</sub>O<sub>3</sub>, Fe<sub>2</sub>O<sub>3</sub> and CaO. In the trace elements, the means of Pb, Th, Rb, Sr, Y, Zr, Cu, Ni, La, Ga, As and S are comparatively depleted while those of Cr, Ce, V and Zn are slightly elevated. The PABQ samples also have relatively low SiO<sub>2</sub> and elevated Fe<sub>2</sub>O<sub>3</sub>, MgO, Na<sub>2</sub>O and CaO contents. There is more Na<sub>2</sub>O than CaO, more CaO than K<sub>2</sub>O, and more Sr than Rb. The concentrations

of Ni, La, Ga, As and P2O5 are low, while those of S, CO2, Cr, Ce, V, Ba and Cu are elevated. Cu and S are very high (1279 ppm and 1.38% respectively in sample 79-72, and 3.37% S in 79-151) in samples which contain abundant disseminated pyrite.

#### 6.4 Wall Rock to the Main Shear mineralization (WAL/RX)

Samples which make up this group are graphite, sericite-chlorite and chlorite schists. The mean SiO2 content is low, but the means for TiO2, Al2O3, Fe2O3, MnO and P2O5 are elevated. According to mean values, CaO is greater than K2O, however the CaO is influenced by samples that are especially carbonate-rich (eg. 80-61H, 80-61L, 80-64, 80-66A and PB38-36), and which constitute ~ 50% of the group, in other samples, K2O is greater than CaO. Na2O is much lower than the values of K2O and CaO. Mean Rb and Sr contents are approximately equal, but in individual samples the Rb/Sr ratio is either >1 or <1. In the trace elements, contents of Zr, Nb, Ni, Ga, U, Th, Rb and Sr are low. Mean Y, Cu, Zn, La, Ce, Cr and Au values are unremarkable. Mean Ba, Ag, As, Pb and V values are high but are influenced by single sample values. In sample 80-61I, Pb (542 ppm), Zn (197 ppm), Cu (206 ppm), U (74 ppm), Ba (801 ppm), Cr (284 ppm), V (4103 ppm), Ni (51 ppm), As (221 ppm) and Ag (7100 ppb) are very elevated in



concentration. This particular sample (from the heart of the Main Shear) has slight quartz veining and is extensively brecciated. Similar high values of Zn in samples 80-61H and 80-182, Pb and Ag in 80-65C, and Pb, Zn, Cu and S in PB38-5B distort the generally lower contents in the other samples.

The mean composition of the WAL/RX samples has a barely perceptible elevation in metal contents when compared to the means of groups from unmineralized areas. However, certain samples within the WAL/RX group have great enrichments, indicating mineralization was selectively superimposed on its wall rocks. The maximum observed metal enrichments in the WAL/RX samples will now be examined.

#### 6.4.1 Volume/Density Relationships

When examining a suite of rocks for the relative loss or gain of selected elements, it is not sufficient to just examine the quoted analytical figures for differences, since the elements are measured and reported in percentage terms and this can yield erroneous results because great changes in a single significant component can mask, or produce apparent, changes in other elements. The only way to determine fundamental physical-chemical changes is to add volume/density relations as intensive variables to the ratioed chemical data. The mathematical formulation for

these inter-relationships (after Gresens, 1967; Babcock, 1973) is:

$$\chi_n = 100 [f_v (g_B/g_A) C_n^B - C_n^A]$$

where  $\chi$  = amount of change (gain or loss) in component  $n$  (eg. SiO<sub>2</sub>, etc.);  $f_v$  = volume factor;  $g_B$  and  $g_A$  = specific gravity of rock samples B and A;  $C_n^B$  and  $C_n^A$  = amount of component  $n$  in samples B and A.

Which simplifies to:

$$f_v = \chi_n \left( \frac{g_A}{g_B C_n^B} \right) + \frac{C_n^A}{(g_A/g_B C_n^B)}$$

(or a straight line equation). In ideal systems the volume factor will become evident as  $f_v$  values should converge (ie. when  $\chi$  is set to equal 0) to approximately the same value (Gresens, 1967), indicating that the components, for which these volume factors have been defined, were immobile during transition from one rock to another.

In order to examine the elemental gains or losses in the WAL/RX samples produced by the Au-bearing hydrothermal fluids, volume factors for each sample were defined using the equations as above. The WAL/RX samples are made up of rock types represented by the other schist groups. Three  $f_v$ 's were determined for each WAL/RX sample that contained the full range of chemical analyses, using the samples with maximum and minimum specific gravities in the relevant non-wall rock unit and the mean hydrated chemical composition of this non-wall rock unit (+ mean S.G.); eg. to determine the three  $f_v$ 's for WAL/RX sample PB28-13,

which is SER/SC, was compared with sample 79-137, which has the highest S.G. in unit SER/SC; with sample 79-85, which has the lowest S.G. in SER/SC; and finally with the hydrated mean of SER/SC (+ mean S.G. of 2.62). Three  $fv$ 's were calculated to give the maximum range of possible changes, because none of the WAL/RX samples is in actual contact (or even near) non-wall rock samples, and the chemical data described above shows that there are wide compositional variations between samples in any given group. The sample names and S.G.'s used in the calculations are given in Table XI.

When these  $fv$ 's were calculated, there was no significant convergence of values, indicative of the wide intra-group chemical variations, so  $Al_2O_3$  was arbitrarily defined as having been immobile to the hydrothermal fluids. (This is not necessarily correct, but as shown by numerous authors (eg. Gresens, 1967; Hynes, 1980; Kerrich and Fyfe, 1981; Ferry, 1982; Strong, 1982), it is the one oxide (element) that has consistently proved immobile, or least mobile). The  $fv$  value from  $Al_2O_3$  was then used to solve the  $fv$  equations for all the other components (elements) so that gains and/or losses of each was determined. The supposition of  $Al_2O_3$ -immobility was further substantiated in these determinations as it was found that compositions of other typically immobile elements, eg.  $TiO_2$ ,  $MnO$ , etc., were relatively unchanged.

TABLE XI Samples and Specific Gravities for Volume/Density Calculations

<u>ROCK TYPE</u>	<u>Max. S.G.</u>	<u>Sample</u>	<u>Min. S.G.</u>	<u>Sample</u>	<u>Mean S.G.</u>
Graphite Schist	3.51	PB38-41	2.16	PB41-4	2.65
Sericite Schist	2.87	79-137	2.07	79-85	2.62
Sericite/chlorite Schist	2.74	PB38-8	2.29	PB4-2	2.54
Chlorite Schist	2.82	79-43	2.30	PB7-13	2.56

Most elements have erratic relationships indicating both losses and gains. The SE/CL-type WAL/RX samples have the widest variations but also the largest number of samples (5), whereas the sole SER/SC-type sample (PB28-13) shows the most consistent variations. There are, however, some elements which show consistent gain/loss relationships through the different rock types. In the major oxide elements K<sub>2</sub>O has been added to all WAL/RX's (except PB28-13, SER/SC, where there was minimal K<sub>2</sub>O removal) and Na<sub>2</sub>O and MgO have been removed. The chalcophile elements Pb (except in SER/SC), Ga and As (except in SER/SC) were gained by WAL/RX samples, whereas Ni was removed. La, Rb, Ce and CO<sub>2</sub> are similarly gained, and Cr seems to be lost (except in GAST).

In summary, the hydrothermal fluids which deposited the Au/sulphide -bearing quartz veins were potassic (rather than sodic) and produced minor chalcophile element haloes. Au is most often slightly depleted according to these data.

#### 6.4.2 Rare Earth Elements in wall rock samples

The chondrite-normalized REE patterns for five wall rock samples (80-61H, 80-61I, 80-65C, 80-66A and PB38-36) are illustrated on Figure 34 (along with NAS, NASC, PAAS and AAS). All five wall rock samples have much flatter patterns than those of the averages, with lower LREE's and

## WALL ROCKS

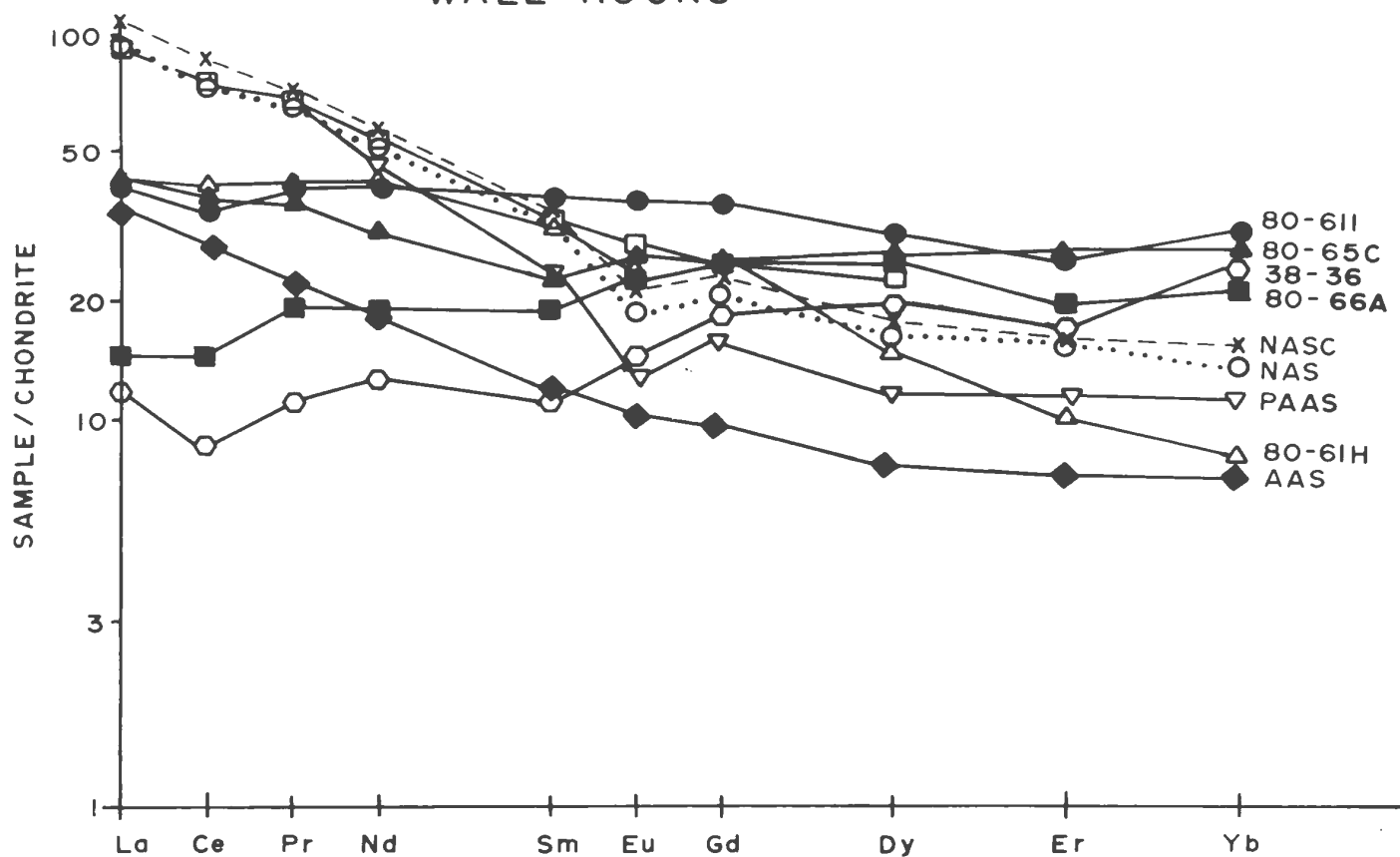


Figure 34 Chondrite-normalized REE patterns for wall rocks to the Main Shear Showing. Also outlined are patterns of NAS, NASC, AAS, and PAAS (see caption Figure 32 for details).

higher HREE's (except 80-61H). There is either a normal Eu distribution or a positive Eu anomaly (except 80-61H which has a very small negative anomaly), again unlike the average patterns (*ie.* they have negative Eu anomalies).

Sample 80-61I has a depleted LREE and equivalent HREE pattern when compared to the non-wall rock graphite schist samples 80-38 and PB38-42. Similarly in Figure 32, 80-65C and 80-66A, samples of SE/Cl, have depleted LREE's when compared to the non-wall rock SE/CL sample, 79-78C, and much higher HREE's. Samples PB38-36 and 80-61H are of CHL/SC and due to their more mafic composition would be expected to have a flatter REE pattern, however, PB38-36 is distinctly LREE-depleted. The LREE-depletions of these wall rocks are illustrated in Figure 35, where the REE concentrations are ratioed with respect to NAS.

Since these depleted patterns occur within those samples which obviously experienced a hydrothermal event (*ie.* deposition of gold/sulphide-bearing quartz veins), the depletion is logically attributable to alteration produced by hydrothermal overprinting. Flynn and Burnham (1978) suggest that REE's are complexed by F- and Cl-, but not by CO<sub>3</sub>-, and are preferentially partitioned into a fluid phase. They also show that Cl- more readily complexes LREE's. However in very high temperature experiments (1200-1300° C), Wendlandt and Harrison (1979) found that CO<sub>2</sub>-rich vapour is enriched in REE's, but

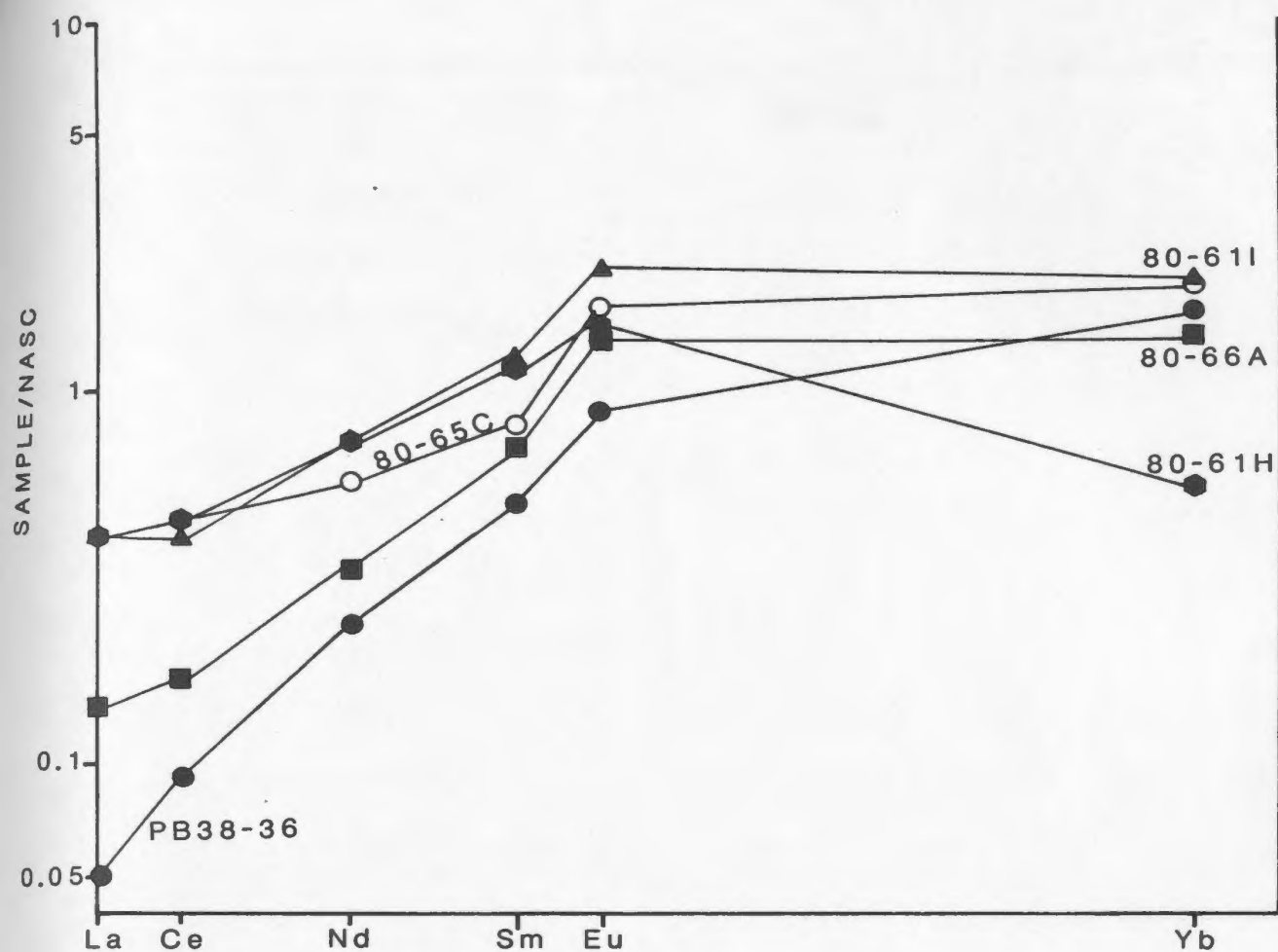


Figure 35 REE patterns for wall rocks to the Main Shear Showing ratioed to NASC values. North American Shale Composite (NASC) values from Haskin *et al.* (1968). The diagram illustrates the LREE-depletions found in the wall rocks.



especially LREE's.

Empirical evidence (eg. Kerrich and Fryer, 1979; Taylor and Fryer, 1980, 1982, and in press) is in agreement with the experimental studies of Flynn and Burnham (1978), and indicates that in mineral deposits, where the nature of the hydrothermal/mineralizing fluid is known (eg. porphyry copper, or sedimentary uranium deposits),  $\text{Cl}^-$  complexes and transports LREE's, while  $\text{F}^-$  and  $\text{CO}_3^-$  do the same for HREE's.  $\text{CO}_3^-$  could also complex and remove LREE's from some environments while precipitating HREE's, but the resulting REE patterns are quite distinctive as any semblance to a normal distribution is obliterated (eg. the gold deposit at the Dome Mine Ontario, Kerrich and Fryer (1979) and the uranium deposits in the Pine Creek Geosyncline, Australia, McLennan and Taylor (1979)).

It is therefore assumed that the LREE depletion visible in the WAL/RX samples is due to leaching by  $\text{Cl}^-$ -bearing hydrothermal fluids and these fluids were the same as those involved in precipitating the ore-bearing quartz veins. Samples 80-66A and 80-61H are carbonate-rich and some of the carbonate was obviously deposited from the same hydrothermal activity and thus some of the HREE's may have also been introduced into the wall rock. However, neither sample shows evidence for  $\text{CO}_3^-$  complexing having been important.

### 6.5 Comparison with the data of others

Devonian to Carboniferous rhyolites from Nova Scotia (Dostal et al., 1983) have very similar compositions to those of the WPGIG (see Table XII). The Nova Scotian rhyolites have lower CaO and P<sub>2</sub>O<sub>5</sub> concentrations than WPGIG, and elevated contents of Th, Sr (>2x), Zr (~2x), Nb and Ce. Geochemically the WPGIG samples are quite similar to the average analyses for four rhyolite sands (Webb and Potter, 1969, see Table XII) from Mexico, except the latter contains more TiO<sub>2</sub>, Al<sub>2</sub>O<sub>3</sub> and CO<sub>2</sub>, and less K<sub>2</sub>O than the WPGIG. The reason for comparing these two groups is that some of the WPGIG samples have undergone minor reworking as close-to-source volcanic debris.

Compared to Shaw's (1956) average composition of 155 pelitic schists (see Table XII), the Windsor Point Group schists are roughly similar except they have decidedly lower Al<sub>2</sub>O<sub>3</sub> concentrations and elevated CaO contents. The CO<sub>2</sub> values in Shaw's pelites are like those of the GAST, or WAL/RX samples. All other elemental contents are bracketed by those in the Windsor Point Group schists. Pelitic schists from the Upper Wakatipu area of New Zealand (after Kawachi, 1974; see Table XII) are very enriched in Al<sub>2</sub>O<sub>3</sub>, and slightly so in Na<sub>2</sub>O, with respect to the schists of this study. In terms of MgO, MnO and CaO  $\Sigma$ 's, Kawachi's schists resemble the SE/C1 samples, but the K<sub>2</sub>O contents

TABLE XII Average Chemical Data from Other Authors

	(1)	(2)	(3)	(4)	(5)	(6)	(7)	(8)	(9)	(10)	(11)	(12)	(13)	(14)	(15)	(16)	(17)
	MEAN	MEAN	MEAN	MEAN	MEAN	MEAN	MEAN	MEAN	MEAN	MEAN	MEAN	MEAN	MEAN	MEAN	MEAN	MEAN	MEAN
wt %																	
SiO <sub>2</sub>	70.39	70.7	61.54	60.04	54.20	69.70	55.74	55.00	59.22	--	70.47	--	--	58.81	65.91	54.32	--
TiO <sub>2</sub>	0.23	0.49	0.82	0.73	0.76	0.79	0.90	0.92	1.41	0.33	0.60	0.54	0.84	0.64	0.61	--	--
Al <sub>2</sub> O <sub>3</sub>	12.31	14.30	16.95	18.73	16.65	18.00	18.16	19.50	20.73	13.27	8.32	12.00	17.04	11.44	13.16	--	--
Fe <sub>2</sub> O <sub>3</sub>	1.22	0.71	2.34	1.54	0.45	7.63	9.36	9.50	1.10	2.84	5.29	--	4.62	0.80	12.29	--	--
P <sub>2</sub> O <sub>5</sub>	0.96	2.25	3.90	3.90	--	--	--	--	8.10	--	--	--	3.77	2.04	--	--	--
MnO	0.48	0.05	--	0.11	0.42	0.13	0.54	0.24	0.13	0.02	0.22	0.07	0.08	0.06	0.06	--	--
MgO	0.57	0.67	2.52	2.30	3.71	3.44	3.80	4.09	2.60	1.12	1.32	0.60	2.79	3.22	3.89	--	--
CaO	0.38	1.50	1.75	2.30	2.66	1.21	2.43	1.89	1.26	2.1	1.60	0.01	1.97	1.66	3.00	--	--
Na <sub>2</sub> O	1.79	2.50	1.82	1.84	1.59	1.45	1.52	1.88	1.82	0.94	2.02	0.88	1.60	0.47	1.29	--	--
K <sub>2</sub> O	6.28	3.56	3.45	3.05	3.30	3.70	4.16	4.50	3.56	2.4	2.5	3.49	3.58	2.80	2.88	--	--
P <sub>2</sub> O <sub>5</sub>	0.04	0.03	--	0.20	0.16	0.11	0.27	0.14	0.26	--	--	0.07	0.13	0.08	0.07	--	--
LOI	1.72	2.03	3.47	3.1	6.43	3.07	2.54	1.67	--	--	--	--	4.44	3.47	8.06	--	--
ppm																	
Pb	--	--	--	--	--	--	--	--	--	20	50	101	--	--	--	--	--
Zn	21	--	--	--	--	--	--	--	--	--	--	--	--	--	--	--	--
V	6	--	--	--	--	--	--	--	--	--	--	--	--	--	--	10-40	--
Fe	182	--	--	--	--	--	--	--	109	--	89	283	251	--	--	--	--
Se	118	--	--	--	--	--	--	--	168	200	65	419	272	--	--	--	--
Y	--	--	--	--	--	--	--	--	--	30	28	--	43	--	--	--	--
Er	454	--	--	--	--	--	--	--	--	70	134	179	173	--	--	--	--
Mo	31	--	--	--	--	--	--	--	--	--	--	--	12	--	--	--	--
Sn	--	--	--	--	--	--	--	--	149	300	30	--	144	--	--	--	1000
Cu	--	--	--	--	--	--	--	--	--	70	64	202	48	--	--	40-70	650
Bi	--	--	--	--	--	--	--	--	--	50	--	51	92	--	--	80-150	510
La	61	--	--	--	--	--	--	--	--	30	--	--	30	--	--	--	--
Ba	641	--	--	--	--	--	--	--	700	300	--	870	632	--	--	--	150
V	--	--	--	--	--	--	--	--	--	150	--	389	--	--	--	150-300	--
Co	126	--	--	--	--	--	--	--	--	--	--	--	66	--	--	--	--
Cr	--	--	--	--	--	--	--	--	--	100	--	211	135	--	--	--	100
Ga	--	--	--	--	--	--	--	--	--	20	--	18	20	--	--	--	--
As	--	--	--	--	--	--	--	--	--	--	--	25	--	--	--	20-40	--
wt %																	
H	--	0.008	--	--	--	--	--	--	0.35	--	--	1.01	0.61	3.43	9.02	--	--
OH	--	0.10	1.67	--	--	--	--	--	--	3.53	--	--	1.01	1.47	1.17	--	--
ppb																	
Ag	--	--	--	--	--	--	--	--	--	1000	--	--	--	--	--	--	--

Basal et al. (1983) = (1); Webb and Potter (1969) = (2); Shaw (1954) = (3); Kamachi (1970) = (4); Ferry (1980), chlorite zone = (5); biotite zone = (6); garnet zone = (7); staurolite zone = (8); Yardley (1977) = (9); Vane and Tourbatolet (1970) = (10); Stephens et al. (1975) = (11); Spencer (1964) = (12); Van de Kamp et al. (1979) = (13); Ferry (1981), biotite zone = (14); garnet zone = (15); Leventhal and Rastrom (1984) = (16); Harris (1960) = (17)

-- Not Determined

resemble those of the GAST or WAL/RX units. Ferry's (1982) chemical analyses for schists from the chlorite, biotite and garnet zones within the Waterville Formation of Maine are grossly similar to the Windsor Point Group samples except  $Al_2O_3$  has a greater concentration,  $MnO$  and  $K_2O$  contents are generally more elevated, and  $SiO_2$  and  $CaO$  are slightly depleted in the former schists.

The consistently higher  $Al_2O_3$  contents described in pelites from elsewhere compared, to the schists of this study, reflect variations in the provenance of detritus (and depositional environment) in the parental sediments from which the schists were derived.  $Al_2O_3$  is enriched in most sedimentary rocks relative to igneous rocks because of removal of  $Al_2O_3$ -poor phases during transport to a depositional area etc. (cf. Garrels and MacKenzie, 1971). However the Windsor Point Group schists were derived from volcanic debris deposited close-to-source without much transport modification, thus resulting in their low- $Al_2O_3$  contents.

The PAB/GN samples, when compared to staurolite-grade pelites (Yardley, 1977; Ferry, 1982) from elsewhere, are relatively enriched in  $SiO_2$ ,  $CaO$ ,  $Na_2O$  and  $K_2O$ , but are depleted in  $Al_2O_3$  and to lesser extents in  $Fe_2O_3$  and  $TiO_2$ , indicating the PAB/GN samples are more felsic.

In their classic study, Vine and Tourtelot (1970), analysed the trace metal contents of 779 shale samples from

various localities through Canada and the United States in order to determine the average geochemical composition of black shales (presented in Table XII). When compared to the elemental concentrations in these North American shale averages, the GAST samples are enriched in all elements except Y, Zr, Ni, La and Ga which are equivalent in concentration, and Na<sub>2</sub>O, Sr, Cr and CO<sub>2</sub> which are depleted. Except for depletions in SiO<sub>2</sub>, TiO<sub>2</sub> and Na<sub>2</sub>O, the GAST samples are enriched or equivalent in most elements when compared to Stephens *et al.*'s (1975) average data for graptolitic shales in Scotland,

A Silurian shale band from Wales, Spencer (1966), contains lesser amounts of the more mafic major oxides, yet more of the trace elements (especially Rb, Sr and Cu) and Na<sub>2</sub>O than the GAST samples. The average chemical composition of thirteen shales from the Santa Ynez Mountains of California (Van de Kemp *et al.*, 1976; see Table XII) more closely resemble those in the GAST samples, except for strong depletions in Rb and Sr in the GAST.

Ferry (1981) has described the major element concentrations (see Table XII) of graphitic schists, in a prograde metamorphic environment with both biotite and garnet zones (*ie.* equivalent metamorphic grade of the GAST samples). When compared to the GAST rocks, Ferry's samples have minor enrichments in Fe<sub>2</sub>O<sub>3</sub> and MgO, minor depletions in MnO and P<sub>2</sub>O<sub>5</sub>, but all other elements are roughly the

same. The GAST samples contain more Cu, V and As, but less U and much less Ni than black shale deposits of similar Devonian age in the southern Appalachians (Leventhal and Hosterman, 1982).

According to their geochemical compositions, the GAST samples are not significantly anomalous when compared to other graphitic shale units. In fact the literature survey has shown that these rock types can have a range in elemental abundances. The enrichment of the ferro-magnesium elements in the GAST samples relative to most studies (eg. Vine and Tourtelot, 1970), is probably indicative of the proximity to a volcanic source (and thus the presence of volcanic debris) of the depositional area. The chemically similar shales from the Santa Ynez Mountains are also thought to have had an effective volcanic component in their source regions (Van de Kemp et al., 1976):

In order to define the compositions of metal-rich shales, Vine and Tourtelot (1970) used statistical methods to produce minimum enrichment values and a minor-element enrichment index for shales. These minimum enrichment values are listed in Table XIII. Of nineteen samples of GAST (only 10 with major element analyses), eight (or 80%) contain higher MnO values, three (or 16%) have higher Ba, two (11%) have higher Pb, and one (5%) has higher Cu concentrations than their respective enrichment values,

<u>ELEMENT</u>	<u>MIN. ENRICHMENT VALUE</u>
TiO <sub>2</sub>	1.17 %
MnO	0.13 %
Pb	100 ppm
U	30 ppm
Sr	1500 ppm
Y	70 ppm
Zr	200 ppm
Zn	1500 ppm
Cu	200 ppm
Ni	300 ppm
La	70 ppm
Ba	1000 ppm
V	1000 ppm
Cr	700 ppm
Ga	50 ppm
Ag	7000 ppb

TABLE XIII Enrichment Values (after Vine and Tourtelot, 1969)

which yield an enrichment index of 112 out of a possible 1600. Aside from MnO, which is enriched in the sedimentary environment and has no relation to the gold-sulphide mineralization, the GAST samples are not metal-rich.

This is even more strongly borne out when the GAST samples are compared to sulphide-bearing graphite schists from Finland (Marmo, 1960; see Table XII) which contain very high concentrations of Zn, Cu and Ni.

The WAL/RX samples (11 with major element analyses; 15 with trace element analyses) have seven samples (64%) with higher MnO, six with elevated Zr (33%), three (20%) with higher Pb and Y, two (13%) with elevated Cu and La, and one (6%) each of higher TiO<sub>2</sub>, V and Ag when compared to Vine and Tourtelot's (1970) enrichment factors. Not all samples of WAL/RX are graphitic schist, and the high Zr contents occur in SE/CL samples and the high TiO<sub>2</sub> value occurs in a CHL/SC sample. All the other enriched metal values in these samples are greater than the typical background contents in their respective rock types and therefore are indicative of anomalous concentration. Disregarding TiO<sub>2</sub> and Zr, the enrichment index for the WAL/RX samples is 142 out of a possible 1600 (i.e. only slightly greater than non-wall rock graphitic schists).



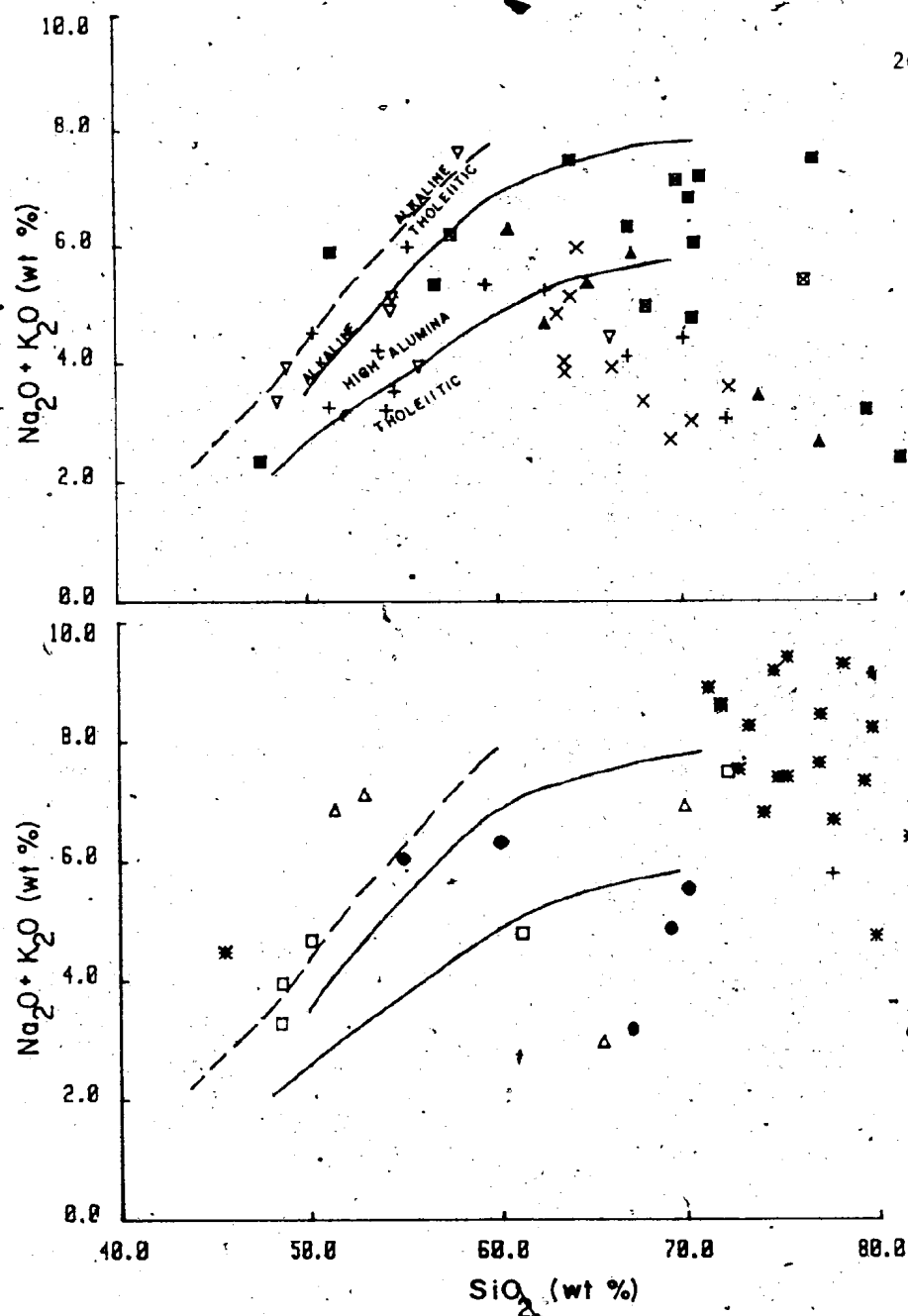
### 6.6 Variation and Discrimination Diagrams

According to Irvine and Barager's (1971) dividing line, as illustrated on the  $\text{Na}_2\text{O}+\text{K}_2\text{O}$  vs.  $\text{SiO}_2$  plot (Figure 36), all the rocks from this study are tholeiitic (except for the lone mafic WPGIG sample and half each of the PABQ and WPGQ groups which are indicated as alkaline). The only schists mafic enough to really apply this diagram, CHL/SC, plot mainly in the high alumina basalt field (after Kuno, 1968).

The  $\text{K}_2\text{O}$  vs.  $\text{Na}_2\text{O}$  and  $\text{Rb}$  vs.  $\text{Sr}$  plots (Figures 37 and 38) provide excellent diagrams for differentiation between the various groups. In the former, the WAL/RX, GAST and SER/SC samples are definitively potassic (i.e.  $\text{K}_2\text{O}/\text{Na}_2\text{O} > 1$ ), while the CHL/SC, CL/BIO, WPGQ, PABQ and PAB/GN are sodic. The SE/CL and WPGIG samples straddle the two zones with strong negative correlations (the WPGIG ones occur at distinctly higher overall values). On the latter diagram, the GAST and WPGIG (with some slope) values are dominantly in the Rb field, the CHL/SC, WPQ, PABQ and PAB/GN samples are in the Sr field, and all the other groups straddle both fields with characteristically inverse relations.

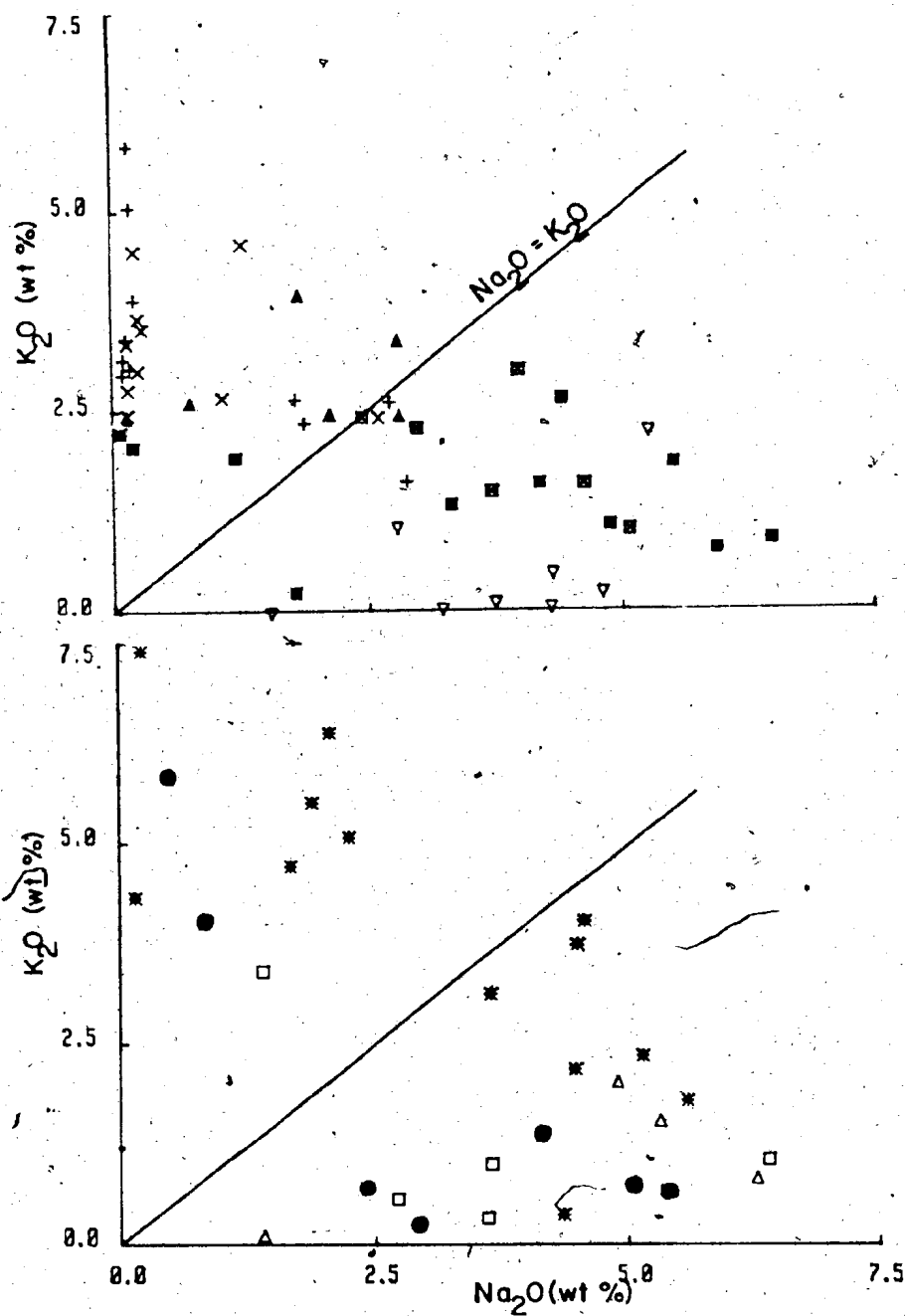
Figures 39a and 40a ( $\text{Na}_2\text{O}/\text{Al}_2\text{O}_3$  vs.  $\text{K}_2\text{O}/\text{Al}_2\text{O}_3$ , and  $\log (\text{SiO}_2/\text{Al}_2\text{O}_3)$  vs.  $\log [(\text{CaO}+\text{Na}_2\text{O})/\text{K}_2\text{O}]$ ) are plots of the group averages in relation to fields of average sedimentary vs. igneous rocks from Garrels and MacKenzie (1971) (the averages from Chorlton (1980b) are also plotted on this diagram). Figures 39b and 40b contain plots of individual samples. On both diagrams the GAST, WAL/RX and

Figure 36 Total alkalis vs. SiO<sub>2</sub> diagram for Windsor Point Group schists and ignimbrites, and Port aux Basques Gneiss samples. Alkaline-tholeiitic dividing line from Irvine and Baragar (1971), alkaline- high alumina-tholeiitic fields from Kuno (1968). Most units are tholeiitic. See Key for group identification.



- CHLORITE/BIOTITE SCHIST
- ▼ CHLORITE SCHIST
- ▲ SERICITE SCHIST
- + WALL ROCK
- × GRAPHITE SCHIST
- SÉRICITE/CHLORITE SCHIST
- PORT AUX BASQUES GNEISS
- \* WINDSOR POINT GROUP IGNIMBRITE
- △ RETROGRESSED PORT AUX BASQUES GNEISS
- WINDSOR POINT GROUP (?)

Figure 37 K<sub>2</sub>O vs. Na<sub>2</sub>O diagrams for the Windsor Point Group schist  
and ignimbrite, and the Port aux Basques Gneiss samples.  
See Figure 36 for sample key. See text for discussion.



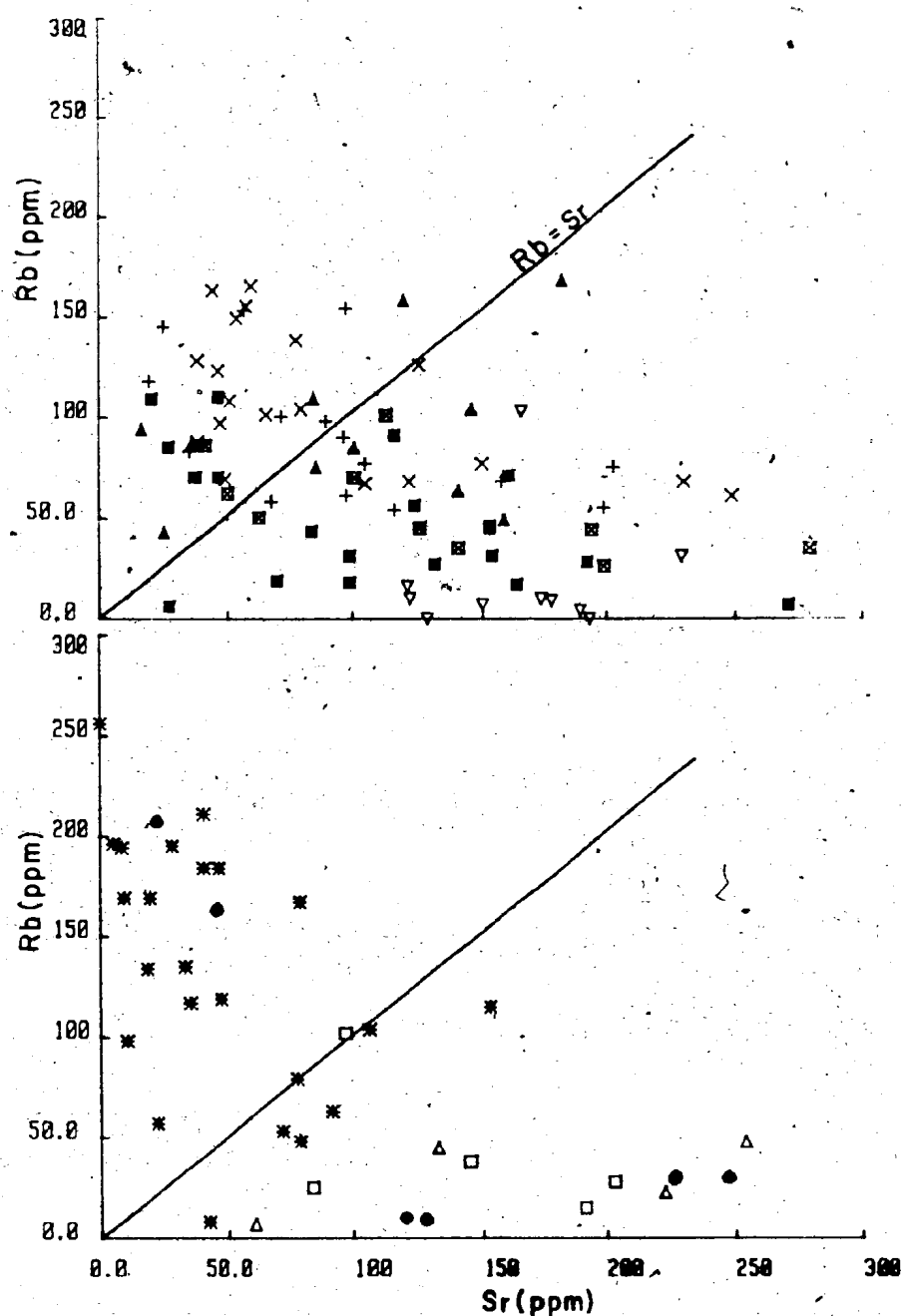


Figure 38 Rb vs. Sr diagrams for the Windsor Point Group and Port aux Basques Gneiss samples. See Figure 36 for sample key.

Figure 39a Na<sub>2</sub>O/Al<sub>2</sub>O<sub>3</sub> vs. K<sub>2</sub>O/Al<sub>2</sub>O<sub>3</sub> diagram for Windsor Point Group and Port aux Basques Group averages (see Figure 36 for the group key). Fields from Garrels and McKenzie (1971). Numbers indicate averages for Chorlton's (1980b) data, viz.; 1 = Billiards Brook flows; 2 = Piglet Brook rhyolite; 3 = Dolman Formation; 4 = Hawk's Nest porphyry; 5 = Bay du Nord Group felsites; 6 = Georges Brook Formation crystal tuff; 7 = Georges Brook Formation felsic flows; 8 = Georges Brook Formation fine tuff; 9 = Georges Brook Formation mafic flows. This diagram shows the igneous nature of most schists in the Windsor Point Group and the sedimentary nature of sericite, graphite and wall rock schists (wall rocks are actually composed of these other schists). The diagram also shows the great differences between units in the Cape Ray Fault Zone and the Bay du Nord/La Poile Groups described by Chorlton (1980b).

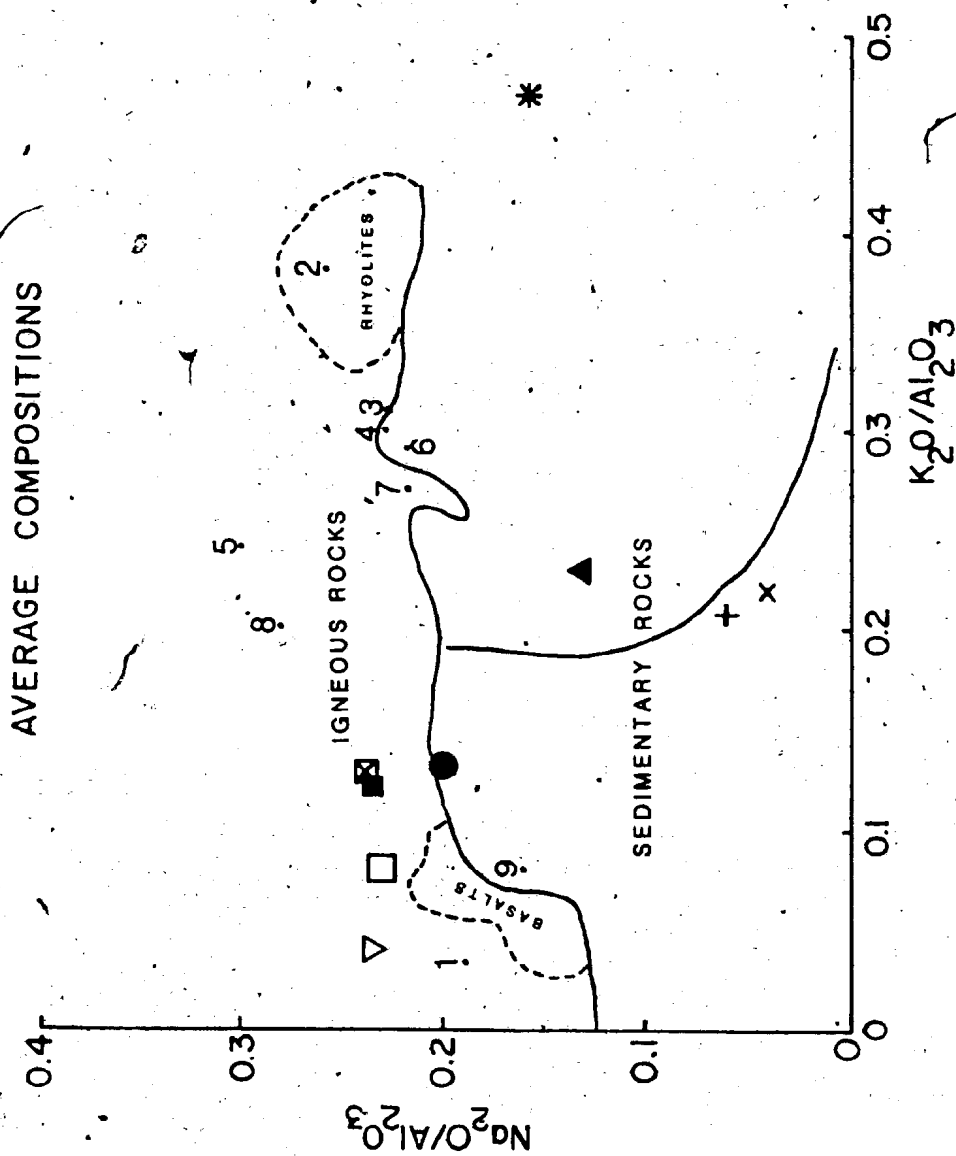




Figure 39b  $\text{Na}_2\text{O}/\text{Al}_2\text{O}_3$  vs.  $\text{K}_2\text{O}/\text{Al}_2\text{O}_3$  diagram for the Windsor Point Group schists and ignimbrites, and the Port aux Basques Gneiss samples. Plot of individual samples making up the averages in Figure 39a.

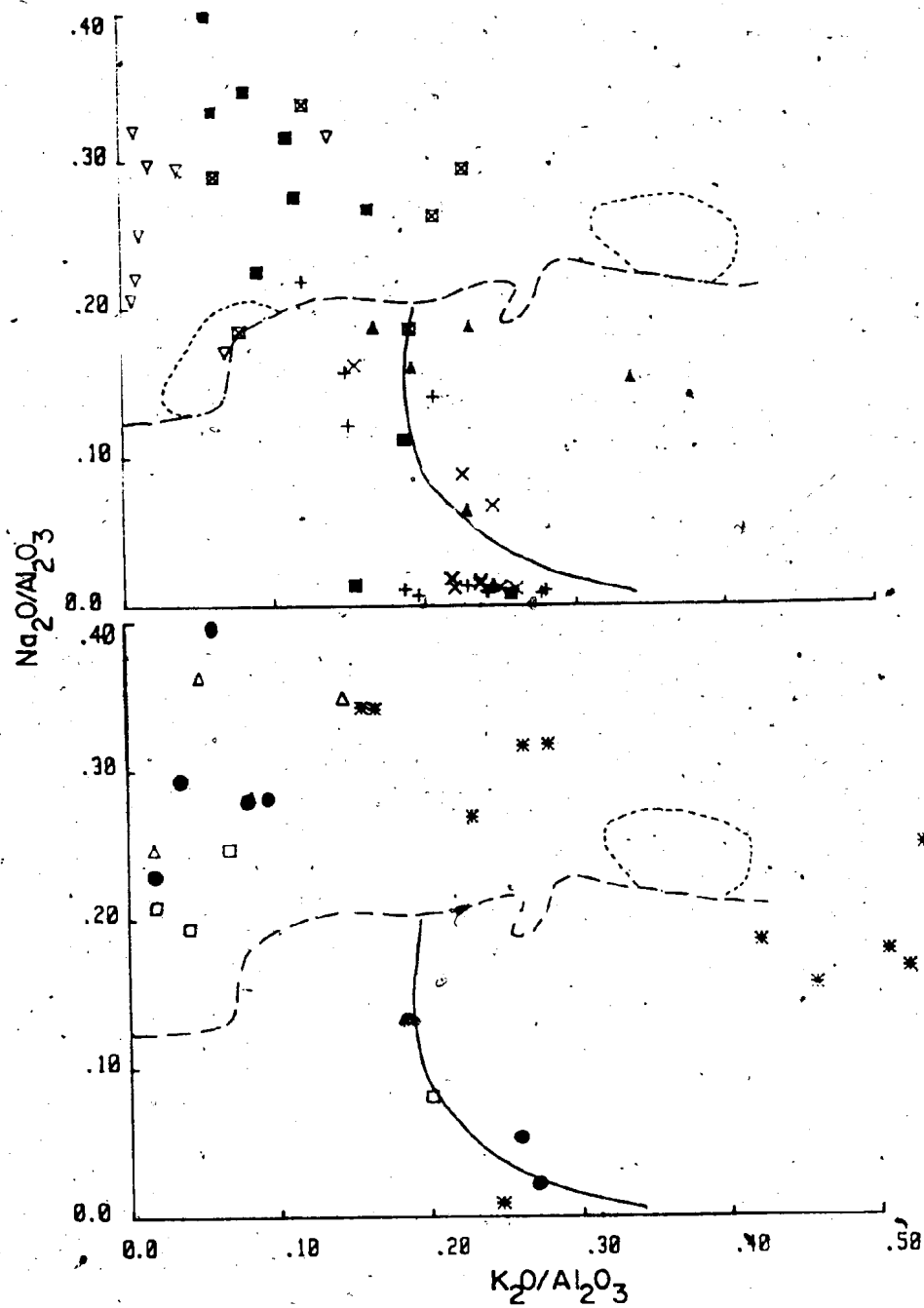


Figure 40a Log (SiO<sub>2</sub>/Al<sub>2</sub>O<sub>3</sub>) vs. log ((CaO+Na<sub>2</sub>O)/K<sub>2</sub>O) for Windsor Point Group and Port aux Basques Gneiss averages. Also included are averages from Chorlton's (1980b) data (see Figure 39a for key). Fields from Garrels and McKenzie (1971). This diagram illustrates the strong igneous imprint on all units in the Cape Ray Fault Zone (ie. the sediments were derived from volcanic terranes and activity).

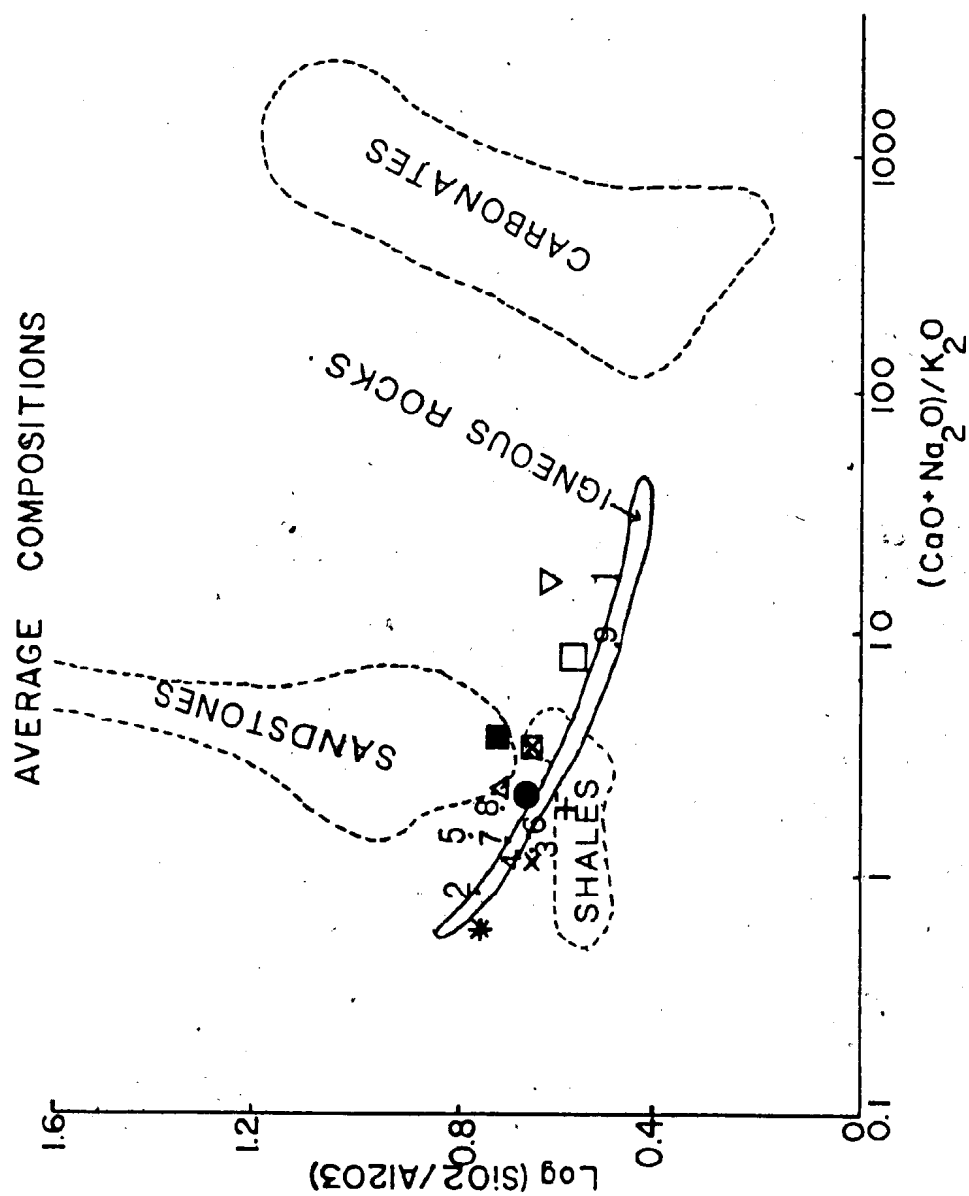
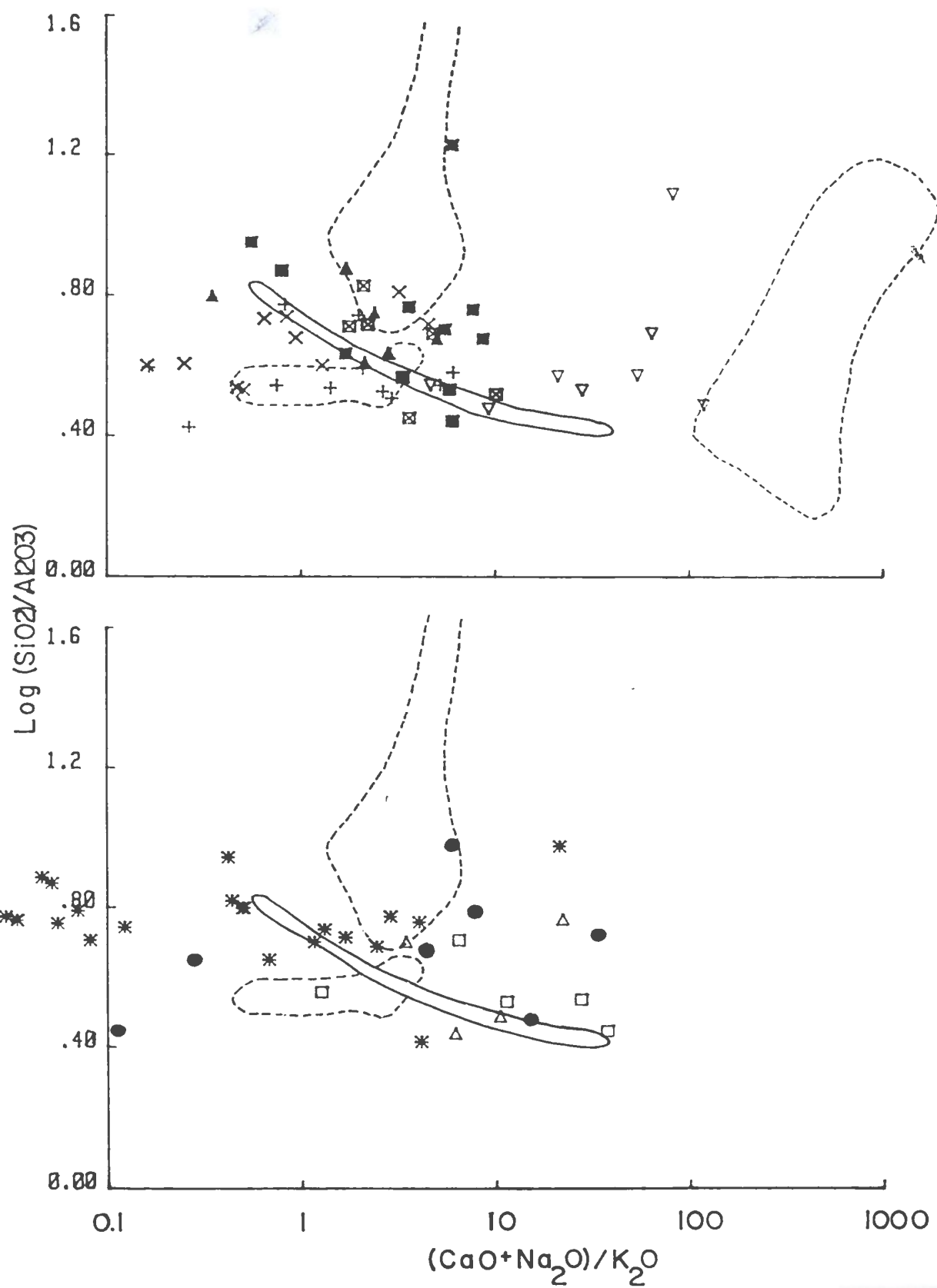


Figure 40b Log (SiO<sub>2</sub>/Al<sub>2</sub>O<sub>3</sub>) vs. log ((CaO+Na<sub>2</sub>O)/K<sub>2</sub>O) for the Windsor  
Point Group and the Port aux Basques Gneiss samples. Plot  
of individual samples making up the averages in Figure 40a.



SER/SC rocks are defined as sedimentary in origin. The other groups are igneous on the  $\text{Na}_2\text{O}/\text{Al}_2\text{O}_3$  vs.  $\text{K}_2\text{O}/\text{Al}_2\text{O}_3$  diagram but fall off the igneous trend on the other (i.e. Figure 40b). On this latter diagram the fields are probably too restrictive. On the former diagram (see Figure 39b) the CHL/SC, and to a lesser extent, the CL/BIO, SER/SC, WPGQ and PABQ samples, are distinctly igneous. The WPGIG samples just fall off the end of the rhyolitic field into the sedimentary field, but remembering the potash metasomatism which affected this group, classification problems are to be expected and the ignimbrites have also undergone slight sedimentation. The average PAB/GN is just within the sedimentary field, but the actual samples plot with wide variation in both fields. Because the Windsor Point Group sediments are made up of volcanic debris and the volcanic eruptions have been modified by sedimentary processes the rocks straddle the igneous/sedimentary spectrum.

The average values from Chorlton (1980b) for the Bay du Nord/La Poile Groups plot in distinctly different regions of these diagrams compared to the Cape Ray Fault Zone data. The Billiards Brook flows and Georges Brook mafic flows plot in the basaltic area and those of the Piglet Brook rhyolite plot in the rhyolite/ignimbrite field. The other averages plot with intermediate and granitic rocks.

#### 6.6.1 Summary of geochemical data

Conclusions to be drawn from the foregoing descriptions are:

- 1) There are no great chemical differences between the schist samples, and the only distinct group is felsic volcanic rocks of the Little Barachois Formation. The Port aux Basques Gneiss samples are similar to the Windsor Point Group schists, yet are unlike the Port aux Basques Gneiss reported by Taylor (1970) and the Bay du Nord/La Poile Groups reported by Chorlton (1980b).
- 2) The schists resemble typical sediments/schists reported elsewhere except they are slightly more mafic than most, due to the close-to-source volcanic derivation.
- 3) The graphite schist (GAST) and wall rock (WAL/RX) samples are not like ore-bearing sediments found elsewhere because they have chemical compositions typical of sedimentary rocks.
- 4) Samples in the WAL/RX group have slight increases in some chalcophile elements compared to unmineralized samples.
- 5) Elevated, anomalous concentrations of chalcophile elements in certain samples can be traced back to epigenetic quartz veining.



### 6.7 Intermediate to Mafic Intrusives

The average anhydrous elemental concentrations and standard deviations for the intermediate to mafic intrusives occurring within the Cape Ray Fault, Zone are listed in Table IX (the complete data are in Appendix IV). Amphibolites from the Port aux Basques Gneiss are listed as PABAM; metagabbros of the Long Range Mafic/Ultramafic Complex as LRM/UM; gabbros in the Windsor Point Group as GABB; metagabbros along the southern margin of the Windowglass Hill Granite as GABWG; basic dykes cutting the Cape Ray Granite as BSC/DK; dioritic layers associated with the Windowglass Hill Granite (in drill core) as DIOR; and silicious gabbroic rocks within the Windsor Point Group as GRANO.

As is evident from the table of average analyses, these units are chemically similar. The LRM/UM rocks have higher MgO, Ni, Ba and K<sub>2</sub>O than the other groups, but since these rocks are ophiolitic, the elevations in MgO and Ni contents are understandable, and the higher K<sub>2</sub>O and Ba concentrations are indicative of the extensive hydrothermal alteration experienced by these rocks. The GABB samples have the highest average Na<sub>2</sub>O contents for the mafic rocks. The most elevated concentrations of TiO<sub>2</sub>, Sr, V and Ce occur in the BSC/DK rocks (indicative of their basaltic nature). The DIOR samples contain more Pb, Zr, Ce, As and S than any of the other units. The elevated Zr (seen in GRANO samples also) is a result of the more silicious

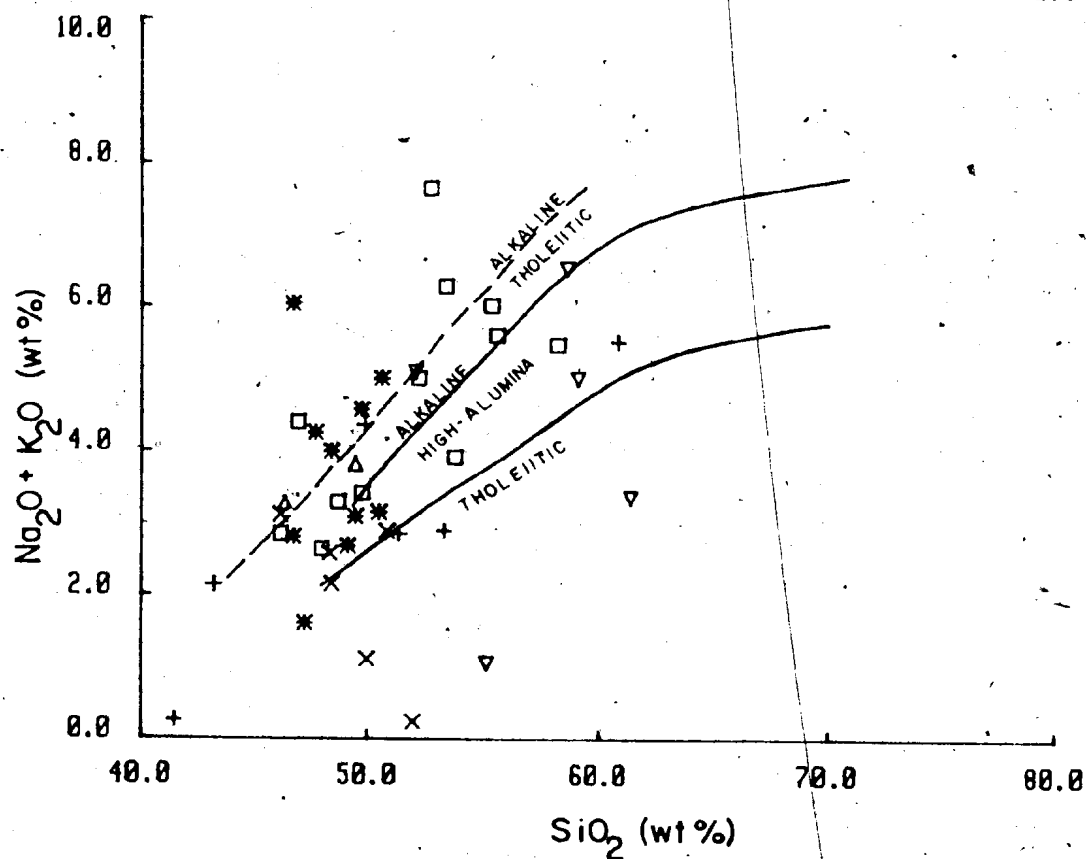
compositions, while Pb, As and S are probably tied up in the abundant disseminated pyrite. The GRANO rocks are the most silicious and accordingly contain the highest concentrations of Na<sub>2</sub>O and Rb, and with DIOR, the lowest mean Cr.

#### 6.7.1 Variation and Discrimination Diagrams

On a total alkalis vs. silica diagram (Figure 41), all samples generally plot as tholeiites, however 50 % of the GAB/WG and three of the GABB samples occur in Irvine and Barager's (1971) alkaline field. These "alkali" samples are seemingly more highly altered than the others, thus the higher alkali content is a secondary feature rather than a petrogenetic one. All other units have compositions ranging from high alumina to tholeiitic (after Kuno, 1968) except the LRM/UM samples which have lower alkali contents and thus are distinctly tholeiitic.

The AFM plot (Figure 42) indicates that all units are calc-alkaline to tholeiitic, but they define no discernable intergroup trends (ie. they don't appear to be related). The LRM/UM samples plot as a very primitive composition which could yield either calc-alkaline or tholeiitic trends (as would be expected since these samples are of ophiolitic gabbros).

Except for LRM/UM, every group plots in the Na<sub>2</sub>O>K<sub>2</sub>O



- X LONG RANGE MAFIC/ULTRAMAFIC COMPLEX
- + PORT AUX BASQUES COMPLEX AMPHIBOLITE
- GABBRO
- \* GABBRO (S of Windowglass Hill)
- △ BASALTIC DYKE
- ▽ DIORITE
- GRANODIORITE

Figure 41 Total alkalis vs. SiO<sub>2</sub> diagram for the mafic volcanic/plutonic rocks of the Cape Ray Fault Zone. (See Figure 36 for references to fields).

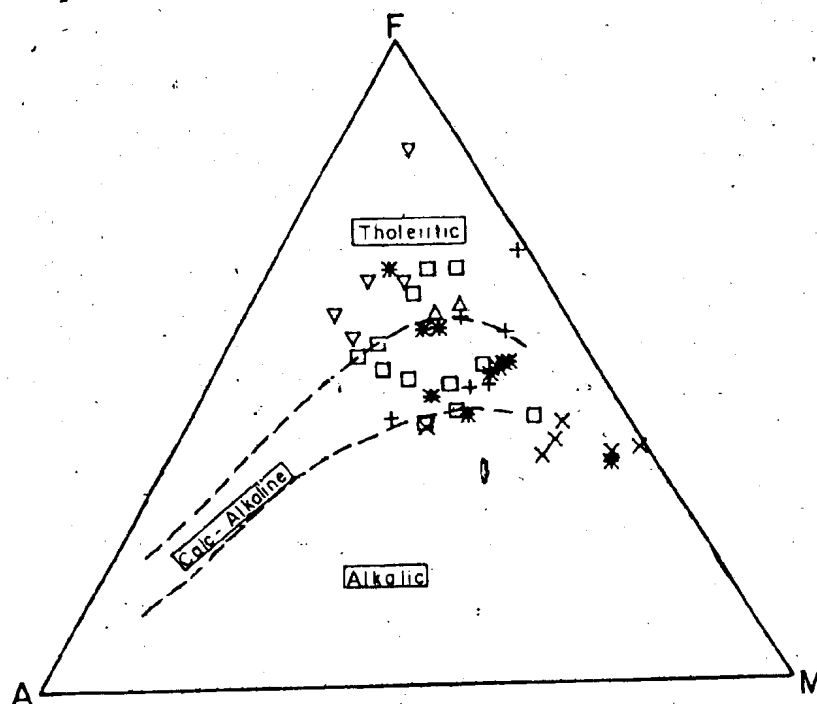


Figure 42 AFM diagram for volcanic/plutonic rocks in the Cape Ray Fault Zone. Sample key as Figure 41. A = Na<sub>2</sub>O + K<sub>2</sub>O; M = MgO; Fe = Total Fe as FeO. Fields from Irvine and Baragar (1971).

field on a  $\text{Na}_2\text{O}$  vs.  $\text{K}_2\text{O}$  diagram (Figure 43a). The higher  $\text{K}_2\text{O}$  contents seem to reflect potash metasomatism, and on a  $\text{Rb}$  vs.  $\text{Sr}$  diagram (Figure 43b), the LRM/UM rocks plot with all the others in having  $\text{Sr} \gg \text{Rb}$  (ie. the low  $\text{Rb}$  concentrations don't match the  $\text{K}_2\text{O}$  enrichment; further supporting the supposition that potash metasomatism is the cause of the "alkalic" features in the LRM/UM).

The  $\text{Ti/Zr/Y}$  and  $\text{Zr/Y}$  vs.  $\text{Zr}$  diagrams of Pearce and Cann (1973), Figures 44a and 44b, have direct petrogenetic implications for their different fields. On the  $\text{Ti/Zr/Y}$  plot, most GABB, GAB/WG and BSC/DK samples are classified as being either mid-ocean ridge basalts (MORB) or volcanic arc basalts (VAB), while the PABAM samples are just VAB's. The samples of the other groups don't concentrate in any of the fields. According to the  $\text{Zr/Y}$  vs.  $\text{Zr}$  diagram, the GABB, GAB/WG and BSC/DK samples plot as ocean floor basalts (OFB), some of the LRM/UM samples plot as VAB, and the PABAM samples plot as either within plate basalts (WPB) or ocean floor basalts.

Two more recent discrimination diagrams (from Gale and Pearce, 1982), viz.  $\text{TiO}_2$  vs.  $\text{Zr}$  and  $\text{Cr}$  vs.  $\text{Y}$ , have been successfully used for modelling Norwegian greenstones. On the former diagram (see Figure 45a), the PABAM samples are classified as island arc lavas, most of the GAB/WG samples as mid-ocean ridge basalts, and the GABB samples as both MORB and WPB. The LRM/UM samples plot well outside of the

Figure 43a Na2O vs. K2O diagram for mafic volcanic/plutonic rocks of the Cape Ray Fault Zone. Sample key as in Figure 41.

Figure 43b Rb vs. Sr diagram for the mafic volcanic/plutonic rocks of the Cape Ray Fault Zone. Sample key as in Figure 41.

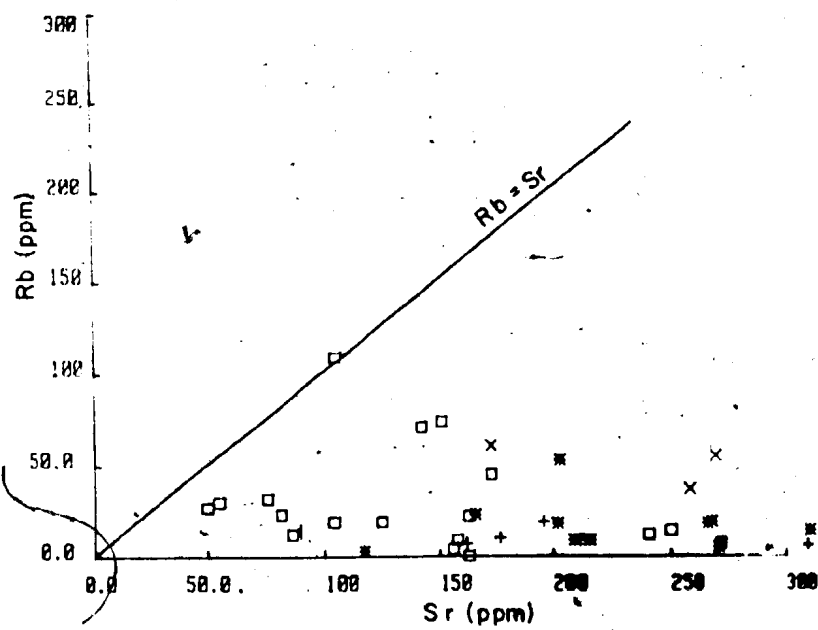
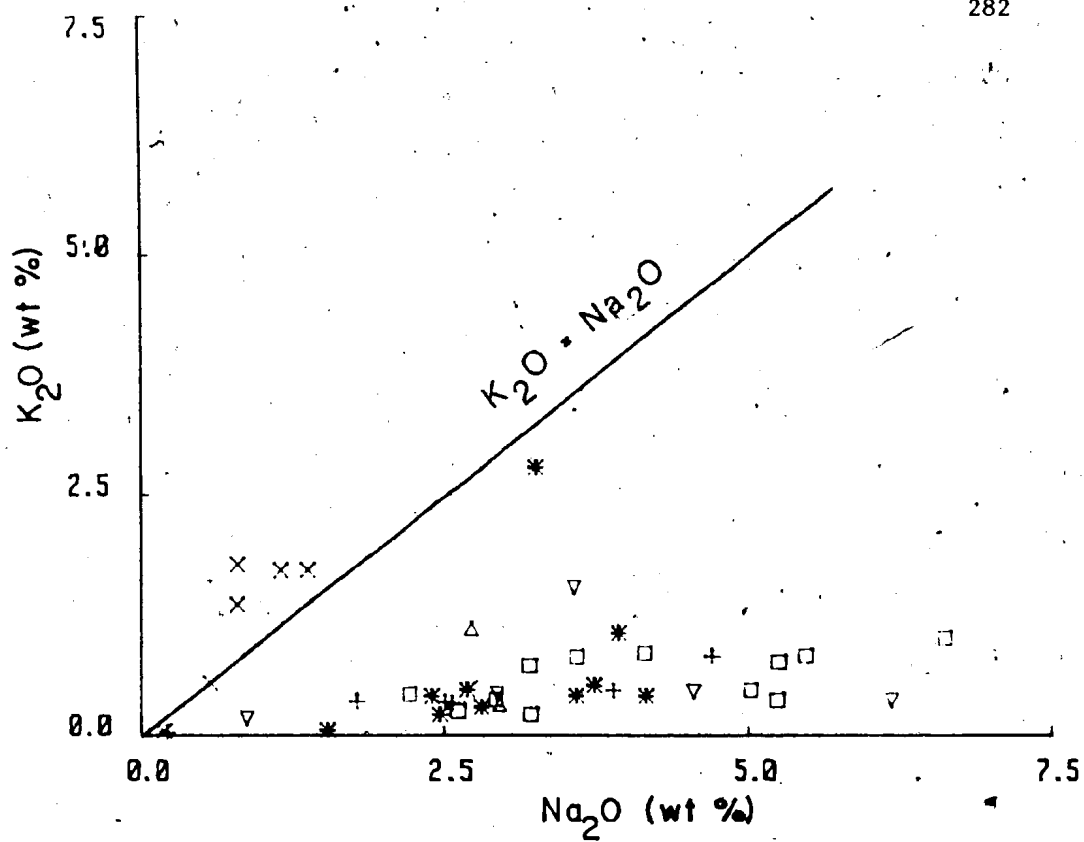


Figure 44a Ti/Zr/Y diagram for the mafic volcanic/plutonic rocks of the Cape Ray Fault Zone. Fields are from Pearce and Cann (1973). WPB = within plate basalt; VAB = volcanic arc basalt; MORB = mid-ocean ridge basalt. Sample key as in Figure 41.

Figure 44b Log (Zr/Y) vs. log (Zr) diagram for the volcanic/plutonic rocks of the Cape Ray Fault Zone. Fields are from Pearce and Cann (1973). OFB = ocean floor basalt. Sample key as in Figure 41. This diagram indicates that the gabbro and gabbro south of Windowglass Hill, most closely resemble ocean floor basalts.



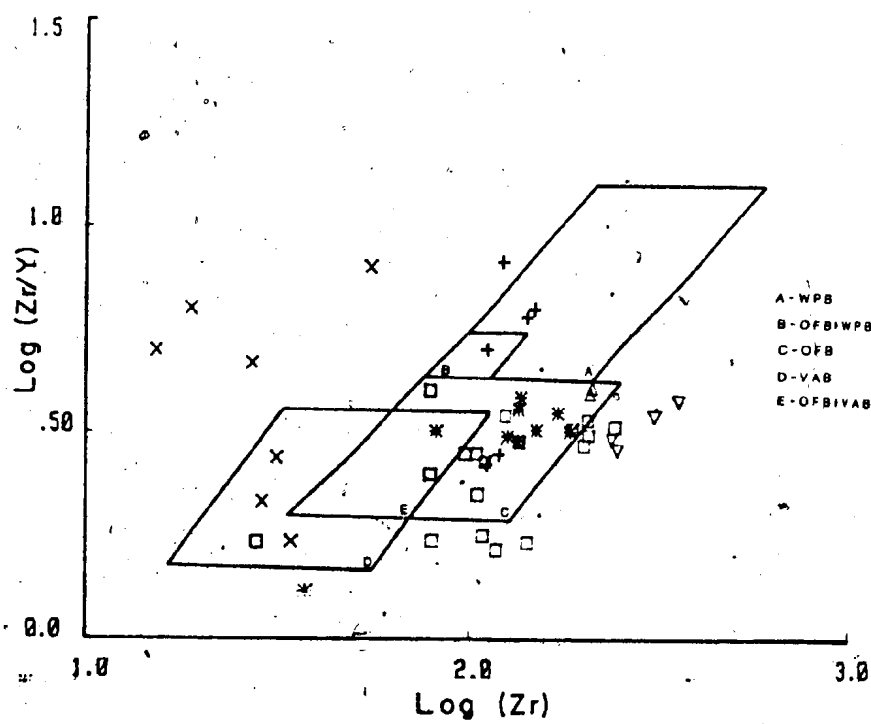
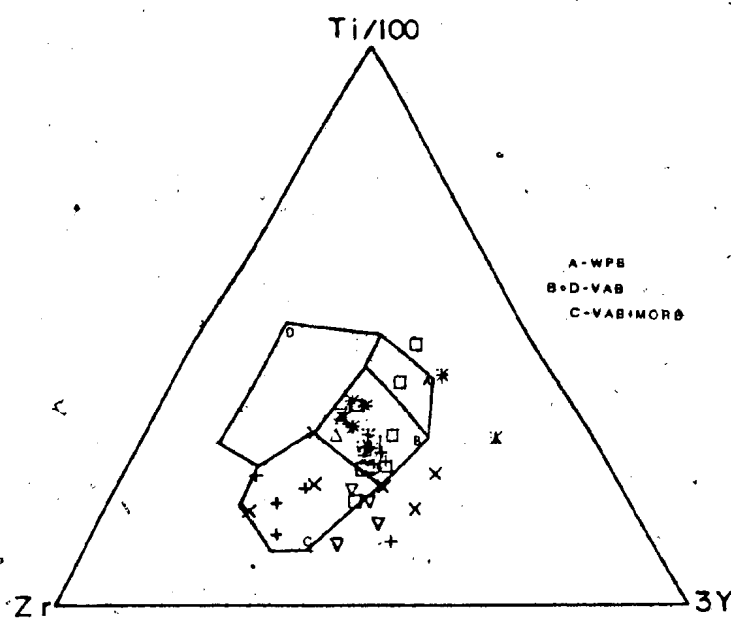
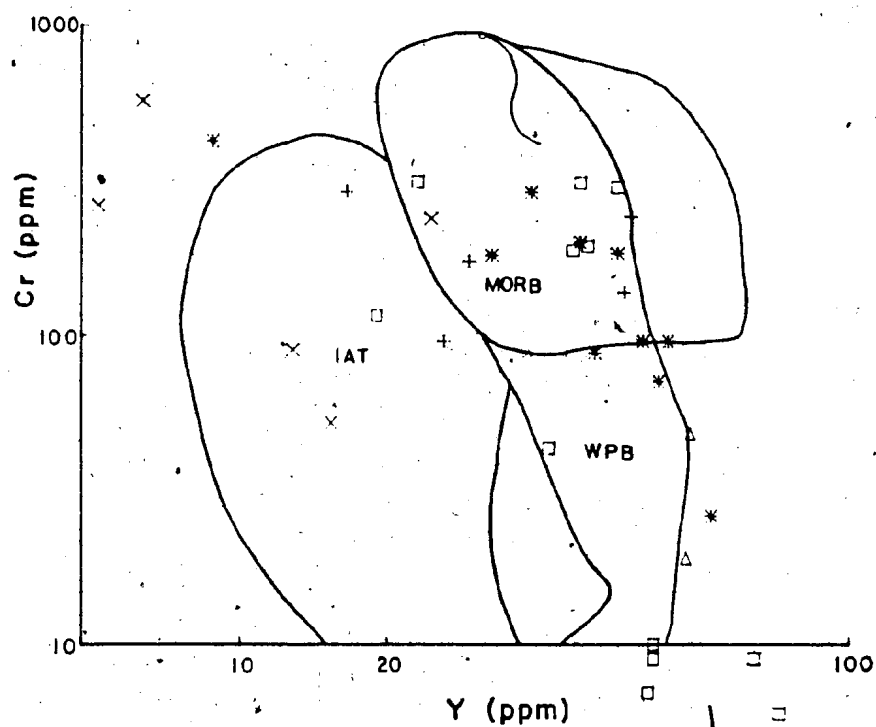
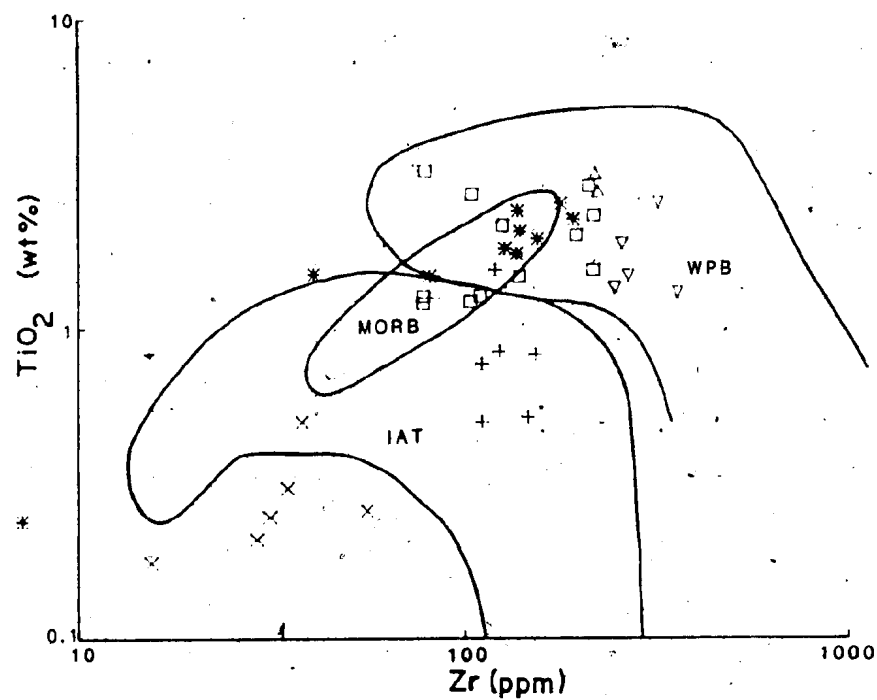


Figure 45a TiO<sub>2</sub> vs. Zr diagram for volcanic/plutonic rocks of the Cape Ray Fault Zone. Fields from Pearce and Gale (1982). IAT = island arc tholeiite; MORB = mid-ocean ridge basalt; WPB = within plate basalt. Sample key as in Figure 41. Amphibolites from the Port aux Basques Gneiss plot as IAT, while the other groups (except the ophiolitic fragments - Long Range Mafic/Ultramafic Complex) plot as WPB.

Figure 45b Cr vs. Y diagram for the volcanic/plutonic rocks of the Cape Ray Fault Zone. Fields from Pearce and Cann (1982). Sample key as in Figure 41. There are no consistent trends for any of these groups.



MORB field towards the origin of the diagram. G. Dunning (pers. comm, 1983) found that diabase dykes from the Annieopsquotch Ophiolite Complex plotted right in the MORB field (on a similar diagram), that pillow lavas from the same complex were too altered to use for the chemical classification scheme, and that the gabbros plot off the MORB field in the same region as the LRM/UM samples. Dunning feels this offset may be a function of fractionation processes operative within the gabbros. The LRM/UM metagabbros, however have a visible metasomatic overprint, so in their case, alteration has to be postulated as a reason for the offset.

On the second diagram (Figure 45b), the various groups have a larger spread through the designated fields. The GABB and GAB/WG rocks plot as either MORB or WPB; the BSC/DK samples as WPB; the PABAM as VAB, MORB or WPB; and two LRM/UM samples as VAB and one as MORB rocks.

In conclusion all the units have undergone varying degrees of alteration and trace element mobilization, thus the use of the foregoing discriminant diagrams must be done with caution (eg. the LRM/UM samples are too altered to exhibit typical ophiolitic characteristics). The PABAM rocks seem to be derived from island arc-type volcanism (which is what Chorlton, 1982, suggested for the whole Port aux Basques Complex). Samples from GABB and GAB/WG, generally have the chemical characteristics of ocean floor

basalts etc., however these units are plutonic and are intrusive into a continental terrain, thus their chemistry may simply reflect their primitive nature (ie. lack of fractionation). The chemical natures of the BSC/DK samples seem to be more typical of within plate basalts. These dykes probably represent a basaltic phase of the gabbro samples (GABB and GAB/WG).

#### 6.7.2 Rare Earth Elements

The chondrite-normalized REE patterns for two samples (79-170A and 80-57) of PABAM are plotted on Figure 33 (along with the PAB/GN samples). These samples have only slight LREE enrichments, small positive Eu anomalies, and Yb is elevated in 79-170A. The patterns most strongly resemble those of basic arc rocks (after descriptions of Anon, 1981- Basaltic Volcanism Study Group). They are distinctly unlike ocean floor volcanics (which have low overall REE contents and depleted LREE's), and are not very similar to continental basic volcanics. If they are arc-type patterns, this is the only direct chemical evidence of arc volcanism in the Port aux Basques Complex (ie. the gneisses seem to be metasediments).

### 6.8 Granitoids

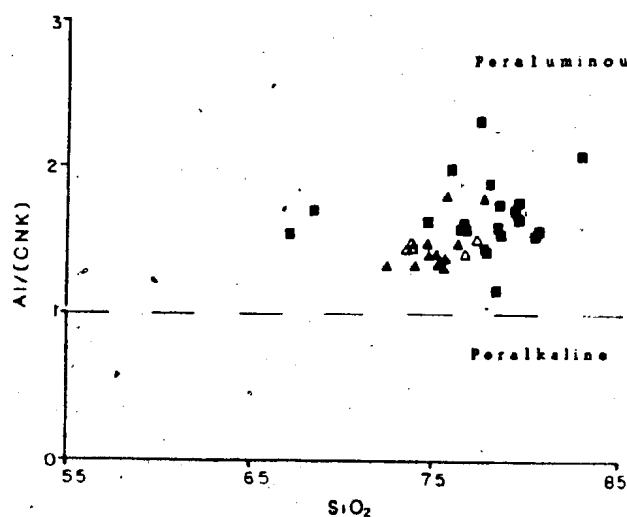
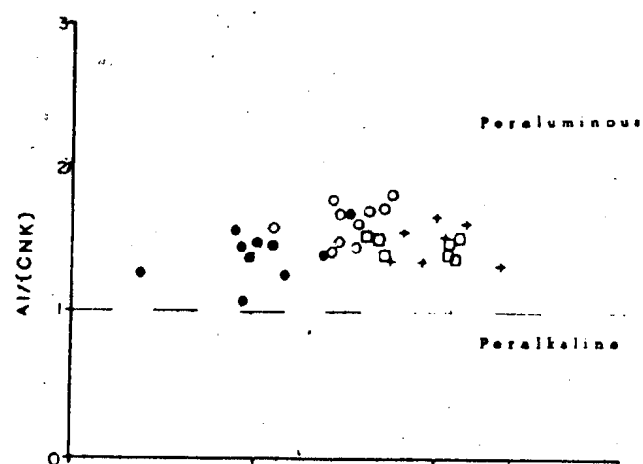
The means (and standard deviations) of chemical composition of each granitoid in this area are listed in Table IX (full data in Appendix IV). There are low MgO, K<sub>2</sub>O and Rb vs. elevated Na<sub>2</sub>O, Pb, Zn, Cu, Y, As, S, Au and Ag concentrations in the Windowglass Hill Granite (WGHGR) with respect to the other granites (the means for the chalcophile elements (Pb, Zn, Cu, As, S, Au and Ag) in this granite are high due to two samples with anomalously high concentrations of the elements, eg. samples WGH SH2B and WGH SH3 which are wall rock to gold/sulphide-bearing quartz veins). The high Na<sub>2</sub>O values are indicative of sodic metasomatism which has affected all samples of this granite. The low MgO results from the lack of a mafic mineral phase. The REE's, La and Ce, have amongst the highest means for all granites.

The Port aux Basques Granite (PABGRN) is distinctive due to the second highest mean Ce content. The tonalite phase of the Cape Ray Granite (CRG-TN) has a chemistry consistent with its mafic nature, particularly with the highest mean V concentration. The megacrystic phase of this same granite (CRG-MX) has the highest mean P<sub>2</sub>O<sub>5</sub>, Sr, Ba and Ce concentrations. Since Sr and Ba typically occur within feldspars, the elevated concentrations in this granite phase are accountable by the microcline megacryst component. P<sub>2</sub>O<sub>5</sub> occurs in apatite which is also abundant in this granite.

The Red Rocks Granite (RD-R-G) has very high mean values of Sr, Ba and Ag. The high mean of Ag is due to a single anomalous value in sample RRG-5, but Sr and Ba are intrinsic to the chemistry of this feldspar-rich leucocratic granitoid. The Strawberry (STG) and Isle aux Morts Brook (IAM/GR) Granites are chemically unremarkable when compared to the others except for the highest Ni contents, and the highest Ga values in the latter. The U and Th concentrations in these post-tectonic granitoids are also elevated when compared to the rest.

All the granites have very similar Barth (1961) mesonorm mineralogies. The most typical composition for all granites is quartz -albite -orthoclase -anorthite -corundum -biotite -sphene -zircon -apatite (except the WGHGR samples which have no normative apatite). Normative actinolite is present in some PABGRN, CRG-TN, CRG-MX, and RD-R-G samples. Chromite is likewise present in norms for the Cape Ray and Port aux Basques Granites. Normative pyrite occurs in those granites with sufficient S. The common presence of normative corundum indicates all these granites are peraluminous (ie.  $Al_2O_3 > Na_2O + K_2O + CaO$ ). This is further illustrated in Figure 46, where all samples plot in the peraluminous field.

According to the normative composition granite classification scheme of O'Conner (1965), as outlined on Figure 47; the PABGRN samples range from trondhjemite to



- CAPE RAY GRANITE (tonalite)
- CAPE RAY GRANITE (megacrystic)
- ◉ (feldspar separate)
- RED ROCKS GRANITE
- + PORT AUX BASQUES GRANITE
- WINDOWGLASS HILL GRANITE
- ▲ STRAWBERRY GRANITE
- △ ISLE AUX MORTS BROOK GRANITE

Figure 46 Al/(CNK) vs. SiO<sub>2</sub> diagram for granitoids in the Cape Ray Fault Zone. Al = Al<sub>2</sub>O<sub>3</sub>; C = CaO; N = Na<sub>2</sub>O; K = K<sub>2</sub>O. All granitic rocks are definitely peraluminous.



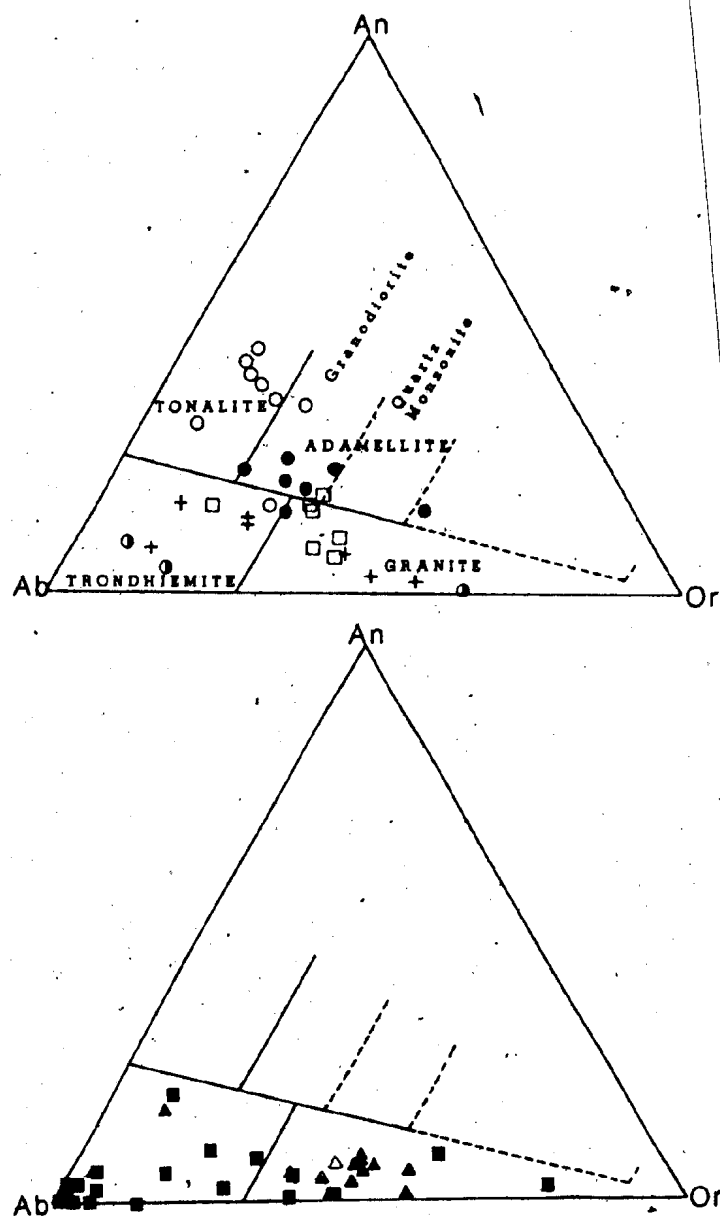


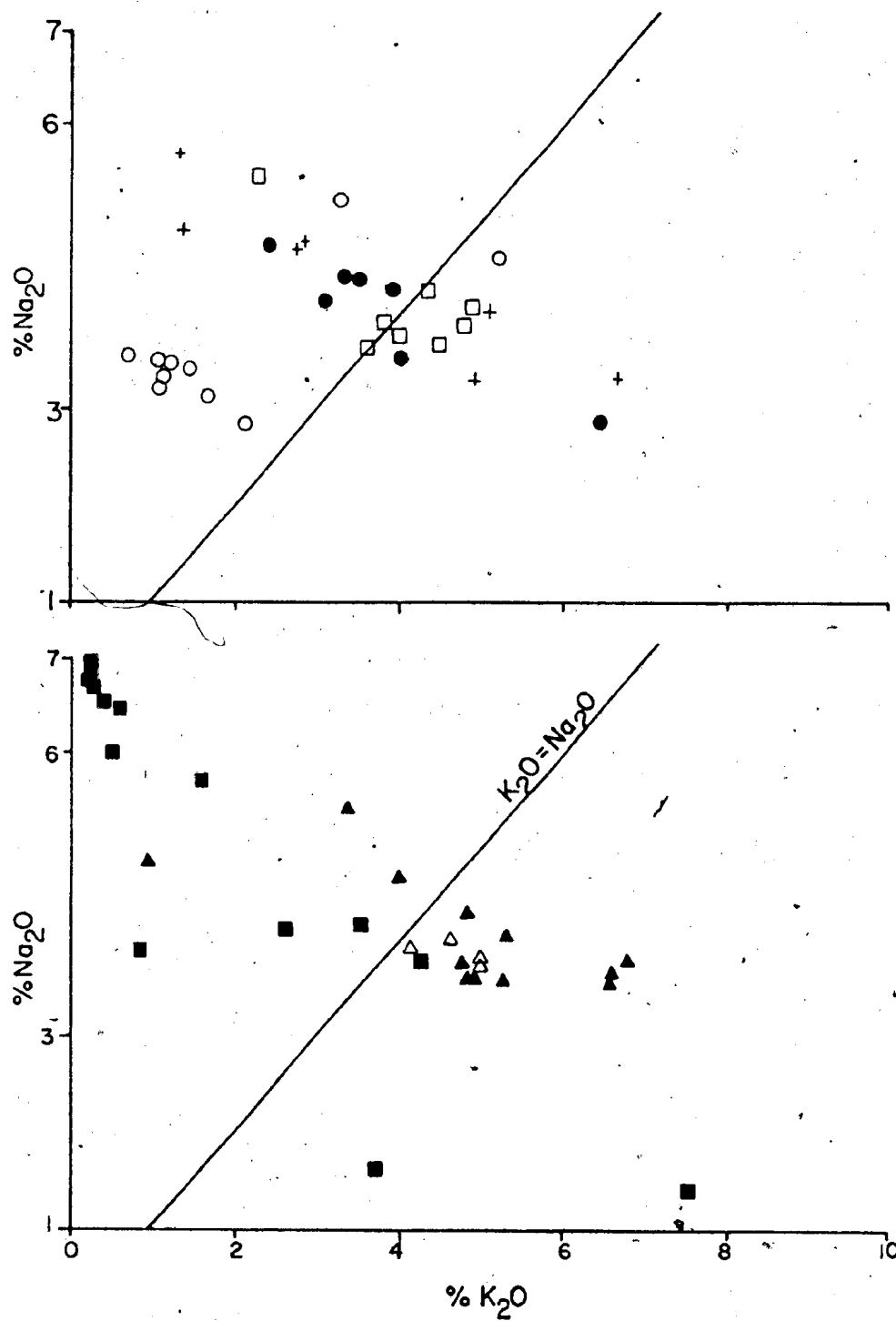
Figure 47 Normative Ab-An-Or diagram for granitoids in the Cape Ray Fault Zone. The classification fields are from O' Conner (1965). Sample key as in Figure 46.

granite; the CRG-TN's are tonalites (with one granodiorite and one trondhjemite); the CRG-MX are adamellites (+ one granite); the RD-R-G's are granite to adamellite; the WGHGR samples are dominantly trondhjemitic with some granite; the STG are granites with a couple of trondhjemite; and all the IAM/GR are granite. The concentration of WGHGR samples in the albite corner illustrates the soda metasomatism experienced by this granite and therefore the distribution is skewed from what the primary compositions should be. The CRG-TN, CRG-MX and RD-R-G samples seem to define a subtle trend from An-rich to An-poor.

As a broad generalization, the granites can be broken down into three main groups, viz.; 1) the Port aux Basques Granite, 2) both phases of the Cape Ray Granite and the Red Rocks Granite, and 3) the Windowglass Hill, Strawberry, and Isle aux Morts Brook Granites. This grouping is also applicable to physical characteristics of these granites, because in Buddington's (1959) classical subdivision, the PABGRN is a catazone granite, the CRG-TN, CRG-MX and RD-R-G granites are of the mesozone, and WGHGR, STG, and IAM/GR granite are of the epizone.

When the alkali contents of these granites are compared to each other (Figure 48) most the granites show a negative correlation to varying degrees, except RD-R-G which plots more as a group. The granites straddle the

Figure 48 Na<sub>2</sub>O vs. K<sub>2</sub>O diagrams for granitoids in the Cape Ray Fault Zone. Sample Key as in Figure 46. See text for discussion.



K<sub>2</sub>O/Na<sub>2</sub>O equal oxide line, except CRG-TN which is on the Na<sub>2</sub>O-rich side. The WGHGR samples generally plot in the very high Na<sub>2</sub>O- low K<sub>2</sub>O end, but there is a minor scatter of values through the K<sub>2</sub>O-rich portion. The 'noise' in the RD-R-G and WGHGR plots indicates a metasomatic overprint on the distribution of these two elements. The extensive consanguineous, inversely-related sodic vs. potassic metasomatism Dingwell (1980) found overprinting the PABGRN, is also reflected in this data.

On the Rb vs. Sr diagram (Figure 49) the RD-R-G, CRG-TN and CRG-MX granites plot in the Sr>Rb field. There is no correlation between Rb and Sr in these units, and the Sr is Rb-independent. The PABGRN samples straddle the two fields and there is a general negative correlation between Rb and Sr (further indicative of the metasomatism). The WGHGR, STG and IAM/GR granites, on the other hand, plot in the Rb>Sr field, contain very little Sr, and the Rb is Sr-independent. The three-fold grouping of the granites is further illustrated when K/Rb is plotted against Rb/Sr (Figure 50). On this diagram the two Cape Ray Granites have wide variations in K/Rb ratios, yet very restricted Rb/Sr ratios (<1). The RD-R-G samples generally parallel this trend with minor scatter. The STG and IAM/GR granites conversely have variable Rb/Sr ratios (>1) yet narrow K/Rb variations. The WGHGR is most similar to the post-tectonic granites but does have a majority of samples in the Rb/Sr <

Figure 49 Rb vs. Sr diagrams for the granitoids in the Cape Ray  
Fault Zone. Sample key as in Figure 46. See text for  
discussion.

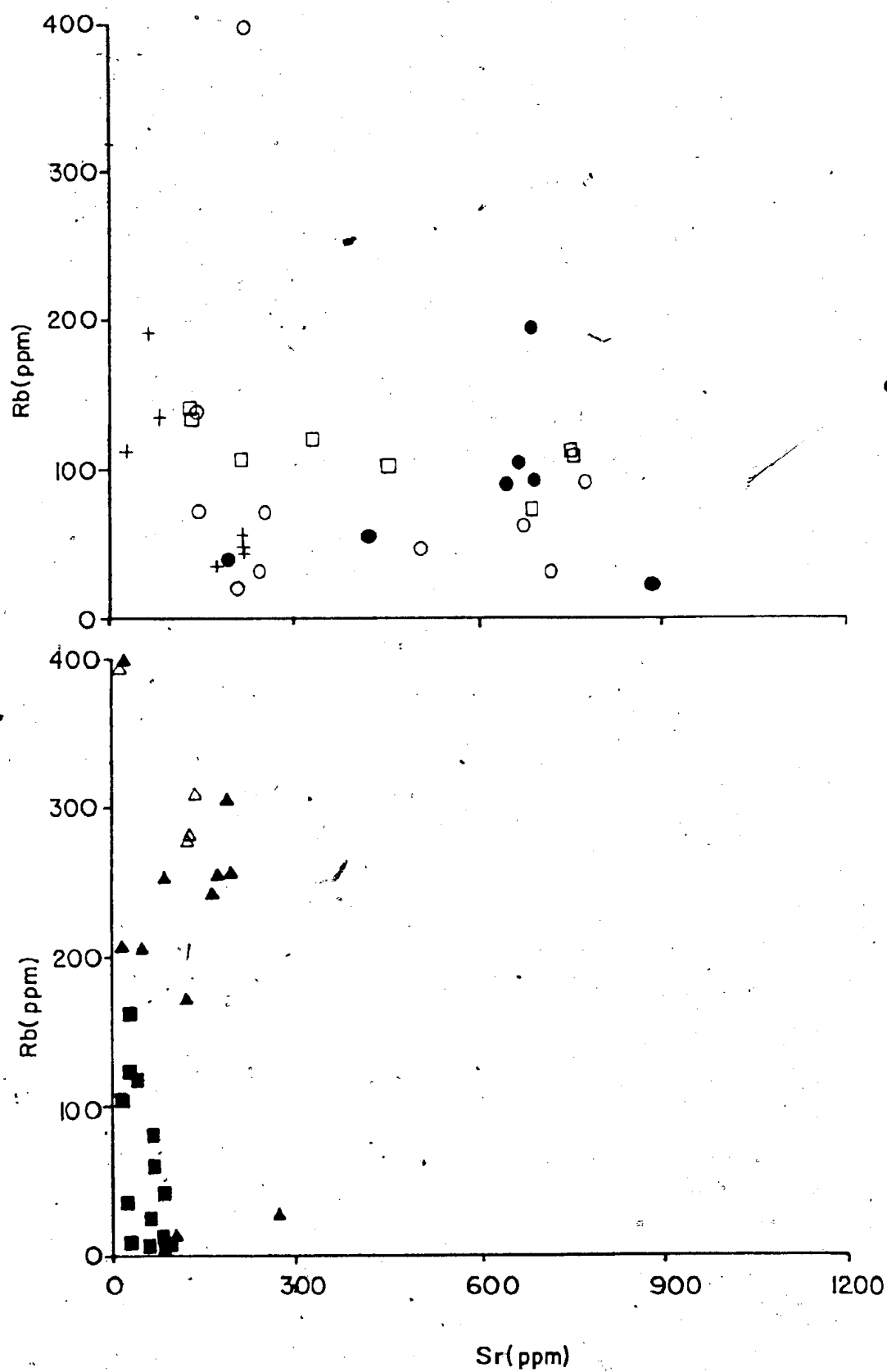
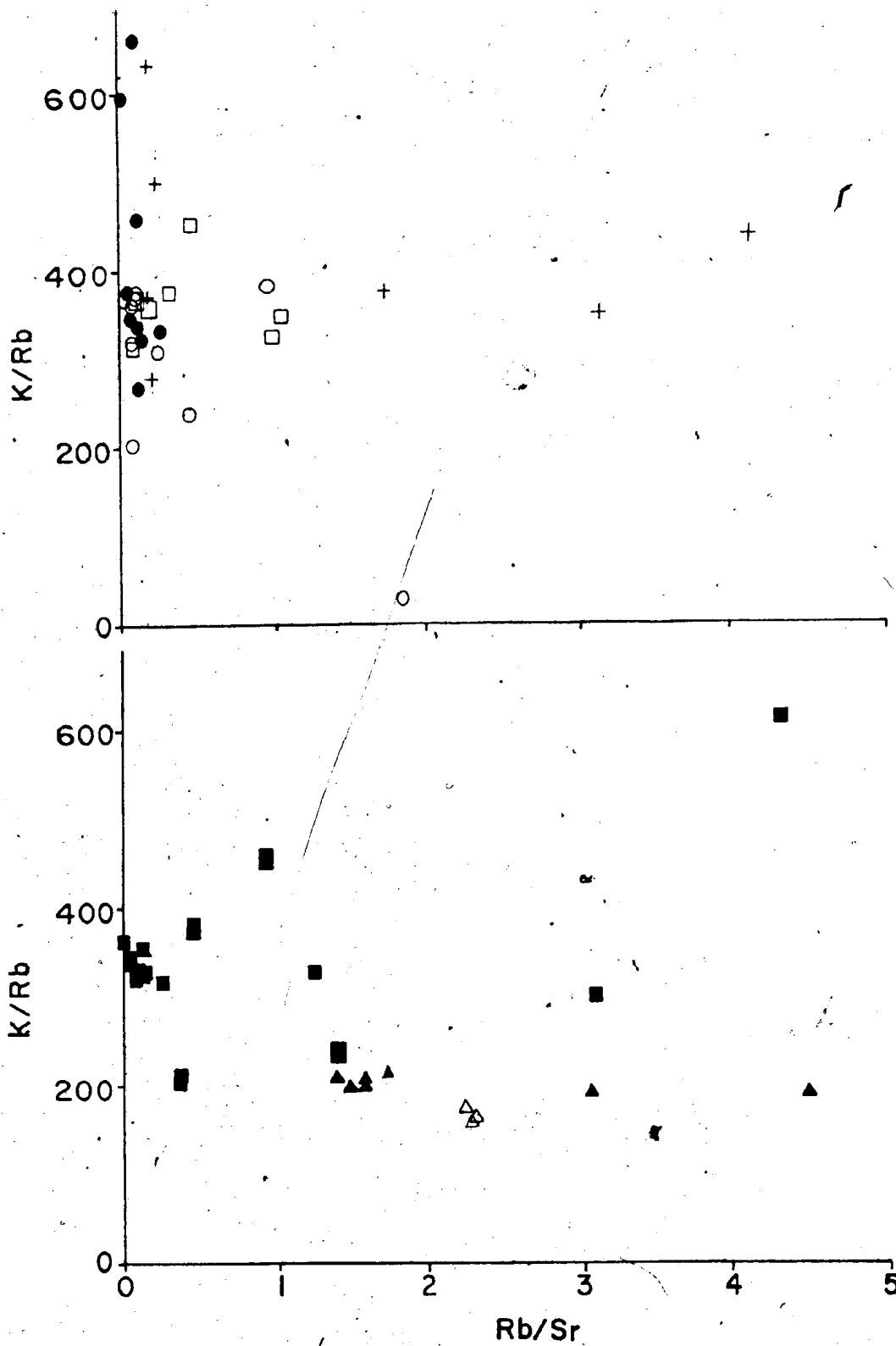


Figure 50  $K/Rb$  vs.  $Rb/Sr$  diagrams for granitoids in the Cape Ray  
Fault Zone. Sample key as in Figure 46. See text for  
discussion.





1 range. The PABGRN samples typically straddle both extremes.

The relationship between Rb and  $K_2O$  in these granites is very uniform (see Figure 51) with mean K/Rb ratios of 364 in PABGRN, 267 in CRG-TN, 355 in CRG-MX, 299 in RD-R-G, 288 in WGHGR, 163 in STG and 115 in IAM/GR samples. The WGHGR, CRG-TN, CRG-MX and RD-R-G samples all lie within Taylor's (1965) coherent field (*ie.* the elements vary systematically). The post-tectonic granites fall in Taylor's (1965) late stage granite field, where Rb is quite enriched relative to normal abundances. This indicates that Rb had increased partitioning into the melt phase (be it partial melt or differentiate) relative to the source. If these granites resulted from fractional crystallization, then they would have to represent very late stages in melt evolution since K would be relatively depleted relative to Rb. On the other hand, if they were partial melts they would have to be either the very first melts (unlikely due to the general granitic composition), or melts from an already depleted source (*ie.* one that's missing K to begin with). The PABGRN, typically, is not restricted to any field on this diagram.

The CRG-TN, CRG-MX and RD-R-G granites define a general trend on an AFM diagram (Figure 52) within the calc-alkaline field and parallel to the trondhjemitic trend of Barker and Arth (1976). The PABGRN samples occur in the

Figure 51 K vs. Rb diagrams for granitoids in the Cape Ray Fault Zone. Fields of normal ratios and late stage granites from Taylor (1965). Sample key as in Figure 46. See text for discussion.

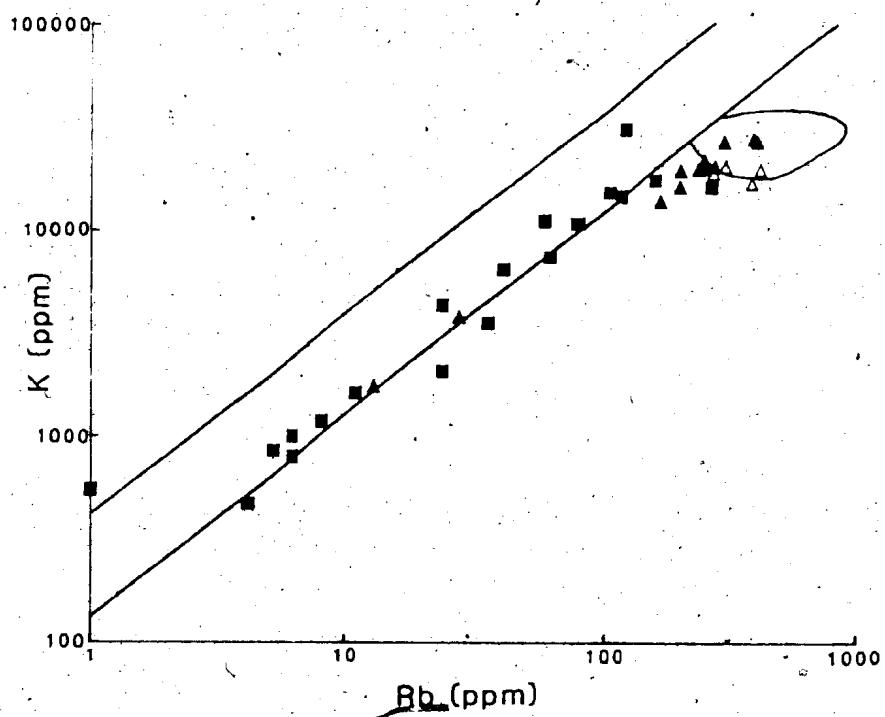
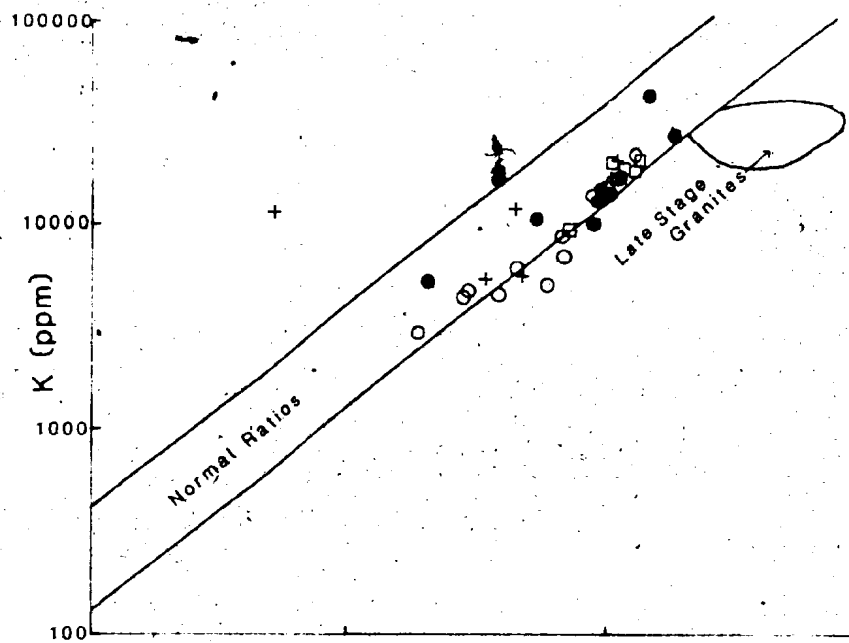
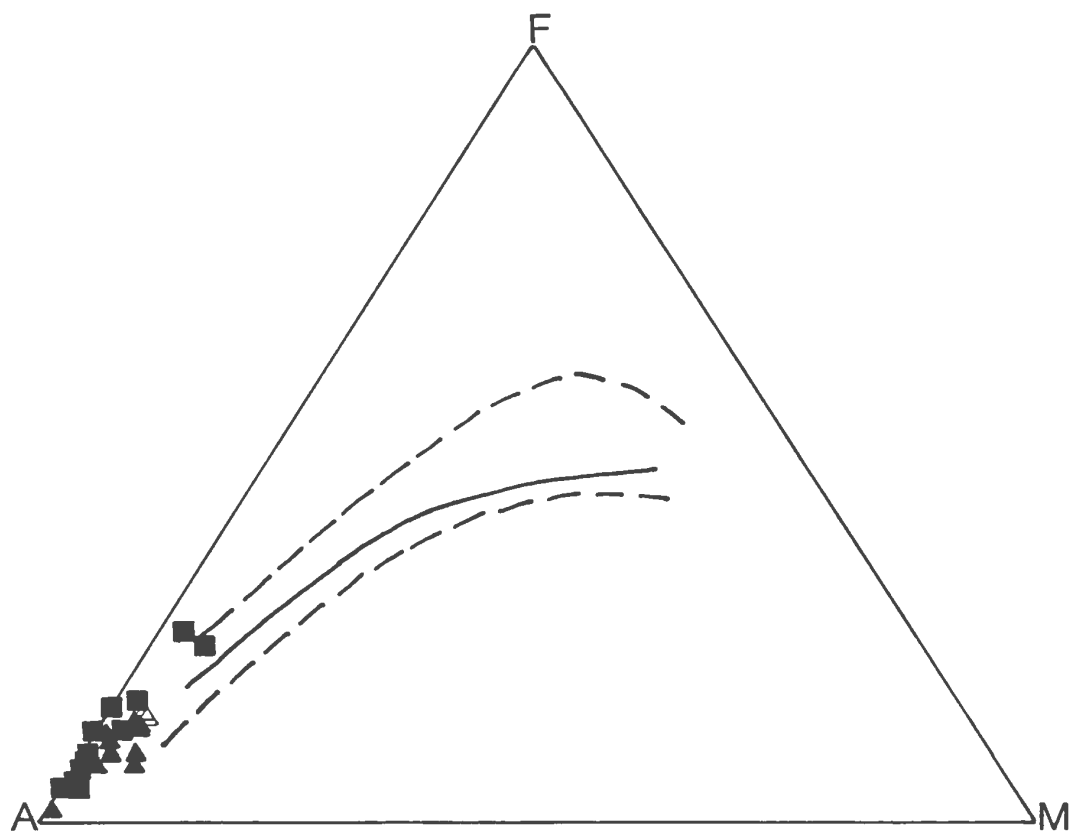
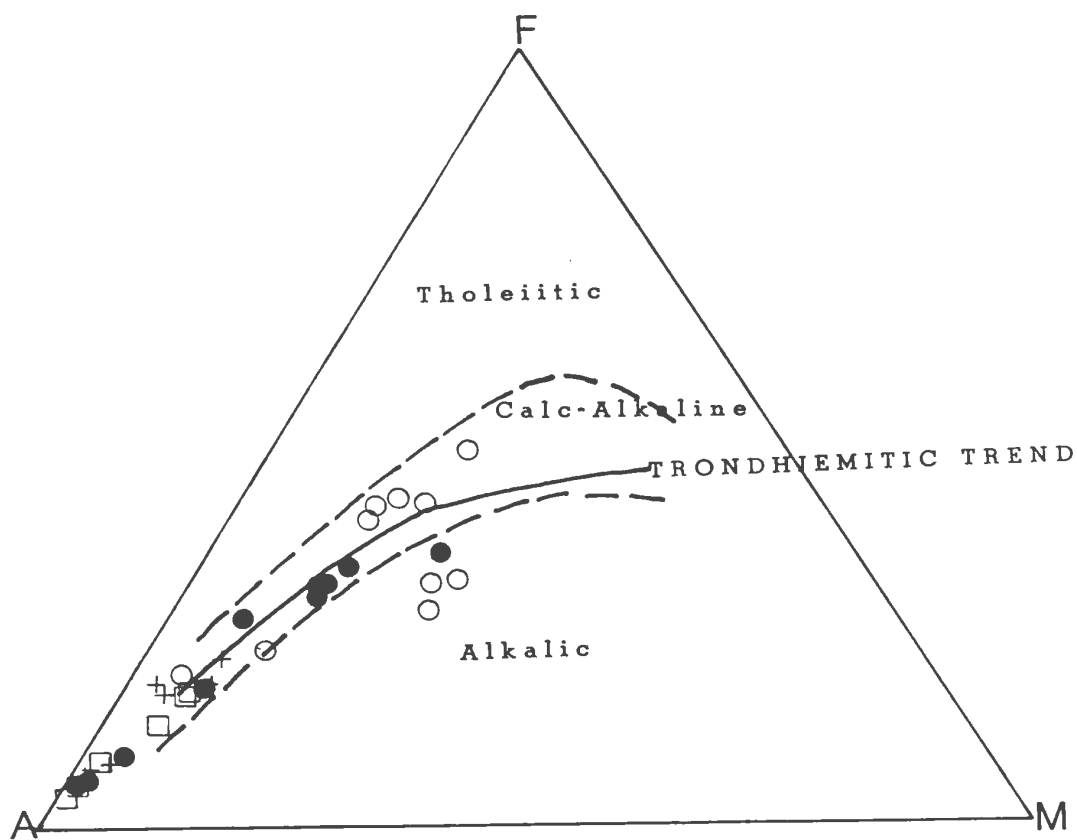


Figure 52 AFM diagrams for granitoids in the Cape Ray Fault Zone.

Sample key as in Figure 46. A =  $\text{Na}_2\text{O} + \text{K}_2\text{O}$ ; F = total Fe as FeO; M = MgO. Tholeiitic, calc-alkaline and alkalic fields are from Irvine and Baragar (1971). Trondhjemitic trend is from Barker and Arth (1975).



lower left hand corner, while the WGHGR, STG and IAM/GR samples plot on the A-F (ie. felsic) join seemingly without a discernable trend.

The calc-alkaline and trondhjemitic trends are separable on a Na<sub>2</sub>O-K<sub>2</sub>O-CaO diagram, Figure 53 (after Barker and Arth, 1976), and the CRG-TN, CRG-MX and RD-R-G granites follow the calc-alkaline trend (going progressively from more mafic tonalite through megacrystic granite to true granite). The PABGRN falls off the trend and its samples are scattered. The STG, IAM/GR and WGHGR granites, as shown on this diagram, have a very small CaO component, and are essentially defined by varying contents of Na<sub>2</sub>O vs. K<sub>2</sub>O.

The apparent common fractionation trend defined by the Cape Ray and Red Rocks Granite is bisected by the 5 kb cotectic of Winkler et al. (1977) in the Q-Ab-Or-An-H<sub>2</sub>O system (Figure 54a). The tonalites plot around the dotted line (ibid.) which divides the melt system into two assemblages; one which contains Or as a component (ie. to the Or-side of the line), and an Or-absent one. The RD-R-G occurs near the cotectic and the CRG-MX samples are on the Q-poor side of the cotectic. According to such positioning, these granites could not represent a fractionation trend, from CRG-TN to RD-R-G through CRG-MX, as the cotectic would have to be crossed in going from CRG-TN to CRG-MX and then the system would have to

Figure 53 CNK diagrams for granitoids in the Cape Ray Fault Zone.

Sample key as in Figure 46. Calc-alkaline and trondhjemitic trends are from Barker and Arth (1975). C = CaO; N = Na<sub>2</sub>O; K = K<sub>2</sub>O.



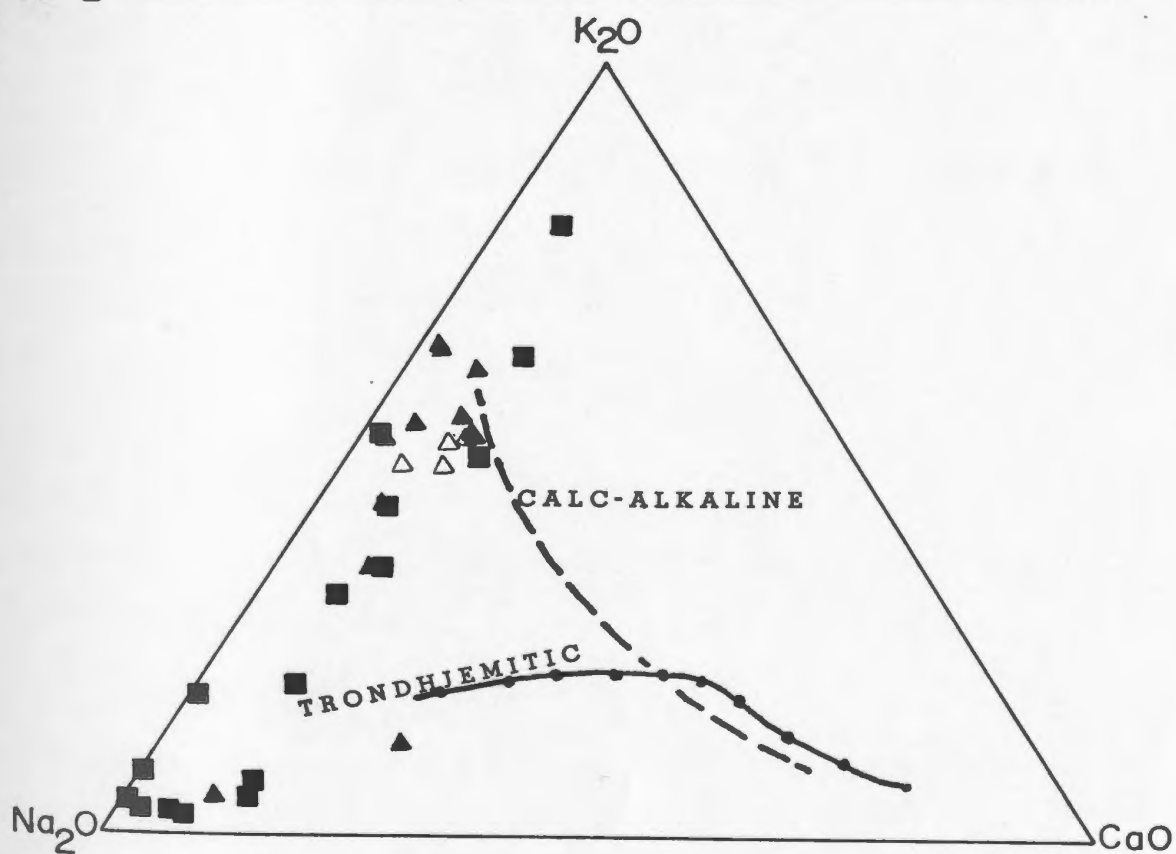
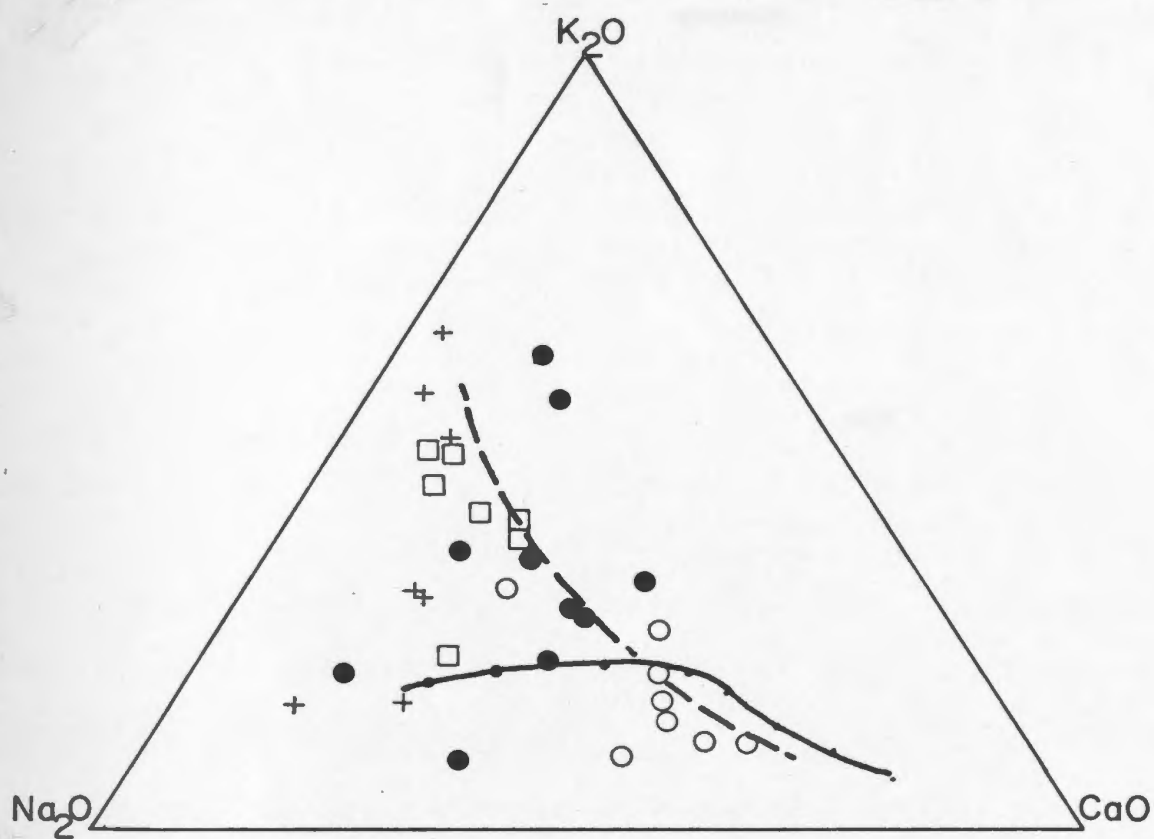
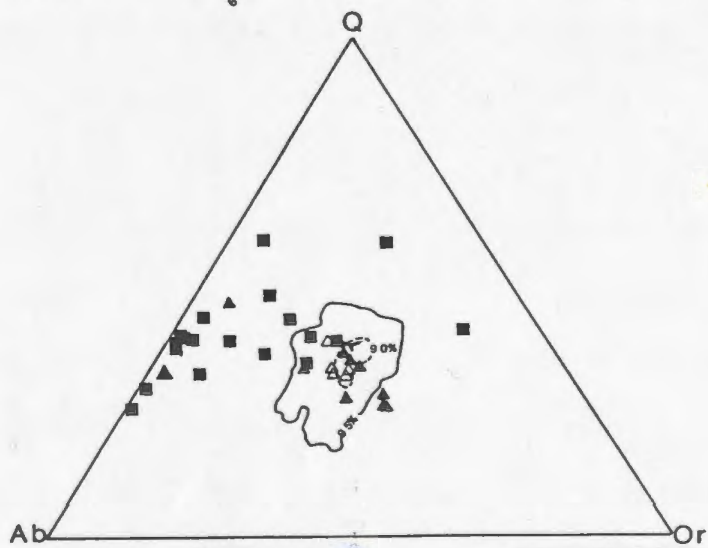
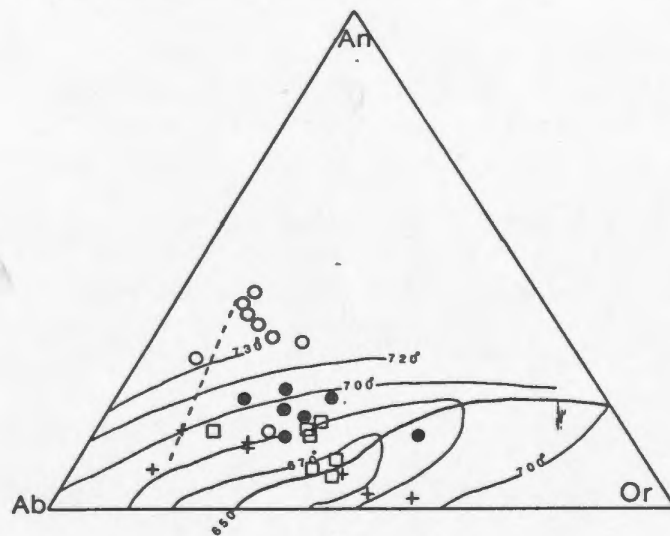
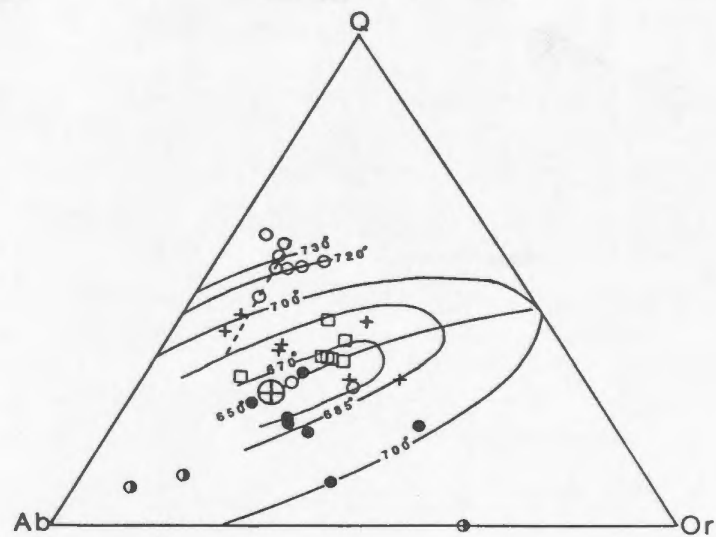


Figure 54a Normative quartz-albite-orthoclase diagram for the Red Rocks, Port aux Basques, megacrystic and tonalitic Cape Ray Granites. The cotectic line and isotherms are from Winkler et al. (1977). Dashed line indicates the dividing line between Or-present and Or-absent assemblages.

Figure 54b Normative albite-anorthite-orthoclase diagram for the Red Rocks, Port aux Basques, megacrystic and tonalitic Cape Ray Granites. The cotectic line and isotherms are from Winkler et al. (1977). Dashed as in Figure 54a.

Figure 54c Normative quartz-albite-orthoclase diagram for the Windowglass Hill, Strawberry and Isle aux Morts Brook Granites. Y represents the the 1 kb cotectic from James and Hamilton (1970), and the contours are areas of predominant granite compositions from Luth et al. (1964).



back-track again from the CRG-MX to RD-R-G, a procedure that is unlikely. However, this diagram contains only three components of a four component system, and the remaining component, An, is a major normative phase in each granitoid (up to 25 wt. % in CRG-TN, 18 wt. % in CRG-MX and 11 wt. % in RD-R-G). When the granites are plotted around the An-Ab-Or cotectic, Figure 54b, (from Winkler et al., 1977), the fractionation trend reappears. The trend approximates decreasing liquidus temperatures until the cotectic is encountered at which time the RD-R-G would finish crystallization. The tonalites again plot on the Or-absent dividing line.

The PABGRN does not fall on any readily defineable isothermal or cotectic surface trends. As described by Dingwell (1980), the extensive Na<sub>2</sub>O/K<sub>2</sub>O metasomatism of this granite yields non-liquidous normative compositions. The WGHGR samples (Figure 54c) likewise yield unreasonable normative concentrations due to sodic metasomatism.

The IAM/GR samples define a fairly coherent grouping when plotted in the normative Q-Ab-Or system (Figure 54c). They fall within Luth et al.'s (1964) 90 % average <sup>17</sup> granite composition and close to the 1 kb ternary minimum from Tuttle and Bowen (1958). However since IAM/GR contains ~ 3 % An, the granite samples more closely approximate the ternary minimum for 3 % An derived by James and Hamilton (1969). This 1 kb crystallization range is consistent with

the andalusite grade (ie.  $< 3$  kb) at intrusive contacts of this granite. The STG samples show more scatter around the IAM/GR samples which probably indicates they represent different levels of crystallization (ie. the IAM/GR is a small homogeneous pluton, while the STG samples were collected from throughout this much larger (and more complex) granite).

#### 6.8.1 Petrogenesis of the Granitoids

Granites can theoretically form as either differentiation products of a more mafic magma, or as partial melts of some pre-existing lithology. Those granites derived by partial melting, resist generalizations regarding chemical and physical properties because of the almost infinite varieties of possible parental material available in the crust and also because of the possible masking effects of magma mixing (eg. a basic magma encounters a solid material in the crust, melts it and then the two melts mix, producing a hybrid magma which owes its fundamental properties to two, possibly completely different, lithologies). One approach that offers at least a qualitative way of examining partial melt granitoids, is that of Chappell and White (1974), and White and Chappell (1977), who divided granites into I (igneous) or S (sedimentary) -types based on whether the source was an

igneous or sedimentary rock. The basis of this subdivision (after Chappell and White, 1974) is:

I-TYPE

S-TYPE

high Na <sub>2</sub> O; >3.2 % in felsic rocks	low Na <sub>2</sub> O; <3.2 % in rocks with up to 5% K <sub>2</sub> O
> 2.2% in mafic rocks;	<2.2 % in rocks with up to 2% K <sub>2</sub> O
Molecular Al <sub>2</sub> O <sub>3</sub> /(Na <sub>2</sub> O+K <sub>2</sub> O+CaO)<1.1	>1.1
CIPW normative diopside or <1% normative corundrum	>1% CIPW normative diopside
broad spectrum of composition from felsic to mafic	relatively restricted in composition to high SiO <sub>2</sub> types
regular inter-element variations within plutons; linear or near linear variation diagrams	variation diagrams irregular

These groups are based on broad generalizations with respect to the chemical compositions of igneous vs. sedimentary rocks (eg. that Na<sub>2</sub>O is removed during sedimentary processes and replaced by K<sub>2</sub>O). The irregularity of variation diagrams in S-type melts reflects the idea that a sedimentary rock is by definition rather chemically inhomogeneous and thus any derived melt would be inhomogeneous. A logical extension of this same argument

is that the MSWD's in Rb/Sr isochron determinations would be large for S-type melts (since the MSWD measures sample variation vs. machine error).

Pre-supposing that the granites in the Cape Ray Fault Zone were partial melts, according to Chappell and White's (1974) definitions, the WGHGR, STG and IAM/GR granites are S-type, the CRG-TN, CRG-MX and RD-R-G are I-type, and the PABGRN is questionably I-type.

To this pantheon of partial melt types (or alphabetical Australian granitoids) a new one has been added, the A-type (or anorogenic) after Collins et al. (1982). As defined by these authors, the A-type granites result from partial melting of a lower crustal felsic granulite that was depleted in the more compatible elements due to production of a previous melt. In comparison with the I-type granites, A-types contain higher abundances of Na<sub>2</sub>O+K<sub>2</sub>O, Nb, Ga, W, Mo, Sn, Zr, Y, REE, Pb and Zn, and lower concentrations of MgO, CaO, V, Ni, Co and Cr. As will be described below, the STG and IAM/GR granites most closely resemble the A-type when compared to the other granites in the area.

Numerous recent studies from regional terrains in such diverse areas as New Mexico (Condie, 1978); New Mexico and Colorado (Barker et al., 1976); Newfoundland (Strong, 1980); Minnesota (Arth and Hanson, 1975); Scotland (Pankhurst, 1979); Australia (Price and Taylor, 1977);

and South Africa (Condie and Hunter, 1976) have shown that groups of granitoids in a given area can have totally different petrogenetic origins, ranging from differentiation to partial melting of various and sundry parental lithologies. The aim of the remainder of this chapter is to provide petrogenetic models for the various granitoids in the Cape Ray Fault Zone. Also included in these discussions, are descriptions of the REE contents of the granites, since REE's have proven to be a powerful petrogenetic evaluator (eg. Hanson, 1978, 1980; Arth, 1979; Strong and Dupuy, 1982; Fourcade and Allegre, 1981; Muecke and Clarke, 1981).

#### 6.8.1.1 The Port aux Basques Granite

Brown (1975) alluded to the possibility that this granite originated as a partial melt of the enclosing Port aux Basques Gneiss (ie. was migmatitic). On the basis of geochemical and gravity data, Dingwell (1980) also concluded that the granite was derived from partial melting of the gneiss. Although not necessarily formed as an in situ melt, he suggested that the granite was intruded very close to its region of generation.

Chondrite-normalized REE patterns for three samples from this granite are illustrated in Figure 55. Two samples, A-3 and A-6, have very similar patterns with



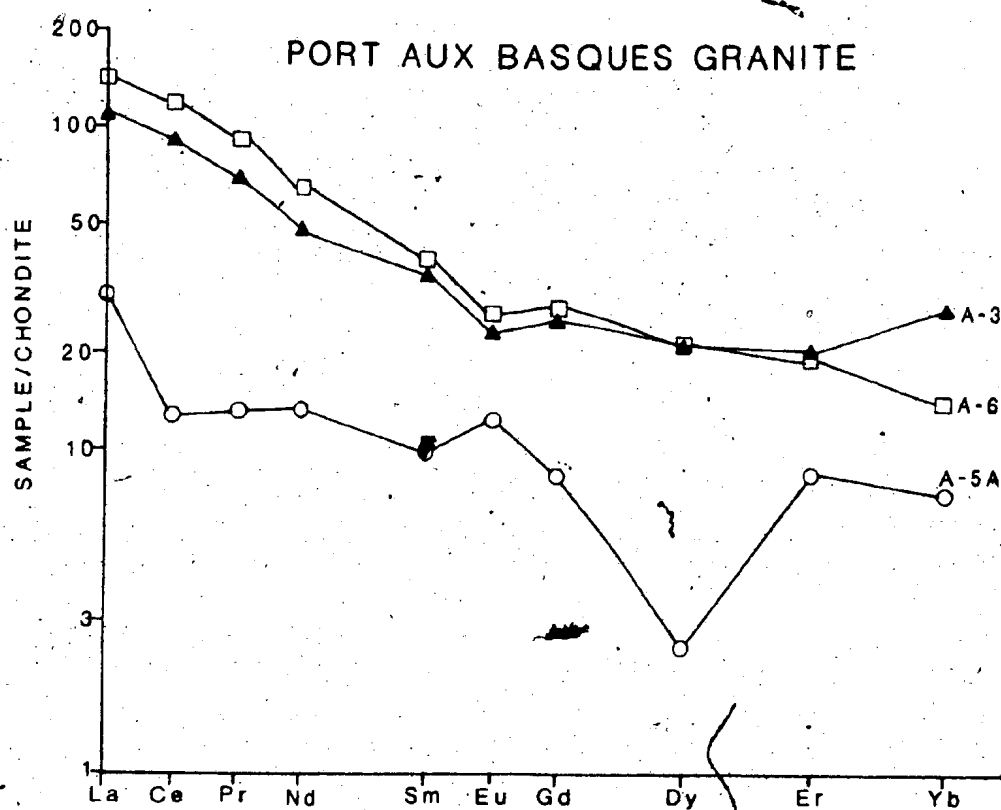


Figure 55 Chondrite-normalized REE patterns for the Port aux Basques Granite. Normalized to Taylor and Gorton's (1977) chondrite values.

enriched LREE's, depleted HREE's, and a small negative Eu anomaly. A-5A, however, has distinctly lower total REE concentrations, a positive Eu anomaly, and a Dy depletion. The CaO, Na<sub>2</sub>O and K<sub>2</sub>O wt. % contents of samples A-3, A-6 and A-5A are 0.48, 3.28, 4.87; 0.38, 3.3, 6.6; and 1.59, 4.73 and 2.82 respectively. Dingwell (1980) showed that accompanying the extensive sodium metasomatism, that overprinted portions of this granite, were enrichments in CaO, Sr and Rb. Sample A-5A has obviously undergone Na<sub>2</sub>O and CaO enrichments relative to the other samples (which resemble the non-metasomatized portions of the granite as reported by Dingwell). The overall REE depletion in A-5A would seem to result from this same metasomatic event. As CaO and Sr were also added to the granite during the metasomatism, and since Eu is chemically similar to these two elements (the so-called Eu anomalies in whole rock samples are due to the strong preferential siting of Eu in feldspars where it substitutes for Ca and Sr), the altered sample also has a positive anomaly. The Dy depletion is most likely a result of analytical error.

The REE patterns for the gneiss samples (Figure 33) are quite similar to those of the granite except for a slight overall REE enrichment and negative Eu anomaly in the PAB/GN. The patterns are consistent with the partial melting of the PAB/GN to yield the PABGRN with only plagioclase as a minor residual mineral (biotite could also

be residual, but would have a negligible effect on the REE distributions (cf. Hanson, 1978, 1980)).

Dingwell (1980) correlated the Port aux Basques Granite with the two-mica leucogranites of the northern Gander Zone as described by Strong and Dickson (1978). These latter two authors suggested that these granites were probably anatectic melts of Gander Zone metasediments. Strong (1980), however, suggested that the Gander Zone and Port aux Basques Granites, though produced by partial melting of metasediments, were also generated by extra heat in the form of frictional heating along major shear belts. He interpreted the Cape Ray Fault Zone and other faults in the Port aux Basques Complex as representatives of such frictional heat-producing shear belts. However, the prograde regional metamorphism described above, reached such intensities, that the partial melting of surrounding metasediments can be ascribed to it alone. Elias and Strong (1982) suggest that granites in the southern portion of the Gander Zone were derived by partial melting of lithologies induced by a combination of mafic mantle-type magmas (produced by subduction) and shear heating, produced by compressive stresses.

#### 6.8.1.2 The Cape Ray and Red Rocks Granites

##### 6.8.1.2a The tonalite

Tonalites are often included in discussions of

trondhjemites, since the latter are by definition, leucotonalites (Barker, 1979). According to Barker and Arth (1976) low Al<sub>2</sub>O<sub>3</sub> (<14.5 % Al<sub>2</sub>O<sub>3</sub>) tonalitic magmas are generated either by crystal fractionation of low potassium andesite magmas, or were generated in the Precambrian by partial melting of amphibolite with residual plagioclase (and thus a negative Eu anomaly in the tonalite melt). High Al<sub>2</sub>O<sub>3</sub> tonalites, on the other hand, are produced by hornblende fractionation of a basaltic magma, or partial melting of metabasalt with residual hornblende and/or garnet (the tonalite magmas thus have a positive Eu anomaly). However Albuquerque (1977) reports tonalites derived by partial melting of metasedimentary rocks.

Figure 56 is Arth's (1979) Yb vs. Al<sub>2</sub>O<sub>3</sub> plot with defined oceanic and continental fields. Two of the CRG-TN samples occur in the low Al<sub>2</sub>O<sub>3</sub> oceanic field (the third has a much lower Yb content than the others and thus falls off the field). The CRG-MX samples occur to the high Al<sub>2</sub>O<sub>3</sub> side, but are not in the continental field (i.e. they have oceanic Yb contents).

The close association of the CRG-TN (and CRG-MX) granites with the ophiolitic remnants of the Long Range Mafic/Ultramafic Complex are superficially suggestive of a genetic link. The ubiquitous amphibolite xenoliths are themselves ophiolitic remnants and they exhibit reaction

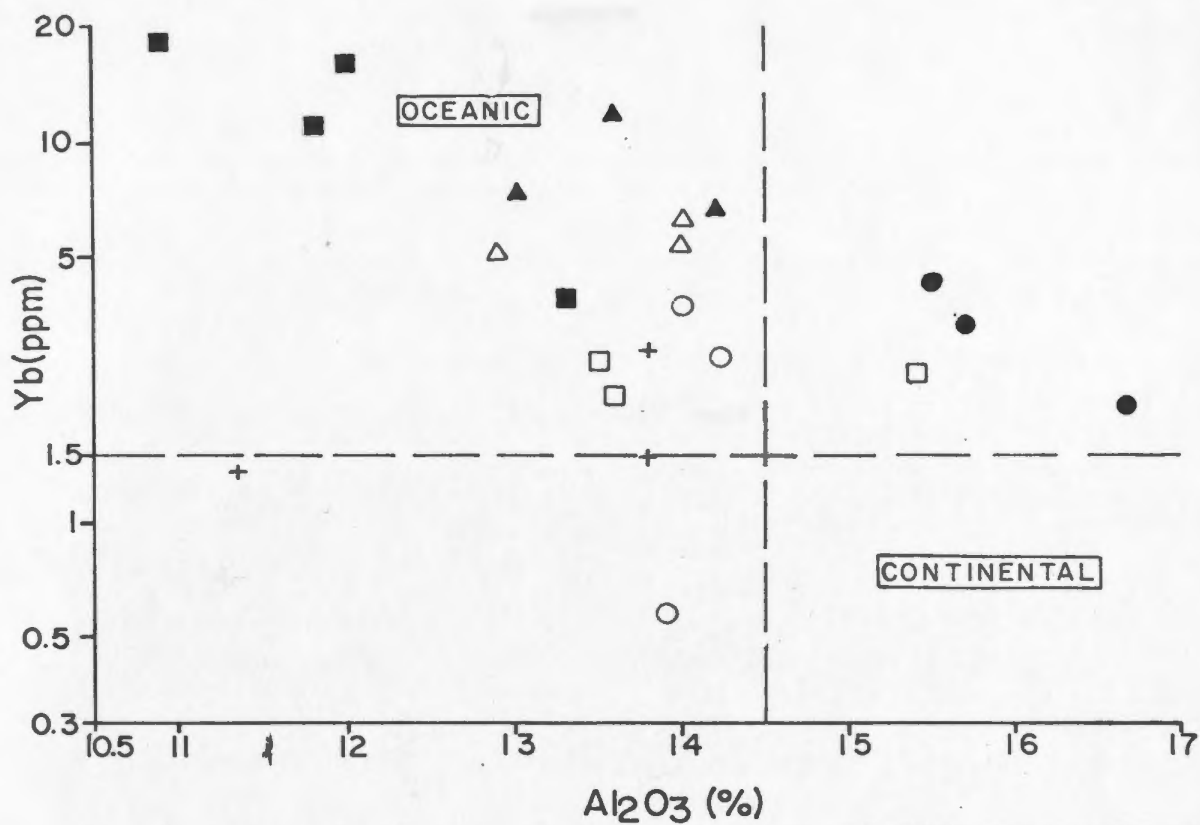


Figure 56 Yb vs.  $Al_2O_3$  diagram for granitoids in the Cape Ray Fault Zone. Sample key as in Figure 46. Oceanic and continental fields from Arth (1979).

rims with the enclosing tonalite reminiscent of the restite-type relations described by White and Chappell (1978). When compared to oceanic plagiogranite (or tonalite-like melts derived by fractional crystallization from mafic magmas), the CRG-TN and CRG-MX samples plot well away from all of Coleman and Peterman's (1975) definitive fields (for example see Figure 57).

The chondrite-normalized REE patterns for the CRG-TN are illustrated on Figure 58a. Also shown are the fields for Nova Scotian tonalites from Albuquerque (1977), and the Saganaga tonalite from Arth and Hanson (1972). The CRG-TN samples have low overall REE contents ( $< 50\times$  chondrite) and positive Eu anomalies. Except for sample 79-68B, the patterns are relatively flat with only minor HREE depletion. In fact the patterns resemble those of weathered sea-floor basalts (eg. Floyd, 1977; Ludden and Thompson, 1979).

Albuquerque's (1977) tonalites, derived from partial melting of metasediments, have enriched LREE's relative to the CRG-TN and a negative Eu anomaly. The LREE-enrichment is a result of higher LREE contents in the source (ie. Albuquerque's patterns resemble NASC). The Saganaga tonalite, derived from partial melting of amphibolite (or eclogite) of basaltic/gabbroic composition, has similar patterns to those of the CRG-TN samples but with depleted concentrations overall. Similar REE patterns to those in

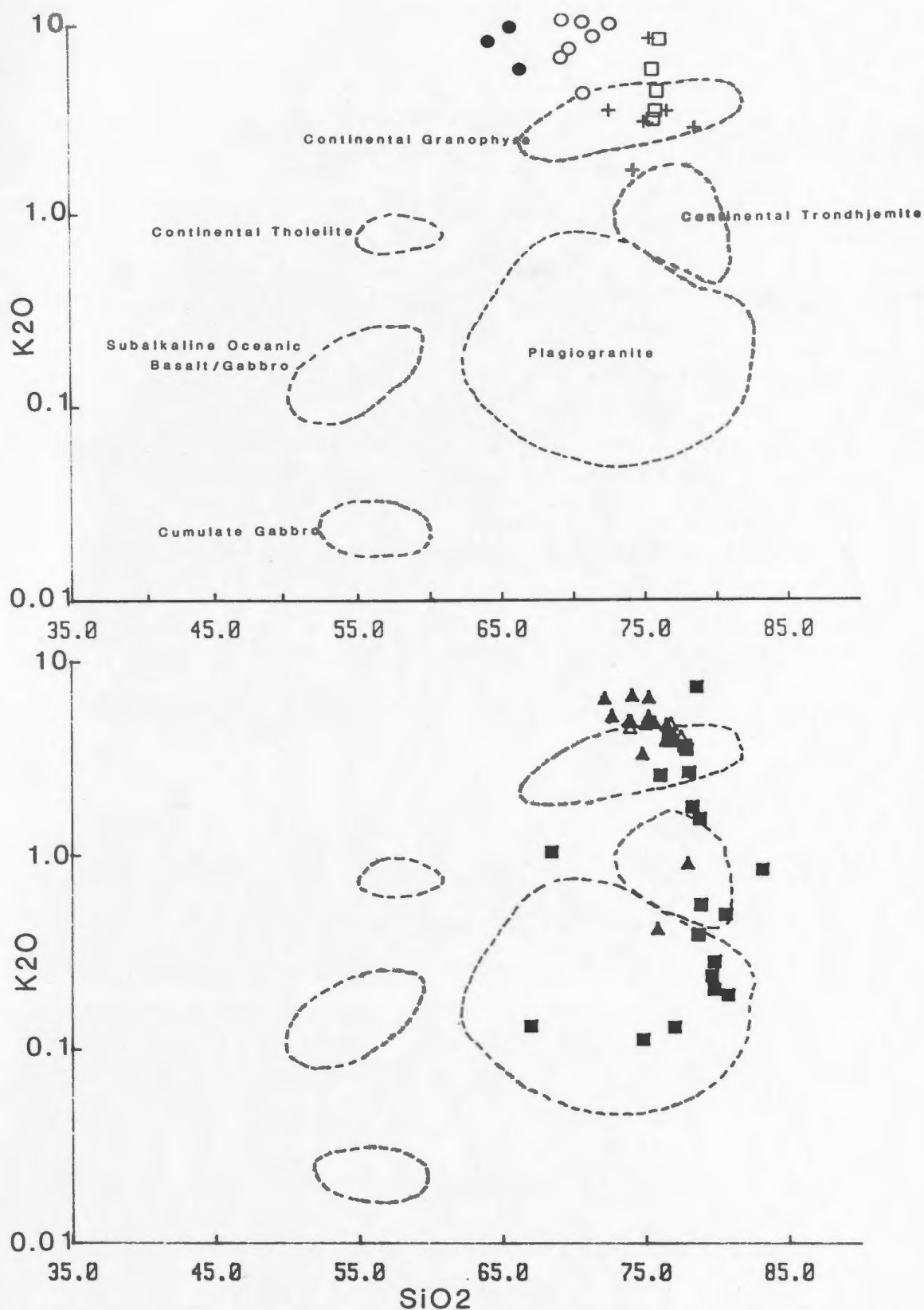


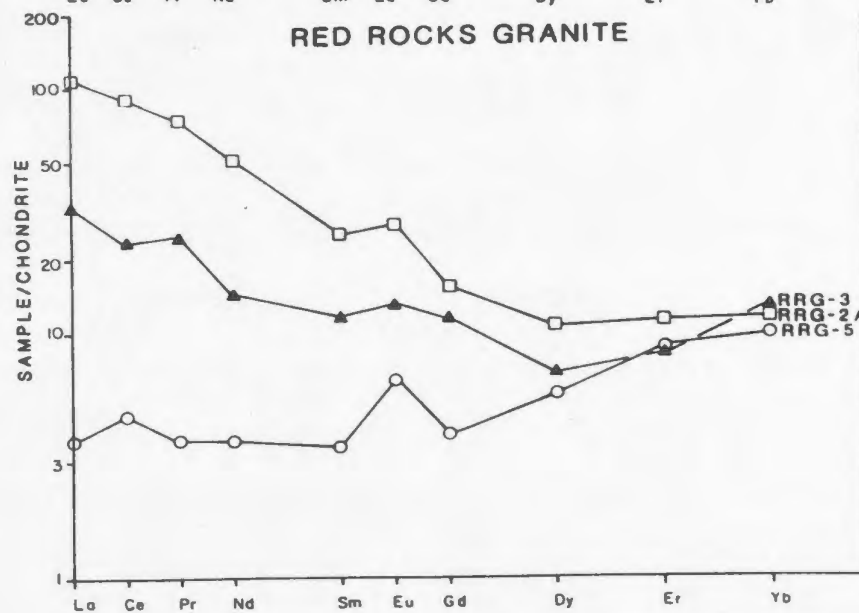
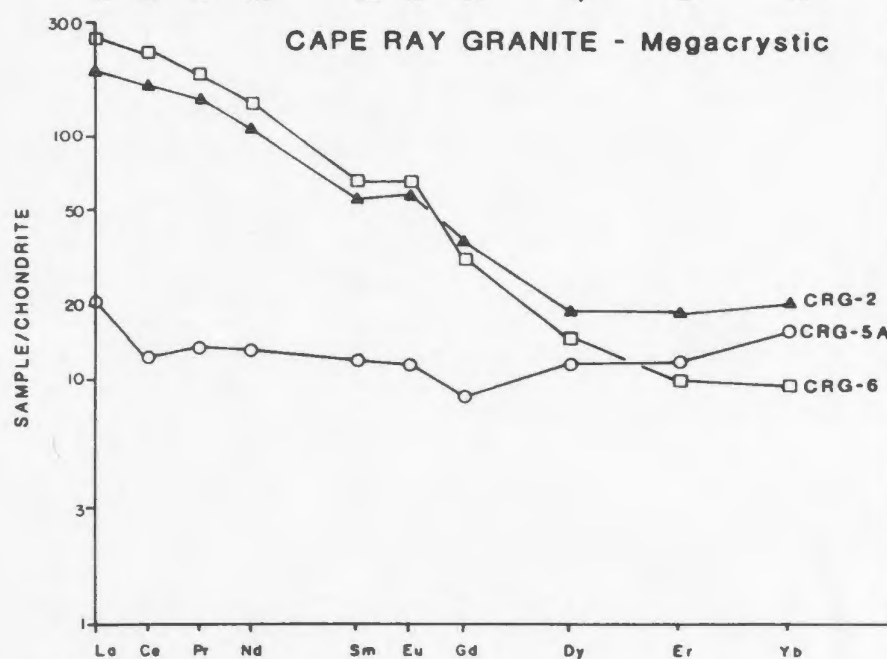
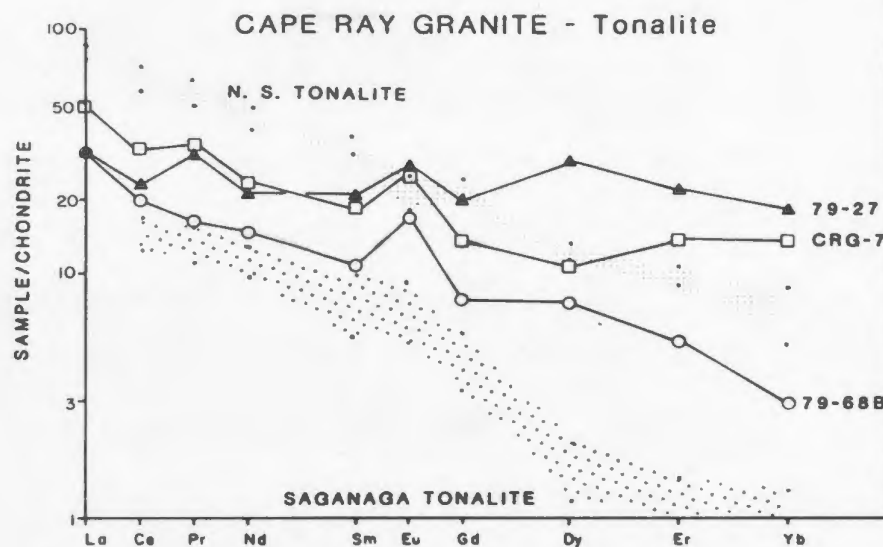
Figure 57  $\text{K}_2\text{O}$  vs.  $\text{SiO}_2$  diagram for granitoids in the Cape Ray Fault Zone. Sample key as in Figure 46. Outlined fields are from Coleman and Peterman (1975).

Figure 58a Chondrite-normalized REE patterns for the tonalitic Cape Ray Granite. Patterns for Saganaga Tonalite are from Arth and Hanson (1972) and for Nova Scotian Tonalites are from Albuquerque (1977).

Figure 58b Chondrite-normalized REE patterns for the megacrystic Cape Ray Granite.

Figure 58c Chondrite-normalized REE patterns for the Red Rocks Granite. All samples were normalized to Taylor and Gorton's (1977) chondrite values.





the CRG-TN have also been reported by Condie et al. (1982) for tonalitic gneisses of southern India, which they state were derived originally from partial melting of mafic volcanic sources, and by Tarney et al. (1979) for tonalites derived by partial melting of amphibolite in the Archean of Scotland and East Greenland.

Overall the CRG-TN tonalite appears to have been derived by partial melting of ophiolitic material such as that represented by the Long Range Mafic/Ultramafic Complex. The positive Eu anomaly suggests that hornblende was a residual mineral, but that plagioclase was not. Furthermore in the remnant xenoliths that are almost totally replaced by tonalite, hornblende is the only visibly residual phase. This is problematical since it is usually suggested (eg. Arth and Hanson, 1972; Barker and Arth, 1976; Arth, 1979) that plagioclase is a residual phase in oceanic environments.

Arth (1979) suggests that the high Al<sub>2</sub>O<sub>3</sub> tonalite-trondhjemites (or those from continental margins/interiors) are derived by partial melting of meta-basaltic material at intermediate crustal levels with residual hornblende. Conversely he suggests that low Al<sub>2</sub>O<sub>3</sub> tonalite/trondhjemites can be the products of partial melting of basalt at shallow depths leaving residual plagioclase. According to Arth, this 14.5 to 15 wt. % Al<sub>2</sub>O<sub>3</sub> subdivision is not a hard and fast rule as both types

often occur in the same environment. The CRG-TN samples have definite oceanic affinities (ie. since the xenoliths are ophiolitic), and also have oceanic REE patterns except for the positive Eu anomaly, typical of continental derivation.

The SiO<sub>2</sub> wt. %s for samples 79-27, CRG-7 and 79-68B are 66.7, 69.1 and 71.7 respectively, ie. the more siliceous the sample, the lower its HREE concentration. Arth et al. (1978) have reported similar inverse relationships between HREE's and SiO<sub>2</sub> in tonalites/trondhjemites from the Kalanti area of southeast Finland which they thought reflected the fractional crystallization of hornblende from a calc-alkaline sequence with a parental<sup>0</sup> gabbroic magma, however they state partial melting of amphibolite may have contributed tonalitic magma. Since there is absolutely no evidence for more mafic parental magmas to the CRG-TN (the tonalite visibly replaces and melts out the only prospective parental material - the ophiolite), the increase of HREE's with decreasing SiO<sub>2</sub> indicates different degrees of partial melting such that 79-68B (the most siliceous) would represent the initial melt while 79-27 represents a higher degree of partial melting. The controlling factor is the greater breakdown of the residual hornblende or zircon (thus releasing the HREE's) with increased partial melting.

The CRG-TN and its associated ophiolitic xenoliths

resemble the Little Port Complex of western Newfoundland (Malpas, 1979) and the Twillingate Trondhjemite of north-central Newfoundland (Payne and Strong, 1979). In the former occurrence, quartz diorites were intruded into ophiolitic metagabbros and amphibolites in much the same manner as the CRG-TN. Malpas (1979) described this sequence as the basal portion of an island arc terrain, and the quartz diorites themselves as partial melts of amphibolites. Payne and Strong (1979) also define the metabasalts and amphibolites of the Sleepy Cove and Moreton's Harbour Groups as representing the base of an island arc. The Twillingate Trondhjemite is intrusive into these metabasic rocks, which Payne and Strong state were partially melted to produce the trondhjemitic magma.

Dunning and Chorlton (1983), and Dunning (1983, pers. comm.) include the CRG-TN within the tonalitic terrain which they define as extending from the Cape Ray area inland to the Annieopsquotch Ophiolite Complex (a distance of over 200 km). Dunning has completed chemical analyses on some of the tonalites intrusive into the Annieopsquotch ophiolites and they are chemically similar to the CRG-TN as reported herein. Dunning's (1983, pers. comm.) tonalites are fairly fresh (unlike the CRG-TN) and though he postulates their origin as resulting from partial melting of the ophiolites, he is also of the opinion that there was some basal continental crust involvement in the melting

processes (this is based on U/Pb isotopic and chemical evidence). This chemical evidence (ie. fresh chemistry and high Al<sub>2</sub>O<sub>3</sub> nature) is lacking in the CRG-TN and there is no direct chemical evidence for crustal involvement in the origin of the CRG-TN itself.

#### 6.8.1.2b The megacrystic phase

Chemically the CRG-MX granitoid is quite similar to that of the CRG-TN (vs. the other granitoids) and forms geochemically coherent trends with the more mafic CRG-TN samples transitional into the felsic CRG-MX samples. On the basis of field evidence (ie. identical xenolith contents and deformational overprinting) and a transitional contact, the CRG-MX and CRG-TN appear to be phases of the same plutonic suite.

The chondrite-normalized REE patterns for the CRG-MX (Figure 58b) differ somewhat from those of the CRG-TN in that they have elevated LREE concentrations. One sample, CRG-5A, however, has a similar pattern. This sample is from a megacryst-poor layer in a region of crystal layering. If the CRG-MX is a more differentiated, or alkali feldspar rich-portion, of the CRG-TN magma, then the higher LREE's represent some combination of residual biotite, (+ hornblende) in the CRG-TN melt, and partitioning of K-feldspar into the CRG-MX (after the

mineral-melt  $K_d$ 's for REE's from Hanson, 1980). Samples CRG-2 and CRG-6 contain 60.8 and 61.5 wt. %  $SiO_2$  respectively, which is up to 10 wt % less than the CRG-TN samples, thus the higher LREE's indicate less dilution of the total REE content by quartz. The low contents of LREE's in sample CRG-5A reflect the lack of sphene and apatite relative to the megacrystic/biotite-rich portions of this phase.

The initial  $^{87}Sr/^{86}Sr$  ratio of 0.709, as determined for this granite, is too high for a magma derived solely from partial melting of mantle (ophiolitic) material and therefore implies involvement (or mixing) of continental-type melts in the more mafic tonalitic magma to produce the megacrystic phase.

#### 6.8.1.2c The Red Rocks Granite

The RD-R-G, like the CRG-MX, occurs as a small, isolated pluton within (and thus in contact with only) the CRG-TN terrain. Lithologically the RD-R-G is unlike these other two granitoids due to the lack of deformation and a finer-grained, more leucocratic texture. The abundant biotite schlieren superficially resemble the xenoliths of the Cape Ray Granites (in the most extreme replacement in these latter granites, the xenoliths become masses of chloritized biotite).

Geochemically the RD-R-G is readily classifiable as a granite. However it contains normative anorthite, very high Sr concentrations, and generally elevated contents of the more 'mafic-type' trace elements (eg. V, Cr, etc.), yet lower abundances of 'felsic-type' trace elements, (eg. Nb, Rb, etc.). The RD-R-G also forms the felsic end member to geochemical trends beginning with the CRG-TN, therefore the RD-R-G appears to be still another phase of the Cape Ray Granite suite.

The chondrite-normalized REE patterns for the RD-R-G (Figure 58c) are similarly transitional into those of the CRG-TN and CRG-MX. All three granitoids have positive Eu anomalies which stand in marked contrast to other granites in the region, which have negative Eu anomalies. Sample RRG-2A (a granite) has a REE pattern quite similar to those of the CRG-MX (ie. CRG-6 and CRG-2). Sample RRG-3 has lower REE contents than RRG-2A, but it also has decreased contents of zircon, sphene and apatite along with elevated SiO<sub>2</sub>, and thus its REE pattern is a reflection of this difference in mineralogy (after the mineral-melt Kd's for those minerals from Hanson, 1978, 1980).

Sample RRG-5 is of a pegmatitic phase. Its lower REE contents are to be expected as it represents a fluid phase evolved from the same melt (ie. a pegmatite) as the other granites (after Hanson, 1980). The enriched HREE of RRG-3 may be due to the influence of carbonate and/or fluorine

complexing within such a late stage fluid (cf. Taylor and Fryer, 1982). The presence of late stage fluids within this granite system is further indicated by chalcopyrite/pyrite-coated quartz veinlets which occur through the granite (ie. like a porphyry-type system) and the saenitic textures in biotite (produced by externally-derived volatile fluxing). The pegmatite (RRG-5) has an even more pronounced HREE-enrichment probably also showing carbonate-complexing in late stage fluids.

#### 6.8.1.2d Conclusions regarding the Cape Ray and Red Rocks Granites

The CRG-TN is easily modeled as the product of amphibolite (meta-ophiolite) partial melting with residual hornblende. Whether the melt represents the root zone of oceanic crust remains to be investigated. The overall physical environment resembles that of the Little Port Complex (Malpas, 1979), or of other terrains such as the Himalayas, which have evidence of large scale regional tectonism resulting from continental collision and/or ocean closure. In the Himalayan examples, oceanic crust is extensively intruded by dioritic-type plutons, the origin of which is a matter of debate. Honegger *et al.* (1982) assume the magmas are the final products of fractionation



from the original mafic parent, while Coward et al. (1982) found the magmas post-dated the mafic volcanics and are associated with their actual deformation (they leave the actual generation of the magmas open for study, but presumably it can't be fractionation from the mafic lavas).

The isolated fragments representing the Long Range Mafic/Ultramafic Complex are remnants of the Iapetus Ocean that probably covered most of the area northwest of the Cape Ray Fault Zone and into the map areas of Brown (1977), Chorlton and Dingwell (1980) and Chorlton (1982) as a continuous sheet and probably was connected with the Annieopsquatch Ophiolite Complex (Dunning, 1981). This ophiolite sheet was subsequently deformed and engulfed by tonalitic intrusives such as that represented by the CRG-TN. Since the ophiolite represents ocean floor material, to melt the ophiolite and produce a tonalite magma, the oceanic geotherm of  $\sim 100^\circ\text{C}/\text{km}$  (Bottinga and Allegre, 1978) would have to be exceeded. However, if the root zone of the ophiolite sheet was continuous to mantle depths (i.e. like typical oceanic crust), there would be no cause to exceed solidus temperatures.

One method of producing temperatures high enough to exceed both the oceanic geotherm and solidus temperatures would be to drastically thicken the ocean crust such that its basal P-T conditions were out of equilibrium causing melting (eg. 5

kb as in the Q-An-Ab-Or system after Winkler et al., 1977). In order to thicken the oceanic crust it would either have to be overlain, or would itself have to overlie other crustal material. Since there is no evidence of any great thickness of sediments overlying the ophiolites, the ophiolites must themselves be thickened by mechanisms like thrusting or obduction, which are commonly accepted as the origins for the Bay of Islands and Hare Bay allocthons (eg. Williams, 1979).

Alternatively the actual obduction process, somewhat akin to large scale thrust faulting, may have generated sufficient mechanical heat to begin melting (cf. LeFort, 1978; Strong, 1980). Whatever the mechanism (or combination of mechanisms) for melting of the ophiolitic material, the production of the CRG-TN implies some large-scale deformational tectonics involving the Long Range Mafic/Ultramafic Complex as an allocthonous layer. Beneath this complex is either more oceanic crust or continental crust of the western margin of the Iapetus.

The CRG-MX and RD-R-G granites appear to be isolated pockets within the tonalite terrain produced by differentiation and/or mixing (involving basal continental crust) processes from the tonalitic magma. Support for such a model comes from the experimental work of Whitney (1977), who showed that during cooling of tonalite magma, at up to 2 kb and with 2-4 % H<sub>2</sub>O, pockets (or caps) of an

aqueous vapour phase will evolve from the melt (ie. as lower temperature zones). Alkali feldspar (+ quartz and plagioclase) are concentrated in this vapour phase, leaving the melt more enriched in plagioclase and quartz (ie. tonalitic) components. The RD-R-G would represent an even more evolved vapour phase-type assemblage. Wyllie (1977) suggested that in the deeper parts of some batholithic regions, the removal of interstitial granitic liquid from more refractory crystals (tonalitic) can produce small plutons enriched in alkali feldspars at higher levels. Finally, Naney and Swanson (1980) have shown that Mg and Fe can cause rapid crystallization of mafic phases relative to alkali feldspar and quartz (in their experiments, crystallization of felsic material often could not be achieved, while more Fe/Mg-rich melts readily crystallized). This means that any pockets of the more felsic material may remain liquid within the crystallized (or crystallizing), more mafic, host. If such a liquid could be tapped or collected, felsic zones could be produced.

Rollinson and Windley (1980) have described a very similar sequence in the Lewisian complex of the Scourie-Badall area, Scotland, wherein a tonalitic melt was parental to granitoid sheets ranging from trondhjemite to granite. The tonalite is intrusive into gabbro-ultramafic complexes and the felsic sheets in turn intrude the

tonalite and ultramafics. Fractional crystallization of hornblende and/or plagioclase from the tonalite produced the trondhjemite and fractional crystallization of plagioclase from the trondhjemite, produced the granites (+ granodiorites). These authors state the tonalite was derived by partial melting, or hornblende and/or garnet fractionation, from a basic parent but the actual mechanics and source are at present indecipherable.

The initial  $87\text{Sr}/86\text{Sr}$  ratio of the RD-R-G (as derived in the poorly fitted errorchron of Figure 8) is 0.708, which is high for a melt supposedly derived solely from an oceanic source. Because of this, contamination of the differentiated tonalite-derived melt by continental crust is a likely possibility. If this is indeed the case, then the ophiolitic sheets are ultimately underlain by continental crust.

#### 6.8.1.3 Windowglass Hill Granite

This is the most felsic granitoid in the area. In terms of Chappell and White's (1974) classification, it would be a typical S-type granite (high  $\text{SiO}_2$ , non-linear variation diagrams, etc.), except  $\text{Na}_2\text{O}$  is much greater than  $\text{K}_2\text{O}$ . The initial  $87\text{Sr}/86\text{Sr}$  ratio of 0.710 is high enough to be indicative of crustal (vs. mantle or mafic) derivation. The granite was subjected to sodic

metasomatism, however this event could not have occurred at any significantly later post-intrusive (or crystallization) period because; a) overall chemistry (eg. Rb-K covariance) has not been strongly affected, b) the Rb/Sr radiometric date was based on samples from throughout the pluton, and its well-fitted isochron indicates isotopic, and thus elemental, equilibrium, c) the late Devonian age itself is geologically reasonable, and if metasomatically re-set, the re-setting had to be close to the actual age. Thus the alteration seems to be deuteric. Deuteric (hydrothermal) alteration, according to Barker (1970), is a typical effect within granophyric granites such as the WGHGR. (He suggests derivation of the fluids, as an aqueous phase, is due to rapid crystallization).

The chondrite-normalized REE patterns for five samples of this granite are illustrated on Figure 59. Samples WGH-1 and 79-112 are typical of this granite and have very elevated overall REE concentrations with highly enriched LREE's to HREE's. They also have a negative Eu anomaly. Sample 79-74 is from the mylonitized northeastern extension of this granite in H Brook and it differs from the other samples because of depleted HREE contents. This depletion is strong enough to mask the negative Eu anomaly and it is reasonable to assume the depletion is the result of hydrothermal alteration. Since this sample is from a mylonitized zone, the alteration was probably initiated

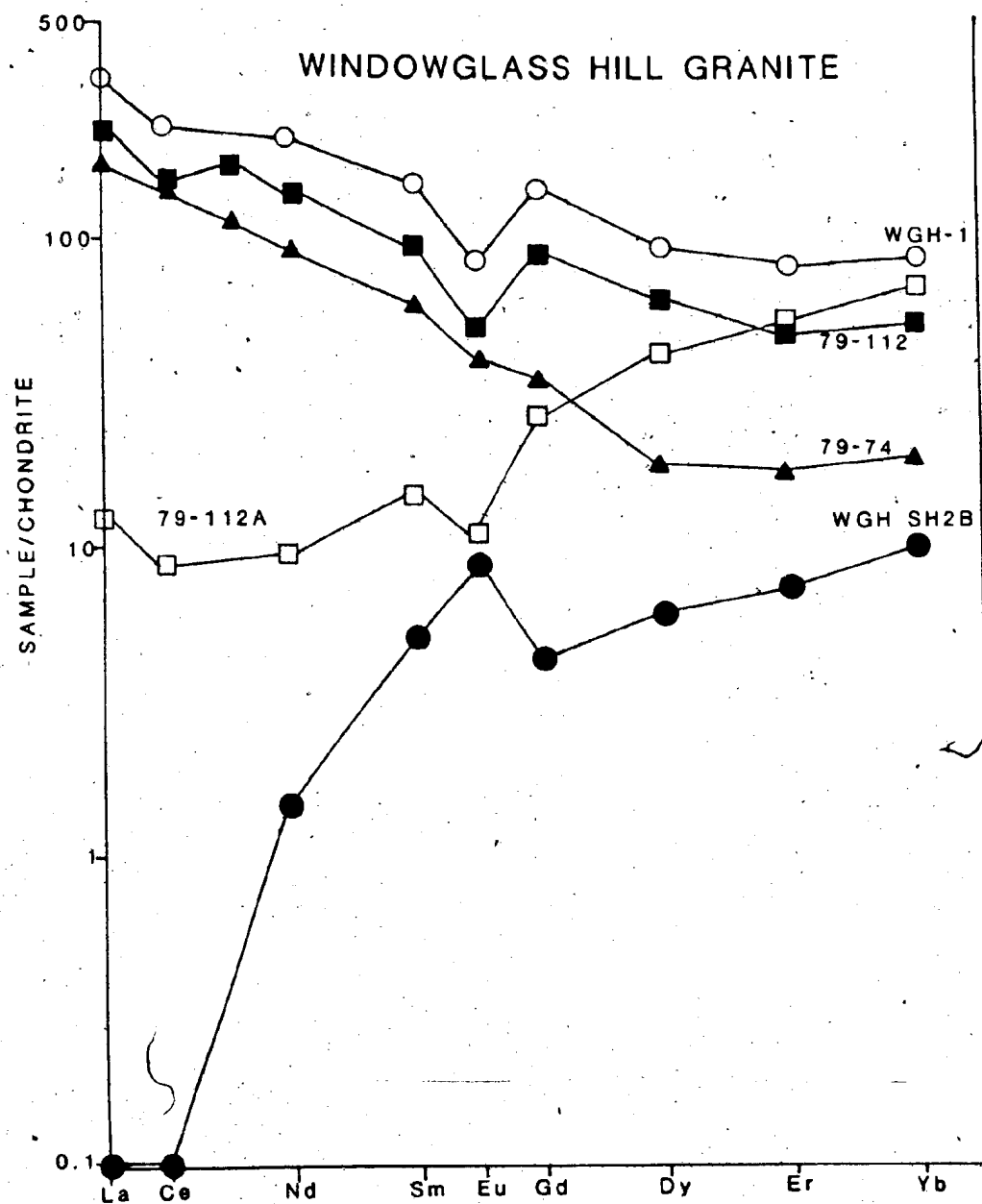


Figure 59 Chondrite-normalized REE patterns for the Windowglass Hill Granite.

during deformation. Taylor and Fryer (1982) report similar HREE depletions during leaching at Climax, Colorado.

Sample 79-112A on the other hand has a very intense LREE-depletion in comparison with the other WGHGR samples. It comes from within the main mass of the pluton and has no petrographic differences from the other samples. However, it has much lower CaO and K<sub>2</sub>O concentrations and elevated Na<sub>2</sub>O (6.56 wt. %). It also has lower Rb, Ni and higher Nb than typical WGHGR. The LREE-depletion therefore seems to result from the albitization experienced by this granite.

Mineyev (1963) reported removal of LREE's during albitization of granites in Kazakhstan. He found that there was a progression of depletion with increasing degrees of alkali metasomatism and Ca-removal. According to Mineyev this zonation results from increasing acidity of the hydrothermal solutions and he likens the albitized granitoids to pegmatites.

Sample WGH SH2B shows an extreme degree of LREE-depletion. This particular sample is from altered granite that forms the actual host (ie. selvage) to a gold/sulphide-bearing quartz vein. This LREE-depletion is coupled with a decrease in CaO, K<sub>2</sub>O, U, Zr, Nb and Ni, and an increase in V, Cr, Ga and SiO<sub>2</sub> contents relative to unaltered granite. Since the LREE-depletion accompanies both mineralization processes (cf. the LREE-depletion in

wall rocks to the Main Shear Showing also had LREE-depletions) and albitization in the WGHGR, the hydrothermal ore fluids and deuteric alteration fluids appear to have been one and the same.

In order to ascertain the relative losses or gains incurred by the granite due to hydrothermal fluids, volume factors (fv's) were determined between sample WGH SH2B and the non-wall rock granite sample with the highest S.G., the sample with the lowest S.G., and the mean hydrated granite (with mean S.G.) in the same manner as outlined in section 6.2.6.1 above. Al<sub>2</sub>O<sub>3</sub> was again assumed to be immobile and the relative gains and/or losses were determined using the Al<sub>2</sub>O<sub>3</sub> fv (see Table XIV for sample identification and S.G.).

MAX. S.G.	SAMPLE	MIN. S.G.	SAMPLE	MEAN S.G.
2.700	80-186	2.341	WGH-4	2.525

TABLE XIV Samples and Specific Gravities for Volume/Density Calculations

A significant amount of SiO<sub>2</sub>, and smaller amounts of Fe<sub>2</sub>O<sub>3</sub> and MgO, were added, and a noticeable Na<sub>2</sub>O and minor CaO depletions were superimposed on the wall rock. The other major oxides show negligible change. In the trace elements, extremely large quantities of Pb, Zn, Cu, V, Cr, Ga, Au, and especially Ag were introduced into the wall rock, while significant quantities of Th, Sr, Y, Zr, Nb and Ce were removed (La is depleted in the min. and mean S.G.



samples and only slightly added in max. S.G. computations). The most striking characteristics of the alteration induced by ore-bearing hydrothermal fluids was extreme enrichment in the chalcophile elements, and depletion in some of the 'felsic' elements. The depletion in Na<sub>2</sub>O and addition of Ca, Pb and Ag are the only alteration effects in common with the WAL/RX samples.

Volume/density relationships were also examined in sample 79-112A (i.e. with the LREE depletion). Additions include SiO<sub>2</sub>, Fe<sub>2</sub>O<sub>3</sub>, MgO, Th, Nb, Cr and Au (+ S), while CaO (minor), U, Sr (significant), Cu, Ni, Ba, Ce and Ag, are depleted. The alteration changes in this sample closely parallels those in the wall rock samples with additions of SiO<sub>2</sub>, Fe<sub>2</sub>O<sub>3</sub>, MgO and Au, and depletion of CaO, Sr, La and Ce. Na<sub>2</sub>O is not a factor in these volume/density relationships as the entire granite has undergone such a pervasive sodic metasomatism that relative changes between selected samples are not as significant as the increase in Na<sub>2</sub>O content through the whole granite when compared to other granites.

Very similar REE patterns (except for the HREE or LREE-depleted samples) have been reported by Walsh and Henderson (1977) for the granophyre intrusion in Centre 3 at Ardnamurchan. Though the basic rocks (eucrites, gabbros and dolerites) in this centre formed by fractionation from a single mafic parent, Walsh and Henderson found that the

granophyre would not fit this model and had to be derived by some other melting event.

Nicollet et al. (1979) have also reported very similar REE patterns, including a sample with the same LREE-depletion, from the Southern Massif Central in France. The authors call the unit a trondhjemite, yet it has similar chemical characteristics to the WGHGR except for higher CaO, MgO, Sr and Cr, and lower Na<sub>2</sub>O, K<sub>2</sub>O and Rb concentrations (ie. slightly more mafic). Their LREE-depleted sample (No. 6) has the lowest Na<sub>2</sub>O concentration of all their samples and has no evidence of albitization, so the authors feel the depletion resulted from fractionation of zoisite out of the sample (they feel that zoisite has a LREE enrichment like allanite, and No. 6 has no zoisite unlike the other samples). As for the origin of the trondhjemites themselves, Nicollet et al. (1979) feel that they must have resulted from partial melting of an igneous felsic parent with trondhjemitic affinities, due to their very felsic and differentiated natures.

The REE-enriched composition of the WGHGR also implies that its parent must likewise have elevated REE concentrations. The negative Eu anomaly implies either residual plagioclase in, or plagioclase fractionation from, the source, however since the WGHGR represents such a low temperature melt (ie. granite minimum) and since the

residual, or fractionated, feldspar (with its very high residual/melt  $K_d$  for Eu) must be minor, the source itself be very felsic (*ie.* to have such a small amount of fractionated or residual plagioclase).

The WGHGR is chemically similar to the basal Windsor Point Group ignimbrite (WPGIG), except that the latter underwent potassic deuteric alteration. However, these deuteric alterations indicate both units had magmatic vapour/fluid phases. Both units have a similar initial  $^{87}\text{Sr}/^{86}\text{Sr}$  ratios (of 0.710 and 0.709) and are about the same age (*ie.* 368 and 377 Ma respectively), thus the WGHGR may represent a sub-volcanic equivalent of the WPGIG. As such the granite would be derived from the same source as the felsic volcanics but may have undergone some plagioclase fractionation. As postulated above, the volcanics were probably derived by partial melting of continental crust at depths of up to 20 km (after Hildreth's (1981) model).

#### 6.8.1.4 Strawberry and Isle aux Morts Brook Granites

These post-tectonic granites have characteristics of both the biotite granite and alkaline (peralkaline) granite subdivisions of Newfoundland granitoid rocks as outlined by Strong (1980). The biotite granites, according to Strong, are both pre and post-tectonic (440-312 Ma), are high

level, and in the case of the Ackley City batholith, contain molybdenite. The STG and IAM/GR granites easily fit in this classification.

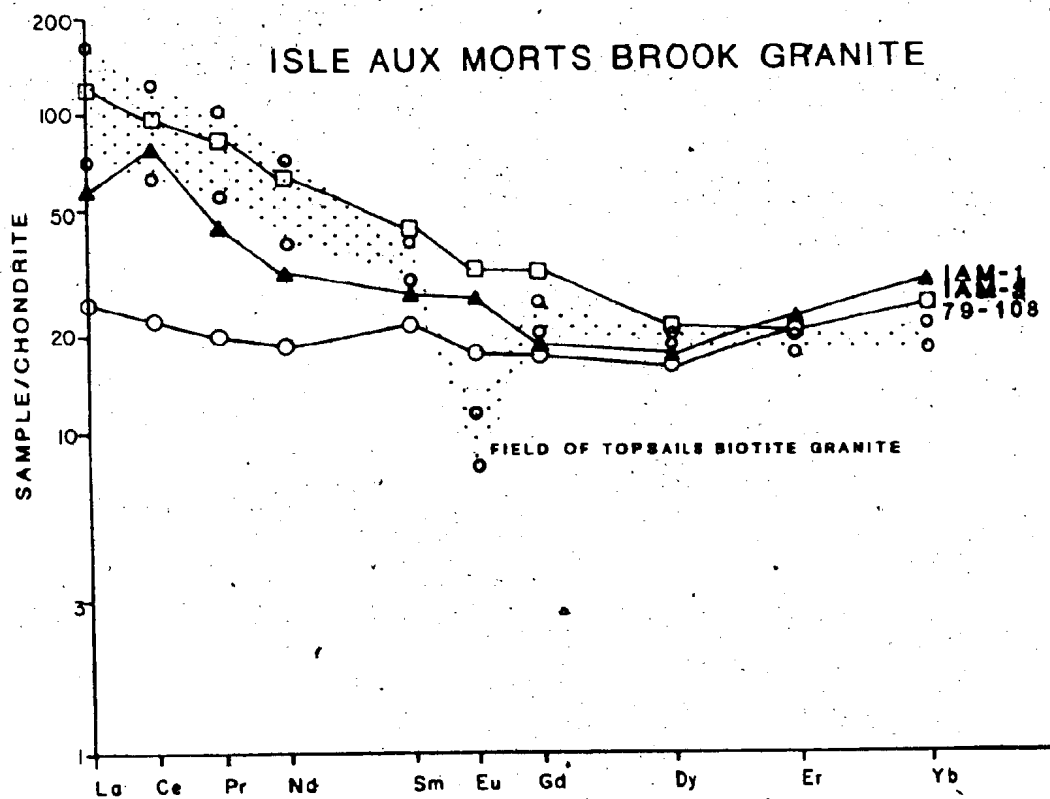
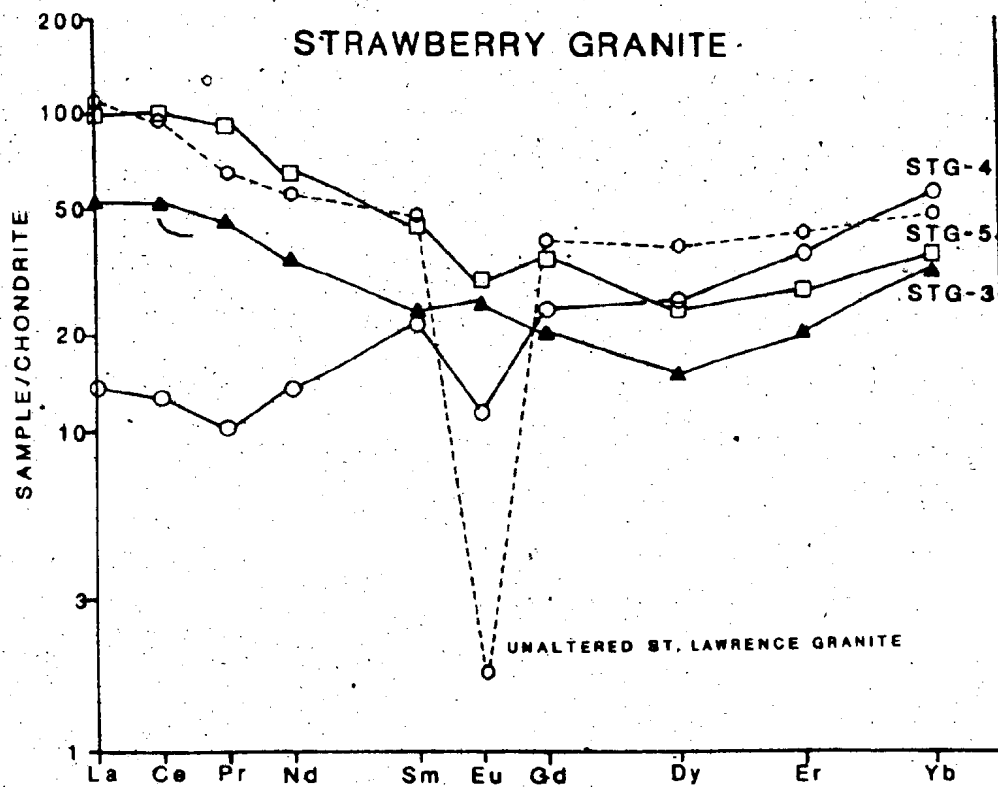
The alkaline (peralkaline) granites on the other hand, are mainly alkali feldspar-granite with peralkaline phases, in the case of the Topsails Granite (Taylor et al., 1980), or are alkaline-peralkaline granites with extensive vapour phase fluorite veining (as in the St. Lawrence Granite, Strong and Teng (1975)). The STG-IAM/GR granites are not alkaline, but resemble the main mass of the Topsails Granite and have some fluorite veining (ie. indicative of a late stage vapour phase typical of those evolved in peralkaline granitoids (cf. Taylor et al., 1981)).

The initial  $^{87}\text{Sr}/^{86}\text{Sr}$  ratios of these two granites (0.707 and 0.708) are high enough to indicate some involvement of continental crustal material in generation of the magmas, yet are not high enough to prove total continental crust derivation (unless it was rather primitive crust).

Figure 60 has the chondrite-normalized REE patterns for the STG and IAM/GR granites, along with an average pattern for the St. Lawrence Granite (from Strong, 1982) and a range of values for the Topsails Granite (from Taylor et al., 1981). The patterns for both granites are very similar both to each other (they are the same, with slightly elevated LREE's, decreasing in the middle REE's,

Figure 60a Chondrite-normalized REE patterns for the Strawberry Granite. Pattern for unaltered St. Lawrence Granite is from Strong (1982).

Figure 60b Chondrite-normalized REE patterns for the Isle aux Morts Brook Granite. Field of REE patterns for the Topsails Granite is from Taylor et al. (1981).



and elevated in HREE's) and to the Topsails and St. Lawrence Granites. Two samples of each granite have small negative Eu anomalies and one of each has a positive Eu anomaly. Samples 79-108 and STG-4 are aplites from their respective granites and thus their REE depletions are explicable in terms of derivation as fluid phases from the magmas (cf. Hansen, 1980). STG-4 has a strong Eu depletion indicating that plagioclase was residual in the magmatic phase.

The saucer shape (ie. HREE-enrichment) of these patterns is very reminiscent of the Topsails Granite (Taylor et al., 1981), and by inference, those of the Oslo Rift, Norway (after Neumann et al., 1977). Such patterns are also seen to a lesser extent in the Gabo and Mumbulla Granitic Suites of Australia (Collins et al., 1982). Taylor et al. (1981) imply that these patterns result from the preferential concentration of HREE's (due to CO<sub>3</sub>- or F-complexing) into the vapour phase of a magmatic system. The common occurrence of fluorine and/or carbonate-bearing phases in such granitoids is taken as proof of the existence of such a fluid (ibid.).

Chemically and physically (ie. high level, hot, anhydrous, etc.) the STG and IAM/GR granites resemble the A-type granitoids described by Collins et al. (1982) from Australia. These authors infer the origin of these granites as partial melts from a deeper, depleted felsic

granulite source (depleted by earlier partial melting episodes). A similar model is favoured for the STG and IAM/GR granites. The overall lower REE contents and minimal Eu fractionation imply that the source does not contain extensive residual plagioclase (ie. is felsic), yet the non-alkalinity and moderate concentrations of large cations (such as Nb, Ga and Y) show the source was not necessarily as depleted or totally melted as in the other examples.

Since the STG intrudes both the CRG-TN and Long Range Mafic/Ultramafic Complex ophiolite remnants, it implies the presence of a felsic granulite basement beneath the ophiolitic terrain. This in turn implies that the entire ophiolitic sheet is allocthonous onto continental crust, and therefore, that at least in southwestern Newfoundland, there is extensive underplating by proto-North American crust (ie. Grenvillian).



## CHAPTER 7

### THE ORE DEPOSITS

#### 7.1 Sulphide Mineral Occurrences

The main metallogenic aspect of this thesis was the examination of the gold/base metal sulphide quartz veins of the Main Shear and Windowglass Hill Showings, however during the course of this research, other sulphide showings were discovered and/or re-investigated in almost all the lithologic units within the Cape Ray Fault Zone. These smaller occurrences are briefly described in Table XV (see mineral locations on Map 1 in pocket).

##### 7.1.1 Windowglass Hill Showings

There are two sets of sulphide-bearing quartz veins within this granite. The oldest and best mineralized set has a general strike of 0/25W, parallel to a joint set. These veins occur as 1-2 mm thick sets spaced 10 cm apart, but there are larger veins up to 1 m thick. These large veins pinch and swell extensively, and the best sulphide mineralization is encountered in these zones of maximum swell.

Most of these veins contain galena, chalcopyrite,

OTHER SULPHIDE OCCURRENCES IN THE CAPE RAY FAULT ZONE

<u>LITHOLOGIC UNIT</u>	<u>MINERALS</u>	<u>FORM</u>	<u>LOCATION</u>	<u>COMMENTS</u>
Port aux Basques Gneiss (a)leucocratic bands	py	disseminated in gneiss	throughout	up to 20-30% py in particular bands
(b)amphibolite	po	massive syngenetic layers in amphibolite	Bailey's Brook	
Cape Ray Granite (a)hornblende	py-graphite	quartz veins	throughout	
(b)pegmatitic (i)	cpy-py	quartz veins	near lighthouse at Cape Ray	Stackhouse Showing - two subhorizontal quartz veins, 2-8 cm thick, interconnected - lateral extent of 10 m - cpy masses up to 8 mm in dia. - assay 7.7% Cu, 1.03 gm/m.t. Au, and 69.9 gm/m.t. Ag.
(ii)	cpy-py-gal	quartz veins	near Billy's Pond	
(c)Red Rocks Granite (i)	py-cpy	quartz veins	throughout	sulphide masses on quartz fracture-fillings - assay 600 ppm Cu, 100 ppm Pb and trace Au
(ii)	gal	shear zones	throughout	found in zones of cataclastic (brittle) deformation
Windsor Point Group (i)	py (± cpy, po)	quartz veins	Jerret Point to contact with Port aux Basques Complex	maximum assay: 100 ppm Cu and trace Au
(ii)	py	quartz veins	along shore of Little Barachois	boudined, pyritiferous quartz veins in graphite schists - maximum assay: ~250 ppm Cu and nil Au
(iii)	gal-py	quartz vein (up to 0.3 m thick)	Red Rocks Point	along contact of quartz-feldspar porphyry dyke and host granite
(iv)	gal-py	disseminated	Trans-Canada Highway	in mylonite outcrop on TCM - disseminated pyrite cubes (1-3 mm in width) and galena grains (~0.02 mm)
Strawberry Granite (i)	molybdenite-py	disseminated	Isle aux Morts Brook	
(ii)	fluorite	cement		cement to gas breccia
Isle aux Morts Brook Granite	molybdenite	disseminated	south of Big Pond	flakes in aplite dyke cutting gneiss roof pendant

Abbreviations: py = pyrite; po = pyrrhotite; cpy = chalcopyrite; gal = galena.

TABLE XV Other Mineral Occurrences in the Cape Ray Fault Zone

pyrite and minor sphalerite. The sulphides range from small disseminations to network masses, up to 10x5 mm, through the quartz veins. The pyrite is present as subhedral cubes (as is coarse-grained galena), while the other sulphides are totally anhedral masses often with thin stringers leading out from the main mass. In general there are two groups of sulphide associations in the veins, both of which have ore-grade concentrations of Au viz.; galena-rich with pyrite and minor chalcopyrite (most common); and chalcopyrite-pyrite with minor galena.

There are often haloes of up to 2-3 % disseminated pyrite in the host granite to the veins, and the best gold/sulphide mineralization is found in those veins with the greatest pyrite haloes. The small pond within the centre of this granite contained the highest Pb, high Cu and the only detectable Au concentrations found in any ponds silt sampled by geologists from Riocanex Ltd. through the whole concession area of the Cape Ray Fault Zone.

The second quartz vein set consists of 5 mm to 10 m wide veins which strike northeasterly (~45°) and dip steeply SE (~82°), or parallel to main fabric developed in schists surrounding the granite (ie. parallel to D1). Veins of this second set post-date those of the first group, and are only mineralized where they intersect strongly mineralized veins of the first set (ie. the

sulphide is remobilized).

Drilling and geophysical studies conducted by geologists of Riocanex Ltd. indicate that some mineralization occurs in narrow linear zones which plunge at shallow angles to the southeast. These zones correspond to lines of intersection between the two vein sets and represent ore mineral remobilization from the first set by the veins, and deformational effects of the second set.

#### 7.1.1.1 The H and I Brook Showings

These showings consist of sulphide-quartz veins cutting the mylonitized extension of the Windowglass Hill Granite in H and I Brooks (see Map 1 in pocket). The mylonitized granite hosts are 3-5 m wide zones of pink to green, aphanitic mylonite, that are cut by numerous quartz veins, and are folded and interbedded within chloritic schists of the Windsor Point Group. There was also a very small showing of the same granite in J Brook along strike from these first two showings, however repeated sampling has so degraded the mineralization that there is none visible now.

The quartz veins average 10-20 mm in width and contain coarse "knots" of galena-sphalerite-pyrite (+ chalcopryite), up to 10 mm in diameter (Plate 7-1A). There are also smaller disseminations of these sulphides

scattered through the veins and occasional disseminated pyrite cubes in the mylonitized granite host.

The veins are generally axial planar to F2 folds and thus parallel/subparallel to the main D1 regional fabric. There are however irregular pods of quartz with galena, sphalerite and chalcopyrite. The axial planar veins appear to be correlative with the second vein set as seen in the main granite body and as such would result from remobilization of earlier deposited material (possibly represented by the isolated pods).

The model of remobilization is further supported by the very low Au (and Ag) contents of these veins. In direct contrast to Au ore grade values found in primary sulphide veins in the granite proper, those veins in the H and I Brooks most frequently have low to trace gold values (as evidenced by assays from Riocanex Ltd.). Zones of strong remobilization in the Main Shear showings also indicate a relative decrease in Au concentration with remobilization (described below). There are scattered zones within these showings (as determined from drilling) which achieved assays of 0.04 oz/ton Au and a single basal quartz vein (ie. between the granite and underlying schist, thus possibly representative of earlier mineralization) which had 2 oz/ton Au and 0.16 oz/ton Ag.

Phillips Management Ltd., however, in their investigation of the mineralized horizon represented by the

H and I Brook showings, derive a tentative average grade for the zone of 0.39 % Cu, 2.51 % Pb, 2.04 % Zn, 0.48 oz/ton Ag, and 0.84 oz/ton Au. This average probably includes vein samples from the Main Shear showing (as Phillips geologists did not recognize this separate horizon) and thus is not a true representative of the H and I Brook showings.

#### 7.1.2 The Main Shear

This zone crops out nowhere through its length, but is readily traceable by VLF-EM geophysical methods just to the south of the northeastern mylonitized extension of the Windowglass Hill Granite (see Figure 61). The VLF-EM anomaly for this, and other secondary shear fracture zones, is traceable for over 6 km from the Gulch to past the western edge of the Windowglass Hill Granite. The Main Shear anomaly passes quite close to the southern contact of the main part of Windowglass Hill Granite and may pass into the granite at depth. The most significant expression of this geophysical pattern occurs on its eastern portion (ie. south of the Isle aux Morts Brook). IP surveys yield identical subsurface projections for this feature.

Lithologies (as found in drill core) in the Main Shear consist largely of graphitic schist, with extensively interbedded chloritic and sericitic schist of the Windsor

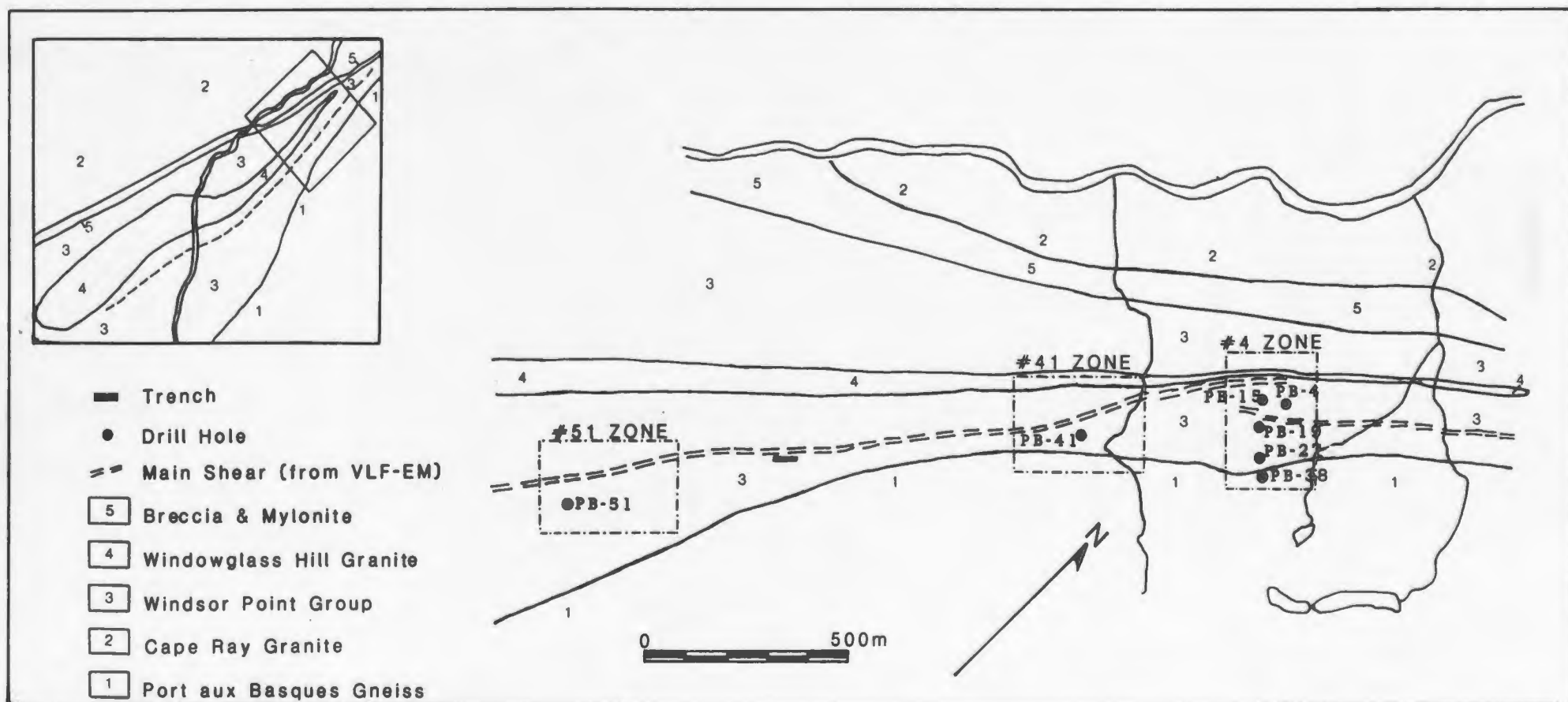


Figure 61 Location of the Main Shear, number four, forty-one and fifty-one zones. Also indicated are the defining drill holes and also the holes forming the cross-section in Figure 62. Inset map indicates location with respect to the Windowglass Hill Granite. Note location of trench which is detailed in Figure 63.

Point Group. The geophysical signature of this zone is produced by the conductive ability of the graphitic schist, which, due to its pronounced friability, is often broken fault gouge (hence the "Shear"). The schists have extensive quartz veins, which themselves are often broken and fractured.

Within the Main Shear there are three significant mineralized zones (see Figure 61), viz.; the four, forty-one and fifty-one (named after the drill holes which first encountered them). These zones appear to be isolated pockets of ore grade material, separated by weakly mineralized to barren intervals, in the rest of the Main Shear. The number four zone, the most easterly, was discovered by Riocanex Ltd. geologists while drilling between the H and I Brooks to locate the strike extensions of the showings within these brooks. Subsequent drilling, along the VLF-EM defined subcrop of the Main Shear, revealed the forty-one and fifty-one zones further to the west. These three zones constitute a strike length of over 2 km. Further drilling outside this strike length has yet to reveal further significant mineralized pockets, and these three may represent the final ore grade section within the Main Shear horizon. The final results of drilling by Riocanex Ltd. has indicated a combined total of 750,000 t, after dilution, of 9 gm/m.t. Au in the three zones within the Main Shear.



The best plan and three dimensional views of the Main Shear horizon occur in a 61.5 m long trench that was dug along the Main Shear just east of the fifty-one zone (Figure 63).

#### 7.1.2.1 The Four Zone

Drill holes fifteen, nineteen, twenty-seven and thirty-eight represent a cross-section through the four zone, 60 m west of hole number four (cross-section in Figure 62). In order to describe the form and nature of the mineralization within the Main Shear showing, assay values and rock types from these drill holes are listed in Table XVI. Graphite schist is the major component in hole fifteen but is less common in the other holes. Overall the lithologies consist of extensively interbedded and interbanded chlorite, -sericite, silicic sericite, and graphite schists. There are also numerous interbands of mylonitized granite (Windowglass Hill Granite) and mylonite. Definitive Windowglass Hill Granite occurs at the bottoms of holes nineteen and twenty-seven.

The following points best summarize the appearance of the Au-bearing quartz vein horizons in the Main Shear, as seen in drill core:

- 1) The majority of veins occur in graphitic schist zones, though other rock types may form the actual wall

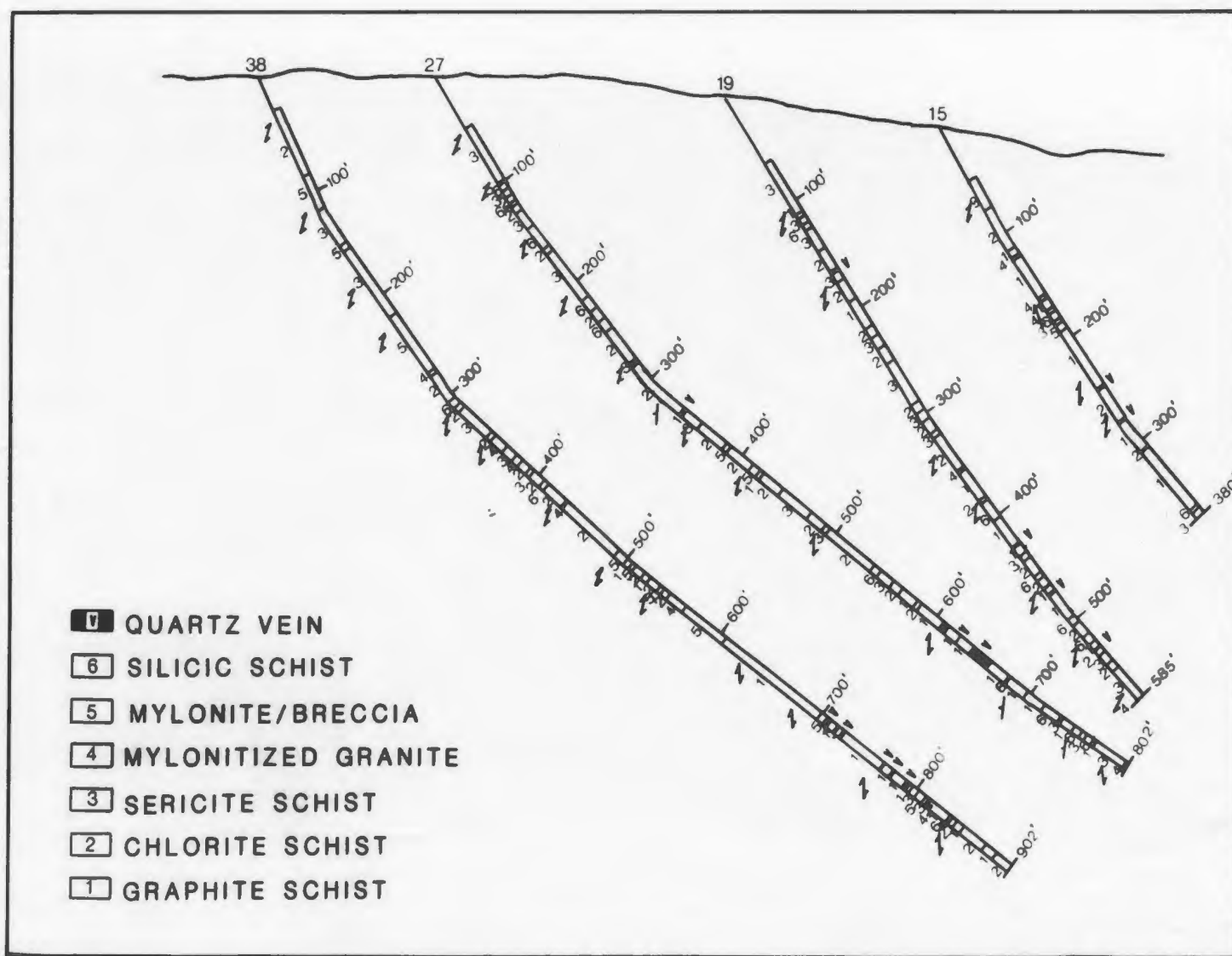


Figure 62 Cross-sectional view of the number four zone. This section is based on drill hole intersections in holes PB-15, PB-19, PB-27 and PB-38.

INTERVAL(ft)	Au oz/t	Ag oz/t	% Cu	% Pb	% Zn	SAMPLE NUMBER	MINERALOGRAPHY	HOST
						<u>HOLE 15</u>		
245-248	0.201	0.10	-0.01	0.02	0.03		gal-cpy-sphal-py	graphitic schist in contact with chloritic schist
276.5-278	0.513	0.36	0.02	1.33	0.60		"	graphitic schist
278-279	0.554	0.43	0.13	0.86	0.63		"	graphitic schist
						<u>HOLE 19</u>		
429-432	0.26	0.44	0.10	1.04	1.05	PB19-14	gal-sphal-cpy-py	graphitic schist
471.2-473.1	0.05	1.01	0.44	1.57	1.26	PB19-18	"	graphitic/chloritic schist breccia
529.8-531.8	0.02	0.58	0.06	1.45	0.24		"	graphitic schist in contact with chloritic schist
						<u>HOLE 27</u>		
339.4-340.2	0.24	0.88	0.19	2.70	4.27		-2 % gal-sphal, 1-2 % cpy, -1%py	graphitic schist in contact with chloritic schist
607.5-609.1	nil	nil	--	--	--	PB27-33	py-breccia	graphitic schist
614.4-616.2	0.08	0.42	0.06	trace	trace		1-2%py +sphal	graphitic schist
624.4-626.4	trace	trace	--	--	--		massive py	graphitic schist
639-642	0.52	1.12	0.17	1.74	1.84	PB27-25	gal-sphal-cpy-py	graphitic schist
642-644	0.09	0.25	0.03	0.58	0.27		1-2% gal, trace py-cpy-sphal	graphitic schist
644-649	-0.02	trace	--	0.05	--		trace gal-py- cpy-sphal	chloritic schist
649-653.5	trace	trace	--	0.07	--	PB27-26	sphal-gal	chloritic schist
653.5-658.5	0.17	0.23	0.01	0.18	0.09	PB27-27 &-28	0.1-0.5% gal	chloritic and graphitic schist
						<u>HOLE 38</u>		
501.8-504.2	0.12	trace	0.09	0.32	0.12	PB38-22 &-23	py with inter- granular gal-cpy	graphitic and sericitic schist
506.2-507.8	0.10	0.30	0.26	0.99	1.49	PB38-24	sphal-gal-py	graphitic schist gouge
708.5-712	0.96	1.58	0.22	4.21	3.07	PB38-32	sphal-gal-cpy-py	graphitic schist
717.2-719	0.52	1.26	0.12	2.10	1.57		"	graphitic schist
765-766.3	0.02	trace	0.01	0.14	0.52		"	graphitic schist gouge
766.3-769	0.13	trace	0.01	0.90	0.36		"	graphitic schist
776-777	0.28	0.94	0.04	1.95	1.34		"	graphitic schist gouge
789.8-793.3	0.94	2.70	0.86	5.80	4.97	PB38-35	"	graphitic schist
806-808.9	0.70	3.98	0.50	5.39	3.56	PB38-37	"	chloritic and sericitic schist

TABLE XVI Data for Cross-section through the Number Four Zone

Mineralography: gal = galena; cpy = chalcopryite; sphal = sphalerite; py = pyrite.

rock.

2) No visible gold is present, but the best Au and Ag values occur in veins with similarly elevated Pb and Zn concentrations.

3) Inter-hole stratigraphic correlation is tenuous at best, and no single veins can actually be traced from one hole into another.

4) There is an apparent decrease in the quantity and quality of sulphide-bearing quartz veins with depth through the Main Shear region.

5) There is no direct correlation between the presence of Windowglass Hill Granite dykes and sulphide-bearing quartz veins in the graphitic areas, however, in at least one zone (ie. the number four), gold values occur in those quartz veins closer to the granite.

#### 7.1.2.2 The Trench Showing

The trench (Figure 63) actually consists of five connected trenches, viz.: 80-1, 80-2, 80-3, 80-4 and 80-5, as designated by Riocanex Ltd. geologists. The trenches were dug to intersect a particularly thick, shallow and well mineralized quartz vein horizon as found in drill holes eighty-nine, one hundred thirty-six and ninety-eight, 330 m, 360 m, and 390 m respectively east of hole sixty-three (part of the number fifty-one zone). The total

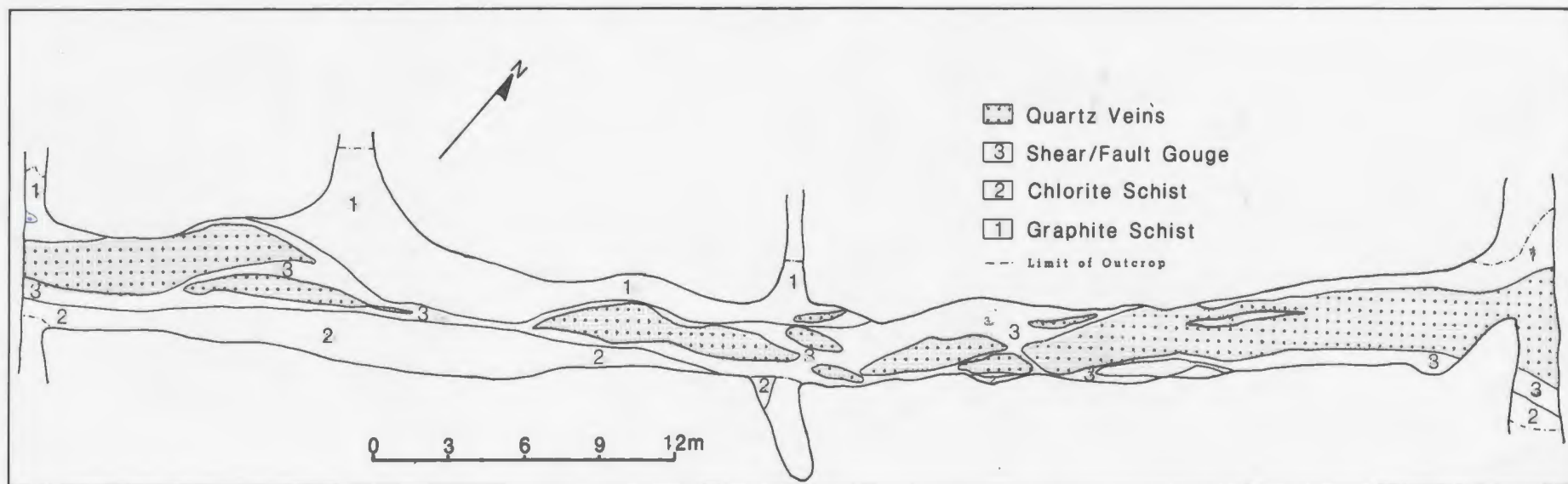


Figure 63 Map of veins in the Trench Showing. Note boudinage and general deformed nature of the veins.

length of the trench(es) is 61.5 m with an average grade of 0.29 oz/t Au for the horizontal width, and 0.95 oz/t Au for the true width.

Bedrock in the trench consists of numerous vein pods, that pinch and swell extensively (from nil to 2.4 m thick), hosted by graphitic and chloritic schist. The pods are up to 21 m long and the host rocks are often broken into gouge and breccia zones. The podiform nature of the veins results from boudinage of a more continuous quartz vein horizon. At their edges the pods have typical rounded/pinched boudin forms (Plate 7-1B). The elongate axes of these boudins is parallel (ie. northeasterly trend) to the dominant D1-fabric developed in the country rock. There is also a strong fracture/cleavage (Plate 7-1C), parallel to the elongate direction and host rock schistosity, which strikes between 40 to 58° with a steep southeastern dip. A second fracture/cleavage, with a due east strike (ie 90°) and near vertical dip (both N and S), dissects more competent vein pods. The angle at which these secondary fractures cut the main fabric indicates sinistral simple shear during deformation. The first cleavage is sinistrally offset by this second cleavage.

Schist fragments within the quartz are stretched and quite often smeared out along a fracture. The wall rocks themselves are similarly fractured and sheared (Plate 7-1C) with an occasional minor fold (Plate 7-1D).

PLATE 7-1 A) "Knots" of galena in quartz veins cutting mylonitized Windowglass Hill Granite in M. Brook. The galena is visible as black masses in white vein above pen.

B) Boudinaged quartz veins in the Trench Showing. The hammer is resting on the end of the boudin. The host rocks are sheared graphitic schists.

C) Sheared quartz veins in Trench Showing. The pen is resting on sheared graphitic schist interlayers in the vein. On the upper left hand side of the pen is a massive galena pocket (light grey).

D) Graphitic schist host to quartz veining in the Trench Showing. The hinge of an F2 fold occurs just to the right of the hammer.





Sulphide mineralization is best developed in the more undeformed portions of the quartz vein pods. Typically sphalerite-galena-chalcopyrite, with lesser cubic pyrite, are intergrown in coarse network patches. Stringers and disseminations are also common sulphide forms. The sulphides appear to form discrete massive layers, with minor disseminations away from the layer, but this is usually quite difficult to discern due to the intense shearing experienced by the veins. The sulphides range from complete intergrowths to local areas of solitary concentration. In a couple of pods, layers (up to 4 mm thick) of arsenopyrite are intergrown with the other sulphides. No visible gold was found in any of the pods.

Deformation-induced sulphide remobilization is quite apparent through the pods. In its most extreme form, small pockets of almost solid galena (Plate 7-1C) occur along the edges of the quartz pods. These pockets consist of totally recrystallized, massive, galena cement to isolated quartz vein fragments, up to 5 mm in diameter. Smeared out, recrystallized, mixed pyrite/chalcopyrite is intergrown with the galena. Such pockets represent extreme brecciation (and strong confining pressures) along the edges of the shear zones. Galena is particularly well-suited to be a breccia cement, because, as shown by various authors (eg. Vokes, 1969; Stanton and Wiley, 1972; Mookherjee, 1976; McClay, 1980) it behaves

plastically during deformation.

In other areas chalcopyrite, pyrite and galena are remobilized into crosscutting fracture/shears. It appears that sphalerite is destroyed during deformation as it is seldom found in highly deformed portions of the quartz pods, and is not remobilized into fractures. Au also seems to dissipate with deformation because the best Au values occur in the undeformed, massive sulphide layers but are reduced in those areas where deformation has decreased sulphide content. In the galena pockets, which are obviously relics of very high grade sections, Au concentration is very low (eg. sample 80-61C is from one of these galena pockets).

The very strong deformation that this vein zone has undergone (with attendant sulphide mobility) is the reason for the lack of correlation between drill holes, the bifurcated, brecciated irregular form of the veins, and the inconsistency in Au values between different horizons. Poor intersections within some holes could result from directional changes in the drill path towards the softer zones near the boudin necks of the quartz veins.

The quartz veins and their mineralization very obviously pre-date the deformation of the vein horizons. These deformations are co-planar to, and have the same general structural sequence as the three phase deformational event which affected all regional

lithologies, and therefore must be the same. Mineralization in the Windowglass Hill Granite is similarly pre-deformation. Since the Strawberry and Isle aux Morts Brook Granites are post-tectonic, a lower limit on the age of the Main Shear and Windowglass Hill Granite showings can be placed at  $362 \pm 16$  Ma (ie. the combined isochron).

## 7.2 ASSAY DATA

### 7.2.1 Introduction

In order to understand the relative distributions and inter-relationships of Au, Ag and the base metal sulphides, assay values for these elements, as produced for Riocañex Ltd., were statistically analysed. These assays provide the most complete data base available for the various deposits, but unfortunately (for statistical purposes), the assay intervals were not of a consistent length, thus all the data available could not be used. Arbitrary assay lengths of 2' (0.6 m) and 5' (1.5 m) were chosen for the computations, and where the actual assay intervals were not of these lengths, adjacent intervals were weighted and combined to produce an assay interval of the correct length. These combined assay lengths range from 1.9-2.1' and 4.8-5.2' to accomodate as much data as possible, though even with this liberal proviso (ie. up to 5% error in

length), a very large amount of the available data were unusable.

The assays are for vein zones and surrounding host rock, sampled from both drill core and trench intersections. Based on the lithological descriptions in the core logs by Riocanex Ltd. geologists, the assays can be broken down into zones within four rock types viz.; graphite schist, chlorite schist, sericite schist and Windowglass Hill Granite. Where the abundance of a given element was defined as "trace" in an assay, the element was assigned a value of 0.001 oz/t for Au and Ag, or 0.001% for Cu, Pb and Zn for the statistical comparisons. This is not stringently correct, however the detection levels could not be used as the assays were completed at different times by different labs (ie. there is no consistent detection level).

The vein zones sampled are necessarily those which had some visible mineralization. The 2' assay intervals generally should have elevated concentrations, since the mineralized veins are thin (usually <2' thick) and the sampling was biased towards the vein zone. The 5' assay intervals are more representative of wing samples taken out from the actual vein. Means for Au, Ag, Cu, Pb and Zn in the eight assay types are given in Table XVII.

<u>Rock Type</u>	<u>Assay Lengths</u>	<u>N</u>	<u>Au(oz/t)</u>	<u>Ag(oz/t)</u>	<u>Cu(%)</u>	<u>Pb(%)</u>	<u>Zn(%)</u>
Graphite schist	2'	181	0.085	0.377	0.137	0.597	0.292
Graphite schist	5'	270	0.079	0.240	0.088	0.353	0.191
Chlorite schist	2'	53	0.033	0.287	0.079	0.312	0.307
Chlorite schist	5'	90	0.036	0.150	0.072	0.234	0.144
Sericite schist	2'	19	0.008	0.100	0.083	0.162	0.081
Sericite schist	5'	36	0.007	0.046	0.063	0.114	0.049
Windowglass granite	2'	42	0.021	0.088	0.062	0.271	0.090
Windowglass granite	5'	175	0.018	0.021	0.030	0.088	0.044

TABLE XVII - Mean assay values

(N = no. of samples)

The highest average Au, Ag, Cu and Pb contents occur in the graphite schist samples, the highest Zn values are in the chlorite schist 2' assays. On the basis of the ore values, the 2' intervals rank above their respective 5' intervals and the overall ranking is graphite schist > chlorite schist > Windowglass Hill Granite > sericite schist. The assay values for each element in all sample groups are log normally distributed with the vast majority of samples in the low to nil concentration end.

Correlation coefficient matrices for the eight groups are listed in Table XVIII. In the 5' assays from all groups, all elements have statistically significant correlations (at 98% probability level) except Au with Zn in the granite samples and Cu with Au in those of the

Graphite schist 2' assaysn=181  $r_{98} = 0.13$ 

	Au	Ag	Cu	Pb	Zn
Au	1.0				
Ag	<u>0.61</u>	1.0			
Cu	<u>0.58</u>	<u>0.44</u>	1.0		
Pb	<u>0.62</u>	<u>0.48</u>	<u>0.55</u>	1.0	
Zn	<u>0.22</u>	<u>0.25</u>	<u>0.12</u>	<u>0.59</u>	1.0

Graphite schist 5' assaysn=270  $r_{98} = 0.03$ 

	Au	Ag	Cu	Pb	Zn
Au	1.0				
Ag	<u>0.82</u>	1.0			
Cu	<u>0.72</u>	<u>0.82</u>	1.0		
Pb	<u>0.73</u>	<u>0.69</u>	<u>0.62</u>	1.0	
Zn	<u>0.62</u>	<u>0.52</u>	<u>0.50</u>	<u>0.84</u>	1.0

Chlorite schist 2' assaysn=53  $r_{98} = 0.32$ 

	Au	Ag	Cu	Pb	Zn
Au	1.0				
Ag	<u>0.53</u>	1.0			
Cu	<u>0.46</u>	<u>0.58</u>	1.0		
Pb	<u>0.70</u>	<u>0.83</u>	<u>0.62</u>	1.0	
Zn	<u>0.20</u>	<u>0.33</u>	<u>0.20</u>	<u>0.80</u>	1.0

Chlorite schist 5' assaysn=90  $r_{98} = 0.25$ 

	Au	Ag	Cu	Pb	Zn
Au	1.0				
Ag	<u>0.83</u>	1.0			
Cu	<u>0.36</u>	<u>0.40</u>	1.0		
Pb	<u>0.56</u>	<u>0.53</u>	<u>0.57</u>	1.0	
Zn	<u>0.37</u>	<u>0.32</u>	<u>0.27</u>	<u>0.86</u>	1.0

Windowglass Hill 2' assaysn=42  $r_{98} = 0.36$ 

	Au	Ag	Cu	Pb	Zn
Au	1.0				
Ag	<u>0.90</u>	1.0			
Cu	<u>0.69</u>	<u>0.81</u>	1.0		
Pb	<u>0.21</u>	<u>0.20</u>	<u>0.13</u>	1.0	
Zn	<u>0.14</u>	<u>0.14-0.06</u>	<u>0.67</u>	<u>1.0</u>	

Windowglass Hill 5' assaysn=175  $r_{98} = 0.13$ 

	Au	Ag	Cu	Pb	Zn
Au	1.0				
Ag	<u>0.64</u>	1.0			
Cu	<u>0.25</u>	<u>0.34</u>	1.0		
Pb	<u>0.23</u>	<u>0.51</u>	<u>0.15</u>	1.0	
Zn	<u>0.09</u>	<u>0.20</u>	<u>0.02</u>	<u>0.68</u>	1.0

Sericite schist 2' assaysn=19  $r_{98} = 0.53$ 

	Au	Ag	Cu	Pb	Zn
Au	1.0				
Ag	<u>0.78</u>	1.0			
Cu	<u>0.14</u>	<u>0.47</u>	1.0		
Pb	<u>0.75</u>	<u>0.82</u>	<u>0.09</u>	1.0	
Zn	<u>-0.03</u>	<u>0.27-0.08</u>	<u>0.62</u>	<u>1.0</u>	

Sericite schist 5' assaysn=36  $r_{98} = 0.39$ 

	Au	Ag	Cu	Pb	Zn
Au	1.0				
Ag	<u>0.73</u>	1.0			
Cu	<u>0.75</u>	<u>0.82</u>	1.0		
Pb	<u>0.57</u>	<u>0.90</u>	<u>0.67</u>	1.0	
Zn	<u>0.36</u>	<u>0.78</u>	<u>0.46</u>	<u>0.86</u>	1.0

TABLE XVIII Correlation Coefficients for Assay Data

(those correlations which are significant to at least 98% probability level are underscored -  $r_{98}$  indicates the 98% probability level for the relevant number of samples)

sericite schist. In the 2<sup>nd</sup> assay intervals, correlations are not as good; in the graphite and chlorite schists all elements occur together significantly except Cu and Zn in the former, and Zn with Au or Cu in the latter; in the granite, Au correlates with Cu and Ag, Ag with Cu, and Pb with Zn; and in the sericite schists, Au, Ag and Pb correlate as do Pb and Zn.

R-mode factor analyses of the assays were conducted using the SPSS system (Nie, et al.; 1970, 1975, with particular reference to Kim, 1975). (For a detailed explanation of factor analysis and its applications to geological problems see Joreskog et al., 1976). The Varimax rotated factor loadings for all groups are listed in Table XIX. In all groups four factors accounted for over 95% of the variance, except the 2<sup>nd</sup> assays of sericitic schist for which only two factors could be calculated since communalities were exceeded with further computations, due to the small number of samples, 19. The factors thus determined are very similar to the correlation relationships.

#### 7.2.2 Conclusions on Assay Data

Conclusions to be derived from the study of these assays are:

- 1) Au and Ag occur with base metals (as shown by their

TABLE XIX Varimax Rotated Factors in Assay Data (those elements significant in each factor are underscored)

VARIMAX ROTATED FACTOR MATRIX FOR 2' ASSAYS IN GRAPHITIC SCHIST

	FACTOR 1	FACTOR 2	FACTOR 3	FACTOR 4
Au	<u>0.80690</u>	-0.29889	0.13073	<u>-0.13218</u>
Ag	0.66384	-0.18180	<u>0.26970</u>	0.09970
Cu	0.66334	-0.29849	<u>-0.24953</u>	<u>0.10688</u>
Pb	<u>0.89617</u>	0.29378	-0.19719	-0.05902
Zn	0.48910	<u>0.60638</u>	0.11800	0.04595

VARIMAX ROTATED FACTOR MATRIX FOR 5' ASSAYS IN GRAPHITIC SCHIST

Au	<u>0.71916</u>	0.48337	<u>0.23733</u>	0.01126
Ag	<u>0.90998</u>	0.31586	0.05875	<u>0.10487</u>
Cu	<u>0.80623</u>	0.32125	-0.06326	-0.08053
Pb	0.44675	<u>0.83859</u>	0.02035	<u>0.11546</u>
Zn	0.27570	<u>0.85637</u>	0.04223	-0.06465

VARIMAX ROTATED FACTOR MATRIX FOR 2' ASSAYS IN CHLORITIC SCHIST

Au	0.08910	0.41334	<u>0.69312</u>	-0.00179
Ag	0.20997	<u>0.77382</u>	0.22084	-0.04178
Cu	0.10915	<u>0.75513</u>	<u>0.53135</u>	<u>0.09627</u>
Pb	<u>0.90519</u>	0.13662	0.31605	<u>0.08437</u>
Zn	<u>0.94152</u>	0.17298	-0.08592	-0.06632

VARIMAX ROTATED FACTOR MATRIX FOR 5' ASSAYS IN CHLORITIC SCHIST

Au	<u>0.82764</u>	0.21201	0.17856	<u>0.12362</u>
Ag	<u>0.82286</u>	0.16992	0.26475	-0.00657
Cu	0.23729	0.18527	<u>0.67862</u>	0.04615
Pb	0.34571	<u>0.73134</u>	0.41888	<u>0.40713</u>
Zn	0.17691	<u>0.91065</u>	0.14932	-0.01930

VARIMAX ROTATED FACTOR MATRIX FOR 2' ASSAYS IN SERICITIC SCHIST

	FACTOR 1	FACTOR 2	FACTOR 3	FACTOR 4
Au	<u>0.85546</u>	0.07275		
Ag	<u>0.92352</u>	0.27227		
Cu	0.32205	-0.08157		
Pb	<u>0.73347</u>	<u>0.66243</u>		
Zn	-0.05518	<u>0.99640</u>		

VARIMAX ROTATED FACTOR MATRIX FOR 5' ASSAYS IN SERICITIC SCHIST

Au	0.21808	<u>0.81473</u>	-0.01499	-0.07081
Ag	<u>0.68286</u>	<u>0.70950</u>	<u>0.15247</u>	0.00394
Cu	0.31801	<u>0.84264</u>	-0.00089	<u>0.09463</u>
Pb	<u>0.83798</u>	0.47700	-0.11120	-0.00410
Zn	<u>0.92060</u>	0.19418	0.05163	0.01045

VARIMAX ROTATED FACTOR MATRIX FOR 2' ASSAYS IN WINDOWGLASS HILL GRANITE

Au	<u>0.89767</u>	0.13140	-0.11853	<u>0.10976</u>
Ag	<u>0.98727</u>	0.12504	-0.01244	<u>-0.09578</u>
Cu	<u>0.82248</u>	-0.02593	<u>0.34115</u>	-0.00478
Pb	0.12083	<u>0.80627</u>	0.12434	0.04718
Zn	0.02145	<u>0.84224</u>	-0.14371	-0.04416

VARIMAX ROTATED FACTOR MATRIX FOR 5' ASSAYS IN WINDOWGLASS HILL GRANITE

Au	0.06674	<u>0.73039</u>	0.23224	-0.03589
Ag	0.25780	<u>0.71757</u>	<u>0.47641</u>	<u>0.25850</u>
Cu	0.02232	0.20597	<u>0.37629</u>	0.01236
Pb	<u>0.85738</u>	0.18161	<u>0.21022</u>	<u>0.22447</u>
Zn	<u>0.81704</u>	0.04960	-0.04211	-0.09837



common correlations). In the schist samples, Au and Ag correlate well with all the other assayed metals, but in the Windowglass Hill Granite there is a tendency for them to occur with Cu, while Pb and Zn occur together (ie. Au-Ag with chalcopyrite - the only Cu-bearing mineral present).

The factor analyses indicate that all five elements occur together to some degree, but detailed examination shows that there are two main groupings, viz., Au and Ag (+ Cu); and Pb with Zn. Also the Au/Ag values are most strongly correlative with Cu indicating the most common host of the precious metals in the veins, according to statistical comparisons, is chalcopyrite. Zn (ie. sphalerite) is the most solitary of the elements.

2) The highest assay values for Ag, Pb and Zn occur in 2' assay intervals from the graphitic schists, the highest Au is in a 5' assay from graphitic schist and the highest Cu is from a 2' assay in chlorite schist. The actual highest assays are : 1.58 oz/t Au, 12.1 oz/t Ag, 2.61% Cu, 10.2% Pb and 5.51% Zn.

3) Zn has much reduced concentrations in the granite relative to the schists.

4) All elements have strong log normal distributions.

5) Overall ore grade values for Au, Ag, Cu, Pb and Zn are usually greater than 0.025 oz/t, 0.126 oz/t, 0.022%, 0.022% and 0.022% respectively.

6) Through most assay intervals, the elements have effective (or practical) detection limits higher than their stated (ie. from the analytical laboratories) detection limits. This may prove of importance in ore grade or ore reserve calculations as the actual lower (or practical) detection limit occurs at concentrations below those stated as the analytical detection limits. Ag is the only element which does not have significant differences between probable detection levels and actual determined concentrations (because of its relative ease of analysis).

#### 7.2.3 Discriminant Function Analyses

Discriminant function analyses, from the SPSS system (see Klecka, 1976), were performed on assay values from the graphitic schist and Windowglass Hill Granite groups to see if there is a defineable statistical difference between the two groups (based on their ore element distributions). 2' and 5' assays from each group were combined to create the end members for the function analyses (ie. the schist end member contained 451 samples, and the granite end member has 210 samples). When these groups were processed, they defined two functions separating the two groups viz. :

schist-hosted samples=

$-0.9+2.21Au-0.077Ag+1.6Cu+0.032Pb+0.3Zn$

granite-hosted samples=

$-0.72+0.43Au-0.19Ag+1.01Cu+0.045Pb+0.059Zn$

However when all the samples were entered into these equations, one at a time, to develop a discriminant function histogram for the two groups (Figure 64), it was found that the two groups were superimposed on one another. Detailed examination of group memberships indicates 301, or 66.7%, of the schist samples actually belong in the granite group, while only 8.1% of the granite samples were wrongly classified. What this analysis essentially shows, is that, in terms of assay values and metal distributions, there is no difference between the Main Shear and granite-hosted mineralization (ie. the two vein systems have the same assay compositions).

### 7.3 Ore and Trace Element Concentrations in the Showings

Trace element, gold and silver analyses were conducted on forty-three grab samples from the Main Shear showing and six grab samples from the Windowglass Hill Granite veins. Results of the analyses are reproduced in Appendix IV. The samples are quartz veins with visible sulphide (of varying concentrations), and occasional fragments of wall rock (usually <10% of the sample).

#### 7.3.1 Means and Distributions

The means and standard deviations for all the trace

# CANONICAL DISCRIMINANT FUNCTION

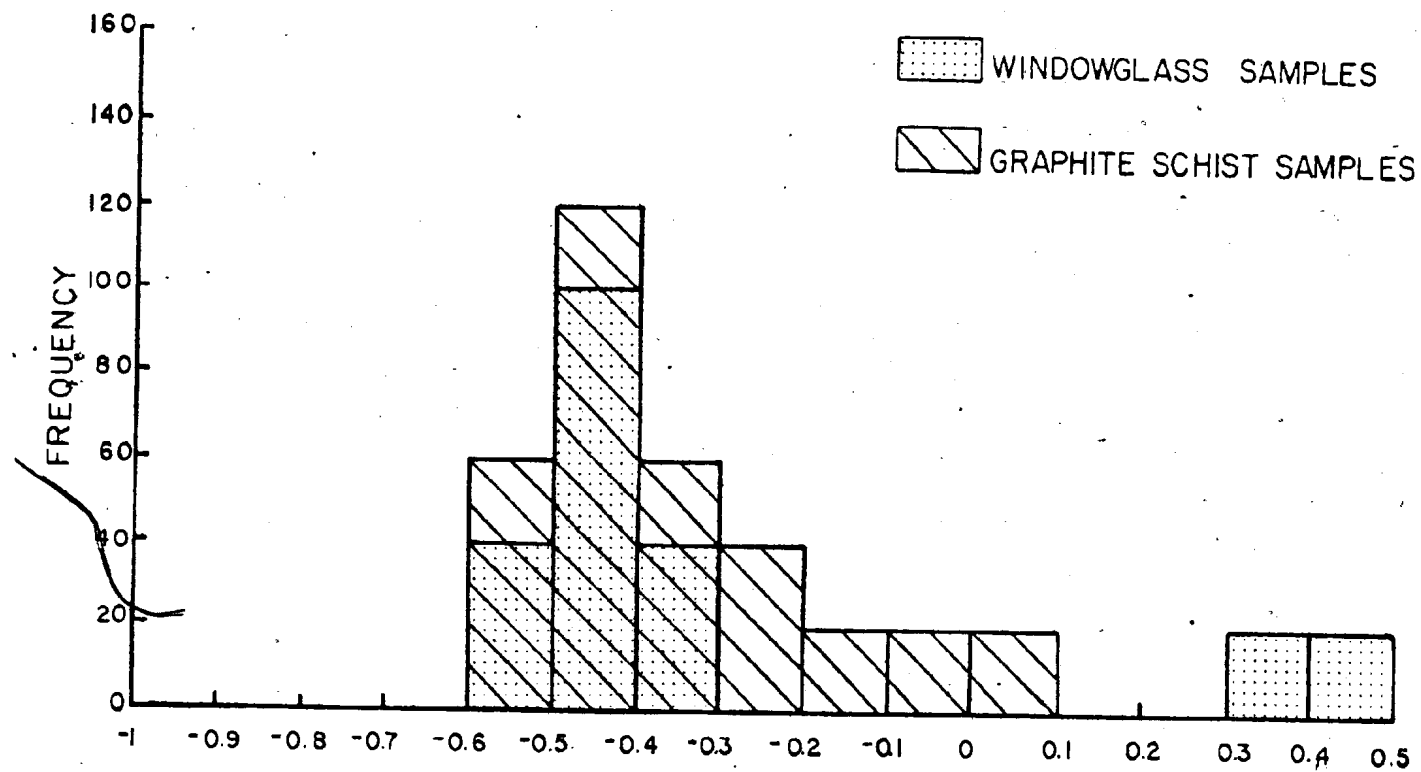


Figure 64 Histogram of the canonical discriminant function for assay data. The discriminant function was derived to differentiate between assays from the Windowglass Hill and graphitic schist-hosted samples. The two groups are effectively the same.

elements in both horizons are listed in Table XX. The samples from the Main Shear have very elevated Pb, Zn, Cu, Ga, As, S, CO<sub>2</sub>, Au and Ag concentrations, and noticeably depleted Rb, Sr, Zr and Nb contents. The standard deviations indicate that Pb, Th, Zn, Cu, Ba, Ga, As, Au and Ag have very wide ranges in concentration. The averages from the Windowglass Hill Granite samples show elevations in most of the same elements, but to a much lesser degree. Zn, Ga, As and Ba have much reduced concentrations, and most background levels for the other elements are lower. The ore elements have similar wide dispersions of values as seen in the schist samples.

All the elements in the Main Shear samples have log normal distributions except Cr which has regular arithmetic variations and a negatively skewed log distribution. The log normal plots indicate that some elements have unimodal, bimodal, or even trimodal distributions. These are described in Table XXI along with the concentration means for each distribution.

In summary, there appear to be two levels of concentration distributions within the chalcophile (ore) elements, unlike the other non-ore elements, which are generally unimodally distributed. The main sulphide element, S, however, has a definite unimodal distribution which may be due to the presence of some sulphide (if only

TABLE XX MEAN TRACE ELEMENT CONTENTS

	MAIN SHEAR SHOWING		WINDOWGLASS SHOWING	
	MEAN	STD. DEV.	MEAN	STD. DEV.
	n-43		n-6	
ppm				
Pb	48197	88160	20003	21613
Th	22	110	7	11
U	6	8	5	7
Rb	27	33	9	5
Sr	30	49	19	28
Y	16	20	30	30
Zr	55	86	58	56
Nb	4	6	4	6
Zn	19571	34202	618	982
Cu	9371	22016	5021	5148
Ni	30	55	2	3
La	18	11	9	7
Ba	311	971	47	32
V	76	75	6	3
Ce	21	20	20	16
Cr	36	24	33	23
Ga	1163	2267	315	414
As	1036	2295	349	414
wt %				
S	4.3	4.1	4.2	4.4
CO <sub>2</sub>	0.54	0.68	0.33	0.32
ppb				
Au	6464	8521	19260	28111
Ag	59224	131311	44192	27197

TABLE XXI Element Distributions in Ore Samples

<u>ELEMENT</u>	<u>LOG DISTRIBUTION</u>	<u>MEANS OF THE DISTRIBUTIONS</u>
Pb	trimodal	133, 1778, 74989 ppm
Zn	bimodal	422, 42170 ppm
Cu	bimodal	75, 7500 ppm
Ga	bimodal	79, 1995 ppm
As	bimodal	50, 631 ppm
Au	bimodal	316, 4217 ppb (background at 32 ppb)
U	bimodal	3, 18 ppm
Ag	unimodal	74989 ppb (background at 1000 ppb)
Rb	unimodal	20 ppm
Sr	unimodal	16 ppm
Y	unimodal	17 ppm
Zr	unimodal	28 ppm
Nb	unimodal	4 ppm
La	unimodal	22 ppm
Ba	unimodal	100 ppm
V	unimodal	71 ppm
Ce	unimodal	18 ppm
Th	unimodal	4.5 ppm
Cr	unimodal	56 ppm
Ni	unimodal	28 ppm
S	unimodal	5
CO <sub>2</sub>	unimodal	0.8

pyrite) in all samples selected. Thus the actual variation in S is not a function of its presence or absence within a vein (eg, whereas galena is not present in all samples, Pb may have more than one distribution curve). The lower concentration peaks in these elements represent background, or non-ore grade, contents, while the second levels are ore grade. The respective means for these ore distributions are; 74,989 ppm, 42,170 ppm, 7,500 ppm, 1,995 ppm, 631 ppm and 4,217 ppb in Pb, Zn, Cu, Ga, As and Au, and threshold values (estimated visually from the log plots) are 7500, 3162, 316, 1000 and 100 ppm and 1000 ppb respectively.

#### 7.3.2 Correlation Coefficients and Factor Analyses

A correlation coefficient matrix for the Main Shear data (log normally transposed) (Table XXII) show numerous significant (at 98%) element correlations in the Main Shear Showings and much fewer in the granite. In the Main Shear samples there are two groups of elements (based on their correlations) viz.; 1) a sulphide phase consisting of Pb, Zn, Cu, La, Ga, As, S, Ag and Au (the chalcophile elements, except La), 2) the second group consists of Th, U, Rb, Y, Zr, Nb, V, Ce, Sr and Ba (ie. definitely non-sulphide) and seems to be a silicate or oxide phase. These two groups are apparently opposed as there are negative correlations of Y with Pb, As, Ag and S. Au correlates directly with



TABLE XXII Correlation Coefficient matrix for trace elements in samples from  
the Main Shear Showing.  $n=43$ ;  $r_{98}=0.35$ . Those correlations that are  
significant at 98% probability level are underscored.

	Pb	Th	U	Rb	Sr	Y	Zr	Nb	Zn	Cu	Ni	La	Ba	V	Ce	Cr	Ga	As	S	Au	Ag
Pb	1.00																				
Th	-0.28	1.00																			
U	-0.23	0.30	1.00																		
Rb	-0.21	0.45	0.45	1.00																	
Sr	0.12	0.15	0.23	0.46	1.00																
Y	-0.46	0.17	0.62	0.57	0.51	1.00															
Zr	-0.17	0.33	0.42	0.65	0.51	0.52	1.00														
Nb	-0.22	0.19	0.42	0.35	0.21	0.45	0.56	1.00													
Zn	0.84	-0.37	-0.09	-0.20	0.19	-0.28	-0.01	-0.14	1.00												
Cu	0.65	-0.22	0.09	-0.22	-0.08	-0.31	-0.16	0.05	0.56	1.00											
Ni	-0.11	-0.22	0.23	0.08	0.17	0.24	-0.18	0.14	-0.17	0.07	1.00										
La	0.35	-0.03	0.13	0.02	0.35	0.11	0.28	0.26	0.33	0.38	0.08	1.00									
Ba	-0.11	0.02	0.22	0.47	0.56	0.52	0.38	0.47	-0.13	-0.08	0.36	0.47	1.00								
V	-0.24	0.25	0.34	0.49	0.45	0.50	0.45	0.34	-0.19	-0.26	0.27	0.26	0.69	1.00							
Ce	-0.29	0.32	0.10	0.34	0.23	0.28	0.40	0.41	-0.17	-0.28	-0.13	-0.02	0.30	0.35	1.00						
Cr	-0.10	0.01	0.09	-0.10	-0.12	-0.07	-0.07	-0.14	-0.03	-0.09	0.12	-0.13	-0.12	0.35	-0.06	1.00					
Ga	0.72	-0.29	-0.32	-0.07	0.26	-0.31	-0.12	-0.22	0.60	0.16	-0.01	0.33	0.07	-0.08	-0.15	-0.14	1.00				
As	0.69	-0.18	0.05	-0.18	-0.12	-0.39	-0.18	0.03	0.53	0.60	-0.00	0.22	-0.10	-0.21	-0.25	-0.02	0.34	1.00			
S	0.64	-0.23	0.14	-0.29	0.02	-0.35	-0.03	0.01	0.64	0.75	0.03	0.46	-0.10	-0.25	-0.24	-0.01	0.25	0.74	1.00		
Au	0.68	-0.05	0.08	-0.20	0.16	-0.23	0.01	-0.15	0.67	0.69	-0.13	0.53	-0.12	-0.09	-0.20	0.05	0.36	0.53	0.73	1.00	
Ag	0.83	-0.01	-0.03	-0.08	0.07	-0.38	-0.07	-0.12	0.64	0.78	-0.07	0.47	-0.08	-0.16	-0.21	-0.16	0.41	0.65	0.67	0.77	1.00

n = number of samples,  $r_{98}$  = significant correlation at 98 % probability level).

Pb, Zn, Cu, La, Ga, As, S and Ag.

R-mode factor analysis of the Main Shear ore samples indicates twelve factors (listed in Table XXIII) account for 95.9% of the variance. The elements loaded on each factor are: Factor 1 (F1), Rb-Y-Zr-Nb-La-Ce (indicative of a silicate component); F2, Pb-Ni-Ga + partially S (a sulphide factor - mainly galena); F3, Th-Ag, the reason for the occurrence of this factor, which accounts for 11% of the variance, is not readily explicable and is probably happenstance (the chemical similarities of Ag and Th are unremarkable, and there is no mineral phase which would preferentially accomodate these two elements); F4, Zn-Au + partial S (a gold factor - unlike the assay data, Au correlates best with Zn in these grab samples, i.e. it would appear that Au occurs in sphalerite-rich areas thus this is a sphalerite-Au factor); F5, V-Cr (probably a mica factor); F6 Cu + partial S (a chalcopyrite factor); F7, Sr + partial La (carbonate factor); F8 U + partial Y and V, opposed by partial Ga (a mica (?) factor opposed by the sulphide factor); F9, Ba (a barite factor); F10, Au-As (gold- arsenopyrite factor); F11, Pb opposed by S (since Pb is so overwhelming in some of the samples, this factor probably indicates that not all S is tied up in galena since there are other sulphides present - at 1.6% of the variance, an insignificant factor); F12, Rb-La-V opposed by Zr (a feldspar factor probably resulting from wall rock

TABLE XXIII

VARIMAX ROTATED FACTOR MATRIX FOR SAMPLES FROM THE MAIN SHEAR SHOWING

	FACTOR 1	FACTOR 2	FACTOR 3	FACTOR 4	FACTOR 5	FACTOR 6	FACTOR 7	FACTOR 8	FACTOR 9	FACTOR 10	FACTOR 11	FACTOR 12
Pb	-0.09782	<u>0.83572</u>	0.14367	0.18574	-0.12701	0.19000	-0.07396	-0.25968	-0.07290	0.19597	<u>0.23865</u>	0.00181
Th	-0.00448	-0.5138	<u>0.78291</u>	-0.08391	-0.03478	-0.06732	0.03327	-0.04350	-0.01099	0.00104	-0.06674	0.00728
U	0.09961	-0.13189	-0.08177	-0.00896	0.07997	-0.05613	-0.05325	<u>0.61699</u>	-0.08253	0.14458	-0.00595	0.00176
Nb	<u>0.78712</u>	-0.09547	0.16539	-0.16100	0.28751	-0.02815	-0.04258	0.15104	0.16043	-0.05735	0.02569	<u>0.15816</u>
Cr	0.27108	-0.10752	0.01860	-0.11047	0.15600	-0.05998	<u>0.76070</u>	-0.06460	-0.08706	-0.08348	0.00073	-0.00483
Y	<u>0.90979</u>	-0.12608	-0.12490	-0.13212	-0.11685	-0.11167	0.10602	<u>0.21234</u>	0.01583	-0.03469	0.08244	0.02262
Zr	<u>0.93470</u>	-0.09843	-0.00020	-0.03479	-0.18204	-0.08688	0.10286	-0.04496	0.07947	-0.02487	0.01060	<u>-0.13783</u>
Nb	<u>0.91497</u>	-0.09950	-0.11728	-0.06795	-0.02959	0.02755	0.04890	-0.09610	0.11781	-0.03237	-0.05265	-0.01799
Zn	-0.04841	0.14730	-0.01608	<u>0.86152</u>	-0.03734	0.14227	-0.04357	-0.02647	-0.03470	-0.06121	0.04112	-0.00763
Cu	-0.09249	0.20656	0.00775	0.18886	-0.16856	<u>0.83554</u>	-0.03780	-0.09416	-0.01503	0.02670	0.02304	0.00223
Ni	-0.10993	<u>0.81043</u>	-0.05683	-0.02839	-0.03128	0.15669	0.00713	0.13691	0.06808	-0.07581	<u>-0.15208</u>	-0.01304
La	<u>0.71426</u>	0.30575	0.00441	0.40015	0.18395	0.09575	<u>0.35271</u>	0.01834	0.09847	-0.04310	-0.02314	<u>0.10355</u>
Ba	0.14728	-0.02516	-0.03240	-0.08447	0.24961	-0.01886	-0.07599	-0.09461	<u>0.73973</u>	-0.04480	-0.00312	-0.00008
V	0.21616	-0.06315	0.02878	-0.16226	<u>0.72655</u>	-0.03044	0.14740	<u>0.28565</u>	0.26503	-0.17551	0.03843	<u>0.11021</u>
Ce	<u>0.85525</u>	-0.09420	0.01016	-0.15033	0.31686	-0.08486	0.11672	0.08981	-0.14790	-0.16313	-0.03449	0.00652
Cr	-0.07107	-0.14749	-0.17854	0.05757	<u>0.74757</u>	-0.19534	0.08410	-0.04162	0.12432	-0.01701	-0.02606	-0.06150
Ga	-0.08231	<u>0.90051</u>	0.10274	0.19426	-0.10633	-0.00427	-0.08135	<u>-0.26878</u>	-0.07725	0.17622	0.03306	0.01766
As	-0.08422	0.10103	0.02947	0.08819	-0.07581	0.02304	-0.04789	0.11347	-0.02607	<u>0.50602</u>	0.00235	-0.00129
S	-0.16368	<u>0.46062</u>	-0.03286	<u>0.58284</u>	-0.20748	<u>0.48668</u>	-0.11551	0.09573	-0.03669	0.09986	<u>-0.20501</u>	-0.01058
Au	-0.18104	-0.00395	-0.01967	<u>0.71164</u>	0.01796	0.02326	-0.05688	-0.03251	-0.08565	<u>0.38287</u>	-0.00293	0.00236
Ag	-0.07223	0.15552	<u>0.96472</u>	0.05054	-0.10656	0.07851	-0.01706	-0.06940	-0.02480	0.04585	0.08100	-0.00254

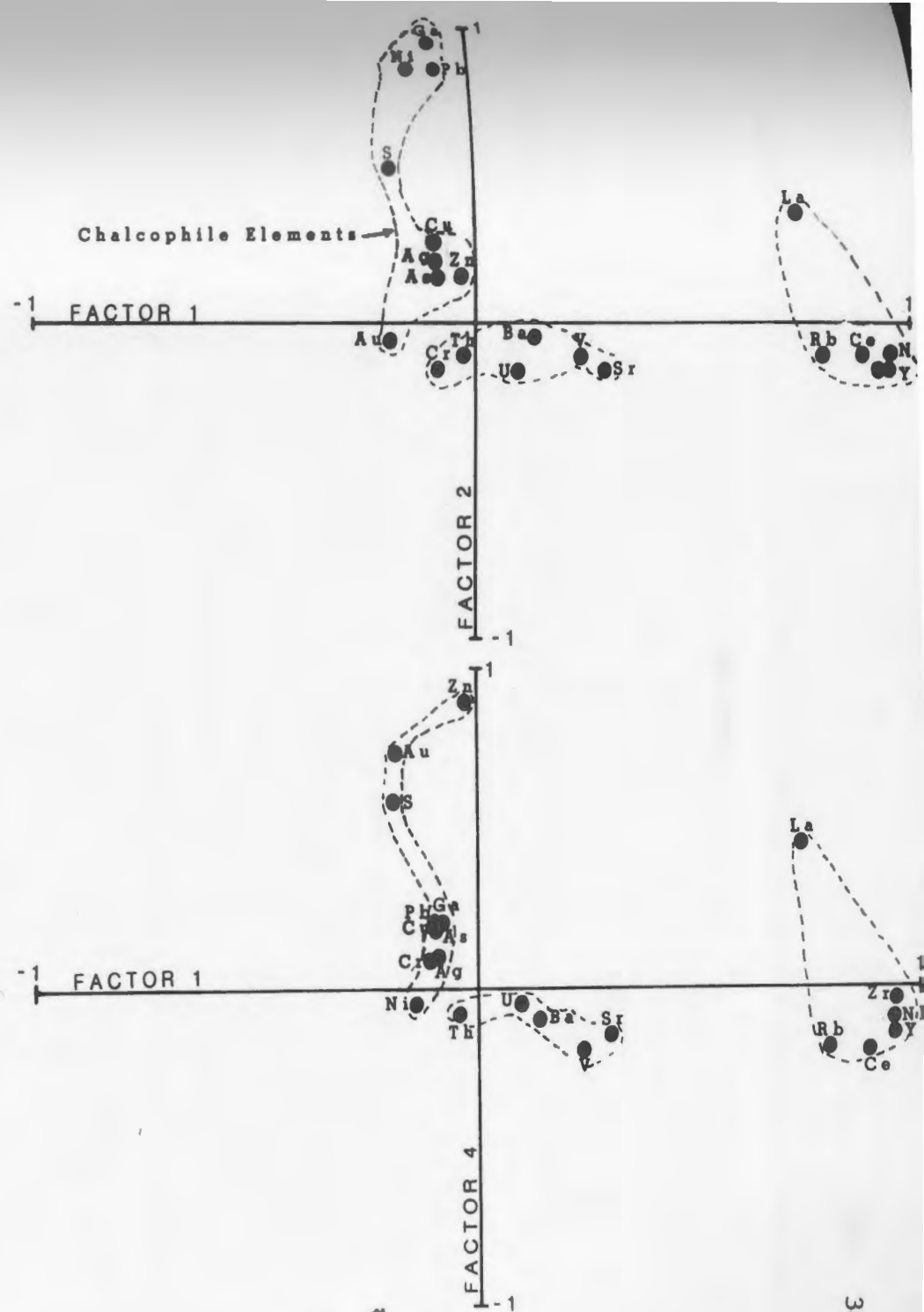
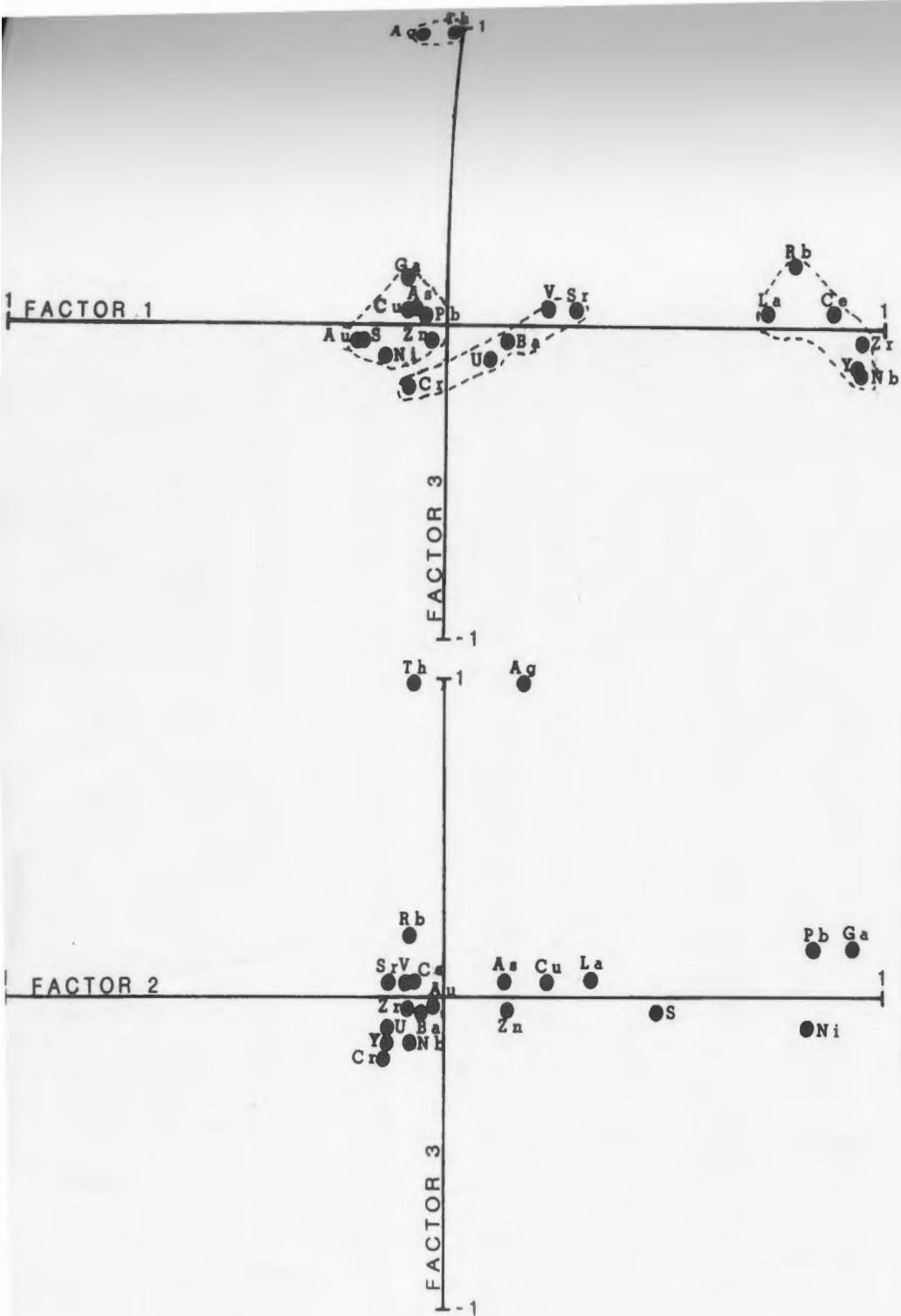
inclusions, opposed by a mica (?) factor).

When these factors are compared to each other, as in Figure 65, fundamental elemental groupings are discernable. These groups consist of (a) La-Ce-Rb-Nb-Y (a silicate component), (b) Au-Ag-As-Cu-Zn-Pb-Ga-S (a sulphide component), and (c) Cr-Th-U-Ba-V-Sr (a carbonate/clay(?) component). The groups consistently occur through comparisons of F1 with all others (except for local permutations such as F3 which shows an inter-relationship between Ag and Th), and group (a) is the most unique (ie. groups (b) and (c) are sometimes intermixed). When other factors beyond F1 are compared, the groups merge because the actual variance decreases rapidly after F1 (ie. it accounts for 30% of total group variance).

In deposits of the Cortez quadrangle of Nevada, some of which are granite-hosted, Elliot and Wells (1968) found good positive correlations between similar chalcophile and noble metals (ie. Au-Ag-Pb-Fe-Sb-Cu), but As was correlative in only the surrounding country rocks. In silicified rocks of the Goldfield Mining District of Nevada, Ashley and Keith (1976), found good correlations between Au and Ag-Pb-Bi-As. However in the Carlin deposit of Nevada, which was deposited from meteoric waters (Radtke et al., 1980), Harris and Radtke (1976) found that Au correlates very poorly with Cu-Pb-Mo-Ba, but that these other elements have strong intercorrelation.

Figure 65 Plots of Varimax rotated factors in the Main Shear samples.

The factors consistently indicate the three main groupings through the samples. By Factor 3, the variance within the group becomes minimal.



### 7.3.3 Relative Enrichment Factors

Average enrichment factors, of ore and trace elements between the Main Shear samples and an average of schist samples (eg. GAST, SE/CL, SER/SC, CL/BIO and CHL/SC), and between granite ore veins and average Windowglass Hill Granite (without the wall rock samples WGH SH2B and WGH SH3) were calculated and are represented in Figures 66a and 66b. In the Main Shear samples, all the chalcophile elements, Th and U are enriched to varying degrees, while the other elements are depleted. The greatest enrichments are Ag (871x background schist), Au (718x), Pb (332x), Zn (157x), Cu (76x) and As (31x). S (8x) and Th (2.8x) are moderately enriched, and U (1x) and Ni (1x) are only slightly enriched in the veins relative their host schists.

The veins in the granite have extremely elevated average Au contents (2751x background granite), but due to the small number of vein samples (6), this mean value is positively skewed by the undue influence of a single high concentration (ie. sample WGH SH2A contains 73,730 ppb Au). The other chalcophile elements (except Ni), Cr, U and CO<sub>2</sub> have positive enrichments which range from high in Pb (54x), Cu (34x), Ag (29x), Cr (17x), As (15x), Ga (14x) and S (10.8x), to moderate in Zn (2.5x), and low in U (1.2x) and CO<sub>2</sub> (1.1x). The elevated Cr is probably contained in Cr-bearing micaceous minerals in the veins vs. granite

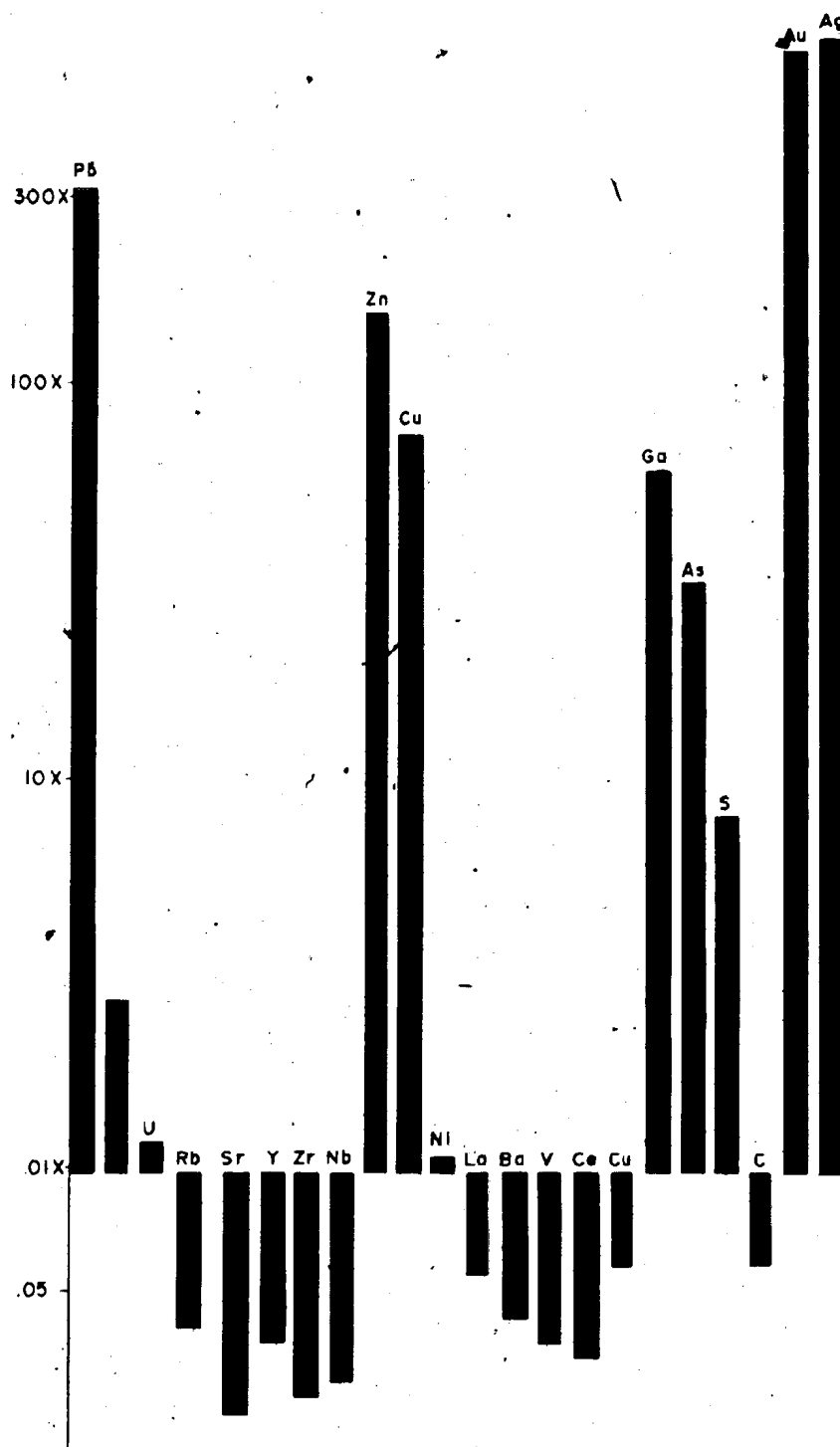


Figure 66a Enrichment/depletion factors for elements in the Main Shear Showing. The chalcophile/ore elements have intense enrichments, while the other trace elements generally are depleted.

Figure 66b Enrichment/depletion factors for elements in the Windowglass Hill Showing. Chalcophile/ore enrichments are noticeably less than in the Main Shear Showing.

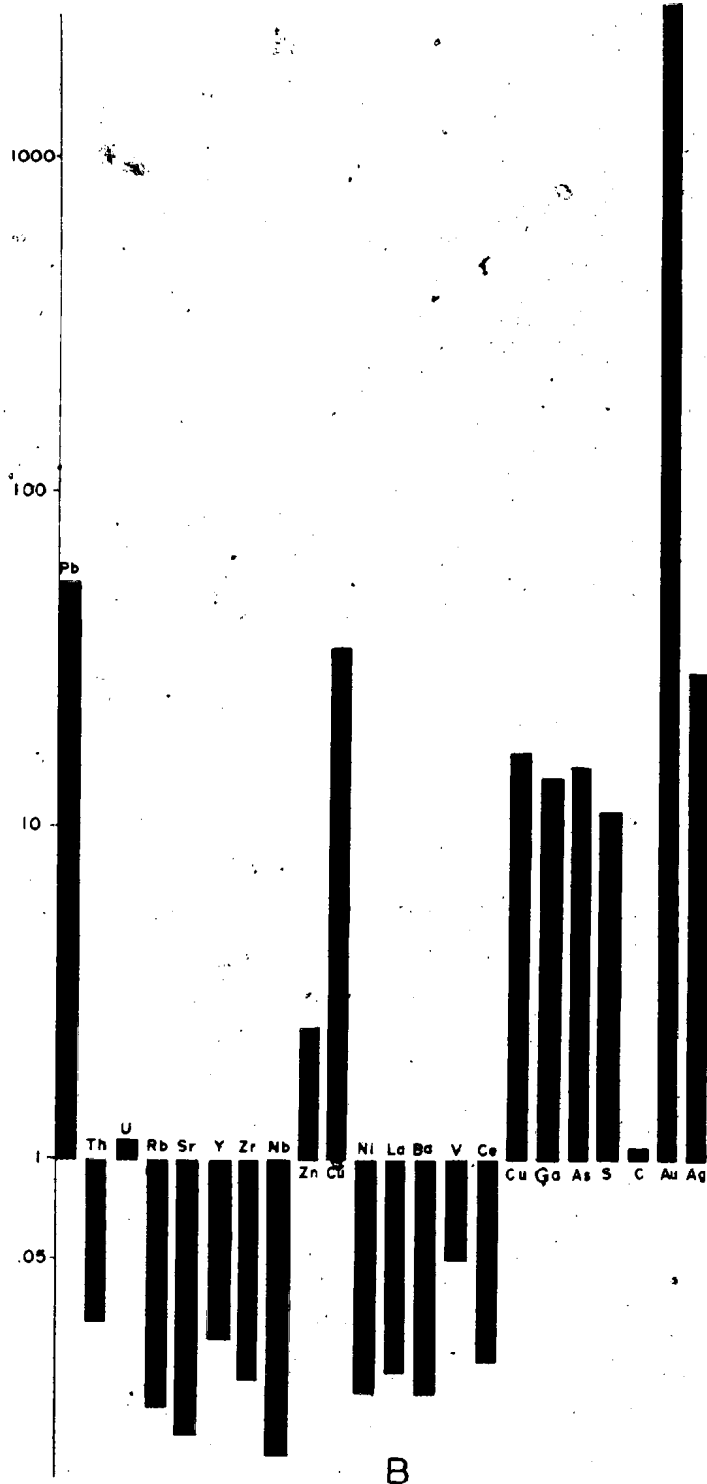
Figure 66c Enrichment/depletion factors for Main Shear samples vs. background Windowglass Hill Granite. The enrichment factors are intermediate between those in Figures 66a and 66b.

## MAIN SHEAR SHOWING



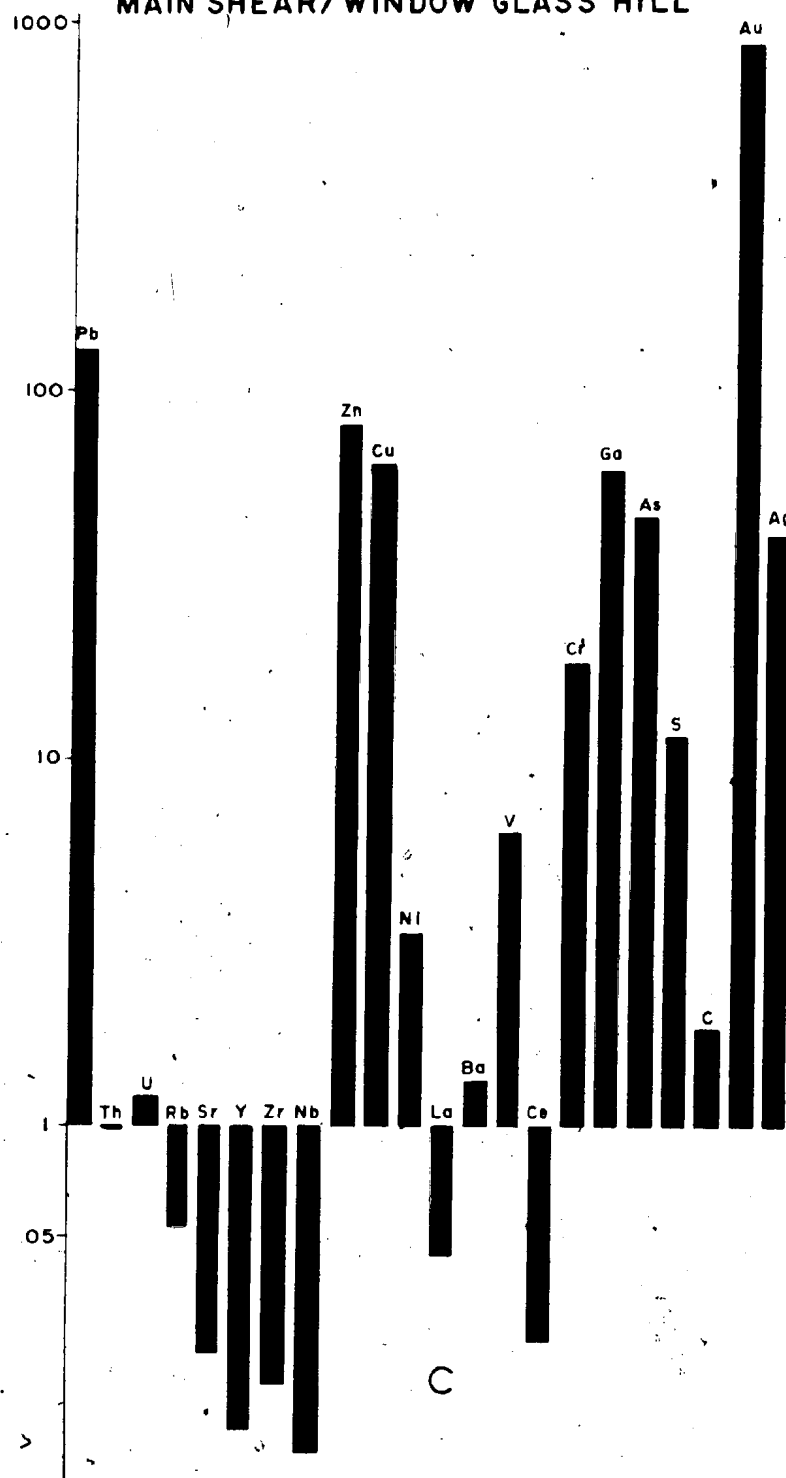
A

## WINDOW GLASS HILL SHOWING



B

## MAIN SHEAR/WINDOW GLASS HILL



(cf. Kerrich, 1980). Similarly higher CO<sub>2</sub>, indicates more carbonate in the veins than granite. Silicate elements are more depleted in the granite than in the Main Shear veins possibly because of the generally higher concentrations of those elements in the granite vs. schists (ie. a host rock influence).

There are significant differences in the relative enrichments of the sulphide elements between veins in the two showings. Au is greatly enriched in the granite veins (possibly sample bias), but all the other elements (except S) have much lower enrichments than in the Main Shear veins (eg. Pb is 332x background in the Main Shear veins, but only 54x in the granite), and Zn is very much less enriched (ie. 157x vs. 2.7x). (This lower concentration of Zn was also found in the assay data described above).

In order to determine if the differences in enrichment factors solely reflected differences in background concentrations, the enrichment ratios between Main Shear ore veins and the average Windowglass Hill Granite were calculated (Figure 66c). The relative enrichments are similar to those in Figure 66b (ie. granite quartz veins/background granite) indicating the granite does have some higher background contents of Pb and Ag, similar concentrations of Zn, Cu, Ga and As, and lower S. The Zn ratio is higher than that in Figure 66b, but not as high in Figure 66a, thus the Zn backgrounds in the granite are

higher, than those in the schists, yet the content of Zn in granite-hosted quartz veins is significantly lower than that in the Main Shear veins. A final conclusion to be reached is that the lower enrichment factors in the granite-hosted veins show that these veins are more chemically similar to their host than the Main Shear veins are to their enclosing schists.

As a broad generalization, Kerrich (1980), Kerrich et al. (1981), Kerrich and Fryer (1981) and Kerrich (1983a) have concluded that in Archean lode gold deposits, Au, Ag and As (or "rare elements") are greatly enriched relative to nearby host volcanic rocks, whereas Pb, Zn and Cu are only slightly enriched. Quoted enrichment factors for a) world-wide mafic, igneous rock-hosted lode deposits are 15,000x for Au, and 80x for Ag, but only 0.2-5x for Pb, Zn and Cu (Kerrich and Fryer, 1981), b) and 10,000x (ibid.) for As in the Yellowknife district. In particular, for the Dickenson Mine, Red Lake, Ontario, Kerrich and Fryer (1981) and Kerrich (1983a) show enrichments of ~ 18,000x Au, 1,800x As and 40x Ag, yet only 18x for Zn and <2x for Cu and Pb in ore relative to host basalts.

These authors state that extremely high and preferential enrichments of Au, Ag and As vs. base metals are an intrinsic result of low water/rock ratios in the source regions of the mineralizing fluids. They feel that such source regions are best conceptualized as zones of

metamorphic outgassing produced by amphibolite grade metamorphism (cf. Fyfe and Henley, 1973; Henley et al., 1975; Kerrich and Fyfe, 1981).

Such relationships do not hold for the Cape Ray Fault Zone deposits. In both environments all the chalcophile elements are enriched to similar degrees (ie. there is no separation of base metal vs. "rare" elements). The Pb and Cu enrichment factors exceed 30x, yet the Au, As or Ag enrichments do not exceed 800x background (except Au in the granite-hosted veins), and both Pb and Cu have greater enrichments than Ag in the granite showing.

Kerrich (1983a) subdivided Au-bearing deposits into two groups (viz.; lode gold deposits and base metal deposits), on the basis of their relative Au enrichments vs. enrichment of Cu + Zn (the former is highest and the latter lowest in the lode gold deposits, and the reverse is true for the base metal deposits - see Figure 67). However of the two lode gold deposits in this study, the Main Shear veins plot with the base metal deposits and the Windowglass Hill Granite veins are transitional between the two groups. Therefore this enrichment classification scheme is not applicable to the Cape Ray Deposits. The granite-hosted veins are transitional solely because of the relative Zn depletion (ie. the other base metals, Cu and Pb, have enrichment patterns comparable with the base metal deposits).

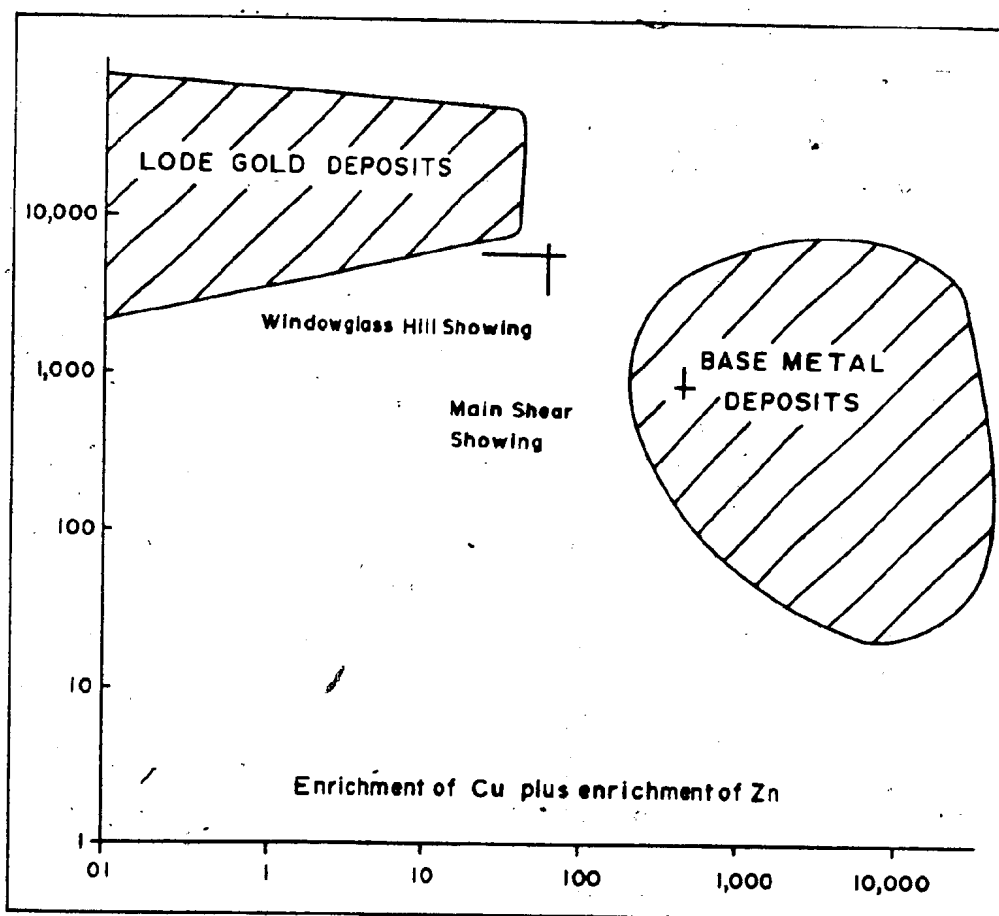


Figure 67 Au enrichment vs. Cu + Zn enrichment diagram for the Windowglass Hill and Main Shear Showings. Diagram and fields are from Kerrich (1983a). This diagram indicates that the Main Shear Showing would be classified as a base metal deposit, while the Windowglass Hill Showing is transitional between lode gold and base metal deposits.



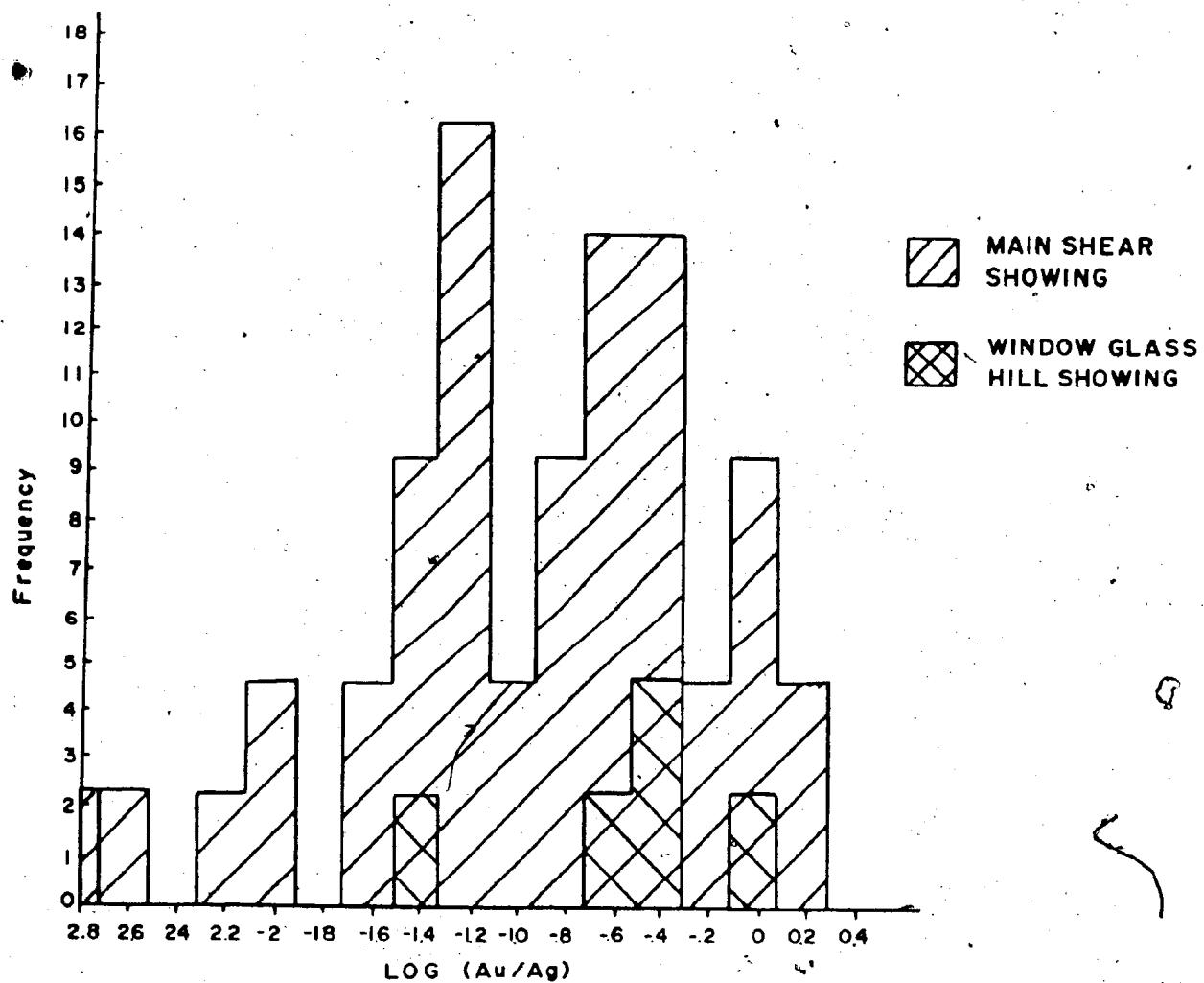
#### 7.3.4 Au/Ag Ratios

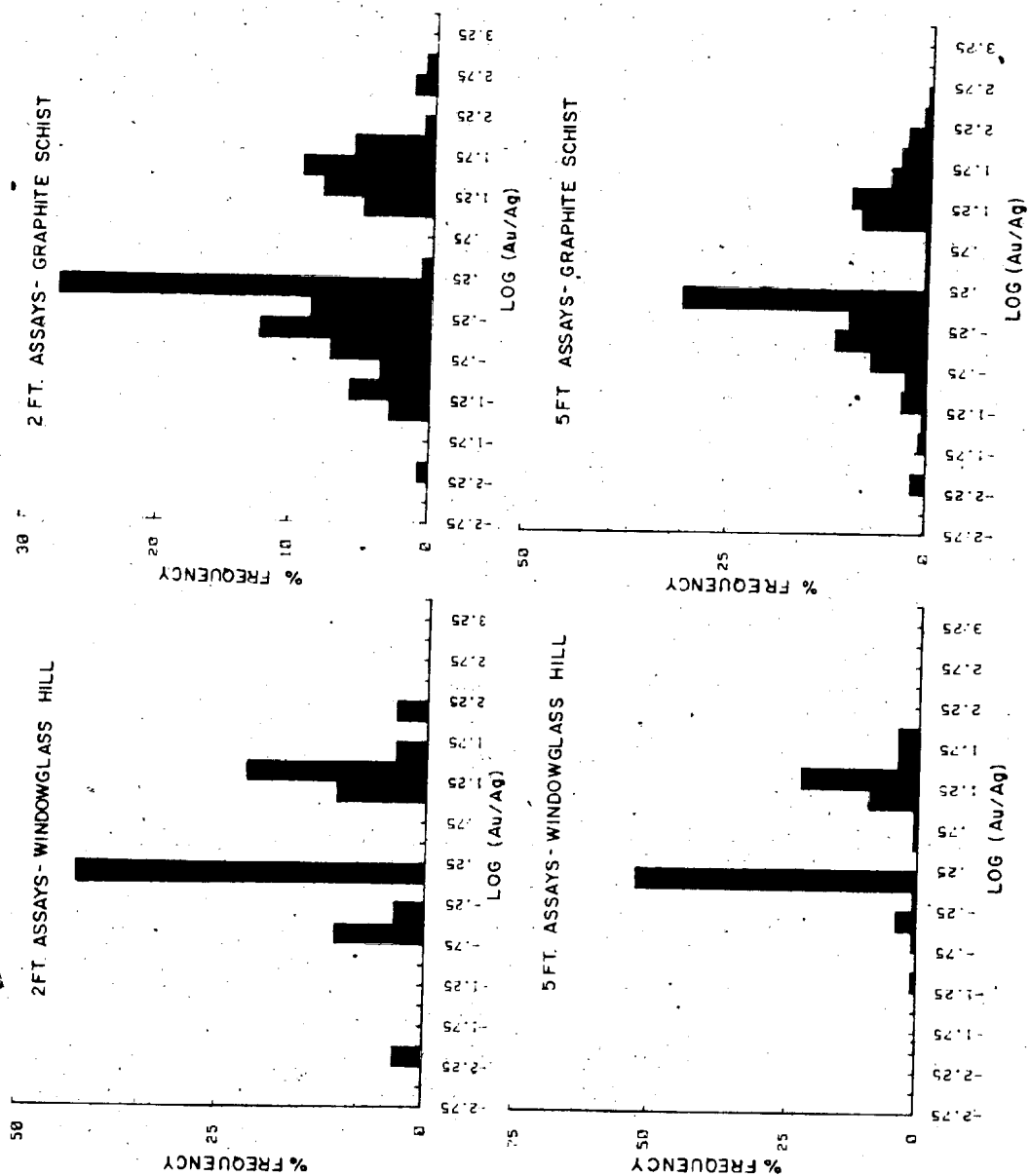
The Au/Ag ratios of ore samples from both vein systems are typically less than 1, grading from 0.002 (sample PB53-2) to 3.3 (sample PB27-33) in the Main Shear samples, and 0.001 (sample PB133-6A) to 0.39 (sample PB38-5A) in the granite. The ratios have a log normal distribution (Figure 68a), with a broad three-pronged set of peaks for the Main Shear (general mean of ~0.25) and general maxima for the granite samples of about 0.32. Though based on a small sample size, the Au/Ag ratios in the granite-hosted veins are slightly higher than in the Main Shear samples. This general relationship is visible in the assay sample also, where, in the lognormal distributions of the ratios (Figure 68b), there are two peaks in the schist samples below and above 1:1, with a preponderance of samples in the lower ratio area; however in the Windowglass assay samples, aside from the central peak 1:1 peak, ratio values are concentrated above 10 (though there is a small scatter below 1:1).

The importance of Au/Ag ratio distributions to ore deposit zonation is a controversial, much discussed, yet little understood phenomena. Boyle (1979, pp. 197-207) presents an overview and synthesis on this particular subject and according to this compilation, gold-quartz vein lodes generally have Au/Ag ratios of 1.37-12.5 (average

Figure 68a Histogram of Au/Ag ratios in the Windowglass Hill and Main Shear Showings. Ratios are quite similar, if slightly higher in the Windowglass Hill Showing.

Figure 68b Histogram of Au/Ag ratios in the assay samples. See text for discussion.





4.2), ie. unlike the Cape Ray deposits. The only analogous ratio groupings (to the Cape Ray Deposits) are found in the Tertiary gold-quartz vein lode deposits (0.005-0.33, average 0.05) in acidic volcanic rocks (eg. Cripple Creek, Colorado, etc).

As to actual intra-deposit variations, Boyle found that Au/Ag ratios most frequently increase with depth, or increasing temperatures of deposition. The subtle Au/Ag variations between the Main Shear and Windowglass showings might therefore signify slightly higher ore-forming temperatures for those veins in the granite.

#### 7.4 Background Au-Ag Abundances in the Regional Lithologic Units

The background Au and Ag contents within the surrounding lithological units of the ore deposits were examined in order to: 1) locate any anomalous values indicative of further mineralization, 2) determine if any of these units can be demonstrated to be sources of these elements, 3) evaluate the relative abundances of these elements in the different rock types, and 4) compare and contrast these abundances with those derived elsewhere by other authors for similar rock types.

Because of the very low concentrations of these elements in the various rock types (Au is usually < 10 ppb and Ag is generally < 200 ppb), there are numerous problems

associated with such analyses. Contamination from analytical reagents and general sample preparation can produce "anomalous values" (cf. Gottfried *et al.*, 1972), therefore elevated concentrations must be evaluated with such problems in mind. The overall consistency of values within each group is good, though there are differences between groups, indicating the analyses are acceptable (as are the conclusions to be drawn from them). The most striking feature of the Au and Ag is the overall low concentrations and lack of anomalously higher values. The actual number of analyses per lithologic unit is small, but where there are sufficient data, the Au and Ag distributions are log normal.

#### 7.4.1. Windsor Point Group Schists

The highest Au contents are found in the three samples of the chlorite schist, *viz.*: 30.2 ppb in 79-73, 25.5 ppb in PB7-13 and 38 ppb in sample PB51-12. All three are from the ore deposit region. 79-73 occurs <10 m to the south of the granite-hosted H Brook Showing. The other two are of drill core. In individual samples from each of the other schist units, Au is < 17 ppb, and usually <10 ppb, and means for each group are 6-7 ppb (compare with 15.8 ppb for CHL/SC), and higher Au contents usually occur in those samples with disseminated pyrite.

Ag is usually < 100 ppb, except in the WAL/RX samples which have a mean of 779 ppb, the single largest concentration (ie. 7100 ppb in sample 80-611), and three other samples with > 120 ppb. These schist samples are wall rock to the Main Shear mineralization, thus their elevated Ag is probably due to this proximity to the ore-forming fluids. However, Au is not elevated in these same samples possibly because Ag is more mobile than Au (Boyle, 1979).

The SER/SC samples also have an elevated Ag concentrations and a higher than typical mean (217 ppb). The GAST group has a single sample (PB41-7) with enriched Ag (333 ppb) but its mean of 74 ppb is in line with those of CL/BIO (58 ppb), SE/CL (35 ppb) and CHL/SC (33 ppb).

Table XXIV contains the correlation coefficients for Au and Ag vs. other major and trace elements. There are no significant correlations (at 98% probability) of background Au and Ag in the CHL/SC and SE/CL samples. In the GAST samples, Ag contents correlate positively with those of Pb and LOI, indicating Ag resides in a chalcophile-sulphide phase. In the WAL/RX samples Ag has strong correlations with Pb, U, Y, Cu, V, Cr, Ga, As, CO<sub>2</sub> and P<sub>2</sub>O<sub>5</sub>. This list presents a problem as all the elements do not have a readily identifiable common denominator, but may reflect those elements added to the wall rock by hydrothermal ore fluids. The Gresen's density/volume relations showed that

TABLE XXIV. Correlations of Au and Ag with other elements

UNIT	No. of Samples	$r_{\text{Ag}}$	Element(s) correlating significantly with Au and/or Ag and correlation coefficient
Windowglass Hill Granite	19	0.53	<u>Au</u> : Pb, 0.69; Cu, 0.88; Ga, 0.83 * <u>Ag</u> : Cr, 0.67; Ga, 0.63
Port aux Basques Granite	4	0.98	<u>Ag</u> : MnO, 0.99; CaO, 0.99
Sericite/chlorite schist	6	0.88	<u>Au</u> : Ag, -0.89
Chlorite/biotite schist	3	1.00	<u>Ag</u> : MnO, -1.00
Windsor Point Group Ignimbrite	18	0.54	<u>Ag</u> : Pb, 0.78; Sr, 0.88
Port aux Basques Gneiss	5	0.93	<u>Ag</u> : Th, 0.99
Retrogressed Port aux Basques Gneiss	3	1.00	<u>Au</u> : MgO, 1.00, LOI., 1.00
Diorite	5	0.93	<u>Au</u> : MgO, -0.99
Strawberry Granite	9	0.75	<u>Ag</u> : U, 0.87; Nb, 0.80; Ni, 0.90
Gabbro	6	0.88	<u>Au</u> : MnO, 0.94; LOI., -0.91
Long Range Mafic/Ultramafic Complex	4	0.98	<u>Au</u> : La, 0.99; Ce, 1.00
Wall Rock	9	0.75	<u>Ag</u> : P <sub>2</sub> O <sub>5</sub> , 0.90; Pb, 0.96; U, 0.99; Y, 0.85; Cu, 0.82; V, 0.99; Cr, 0.94; Ga, 0.92; As, 0.89
Graphite schist	10	0.72	<u>Ag</u> : LOI., 0.83; Pb, 0.78
Sericite schist	3	1.00	<u>Au</u> : Al <sub>2</sub> O <sub>3</sub> , -1.00
Tonalitic Cape Ray Granite	5	0.93	<u>Au</u> : Ga, 0.94
Megacrystic Cape Ray Granite	9	0.75	<u>Au</u> : Na <sub>2</sub> O, 0.83; Th, -0.76; V, -0.80
Red Rocks Granite	4	0.98	<u>Au</u> : Al <sub>2</sub> O <sub>3</sub> , 0.99; K <sub>2</sub> O, -0.99



Ga, As and Co<sub>2</sub> were gained by the wall rocks from the hydrothermal ore fluids (but Cr was lost). CL/BIO samples have negative correlations of Ag with MnO. In the SER/SC, Au has a negative correlation with Al<sub>2</sub>O<sub>3</sub> indicating Au doesn't occur in aluminosilicates. There is no correlation between Au and Ag contents in any of the units.

#### 7.4.2 The Port aux Basques Gneiss, WPGQ and PABQ samples

The background Au abundances in each of these three units has a bimodal character in that there are low values, < 7 ppb, and also more elevated ones (up to 49 ppb in sample 79-122 of WPGQ). Sample 79-122 occurs south of the Windowglass Hill Granite and is cut by sulphide-bearing quartz veins apparently from the granite. In the gneiss samples, one has 11.4 ppb Au (79-170S) while another has nil (79-77). The former contains disseminated pyrite and occurs just outside the southeastern boundary at the southwestern edge of this map area. The two samples of PABQ with elevated Au (79-151 and 79-152 with 9.9 and 13.8 ppb respectively), contain > 5 % disseminated pyrite.

Ag is very low in all samples (< 120 ppb) except 79-71 (PAB/GN) which contains 14,813 ppb Ag, but there is also 0.43 % S in this sample.

Correlation coefficients for the Port aux Basques

Gneiss (Table XXIV) indicate Ag has a significant positive correlation with Th. Au in the PABQ samples correlates positively with MgO and LOI (the LOI correlation may indicate Au is in altered zones, and the correlation with MgO is inexplicable except perhaps the Au occurs in more mafic areas). In the WPGQ samples the noble metals have no correlations with other elements.

#### 7.4.3 Windsor Point Group ignimbrites

The felsic volcanic samples have low Au concentrations when compared to the schists. The mean of eighteen samples is 3 ppb with a maximum of 7.8 ppb. The log distributions indicate a mean at 2.6-3.2 ppb. Ag is generally low, <130 ppb, except in two samples, 79-15 (7967 ppb) and 79-19 (460 ppb), both of which are from feldspar porphyry dykes intrusive into the Cape Ray Granite near Red Rocks Point. The galena showing near Red Rocks Point occurs in a quartz vein associated with the 79-15 dyke. The log distribution indicates indicate a more typical Ag mean (ie. without 79-15 and 79-19) of 63-100 ppb.

Table XXIV indicates that the only significant positive inter-element correlation of these noble metals is Ag with Pb and Sr. The high Ag in samples 79-15 and 79-19 are therefore directly correlative with the galena showings. The Sr correlation may indicate that Ag occurs

with carbonate alteration elsewhere.

#### 7.4.4 The mafic units

The Au contents in the basic dyke and gabbro samples are quite low < 3 ppb and < 6 ppb respectively. Similarly the Long Range Mafic/Ultramafic Complex samples have low Au abundances except sample 80-78 which is an altered metagabbro. The Port aux Basques amphibolites generally have < 9 ppb Au, but one sample, 79-63, from near Big Barachois, has 23.6 ppb Au. The gabbro south of Windowglass Hill, and the diorite in contact with this granite in drill core, have somewhat higher Au contents than those in the other mafic rocks. The Ag contents of these two units are consistently higher than those in the other units with means of 62.6 ppb in the diorite, 59.8 ppb in the gabbro; vs. 25, 54.3, 42 and 38 in the ophiolites, amphibolites, gabbros and dykes respectively.

In the gabbro samples, Au has a positive correlation with MnO and negative correlation with LOI. (Table XXIV). It would appear that the Au in the gabbro is primary (ie. correlates with primary mineralogy) and may have been removed during alteration (ie. hence negative correlations with LOI.). Au in the ophiolite remnants correlates with La and Ce. Rocks of this lithology and environment usually have low concentrations of these elements (ie. LREE's)

when fresh, but with increasing seawater-induced alteration (such as that which affected these ophiolitic rocks), La and Ce contents increase. Since both La and Ce were added to these samples, and since both elements correlate with Au, the Au may have been introduced during the ocean floor alteration (cf. Keays and Scott, 1976). In the diorite, Au has a negative correlation with MgO (ie. Au is not associated with mafic silicates).

#### 7.4.5 The granites

Background Au contents in the Port aux Basques (< 4ppb) and Isle aux Morts Brook (< 6 ppb) Granites are quite low. The tonalitic Cape Ray Granite (mean 5.4 ppb) and Red Rocks Granite (mean 4.1 ppb) also have low Au concentrations except for single samples at 13 and 11 ppb respectively (these samples are not significantly different from any others in their groups). The Strawberry Granite has low level Au abundances (<10 ppb), but there are also two enriched samples, STG-2 (19.8 ppb) and STG-5 (16.7 ppb). STG-5 is an aplite sample and STG-2 is a regular granite but with disseminated pyrite. (Note that the pyrite-molybdenite bearing sample, 79-94, contained only 2.1 ppb Au). The megacrystic Cape Ray Granite has a wide range of Au concentrations with three samples (ie. CRG-1F, 14.8 ppb; CRG-2F, 26.8 ppb; and CRG-3AF, 21.3 ppb) having

anomalously high concentrations. These particular samples are feldspar megacryst splits from this granite but the regular granite samples (with megacrysts) have lower Au contents (mean of 5 ppb).

The Windowglass Hill Granite has the most consistently elevated Au contents. The samples with 3419 ppb (WGH SH2B) and 329 ppb (WGH SH3) Au are wall rock to mineralized quartz veins, thus their high values reflect the introduction of Au into the granite (ie. they are the only significant Au haloes found in this study). Aside from these two samples, the log distribution of Au values indicates a mean of approximately 7.9 ppb.

The Ag contents show wide variability in nearly all the granites (except the tonalite and Isle aux Morts Brook Granite). The values are typically higher than those found in the other regional units. The Windowglass Hill Granite has the highest values and the largest spread of any unit sampled in this study. Rejecting the wall rock samples, the log Ag distribution in this granite has a mean of 158 ppb. The Strawberry Granite has a high mean (259 ppb), but this is produced by the inclusion of sample STG-4 which has an inexplicable Ag content of 1,000 ppb.

Au has positive correlations with Ga in the tonalite (ie. a chalcophile phase); positive correlation with Na<sub>2</sub>O, but negative correlation with Th and V in the megacrystic Cape Ray Granite (ie. the higher Au values in

the feldspar megacrysts result in the correlation with Na<sub>2</sub>O, while Th and V may be in biotite phase); positive correlations with Al<sub>2</sub>O<sub>3</sub> and a negative correspondence with K<sub>2</sub>O in the Red Rocks Granite (ie. Au is with mafic silicates). Ag has significant positive inter-relations with U, Nb and Ni in the Strawberry Granite (ie. the Ni may indicate a common sulphide phase, relations with the other elements are not understood); with MnO and CaO in the Port aux Basques Granite (ie. Au is within silicates); and Pb, Cu, Ga and As in the Windowglass Hill Granite (ie. a definite common sulphide phase).

#### 7.4.6 Comparison of background Au and Ag contents with other reports

##### 7.4.6.1 Au abundances

The background Au abundances as determined in this study are similar to those reported elsewhere by other authors for different rock types in different terrains. Au abundance in all terrestrial rock types is generally less than 20 ppb (Tilling et al., 1973, quote 10 ppb as the general maxima for unaltered igneous rocks, and Kwong and Crockett, 1978, state that Au analyses of > 10 ppb are anomalous in an Ontario greenstone belt), but there are of course exceptions. Various authors have tried and failed

to show that certain rock types contain intrinsically elevated Au contents (eg. the so-called elevated Au contents in ultramafic rocks described by Viljoen et al., 1969, which were subsequently shown to be lower than typical basic rocks by Anhaeusser et al., 1975). Another major problem with using data from other authors, is that analyses from pre-1960 are often suspect due to analytical difficulties involved in determining such low element abundance levels with the equipment available at the time. In her compilation of Au abundances, Jones (1969) reports data as pre-1955 and post-1955, emphasizing the greater reliability of the latter group. Boyle's (1979) compilations similarly suggest caution with older data.

Sulphide phases (typically pyrite) have repeatedly been shown to contain the bulk of the background (or elevated) Au in any given rock type. This relationship has been shown a) empirically, such that sulphide-bearing samples contain greater amounts of Au than nonsulphide-bearing samples of the same rock type (eg. Vikhter et al., 1968; Gavrilenko et al., 1976; Boyle, 1979; Keays, 1979; Saager et al., 1982); b) by separating sulphide and non-sulphide phases from a given rock, and analysing each separately (eg. Gureyev, 1968; Jones and Fleischer, 1969; Zvereva and Gavrilenko, 1971; Kwong and Crockett, 1978; and Glasson and Keays, 1978); c) the common correlation of Au and S in both enriched and

depleted zones (eg. Keays and Scott, 1976; and Kuo and Wilson, 1976); and d) experimental data such as that of Mironov et al. (1978) which indicated that a doped isotope of Au ( $^{195}\text{Au}$ ), when placed in a reaction vessel with a basaltic liquid, concentrated in a sulphide phase but if the sulphide phase was absent, the Au was adsorbed onto the reaction vessel wall and did not enter the silicate glass.

In non-sulphide phases, Au is apparently enriched in the more mafic silicates (Jones and Fleischer, 1969; Tilling et al., 1973; and Boyle, 1979), while the more felsic silicates have lower Au contents (eg. Davletov, 1970; Zvereva and Gavrilenko, 1971; and Boyle, 1979). Keays and Scott (1976) state that aside from sulphide sites, Au also occurs in higher temperature oxide and silicate sites in basalts. Iverson et al (1974, p.244) said that Au content "increases not only with basicity but also with sodium content".

The lithologic units with a wide variation in Au contents (eg. GAST), generally have disseminated pyrite as a typical constituent in those samples with the higher Au values, therefore the Au is probably resident in the sulphide phase. However, the definitively mafic-poor Windowglass Hill Granite has higher gold contents than other granitoid and the microcline megacrysts in the megacrystic Cape Ray Granite have Au contents in excess of the granite itself (i.e. including the mafic phases).



These elevated Au contents are the opposite of what would be expected.

Correlations of background Au contents with other trace elements have been attempted by some authors. Zvereva and Gavrilenko (1971) report Au correlations with Cu, Mg and V in granitic intrusions. Keays and Scott (1976) show positive correlations of Au with MgO, Cr and Ni in pillow basalts. However, Saager *et al.* (1982), having analysed the same elements in greenstone belts, found no correlations with Au, and that in factor analysis, Au stood apart from the other elements as a unique factor. Kwong and Crockett (1978) also found no correlations between Au and Na<sub>2</sub>O, K<sub>2</sub>O or MgO. Similarly the samples analysed in this study contained only a few erratic inter-element correlations with Au (mainly indicative of the presence of Au in a sulphide or mafic phase).

The average background Au contents as determined by other authors for mafic volcanic, felsic volcanic and metamorphic rocks are illustrated in Tables XXVa to XXVc. Metamorphic rocks have wide variations in their quoted background values, and sulphide-bearing units have more Au than barren rocks. The Cape Ray Fault Zone schist and gneiss samples are within the general realm of background values (especially those reported by Boyle (1979), whose compilations are of a wide source of data, though the averages appear to be somewhat high and may be so due to

TABLE XVa Background Gold Abundances in Mafic Rocks

<u>Mean Au(ppb)</u>	<u>Rock Type</u>	<u>Reference</u>
0.78	mafic/ultramafic intrusives	Kwong and Crockett, 1978
1.75	mafic volcanics	"
-5	gabbros	Sighinolfi and Gorgoni, 1977
1.8-4.2	diabase	Gavrilenko <i>et al.</i> , 1976
4-5.4	metagabbros	"
4.4-6.8	diabase	Ivensen <i>et al.</i> , 1974
4.2	basalt	"
6.5	gabbros	Shcherbakov and Perezhogin, 1963
4	gabbro	Tilling <i>et al.</i> , 1973
0.8-5.4	basalt	"
11.4	ultramafics	Boyle, 1979
23	gabbros	"
1.6	lamprophyres	"
17	basalt	"
17.9	ultramafics (southern Africa)	Saager <i>et al.</i> , 1982
6.9	basalts	"
0.8-5.7	ultramafics (Europe)	"
0.5	mafic volcanics	"
8.2	dunite	Jones, 1969
5.4	gabbro	"
3.2	basalt	"
12	kimberlites	Paul <i>et al.</i> , 1979
18.2	gabbros and diabases	Stephens and Ehman, 1971

TABLE XXVb Background Gold Abundances in Felsic Rocks

<u>Mean Au (ppb)</u>	<u>Rock Type</u>	<u>Reference</u>
0.5	alkali monzodiorite	Tilling et al., 1973
0.6	quartz monzonite to granite	"
2.6	granodiorite	"
2-6	diorite and tonalite	"
-1	rhyolite/rhyodacite	"
7.1	granite	Ivensen et al., 1974
5	alaskite	"
3.1-3.6	granodiorite	"
1.5	aplite	"
3.5-6.2	granitic intrusives	Zvereva and Gavrilenko, 1977
2.8	granite	Jones, 1969
3.5	diorite	"
12	rhyolite	"
2.4-4	diorite	Davletov and Dzhakshibayev, 1970
1.1-7.1	hornblende-biotite granite	"
2.8-3.3	leucocratic granite	"
11.4	granite	Boyle, 1979
7.5	granodiorite	"
3.7	rhyolite	"
2.8	granites and silicic volcanics	Shcherbakov and Perezhogin, 1963
3.5	diorite	"
1.9	quartz diorite	Stephenson and Ehmann, 1971
0.3	quartz monzonite	"
6.1	feldspar porphyry dyke	"
1.05-1.47	felsic intrusives	Kwong and Crockett, 1978

TABLE XXVc Background Gold Abundances in Metamorphic Rocks

<u>Mean Au (ppb)</u>	<u>Rock Type</u>	<u>Reference</u>
31.7	quartzites	Boyle, 1979
2.2	slates	"
3.1	gneiss	"
7.1	amphibolites	"
18.6	schists	"
3.8	chloritized-epidotized tuffs	"
10.9	all metamorphic rocks	"
0.5-200	sulphide-bearing quartzite	Gavrilentz et al., 1976
-0.5	biotite gneiss	"
0.5-3.2	garnet-sillimanite- biotite gneiss	"
0.5-16	aluminous gneiss with sulphide	"
0.6	paragneiss	Stephenson and Ehman, 1971
0.3	metavolcanics	"
2.1-3.9	amphibolite schists	Pchelintseva and Pel'dman, 1973
0.8-4.9	metabasic rocks	"
8.3	argillite	Jones, 1969
1.2	phyllite	"
5.0	schist	"
1.8	gneiss	"
5	metasediments	Glasson and Keays, 1978
14.5	black and grey (pyritic) slates	"
22.4	pyritic black slates	"

inclusion of poorer quality earlier data), but the schists in the ore deposit region have anomalously higher Au contents.

As for the mafic rocks, the basic dyke and gabbro (excluding samples from south of Windowglass Hill) have the same low Au contents reported for mafic rocks by other authors. Amphibolites from the Port aux Basques Complex have an anomalously high mean due to the influence of a single sample. The other samples have typical metabasic rock values. The Long Range Mafic/Ultramafic Complex samples have slightly higher Au contents, but there is a wide variation of quoted abundances in ultramafic rocks (eg. Saager *et al.*, 1982). The diorite, and to a lesser extent, the gabbro from the contact region south of the Windowglass Hill Granite have anomalously high values when compared to their respective rock types from elsewhere.

In terms of felsic/granitic rocks, the Windsor Point Group ignimbrites, and the Port aux Basques, Isle aux Morts Brook, Red Rocks and tonalitic Cape Ray Granites have normal Au concentrations (if somewhat higher than those of Tilling *et al.*, 1973; and Kwong and Crockett, 1978). The megacrystic Cape Ray (due to anomalous values in the feldspar megacryst splits), Strawberry and Windowglass Hill Granites have enriched Au contents. The mafic and sulphide-poor nature of this latter granite is, again, particularly unexpected.

Gottfried et al. (1972), Tilling et al. (1973) and Kwong and Crockett (1978) state that normal Au abundances in fresh rocks are less than 10 ppb except in those rocks which have undergone alteration and secondary introduction or remobilization due to fluid interactions. All lithologic units in this map area are altered and deformed, sometimes to a great degree, except for the post-tectonic granites and portions of the Little Barachois Formation (these units also have the lowest general Au abundances). The slightly elevated background contents in the schists etc. are therefore most likely attributable to secondary hydrothermal influences.

Truly anomalous Au values (ie. > 50 ppb) were found in only the granitic wall rocks to ore veins, but not in the Main Shear Showing wall rocks. Stephenson and Ehmann (1971) report a sample of diabase wall rock to Au-bearing quartz veins with 325 ppb Au (the normal diabase contains Au contents as low as 0.5 ppb). Kwong and Crockett (1978) found that one sample of basalt selvage to a quartz vein with 8 ppm Au, contained >2 ppm Au, yet the remainder of the basalt contained < 10 ppb Au. The lack of distinctive Au haloes around Au-bearing quartz veins is therefore a typical feature of such deposits.

As a very general conclusion it appears that the greatest degree of background Au enrichment (which itself is rather small) in the various rock types, occurs within

the vicinity of the Windowglass Hill Granite (except in the unusual megacryst contents). This granite has quite unusual background gold values and has undergone distinctive sodic metasomatism. All attempts to link the more enriched Au concentrations in this granite with degree of alteration, as shown in Figure 69a, have been unsuccessful. Similarly the LREE-depletions in the granitic wall rocks to ore veins (and to a lesser extent elsewhere in the granite; *ie.* indicative of the hydrothermal alteration experienced by the granite), can not be linked directly to the background Au contents (see Figure 69b where  $La/Y$ , an indication of LREE/HREE fractionations, is plotted *vs.* Au). The Au distribution in the granite is also independent of S (or sulphide phase) content (Figure 69c). Since the Au can't reside in a mafic or sulphide phase (because there are none), and since the felsic minerals have lower Au abundances, the Au in the granite probably exists as intergranular particulate material (as suggested by Saager *et al.* (1982) for Au in greenstones, or by Keays and Scott (1976) for Au in pillow basalts).

In order to define the location of Au and Ag in the Windowglass Hill Granite, R-mode factor analysis was performed on non-wall rock samples of this granite. When all elements are compared seven factors account for 90% of the variance. These factors (listed in Table XXVI)

Figure 69a Plot of Au vs. Na2O in the Windowglass Hill Granite.

Figure 69b Plot of La/Y vs. Au in the Windowglass Hill Granite.

Figure 69c Plot of Au vs. S in the Windowglass Hill Granite. Note the lack of correlation between Au and the other elements in all of these figures.



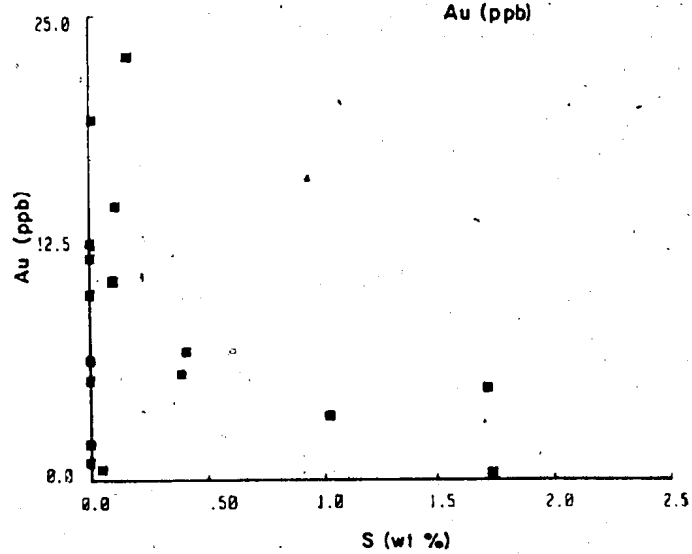
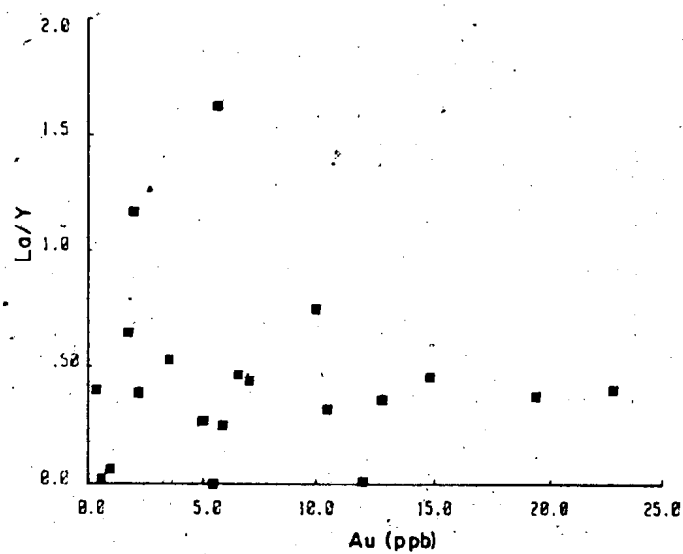
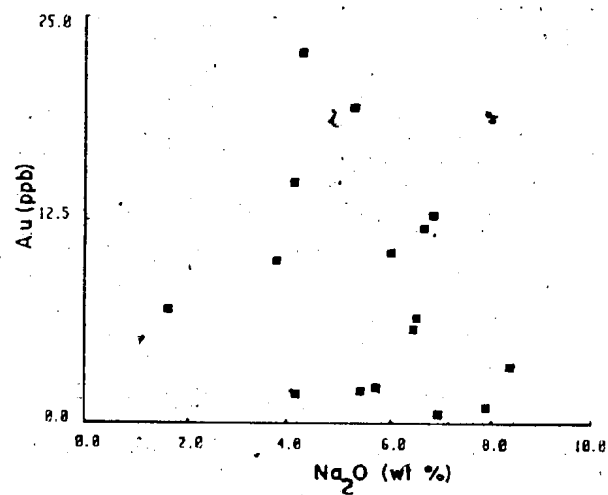


TABLE XXVI VARIMAX ROTATED FACTOR MATRIX FOR SAMPLES FROM THE WINDOWGLASS HILL GRANITE

	FACTOR 1	FACTOR 2	FACTOR 3	FACTOR 4	FACTOR 5	FACTOR 6	FACTOR 7
SiO <sub>2</sub>	-0.89135	0.13005	-0.14273	-0.09107	-0.05399	-0.12599	0.33552
TiO <sub>2</sub>	0.64774	0.47807	0.20682	-0.18707	0.11395	-0.06053	-0.33174
Al <sub>2</sub> O <sub>3</sub>	0.80898	-0.19408	0.02498	-0.00152	0.12379	0.05851	-0.46191
Fe <sub>2</sub> O <sub>3</sub>	0.45505	0.40209	0.41145	0.31052	-0.03373	-0.07992	0.34385
MnO	0.59647	0.19894	-0.19494	0.46185	-0.04496	0.36698	-0.13117
MgO	0.91594	0.03616	-0.09462	0.22881	0.09524	-0.11874	0.08511
CaO	0.83690	-0.05957	-0.25265	-0.03517	0.02626	0.03465	0.19883
Na <sub>2</sub> O	0.13039	-0.66781	0.22549	-0.54350	-0.22041	-0.01218	-0.37156
K <sub>2</sub> O	-0.01239	0.89272	-0.16434	0.32049	0.10532	0.05601	0.08080
P <sub>2</sub> O <sub>5</sub>	0.25863	0.16638	-0.23940	0.02227	-0.19547	-0.13673	-0.62591
LOI	0.52165	0.13678	-0.00608	0.64261	0.20654	0.33012	0.20218
Pb	-0.04580	0.12203	0.14318	0.91965	-0.01807	-0.04429	-0.03681
Th	-0.77484	0.28795	0.28721	0.13868	0.05489	0.06751	0.28038
U	-0.036450	0.31595	0.18720	0.15267	0.03952	0.64498	0.27931
Rb	-0.03868	0.93523	-0.14001	0.24279	0.13274	0.01125	-0.13977
Sr	0.85621	-0.32526	-0.09255	-0.16224	-0.00956	-0.20182	0.19110
Y	-0.64908	0.54287	-0.03183	-0.02394	-0.18811	0.38296	0.22731
Zr	-0.81743	-0.15209	-0.00487	-0.01233	-0.04872	0.28743	-0.03331
Nb	-0.90928	0.21279	-0.02143	-0.10365	-0.10372	0.08139	0.12679
Zn	-0.00174	0.11674	-0.00665	0.85326	0.32975	0.17444	-0.04108
Cu	0.28666	-0.23605	0.20735	0.30411	0.72767	0.16642	0.11473
Ni	-0.34645	0.66940	-0.15154	0.19606	-0.58327	-0.01414	0.09668
La	-0.25392	0.88349	0.09195	-0.05072	-0.09553	0.18694	0.04347
Ba	0.268628	0.49288	-0.22712	0.28691	0.63350	0.31314	0.07826
V	0.94741	-0.24128	-0.04976	-0.05306	-0.04598	-0.06549	-0.07091
Ce	-0.19616	0.83886	0.14142	-0.09979	-0.14365	0.14212	-0.02713
Cr	-0.01002	-0.20211	0.64246	-0.23529	0.19488	-0.32480	0.12105
Ga	-0.30468	0.15665	0.36670	0.39166	0.57186	-0.09756	0.17776
As	-0.20168	0.03504	0.82128	0.11834	0.01505	-0.13614	-0.21861
S	0.03306	-0.05651	0.87190	0.29086	0.12035	0.05796	0.09292
Au	-0.23552	0.14963	-0.25050	0.10514	0.26077	0.57862	-0.02517
Ag	-0.09827	-0.00393	0.85420	-0.15715	-0.04849	0.13548	0.19200

indicate normal relations between elements (ie. felsic vs. mafic type etc.). Factor 3 (F3) is a sulphide factor and is heavily loaded on Cr (mica ?), As, S and Ag with minor Fe and Ga contributions. Au only becomes significant in factor 6 which has heavy U and Au loadings with lesser MnO, LOI., Y and Ba, and negative Cr loadings. It's difficult to envisage what this factor actually represents, however since U and Ba are associated with carbonate solutions, and the presence of LOI. in the factor, may indicate a hydrothermal/carbonate association. Graphs of these factors (Figure 70) show that all the elements have a broad dispersion and correlations are random.

When only the trace elements are compared, seven factors account for 92% of the variance (Table XXVII). F3 is also a sulphide-Ag factor and Au is significant in only F6, where it is, again, the major component with lesser U and minor Ba and negative Cr.

Elevated Au contents in granitoids containing gold-bearing quartz vein occurrences have been described elsewhere by Mantei and Brownlow (1967); Wolfe (1976); Kwong and Crockett (1978); and Churchill et al. (1980). Actual haloes of enriched Au contents in country rocks surrounding such granitoids have not been widely described but are mentioned by Shcherbakov and Perezhugin (1963); Mantei and Brownlow (1967- whose data was re-checked by Tilling et al., 1973); Elliot and Wells (1968); and

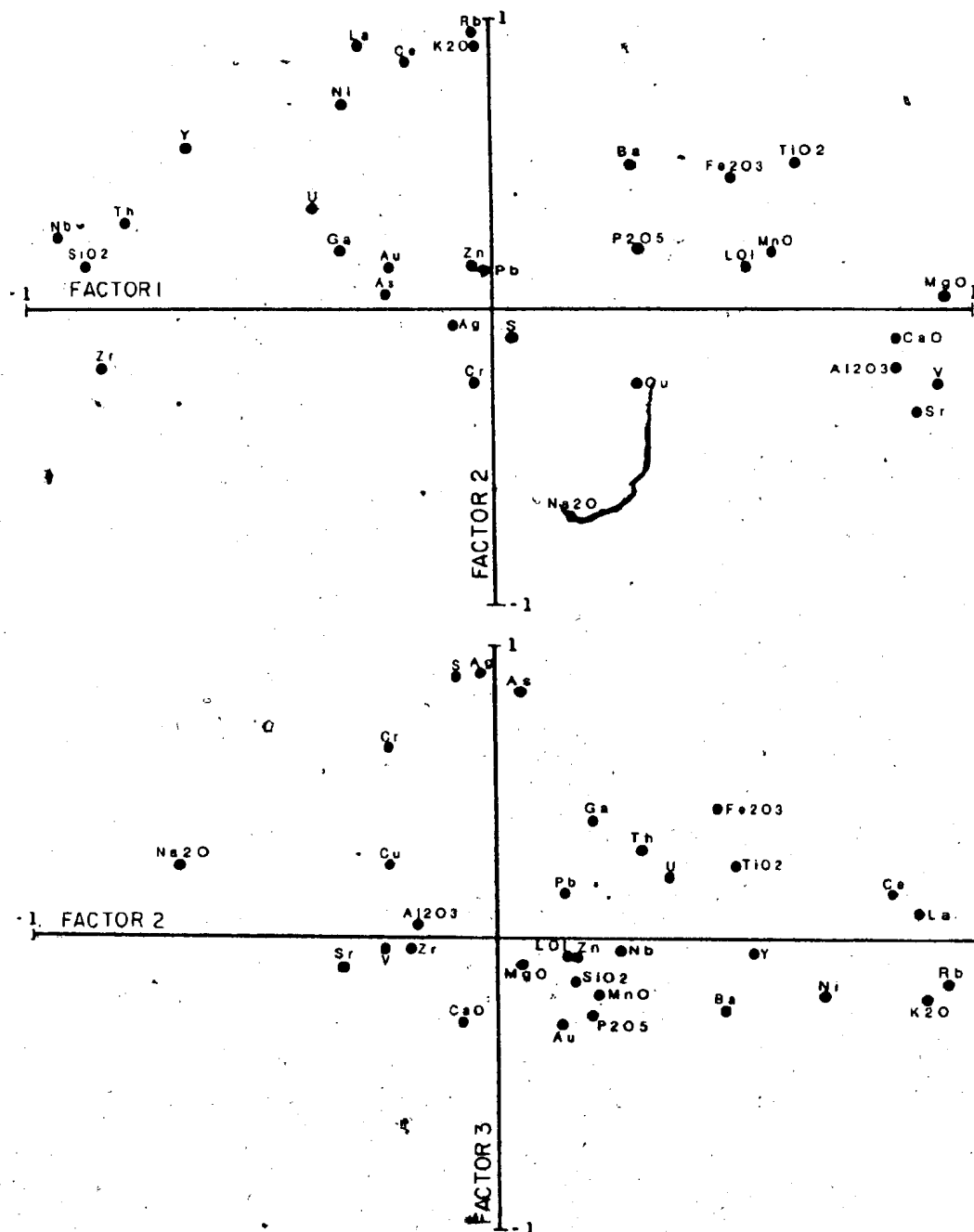


Figure 70 Plot of Varimax rotated factors in the Windowglass Hill Granite. The widespread nature of these distributions indicates a fundamental lack of correlation between the elements.

TABLE XXVII VARIMAX ROTATED FACTOR MATRIX FOR TRACE ELEMENTS IN THE WINDOWGLASS HILL GRANITE

	FACTOR 1	FACTOR 2	FACTOR 3	FACTOR 4	FACTOR 5	FACTOR 6	FACTOR 7
Pb	0.07715	0.08990	0.11023	0.08209	<u>0.94200</u>	-0.05322	0.00321
Th	<u>0.76466</u>	0.25911	0.29132	0.03259	0.15361	0.10603	0.02460
U	0.46139	0.27120	0.21301	0.07562	0.14874	<u>0.56606</u>	<u>0.37156</u>
Rb	0.04631	<u>0.85993</u>	-0.18063	0.18051	0.28067	0.13290	-0.13695
Sr	-0.83847	-0.30335	-0.07226	0.01498	-0.15228	-0.19220	0.15678
Y	<u>0.72286</u>	0.56988	-0.03688	-0.06951	-0.04496	0.21847	<u>0.27982</u>
Zr	<u>0.84625</u>	-0.12957	-0.00780	-0.08316	0.00217	0.07270	0.12238
Nb	<u>0.94646</u>	0.19503	-0.01332	-0.11987	-0.09861	0.02480	0.00695
Zn	0.03374	0.03911	-0.01385	0.40017	<u>0.81993</u>	0.24288	-0.02087
Cu	-0.26165	-0.30002	0.20977	<u>0.75038</u>	0.19900	0.18136	0.01530
Ni	0.35577	<u>0.73237</u>	-0.18612	-0.42854	0.24823	-0.11544	0.18582
La	0.30593	<u>0.91701</u>	0.05080	0.07150	-0.05757	0.05376	0.12357
Ba	-0.20136	0.38956	-0.23922	<u>0.72292</u>	0.21827	0.38716	0.07895
V	<u>-0.94049</u>	-0.22599	-0.04391	-0.04573	-0.04185	-0.02148	0.06736
Ce	0.20626	<u>0.86381</u>	0.11355	-0.08103	-0.06167	0.12323	-0.05464
Cr	0.01142	-0.18507	<u>0.63576</u>	0.18755	-0.23732	-0.36635	-0.12595
Ga	0.37501	0.08576	0.35696	<u>0.72623</u>	0.32579	-0.15155	-0.03916
As	0.14311	0.04273	<u>0.87118</u>	-0.12314	0.20672	0.02252	-0.39465
S	-0.03265	-0.03558	<u>0.84183</u>	0.20993	0.24010	0.00670	0.06709
Au	0.25468	0.09372	-0.20292	0.19720	0.02725	<u>0.77492</u>	-0.07576
Ag	0.14768	0.03862	<u>0.87872</u>	0.00444	-0.14195	-0.04295	<u>0.32196</u>

Davletov and Dzhakshibayev (1970). The origin of hydrothermal fluids responsible for these enrichments is discussed below.

#### 7.4.6.2 Ag abundances

Ag has much higher crustal abundances than Au, Table XXVIII (after compilations of Boyle, 1968, 1979) shows most rock types have > 50 ppb background Ag, and metamorphosed rocks have > 150 ppb Ag. Boyle (1968) reports Ag contents of 300-1700 ppb in hornblende; 100 to 1000 ppb in biotite; 200-5000 ppb in garnet; trace to 6000 ppm in chlorite (common metamorphic minerals in the fault zone). Dostal et al. (1979) found that Ag abundances in fresh alkalic basalts ranged from < 20 (the detection limit) to 140 ppb, while rhyolitic rocks contained higher average abundances of 24-148 ppb (with biotite separates containing 259-770 ppb Ag). Keays and Scott (1976) showed that Ag distributions were similar to those of Au, in that they were higher in sulphide/refractory oxide/silicates, and were remobilized and concentrated during alteration.

<u>Rock Type</u>	<u>Mean Silver Content (after Boyle, 1968, 1979)</u>
Ultramafics	80 ppb
Gabbro	140 ppb
Basalt	110 ppb
Granodiorite	50 ppb
Andesite	80 ppb
Granite	50 ppb
Rhyolite	50 ppb
All Igneous Rocks	70 ppb
Slate	200 ppb
Amphibolite	250 ppb
Schist	200 ppb
All Metamorphic Rocks	150 ppb

TABLE XXVIII Background Silver Contents in Common Terrestrial Rocks

All the mafic volcanic units have similar Ag contents to those reported by Boyle (1968, 1979) in equivalent rocks, except that the ophiolite fragments are somewhat depleted. Similarly, the Ag values for most schist samples are normal. The gneiss samples have a high mean value influenced by a single sample with extremely high concentration (the maxima is inexplicable except as a result of disseminated sulphide). The Strawberry and Red Rocks Granites have anomalously high means biased by single samples, but both granites are sulphide-bearing (ie. Ag with a sulphide phase).

The only definitively elevated Ag concentrations occur

in the Windowglass Hill Granite wall rock samples (ie. WGH SH2B and WGH SH3), the wall rocks to the Main Shear mineralization, and the feldspar porphyry dykes with associated galena mineralization. Though the number of very anomalous Ag samples is low, it is still greater than the number of anomalous Au samples, and therefore Ag is a better ore indicator (or 'pathfinder element'). The Ag concentrations, however, do not have an enriched halo surrounding the Windowglass Hill Granite (like that of Au), even though this granite has a somewhat higher than normal background Ag content.

#### 7.5 Ore Petrography and Microprobe Analyses

The mineralogy of the two vein showings is fairly simple, consisting of varying amounts of galena, sphalerite, chalcopryite and pyrite with associated electrum. Pyrrhotite occurs as minute inclusions within the larger sulphide grains and arsenopyrite is found only in the more gold/silver-rich portions of the Main Shear horizon. The primary Fe-oxide is magnetite, which is found predominantly in wall rock fragments rather than in the veins sensu stricto. Supergene oxidation has produced hematite from pyrite and magnetite, and covellite (+ cuprite) from chalcopryite.

All sulphides are complexly intergrown, with any one



occurring as inclusions within another, but pyrite and arsenopyrite have the only euhedral forms. Sphalerite contains varying amounts and sizes of chalcopyrite inclusions throughout. The paragenetic sequence indicates pyrite/arsenopyrite formed first, followed by the simultaneous deposition of the other sulphides.

Each of the sulphides is disseminated in wall rock selvages and fragments from the main quartz vein, and there are abundant minute veins dispersed into such zones. The intense deformation has also recrystallized the more ductile galena and chalcopyrite, shattered pyrite and arsenopyrite, and remobilized sphalerite.

#### 7.5.1 Pyrite

Pyrite in some schists has been extensively flattened and elongated (length/width ratios vary from 4:1 to almost 1:1) by superimposed deformation (Plate 7-2A). According to Graf et al. (1981), the activation temperature for the deformation must be  $> 200^{\circ}\text{C}$  but  $< 400^{\circ}\text{C}$  to produce such plastic deformation of pyrite (this is also the general temperature conditions ascertained from metamorphic mineral assemblages).

Microprobe analyses for various pyrites are listed in Table XXIX. The pyrites are  $\text{FeS}_2$  with only minor (statistically insignificant) amounts of Cu, Zn or As.

TABLE XXIX

PYRITE COMPOSITIONS ( wt % and atomic proportions)

<u>ANALYSIS</u> <u>SAMPLE</u>	<u>1</u> 80-61K	<u>2</u> 80-61K(B)	<u>3</u> WGH SH3B	<u>4</u> PB28-5D
S	52.34	52.71	53.49	51.66
Fe	47.50	47.07	47.47	46.71
Cu	<u>0.08</u>	<u>--</u>	<u>0.07</u>	<u>0.04</u>
Total	99.92	99.78	101.03	98.41
S	1.969	1.980	1.984	1.973
Fe	1.027	1.016	1.012	1.023
Cu	<u>--</u>	<u>--</u>	<u>--</u>	<u>--</u>
Total	2.996	2.996	2.996	2.996

substituting for Fe. The rare pyrrhotite inclusions indicate that during the waning stages of pyrite crystallization, local zones deficient in S, produced iron sulphide without the pyrite stoichiometry.

#### 7.5.2 Chalcopyrite

Chalcopyrite behaves ductilely in comparison to pyrite during deformation and is remobilized into shear/fractures, or is totally recrystallized and intergrown with galena (Plate 7-2B). Secondary oxidation has produced intergrowths of hematite and covellite after chalcopyrite.

Microprobe analyses of six chalcopyrite grains are presented in Table XXX. The compositions are  $\text{CuFeS}_2$  with only minor amounts of other cations, the most noticeable is 0.11 wt % Zn in chalcopyrite from sample PB41-2B.

#### 7.5.3 Sphalerite

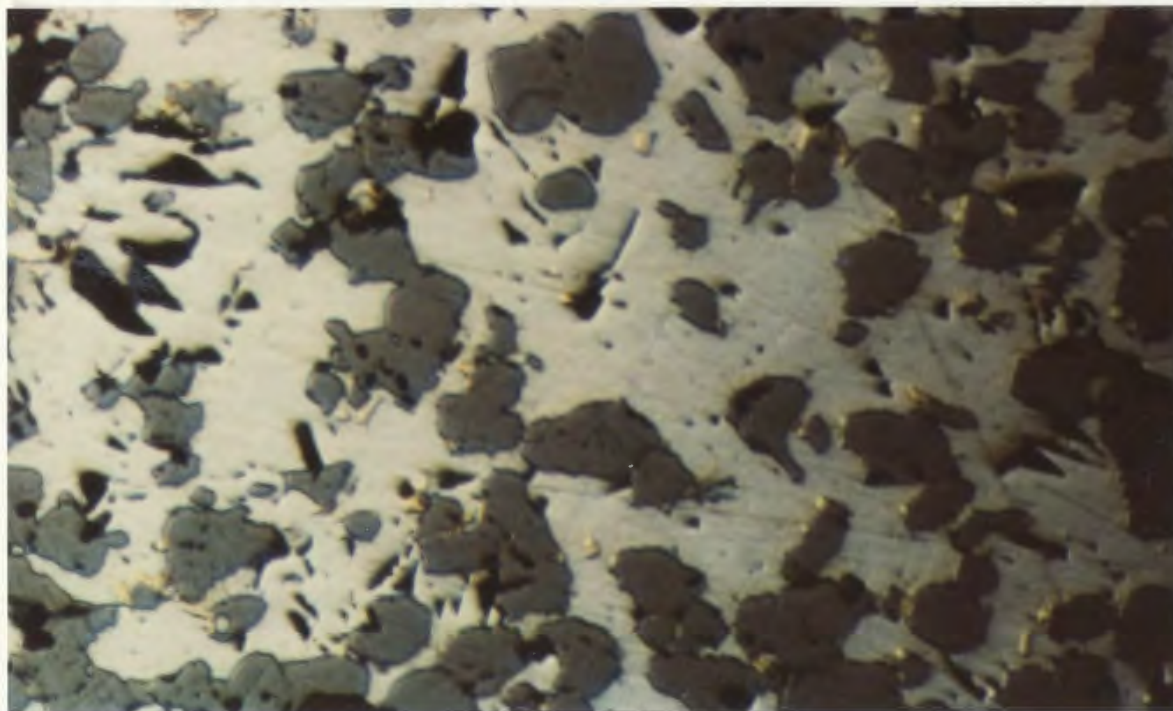
Sphalerite occurs in those Main Shear veins which also contain massive galena and chalcopyrite; it is rare as a solitary sulphide but is usually intergrown the other sulphides. Sphalerite is found in the Windowglass Hill Granite veins, but is much less abundant. Sphalerite grains are totally anhedral masses, up to 10x5 mm. The larger grains form boxwork intergrowths with galena and/or

PLATE 7-2 A) Elongate pyrite grain in country rock to Main Shear Showing. The pyrite was flattened during the D1 deformation and thus is pre-deformation. This section is about 0.8 mm across.

B) Intergrown galena (light grey), quartz (dark grey) and chalcopyrite (yellow). This rock has been deformed and is consequently totally recrystallized. The chalcopyrite occurs as isolated blebs scattered through the galena. This section is 0.08 mm across.



A



B

TABLE XXX

CHALCOPYRITE COMPOSITIONS (wt % and atomic proportions)

<u>ANALYSIS</u> <u>SAMPLE</u>	<u>1</u> <u>80-61K(B)</u>	<u>2</u> <u>PB41-2B</u>	<u>3</u> <u>PB41-2B</u>	<u>4</u> <u>PB41-2B</u>	<u>5</u> <u>80-61K(B)</u>
S	34.85	35.58	34.45	34.10	34.38
Fe	31.13	31.44	30.85	30.86	31.43
Cu	33.99	33.86	34.38	33.59	34.31
Zn	--	0.11	0.11	0.05	--
Total	<u>99.97</u>	<u>100.99</u>	<u>99.89</u>	<u>98.70</u>	<u>100.12</u>
S	1.496	1.512	1.488	1.488	1.476
Fe	0.766	0.762	0.735	0.774	0.774
Cu	<u>0.734</u>	<u>0.726</u>	<u>0.750</u>	<u>0.738</u>	<u>0.744</u>
Total	2.996	3.000	2.973	3.000	2.994

chalcopyrite (Plate 7-3A). Sphalerite grains within the granite-hosted veins are generally  $\leq 0.01$  mm in diameter, with the largest about  $1 \times 0.25$  mm.

The most consistent feature in the sphalerite is the presence of chalcopyrite inclusions. These round inclusions are usually  $\leq 0.002$  mm in diameter (Plate 7-3B) and only rarely have a crystallographic orientation (i.e. non-coherent exsolution). The chalcopyrite inclusions are scattered throughout smaller sphalerite grains, but in the larger sphalerite grains, the cores are inclusion-free and inclusions are concentrated along the rims. Similar textures are reported by Figueiredo *et al.* (1980). These inclusions were exsolved from the sphalerite host and therefore represent unmixing products from a higher temperature solid solution of chalcopyrite and sphalerite.

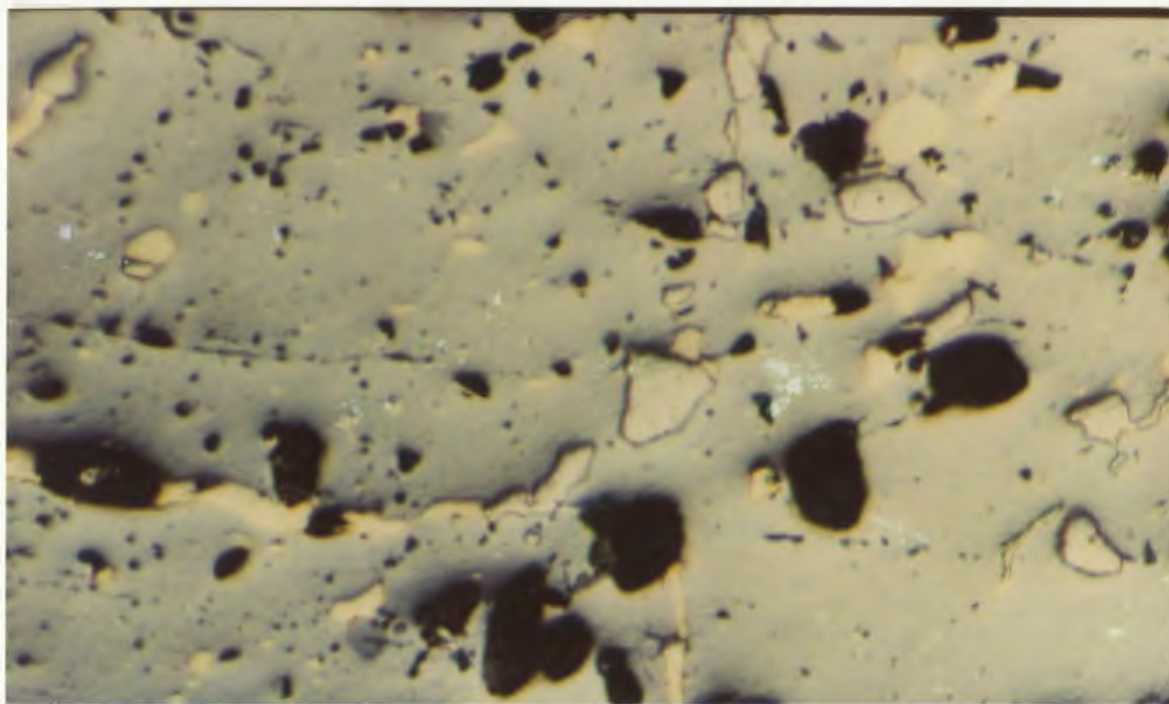
The chemical compositions of a series of sphalerite grains (from microprobe analyses) are presented in Table XXXI. One sphalerite grain was analysed as having 0.11 wt % Au.

The mole % of FeS in sphalerite is buffered by equilibrium assemblages of pyrite and pyrrhotite over wide temperature ranges but is strongly dependent on pressure, as a result, geobarometers have been developed using sphalerite (cf. Scott and Barnes, 1971; Scott, 1973). According to Wiggins and Craig (1980), and Hutchison and Scott (1981), the presence of significant chalcopyrite has

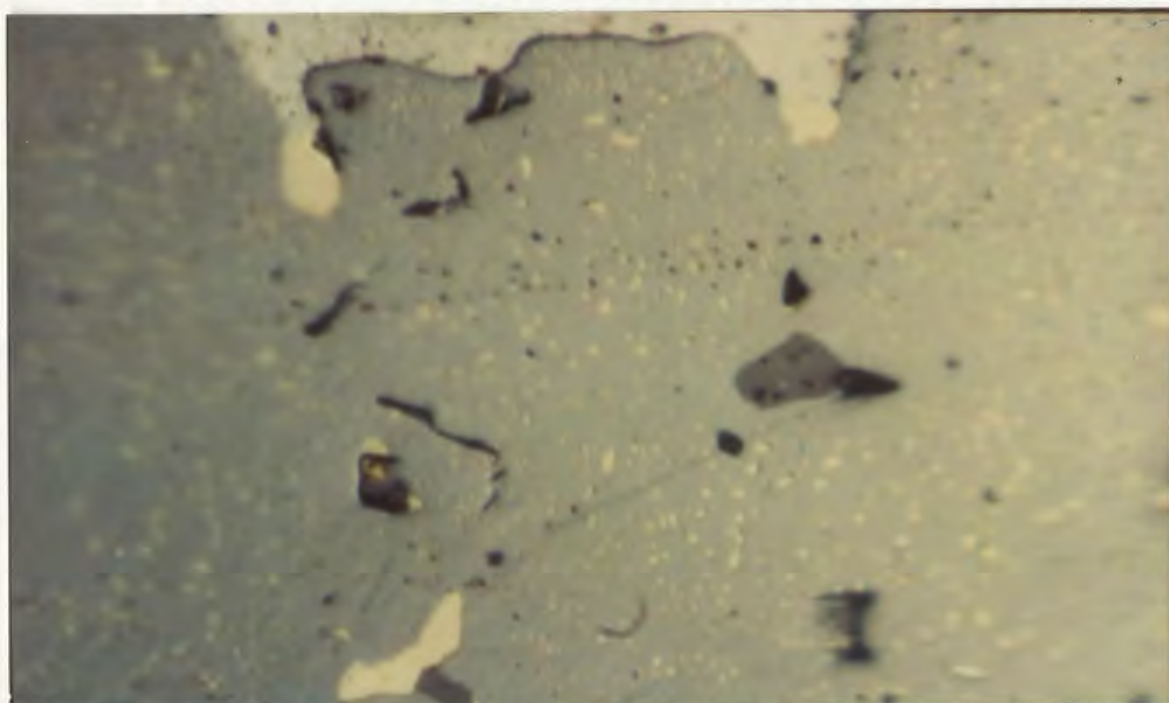
PLATE 7-3 A) Massive sphalerite (light grey) with galena (white grey) and chalcopyrite (yellow) inclusions and fracture-fillings. This section is 0.08 mm across.

B) Sphalerite (grey) with non-coherent chalcopyrite (yellow) exsolution blebs). Galena (white-grey) occurs along the upper portion of the plate and larger chalcopyrite grains occur at this interface. This section is 0.08 mm across.





A



B

TABLE XXXI

ZEPHALERITE COMPOSITIONS (wt % and atomic proportions)

ANALYSIS SAMPLE	1 PB38-42B	2 PB38-42B	3 PB38-35B	4 PB27-25D	5 PB27-25D	6 PB27-25D	7 PB41-6D	8 PB41-6D
S	31.76	31.32	32.34	33.76	32.39	31.80	33.30	32.32
Fe	7.80	7.59	3.38	6.00	5.04	5.56	5.80	6.01
Cu	0.07	--	0.95	0.10	0.96	--	0.53	0.03
Zn	59.23	58.62	63.29	60.98	60.67	60.73	59.85	60.81
Cd	<u>0.36</u>	<u>0.70</u>	<u>0.62</u>	<u>0.09</u>	<u>0.46</u>	<u>0.57</u>	<u>0.61</u>	<u>0.65</u>
Total	<u>99.22</u>	<u>98.23</u>	<u>100.58</u>	<u>100.93</u>	<u>99.53</u>	<u>98.67</u>	<u>100.09</u>	<u>99.83</u>
S	0.968	0.968	0.980	1.006	0.987	0.980	1.000	0.980
Fe	0.140	0.132	0.060	0.101	0.089	0.099	0.102	0.105
Cu	--	--	0.015	0.003	0.015	--	0.008	--
Zn	0.890	0.890	0.940	0.891	0.906	0.917	0.883	0.906
Cd	--	<u>0.008</u>	<u>0.005</u>	--	<u>0.005</u>	<u>0.005</u>	<u>0.004</u>	<u>0.004</u>
Total	1.998	1.998	2.000	2.001	2.002	2.001	1.996	1.996
ANALYSIS SAMPLE	9 PB41-6D	10 PB41-6D	11 79-74					
S	31.25	31.94	32.44					
Fe	0.33	6.21	2.82					
Cu	0.05	1.61	0.43					
Zn	66.93	61.75	63.94					
Cd	<u>0.96</u>	<u>0.48</u>	<u>0.71</u>					
Total	<u>99.51</u>	<u>101.99</u>	<u>100.34</u>					
S	0.969	0.957	0.957					
Fe	0.004	0.105	0.047					
Cu	--	0.023	0.062					
Zn	1.016	0.906	0.925					
Cd	<u>0.008</u>	<u>0.004</u>	<u>0.006</u>					
Total	1.996	1.996	1.997					

no effect on the FeS-ZnS system, though the former authors developed a CuS-dependant geothermometer for sphalerite.

However, the geothermometer of Wiggins and Craig (1980) and the geobarometer/geothermometer from Hutchison and Scott (1981) have proved unusable in the Cape Ray sphalerites, because they were derived for sphalerites formed above 500° C. The one point these unusable thermometers do indicate, though, is that the sphalerites in question formed < 450° C.

#### 7.5.4 Galena

Galena has the best equilibrium intergrowths with the quartz gangue of any of the sulphides, and sometimes single euhedral hexagonal quartz crystals occur within galena grains (Plate 7-4A).

As previously stated, galena behaved more ductilely during deformation than any of the other sulphides. On unetched surfaces, the galena in these deformed areas has become massive and amorphous with no visible shears, fractures, or kink-type folds (*ie.* no preferred orientations). According to Stanton and Wiley (1972), unfoliated deformed galena probably occurs when the sulphide has been subjected to temperatures of 300° C, or greater, (*ie.* the greenschist facies) for sustained periods.

Microprobe analyses for nineteen galena grains are listed in Table XXXII. The most consistent trace metal in the galena is Bi which reaches up to 0.93 wt%. Ag is occasionally present in trace amounts. Samples 79-16, from the quartz/feldspar porphyry dyke near Red Rocks Point, and 79-56A, from the mylonite outcrop on the Trans-Canada Highway, have trace amounts of Au in single galena patches, and 0.17 wt % Au occurs in a galena grain from the Windowglass Hill Granite veins (sample WGH SH2A(B)).

#### 7.5.5 Arsenopyrite

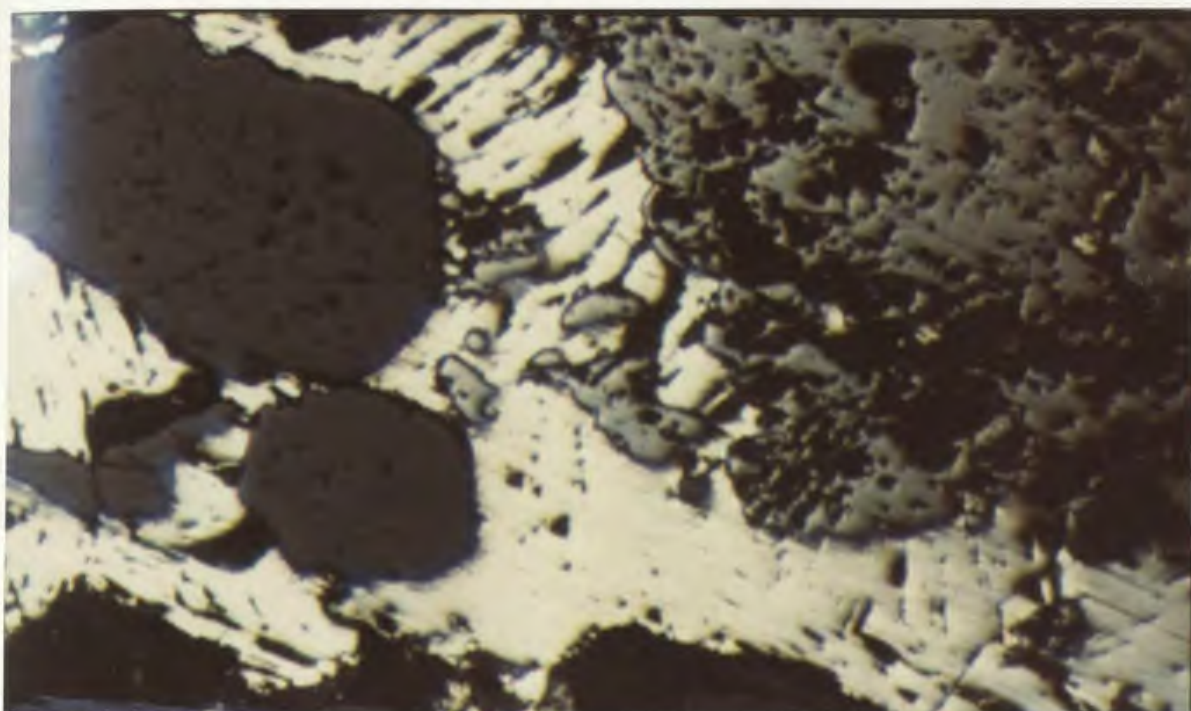
Arsenopyrite was found in only a few samples from the Main Shear horizon, and never in the Windowglass Hill Granite. It occurs as euhedral diamond-shaped grains, up to  $3 \times 0.5$  mm, or in massive layers up to 10 mm thick (Plate 7-4B).

Microprobe analyses of arsenopyrite grains (Table XXXIII) indicate a stoichiometric composition of  $(\text{Fe}, \text{As})_{0.9}\text{S}_{1.1}$  for this sulphide. Since arsenopyrite of this composition is in equilibrium with pyrite, but not with pyrrhotite, its temperature of formation, can be determined using the detailed map of the Fe-As-S system (Figure 71) from Kretschmar and Scott (1976).  $(\text{Fe}, \text{As})_{0.9}\text{S}_{1.1}$  would only be in equilibrium with both pyrite and pyrrhotite at temperatures less than or equal to  $300^\circ \text{C}$ .

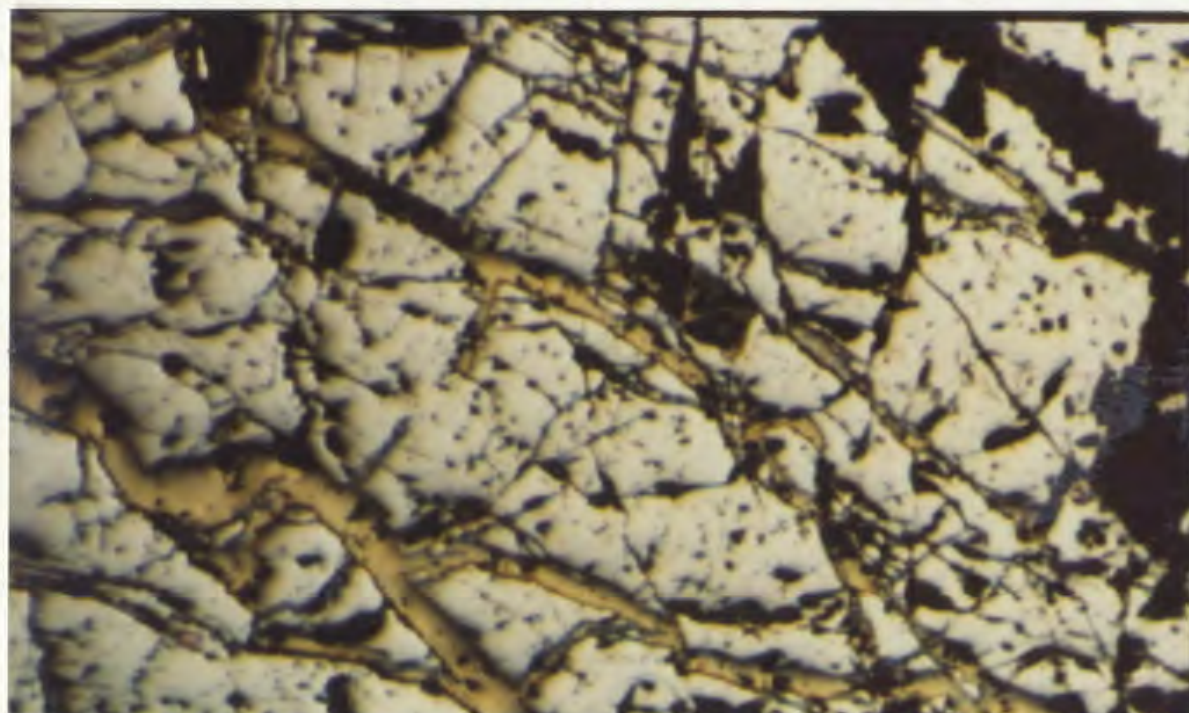
PLATE 7-4 A) Galena (white) intergrown with quartz gangue (black) and sphalerite (dark grey - to the right). The quartz gangue contains euhedral hexagonal crystal forms. This section is 0.08 mm across.

B) Massive arsenopyrite cut by chalcopyrite (yellow) fracture-fillings. This section is 0.4 mm across.





A



B

TABLE XXXII GALENA COMPOSITIONS (wt % and atomic proportions)

ANALYSIS SAMPLE	<sup>1</sup> 80-61K(B)	<sup>2</sup> 80-61K(B)	<sup>3</sup> 80-61K(B)	<sup>4</sup> PB41-2B	<sup>5</sup> PB41-2B	<sup>6</sup> PB38-42B	<sup>7</sup> PB38-42B	<sup>8</sup> WGH SH2A(B)
S	14.83	13.97	15.07	13.54	14.08	13.95	14.25	13.94
Pb	83.79	87.24	85.05	84.53	83.43	86.96	85.80	87.02
Bi	0.13	0.01	0.20	0.58	0.68	0.39	0.14	--
Ag	--	--	--	0.18	0.29	--	--	0.03
Au	--	--	0.09	0.01	0.01	0.14	0.04	0.04
Total	98.75	101.22	100.41	98.84	98.49	101.44	100.23	101.03
S	0.531	0.508	0.531	0.506	0.518	0.508	0.516	0.508
Pb	0.465	0.492	0.465	0.489	0.475	0.488	0.480	0.490
Bi	--	--	--	0.004	0.004	0.004	--	--
Ag	--	--	--	0.002	0.004	--	--	--
Au	--	--	--	--	--	--	--	--
Total	0.996	1.000	0.996	1.001	1.001	1.000	0.996	0.998

ANALYSIS SAMPLE	<sup>9</sup> PB38-42C	<sup>10</sup> 79-56A	<sup>11</sup> 79-56A	<sup>12</sup> 79-16	<sup>13</sup> 79-16	<sup>14</sup> PB38-35B	<sup>15</sup> PB38-35B	<sup>16</sup> PB38-35B
S	14.69	13.96	14.15	13.70	14.23	15.36	14.66	14.39
Pb	86.52	87.46	86.79	87.11	86.00	85.78	83.70	84.16
Bi	0.26	0.03	0.33	0.23	0.47	NA	NA	NA
Ag	--	--	0.20	0.08	0.16	0.13	0.02	0.04
Au	--	0.14	--	0.11	0.02	0.04	--	0.07
Total	101.47	101.59	101.47	101.23	100.88	101.31	98.38	98.66
S	0.523	0.508	0.512	0.502	0.514	0.535	0.531	0.533
Pb	0.477	0.491	0.485	0.494	0.481	0.461	0.469	0.477
Bi	--	--	0.002	--	0.002	NA	NA	NA
Ag	--	--	0.002	--	0.002	--	--	--
Au	--	--	--	--	--	--	--	--
Total	1.000	0.999	1.001	0.996	0.999	0.996	1.000	1.000

TABLE XXXIII ARSENOPYRITE COMPOSITIONS (wt % and atomic proportions)

ANALYSIS SAMPLE	<sup>1</sup> 80-61K	<sup>2</sup> 80-61K(B)	<sup>3</sup> 80-61K(B)	<sup>4</sup> 80-61K(B)	<sup>5</sup> 80-61K(B)	<sup>6</sup> 80-61K(B)
S	21.44	22.04	20.89	21.91	20.63	21.29
Fe	36.52	36.03	36.08	36.25	35.80	36.23
As	42.16	41.97	43.21	42.57	42.54	42.88
Zn	0.02	0.10	0.09	0.04	0.05	0.14
Total	<u>100.14</u>	<u>100.14</u>	<u>100.27</u>	<u>100.77</u>	<u>99.02</u>	<u>100.54</u>
S	1.063	1.086	1.043	1.079	1.043	1.055
Fe	1.039	1.020	1.031	1.020	1.037	1.032
As	0.895	0.887	0.922	0.897	0.920	0.908
Zn	--	0.004	0.004	--	--	0.006
Total	<u>2.996</u>	<u>2.996</u>	<u>3.000</u>	<u>2.996</u>	<u>3.000</u>	<u>3.001</u>



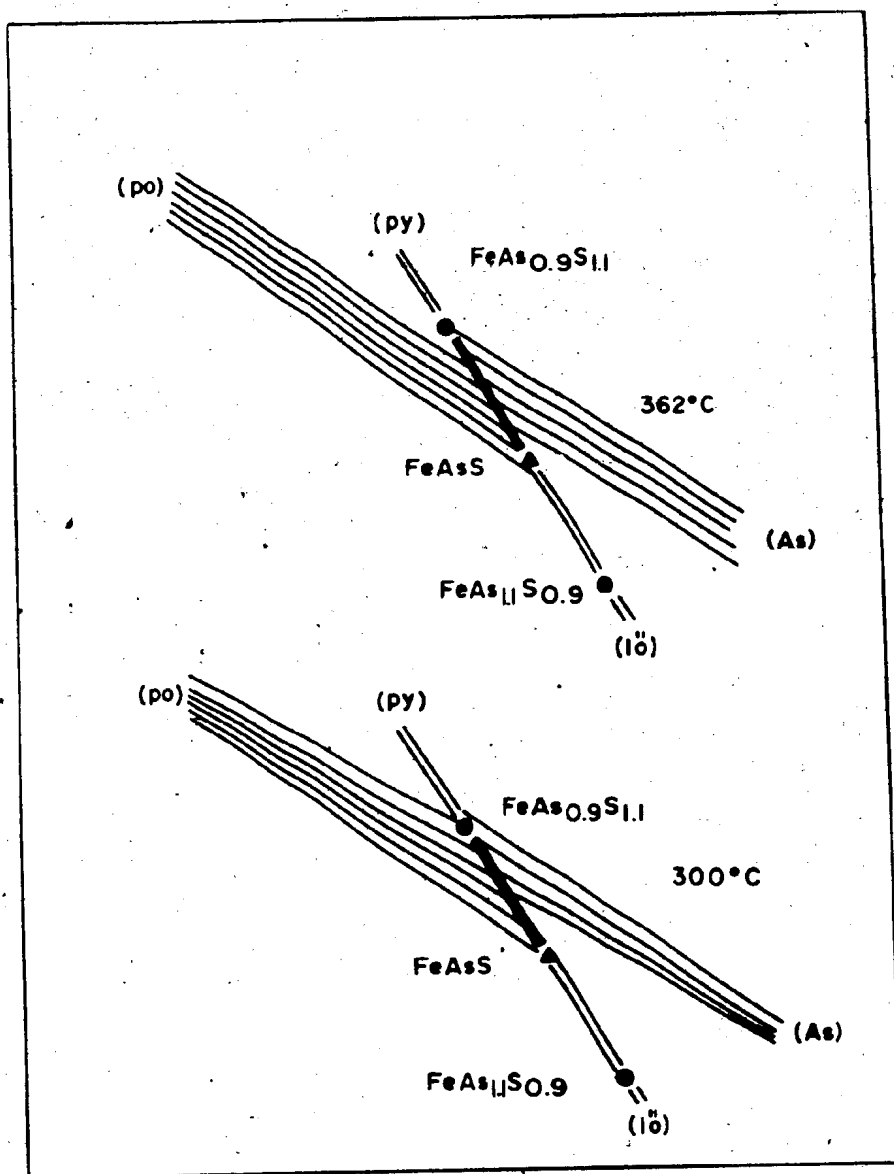


Figure 71 Detailed map of the Fe-As-S system (from Kretschmer and Scott, 1976). There are equilibrium intergrowths of arsenopyrite-pyrite and pyrite-pyrrhotite, but not arsenopyrite-pyrrhotite, in the Main Shear Showing. According to this diagram such intergrowths must form above 300 °C, since arsenopyrite of composition  $(\text{Fe, As})_{0.9}\text{S}_{1.1}$  is in equilibrium with pyrite at this temperature.

Figure 72 (after Kretschmar and Scott, 1976) is a log  $a_{S2}$  vs. temperature diagram for arsenopyrite. According to the analyses in Table XXIII, the atomic % As in the Main Shear arsenopyrites is 29.18 to 30.67 %, which indicate a temperature range of 315 to 352 °C for formation of the arsenopyrite (based on arsenopyrite-pyrite equilibrium). It also indicates a log  $a_{S2}$  of -10 to -8 for the ore-forming system.

#### 7.5.6 Gold/Silver (Electrum)

The chemical compositions of thirteen gold (and silver) grains are listed in Table XXXIV (microprobe analyses). In all cases the grains contained significant silver and thus are actually electrum (*ie.*  $\geq 25$  % Ag, Uytendogaardt and Burke, 1971; or  $\geq 20$  % Ag, Gasparrini, 1983), though the grain in sample PB38-35(B) contained only 15 mole % Ag. The Au/Ag wt % ratios range from 1.01 to 10.53. The mole % Ag ranges from 15 to 64 %, with both extremes occurring in samples from the Main Shear. The granite-hosted vein samples contain Ag > Au (Au/Ag mole % ratios of 0.76, 0.74, 0.72, 0.69 and 0.61), while the Main Shear samples contain Au > Ag (Au/Ag mole % ratios of 5.83, 3.63, 1.98, 1.28, 1.25, 1.23, 0.89 and 0.55). The electrum grains with the highest Au/Ag ratios (from sample 80-65D(H)) are solitary (*ie.* they are not in contact with

Figure 72 Log  $a_{S_2}$  vs. temperature diagram for the Fe-As-S system (after Kretschmer and Scott, 1976). The 30% As tie line is highlighted on this diagram since it represents the composition of arsenopyrites in the Main Shear Showing.

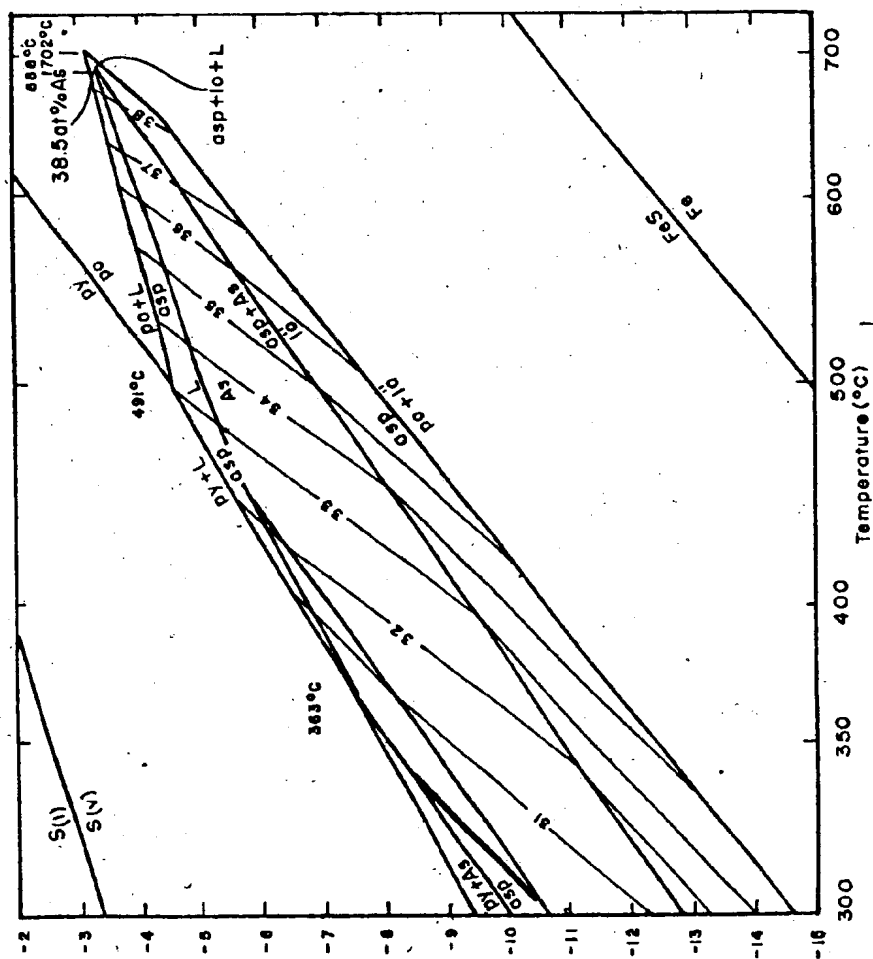


TABLE XXXIV ELECTRUM COMPOSITIONS (wt % and atomic proportions)

ANALYSIS SAMPLE	1 PB41-2B	2 PB41-2B	3 PB41-2B	4 PB41-2B	5 80-65P(B)	6 WGH SHOW	7 WGH SHOW	8 PB38-35B
S	0.08	0.09	0.07	0.01	0.18	0.13	0.14	0.19
Pb	1.22	1.34	1.57	1.17	--	--	0.07	--
Bi	0.23	0.37	0.24	0.13	0.54	0.50	0.23	0.30
Ag	30.55	29.22	29.97	30.46	37.51	41.39	43.82	48.77
Au	71.80	68.12	67.86	69.12	60.92	57.24	54.42	49.04
Total	103.88*	99.14	99.71	100.89	99.14	99.26	98.68	98.03
S	0.004	0.004	0.004	--	0.008	0.006	0.006	0.008
Pb	0.008	0.012	0.012	0.008	--	--	--	--
Bi	--	0.004	--	--	0.004	0.004	0.002	0.004
Ag	0.430	0.430	0.438	0.441	0.524	0.565	0.590	0.637
Au	0.555	0.551	0.543	0.547	0.465	0.428	0.403	0.357
Total	0.996	1.000	0.996	0.996	1.001	1.003	1.001	1.000

\*This was such a small grain that it was difficult to analyse, so even though the analysis is not within the usually accepted limits (i.e. 98 to 102 total wt %), it is reported here.

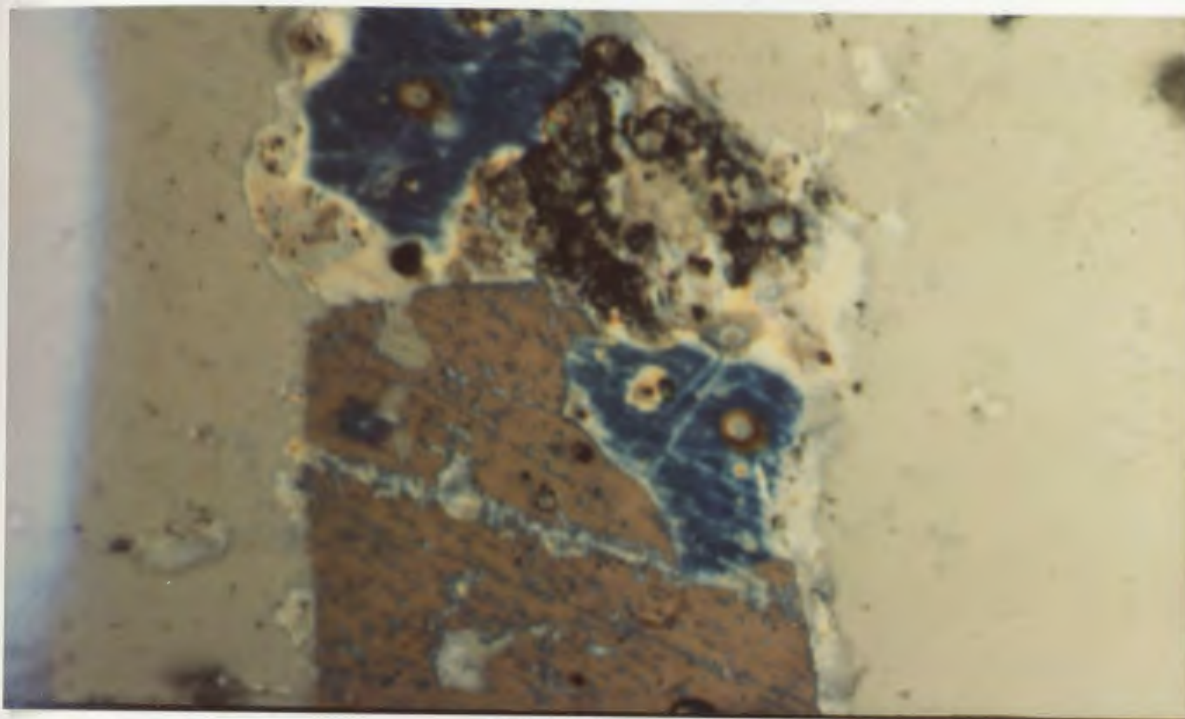
any sulphide).

No electrum (or gold) is visible in hand specimen from either of the two showings. In polished sections these grains are rather difficult to identify because the presence of such large amounts of Ag, changes the optical properties from those that are very distinctive and diagnostic of pure gold (cf. Ramdohr, 1969), to a much paler yellow material that resembles chalcopyrite (eg. Eales, 1961; Uytendogaardt and Burke, 1971; Henley, 1975). However when the polished sections were coated with graphite for microprobe analysis, the electrum grains become a bright blue (Plate 7-6A), which is quite distinctive compared to the masked colours of the other minerals. This blue colouration was subsequently used for reliable identification and numerous previously unnoticed Au/Ag grains were detected.

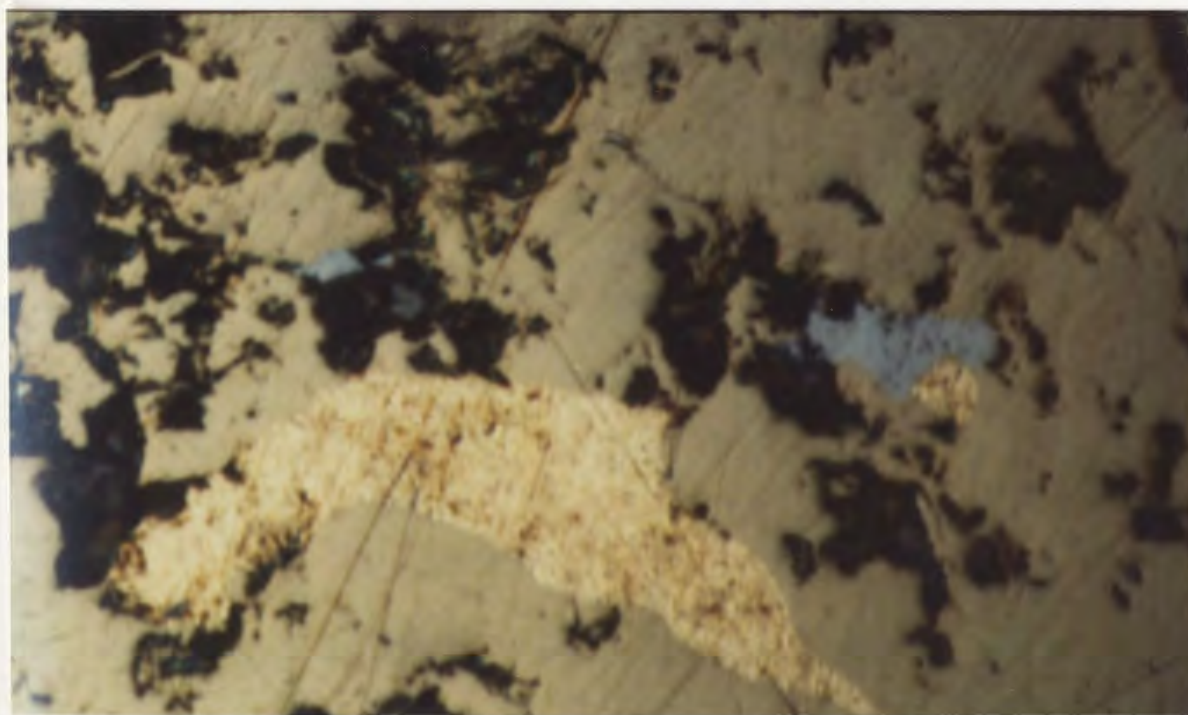
The electrum occurs as minute grains, up to 0.8 mm in diameter but usually  $\leq$  0.02 mm, intergrown with pyrite (Frontispiece), chalcopyrite (Plate 7-6B), galena (Plate 7-7A) and sphalerite (Plate 7-7B) (or some combination of these (Plate 7-8A)), or as solitary grains disseminated through the quartz vein in regions of sulphide concentration (Plate 7-8B). Such intergrowths are typical of most other gold/base metal sulphide deposits (eg. Henley, 1975; Boyle, 1979, etc.) However, according to Gasparrini (1983), the occurrence of gold in chalcopyrite

PLATE 7-5 A) Electrum (blue) intergrown with pyrite (brownish purple). . This plate is the same as that in the frontispiece except the section is coated with graphite.

B) Electrum (bright-yellow) intergrown with chalcopyrite (dark yellow background). The blue-coloured mineral is graphite-coated chalcopyrite. This section is 0.08 mm across.



A

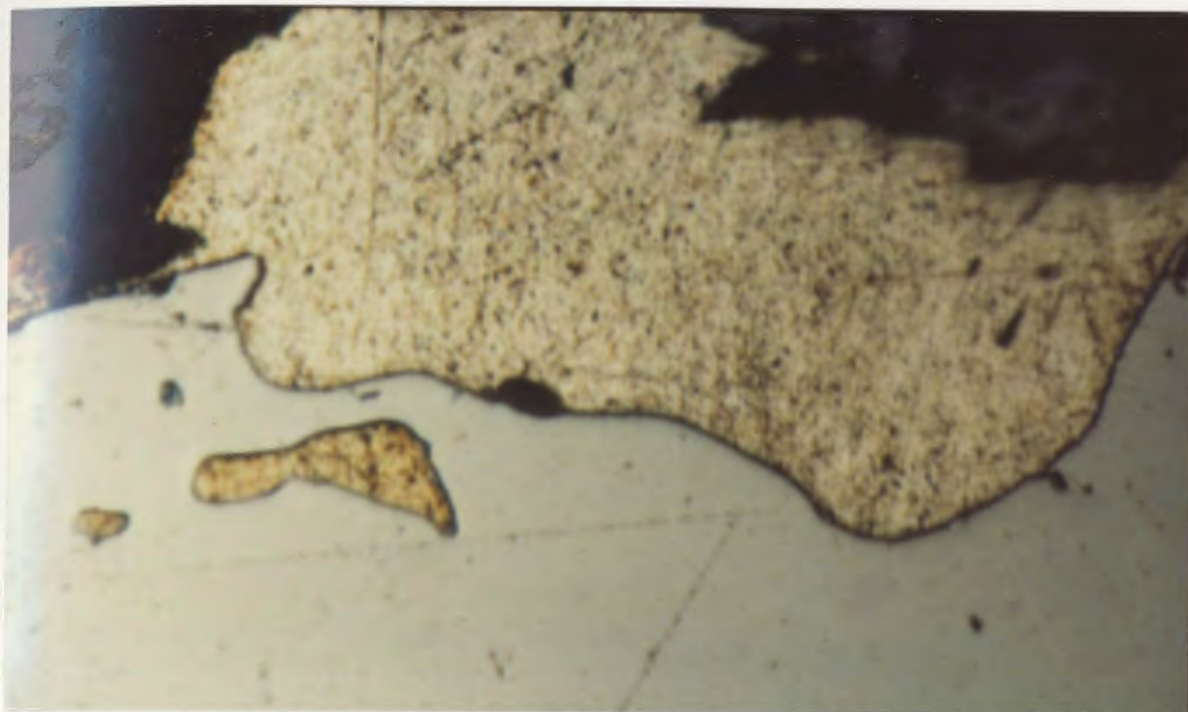


B

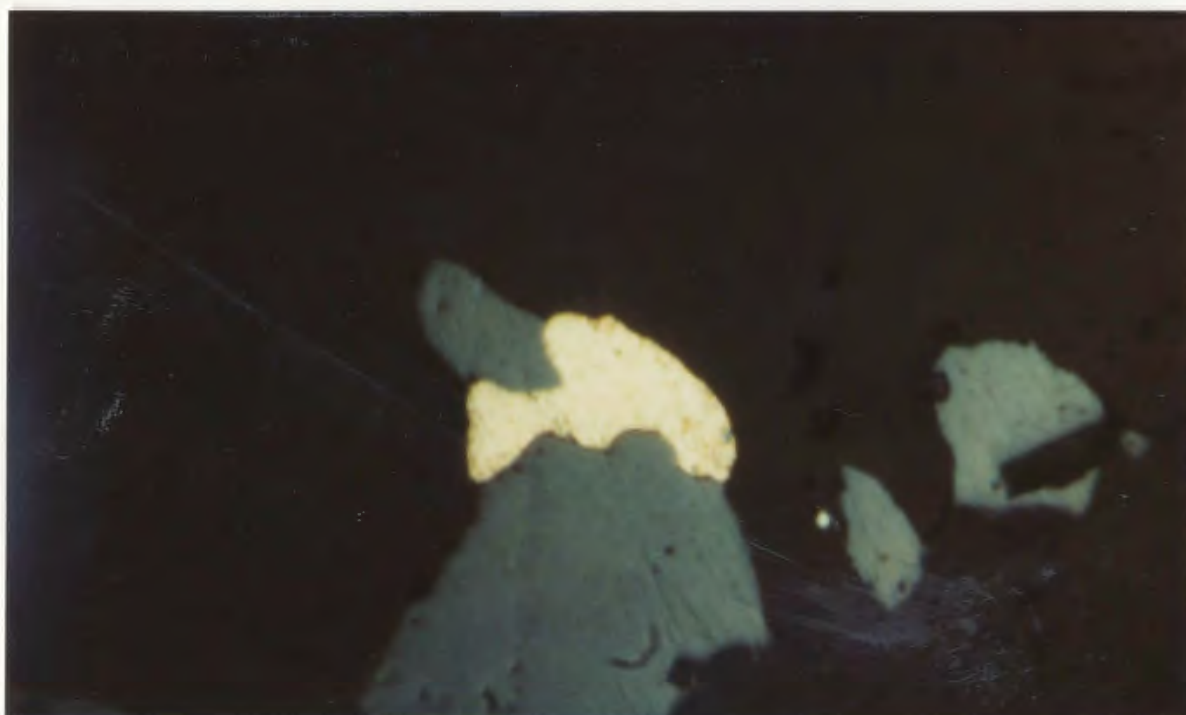


PLATE 7-6 A) Electrum (yellow) intergrown with and included in galena (white grey) and in contact with quartz gangue (black). This section is 0.08 mm across.

B) Electrum (yellow) intergrown with sphalerite (dark grey) and quartz gangue (black). This section is 0.08 mm across.



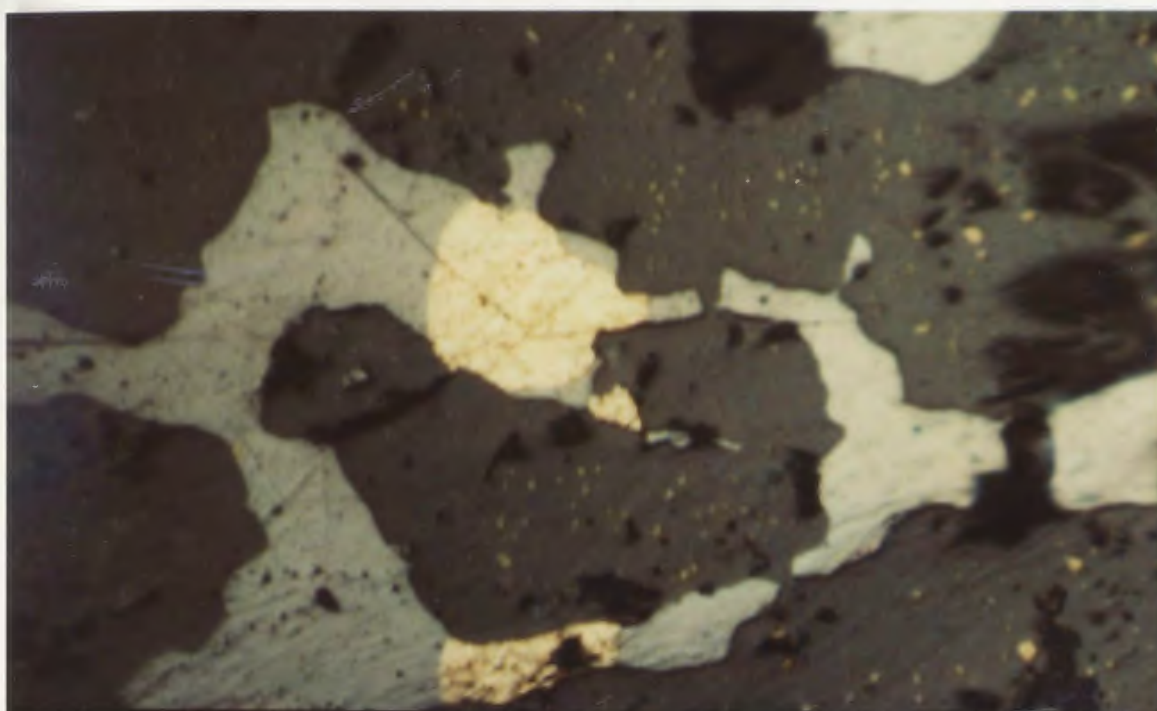
A



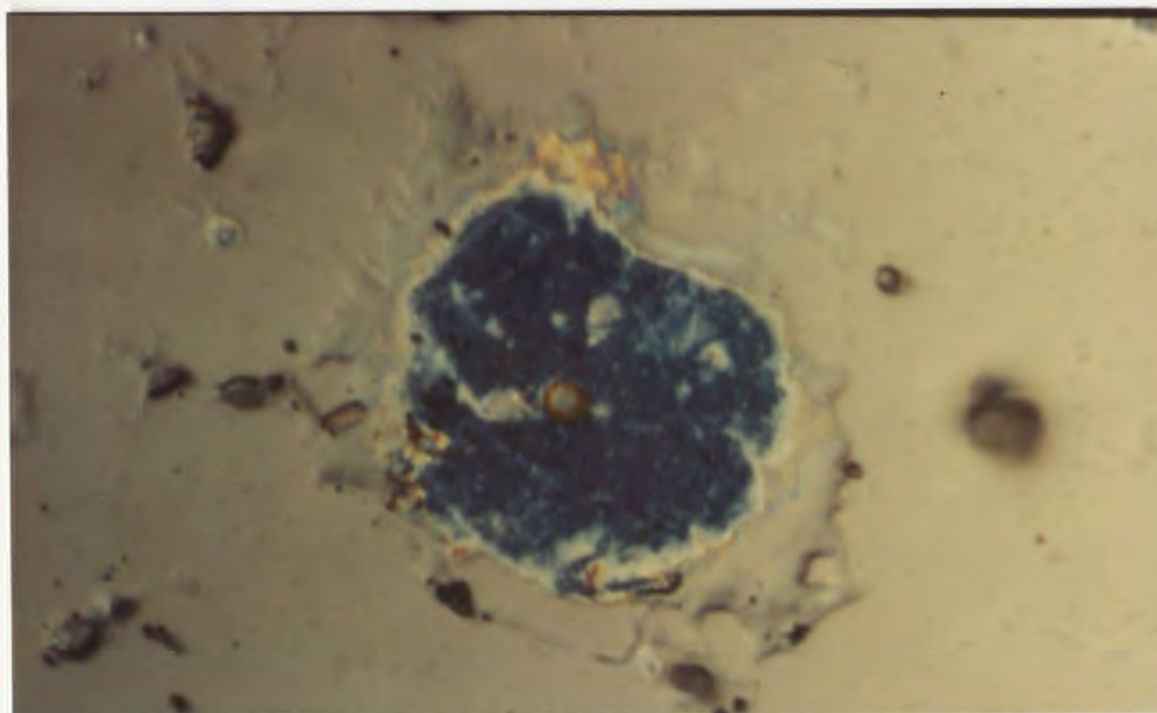
B

PLATE 7-7 A) Electrum (bright yellow) intergrown with galena (grey) and sphalerite (dark grey). The sphalerite contains exsolved blebs of chalcopyrite (yellow). This section is 0.08 mm across.

B) Solitary electrum grain (dark blue) intergrown with quartz gangue. The electrum has a graphite coating. This section is 0.08 mm across.



A



B

is much less common than in the other sulphides.

In the Windowglass Hill Granite-hosted samples, electrum is usually found with pyrite in pyrite-chalcopyrite-galena rich portions of the veins, while in the Main Shear veins the electrum is more typically with other sulphides.

#### 7.5.7 Other Minerals

Magnetite occurs as euhedral octahedra (up to 0.15 mm in diameter), or in patches of octahedra (up to 0.8 mm in diameter) in the Windowglass Hill Granite, and in schist wall rocks. Magnetite grains occur rarely in quartz veins intergrown with pyrite-chalcopyrite-sphalerite.

Pyrrhotite occurs as inclusions within sphalerite, galena and pyrite crystals, up to, but usually less than, 0.15 mm in diameter. It is not found in the granite-hosted quartz veins.

#### 7.6 Significance of Intergrowth Textures and Compositions

According to the experimental work of Brett and Kullerud (1967), mixtures of galena (70 %) and pyrite (30 %) can crystallize from a liquid at temperatures below 716° C (above 719° C pyrrhotite is the stable Fe sulphide). However the presence of appreciable sphalerite can lower

this temperature considerably. The main conclusion, though, is that the Cape Ray ores were formed at  $< 700^{\circ} \text{C}$ .

Experimentally-derived phase relations in the system Fe-Cu-S can better define the temperature range of formation. As shown by Barton and Skinner, 1979, at  $500^{\circ} \text{C}$ , pyrite and chalcopyrite may coexist in equilibrium, as can pyrite and pyrrhotite, but chalcopyrite-pyrrhotite are out of equilibrium due to the presence of an intervening intermediate solid solution (iss). At  $300^{\circ} \text{C}$  however, the iss field is reduced and equilibrium is possible between all three phases (as found in the Main Shear quartz veins). Therefore the ore formation had to be at temperatures of less than  $500^{\circ} \text{C}$ .

Sugaki et al. (1975) showed that the tie line change from intermediate solid solution-pyrite to chalcopyrite-pyrrhotite (ie. the stabilities present here) occurs at  $328 \pm 5^{\circ} \text{C}$ , thus the ores probably equilibrated near or below this change. Hutchison and Scott (1981) suggest that increasing pressures to 5 kb raises the temperature range of the tie line change to  $353\text{--}400^{\circ} \text{C}$ .

Figueiredo et al. (1980) studied the thermal behaviour of sphalerites containing chalcopyrite inclusions. (One set of samples from Ivigtut, Greenland, consisted of sphalerite with coexisting chalcopyrite, pyrite, galena and minor pyrrhotite, ie. similar to the Cape Ray samples). They found that complete homogenization

occurs at  $690^{\circ}\text{C}$  after only six days of heating. They concluded that during the cooling of sphalerite, "surplus copper had to leave the sphalerite lattice" (*ibid.*, p. 285). (*ie.* exsolution). Sphalerite from the Cape Ray deposits would be expected to behave similarly. From experimental results in the pseudobinary system chalcopyrite-sphalerite, Moh (1975), found that inversion of a pre-existing solid solution occurs below  $500^{\circ}\text{C}$ .

Electrum is apparently the typical Au-bearing phase in epithermal-type Mesozoic-Cenozoic gold deposits (eg. Henley, 1975; Boyle, 1979), whereas native gold is more typical of older deposits. There is a general paucity of information concerning relationships in the Au-Ag (electrum) system, but Barton (1980) was able to define the  $\log f_{\text{S}_2}$  vs.  $T$  relations of different electrum compositions in equilibrium with Ag/Au/S. solid solutions over the range of interest.

Interpretations of the variations in Au/Ag ratios (or fineness) within gold/electrum grains through different deposits are ambiguous. Eales (1961) found that earlier-formed native gold enclosed in sulphides (such as chalcopyrite or sphalerite) is more silver-rich than later-formed solitary disseminated gold grains. Eales also stated that high-grade ore contains silver-poor gold, and low-grade ore has silver-rich gold. Sakharova (1969) found a similar relationship, in that native gold enclosed in

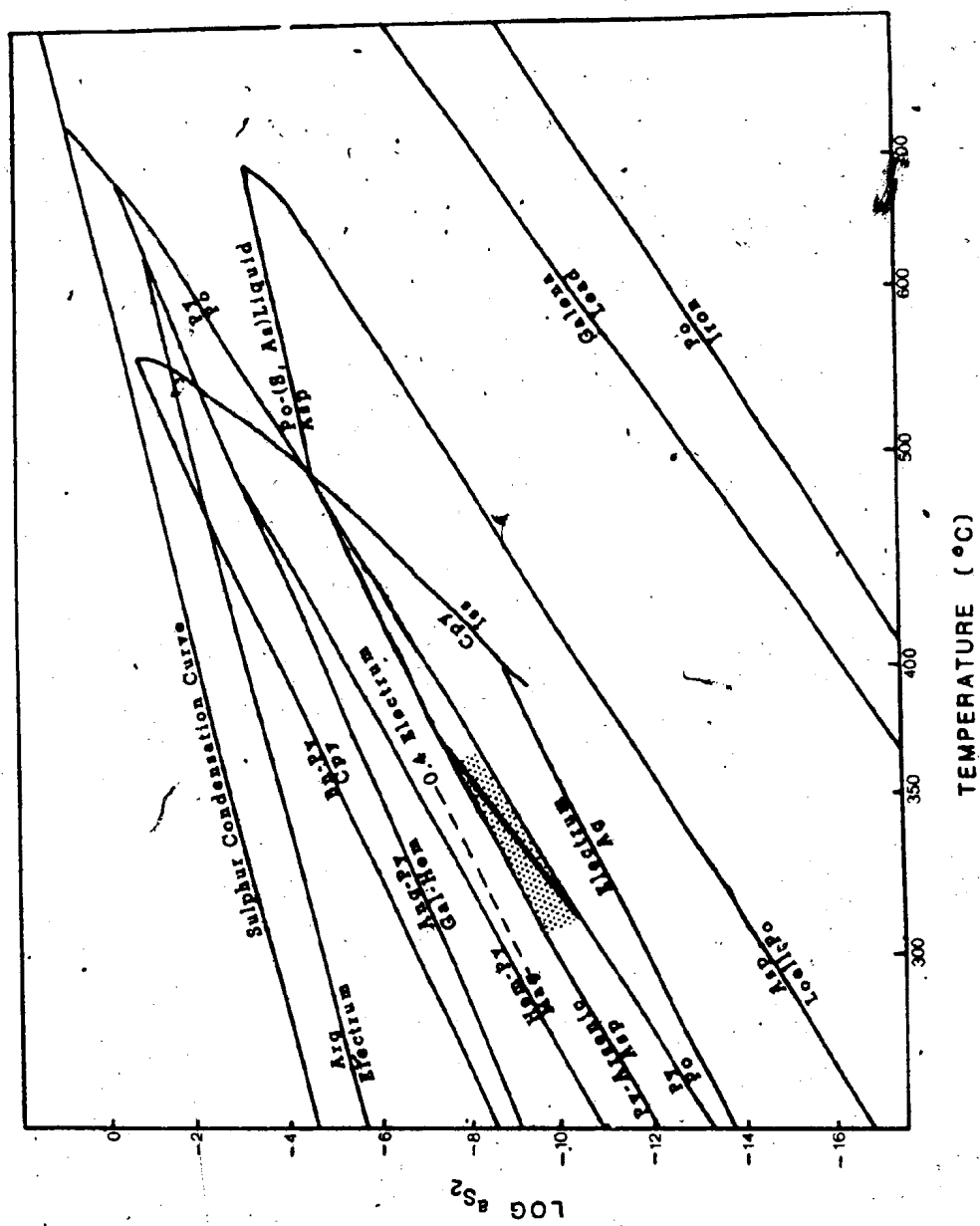
sulphide has increased Ag contents in rims vs. cores, while disseminated solitary gold has no zonation.

The same kind of relationship is visible in the Main Shear veins, as the discrete disseminated electrum grains have the lowest Ag contents, and, according to the previous authors, this Au-rich electrum formed later than the more Ag-rich grains. Boyle (1979), however, stated that this relationship holds only for Paleozoic and Precambrian deposits, because the reverse is true in deposits of Mesozoic-Cenozoic age as these later systems are enriched in Ag.

The log  $a_{S_2}$  vs. temperature grid for all relevant phases in the Cape Ray Deposits is illustrated in Figure 73 (from Barton and Skinner (1979), with the arsenopyrite data of Kretschmer and Scott (1976), and the Ag/electrum data of Barton (1980)). A major constraint on the ore-forming system is the presence of  $(Fe, As)_{0.9}S_{1.1}$ , however the electrum grains generally have  $> 0.4$  mole % Ag, which further constrains the system around the 30 % As line (see Figure 73). The chalcopyrite-pyrite and chalcopyrite-pyrrhotite equilibrium lines, with an intermediate solid solution, also restrict ore-forming compositions to the same area. The other equilibria for all the other phases are consistent. These phase relations indicate a log  $f_{S_2}$  range of -7.6 to -10.7 and temperatures ranging from 308 to 360° C. According to Barton and



Figure 73 Log  $a_{S_2}$  vs. temperature grid for sulphide phases relevant to the Main Shear mineralization. The diagram is based on that of Barton and Skinner (1979) with arsenopyrite data from Kretschmar and Scott (1976) and the electrum data of Barton (1980). The shaded area represents the compositional field for Main Shear intergrowths, the heavy line is the 30 % As compositional tie line for arsenopyrite.



Skinner (1979) pressures of 2 to 3 kb, only slightly change the temperatures of these univariant curves, and therefore the relations as illustrated are relevant to the ore-forming system.

### 7.7 Sulphur Isotopes

The basis for the use of sulphur isotopes in petrogenetic considerations is the isotopic differentiation between  $^{34}\text{S}$  and  $^{32}\text{S}$  in different environments, minerals and ore-forming systems. Detailed reviews of sulphur isotope systematics are given by Rye and Ohmoto (1974) and Ohmoto and Rye (1979). This differentiation, or the isotopic fractionation factor, is expressed in ‰ (per mil) and is defined in terms of the difference in the  $^{34}\text{S}/^{32}\text{S}$  isotopic ratio between a given sample and the standard (the standard being troilite from the Canyon Diablo meteorite (McNamara and Thode, 1950)). The formulation of the fractionation factor is:

$$\delta^{34}\text{S}(\text{sam})(\text{‰}) =$$

$$(((^{34}\text{S}/^{32}\text{S})_{\text{sam}} - (^{34}\text{S}/^{32}\text{S})_{\text{std}}) / (^{34}\text{S}/^{32}\text{S})_{\text{std}}) \times 1000$$

where sam=sample and std=standard.

Ultimately the  $\delta^{34}\text{S}$  composition of sulphides deposited from hydrothermal fluids is dependant on; a) the source of the sulphur in solution, b) mechanics of deposition, c) mineralogy, and d) the physical conditions at the time of

deposition. As a very broad generalization, sulphides deposited from igneous systems have  $\delta^{34}\text{S}$  of around 0 ‰ (ie. not fractionated with respect to the meteoritic composition), sedimentary sulphides range from  $< -40 \delta^{34}\text{S}$  to  $> 40 \delta^{34}\text{S}$ , with a maximum around  $-15 \delta^{34}\text{S}$  (ie isotopically lighter than the meteorite), and oceanic and evaporite sulphides have a  $\delta^{34}\text{S}$  of about  $+20 \delta^{34}\text{S}$  (isotopically heavier) (after Ohmoto and Rye, 1979).

The  $\delta^{34}\text{S}$  data for twenty-seven sulphide separates (fourteen from the Main Shear, and thirteen from the Windowglass Hill Granite) are listed in Table XXXV. Seven galena, five pyrite and one chalcopryrite separates were analysed from the granite; five galena, four pyrite, three sphalerite and two chalcopryrite separates were analysed from the Main Shear. In most cases, it was attempted to separate more than one mineral in order to get a range of  $\delta^{34}\text{S}$  values for a sample (in some cases this was impossible as the samples were monomineralic at the sample collection scale, and three separates were lost during analysis).

The range in  $\delta^{34}\text{S}$  values for these various sulphides are illustrated in Figure 74. In general the fractionation factors are positive but average close to zero. There is a mineralographic trend in values, with isotopic heaviness increasing from galena through chalcopryrite, sphalerite to pyrite. This trend is a normal feature of other ore systems (cf. Ohmoto and Rye, 1979). (The pyrite samples

TABLE XXXV  $^{63}\text{S}$  DATA

<u>SEPERATE#</u>	<u>SULPHIDE</u>	<u>SAMPLE #</u>	<u><math>^{63}\text{S}</math></u>	<u>SHOWING</u>
DHCW1	galena	WGH Show	+3.1	Windowglass Hill
DHCW2	pyrite	WGH Show	+3.6	Windowglass Hill
DHCW3	sphalerite	PB63-5	+3.2	Main Shear
DHCW4	galena	PB63-5	-0.5	Main Shear
DHCW4 (dup.)	"	"	+0.4	"
DHCW5	pyrite	PB63-5	+4.6	Main Shear
DHCW6	sphalerite	80-65B	+3.0	Main Shear
DHCW7	galena	80-65B	+1.5	Main Shear
DHCW8	pyrite	80-65B	-4.6	Main Shear
DHCW9	galena	80-65A	+1.5	Main Shear
DHCW10	sphalerite	PB41-6	+2.5	Main Shear
DHCW12	galena	PB133-9	+0.1	Windowglass Hill
DHCW14	pyrite	PB133-9	+4.4	Windowglass Hill
DHCW15	chalcopryrite	80-61F	+1.4	Main Shear
DHCW19	galena	79-78B	+2.0	I Brook (Windowglass Hill)
DHCW21	pyrite	80-66C	-5.2	Main Shear
DHCW23	pyrite	PB28-5D	+6.9	Main Shear
DHCW24	galena	PB28-5D	+2.2	Main Shear
DHCW25	galena	PB38-37	+1.3	Main Shear
DHCW26	chalcopryrite	Pb38-37	+3.1	Main Shear
DHCW28	galena	WGH SH1	+2.9	Windowglass Hill
DHCW29	chalcopryrite	WGH SH1	+4.2	Windowglass Hill
DHCW30	galena	WGH SH1	-1.0	Windowglass Hill
DHCW32	pyrite	80-149	+2.7	I Brook (Windowglass Hill)
DHCW33	galena	80-148	+3.7	H Brook (Windowglass Hill)
DHCW34	pyrite	80-148	+4.2	H Brook (Windowglass Hill)
DHCW35	galena	WGH SH2	+2.7	Windowglass Hill
DHCW37	pyrite	WGH SH3	+5.9	Windowglass Hill

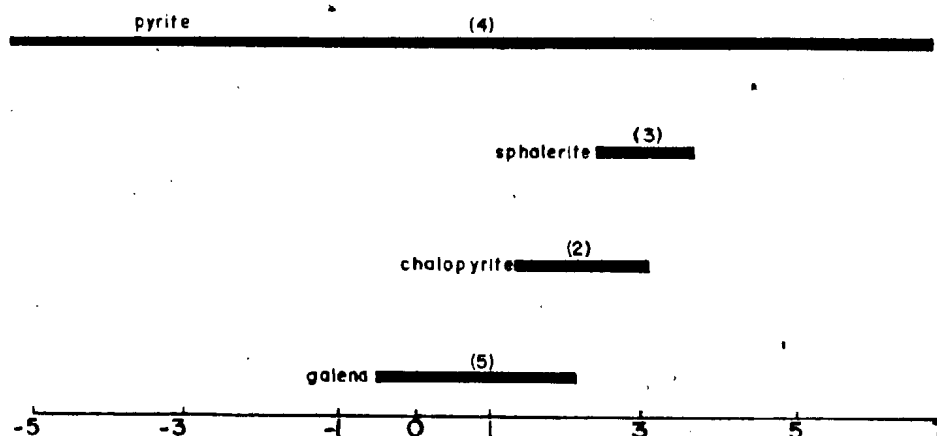
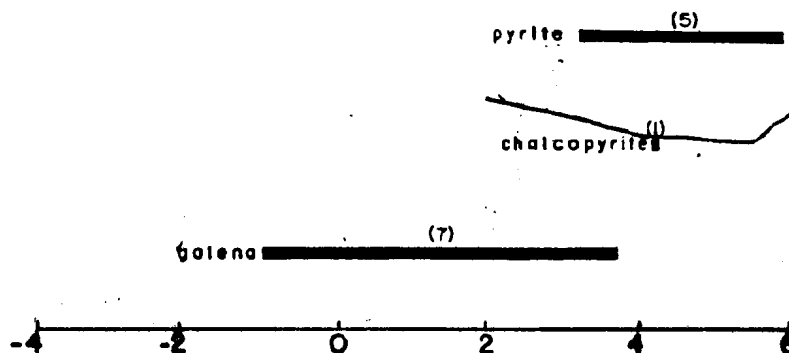
$\delta^{34}\text{S}\text{‰}$  MAIN SHEAR SAMPLES $\delta^{34}\text{S}\text{‰}$  WINDOWGLASS SAMPLES

Figure 74 Range of  $\delta^{34}\text{S}$  (‰) values for sulphide separates from the Main Shear and Windowglass Hill Showings. Bracketed numbers indicate number of defining samples.

from the Main Shear have a very broad range based on two positive samples, + 4.6 and + 6.9 (the overall highest of all) and two negative samples, - 4.6 and - 5.2, so the range is not a complete continuum but is more like that of two end members).

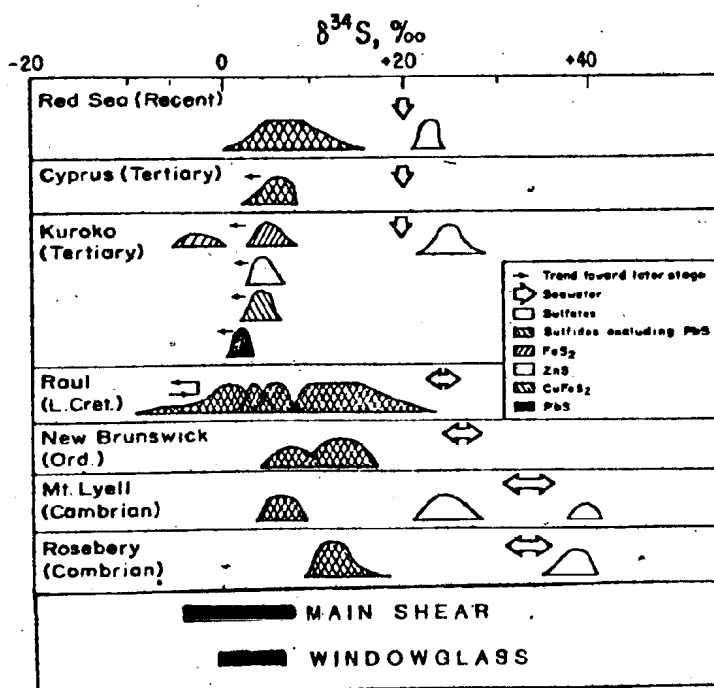
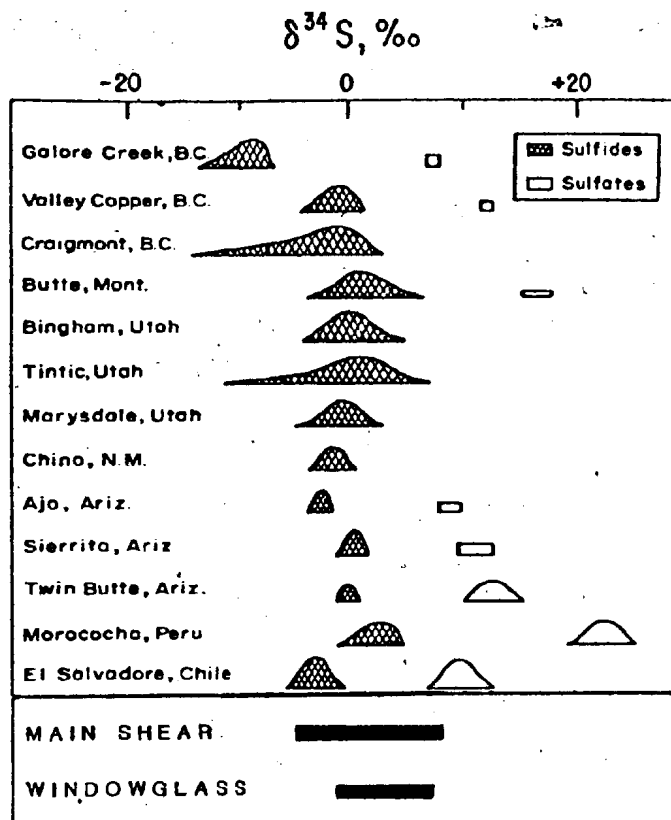
When the overall ranges of  $\delta^{34}\text{S}$  in each of the quartz vein systems is compared to those of other hydrothermal deposits (Figure 75, after Ohmoto and Rye, 1979), they are the same as those ranges found in porphyry copper systems; which according to Ohmoto and Rye (1979) average -3 to +9 ‰. However, they also overlap with the ranges found in stratabound massive sulphide deposits (Figure 75). The ranges typical of Mississippi Valley-type deposits, around + 20 ‰ with wide variation (*ibid.*), are distinctly different.

The latter deposits are definitively sedimentary deposits and their sulphur is non-volcanic. The porphyry copper type, on the other hand, are definitively magmatic (as is reflected by the low to zero  $\delta^{34}\text{S}$  values). The massive sulphides involve hot submarine volcanic rocks and circulating seawater, leading Ohmoto and Rye to conclude that the sulphur is from reduction of seawater sulphate by the volcanics, but some of the sulphur may be of direct igneous derivation.

Sulphur in the Cape Ray samples is definitely not of sedimentary origin, and is most likely of magmatic affinity.

Figure 75 Comparison of  $\delta^{34}\text{S}$  values in the Cape Ray showings with those of porphyry copper and volcanogenic massive sulphide deposits. This diagram is from Ohmoto and Rye (1979). The Cape Ray showings are quite similar to the porphyry copper systems (ie. are composed of magmatic sulphur), and are slightly less fractionated than the massive sulphides.





(there's no evidence of submarine mafic volcanism in the whole fault zone, let alone intimately associated with ore deposition). The sulphur could conceivably have been derived by leaching of disseminated sulphides in volcanic rocks but; 1) there is a paucity of actual mafic volcanic rocks in the region, 2) the local schists were derived from tuffaceous rocks with a dominant sedimentary influence and thus any leached sulphur would have a strong sedimentary (ie isotopically heavy) signature (eg. pyrite in the pyritiferous graphitic schists was probably diagenetic feature during deposition of the muds (cf. Ferry, 1981)), 3) these schists have vastly greater volumes than any of the mafic volcanic rocks in the fault zone, so the sulphur-deriving fluid would have to affect them as well as the mafic volcanics (leading to a sedimentary signature on  $^{34}\text{S}$ ), and finally, 4) equilibrium between the leaching fluids and the volcanic sulphur source would have to be achieved in order to yield the non-fractionated sulphur ratios, although the fluids which obviously traversed the country rocks have affected these rocks extensively (ie. there could not have been fractionation during the leaching). The overall conclusion is that the sulphur in the sulphides of both ore horizons is of magmatic (probably granitic) derivation.

#### 7.7.1 Temperatures

Isotopic fractionation between an equilibrium

sulphide-mineral pair is temperature dependant. Accordingly, various authors (eg. Kajiwarra and Krouse, 1971; Czamanske and Rye, 1974) have defined geothermometers, based on experimentally-derived fractionation values for selected mineral pairs. Skirrow and Coleman (1982) found, when studying an inactive sulphide mound near the Galapagos Rift and comparing temperatures derived by sulphur isotope analysis using Kajiwarra and Krouse's (1971) data for pyrite-chalcopyrite, that these calculated temperatures ( $390^{\circ}\text{C}$ ) are almost identical with those ( $380^{\circ}\text{C}$ ) determined by examination of an active mound.

Using the fractionation factors from Kajiwarra and Krouse (1971) for the mineral pairs pyrite-galena, pyrite-chalcopyrite, pyrite-sphalerite, chalcopyrite-galena and chalcopyrite-sphalerite, the temperatures for various samples from the two ore horizons were determined (see Figure 76). There is a wide range of temperatures so determined from the granite-hosted sulphides. Three are abnormally high at  $980$  and  $1210^{\circ}\text{C}$ , and of the other two ( $434$  and  $233^{\circ}\text{C}$ ), only the lower is reasonable based on ore mineral intergrowths (ie. equilibrium textures), etc. The Main Shear samples have a peak of calculated temperatures around  $200^{\circ}\text{C}$ , with single observations ranging up to  $457^{\circ}\text{C}$ . The intermediate calculations are most reasonable in

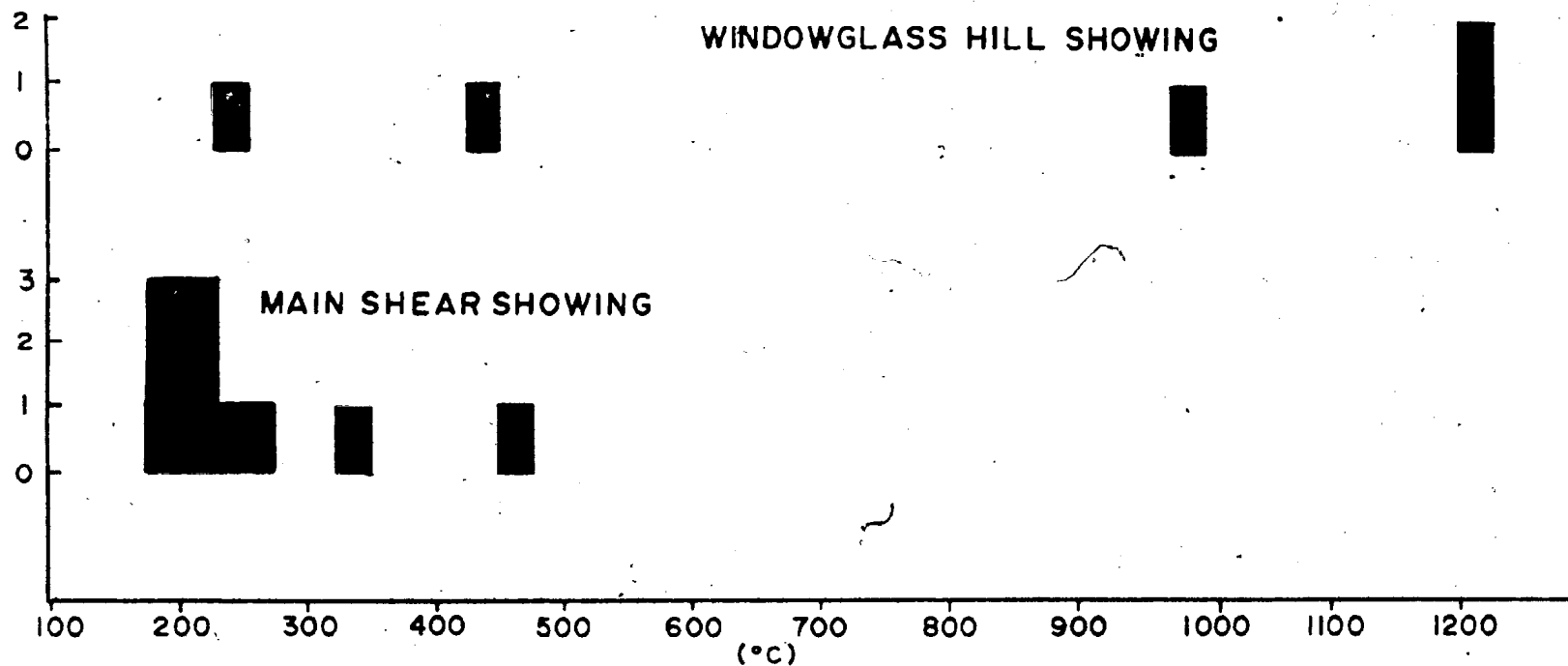


Figure 76 Histogram of temperature determinations for the Main Shear and Windowglass Hill Showings based on sulphur isotope fractionations between co-existing sulphides. The fractionation factors of Kajiwara and Krouse (1971) were used in these determinations.

view of other factors (ie. 239, 261 and 328° C), but the 200° C appears to be low. The main problem lies with the wide range (ie. lack of precision) in replicate analyses, the 200° C peak is marked by five determinations based on the maximum, minimum and mean  $\delta^{34}\text{S}$  value for the galena of sample DHCW-4.

Since these determinations are based on coexisting pairs of sulphide minerals, the lack of precision in analysis casts doubt on the validity of the data. Smith et al. (1977) derived a sulphide geothermometer based on three co-existing sulphides (galena, sphalerite and pyrite). The addition of a third component to temperature determinations provides greater constraints on the variability of the temperature calculation, and thus provides an additional check on the calculation. Co-existing sulphide separates of these three minerals were analysed from only one sample (ie. PB63-5). When these three separates were used (including the min., max. and mean values of galena), they defined a restricted temperature zone on this geothermometer (Figure 77) that indicates a temperature of ore formation around ~ 225° C. The fact that this area lies on, or close, to the linear temperature trend defined by Smith et al. (1977) (using both their own and Kajiwara and Krouse's (1971) experimental data) indicates that this temperature determination is reasonable.

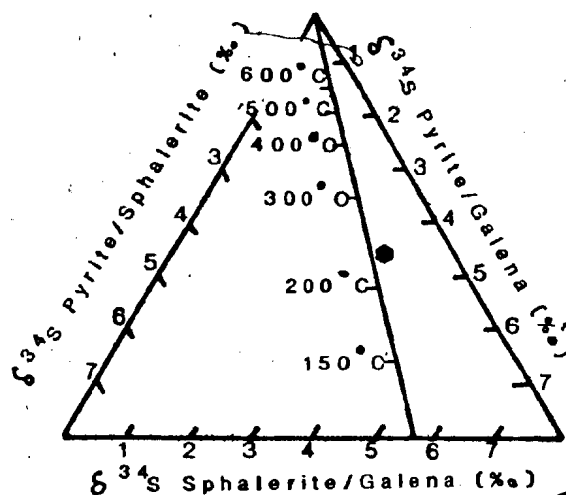


Figure 77 Pyrite-sphalerite-galena sulphur isotope geothermometer for sample PB63-5 from the Main Shear Showing. This diagram is from Smith et al. (1977). The range of fractionation values in the sample is represented by the hexagon point at 225°C.

The composite pyrite-sphalerite geothermometer derived by Lusk et al. (1975) indicates an ore-formation temperature of about 230° C.

#### 7.8 Lead Isotopes

Pb has four naturally occurring isotopes, viz. 204Pb, 206Pb, 207Pb and 208Pb; of which the latter three are produced by radioactive decay of 238U, 235U and 232Th respectively. 204Pb is the only non-radiogenic isotope and it is used to ratio all the other isotopes to each other. Since the amounts of the different radiogenic isotopes increase through time at different rates, the ratios of the different isotopes to one another can be used (knowing the decay constants) to determine the age of the earth. If, however, the lead is separated at some point in time from its decaying parents, then its isotopic ratios will freeze that point of time in whatever new system the lead is incorporated. Complications arise when radiogenic leads, with different ratios, are mixed in a single system, when new concentrations of decaying parents are added to the system, or when there are isotopic fractionations produced by physiochemical conditions extant in either the region of Pb separation or incorporation. An excellent overview of the Pb isotopic system is presented by Koppel and Grunnenfelder (1979).

Early workers (cf. Doe, 1970), using analytical techniques of poorer precision, considered the earth to have been a closed system since its formation such that all stratabound, galena-bearing mafic volcanic deposits lay on a single-stage growth curve from origin to present-day (ie. these deposits were derived directly from the mantle). Subsequently, using better data, it was found that numerous deposits fall off this single-stage growth curve, so two-stage evolutionary curves were developed (eg. Cumming and Richards, 1975; Stacey and Kramers, 1975). In these new models, large scale differentiation between the origin of the earth and the present-day was assumed to have taken place.

Meanwhile other authors (eg. Doe and Delevaux, 1973; Zartman, 1974) were noting that whole rock Pb isotopic compositions had wide regional and lithological variations. Finally Doe and Zartman (1979) produced the latest interpretation of Pb isotopic systematics, "plumbotectonics". This model recognized that different geological environments have specific Pb isotopic ratios intrinsically related to the petrogenesis of the particular environment. Expanding on this, they were able to define four fundamental radiogenic growth curves (viz. for the mantle, the orogene, the upper crust (contributed to the orogene), and the lower crust (contributed to the orogene)), and any combinations thereof, which could be



used to explain the Pb isotopic ratios within a given system. They went beyond the notion of single-stage and two-stage growth and realised that the earth has not been a closed Pb-isotopic system. However, as a best approximation they thought there were four main systems operative in the earth and that, these systems have periodically interacted with each other to such an extent that their defined growth curves are dependant on what happens in the other systems also.

The Pb isotopic compositions for five galena samples from the Cape Ray Fault Zone are listed in Table XXXVI. Sample 79-16 is from the galena showing associated with the quartz/feldspar porphyry dyke at Red Rocks Point (distal feeder of the Windsor Point Group ignimbritic volcanism). 79-58A is from the galena-bearing mylonite on the Trans-Canada Highway (ie the coastal mylonite). WGH Show is from a base metal-bearing quartz vein in the Windowglass Hill Granite and the final two samples (PB38-35 and 80-65B) are from the Main Shear Showing veins. These samples were originally selected to ascertain if there were substantial differences between galenas in the different horizons, however the analyses indicate the Pb isotopic ratios have a restricted range of values and seem to define a communality between the samples. This is not totally unexpected as the time span for deposition is in the late Devonian.

When plotted on Doe and Zartman's (1979) growth curve

TABLE XXXVI LEAD ISOTOPE DATA

(Decay constants used:  $^{238}\text{U} = 0.155125 \times 10^{-9} \text{yr}^{-1}$ ;  $^{238}\text{U} = 0.98485 \times 10^{-9} \text{yr}^{-1}$ )

<u>SAMPLE #</u>	<u><math>^{206}\text{Pb}/^{204}\text{Pb}</math></u>	<u><math>^{207}\text{Pb}/^{204}\text{Pb}</math></u>	<u><math>^{208}\text{Pb}/^{204}\text{Pb}</math></u>
79-16	$18.074 \pm 0.13$	$15.503 \pm 0.17$	$37.594 \pm 0.15$
79-58A	$18.101 \pm 0.11$	$15.516 \pm 0.15$	$37.660 \pm 0.14$
80-65B	$17.923 \pm 0.93$	$15.367 \pm 0.94$	$37.448 \pm 1.0$
PB38-35	$18.452 \pm 0.33$	$15.475 \pm 0.36$	$38.012 \pm 0.38$
WGH Show	$18.120 \pm 0.08$	$15.575 \pm 0.11$	$37.992 \pm 0.11$

diagrams (Figure 78), all these galena samples fall near the 400 Ma time line, further indicating that all the galena samples are of about the same age. They also lie in the oceanic basalt fields and are most closely related to the mantle growth curves. This is unexpected since the environment of deposition is definitively continental, while deposits such as Buchans (Swinden and Thorpe, 1983), a classic volcanogenic massive sulphide deposit, fit in this same oceanic field. Swinden and Thorpe (1983) have shown that the Barasway de Cerf and Strickland deposits of southwestern Newfoundland, island arc-related sulphide deposits, are very radiogenic when compared to the post-Caradocian massive sulphide deposits of the Central Mobile Belt (eg. Buchans, York Harbour). The Pb in these latter deposits is thought to have been derived directly from the mantle (*ibid.*), and the Cape Ray galena Pb ratios are most similar to these type of deposits.

In the case of ore leads there are two important times  $t_1$ , which is the age of the source, and  $t_2$ , the age of the mineralization (or age of deposition). These ages are related by the equation:

$$S = 1/137.88 \times \frac{(e^{\lambda_5 t_1} - e^{\lambda_8 t_1})}{(e^{\lambda_5 t_2} - e^{\lambda_8 t_2})}$$

(after Koppel and Grunfelder, 1979), wherein  $S$  = the slope;

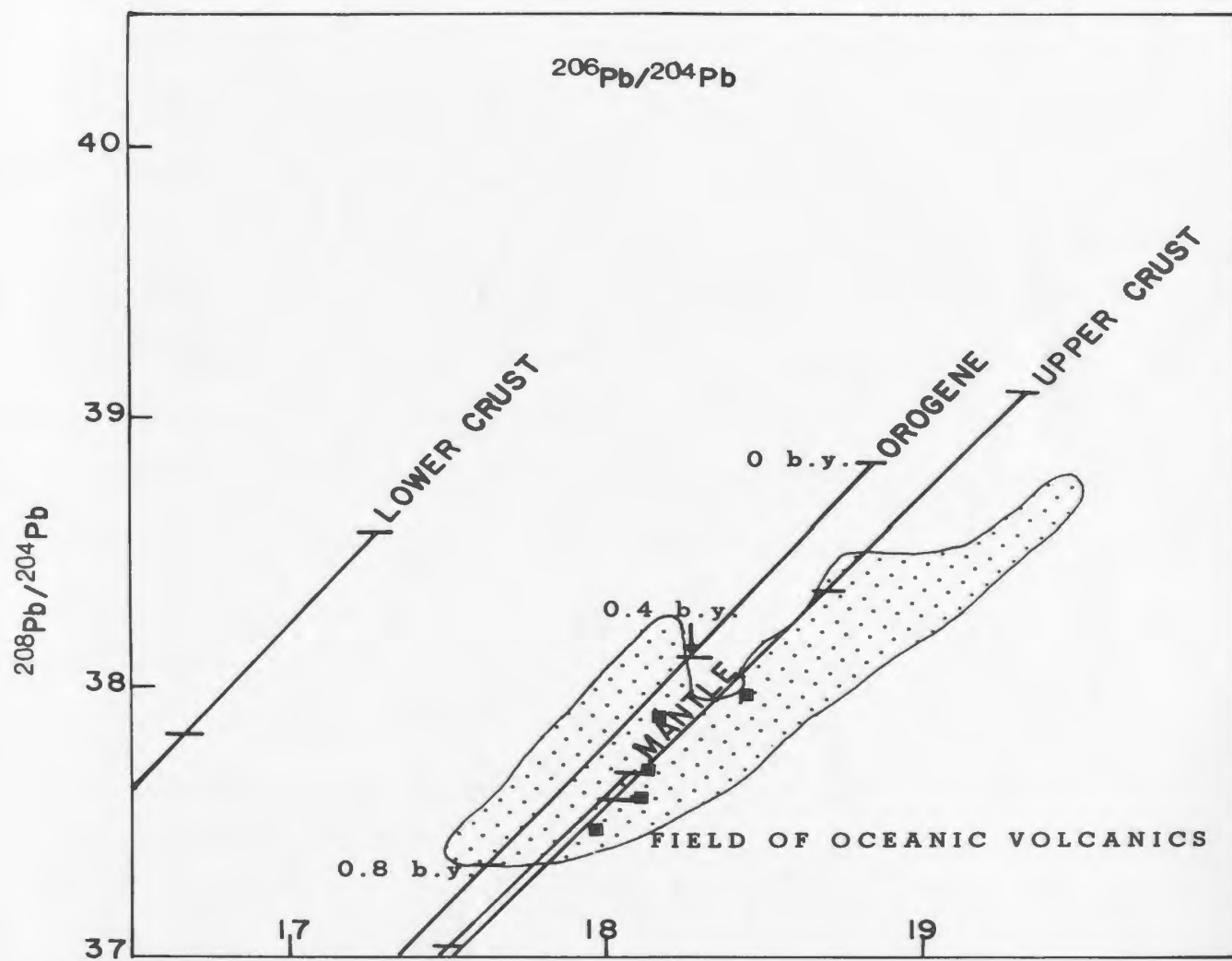
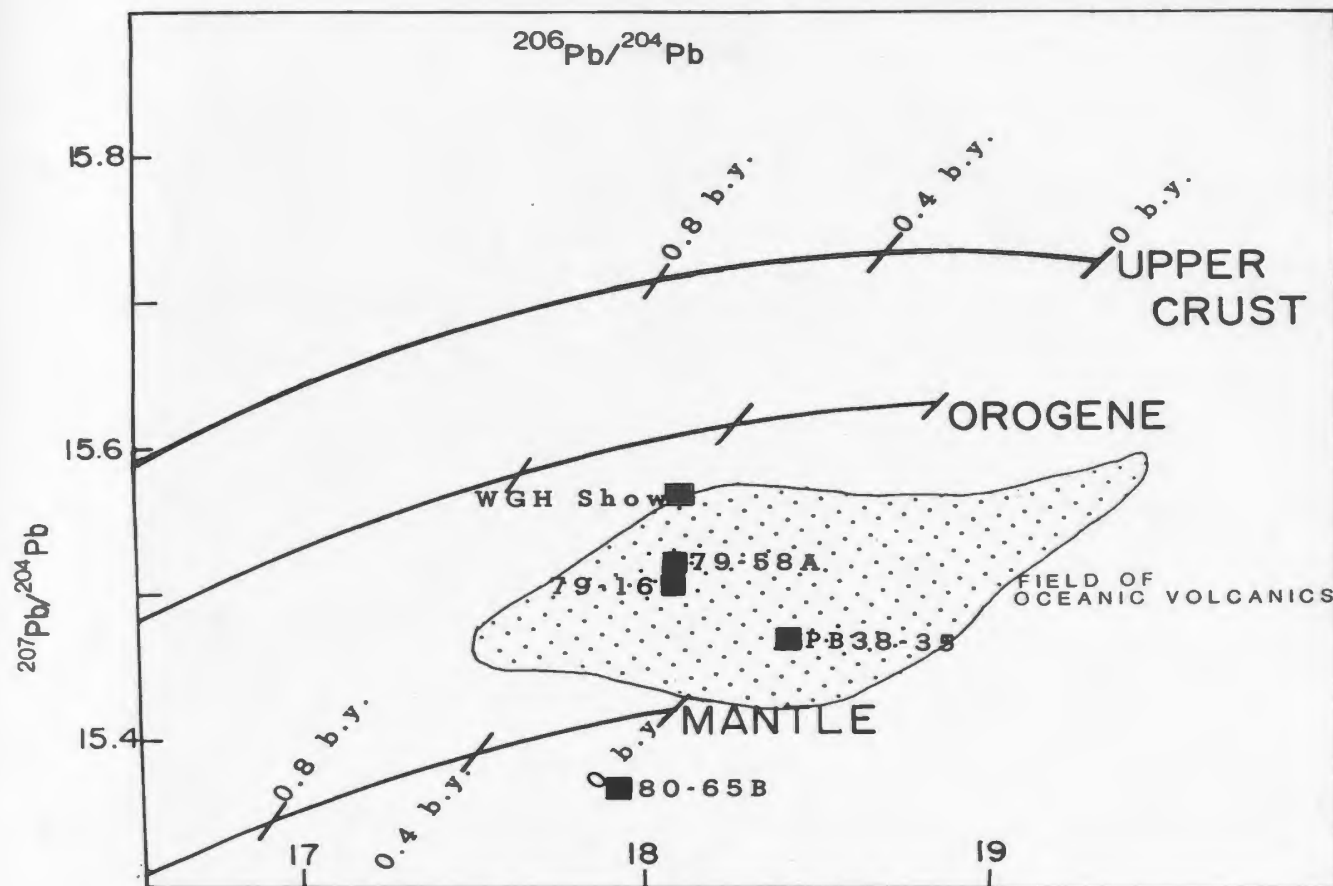
$\lambda_5$  = decay constant of  $^{235}\text{U}$  and  $\lambda_8$  = decay constant of  $^{238}\text{U}$ .

By letting  $t_1=t_2$  the equation simplifies as:

$$S = 1/137.88 \times \frac{\lambda_5 e^{\lambda_5 t_1}}{\lambda_8 e^{\lambda_8 t_1}} \quad (1)$$

Figure 78 Pb isotopic growth curves and the Cape Ray sample data.

These diagrams are from Doe and Zartman (1979). The Cape Ray samples occur within the field of oceanic<sup>3</sup> volcanic rocks as defined by Doe and Zartman, and form a partially linear array close to the 400 Ma time line. On the  $^{207}\text{Pb}/^{204}\text{Pb}$  vs.  $^{206}\text{Pb}/^{204}\text{Pb}$  diagram, the samples appear to be the products of mantle processes, rather than those of the upper crust in which they were deposited.




By solving the equation for  $t_1$ , the minimum age of the source or maximum age of the mineralization can be determined. Regressing the five data points from the Cape Ray Fault Zone (using a slight modification of York's (1969) regression method), produces a slope of 0.124. When this value is entered in equation (1), the determined age is 1,194,600,000 yrs (or  $\sim 1.2$  Ga), which must certainly be the age of the source, as the age of the mineralization is post-Upper Devonian.

The Pb isotopic data present a conundrum for petrogenetic modelling because on the one hand the source environment appears to have been mantle material, but the galenas are intimately associated with both the basal ignimbrites of the Windsor Point Group and the Windowglass Hill Granite. Geochemical evidence indicates these lithological units were derived by partial melting of a felsic source. A second problem is that the derived age of the source is 1.2 Ga, yet the only oceanic crust present in the area (though in minor dismembered portions) is the Long Range Mafic/Ultramafic Complex which is, at the oldest, Lower Ordovician. All other units post-date these ophiolite fragments.

There is however one unseen source of the right age and that is continental crust underlying this complete area. This crust has already been implicated as the source for the partial melts which produced the Windsor Point

Group ignimbrites, Windowglass Hill, Isle aux Morts Brook and Strawberry Granites. Since the ophiolites in this area represent oceanic crust of the Dunnage Zone, such continental crust would have to be basement to the ancient western continental margin (ie. Grenvillian).

This still leaves the problem of the mantle affinity for the lead isotopes, but Fletcher and Farquhar (1982) have recently shown that mineral deposit sulphides (mainly galenas) in the Central Metasedimentary Belt of the Grenville Province in Ontario and Quebec have the similar oceanic affinities. They explain that these ratios result from the special nature of the Grenvillian crust (ie. that it was "crustal material, newly differentiated from mantle reservoirs at approximately 1.3-1.0 Ga" (ibid., p.25). In other words, it was so quickly derived from mantle sources that the Pb's still reflect the mantle growth curve. Most importantly though, Fletcher and Farquhar also examined post-Ordovician vein-Pb isotopic ratios, probably derived by remobilization of the Grenvillian mineralization, and found that they define a secondary isochron which intersects the growth curve at Grenvillian times (~1000 Ma). Though they (ibid.) postulate that the resultant vein ratios are produced by addition of some more radiogenic Pb to the Grenville Pb, overall the post-Ordovician vein lead ratios have retained their mantle volcanic affinities (after Doe and Zartman, 1979).



Thus, the Pb isotopic ratios indicate the Cape Ray galenas can be best explained as having been derived from Grenvillian basement sources. This accords with the geochemical evidence for the origin of the Windsor Point Group, Windowglass Hill Granite and post-tectonic granites as partial melts of felsic sources, and provides a link between mineralization and these magmatic systems (especially the Windowglass Hill Granite). These postulations also further strengthen the supposition that the Windowglass Hill Granite and the Windsor Point Group volcanism are inter-related.

#### 7.9 Conclusions

The electrum/base metal sulphide quartz vein lode deposits in the Cape Ray Fault Zone occur in two distinct horizons, viz.; a schist horizon (mainly graphitic but with chloritic and sericitic components), and the Windowglass Hill Granite. Both vein horizons are deformed (especially those in the schist) and thus formed in the late Devonian. The two vein zones are not directly linked, but geophysical evidence suggests a possible link to the south of the granite.

The ore metals are Au, Ag, Cu, Pb and Zn. Statistical analysis of the assays indicates a common correspondence and distribution for all five elements (Zn is the most



solitary). Discrimination function analysis shows that the schist-hosted and granite-hosted veins have identical assay distributions. When a series of trace elements were examined, there are apparently three main groupings of elements, viz.; a sulphide/chalcophile group, a silicate group, and a carbonate/clay group. Within the sulphide group there are discernible background and elevated (ie. ore grade) concentrations. Element enrichment factors resemble those found in auriferous massive sulphide-type deposits and are distinctly different from Archean lode gold deposits.

Background Au contents in the various lithologies are typically low and resemble reported abundances, except the Windowglass Hill Granite and surrounding country rocks which have slightly anomalous Au concentrations. Ag is highest in quartz-feldspar porphyry dykes of the Windsor Point Group that have associated syngenetic galena-bearing quartz veins.

The base metal sulphide minerals are mainly galena, sphalerite, chalcopyrite and pyrite with lesser arsenopyrite and rare pyrrhotite. Arsenopyrite doesn't occur in the granite-hosted veins and sphalerite is much less abundant in these veins also. Au and Ag occur together as electrum which is intergrown with all the other sulphides and is occasionally solitary. Temperatures of ore formation from mineral intergrowths and compositions (eg.

arsenopyrite) range from about 250 to 400° C, averaging around 300° C.

Sulphur isotope ratios suggest that the sulphur in the sulphides is of magmatic origin, and sulphur isotope geothermometers reveal temperatures of 200-250° C.

Lead isotope ratios are similar in galenas from the granite-hosted veins, the schist-hosted veins and from the quartz-feldspar porphyry dykes/meta-felsic tuffs of the Windsor Point Group. The ratios are of a mantle-type and have a regressed source age of  $\sim$  1.2 Ga. The only plausible source for such ratios would be Pb remobilized from Grenville material.

## CHAPTER 8

### CONCLUSIONS AND TECTONIC/METALLOGENIC MODELS

#### 8.1 Metallogeny of the Fault Zone

Most of the minor occurrences in the fault zone are epigenetic, except the galena in quartz-feldspar porphyry dykes and the coastal mylonite, pyrrhotite in amphibolites of the Port aux Basques Complex, and pyrite-chalcopyrite fractures in the Red Rocks Granite, which are all syngenetic (*ie.* are related to magmatic processes in their hosts). The Main Shear quartz veins are definitely epigenetic, but those in the Windowglass Hill Granite could be either syn- or epigenetic. The timing of the electrum-bearing quartz veining in this granite thus forms the most fundamental question to be answered.

These late Devonian lode deposits contain gold as electrum. The temperatures of formation are ~ 300°C with some evidence of higher temperature assemblages in the granite-hosted veins.

Based on the regional tectonic and lithologic framework for the Cape Ray Fault Zone, there are a number of genetic models, described elsewhere by others for lode gold deposits, which are applicable to the Main Shear and Windowglass Hill Showings. Unfortunately (since these

deposits are Devonian) most of these hypotheses refer to Archean lode gold deposits (Devonian lodes are not well known). The most pertinent of these models are:

(1) The ore fluids formed as a result of metamorphic outgassing (dehydration or degassing) during amphibolite facies metamorphism and subsequently the fluids moved to zones of lower metamorphic grade. The Au was supposedly present at background levels in the proto-amphibolitic rocks, but was preferentially partitioned into a fluid phase relative to the base metals (cf. Fyfe and Henley 1973; Kerrich and Fryer, 1979; Kerrich and Fyfe, 1981).

(2) The fault zone acted as a structural trap, or conduit, into which laterally secreted fluids, moving under a geochemical gradient and influenced by heat from a cooling granitoid body, passed through the surrounding country rock, dissolving minute amounts of background Au and ultimately precipitating the fluids and Au as veins in zones of dilation (cf. Boyle, 1961; Boyle, 1979).

(3) The cooling of magmas induced convection (ie. circulation) of ground waters through regional lithologies scavenging the ore metals and ultimately precipitating them as veins in favourable horizons. (cf. Radtke et al., 1980).

(4) The Windowglass Hill or Strawberry/Isle aux Morts Brook Granites, or the felsic volcanism of the Windsor Point Group directly contributed magmatic fluids

and metallic complexes from their magmas to the hydrothermal fluids, which may also have had some contributions from ground waters passing through regional lithologies (cf. Burnham and Ohmoto, 1980).

The possible role of the Strawberry/Isle aux Morts Brook Granites in the ore-forming process can be ruled out as the granites are post-tectonic, yet the deposits have undergone intense deformation. Conversely, fluids derived by metamorphic outgassing during amphibolite grade metamorphism of the Port aux Basques Complex are ruled out because this peak of metamorphism was reached prior to deposition of the Windsor Point Group (ie. the quartz vein hosts). Similarly the Cape Ray and Red Rocks Granites are too old to have provided magmatic fluids.

The mineralization is thus an intrinsic feature of the Windsor Point Group/Windowglass Hill Granite. This is further strengthened by the similar Pb isotopic signatures of galenas from the ore deposits and from acid volcanics of the Windsor Point Group (these galenas, in a quartz-feldspar porphyry dyke and mylonitized acid tuff, were magmatic products (ie. were syngenetic with the intrusion/extrusion of the hosting magmas)).

The enriched background Au and Ag contents in the Windowglass Hill Granite, and relatively enriched halo of background Au values in units surrounding this granite (ie. units which were intruded by offshoots of the granite or

veinlets from the granite), further indicates that the granite is related to the mineralization. Furthermore, although equivalent quartz-veined graphitic, chloritic and/or sericitic schists occur elsewhere in the fault zone, only those of the Main Shear (ie. in close proximity to the Windowglass Hill Granite) actually contain the Au-Ag base metal sulphide mineralization.

The role of the Windowglass Hill Granite in the ore-forming system is therefore significant, but the larger question is whether cooling of the granitic magma acted simply as a heat source (or pump) for circulating, leaching waters, or whether the resultant fluids and metallic components were produced as primary magmatic solutions emanating from the magma. A number of factors favour a magmatic origin for the fluids, such as:

(1) The Pb isotopes show a magmatic input (assuming the granite is a subvolcanic equivalent or phase of the Windsor Point Group volcanism).

(2) The sulphur isotopes, with low to nil fractionation, resemble those of magmatic sulphides. To derive these same sulphides from the surrounding regional lithologies by circulating ground waters implies total isotopic equilibrium was achieved between the leaching fluid and dissolving sulphides. Yet by their very natures, these fluids would remove only partial amounts of the available sulphide and partial removal would result in only

partial equilibrium and the resultant sulphur would be fractionated.

(3) As a crude approximation, based on Au/Ag ratios, the granite veins are of a higher temperature than the Main Shear veins. If the ore fluids were of magmatic derivation then the granite should have higher temperature veins than the peripheral veins.

(4) The Au, Ag and base metals are enriched to about the same degree in the veins. If these metals were derived by leaching country rocks, and the water/rock ratios were high, then the base metals should be favoured (due to their much greater abundances) for solvation, thus yielding a fluid greatly enriched in base metals relative to Au and Ag. In situations of low water/rock ratios (cf. Kerrich and Fryer, 1981), Au and Ag would be favoured (enriched) over the base metal sulphides. However the equivalent enrichments of all these elements implies a source in which the elements have a consistent ratio relative to average crustal rocks, and this would only occur within a melt (ie. in a melt all the elements would be incorporated totally and not relative to the vagaries of solution).

(5) The granite has undergone deuteric alteration that has albited the granite and altered its REE patterns. Though not directly relateable, the ore fluids and the deuteric fluids left similar chemical alteration signatures (ie. the deuteric fluids were late magmatic and

caused similar changes in granite chemistry as the ore fluids did to granite wall rocks to ore veins).

(6) Ag and Au occur together as electrum. Electrum is a typical ore mineral in Tertiary lode gold deposits (cf. Boyle, 1979) which are thought to be, at least in part, magmatic because they are associated with magmatic systems, eg. the Battle Mountain District, Idaho; Cortez and Carlin, Nevada (Roberts et al., 1971).

(7) On the basis of ore element enrichments and trace element contents, the quartz veins in the granite have a chemical signature more similar to that of their host (and thus magmatic source), than the Main Shear veins have to their hosts.

The common association of Au-bearing quartz veins and granitic rocks has long been noted (eg. Anhaeuser, 1976; Konstantinov, 1977; Kitaev, 1978; Boyle, 1979; Friske et al., 1979; Gorman et al., 1981; Studemeister et al., 1981; Hodgson, 1983; Marmont, 1983), but has also been the subject of controversy as to whether the granitic systems actually contributed metals and fluids to the ore-forming system, or acted simply as a heat pump. In the case of most Precambrian (primarily Archean) deposits, the weight of accumulated evidence suggests that granites only provided the heat (eg. Boyle, 1979; Marmont, 1983; Kerrich, 1983b; etc.). In Phanerozoic deposits, granitic hosts are likewise usually described as heat engines (eg.



Dickson et al., 1979, Radtke et al., 1980). However, in a large number, various authors have also found evidence of magmatic fluid/metal involvement from isotopic, geochemical and/or fluid inclusion data (eg. Guha et al., 1979; O'Neil and Bailey, 1979; Sawkins et al., 1979; Norman and Landis, 1980).

At the other extreme, granites within some deposits have been described as the ultimate source of the metalliferous hydrothermal fluids. Mantei and Brownlow (1967) studied the Marysville quartz diorite stock of Montana which has several peripheral lode gold deposits, and found that these deposits were formed from late-stage magmatic fluids. Richter (1970) described Au-bearing quartz veins in granodiorite dykes and host greywackes of the Nuka Bay area Alaska, that he states were formed by magmatic solutions from an underlying granite. Anhaeusser (1976), in a review of gold mineralization in southern Africa, suggested some deposits may result from epithermal fluids generated by granitic magmas. Glasson and Keays (1978) examined the concentrations and distributions of Au and base metals in metasedimentary rocks of the auriferous Slate Belt of Victoria, Australia. On the basis of mass balance calculations, these authors determined that the hydrothermal fluids which deposited saddle-reef type gold deposits in the area were derived by partial melting of metasedimentary rocks. Young (1979), describing

electrum-bearing quartz veins of the Granite District, Oregon, which occur in both granodiorite and hosting metamorphic rocks, defined the hydrothermal ore fluids as magmatic. Sillitoe (1979) depicted Au in porphyry copper systems as a component of magmatic fluids.

Boyle (1979) argues against the possible role of granitic magmas contributing either fluids and/or metallic components to the ore-forming systems of epithermal gold deposits, mainly based on empirical evidence (cf. Tilling et al., 1973) that gold is not concentrated in the more felsic portions of composite petrogenetic suites. Burnham and Ohmoto (1980) have shown, however, that second boiling of a granitic magma (ie volatile separation during ascent) can produce an aqueous phase separate from the magma, into which base metals, Au, Ag, S and Cl are preferentially partitioned.

According to Burnham and Ohmoto (1980) the 'boiling off' of these late stage fluids could conceivably raise the pressures sufficiently in the magmatic system to fracture surrounding country rock and produce pathways for the fluids to flow along and zones for their precipitation (ie. forming lode deposits). Also in their model the fluids would cause potassic alteration of country rock.

Burnham and Ohmoto (1980) suggest that the metallic components in an evolved aqueous vapour phase would be transported as Cl- complexes. However experimental work on

gold complexing has indicated that  $\text{Cl}^-$  complexes are significant only at higher temperatures (eg. Weissberg, 1970; Rytuba and Dickson, 1974; Letnikov *et al.*, 1975; Romberger, 1982). A more likely complexing candidate at  $< 300^\circ\text{C}$  would be thiosulphide (eg. Seward, 1973; Rytuba and Dickson, 1974; Letnikov *et al.*, 1975). Romberger (1982; and 1983 pers. com.) suggests that bisulphide may also be important. The fact that Au may be complexed by a sulphur species does not rule out Burnham and Ohmoto's modelling because they also note the widespread presence of such ions in magmatic vapour phases.

This magmatic model is directly applicable to the Cape Ray Deposits. The Windowglass Hill Granite appears to be the source of the hydrothermal fluids (as shown by the isotopic evidence *etc.*). Volume/density relationships show that the alteration superimposed on schist wall rocks to ore veins was potassic. The Main Shear veins dip toward the granite and thus look like an offshoot from the granite locus. The REE data indicate LREE depletions in the vicinity of the ore veins and if the empirical evidence is correct (*cf.* Taylor and Fryer, 1982), then the LREE's are preferentially complexed by  $\text{Cl}^-$  ions. Consequently removal of LREE's from the host rocks implies complexing by  $\text{Cl}^-$  ions (rather than  $\text{F}^-$  or  $\text{CO}_3^{2-}$ ) from the hydrothermal fluids. If these fluids carried the metals as  $\text{Cl}^-$  complexes and then conditions were suitable for their precipitation, the

Cl<sup>-</sup> ions remaining in solution would be out of equilibrium with the enclosing rocks and could leach and complex LREE's. However the role of ionic sulphur (eg. thiosulphide) species in transport and/or complexing of REE's is at present unknown. If the Au was transported as thiosulphide (HS<sup>-</sup>) complexes (cf. Seward, 1973) then when precipitation occurred, the H<sup>+</sup> ion concentration in the fluids would be increased, producing a concomitant increase in Cl<sup>-</sup> activity. To buffer this increased acidity the extra Cl<sup>-</sup> could complex the LREE's and remove them from the system.

#### 8.1.1 Metallogenic Conclusions

To sum up the metallogenic conclusions; the Windowglass Hill Granite, derived by partial melting of deeper-seated Grenvillian basement gneiss, evolved an aqueous phase during ascent to its present level of exposure. Base metals (ie. Cu, Pb, Zn, As, etc.), S, Cl, Ag and Au were partitioned into this aqueous phase. The evolution of this fluid phase through second boiling may have raised the internal pressure within the cooling magma and country rocks, shattering ductile (or weaker) horizons, such as the graphitic schists of the Windsor Point Group, to produce zones of dilatency into which the fluids could flow and precipitate their metallic components. It appears

that the graphite schists offered mainly a structural trap for the fluids rather than a chemical one, as chloritic and sericitic schists also host minor veins. The reason for the precipitation is probably a lowering of temperature or pressure as described in the experimental results of various authors (eg. Rytuba and Dickson, 1974; Romberger, 1982).

### 8.2 Tectonic Model

To develop a holistic model for tectonic evolution of the Cape Ray Fault Zone, each of the disparate threads of petrological, geochronological, structural, metamorphic and geochemical evidence as described above must now be woven together. Once this framework has been erected, the metallogeny, which is both an intrinsic result of, and participant in, the evolutionary cycle of this area, can also be placed in perspective. The best means of model design is to describe and interpret each of the different lithologies in a chronological order.

The oldest possible rocks in this region would be remnants of Grenvillian continental crust. As described in this study, there are no visible examples of this basement complex, at the current level of erosion, anywhere in the Cape Ray Fault Zone. Those rocks which were previously interpreted as such have been shown to be Paleozoic

tonalites.

The oldest rocks present in this area then are the ophiolitic remnants of the Long Range Mafic/Ultramafic Complex. These isolated fragments are relicts from the ocean crust and mantle of the Ordovician Iapetus Ocean. Based on the best ages available available for correlative ophiolites (eg. Dunning et al., 1982) these metagabbros are about 480 Ma. Although the allocthonous natures of other ophiolitic terranes in western Newfoundland are readily demonstrable, no such evidence (ie. thrust fault contacts etc.) is visible for the Long Range Mafic/Ultramafic Complex, and on the basis of structural/intrusive relationships, the complex appears to be autocthonous. The portions of this complex mapped for this project are solely metagabbros having no relict cumulate textures and there are no superimposed structural fabrics. Metamorphism is of the greenschist facies, but is dominantly a result of ocean floor/seawater metasomatic interactions (eg. pyroxenes altered to amphibole).

Presumably the next oldest lithology (or possibly contemporaneous with the ophiolitic remnants), is the gneiss unit of the Port aux Basques Complex. This unit consists of paragneiss (though possibly derived from felsic pyroclastic protoliths) and abundant amphibolite bands. These interbands were derived from a mafic volcanic protolith that seems to most resemble basalts of an island

arc environment. Modelling the genetic environment of the leucocratic portions of the gneiss is more difficult than for the amphibolites. The closest approximation in terms of classical plate tectonic models would be some sort of large basin in a tectonically active island arc terrane (eg. a back arc basin). The overwhelming felsic nature of this unit (despite the amphibolite interbands) suggests the involvement of continental crust either as the source of detritus for the basin, as the source for felsic partial melts which produced acid volcanism in the basin, or a combination of the two. The age of this metamorphic complex is not known precisely but if it was involved with island arc tectonics (or the like) of the Iapetus Ocean, then its age could range from mid-Ordovician to Silurian.

The Bay du Nord/La Poile Groups have been modelled as being of island arc derivation, although they are predominantly the products of felsic volcanism. Chorlton (1980b, 1982) has described the Port aux Basques Complex as a distal portion of these same groups and thus she has defined this complex to be a result of island arc volcanism (with no continental crust involvement). However, the chemical composition of the Port aux Basques Gneiss, as described in this study, is different from those of the Bay du Nord/La Poile Groups (as defined by Chorlton 1980b), and therefore their correlation is suspect.

Both current and genetic inter-relationships between

the Long Range Mafic/Ultramafic and Port aux Basques Complexes are nowhere visible. Since the ophiolitic fragments represent remnants of a more complete ocean floor terrane, the gneiss complex, as a back arc-type basin, would of necessity pass laterally into such ocean floor material. The actual nature of this transition is impossible to determine as it could mark an island arc subduction zone, an ocean ridge environment, or the gneisses could even be construed as a microcontinent completely enclosed in ocean crust. In terms of Williams and Hatcher's (1982) terminology this gneiss complex would be a "suspect terrane" and as such it would represent a lithological package from elsewhere plastered unto remnant, telescoped oceanic crust.

The gneiss complex was affected by intense metamorphic/structural tectonism which produced the earliest defineable fabrics in the fault zone, but which were also coplanar to the later deformations which affected all units. Since the resolved principal stress orientations for these later deformations indicate a stress regime of NE/SW-directed compression, the earlier co-planar deformation in the gneiss must have had compression from about the same direction. The coincident metamorphism was of such high temperature and pressure, that it caused partial melting of the gneisses, yielding the synkinematic Port aux Basques Granite. The bulls-eye intrusive pattern



and foliated nature of this granite indicate that the deformation continued after melt production and emplacement. This metamorphic/structural event was probably Acadian (or Late Silurian), but radiometric age dating of this granite could yield a more exact age of deformation.

The ophiolitic terrane also underwent a partial melting episode, much more intense than that of the gneiss, which resulted in the scattered, remnant status of this terrane. The resulting magma is represented by the voluminous tonalites of the Cape Ray Granite. The megacrystic Cape Ray Granite and more leucocratic Red Rocks Granite resulted from crystal fractionation in and crustal contamination of, the tonalitic magma, and the three granitoids form distinct differentiation trends on most chemical variation diagrams. Lithological and geochemical evidence suggest the tonalite was totally derived by partial melting of only the ophiolite, but the geochemistry of the Red Rocks Granite suggests that continental crust was involved in at least the final stages of magma generation.

An oceanic geotherm is not exceeded in normal circumstances, hence derivation of the tonalites involved some mechanism for surpassing, or lowering, solidus temperatures. Crustal thickening by thrusting, or obduction, could provide such a mechanism and is plausible

in this area as even larger scale movements are postulated for other western Newfoundland ophiolites. The felsic nature of the Red Rocks Granite indicates that if the ophiolite layer were allochthonous it may be underplated by continental crust.

If the Port aux Basques Complex formed in an oceanic basin somehow interconnected with the ophiolite horizon, then it would similarly be allochthonous. The postulated general NE/SW-directed compression which deformed the gneiss unit is consistent with thrusting of a complete ocean floor-basin facies sequence. In fact the elevated P-T conditions predicated by such intense tectonic movements, can account for the migmatization and high grade metamorphism superimposed on this unit.

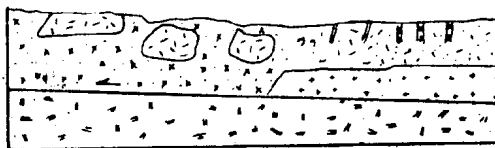
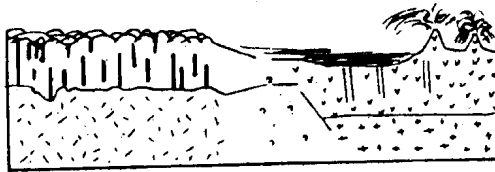
The initial lithological relations of this area are shown in Figure 79a, and the overplating/obduction episode is schematically illustrated in Figure 79b. The most important aspect of this model is that the ophiolite and gneiss complex (basinal material) form a complete allochthonous plate.

The actual contact of between the tonalite-engulfed ocean floor layer and the basin-derived gneiss complex represented a zone of tectonic weakness and the continued (or re-initiated) compression directed from the SW/NE produced the proto-Cape Ray Fault. In most aspects this fault appears to have been a normal fault with the

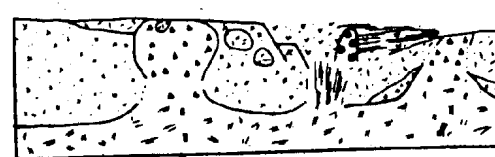
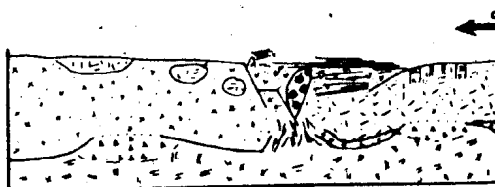
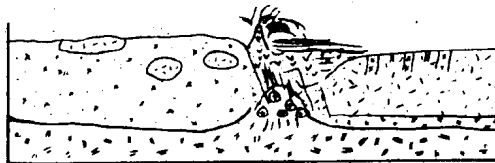
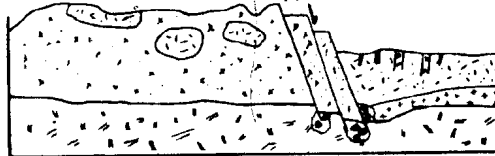
Figure 79 Schematic diagram showing the tectonic evolution of the Cape Ray Fault Zone. The units are: 1 = Grenvillian continental crust; 2 = continental crust of unknown age and/or affinity (possibly Avalonian); 3 to 5 are part of an ophiolite sequence; 3 = the cumulate/plutonic (gabbroic) portions; 4 = sheeted dykes; 5 = pillow lavas; 6 = felsic volcanic and volcanoclastic rocks that were the protoliths of the Port aux Basques Gneiss; 7 = proto-amphibolite interbands (meta-mafic intrusives) of the Port aux Basques Gneiss; 8 = tonalitic Cape Ray Granite; 9 = Port aux Basques Gneiss; 10 = Port aux Basques Granite; 11 = melts incipient to tectonism (normal faulting); 12 = volcanic and associated volcanoclastic and sedimentary rocks of the Windsor Point Group; 13 = Windowglass Hill Granite; 14 = Strawberry/Isle aux Morts Brook Granites. In diagram (A), the ophiolite complex and proto-Port aux Basques Complex are shown with unknown/indecipherable contact relations. The felsic nature of the Port aux Basques meta-volcanics indicates that they were underlain by continental crust. In diagram (B), partial melting of the ophiolite layer produced voluminous tonalitic melts and the xenolithic, remnant status of the ophiolite, at approximately the same time deformation produced the Port aux Basques Gneiss and migmatitic granite. This melting/deformation episode resulted from thrusting of the complete package of

ophiolite-felsic volcanic unto the Grenvillian crust. In diagram (C), thrust faulting has thrown up the ophiolitic side, and melting has commenced in the basal regions of these faults. The faults were initiated along structural weakness between the two terranes (ie. their contact zone). In diagram (D), continental crust partial melts have reached the crustal surface along the normal fault system and have produced the felsic volcanism and associated sedimentary rocks of the Windsor Point Group. This volcanism/sedimentation was deposited mainly on the Port aux Basques Complex along with detritus from the tonalitic terrane. In diagram (E), volcanism of the Windsor Point Group is waning and the Windowglass Hill Granite was intruded into this group. The Main Shear and Windowglass Hill Showings were presumably formed at this time. NE-SW directed compression, probably a continuation of the same stress regime which produced the original thrusting, has deformed the region producing the three-phase deformational episode. The Windsor Point Group was also metamorphosed at this time by the very high, latent heat of the formerly deeper-seated Port aux Basques complex. Further, more extensive, melting of the basal Grenvillian basement also commenced. In diagram (F), the post-tectonic Strawberry/Isle aux Morts Brook Granites were finally intruded at crustal levels. Later reactivation of the stress regime resulted in faulting and brecciation in the complete zone.

\*\*\*\*\* End Caption Figure 79 \*\*\*\*\*



- 14
- 13
- 12
- 11
- 10
- 9
- 8
- 7
- 6
- 5
- 4
- 3
- 2
- 1



tonalite-ophiolite side upthrown (Figure 79c), producing a thin linear basin.

Windsor Point Group ignimbrites and mafic tuffs were erupted (Figure 79d) along the fault trace and into the basin in the late Devonian. Sedimentary detritus, including tonalitic fragments, were intermixed with the tuffs in this basin, producing the interfingering interbedded igneous-sedimentary nature of the basin-fill. There were some actual sedimentary environments present in the basin also, reflected by limestones and lagoonal-type muds (ie. the graphitic schists). The chemical and isotopic properties of the volcanic rocks indicate derivation as partial melts of underplating continental crust (ie. the ophiolite-gneiss layer must be underlain by continental crust).

The Windowglass Hill Granite was similarly derived by partial fusion of deeper-seated felsic material and appears to be a subvolcanic equivalent (or magma chamber) for the felsic volcanism of the Windsor Point Group (Figure 79e). As such the granite intruded some earlier deposited consanguinous material.

Hydrothermal fluids flowed from the underlying magmatic system into this tectonically active basin, and ultimately deposited gold/silver base metal sulphide-bearing quartz veins in both the granite and friable (thus permeable) country rocks. Very slightly

postdating (or maybe coeval with) these fluids, a three-phase deformational event overprinted all lithologies. This event was also controlled by NE/SW-ward directed compression. To separate this deformation sequence from that of the basin-forming stresses is probably incorrect as some deformation must have accompanied deposition of the Windsor Point Group (ie. rather than start and stop, the deformation was progressive and continuous).

The deformation sequences produced both the fabrics and mylonites in the basinal area and also extensively deformed the ore-bearing quartz veins. The overall nature of this deformation is that of a major shear zone with sinistral offset. In this aspect the basin is reminiscent of the much larger fault-induced Carboniferous Deer Lake (cf. Ware and Hyde 1979) and Codroy (Knight, 1983) basins. In both of these larger basins there is some evidence of Devonian felsic volcanic sequences (Hyde, 1983, pers. comm.; Knight, 1983, pers. comm.) at their bases. If these Carboniferous basins are indeed floored by similar Devonian material, then the Cape Ray Fault Zone may represent a failed basin (ie. one which did not grow sufficiently large for influx of voluminous Carboniferous sediments).

The metamorphic grade of the Windsor Point Group is upper greenschist with defineable isograds increasing in

grade to the southeast. The overall aspect of the metamorphic path was apparently isobaric with temperature increasing towards the Port aux Basques Complex. The temperatures of metamorphism increase quite steeply towards the contact, and the metamorphic overprinting possibly results from latent heat in the more highly metamorphosed gneiss complex. Also, the Windsor Point Group in covering this complex could have acted as a thermal blanket, keeping in the heat to metamorphose the sediments and reheat/retrogress the gneiss.

Subsequent to the deformation and metamorphism, two plugs of granite (ie. the Strawberry and Isle aux Morts Brook Granites) intruded the fault zone (Figure 79f). Although not spatially interconnected, these two granites are petrographically, chemically and isotopically alike, and since they intrude either side of the fault zone, they indicate similar zones of origin beneath each terrane (ie. the same source rocks occur beneath the ophiolitic-tonalitic terrane and the felsic volcanic/sedimentary basin). Though these two granites were unaffected by the deformational episodes in the fault zone, their very presence indicates strong tectonic activity because the granitic magmas had to have been generated during the peaks of tectonism (see Figure 79e) and didn't reach their current level of exposure until such activity had ceased. Geochemically and petrographically



the granites resemble A-type (or anorogenic) granitoids that are thought to have been generated by partial melting of depleted granulites. This implies that there is continental crust at depth below the entire map area (possibly depleted due to generation of the Windsor Point Group felsic volcanics and the Windowglass Hill Granite). The only plausible candidate for this granulite is Grenville continental basement (or basement to proto-North American).

Subsequent to intrusion of the post-tectonic granites, the fault zone was reactivated producing brittle deformation, breccias of pre-existing lithologies, and the fault scarp of the present-day Cape Ray Fault.

### 8.3 Prospecting Implications

Though the Cape Ray Deposits appear to be unique in the Appalachians, and especially Newfoundland, in terms of host rocks, Au siting (ie. electrum), age and petrogenesis, this uniqueness seems to result from a lack of known occurrences, as the geological and structural characteristics of the environment for ore deposition are not atypical for the Appalachians. The fundamental prerequisites for the Cape Ray type lode gold/silver -base metal sulphide deposits are:

- (1) A zone of crustal thickening (preferably an

allochthonous terrane) underplated by felsic continental crust.

(2) Derivation of a very felsic granitoid by partial melting of the deeper-seated continental material, which would evolve a vapour/fluid phase upon ascent.

(3) A zone of structural weakness within such a terrane (ie. a major fault/shear zone like the Cape Ray Fault) which partial melts and fluids from the underplating continental crust could use as a pathway.

(4) A layered sequence with ductility contrasts between layers, such as that represented by the Windsor Point Group, into which mineralizing fluids could flow along friable, thus permeable, horizons away from the granitic magma.

ENDISPIECE

"I am standing on the threshold about to enter a room. It is a complicated business. In the first place, I must shove against an atmosphere pressing with a force of 14 pounds on every square inch of my body. I must make sure of landing on a plank travelling at 20 miles a second round the sun. A fraction of a second too early or too late, the plank would be miles away. I must do this whilst hanging from a round planet, head outward into space, and with a wind of ether blowing at no one knows how many miles a second through every interstice of my body. The plank has no solidity of substance. To step on it is like stepping on a swarm of flies. Shall I slip through? No. If I make the venture, one of the flies hits me and I get a boost up again. I fall again, and am knocked upwards by another fly, and so on. I may hope that the net result will be that I remain relatively steady. But if by chance I should slip through the floor, or be boosted too violently up to the ceiling, the occurrence would be not a violation of the laws of nature, but a rare coincidence. Verily, it is easier for a camel to pass through the eye of a needle than for a scientific man to pass through a door."

Sir A.S. Eddington, 1929  
from "The Nature of the Physical World"

# Bibliography

- Albuquerque, C. A. R. de, 1977. Geochemistry of the tonalitic and granitic rocks of the Nova Scotia southern plutons. *Geochim. Cosmo. Acta*, v. 41, pp. 1-13.
- Amit, O., 1976. Retrograde zoning in garnets of Elat-Wadi Magrish metamorphic rocks. *Lithos*, v. 9, pp. 259-262.
- Anhaeusser, C. R., 1976. Archean metallogeny in southern Africa. *Econ. Geol.*, v. 71, pp. 16-43.
- Anhaeusser, C. R., Fritze, K., Fyfe, W. S., and Gill, R. C. O., 1975. Gold in "Primitive" Archean volcanics. *Chem. Geol.*, v. 16, pp. 129-135.
- Anon, 1980. Geochronology report - Newfoundland and Labrador. Nfld. Dept. of Mines and Energy Rept. 80-1, Current Res., pp. 143-146.
- Anon, 1981. Basaltic volcanism study project: Basaltic volcanism on the terrestrial planets. Pergamon Press Inc. New York, 1206 p.
- Arth, J. G., 1979. Some trace elements in trondhjemites - their implications to magma genesis and paleotectonic setting. in *Trondhjemites, Dacites, and Related Rocks*, ed Barker, F., Elsevier Sci. Pub. Co., New York, pp. 123-132.
- Arth, J. G., and Hanson, G. N., 1972. Quartz diorites derived by partial melting of eclogite or amphibolite at mantle depths. *Can. Min. Pet.*, v. 37, pp. 161-174.
- Arth, J. G., and Hanson, G. N., 1975. Geochemistry and origin of the early Precambrian crust of northeastern Minnesota. *Geochim. Cosmo. Acta*, v. 39, pp. 325-362.
- Arth, J. G., Barker, F., Peterman, Z. E., and Friedman, I., 1978. Geochemistry of the gabbro-diorite-tonalite-trondhjemite suite of southwest Finland and its implications for the origin of tonalitic and trondhjemitic magmas. *J. Pet.*, v. 19, pp. 289-316.
- Ashley, R. P., and Keith, W. J., 1976. Distribution of gold and other metals in silicified rocks of the Goldfield Mining District, Nevada. USGS Prof. Pap. 843-B, 17p.
- Atherton, M. P., 1968. The variation in garnet, biotite, and chlorite composition in medium grade pelitic rocks from the Dalradian, Scotland, with particular reference to the zonation in garnet. *Can. Min. and Pet.*, v. 18, pp. 347-371.
- Babcock, R. S., 1973. Computational models of metasomatic processes. *Lithos*, v. 6, pp. 279-290.

- Bacon, C. R., MacDonald, R., Smith, R. L., and Baedeker, P. A., 1981. Pleistocene high silica rhyolites of the Coso Volcanic Field, Inyo County, California. *Jour. of Geophysical Res.*, v.86, pp. 10223-10241.
- Barker, D. S., 1970. Composition of granophyre, myrmekite, and graphic granite. *Geol. Soc. Am. Bull.*, v.81, pp. 3339-3350.
- Barker, F., 1979. Trondhjemite: Definition, environment and hypotheses of origin. *in* Trondhjemites, Dacites and Related Rocks, ed. Barker, F., Elsevier Sci., Pub. Co., New York, pp. 1-12.
- Barker, F., and Arth, J. G., 1976. Generation of trondhjemitic-tonalitic liquids and Archean bimodal trondhjemite-basalt suites. *Geology*, v. 4, pp. 596-600.
- Barker, F., Arth, J. G., Peterman, Z. E., and Friedman, I., 1976. The 1.7 to 1.8 b.y. - old trondhjemites of southwestern Colorado and northern New Mexico. *Geochemistry and depths of genesis. Geol. Soc. Am. Bull.*, v. 87, pp. 189-198.
- Barth, T. F. M., 1961. A final proposal for calculating the mesonorm of metamorphic rocks. *J. Geol.*, v. 70, pp. 497-498.
- Barton, M. D., 1980. The Ag-Au-S system. *Econ. Geol.*, v.75, pp. 303-316.
- Barton, P. B. Jr., Skinner, B. J., 1979. Sulphide Mineral stabilities. *in* Geochemistry of hydrothermal ore deposits, ed. Barnes, H. L., John Wiley and Sons, Toronto, pp. 278-403.
- Bell, T. H., 1978. Progressive deformation and reorientation of fold axes in a ductile mylonite zone: The Woodroffe Thrust. *Tectonophysics*, v. 44, pp. 205-320.
- Bell, T. H., and Etheridge, M. A., 1973. Microstructure of mylonites and their descriptive terminology. *Lithos*, v. 6, pp. 337-348.
- Berthe, D., Choukroune, P., and Jegouzo, P. 1979. Orthogneiss, mylonite and non-coaxial deformation of granites: The example of the South American Shear zone. *Jour. of Struct. Geol.*, v. 1, pp. 31-42.
- Birk, D., 1973. Chemical zoning in garnets of the Kashabowie Group, Shebandowan, Ontario. *Can. Min.*, v. 12, pp. 124-128.
- Black, P. M., 1973. Mineralogy of New Caledonian Metamorphic Rocks. *Con. Min. and Pet.* v. 38, pp. 221-235.
- Blackwood, R. F., 1978. Northeastern Gander Zone, Newfoundland. *Nfld. Dept. of Mines and Energy, Rept. 78-1, Report of Act.*, pp. 72-79.

- Blackwood, R. F., and Kennedy, M. J., 1975. The Dover Fault: Western boundary of the Avalon Zone in northeastern Newfoundland. *Can. Journal. of Earth Sciences.*, v. 12, pp. 320-325.
- Bottinga, Y., and Allegre, C.J., 1978. Partial melting under spreading ridges. *R. Soc. Lon. Philos. Trans., Ser. A*, v. 288, pp. 501-525.
- Boyle, R. W., 1961. The geology, geochemistry and origin of the gold deposits of the Yellowknife District. *G. S. C. Mem.* 310, 193 p.
- Boyle, R. W., 1968. The geochemistry of silver and its deposits. *Geol. Surv. Can. Bull.* 160, 264 p.
- Boyle, R. W., 1979. The geochemistry of gold and its deposits. *Geol. Surv. of Can. Bull.* 280, 584 p.
- Brett, R., and Kullerud, G., 1967. The Fe-Pb-S system. *Econ. Geol.*, v. 62, pp. 354-369.
- Brookes, I. A., 1977. Geomorphology and Quaternary geology of Codroy Lowland and adjacent plateaus, southeast Newfoundland. *Can. Jour. of Earth Sci.*, v. 14; pp. 2101-2120.
- Brooks, C., 1980. The Rb/Sr geochronology of the Archean Chibougamu pluton, Quebec. *Can. Jour. Earth Sci.*, v. 17, pp. 776-783.
- Brooks, C., Hart, S. R., and Wendt, I., 1972. Realistic use of two-error regression treatments as applied to rubidium-strontium data. *Rev. Geophy. and Space Phy.*, v. 10, pp. 551-577.
- Brown, P. A., 1973. Structural and Metamorphic history of the gneisses of the Port aux Basques Region, Newfoundland. Unpub. MSc. thesis, Memorial University of Newfoundland. 113 p.
- Brown, P. A., 1973b. Possible cryptic suture in southwestern Newfoundland. *Nature Phys. Sci.*, v. 245, pp. 9-10.
- Brown, P. A., 1975. Basement-cover relationships in southwest Newfoundland. Unpub. Ph.D. Thesis Memorial University of Newfoundland, 221 p.
- Brown, P. A., 1976a. Geology of the Rose Blanche Map area (110/10) Newfoundland. *Nfld. Dept. of Mines and Energy, Rept.* 76-5, 16 p.
- Brown, P. A., 1976b. Ophiolites in southwestern Newfoundland. *Nature* v. 264, p. 712-715.
- Brown, P. A., 1977. Geology of the Port aux Basques Map area (110/10) Newfoundland. *Nfld. Dept. of Mines and Energy Rept.* 77-2, 11 p.
- Brown, P. A., and Colman-Sadd, S. P., 1976. Hermitage flexure: Fictitious or fact. *Geology*, v.4, pp. 561-564.
- Bryant, B., and Reed, J. C. Jr., 1969. Significance of lineation and minor folds near major thrust faults in the southern Appalachians and the British and Norwegian Caledonides. *Geol. Mag.*, v. 106, pp. 412-429.

- Buddington, A. F., 1959. Granite emplacement with special reference to North America. *Geol. Soc. Am. Bull.*, v. 70, pp. 671-747.
- Burg, J. P., and Laurent, Ph., 1978. Strain analysis of a shear zone in a granodiorite. *Tectonophysics*, v. 47, pp. 15-42.
- Burg, J. P., Iglesias, M., Laurent, Ph., Matte, Ph., and Ribeiro, A., 1981. Variscan intracontinental deformation: the Coimbra-Cordoba shear zone (SW Iberian Peninsula). *Tectonophysics*, v. 78, pp. 161-177.
- Burnham, C. W., and Ohmoto, H., 1980. Late-stage processes of felsic magmatism. *Min. Geol. Spec. Iss.*, No. 8, pp. 1-12.
- Cameron, K. L., and Hanson, G. N., 1982. Rare earth element evidence concerning the origin of voluminous mid Tertiary rhyolitic ignimbrites and related rocks, Sierra Madre Occidental, Chihuahua, Mexico. *Geochim. Cosmo. Acta*, v. 46, pp. 1489-1503.
- Carpenter, R. H., 1974. Pyrrhotite isograd in southeastern Tennessee and southwestern North Carolina. *Geol. Soc. Am. Bull.*, v. 85, pp. 451-456.
- Chappell, B. W., and White, A. J. R., 1974. Two contrasting granite types. *Pac. Geol.*, v. 8, pp. 173-174.
- Chorlton, L. B., 1978a. LaPoile Project, southwestern Newfoundland. in *Nfld. Dept. of Mines and Energy, Rept. 78-1, Rept. of Act. for 1977*, pp. 85-89.
- Chorlton, L. B., 1978b. The geology of the LaPoile map area (110/9), Newfoundland. *Nfld. Dept. of Mines & Energy, Rept. 78-5*, 14p.
- Chorlton, L. B., 1979. LaPoile River map area (110/16), Newfoundland. in *Nfld. Dept. of Mines and Energy, Rept. 79-1, Rept. of Act. for 1978*, pp. 45-53.
- Chorlton, L. B., 1980a. Grandy's Lake, west half. in *Nfld. Dept. of Mines and Energy, Rept. 80-1, Current Research*, pp. 74-78.
- Chorlton, L. B., 1980b. Geology of the LaPoile River area (110/16), Newfoundland. *Nfld. Dept. of Mines and Energy, Rept. 80-3*, 86p.
- Chorlton, L. B., 1980c. Peter Snout, west half. in *Nfld. Dept. of Mines and Energy, Rept. 80-1, Current Research*, pp. 62-73.
- Chorlton, L. B., 1982. General geology and regional significance of the Grandy's Lake area (110/15), Newfoundland, *Nfld. Dept. of Mines and Energy, Rept. 82-1, Current Research*, pp. 65-77.
- Chorlton, L. B., in prep. Geological Development of the southern Long Range Mountains, southwest Newfoundland. A regional synthesis. Ph.D. thesis, Memorial University of Newfoundland.
- Chorlton, L. B., and Dingwell, D. B., 1981. Grandy's Lake (110/15), Newfoundland. *Nfld. Dept. of Mines and Energy Rept. 81-1, Current Research*, pp. 57-69.

- Churchill, R. K., Landis, G. P., and Sawkins, F. J., 1980.  $^{18}\text{O}$  and precious metal data from rocks underlying the Tayoltita Au/Ag deposit, Mexico: - Implications for ore genesis. GSA Abst. with prog., v. 12, p. 403.
- Cobbold, P. R., 1977. Description and origin of banded deformation structure II. Rheology and the growth of banded perturbations. Can. Jour. Earth Sci., v. 14, pp. 2510-2523.
- Coleman, R. G., and Peterman, Z. E., 1975. Oceanic Plagiogranite. J. Geophys. Res., v. 80, pp. 1099-1108.
- Coleman-Sadd, S. P., 1980. Geology of south-central Newfoundland and evolution of the eastern margin of the Iapetus. Am. Jour. of Sci. v. 280, pp. 991-1017.
- Collerson, K. D. and Bridgewater, O., 1979. Metamorphic development of early Archean tonalitic and trondhjemitic gneisses: Saglék area, Labrador. in Trondhjemites, dacites and related rocks, ed Barker, F., Elsevier Sci. Pub. Co. New York. pp. 205-274.
- Collins, W. J., Beams, S. O., White, A. J. R., and Chappell, B. W., 1982. Nature and origin of A-type granites with particular reference to southeastern Australia. Con. Min. Pet., v. 80, pp. 189-200.
- Condie, K. C., 1978. Geochemistry of proterozoic granitic plutons from New Mexico, U.S.A. Chem. Geol., v. 21, pp. 131-149.
- Condie, K. C., Allen, P., and Narayana, B. L., 1982. Geochemistry of the Archean low to high-grade transition zone, Southern India. Con. Min. and Pet., v. 81, pp. 157-167.
- Condie, K. C., and Hunter, D. R., 1976. Trace element geochemistry of Archean granitic rocks from the Barberton Region, South Africa. Earth and Plan. Sci. Lett., v. 29, pp. 309-400.
- Connan, J. and Cassou, A. M., 1980. Properties of gases and petroleum liquids derived from terrestrial kerogen at various maturation levels. Geochem. et Cosmo. Acta, v. 44, pp. 1-23.
- Cooper, J. R., 1954. LaPoile-Cinq Cerf map area, Newfoundland. Geol. Surv. Can. Mem. 276, 62 p.
- Cosgrove, M. E., 1973. The geochemistry and mineralogy of the Permian red beds of southwest England. Chem. Geol., v. 11, pp. 31-47.
- Coward, M. P., Jan, M. Q., Rex, D., Tarney, J., Thirlwall, M., and Windley, B. F., 1982. Structural evolution of a crustal section in the western Himalaya. Nature, v. 295, pp. 22-24.
- Cullers, R. L., Yeh, L. T., Chaudhuri, S., and Guidotti, C. V., 1974. Rare earth elements in Silurian pelitic schists from N.W. Maine, Geochem. et Cosmo. Acta, v. 38, pp. 389-400.
- Cumming, G. L., and Richards, J. R., 1975. Ore lead isotope ratios in a continuously changing earth. Earth Plan. Sci. Lett., v. 28, pp. 155-171.



- Czamanske, G. K., and Rye, R. O., 1974. Experimentally determined sulphur isotope fractionations between sphalerite and galena in the temperature range 600 to 275°C. *Econ. Geol.*, v. 69, pp. 17-25.
- Daveltov, I. K., 1970. Average gold content in essential minerals of intrusive rocks. *Dok. Earth Sci. Sec.* v. 190, pp. 215-217.
- Daveltov, I. K., and Dzhakshibayev, S., 1970. The mineral balance and behaviour of gold during emplacement of an intrusive body. *Geochem. Int.*, v. 7, pp. 997-1005.
- Dickson, F. W., Rye, R. O., and Radtke, A. S., 1979. The Carlin gold deposit as a product of water-rock interactions. *in* Papers on Mineral Deposits of Western North American, *ed.* J. D. Ridge, *Nev. Bur. of Mines and Geol. Rept.* 33, pp. 101-108.
- Didier, J., 1973. *Granites and their Enclaves.*, Elsevier Sci. Pub. Co., Amsterdam. 393 p.
- Dingwell, D. B., 1980. The Geology, Geophysics and Geochemistry of the Port aux Basques Granite., Unpub. Hons. thesis, Memorial University of Newfoundland, 126 p.
- Doe, B. R., 1970. Lead isotopes. Springer-Verlag, Berlin. 137 p.
- Doe, B. R., and Delevaux, M. H., 1973. Variations in lead-isotopic composition in Mesozoic granitic rocks of California: a preliminary investigation. *Geol. Soc. Am. Bull.*, v. 84, pp. 3513-3526.
- Doe, B. R., and Zartman, R. E., 1979. Plumbotectonics, the Phanerozoic. *in* Geochemistry of hydrothermal ore deposits. *ed.* Barnes, H. L., John Wiley and Sons, Toronto. pp. 22-70.
- Dostal, J., Dupuy, C., and Keppie, J. D., 1983. Uranium and thorium in Paleozoic rhyolites of Nova Scotia. *Can. Jour. Earth Sci.*, v. 20, pp. 266-274.
- Dostal, J., Elson, C., and Dupuy, C., 1979. Distribution of lead, silver and cadmium in some igneous rock and their constituent minerals. *Can. Min.*, v. 17, pp. 561-567.
- Dunning, G. R., 1981. The Annieopsquotch ophiolite belt, southwest Newfoundland. *in* Current Research, Part B, *Geol. Surv. Can. Pap.* 81-1B, pp. 11-15.
- Dunning, G. R., and Chorlton, L. B., 1983. Imbricated ophiolite and subduction related intrusions of southwestern Newfoundland. *GSA Abst. with Prog.*, v. 15, p. 188.
- Dunning, G. R., and Herd, R. K., 1980. The Annieopsquotch ophiolite complex, southwest Newfoundland, and its regional relationships. *in* Current Research Part A, *Geol. Surv. Can. Pap.* 80-1A, pp. 227-234.
- Dunning, G. R., and Krogh, T. E., 1983. Tightly clustered, precise U/Pb (zircon) ages of ophiolites from the Newfoundland Appalachians. *GSA Abst. with Prog.*, v. 15, p. 136.
- Dunning, G. R., Carter, P. J., and Best, M. A., 1982. Geology of Star Lake (west half), southwest Newfoundland. *in* Current Research, Part B, *Geol. Surv. Can. Pap.* 82-1B, pp. 21-26.

- Eales, H. V., 1961. Fineness of gold in some southern Rhodesian Mines. 517  
Trans. Inst. Min. and Met., v. 71, pp. 49-73.
- Elias, P., and Strong, D. F., 1982. Paleozoic granitoid plutonism of southern Newfoundland: contrasts in timing, tectonic setting and level of emplacement. Trans. Roy. Soc. Edinburgh; Earth Sci., v. 73, pp. 43-57.
- Elliot, J. E., and Wells, J. D., 1968. Anomalous concentrations of gold, silver and other metals in the Mill Canyon and Cortez Quadrangle, Eureka and Lander Counties, Nevada. USAS Circ. 606, 16 p.
- Ermanovics, I.F., and Froese, E., 1978. Metamorphism of the Superior Province in Manitoba, in Metamorphism in the Canadian Shield. Geol. Surv. Can. Pap. 78-10, pp. 17-24.
- Ewart, A., 1979. A review of the mineralogy and chemistry of Tertiary-Recent dacitic, latitic, rhyolitic, and related salic volcanic rocks. in Trondhjemites, dacites, and related rocks, ed Barker, F., Elsevier Sci. Pub. Co., New York, pp. 13-122.
- Faure, G., 1977. Principles of Isotope Geology. John Wiley and Sons Ltd., New York, 464 p.
- Ferry, J. M., 1981. Petrology of graphitic sulphide-rich schists from south-central Maine: an example of desulfidation during prograde regional metamorphism. Am. Min., v. 66, pp. 908-930.
- Ferry, J. M., 1982. A comparative geochemical study of pelitic schists and metamorphosed carbonate rocks from south-central Maine, USA. Can. Min. and Pet., v. 80, pp. 59-72.
- Figueiredo, B., Spicar, E., and Ekstrom, T., 1980. Exsolution mechanism of chalcopyrite in sphalerite. Geol. Foreningens I Stock. Forhand., v. 102, pp. 284-285.
- Fletcher, I. R., and Farquhar, R. M., 1982. The protocontinental nature and regional variability of the Central Metasedimentary Belt of the Grenville Province: Lead isotope evidence. Can. Jour. Earth Sci., v. 19, pp. 239-253.
- Floyd, P.A., 1977. Rare earth mobility and geochemical characterization of sphinitic rocks. Nature, v. 269, pp. 134-137.
- Flynn, R. T., and Burnham, C. W., 1978. An experimental determination of rare earth element partitioning coefficients between a chloride-containing vapour phase and silicate melts. Geochim. Cosmo. Acta, v. 42, pp. 685-701.
- Fourcade, S., and Allegre, C. J., 1981. Trace elements behaviour in granite genesis: a case study the calc-alkaline plutonic association from the Querigut Complex (Pyrenees, France). Can. Min. Pet., v. 76, pp. 177-195.
- Friske, P., Poulsen, K. M., and Franklin, J. M., 1979. The Beidelman Bay porphyry copper-gold occurrences, northwestern Ontario. GAC Abst. with prog., v. 4, pp. 51.

- Fyfe, W. S., and Henley, R. W., 1973. Some thoughts on chemical transport processes, with particular reference to gold. *Min. Sci. and Eng.*, v. 5, pp. 295-303.
- Gale, G.H., and Pearce, J. A., 1982. Geochemical patterns in Norwegian greenstones. *Can. Jour. Earth Sci.*, v. 19, pp. 385-397.
- Gapais, D., and LeCorre, C., 1980. Is the Hercynian Belt of Brittany a major shear zone? *Nature*, v. 288, pp. 574-575.
- Garrels, R. M., and Mackenzie, F. T., 1971. Evolution of sedimentary rocks. W. W. Norton and Co. Inc., New York. 397 p.
- Gasparrinig, C., 1983. The mineralogy of gold and its significance in metal extraction. *CIMM Bull.*, v. 76, pp. 144-153.
- Garrilehko, B. V., Goryainov, P. M., and Yerdomikov, B. N., 1976. Gold distribution in iron formations of the central part of the Kola Peninsula. *Dok. Akad. Nauk SSSR*, v. 231, pp. 29-31.
- Gillis, J. W., 1972. Geology of Port aux Basques Map-Area, Newfoundland. GSC Paper 71-42, 6 p.
- Glasson, M. J., and Keays, R. R., 1978. Gold mobilization during cleavage development in sedimentary rocks from the auriferous slate belt of central Victoria, Australia: Some important boundary conditions. *Econ. Geol.*, v. 73, pp. 496-511.
- Goldstein, A. G., 1982. Geometry and kinematics of ductile faulting in a portion of the Lake Char mylonite zone, Massachusetts and Connecticut. *Am. Jour. Sci.*, v. 282, pp. 1378-1405.
- Gorman, B. E., Kerrich, R., and Fyfe, W. S., 1981. Geochemistry and field relations of lode gold deposits in felsic igneous intrusions - Porphyries of the Timmins District. *Ont. Geol. Surv. Misc. Pap.* 98, pp. 108-124.
- Gottfried, D., Rowe, J. J., and Tilling, R. I., 1972. Distribution of gold in igneous rocks. *USGS Prof. Pap.* 727, 42 p.
- Graf, J. L., Skinner, B. J., Bras, J., Fagot, M., Levade, C., and Coudrec, J. J., 1981. Transmission electron microscope observation of plastic deformation in experimentally deformed pyrite. *Econ. Geol.*, v. 76, pp. 738-742.
- Grant, J. A., and Weiblen, P. W., 1971. Retrograde zoning in garnets near the second sillimanite isograd. *Am. Jour. of Sci.*, v. 270, pp. 281-296.
- Green, T. H., 1977. Garnet in silicic liquids and its possible use as a P-T indicator. *Can. Min. and Pet.*, v. 65, pp. 59-67.
- Gresens, R. L., 1967. Composition-volume relationships of metasomatism. *Chem. Geol.*, v. 2, pp. 47-65.
- Grocott, J., 1977. The relationship between Precambrian shear belts and modern fault systems. *Jl. Geol. Soc. Lon.*, v. 133, pp. 257-262.

- Guha, J., Leroy, J., and Guha, D., 1979. Significance of fluid phases associated with shear zone Cu-Au mineralization in the Dore Lake Complex, Chibougamau, Quebec. *Bull. Min.*, v. 102, pp. 569-576. 519
- Guidotti, C. V., 1974. Transition from staurolite to sillimanite zone, Rangeley Quadrangle, Maine. *Geol. Soc. Am. Bull.*, v. 85, pp. 475-490.
- Gureyev, V. F., Konstantinov, M. M., and Alysheva, E. I., 1968. Ratio of syngenetic (finely divided) and imposed gold in pyrite. *Dokl. Akad. Nauk SSSR*, v. 181, pp. 164-166.
- Haack, U., Hoefs, J., and Gohn, E., 1982. Constraints on the origin of Damaren granites by Rb/Sr and  $^{18}\text{O}$  data. *Con. Min. and Pet.*, v. 79, pp. 279-289.
- Hansen, E., 1971. *Strain Facies*. Springer-Verlag, New York, 207 p.
- Hanson, G.N., 1978. The application of trace elements to the petrogenesis of igneous rocks of granitic composition. *Earth and Plan. Sci. Lett.*, v. 38, pp. 26-43.
- Hanson, G. N., 1980. Rare earth elements in petrogenetic studies of igneous systems. *Ann. Rev. Earth Plan. Sci.*, v. 8, pp. 371-406.
- Harris, M., and Radtke, A. S., 1976. Statistical study of selected trace elements with reference to geology and genesis of the Carlin Gold Deposit, Nevada. *USGS. Prof. Pap.* 960, 21 p.
- Haskin, L. A., Frey, F. A., and Wildeman, T. R., 1968. Relative and absolute terrestrial abundances of the rare earths. *in* Origin and distribution of the elements, *ed.* Ahrens, L. H., *Int. Ser. Monogr. Earth Sci.*, v. 30, pp. 689-912.
- Henley, K. J., 1975. Gold-ore mineralogy and its relation to metallurgical treatment. *Min. Sci. Eng.*, v. 7, pp. 289-311.
- Henley, R. W., Norris, R. J., and Paterson, C. J., 1976. Multistage ore genesis in the New Zealand geosyncline-A history of post-metamorphic lode emplacement. *Min. Deposita*, v. 11, pp. 180-196.
- Herd, R. K., and Dunning, G. R., 1979. Geology of Puddle Pond map area, southwestern Newfoundland. *in* Current Research, Part A, *Geol. Surv. Can. Pap.* 79-1A, pp. 305-310.
- Higgins, M. W., 1971. *Cataclastic Rocks*, U. S. Geol. Surv. Pap. 607, 97 p.
- Higgins, N. C., and Kawachi, Y., 1977. Microcline megacrysts from the Green Lake Granodiorite, Eastern Fiordland, New Zealand; *N. Z. Jour. of Geol. and Geophys.*, v. 20, pp. 273-286.
- Hildreth, W., 1979. The Bishop Tuff: Evidence for the origin of compositional zonation in silicic magma chambers. *Geol. Soc. Am. Spec. Pap.* 180, pp. 43-79.
- Hildreth, W., 1981. Gradients in silicic magma chambers: Implications for lithospheric magmatism. *Jour. Geophys. Res.*, v. 86, pp. 10153-10192.
- Hine, R., Williams, I. S., Chappel, B. W., and White, A. J. R. 1978. Contrasts between I- and S- type granitoids of the Kosciusko batholith. *Jour. Geol. Soc. Aust.*, v. 25, pp. 219-234.

- Hirschberg, A., and Winkler, H. G. F., 1968. Stabilitätsbeziehungen zwischen chlorit, cordierit und almandin bei der metamorphose. *Con. Min and Pet.*, v. 18, pp. 17-42.
- Hirst, D. M., and Kaye, M. J., 1971. Factors controlling the mineralogy and geochemistry of an Upper Visean sedimentary sequence from Rockhope, County Durham. *Chem. Geol.*, v. 8, pp. 37-59.
- Hobbs, B. E., Means, W. D., and Williams, P. F., 1976. An outline of structural geology. John Wiley and Sons, Inc., Toronto, 571 p.
- Hodgson, C. J., 1983. Preliminary report on a computer file of gold deposits of the Abitibi Belt, Ontario. *Ont. Geol. Surv. Misc. Pap.* 110, pp. 11-37.
- Holdaway, M. J., 1971. Stability of andalusite and the aluminum silicate phase diagram. *Am. Jour. of Sci.*, v. 271, pp. 97-131.
- Holdaway, M. J., Guidotti, C. V., Novak, J. M., and Henry, W. E., 1982. Polymetamorphism in medium-to high-grade pelitic metamorphic rocks, west-central Maine. *Geol. Soc. Am. Bull.*, v. 93, pp. 572-584.
- Hollister, L. S., 1966. Garnet zoning: an interpretation based on the Rayleigh fractionation model. *Science*, v. 154, pp. 1647-1651.
- Honeggor, K., Dietrich, V., Frantz, W., Gansser, A., Thoni, M., and Trommsdorff, V., 1982. Magnetism and metamorphism in the Ladakh Himalayas (the Indus-Tsangpo suture zone), *Earth and Plan. Sci. Lett.*, v. 60, pp. 253-292.
- Hoschek, G., 1969. The stability of staurolite and chloritoid, and their significance in metamorphism of pelitic rocks. *Con. Min. and Pet.*, v. 22, pp. 208-232.
- Hsu, L. C., 1968. Selected phase relationships in the system Al-Mn-Fe-Si-O-H: A model for garnet equilibria. *Jour. of Pet.*, v. 9, pp. 40-83.
- Hutchison, M. N., and Scott, S. D., 1981. Sphalerite geobarometry in the Cu-Fe-Zn-S system. *Econ. Geol.*, v. 76, pp. 143-153.
- Hyde, R. S., and Ware, M. J., 1980. Geology of Carboniferous strata in the Cormack (12H/6) and Silver Mountain (12H/11) map areas in Nfld. Dept. of Mines and Energy, Rept. 80-1, Current Research, pp. 29-36.
- Irvine, T. N., and Baragar, W. R. A., 1971. A guide to the chemical classification of the common volcanic rocks. *Can. Jour. of Earth Sci.*, v. 8, pp. 524-528.
- Ivensen, Y. P., Amuzinskiy, V. A., Korobitsyn, A. V., Kukhtinsky, G. C., and Trunilina, V. A., 1974. Gold distribution in igneous rocks. *Dok. Akad. Nauk SSSR*, J. 216, pp. 242-244.
- Jager, E., 1979. The Rb/Sr method. In *Lectures in Isotope Geology* ed by Jager, E., and Hunziker, J. C., Springer-Verlag, New York, pp. 13-26.

- James, R. S., and Hamilton, D. L., 1969. Phase relations in the system  $\text{NaAlSi}_3\text{O}_8$  -  $\text{KAlSi}_3\text{O}_8$  -  $\text{CaAl}_2\text{Si}_2\text{O}_8$  -  $\text{SiO}_2$  at 1 kilobar water vapour pressure. *Con. Min., and Pet.*, v. 21, pp. 111-141.
- Jones, R. S., 1969. Gold in igneous, sedimentary and metamorphic rocks. *USGS Circ.* 610, 28 p.
- Jones, R. S., and Fleischer, M., 1969. Gold in minerals and the composition of native gold. *USAS Circ.* 612, 17 p.
- Joreskog, K. G., Klován, J. E., and Reymont, R. A., 1976. Geological factor analysis. Elsevier Sci. Pub. Co., Amsterdam, 178 p.
- Jukes, J. B., 1843. General report of the Geological Survey of Newfoundland during the years of 1839 and 1840. Pub. by John Murray, London, 160 p.
- Kajiwará, Y., and Krouse, H. R., 1971. Sulphur isotope partitioning in metallic sulphide systems. *Can. Jour. of Earth Scie.*, v. 8, pp. 1397-1408.
- Kawachi, Y., 1974. Geology and petrochemistry of weakly metamorphosed rocks in the Upper Wakatipu District, southern New Zealand. *N. Z. Jl. Geol. and Geoph.* v. 17, pp. 169-208.
- Kean, B.F., and Herd, R.K., 1982. Geological Association of Canada, Nfld. Sect., Fall Field Trip '82, Burgeo Road, 20 p. Kean, B. F., and Jayasinghe, N. R., (12A/4), Newfoundland. *in* Nfld. Dept. of Mines and Energy Rept. 81-1, Current Research, pp. 32-39.
- Kean, B. F., Deán, P. L., and Strong, D. F., 1981. Regional geology of the central volcanic belt of Newfoundland. *in* the Buchans fifty years of geology and mining. *Geol. Assoc. of Can. Spec. Pap.* No. 22, pp. 65-78.
- Keays, R. R., 1979. Gold deposits and ultramafic rocks: the link with nickel sulphide deposits. *GAC Prog. with Abst.*, v. 4, p. 60.
- Keays, R. R., and Scott, R. B., 1976. Precious metals in ocean-ridge basalts: Implications for basalts as source rocks for gold mineralization. *Econ. Geol.*, v. 71, pp. 705-720.
- Kennedy, M. J., 1975. Repetitive orogeny in the northeastern Appalachians - new plate models based on Newfoundland examples. *Tectonophysics*, v. 9 pp. 452-459.
- Kerrich, R., 1980. Archean gold-bearing chemical sediments and veins: a synthesis of stable isotope and geochemical relations. *Ont. Geol., Surv. Open File Rept.* 5293, *ed.* R.G. Roberts. pp. 137-211.
- Kerrich, R., 1983a. Geochemistry of gold deposits in the Abitibi Greenstone Belt: Part I-a synthesis of data from chemical sedimentary and vein deposit types. *in press*, *CIMM Bull.*
- Kerrich, R., 1983b. Geochemistry of gold deposits in the Abitibi Greenstone Belt: Part II-a revision of hydrothermal fluid properties, alkaline regimes and models. *in press*, *CIMM Bull.* one.

- Kerrich, R., and Fryer, B. J., 1979. Archean precious-metal hydrothermal systems, Dome Mine, Abitibi Greenstone Belt. II REE and oxygen isotope relations. *Can. Jour. Earth Sci.*, v. 16, pp. 440-458.
- Kerrich, R., and Fryer, B. J., 1981. The separation of rare elements from abundant base metals in Archean lode gold deposits: Implications of low water/rock source regions. *Econ. Geol.*, v. 76, pp. 160-166.
- Kerrich, R., Fryer, B. J., Milner, K. J., and Peirce, M. G., 1981. The geochemistry of gold-bearing chemical sediments Dickinson Mine, Red Lake, Ontario: a reconnaissance study. *Can. Jour. Earth Sci.*, v. 10, pp. 624-637.
- Kerrich, R., and Fyfe, W. S., 1981. The gold-carbonate association: source of  $\text{CO}_2$  and  $\text{CO}_2$  fixation reactions in Archean lode deposits. *Chem. Geol.*, v. 33, pp. 265-294.
- Kim, J-O., 1976. Factor Analysis. in SPSS. Statistical package for Social Sciences, 2nd ed. ed. Nie, N. H. et al., McGraw-Hill Book Co., pp. 468-514.
- Kitaev, N.A., 1978. Geology, geochemistry and genetic properties of the formation of gold ores of the Lybavinsk ore deposit (Transbaikal). *Sov. Geol. and Geophysics*, v. 18, pp. 35-40.
- Klecka, W. R., 1976. Discriminant analysis. in SPSS. Statistical package for the Social Sciences, 2nd ed. McGraw-Hill Book Co. ed Nie, N. H. et al., Toronto, pp. 434-467.
- Knopf, E. B., 1931. Retrogressive metamorphism and phyllonitization. *Am. Jour. of Sci.*, v. 21, p. 1-27.
- Konstantinov, M. M., 1977. Geochemical types of gold mineralization in volcanic regimes. *Dokl. Akad. Nauk SSSR*, V. 234, pp. 247-250.
- Koppel, V., and Grunenfelter, M., 1979. Isotope geochemistry of lead. in *Lectures in isotope geology*, ed Jager, E., and Hunziker, J. C. Springer-Verlag, Berlin, pp. 134-153.
- Kretschmar, U., and Scott, S. D., 1976. Phase relations involving arsenopyrite in the system Fe-As-S and their application. *Can. Min.*, v. 14, pp. 364-386.
- Kuno, H., 1968. Differentiation of basaltic magmas. in *Basalts*, vol. 2, H. H. Hess and A. Faldervaart. John Wiley and Sons, New York, pp. 623-688.
- Kuo, H. Y., and Wilson, H. D. B., 1976. Some observations on gold distribution in Archean volcanic rocks. *Univ. Man. Cen. Precambrian Res., Ann. Rept.*, pp. 45-51.
- Kwong, Y. T. J., and Crockett, J. H., 1978. Background and anomalous gold in rocks of an Archean greenstone assemblage, Kakagi Lake area, Northwestern Ontario. *Econ. Geol.*, V. 73, pp. 50-63.

- Lajoie, J., 1980. Volcaniclastic Rocks, *in* Geoscience Canada, Reprint Series I, Facies Models, pp. 191-200.
- Lapworth, C., 1885. The highland controversy in British geology; its causes, course and consequences. *Nature*, v. 32, pp. 556-559.
- LeFort, P., 1978. Relations of two-mica granites with crustal lineaments. Examples of the Haut-Dauphine (French Alps) and Himalayas. *Sci. de la Terre*, v. 11, pp. 31-34.
- Letnikov, F. A., Vibor, N. V., Gantimurova, T. P., Konovalov, I. V., Shkandriy, B. O., and Shkarupa, F. A., 1975. Transport forms of gold and fluid evolution in the production of gold-bearing metamorphogenic quartz veins. *Geochem. Int.*, v. 12, pp. 126-134.
- Leventhal, J. S., and Hosterman, J. W., 1982. Chemical and mineralogical analysis of Devonian black-shale samples from Martin County, Kentucky; Carroll and Washington Counties, Ohio; Wise County, Virginia; and Overton County, Tennessee, U.S.A. *Chem. Geol.*, v. 37, pp. 239-264.
- Loomis, T. P., and Nimick, F. B., 1982. Equilibrium in Mn-Fe-Mg aluminous pelitic compositions and equilibrium growth of garnet. *Can. Min.* v. 20, pp. 393-410.
- Ludden, J. N., and Thompson, G., 1979. An evaluation of the behaviour of the rare earth elements during the weathering of sea floor basalt. *Earth Plan. Sci. Lett.*, v. 13, pp. 85-97.
- Lusk, J., Campbell, F. A., and Krouse, H. R., 1975. Application of sphalerite geobarometry and sulphur isotope geothermometry to ones of the Queмонт Mine, Noranda, Quebec. *Econ. Geol.*, v. 70, pp. 1070-1083.
- Luth, W. C., Jahns, R. H., and Tuttle, O. F., 1964. The granite system at pressures of 4 to 10 kilobars. *Jour. Geophys. Res.*, v. 69, pp. 759-773.
- Malpas, J., 1979. Two contrasting trondhjemite associations from transported ophiolites in western Newfoundland: Initial report. *in* Trondhjemites, dacites and related rocks, ed. Barker, F., Elsevier Pub. Co., New York, pp. 465-488.
- Malpas, J., and Stevens, R. K., 1977. The origin and emplacement of the ophiolite suite with examples from Western Newfoundland. *Geotectonics*, v. 11, pp. 453-466.
- Mantei, E. J., and Brownlow, A. H., 1967. Variation in gold contents of minerals of the Marysville quartz diorite stock, Montana. *Geochim. Cosmo. Acta*, v. 31, pp. 225-235.
- Marmo, V., 1960. On the sulphide and sulphide-bearing graptite schists of Finland. *Finlande Comm. Geol. Bull.*, 190, 80 p. as reported in Tourtelot, E. B., 1970. Selected annotated bibliography of minor-element content of marine black shale, and related sedimentary rocks, 1930-1965. *USAS Bull.* 1293, pp. 54-55.
- Marmont, S., 1983. The role of felsic intrusions in gold mineralization. *Ont. Geol. Surv. Misc. Pap.*, 110, pp. 38-47.



- Mattauer, M., Faure, M., and Malavieille, 1981. Transverse lineation and large-scale structures related to Alpine obduction in Corsica. *Jour. of Struct. Geol.*, v. 3, pp. 401-409.
- McClay, K. R., 1980. Sheared galera; tectures and microstructures. *Jour. Struc. Geol.*, v. 2, pp. 227-234.
- McLennan, S. M., and Taylor, S. R., 1979. Rare earth mobility associated with uranium mineralization. *Nature*, v. 282, pp. 247-250.
- McNamara, J., and Thode, H. G., 1950. Comparison of the isotopic constitution of terrestrial and meteoric sulphur. *Phys. Rev.*, v. 78, pp. 307-308.
- Miller, D. F., and Stoddard, E. F., 1981. The role of manganese in the paragenesis of magmatic garnet: an example from the Old Woman-Piute Range, California. *Jour. of Geol.*, v. 89, pp. 233-246.
- Mineyev, D. A., 1963. Geochemical differentiation of the rare earths. *Geochemistry*. No. 12, pp. 1129-1149.
- Mironov, A. G., Almukhamedov, A. I., Medvedev, A. Ya., and Krendelev, F. P., 1978. Geochemistry of gold in melts of basaltic composition (from experimental data). *Geochem. Int.*, v. 15, pp. 23-35.
- Miyashiro, A., 1973. *Metamorphism and metamorphic belts*. John Wiley and Sons, New York, 492 p.
- Moh, G. H., 1975. Phase relations and mineral assemblages in the Cu-Fe-Zn-An-Sn-S system. *Chemie der Erde*, v. 34, pp. 1-61.
- Mookherjee, A., 1976. Ores and metamorphism: Temporal and genetic relationships. in *Handbook of strata-bound and stratiform ore deposits*, v. 4,, ed. K. H. Wolf, Elsevier Sci. Pub. co., Amsterdam, pp. 203-260.
- Muecke, G. K., and Clarke, D. B., 1981. Geochemical evolution of the South Mountain Batholith, Nova Scotia: rare earth element evidence. *Can. Min.*, v. 19, pp. 133-146.
- Murray, A., 1868. Report of the Newfoundland Geological Survey for 1868 in Murray, A. and Howley, J. P., *Geological Survey of Newfoundland from 1868 to 1880*.
- Nance, W. B. and Taylor, S. R., 1977. Rare earth element patterns and crustal evolution II. Archean sedimentary rocks from Kalgoorlie, Australia. *Geochim. et Cosmo. Acta*, v. 41, pp. 225-321.
- Naney, M. T., and Swanson, S. E., 1980. The effect of Fe and Mg on crystallization in granitic systems. *Am. Min.*, v. 65, pp. 639-653.
- Neumann, E. R., Brunfelt, A. D., and Finstad, K. G., 1977. Rare earth elements in some igneous rocks in the Oslo Ritt, Norway. *Lithos*, v. 10, pp. 311-319.
- Nicollet, C., Leyreloup, A., and Dupuy, C., 1979. Petrogenesis of high pressure trondhjemitic layers in eclogites and amphibolites from southern Massif Central, France. in *Trondhjemites, Dacites and Related Rocks*, ed Barker, F., Elsevier Sci. Pub. Co., New York, pp. 435-463.

- Nicolas, A., and Boudier, F., 1975. Kinematic interpretation of folds in alpine-type peridotites. *Tectonophysics*, v. 25, pp. 233-260.
- Nie, N. H., Benot, D. H., and Hull, C. H., 1970. SPSS statistical package for the Social Sciences. McGraw-Hill Book Co., New York, 343 p.
- Nie, N. H., Hull, C. H., Jenkins, J. G., Steinbrenner, K., and Bent, D. H., 1976. SPSS. Statistical package for the Social Sciences. 2nd ed., McGraw-Hill Book Co., Toronto, 602 p.
- Nitsch, K. H., 1970. Experimental determination of the upper stability limit of stilpnomelane. *Fortschr. Min.*, v. 47, pp. 48-49.
- Nitsch, K. H., 1971. Stability relations of paragneisses containing prehnite and pumpellyite. *Can. Min. and Pet.*, v. 30, pp. 240-260.
- Norman, D. I., and Landis, G. P., 1980. Source of mineralizing components in hydrothermal ore fluids as evidenced by  $^{87}\text{Sr}/^{86}\text{Sr}$  and stable isotope data from the Pasto Bueno Deposit, Peru. *GSA Abst. with Prog.*, v. 12, p. 493.
- O'Brien, S. J., 1982. Geology of the eastern half of the Peter Snoot map area (11P/13E), Newfoundland, in *Nfld. Dept. of Mines and Energy, Prel. Proj. Rept. for 1982*. pp. 58-69.
- O'Conner, J. T., 1965. A classification for quartz-rich igneous rocks based on feldspar ratios. *USGS. Prof. Pap.* 525-B, pp. 1379-1384.
- Odin, G. S., 1982. The Phanerozoic time scale revisited. *Episodes*, v. 1982, pp. 3-9.
- Ohmoto, H., and Rye, R. O., 1979. Isotopes of carbon and sulphur. in *Geochemistry of hydrothermal ore deposits*, ed. Barnes, H. L., John Wiley and Sons, Toronto, pp. 509-567.
- O'Neil, J. R., and Bailey, G. B., 1979. Stable isotope investigation of gold-bearing jasperoid in the Central Drum Mountains, Utah. *Econ. Geol.*, v. 74, pp. 852-859.
- Pankhurst, R. J., 1979. Isotope and trace element evidence for the origin and evolution of Caledonian granites in the Scottish Highlands. in *Origin of Granite Batholiths Geochemical Evidence*, ed. Atherton, M. P., and Tarney, J., Shiva Pub. Ltd., Kent, pp. 18-33.
- Payne, J. G., and Strong, D. F., 1979. Origin of the Twillingate Trondhjemite, north-central Newfoundland: Partial melting in the roots of an island arc. in *Trondhjemites, dacites and related rocks*. ed Barker, F., Elsevier Sci. Pub. Co., New York, pp. 489-516.
- Pearce, J. A., and Cann, J. R., 1973. Tectonic setting of basic volcanic rocks determined using trace element analyses. *Earth Plan. Sci. Lett.*, v. 19, pp. 290-300.
- Phair, G., 1949. Geology of the southwestern part of the Long Range, Newfoundland. Unpub. Ph.D. thesis, Princeton University, 165 p.
- Phillips, F. C., 1971. The use of stereographic projection in structural geology. 3rd ed., Edward Arnold (Publishers) Ltd., London, 90 p.

- Pirie, J., and Mackasey, W. O., 1978. Preliminary examination of regional metamorphism in parts of Quetico metasedimentary belt, Superior Province, Ontario. *in* Metamorphism in the Canadian Shield. Geol. Surv. Can. Pap. 78-10, pp. 37-48.
- Powell, T. G., and McKirdy, D. M., 1973. Relationship between ratio of pristane to phytane, crude oil composition and geological environment in Australia. *Nature Phys. Sci.*, v. 243, pp. 37-39.
- Price, R. C., and Taylor, S. R., 1977. The rare earth element geochemistry of granite, gneiss and migmatite from the Western Metamorphic Belt of southeastern Australia. *Con. Min and Pet.*, v. 62, pp. 249-263.
- Radtke, A. S., Rye, R. O., and Dickson, F. W., 1980. Geology and stable isotopes of the Carlin gold deposit, Nevada. *Econ. Geol.*, v. 75, pp. 641-672.
- Raheim, A., and Green, D. H., 1974. Calibration of garnet-clinopyroxene - Fe/Mg partition as a geothermometer. *Con. Min. and Pet.*, v. 48, pp. 179-203.
- Ramdohr, P., 1969. The ore minerals and their intergrowths. Pergamon Press, Oxford, 1174 p.
- Ramsay, J. G., 1967. Folding and Fracturing of rocks. McGraw-Hill, New York, 568 p.
- Ramsay, J.G., and Graham, R.H., 1970. Strain variation in shear belts. *Can. Jour. Earth Sci.*, v. 7, pp. 786-813.
- Reading, H. G., 1980. Characteristics and recognition of strike-slip fault systems, *in* Sedimentation in oblique-slip mobile zones, ed Ballance, P. F., and Reading, H. G., Blackwell Scientific Publication, Oxford, pp. 7-26.
- Roberts, R. J., Radtke, A. S., and Coats, R. R., 1971. Gold-bearing deposits in North-Central Nevada and southwestern Idaho. *Econ. Geol.*, v. 66, pp. 14-33.
- Rollinson, H. R., and Windley, B. F., 1980. An Archean granulite-grade tonalite-trondhjemite-granite suite from Scourie, NW Scotland: Geochemistry and Origin. *Con. Min. and Pet.*, v. 72, pp. 265-281.
- Roper, P. J. and Dunn, D. E., 1973. Superposed deformation and polymetamorphism, Brevard Zone, South Carolina. *Geol. Soc. Am. Bull.*, v. 84, pp. 3373-3386.
- Rowe, J. J., 1969. Fractionation of gold in a differentiated tholeiitic dolerite. *Chem. Geol.*, v. 4, pp. 421-427.
- Rye, R. O., and Ohmoto, H., 1974. Sulphur and carbon isotopes and ore genesis: A review. *Econ. Geol.*, v. 69, pp. 826-842.
- Rytuba, J. J., and Dickson, F. W., 1974. Reaction of pyrite + pyrrhotite + quartz + gold with NaCl-H<sub>2</sub>O solutions, 300-500°C. 500-1500 bars, and genetic implications. *in* Problems of Ore Deposition, 4th IAGOD symposium, Varna, Bulgaria, v. II, pp. 321-326.
- Saager, R., Meyer, M., and Muff, R., 1982. Gold distribution in supracrustal rocks from Archean greenstone belts of southern Africa and from Paleozoic ultramafic complexes of the European Alps: metallogenic and geochemical implications. *Econ. Geol.*, v. 77, pp. 1-24.

- Sakharova, M. S., 1969. Mineralogy of Darasun gold field in eastern Zabaykaliye. *Int. Geol. Rev.*, v. 11, pp. 45-59.
- Sanderson, D. J., 1973. The development of fold axes oblique to the regional trend. *Tectonophysics*, v. 16, pp. 55-70.
- Sawkins, F. J., O'Neil, J. R., and Thompson, J. M., 1979. Fluid inclusions and geochemical studies of vein gold deposits, Baguio District, Philippines. *Econ. Geol.*, v. 74, pp. 1420-1434.
- Saxena, S. K., 1979. Garnet-clinopyroxene geothermometer, *Con. Min. and Pet.*, v. 70, pp. 229-235.
- Scott, S. D., 1973. Experimental calibration of the sphalerite geobarometer. *Econ. Geol.*, v. 68, pp. 468-474.
- Scott, D. S. D., and Barnes, H. L., 1971. Sphalerite geothermometry and geobarometry. *Econ. Geol.*, v. 66, pp. 653-669.
- Self, S., 1982. Terminology and classifications for pyroclastic deposits in *Pyroclastic volcanism and deposits of Cenozoic intermediate to felsic volcanic islands with implications for Precambrian greenstone-belt volcanoes*. *Geol. Assoc. of Can., Short Course Notes v. 2*, ed L.D. Ayres, pp. 18-37.
- Seward, T. M., 1973. Thiocomplexes of gold and the transport of gold in hydrothermal ore solutions. *Geochim. Cosmo. Acta*, v. 37, pp. 379-399.
- Shaw, D. M., 1956. Geochemistry of pelitic rocks. Part III: Major elements and general geochemistry. *Geol. Soc. Am. Bull.*, v. 67, pp. 919-934.
- Shaw, D. M., 1972. Origin of the Apsley Gneiss, Ontario. *Can. Jour. Earth Sci.*, v. 9, pp. 18-35.
- Shcherbakov, Yu., G., and Perezhugin, G. A., 1963. Geochemical relation between gold mineralization, intrusives and the enclosing rocks in western Siberia. *Geochem. Int.*, No. 9, pp. 882-890.
- Shibata, K., and Ishihara, S., 1979. Initial  $^{87}\text{Sr}/^{86}\text{Sr}$  ratios of plutonic rocks from Japan. *Con. Min. Pet.*, v. 70, pp. 381-390.
- Sibson, R. H., 1977. Fault rocks and fault mechanisms. *Jl. Geol. Soc. Lon.*, v. 133, pp. 191-213.
- Sillitoe, R. H., 1979. Some thought on gold-rich porphyry copper deposits. *Min. Deposita*, v. 14, pp. 161-174.
- Skirrow, R., and Coleman, M. L., 1982. Origin of sulphur and geothermometry of hydrothermal sulphides from the Galapagos Rift, 86°W. *Nature* v. 299, pp. 142-144.
- Slaughter, J., Kerrick, D. M., and Wall, V. J., 1975. Experimental and thermodynamic study of equilibria in the system  $\text{CaO-MgO-SiO}_2\text{-H}_2\text{O-CO}_2$ . *Am. Jour. of Sci.*, v. 275, pp. 143-162.

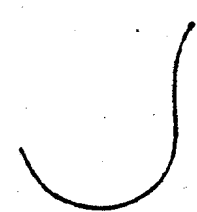
- Smith, J. W., Doolan, S., and McFarlane, E. F., 1977. A sulphur isotope geothermometer for the trisulphide system galena-sphalerite-pyrite. *Chem. Geol.*, v. 19, pp. 83-90.
- Spencer, D., 1966. Factors affecting element distributions in a Silurian graptolite band. *Chem. Geol.*, v. 1, pp. 221-249.
- Spry, A., 1969. *Metamorphic Textures*. Pergamon Press, Oxford. 350 p.
- Stacey, J. S., and Kramers, J. O., 1975. Approximation of terrestrial lead isotope evolution by a two-stage model. *Earth and Plan. Sci. Lett.*, v. 26, pp. 207-221.
- Stanton, R. L., and Willey, H. G., 1972. Experiments on a specimen of galena ore from Coeur d'Alene, Idaho. *Econ. Geol.*, v. 67, pp. 776-788.
- Steiger, R. H., and Jager, E., 1977. Subcommittee on geochronology: convention on the use of decay constants in geo- and cosmochemistry. *Earth Plan. Sci. Lett.*, v. 36, pp. 359-362.
- Stephens, W. E., Watson, S. W., Philp, P. R., and Weir, J. A., 1975. Element associations and distributions through a Lower Paleozoic graptolitic shale sequence in the southern uplands of Scotland. *Chem. Geol.*, v. 16, pp. 269-294.
- Stevens, R. K., 1970. Cambro-Ordovician flysch sedimentation and tectonics in West Newfoundland and their possible bearing on a proto-Atlantic Ocean. *Geol. Assoc. Can. Spec. Pap. No. 7*, pp. 165-177.
- Streckeisen, A., 1976. To each plutonic rock its proper name. *Earth Sci. Rev.*, v. 12, pp. 1-33.
- Strong, D. F., 1977. Volcanic regimes of the Newfoundland Appalachians, in Volcanic regimes of Canada. ed. Baragar, W. R. A., *Geol. Assoc. Can. Spec. Pap. No. 16*, pp. 61-90.
- Strong, D. F., 1980. Granitoid rocks and associated mineral deposits of eastern Canada and western Europe. in the Continental Crust and its Mineral Deposits, ed. Strangway, D. W., *Geol. Assoc. Can. Spec. Pap. 20*, pp. 741-769.
- Strong, D. F., 1982. Carbothermal metasomatism of alaskitic granite, St. Lawrence, Newfoundland, Canada. *Chem. Geol.*, v. 35, pp. 97-114.
- Strong, D. F., and Dickson, W. L., 1978. Geochemistry of Paleozoic granitoid plutons from contrasting tectonic zones of northeast Newfoundland. *Can. Jour. Earth Sci.*, v. 15, pp. 145-156.
- Strong, D. F., and Dupuy, C., 1982. Rare earth elements in the bimodal Mount Peyton batholith: Evidence of crustal anatexis by mantle-derived magma. *Can. Jour. of Earth Sci.*, v. 19, pp. 308-315.
- Studemeister, P. A., Kerrich, R., and Fyfe, W. S., 1981. Geochemistry and field relations of lode gold deposits in felsic igneous intrusions - the Gutcher Lake Stock. *Ont. Geol. Surv. Misc. Pap. 98*, pp. 267-292.
- Sugaki, A., Shima, H., Kitakaze, A., and Havrda, H. 1975. Isothermal phase relations in the system Cu-Fe-S under hydrothermal conditions at 350°C and 300°C. *Econ. Geol.*, v. 70, pp. 806-823.

- Swinden, H. J. S., and Thorpe, R. I., 1983. Variations in style of volcanism and massive sulphide deposition in early-middle Ordovician island arc sequences of the Newfoundland Central Mobile Belt, in press Econ. Geol.
- Tanner, P. W. G., and Miller, R. G., 1980. Geochemical evidence for loss of Na and K from Monian calc-silicate pods during prograde metamorphism. Geol. Mag., v. 117-, pp. 267-275.
- Tarney, J., Weaver, B., and Frury, S. A., 1979. Geochemistry of Archean trondhjemitic and tonalitic gneisses from Scotland and East Greenland in Trondhjemites, dacites and related rocks, ed. Barker, F., Elsevier Sci. Pub. Co., New York, pp. 123-132.
- Taylor, R. P. and Fryer, B. J. 1980. Multiple-stage hydrothermal alteration in porphyry copper systems in northern Turkey: the temporal interplay of potassic, propylitic and phyllic fluids. Can. Jour. Earth Sci., v. 17, pp. 901-926.
- Taylor, R. P. and Fryer, B. J., 1982. Rare earth element geochemistry as an aid to interpreting hydrothermal ore deposits. in Metallization Associated with Acid Magmatism. ed. A. M. Evans, John Wiley and Sons Ltd., pp. 357-365.
- Taylor, R. P. and Fryer, B. J., 1983. Strontium isotope geochemistry of the Santa Rita porphyry copper deposits, New Mexico. in press, Econ. Geol.
- Taylor, R. P. and Fryer, B. J., in prep. Rare earth element lithogeochemistry of granitoid mineral deposits. CIMM Bull.
- Taylor, R. P., Strong, D. F., Fryer, B. J., 1981. Volatile control of contrasting trace element distributions in peralkaline granitic and volcanic rocks. Can. Min. Pet., v. 77, pp. 267-271.
- Taylor, R. P. Strong, D. F., and Kean, B. F., 1980. The Topsails igneous complex: Silurian-Devonian paralkaline magmatism in western Newfoundland. Can. Jour. Earth Sci., v. 17, pp. 425-439.
- Taylor, S. R., 1965. The application of trace elements data to problems in petrology. Phys. and Chem. of the Earth, v. 6, pp. 133-213.
- Taylor, S.R., and Gorton, M.P., 1977. Geochemical application of spark source mass spectrography - III Element sensitivity, precision and accuracy. Geochim. Cosmo. Acta, v. 29, pp. 1243-1261.
- Taylor, S. R. and McLennan, S. M., 1981. The rare earth element evidence in Precambrian sedimentary rocks: implications for crustal evolution. in Precambrian Plate Tectonics, ed. Kroner, A., Elsevier, Amsterdam, pp. 527-548.
- Taylor, W. R., 1970. Geology and geochemistry of a uranium-rich area in southwestern Newfoundland. Unpub. MSc. thesis, Memorial University, 66 p.
- Teng, H. C., and Strong, D. F., 1975. Geology and geochemistry of the St. Lawrence granite and associated fluor spar deposits, southeast Newfoundland. Can. Jour. Earth Sci., v. 13, pp. 1374-1385.
- Tissot, B. P. and Welte, D. H., 1978. Petroleum Formation and Occurrence Springer-Verlag, Berlin, 538 p.
- Tilling, R. I., Gottfried, D., and Rowe, J. J., 1973. Gold abundance in igneous rocks: Bearing on gold mineralization. Econ. Geol., v. 68, pp. 168-186.

- Tracy, R. J., Robinson, P. and Thompson, A. B., 1976. Garnet compositions and zoning in the determination of temperature and pressure of metamorphism, central Massachusetts. *Am. Min.*, v. 61, pp. 762-775.
- Turner, F. J., 1980. *Metamorphic Petrology*. 2nd ed., McGraw-Hill Book Co., New York, 524 p.
- Tuttle, P. F., and Bowen, N. L., 1958. The origin of granite in light of experimental studies in the system  $\text{NaAlSi}_3\text{O}_8$ - $\text{KAlSi}_3\text{O}_8$ - $\text{SiO}_2$ - $\text{H}_2\text{O}$ . *Geol. Soc. Am. Mem.* 74, 153 p.
- Uytendogaardt, W., and Burke, E. A. J., 1971. *Tables for microscopic identification of ore minerals*. Elsevier Pub. Co., Amsterdam, 430 p.
- Van de Kamp, P. C., Leake, B. E., and Senior, A., 1976. The petrography and geochemistry of some Californian arkoses with application to identifying gneisses of metasedimentary origin. *Jour. Geol.*, v. 84, pp. 195-212.
- Vauchéz, A., 1980. Ribbon texture and deformation mechanisms of quartz in a mylonitized granite of Great Kabylis (Algeria), *Tectonophysics*, v. 61, pp. 1-12.
- Vernon, R. H., 1978. Porphyroblast-matrix microstructural relationships in deformed metamorphic rocks. *Geol. Rund.*, v. 67, pp. 288-305.
- Vikjter, B. Y., Razumovo, R. V., Khol, F. I., and Kurvanov, A. Sh., 1968. The form of gold in pyrite deposits, *Dokl. Akad. Nauk SSSR*, v. 178, pp. 152.
- Viljoen, R. P., Saager, R., and Viljoen, M. J., 1970. Some thoughts on the origin and processes responsible for the concentration of gold in the early Precambrian of southern Africa. *Min. Deposita*, v. 5, pp. 164-180.
- Vine, J. D., and Tourtelot, E. B., 1970. Geochemistry of black shale deposits - A summary report. *Econ. Geol.*, v. 65, pp. 253-272.
- Vokes, F. M., 1969. A review of the metamorphism of sulphide deposits. *Earth Sci., Rev.*, v. 5, pp. 99-143.
- Walsh, J. N., and Henderson, P., 1977. Rare earth element patterns of rocks from the Centre 3 Igneous Complex, Ardnamurchan, Argyllshire. *Con. Min. Pet.*, v. 60, pp. 31-38.
- Watterson, J., 1975. Mechanism for the persistence of tectonic lineaments. *Nature*, v. 253, pp. 520-521.
- Webb, W. M., and Potter, P. E., 1969. Petrology and chemical composition of modern detritus derived from a rhyolitic terrain, western Chianua. *Soc. Geol. Mexicana Bol.*, v. 32, pp. 45-61.
- Weissberg, B. C., 1970. Solubility of gold in hydrothermal alkaline sulphide solutions. *Econ. Geol.*, v. 65, pp. 551-556.
- Wendlandt, R. F. and Harrison, W. J., 1979. Rare earth partitioning between immiscible carbonate and silicate liquids and  $\text{CO}_2$  vapour: Results and implications for the formation of light rare earth-enriched rocks. *Con. Min. and Pet.*, v. 69, pp. 409-419.
- White, A. J. R., and Chappell, B. W., 1977. Ultrametamorphism and granitoid genesis. *Tectonophysics*, v. 43, pp. 7-22.

- White, S., 1976. The effects of strain on the microstructures, fabrics and deformation mechanisms in quartzites. *Phil. Trans. R. Soc.*, v. A283, pp. 69-86.
- Whitney, J. A., 1977. A synthetic model for vapour generation in tonalite magmas and its economic ramifications. *Econ. Geol.*, v. 72, pp. 606-690.
- Whitten, E. H. T., 1969. *Structural Geology of Folded Rocks*. Rand McNally and Co., Chicago. 678 p.
- Wiggins, L. B., and Craig, J. R., 1980. Reconnaissance of the Cu-Fe-Zn-S system: sphalerite phase relationships. *Econ. Geol.*, V. 75, pp. 741-751.
- Wilkinson, P., Soper, N. J., and Bell, A. M. 1975. *Skolithos* pipes as strain markers in mylonites. *Tectonophysics*, v. 28, pp. 143-157.
- Williams, H., 1975. Structural succession, nomenclature, and interpretation of transported rocks in western Newfoundland. *Can. Jour. Earth Sci.*, v. 12, pp. 1874-1894.
- Williams, H., (compiler), 1978. Tectonic-lithofacies map of the Appalachian Orogen. Memorial University of Newfoundland Map No. 1.
- Williams, H., 1979. Appalachian Orogen in Canada. *Can. Jour. Earth Sci.*, v. 16, pp. 792-807.
- Williams, H., and Hatcher, R. D., Jr., 1982. Suspect terranes and accretionary history of the Appalachian orogen. *Geology*, v. 10, pp. 530-536.
- Williams, H., and St. Julien, P., 1982. The Baie Verte-Brompton Line: Early Paleozoic continent-ocean interface in the Canadian Appalachians. *in* Major structural zones and faults of the northern Appalachians. *Geol. Assoc. of Can. Spec. Pap.*, No. 24, pp. 177-207.
- Williams, H., Kennedy, M. J., and Neale, E. R. W., 1973. The Appalachian structural province. *in* variations in Tectonic styles in Canada. *Geol. Assoc. Can. Spec. Pap.* 11, pp. 181-261.
- Williams, H., Kennedy, M. J., and Neale, E. R. W., 1974. The northeastward termination of the Appalachian Orogen. *in* Ocean basins and margins, ed. Nairn, A. E. M., vol. 2, Plenum, New York, pp. 79-123.
- Williams, H., and Stevens, R. K., 1974. The ancient continental margin of eastern North America. *in* The geology of continental margins, ed. Burk, C. A., and Drake, C. L., Springer-Verlag. New York, pp. 781-796.
- Williams, H., and McBirney, A. R., 1979. *Volcanology*. Freeman, Cooper and Co., San Francisco, 397 p.
- Wilton, D. H. C., 1981. The Cape Ray cryptic suture is more cryptic than suture. *GAC Prog. with Abst.*, v. 6, pA-62.
- Winkler, H. G. F., 1979. *Petrogenesis of Metamorphic Rocks.*, 5th ed., Springer-Verlag, New York, 348 p.



- Winkler, H. G. F., Das, B. K., and Breitbart, R., 1977. Further data of low-temperature melts existing on the quartz + plagioclase + liquid + vapour isobaric cotectic surface within the system  $Qz-Ab-Or-An-H_2O$ . *N. Jahrb. Min., Mon.*, v. 6, pp. 241-247.
- Wolfe, W. J., 1976. Gold in the early Precambrian Superior Province plutonic rocks: The relation of geochemical abundance and concentration to exploitable levels. *Ont. Div. of Mines, Geoscience study 17*, 11 p.
- Woodsworth, G. J., 1977. Homogenization of zoned garnets from pelitic schists. *Can. Min.*, v. 15, pp. 230-242.
- Wyllie, P. J., 1977. Crustal anatexis: An experimental review. *Tectonophysics*, v. 43, pp. 41-71.
- Yardley, B. W. D., 1977. Relationships between the chemical and modal compositions of metapelites from Connemara, Ireland. *Lithos*, v. 10, pp. 235-242.
- York, D., 1969. Least squares fitting of a straight line with correlated errors. *Earth and Plan. Sci. Lett.*, v. 5, pp. 320-324.
- Young, J. S., 1979. Paragenesis of gold veins in the Granite District, Grant County, Oregon. *GSA Abst. with prog.*, v. 11, p. 306.
- Zartman, R. E., 1974. Lead isotopic provinces in the Cordillera of the Western United States and their geologic significance. *Econ. Geol.*, v. 69, pp. 792-803.
- Zen, E.-An, 1981. Metamorphic mineral assemblages of slightly calcic pelitic rocks in and around the Taconic Allocthon, southwestern Massachusetts and adjacent Connecticut and New York. *USGS Prof. Pap.* 1113, 128 p.
- Zvereva, N. F., and Gavrilenko, B. V., 1971. Gold in rock-forming minerals of the Krykkuduk intrusive complex (Northern Kazakhstan). *Geochem. Int.*, v. 8, pp. 76-80.
- 

- Fryer, B. J., Kerrich, R., Hutchinson, R. W., Pierce, M. G., and Rogers, D. S., 1979. Archean precious-metal hydrothermal systems Dome Mine, Abitibi greenstone belt. I. Patterns of alteration and metal distribution. *Can. Jour. Earth Sci.*, v. 16, pp. 421-439.
- Paul, D. K., Crockett, J. H., and Nixon, P. H., 1979. Abundances of palladium, iridium, and gold in kimberlites and associated nodules. *in* Kimberlites, Diatremes and Diamonds: Their geology, petrology and geochemistry. ed. Boyd, F. R., and Meyer, H. O. A., pp. 272-279.
- Pchelintseva, N. F., and Fel'dman, V. I., 1973. Gold in metamorphic rocks of the Kokchetav uplift. *Geochem. Int.*, v. 10, pp. 1357-1365.
- Richter, D. H., 1970. Geology and lode-gold deposits of the Nuka Bay area, Kenai Peninsula, Alaska. *USGS Prof. Pap.* 625-B, 16p..
- Romberger, S. B., 1982. Transport and deposition of gold hydrothermal systems at temperatures up to 300 C. *GSA Abst. with prog.*, v. 14, p. 602.
- Sighinolfi, G. P., and Gorgoni, C., 1977. Gold distribution in the Ivrea-Verbaro Complex. *Chem. Geol.*, v. 20, pp. 99-107.
- Stephenson, J. F., and Ehmann, W. D., 1971. Neutron activation analysis of gold in Archean igneous and metamorphic rocks of the Rice Lake-Beresford Lake area, southwestern Manitoba. *Econ. Geol.*, v. 66, pp. 933-939.
- e

## Appendix I

### Microprobe Techniques

Electron microprobe analyses were carried out using the JEOL JXA-50A electron probe microanalyser with Krisel control through a PDP-11 mini-computer. Operating conditions were; accelerating voltage of 15 Kv, beam current of around 0.022 microamps, beam size of 1-2 micrometres, and counting rate of up to 60,000 with a default time of 30 seconds. The Krisel Magic correction program was used to correct the sulphide analyses. The Alpha correction program was used for the silicate analyses.

Analyses were termed acceptable if totals equalled between 98 and 102%, except in special cases as noted.

## Appendix II

### Rb/Sr Geochronological Techniques

The analyses were carried out in the laboratories of the Department of Earth Sciences at Memorial University using the same methods as outlined by Taylor and Fryer (1983). Replicate Rb and Sr analyses were completed using standard whole rock pressed pellet X-Ray Fluorescence techniques (see Appendix III). The actual analyses are reported in Table IV.

Sr was separated by standard ion exchange methods and Sr isotopic compositions were measured on a Micromass 30B solid-source mass spectrometer, with computer-controlled magnetic peak switching. The ion beam was collected in a Faraday "cup" collector. Data processing was done with a Hewlett-Packard 2114A computer and a Hewlett-Packard 9845B mini-computer.

The estimated  $2\sigma$  error for Rb and Sr concentrations is  $\pm 1\%$  and for the Rb/Sr ratio is  $\pm 0.5$  ppm. Data were fitted to the isochrons using the regression method of York (1969), with modifications from Brooks *et al.* (1972). The decay constant,  $\lambda_{38\text{Rb}} = 1.42 \times 10^{-11} \text{ yr}^{-1}$ , from Steiger and Jager (1977), was used for computation.

### Appendix III

#### Geochemical Methods

##### III.1 Sample Preparation

The sample sizes had wide variation due to differences in grain size and accessibility. Coarser-grained rocks were consequently of larger bulk sizes (the individual samples of megacrystic Cape Ray Granite were up to 4 kg). Drill core samples from mineralized quartz vein intersections were often smaller than desired, as the interval had previously been split and 1/2 was removed for assay by Riocanex Ltd.. Sometimes the remaining core had been further split by Riocanex geologists, leaving only a 1/4 of the original length. Grab samples of ore from the Trench and Windowglass Hill Granite had no such problems.

Samples were broken into chips by crushing with a hammer on a steel plate. Fragments with visible steel chips were rejected. The fragments were then pulverized for up to two minutes in a tungsten-carbide puck mill, until a powder of at least -100 mesh was produced. If a large quantity of coarse-grained sample was used, the resultant powder was coned and split into halves until just enough powder remained to fill a 125 ml sample bottle. Sample IAM-3, of the Isle aux Morts Brook Granite, was so split and the first half split of powder is now used as an internal standard at Memorial University (ie. MUN-1).

### III.2 Major Element Analyses

Loss on ignition (volatiles) was determined by weighing an amount (weighed accurately to  $10^{-4}$  gms) into a porcelain crucible, heating the crucible to  $1050^{\circ}\text{C}$  for at least two hours, cooling in a desiccator, and then weighing the de-volatized sample for percent loss of volatiles.

P205 was analysed with a Bausch and Lomb Spectronic 20 Colourimeter (*ie.* colourimetrically), based on a modification of the method outlined by Shapiro and Brannock (1962).

$\text{CO}_2$  was determined using a Leco Induction Furnace, Model 523. Samples were placed in a crucible between layers of tin and iron, and were volatilized in the furnace. The resultant vapour was titrated to ascertain the amount of  $\text{CO}_2$ .

The other major element oxides were determined by atomic absorption spectrometry. Samples were prepared using the methods of Langhyr and Paus (1968) and the elements were analysed on a Perkin-Elmer Model 370 atomic absorption spectrometer with digital readout. Occasionally sulphide-rich samples required dissolution in aqua-regia. Precision of this method is indicated in Table A-1.

<u>Element</u>	<u>Published</u>		<u>S.D.</u>	<u>Range</u>	
	<u>Value</u>	<u>Mean</u>		<u>Low</u>	<u>High</u>
SiO <sub>2</sub>	69.11	69.70	0.57	68.20	69.96
Al <sub>2</sub> O <sub>3</sub>	15.40	15.10	0.24	14.75	15.60
Fe <sub>2</sub> O <sub>3</sub>	2.65	2.60	0.02	2.64	2.74
MgO	0.76	0.80	0.005	0.75	0.82
CaO	1.94	2.00	0.10	1.92	2.14
Na <sub>2</sub> O	4.07	4.30	0.02	4.07	4.21
K <sub>2</sub> O	4.51	4.56	0.02	4.50	4.57
TiO <sub>2</sub>	0.50	0.50	0.01	0.47	0.51
MnO	0.03	0.03	0.00	-	-

Table A-1 Precision of Major Element Analyses

(based on four analyses of standard G-2. Published value from Flanagan (1970)).

### III.3 Trace Element Analyses

The trace elements were determined by X-Ray Fluorescence techniques on pressed whole rock powder pellets using a Phillips 1450 automatic X-Ray fluorescence spectrometer with a rhodium tube. The pellets were made from a mixed powder containing 10 gm sample and 1-1.5 gm binding material (Union Carbide Phenolic Resin TR-16933). The powder was pressed at 30 tons psi for a minute before being baked for 10 minutes at 200° C. Data reduction was done with a Hewlett-Packard 9845B mini-computer.

Some grab samples from the showings contained enormous

quantities of Pb (eg. sample 80-61C has > 500,000 ppm Pb) which interfered with and produced artificial peaks in Ga, Th, U, Rb, Sr and Zr. To account for this, the XRF data reduction program was modified to ascertain the true background and peak values of these elements.

Precision and accuracy for the trace element analyses are given in Table A-2 using the standards as listed. Published values from Flanagan (1973).

	<u>W-1</u>	<u>S.D.</u>	<u>N</u>	<u>Pub.</u>	<u>G-2</u>	<u>S.D.</u>	<u>N</u>	<u>Pub.</u>
V	263	4.73	7	240	43	3	10	34
Cr	96.8	2.5	7	120	13	3	10	9
Cu	99.0	2.16	7	110	17	1	10	11
Zn	95.7	1.70	7	86	85	2	10	85
Rb	22.6	2.07	7	21	166	2	10	170
Sr	172	2.94	7	190	477	7	10	480
Y	25.1	3.08	7	25	11	2	11	12
Zr	87.3	1.70	7	105	292	3	10	300
Nb	7.29	1.50	7	9.5	10	1	10	14
Ba	183	10.2	7	160	1865	30	10	1850
Pb	9.86	3.33	7	8	27	2	10	29

Table A-2 Precision and Accuracy of Trace Element Analyses

S.D. = standard deviation; N = no. of analyses; Pub. = published value.

S and As were also determined from the pressed powder



pellets. Precision of the As analyses are shown in Table A-3. S was determined accurately as shown by petrographic observations etc., however, standards determined with the sample runs, indicated much higher values than those published. This discrepancy resulted from contamination of the standard pellets by sulphur-containing instrument oils (due to repeated use of the standard pellets). A fresh standard pellet, yielded S values in good agreement with the published values

As (ppm)

W-1 0.36

S.D. 4.23

N 10

Pub. 1.9 (Abbey, 1975)

SY-2 40.7

S.D. 10

N 7

Pub. 18 (Abbey, 1976)

Table A-3 Precision and Accuracy of As Analyses

III.4 Precious Metal Analyses

The Au and Ag analyses were based on the methods outlined by Fryer and Kerrich (1978). Accordingly, approximately 10 gm of each sample were subjected to repeated HF and aqua-regia attack until all the precious

metals were presumably in aqua-regia solution. A solution of Te was then added to the sample/aqua-regia solution. The resulting solution was titrated with stannous chloride solution which reduced the Te and caused it to precipitate. The precious metals were adsorbed unto the Te and were thus concentrated. The Te/precious metals were then taken to 10 ml volume in a 50:50 HCl:aqua-regia solution.

In the ore samples, Au and Ag<sup>+</sup> concentration was too high for analysis by flameless atomic absorption methods (graphite furnace). These samples were analysed by flame methods with the same machinery as described in Appendix III.2 above. However, to avoid deleterious effects of the acid solution on this machinery, these samples had to be diluted with H<sub>2</sub>O. Unfortunately this dilution led to precipitation of AgCl. So samples with high Ag contents were analysed using the flame atomic absorption methods of Huffman et al. (1966), in which the samples were digested in HNO<sub>3</sub>.

Table A-4 shows the precision of Au analyses, by the flame method, for sample WGH SH1 and its replicates.

To check both the Huffman et al. (1966) method and the Fryer and Kerrich (1978) method, comparisons were made between samples analysed with both methods (to use the flameless atomic absorption methods, the samples were diluted, up to 1000x, with concentrated acid). These comparisons are listed in Table A-5.

	<u>N</u>	<u>MEAN</u>	<u>S.D.</u>	<u>LOW</u>	<u>HIGH</u>
WGH SH1	2	3.22	0.11	3.14	3.29
WGH SH1 (split 1)	1	1.29	-	-	-
WGH SH1 (split 2)	5	2.16	0.24	1.94	2.49

Table A-4 Au(ppm) Precision

<u>Sample</u>	<u>Fryer and Kerrich's method</u>	<u>Huffman et al.'s method</u>
CRG-2F	1324	1000
RRG-5	1728	2000
WGH SH3	14818	18000
WGH SH1	19122	19000
80-66D	42517	51500
133-6	20161	11000

Table A-5 Comparison of Ag Analyses

Ag analyses in the remainder of the samples was accomplished with an HGA-2200 graphite furnace attached to a Perkin-Elmer Model 370 atomic absorption spectrometer. The background Au analyses had to be completed on a Varian Techtron Model 63 Carbon Rod Analyser since the deuterium background corrector on the Perkin-Elmer instrument was broken (this didn't affect the Ag analyses, because the Ag lamp experiences much less matrix interference).

Accuracy of the low level Au and Ag contents was determined using standard samples NIM-G and NIM-N. As quoted by Steele et al. (1978), the Au contents for NIM-G and NIM-N, based on a single reported analysis, are 8 and 4 ppb respectively. Ag contents, quoted by these same authors, for NIM-G and NIM-N are 42-49 ppb and 29-35 ppb respectively. As determined in this study, the gold contents of NIM-G and NIM-N are 2.3 and 8 ppb respectively, and silver contents are 19 and 33 ppb respectively. Five replicate Au analyses of sample IAM-3 have an average of 2.86 ppb with a standard deviation  $\pm 0.91$ . Three replicate Ag analyses of samples IAM-3 and CRG-5A, had means of 121 and 69.3 ppb with standard deviations of  $\pm 51.5$  and  $\pm 24.5$  respectively.

#### III.5 Rare Earth Element Analyses

The rare earth element analyses were carried out by thin film X-Ray fluorescence techniques as outlined by Fryer (1977). In this method 1-2 gm of sample were broken down by HF and the resultant solutions were fed through columns containing ion exchange resin. Calibrated elutions of 2N HCl effectively concentrated the REE's in a final solution. H<sub>2</sub>SO<sub>4</sub> was added to remove Ba, and the solution was dried upon ion exchange paper. This paper was then analysed in the X-Ray Fluorescence spectrometer.

The data are assumed to be accurate to  $\pm 5-10\%$ , or 0.1 ppm, whichever is greater.

Appendix IVIV.1 Major and trace elements, S, CO<sub>2</sub> and Precious metals

Major oxide analyses were not completed in all samples and in these cases the total column is left blank. If an element was not analysed in a particular sample, then the column is left blank. Fe was analysed as total Fe<sub>2</sub>O<sub>3</sub>. S and CO<sub>2</sub> are not included with the major oxide analyses because they were analysed by different methods (S by XRF and CO<sub>2</sub> by volatilization/titration). Also CO<sub>2</sub> analyses were not done for as many samples as were the major oxides.

## Windsor Point Group Ignimbrites (WPGIG)

	WPG-1	WPG-2	WPG-3	WPG-4	W-79-28
Major Elements (Wt %)					
SiO <sub>2</sub>	72.00	67.90	78.30	72.50	68.50
TiO <sub>2</sub>	.69	.61	.13	.13	.95
Al <sub>2</sub> O <sub>3</sub>	11.70	13.40	10.20	12.80	12.40
Fe <sub>2</sub> O <sub>3</sub>	6.17	6.27	1.19	1.84	3.67
MnO	.01	.01	.01	.01	.01
MgO	.33	.16	.11	.06	.54
CaO	.36	.30	.13	.30	.85
Na <sub>2</sub> O	.23	.55	.23	.28	.18
K <sub>2</sub> O	8.36	10.40	7.83	10.46	8.36
P <sub>2</sub> O <sub>5</sub>	.23	.15	.01	0.00	.61
LOI	.79	.47	.49	.53	2.62
TOTAL	100.87	100.22	98.63	98.91	98.69

Trace Elements (ppm)					
Pb	28.00	37.00	18.00	22.00	19.00
Th	9.00	8.00	12.00	15.00	8.00
U	1.00	2.00	2.00	1.00	6.00
Rb	184.00	167.00	169.00	196.00	195.00
Sr	46.00	79.00	19.00	5.00	28.00
Y	90.00	120.00	53.00	108.00	88.00
Zr	382.00	368.00	149.00	283.00	340.00
Nb	16.00	18.00	19.00	19.00	14.00
Zn	38.00	22.00	16.00	15.00	43.00
Cu	11.00	13.00	17.00	26.00	11.00
Ni	25.00	25.00	11.00	23.00	25.00
La	60.00	103.00	40.00	91.00	52.00
Ba	721.00	869.00	595.00	537.00	594.00
V	73.00	35.00	1.00	7.00	105.00
Ce	95.00	165.00	98.00	150.00	93.00
Cr	3.00	0.00	0.00	0.00	0.00
Ga	12.00	3.00	0.00	3.00	22.00
As	23.00	28.00	20.00	5.00	50.00

S & CO <sub>2</sub> (Wt %)					
S	0.00	0.00	0.00	0.00	0.00
CO <sub>2</sub>	0.00			.11	.05

Precious Metals (ppb)					
Au	0.00	1.00	3.90	3.00	
Ag	80.00	67.00	102.00	123.00	

## WPGIG

W-79-143

W-79-32

W-80-76

W-80-83

W-80-88

## Major Elements (Wt %)

SiO2	76.80	71.80	77.50	71.50	67.20
TiO2	.25	.47	.27	.39	.52
Al2O3	10.40	13.20	8.24	14.30	15.10
Fe2O3	1.38	2.43	2.18	3.48	2.44
MnO	.02	.03	.08	.06	.06
MgO	.06	1.76	.51	.90	0.00
CaO	.05	.44	3.57	.14	1.67
Na2O	.40	3.55	4.24	4.55	3.78
K2O	8.70	3.03	.36	4.02	8.00
P2O5	.05	.18	.11	.09	.16
LOI	.32	1.56	3.11	1.03	1.36
TOTAL	98.43	98.45	100.17	100.46	100.29

## Trace Elements (ppm)

Pb	14.00	20.00	1.00	6.00	1.00
Th	19.00	17.00	2.00	16.00	13.00
U	10.00	6.00	3.00	3.00	0.00
Rb	169.00	98.00	8.00	79.00	135.00
Sr	9.00	10.00	42.00	78.00	33.00
Y	90.00	78.00	34.00	27.00	86.00
Zr	368.00	337.00	261.00	166.00	632.00
Nb	33.00	21.00	9.00	8.00	29.00
Zn	18.00	103.00	18.00	48.00	15.00
Cu	7.00	17.00	9.00	22.00	30.00
Ni	16.00	28.00	4.00	0.00	0.00
La	65.00	46.00	17.00	45.00	52.00
Ba	842.00	383.00	66.00	1430.00	672.00
V	12.00	55.00	46.00	86.00	17.00
Ce	135.00	82.00	48.00	78.00	93.00
Cr	0.00	21.00	60.00	15.00	0.00
Ga	10.00	17.00	8.00	17.00	22.00
As	20.00	14.00	0.00	23.00	29.00

## S &amp; CO2 (Wt %)

S	.01	0.00	0.00	0.00	0.00
CO2	.06	.18	.84	.08	

## Precious Metals (ppb)

Au	7.80	0.00	0.00	7.50	
Ag	92.00	86.00	0.00	71.00	

## WPB1G

W-80-135

W-80-146

W-80-208

PB26-4

PB27-32

## Major Elements (Wt %)

SiO2	74.70	.01	76.50	75.80	.01
TiO2	.15	0.00	.21	.13	0.00
Al2O3	12.90	0.00	12.90	12.80	0.00
Fe2O3	1.58	0.00	1.94	.42	0.00
MnO	.01	0.00	.01	.02	0.00
MgO	.26	0.00	.16	.08	0.00
CaO	.05	0.00	0.00	1.78	0.00
Na2O	.26	0.00	.22	4.38	0.00
K2O	9.04	0.00	7.35	2.13	0.00
P2O5	.05	0.00	.02	.01	0.00
LOI	.75	0.00	1.17	2.07	0.00
TOTAL	99.75		100.48	99.62	

## Trace Elements (ppm)

Pb	18.00	4.00	12.00	47.00	765.00
Th	26.00	12.00	26.00	18.00	25.00
U	0.00	3.00	7.00	3.00	9.00
Rb	194.00	57.00	256.00	48.00	63.00
Sr	8.00	22.00	0.00	79.00	92.00
Y	69.00	119.00	114.00	150.00	108.00
Zr	330.00	615.00	346.00	691.00	286.00
Nb	23.00	35.00	28.00	39.00	26.00
Zn	24.00	16.00	90.00	27.00	774.00
Cu	15.00	14.00	13.00	23.00	74.00
Ni	0.00	0.00	0.00	0.00	1.00
La	86.00	62.00	19.00	60.00	52.00
Ba	731.00	296.00	192.00	785.00	288.00
V	8.00	1.00	4.00	0.00	21.00
Ce	160.00	124.00	50.00	111.00	93.00
Cr	0.00	0.00	0.00	0.00	13.00
Ga	23.00	19.00	21.00	23.00	34.00
As	15.00	19.00	3.00	32.00	17.00

## S &amp; CO2 (Wt %)

S	0.00	0.00	0.00	.01	.07
CO2	.51				.16

## Precious Metals (ppb)

Au	1.00		2.80	2.50	
Ag	64.00		17.00	89.00	



## WPGIG

W-79-117

W-79-166

W-79-15

W-79-19

W-80-161

## Major Elements (Wt %)

SiO2	71.80	37.80	71.70	73.50	76.60
TiO2	.40	.62	.23	.20	.06
Al2O3	14.80	14.60	13.90	12.90	12.20
Fe2O3	2.63	6.70	1.46	1.64	.67
MnO	.05	.20	.03	.03	.07
MgO	.80	4.86	.52	.52	.14
CaO	.60	14.75	1.76	1.71	1.18
Na2O	5.08	.13	4.41	5.48	2.04
K2O	2.33	3.60	3.66	1.77	6.34
P2O5	.12	.09	.08	.42	.02
LOI	1.11	15.39	2.51	1.44	1.33
TOTAL	99.72	98.74	100.26	99.61	100.65

## Trace Elements (ppm)

Pb	31.00	30.00	77.00	28.00	27.00
Th	11.00	0.00	13.00	26.00	31.00
U	4.00	0.00	1.00	13.00	4.00
Rb	53.00	115.00	113.00	104.00	119.00
Sr	72.00	153.00	345.00	106.00	47.00
Y	26.00	36.00	9.00	18.00	28.00
Zr	151.00	54.00	130.00	147.00	75.00
Nb	8.00	1.00	10.00	12.00	11.00
Zn	57.00	112.00	41.00	37.00	30.00
Cu	18.00	13.00	19.00	22.00	18.00
Ni	0.00	84.00	2.00	5.00	0.00
La	34.00	27.00	21.00	15.00	26.00
Ba	1854.00	678.00	798.00	231.00	1372.00
V	68.00	174.00	24.00	27.00	7.00
Ce	53.00	41.00	49.00	36.00	73.00
Cr	7.00	181.00	0.00	5.00	0.00
Ga	14.00	11.00	16.00	19.00	12.00
As	23.00	0.00	2.00	0.00	0.00

## S &amp; CO2 (Wt %)

S	0.00	.08	0.00	.01	0.00
CO2	.10				.25

## Precious Metals (ppb)

Au		6.00	2.60	3.70	1.10
Ag		58.00	7967.00	460.00	99.00

## WPGIG.

W-80-163

W-80-112

W-80-122

W-80-210

## Major Elements (Wt %)

SiO2	77.60	80.90	74.00	74.20
TiO2	.09	.21	.24	.26
Al2O3	11.80	9.22	11.80	12.40
Fe2O3	.80	1.80	3.42	3.02
MnO	.01	.02	.04	0.00
MgO	.40	.18	.53	.20
CaO	0.00	.32	.85	0.00
Na2O	2.19	1.65	1.85	.14
K2O	4.97	4.67	5.41	8.96
P2O5	.02	.01	.02	.10
LOI	.76	.61	1.52	.53
TOTAL	98.64	99.59	99.68	99.81

## Trace Elements (ppm)

Pb	2.00	13.00	14.00	19.00
Th	0.00	8.00	9.00	23.00
U	5.00	2.00	4.00	15.00
Rb	117.00	134.00	211.00	184.00
Sr	35.00	18.00	40.00	40.00
Y	17.00	15.00	58.00	74.00
Zr	87.00	107.00	228.00	300.00
Nb	7.00	6.00	12.00	23.00
Zn	35.00	17.00	28.00	22.00
Cu	16.00	19.00	14.00	19.00
Ni	0.00	2.00	10.00	0.00
La	25.00	25.00	43.00	62.00
Ba	1779.00	687.00	615.00	801.00
V	12.00	49.00	91.00	47.00
Ce	46.00	46.00	54.00	107.00
Cr	0.00	31.00	36.00	7.00
Ga	12.00	12.00	15.00	18.00
As	0.00	9.00	0.00	13.00

## S &amp; CO2 (Wt %)

S	.01	0.00	0.00	0.00
CO2		.06	.22	.01

## Precious Metals (ppb)

Au	3.00	.40	6.60	2.50
Ag	62.00	11.00	16.00	7.00

## Chlorite Schist (CHL/SC)

549

W-79-43

W-79-73

W-80-147

W-80-188

W-80-217

## Major Elements (Wt %)

SiO2	47.10	51.60	62.80	0.00	83.50
TiO2	1.79	.99	.87	0.00	.32
Al2O3	15.30	13.80	12.80	0.00	6.80
Fe2O3	11.62	10.35	7.30	0.00	2.28
MnO	.16	.18	.23	0.00	.03
MgO	8.11	5.18	2.54	0.00	.48
CaO	10.00	6.30	4.34	.01	4.34
Na2O	3.16	3.46	4.10	0.00	1.50
K2O	.11	.18	.13	0.00	.07
P2O5	.22	.10	.17	0.00	.04
LOI	2.41	6.70	3.60	0.00	.47
TOTAL	99.98	98.84	98.88		99.83

## Trace Elements (ppm)

Pb	7.00	7.00	9.00	4.00	6.00
Th	0.00	0.00	4.00	4.00	8.00
U	3.00	0.00	8.00	0.00	3.00
Rb	0.00	4.00	9.00	10.00	0.00
Sr	193.00	189.00	177.00	173.00	564.00
Y	28.00	31.00	42.00	29.00	128.00
Zr	93.00	63.00	126.00	97.00	484.00
Nb	6.00	2.00	3.00	6.00	36.00
Zn	94.00	104.00	85.00	82.00	30.00
Cu	58.00	100.00	53.00	52.00	16.00
Ni	106.00	18.00	3.00	11.00	0.00
La	24.00	19.00	24.00	20.00	39.00
Ba	49.00	150.00	71.00	170.00	13.00
V	256.00	372.00	176.00	205.00	13.00
Ce	33.00	26.00	36.00	44.00	95.00
Cr	306.00	30.00	8.00	34.00	0.00
Ga	18.00	9.00	15.00	17.00	14.00
As	10.00	0.00	0.00	7.00	30.00

## S &amp; CO2 (WT.%)

S	0.00	.14	.06	.02	.03
CO2	.04	.41	.28		.04

## Precious Metals (ppb)

Au	4.40	30.20			2.20
Ag	3.00	21.00			3.00

## CHL/SC

	PB4-3	PB27-3	PB38-18	PB51-12	PB38-15
Major Elements (Wt %)					
SiO <sub>2</sub>	51.20	.01	.01	43.70	.01
TiO <sub>2</sub>	1.20	0.00	0.00	1.34	0.00
Al <sub>2</sub> O <sub>3</sub>	15.10	0.00	0.00	14.60	0.00
Fe <sub>2</sub> O <sub>3</sub>	12.00	0.00	0.00	11.87	0.00
MnO	.18	0.00	0.00	.18	0.00
MgO	5.15	0.00	0.00	6.98	0.00
CaO	3.96	0.00	0.00	6.90	0.00
Na <sub>2</sub> O	4.49	0.00	0.00	2.50	0.00
K <sub>2</sub> O	.30	0.00	0.00	1.01	0.00
P <sub>2</sub> O <sub>5</sub>	.13	0.00	0.00	.41	0.00
LOI	4.48	0.00	0.00	9.15	0.00
TOTAL	98.19			98.64	.01

Trace Elements (ppm)					
Pb	9.00	12.00	18.00	8.00	10.00
Th	0.00	1.00	10.00	2.00	8.00
U	0.00	0.00	2.00	0.00	2.00
Rb	7.00	0.00	7.00	31.00	10.00
Sr	150.00	129.00	320.00	230.00	122.00
Y	37.00	27.00	28.00	41.00	21.00
Zr	80.00	114.00	155.00	216.00	108.00
Nb	0.00	6.00	5.00	62.00	3.00
Zn	79.00	119.00	87.00	145.00	101.00
Cu	100.00	172.00	68.00	0.00	357.00
Ni	0.00	5.00	19.00	111.00	13.00
La	12.00	32.00	23.00	49.00	20.00
Ba	225.00	54.00	172.00	303.00	263.00
V	413.00	335.00	202.00	264.00	362.00
Ce	34.00	63.00	40.00	102.00	24.00
Cr	26.00	47.00	57.00	203.00	12.00
Ga	19.00	22.00	13.00	19.00	21.00
As	5.00	44.00	0.00	0.00	6.00

S & CO <sub>2</sub> (WT %)					
S	.14	1.66	.02	0.00	2.13
CO <sub>2</sub>					.31

Precious Metals (ppb)					
Au	8.60			38.00	
Ag	83.00			50.00	

## CHL/SC

PB38-19

PB7-13

## Major Elements (Wt %)

SiO2	49.80	54.20
TiO2	1.53	.48
Al2O3	13.40	15.50
Fe2O3	9.86	6.78
MnO	.20	.13
MgO	5.12	3.51
CaO	6.82	5.21
Na2O	3.95	4.91
K2O	.51	2.17
P2O5	.15	.11
LOI	7.92	5.89

TOTAL	99.26	98.89
-------	-------	-------

## Trace Elements (ppm)

Pb	12.00	3.00
Th	1.00	1.00
U	0.00	4.00
Rb	16.00	103.00
Sr	121.00	166.00
Y	44.00	12.00
Zr	160.00	55.00
Nb	12.00	2.00
Zn	96.00	88.00
Cu	22.00	20.00
Ni	24.00	6.00
La	29.00	11.00
Ba	154.00	423.00
V	328.00	146.00
Ce	60.00	21.00
Cr	75.00	34.00
Ga	12.00	28.00
As	1.00	0.00

## S &amp; CO2 (WT %)

S	.05	.01
CO2	1.13	

## Precious Metals (ppb)

Au	2.00	25.50
Ag	20.00	53.00

## Sericite/Chlorite Schist (SE/CL)

80-27

PB38-17

W-79-7BC

W-80-39

W-80-45

## Major Elements (Wt %)

SiO2	68.70	68.90	79.40	69.00	69.00
TiO2	1.05	.40	.29	.35	.30
Al2O3	11.80	13.70	8.89	14.60	16.10
Fe2O3	6.78	4.58	4.04	4.30	2.43
MnO	.14	.14	.03	.05	.08
MgO	2.22	2.10	1.21	1.17	1.79
CaO	1.75	1.59	1.20	1.57	1.24
Na2O	3.25	4.75	.07	5.82	4.30
K2O	1.38	1.14	2.28	.85	2.67
P2O5	.22	.08	.12	.12	.11
LOI	1.98	2.47	2.48	2.18	2.00
TOTAL	99.27	99.85	100.01	100.01	99.02

## Trace Elements (ppm)

Pb	12.00	7.00	11.00	0.00	56.00
Th	5.00	9.00	9.00	12.00	14.00
U	1.00	3.00	6.00	1.00	7.00
Rb	45.00	27.00	85.00	19.00	86.00
Sr	126.00	132.00	27.00	70.00	38.00
Y	55.00	28.00	31.00	61.00	64.00
Zr	272.00	143.00	317.00	241.00	421.00
Nb	14.00	9.00	9.00	4.00	14.00
Zn	74.00	63.00	48.00	43.00	192.00
Cu	31.00	32.00	14.00	27.00	210.00
Ni	17.00	3.00	11.00	0.00	1.00
La	42.00	13.00	35.00	29.00	47.00
Ba	513.00	559.00	293.00	306.00	1995.00
V	167.00	112.00	85.00	47.00	64.00
Ce	93.00	38.00	56.00	49.00	81.00
Cr	82.00	3.00	118.00	9.00	0.00
Ga	15.00	10.00	11.00	19.00	20.00
As	0.00	0.00	0.00	0.00	0.00

## S &amp; CO2 (WT %)

S	0.00	.16	0.00	0.00	.05
CO2	.12	.10	.34	.38	.29

## Precious Metals (ppb)

Au	4.00	7.30	5.50	13.00	
Ag	48.00	21.00	59.00	22.00	

## SE/CL

	W-80-49	W-80-93	PB4-1	PB4-4	PB15-8
Major Elements (Wt %)					
SiO <sub>2</sub>	89.80	77.70	.01	0.00	47.10
TiO <sub>2</sub>	.17	.62	0.00	0.00	.51
Al <sub>2</sub> O <sub>3</sub>	5.31	10.50	0.00	0.00	17.10
Fe <sub>2</sub> O <sub>3</sub>	1.33	4.18	0.00	0.00	9.98
MnO	.02	.07	0.00	0.00	.18
MgO	.90	.99	0.00	0.00	5.73
CaO	.24	.40	0.00	.01	5.55
Na <sub>2</sub> O	1.77	1.17	0.00	0.00	3.85
K <sub>2</sub> O	.33	1.97	0.00	0.00	1.55
P <sub>2</sub> O <sub>5</sub>	.12	.03	0.00	0.00	.03
LOI	.49	1.97	0.00	0.00	7.73
TOTAL	100.48	99.60			99.31

Trace Elements (ppm)					
Pb	2.00	13.00	8.00	8.00	6.00
Th	8.00	9.00	9.00	6.00	0.00
U	0.00	3.00	5.00	12.00	0.00
Rb	6.00	70.00	43.00	31.00	28.00
Sr	27.00	37.00	84.00	99.00	192.00
Y	13.00	35.00	55.00	51.00	17.00
Zr	86.00	267.00	190.00	256.00	25.00
Nb	5.00	10.00	13.00	20.00	0.00
Zn	25.00	47.00	93.00	156.00	125.00
Cu	15.00	33.00	25.00	48.00	240.00
Ni	4.00	24.00	0.00	0.00	22.00
La	0.00	19.00	31.00	35.00	1.00
Ba	141.00	440.00	849.00	113.00	432.00
V	35.00	93.00	285.00	473.00	297.00
Ce	18.00	57.00	78.00	93.00	11.00
Cr	32.00	107.00	31.00	2.00	72.00
Ga	7.00	12.00	19.00	21.00	16.00
As	0.00	6.00	2.00	33.00	5.00

S & CO <sub>2</sub> (WT %)					
S	0.00	0.00	.30	0.00	.02
CO <sub>2</sub>	.08	.18	.80		1.07

Precious Metals (ppb)					
Au					
Ag					

## SE/CL

	PB19-4	PB19-6	PB27-7	PB38-8	PB38-11
Major Elements (Wt %)					
SiO <sub>2</sub>	.01	.01	76.00	62.00	.01
TiO <sub>2</sub>	0.00	0.00	.10	.38	0.00
Al <sub>2</sub> O <sub>3</sub>	0.00	0.00	13.30	16.90	0.00
Fe <sub>2</sub> O <sub>3</sub>	0.00	0.00	.60	5.48	0.00
MnO	0.00	0.00	.01	.08	0.00
MgO	0.00	0.00	.18	3.76	0.00
CaO	0.00	0.00	1.10	1.01	0.00
Na <sub>2</sub> O	0.00	0.00	6.42	5.34	0.00
K <sub>2</sub> O	0.00	0.00	.97	1.89	0.00
P <sub>2</sub> O <sub>5</sub>	0.00	0.00	.03	.01	0.00
LOI	0.00	0.00	1.23	2.63	0.00
TOTAL			99.94	99.48	

Trace Elements (ppm)					
Pb	1.00	6.00	19.00	33.00	16.00
Th	0.00	14.00	10.00	15.00	15.00
U	0.00	6.00	5.00	1.00	4.00
Rb	56.00	109.00	18.00	45.00	17.00
Sr	124.00	20.00	99.00	153.00	164.00
Y	31.00	45.00	30.00	39.00	32.00
Zr	169.00	155.00	59.00	191.00	192.00
Nb	30.00	19.00	20.00	13.00	28.00
Zn	170.00	94.00	19.00	63.00	52.00
Cu	52.00	16.00	36.00	53.00	176.00
Ni	72.00	27.00	0.00	11.00	46.00
La	43.00	38.00	13.00	32.00	20.00
Ba	201.00	1322.00	640.00	655.00	329.00
V	371.00	191.00	11.00	131.00	118.00
Ce	90.00	71.00	27.00	59.00	55.00
Cr	147.00	71.00	14.00	5.00	75.00
Ga	21.00	23.00	19.00	16.00	16.00
As	38.00	0.00	6.00	0.00	0.00

S & CO <sub>2</sub> (WT %)					
S	.01	0.00	.43	.05	.03
CO <sub>2</sub>	2.00		.24	.07	

Precious Metals (ppb)					
Au			.30	15.50	
Ag			67.00	11.00	



## SE/CL

38-26

PB38-30

PB38-43

PB41-5

PB133-3

## Major Elements (Wt %)

SiO2	.01	.01	.01	0.00	.01
TiO2	0.00	0.00	0.00	0.00	0.00
Al2O3	0.00	0.00	0.00	0.00	0.00
Fe2O3	0.00	0.00	0.00	0.00	0.00
MnO	0.00	0.00	0.00	0.00	0.00
MgO	0.00	0.00	0.00	0.00	0.00
CaO	0.00	0.00	0.00	.01	0.00
Na2O	0.00	0.00	0.00	0.00	0.00
K2O	0.00	0.00	0.00	0.00	0.00
P2O5	0.00	0.00	0.00	0.00	0.00
LOI	0.00	0.00	0.00	0.00	0.00

TOTAL

## Trace Elements (ppm)

Pb	17.00	11.00	4.00	3.00	0.00
Th	15.00	0.00	6.00	3.00	2.00
U	3.00	4.00	1.00	3.00	0.00
Rb	70.00	71.00	7.00	91.00	110.00
Sr	46.00	161.00	271.00	116.00	46.00
Y	68.00	22.00	30.00	76.00	34.00
Zr	287.00	30.00	71.00	228.00	227.00
Nb	17.00	1.00	1.00	13.00	15.00
Zn	71.00	102.00	79.00	75.00	83.00
Cu	17.00	17.00	40.00	22.00	6.00
Ni	16.00	32.00	22.00	0.00	39.00
La	48.00	18.00	7.00	48.00	33.00
Ba	826.00	244.00	160.00	211.00	741.00
V	90.00	322.00	234.00	387.00	115.00
Ce	87.00	26.00	14.00	87.00	67.00
Cr	7.00	49.00	71.00	4.00	101.00
Ga	12.00	17.00	10.00	23.00	20.00
As	3.00	10.00	0.00	38.00	0.00

## S &amp; CO2 (WT %)

S	.16	0.00	.22	.11	0.00
CO2	.95		.46		.27

## Precious Metals (ppb)

Au	1.90
Ag	20.00

## SE/CL

PB4-2

PB3B-16

## Major Elements (Wt %)

SiO2	41.30	0.00
TiO2	2.84	0.00
Al2O3	12.20	0.00
Fe2O3	12.78	0.00
MnO	.24	0.00
MgO	4.64	0.00
CaO	10.82	.01
Na2O	.17	0.00
K2O	1.88	0.00
P2O5	.45	0.00
LOI	11.67	0.00

TOTAL 98.99

## Trace Elements (ppm)

Pb	5.00	8.00
Th	4.00	11.00
U	1.00	2.00
Rb	46.00	31.00
Sr	153.00	154.00
Y	48.00	30.00
Zr	106.00	138.00
Nb	10.00	9.00
Zn	127.00	57.00
Cu	27.00	47.00
Ni	0.00	9.00
La	30.00	32.00
Ba	347.00	804.00
V	629.00	106.00
Ce	70.00	55.00
Cr	0.00	5.00
Ga	21.00	12.00
As	31.00	2.00

## S &amp; CO2 (WT %)

S	.02	.17
CO2		.15

## Precious Metals (ppb)

Au  
Ag

## Sericite Schist (SER/SC)

	W-79-85	W-79-137	W-79-49	W-79-54	W-79-78A
Major Elements (Wt %)					
SiO <sub>2</sub>	57.40	72.60	61.90	54.40	73.30
TiO <sub>2</sub>	1.10	.65	.49	.35	.14
Al <sub>2</sub> O <sub>3</sub>	14.20	11.60	11.00	11.50	9.78
Fe <sub>2</sub> O <sub>3</sub>	9.47	7.94	3.93	3.46	3.68
MnO	.18	.09	.39	.09	.09
MgO	1.45	1.45	1.56	3.65	1.32
CaO	4.37	.19	7.29	9.38	4.00
Na <sub>2</sub> O	2.66	.74	1.68	1.84	.13
K <sub>2</sub> O	3.29	2.65	3.73	2.22	2.40
P <sub>2</sub> O <sub>5</sub>	.47	.17	.13	.06	.11
LOI	7.39	2.27	7.08	11.87	5.04
TOTAL	101.98	100.35	99.18	98.82	99.99

Trace Elements (ppm)					
Pb	13.00	17.00	0.00	8.00	126.00
Th	4.00	15.00	7.00	11.00	9.00
U	0.00	2.00	4.00	4.00	7.00
Rb	158.00	94.00	168.00	75.00	85.00
Sr	120.00	16.00	182.00	329.00	101.00
Y	99.00	33.00	35.00	34.00	35.00
Zr	275.00	309.00	328.00	197.00	302.00
Nb	22.00	19.00	12.00	11.00	10.00
Zn	252.00	74.00	48.00	82.00	177.00
Cu	5.00	28.00	32.00	20.00	14.00
Ni	0.00	31.00	24.00	35.00	21.00
La	46.00	41.00	36.00	36.00	44.00
Ba	718.00	515.00	3320.00	387.00	524.00
V	36.00	117.00	78.00	99.00	82.00
Ce	75.00	62.00	50.00	55.00	59.00
Cr	118.00	78.00	106.00	79.00	95.00
Ga	27.00	13.00	14.00	14.00	15.00
As	32.00	19.00	9.00	1.00	0.00

S & CO <sub>2</sub> (WT %)					
S	0.00	.02	.01	.09	.01
CO <sub>2</sub>		.17	1.58	2.83	.76

Precious Metals (ppb)					
Au				9.10	13.10
Ag				407.00	37.00

## SER/SC

	PB27-2	PB26-10	PB133-10	PB38-7A	PB2B-6
Major Elements (Wt %)					
SiO2	.01	.01	.01	.01	60.20
TiO2	0.00	0.00	0.00	0.00	.54
Al2O3	0.00	0.00	0.00	0.00	14.00
Fe2O3	0.00	0.00	0.00	0.00	7.27
MnO	0.00	0.00	0.00	0.00	.16
MgO	0.00	0.00	0.00	0.00	1.43
CaO	0.00	0.00	0.00	0.00	4.05
Na2O	0.00	0.00	0.00	0.00	2.62
K2O	0.00	0.00	0.00	0.00	2.36
P2O5	0.00	0.00	0.00	0.00	.26
LOI	0.00	0.00	0.00	0.00	5.31
TOTAL					98.20

Trace Elements (ppm)					
Pb	32.00	2.00	15.00	27.00	759.00
Th	10.00	14.00	3.00	12.00	22.00
U	4.00	6.00	1.00	2.00	4.00
Rb	43.00	109.00	87.00	49.00	63.00
Sr	25.00	85.00	36.00	159.00	141.00
Y	35.00	37.00	22.00	28.00	108.00
Zr	406.00	405.00	263.00	145.00	361.00
Nb	11.00	12.00	11.00	10.00	27.00
Zn	33.00	51.00	70.00	65.00	1026.00
Cu	836.00	15.00	8.00	35.00	72.00
Ni	5.00	33.00	24.00	8.00	0.00
La	38.00	29.00	32.00	22.00	49.00
Ba	4318.00	512.00	302.00	617.00	549.00
V	84.00	89.00	97.00	106.00	26.00
Ce	48.00	70.00	52.00	45.00	86.00
Cr	34.00	120.00	95.00	2.00	0.00
Ga	0.00	14.00	16.00	11.00	44.00
As	103.00	16.00	0.00	0.00	41.00

S & CO2 (WT %)					
S	7.71	0.00	0.00	.33	.38
CO2	.15			.35	.80

Precious Metals (ppb)					
Au					1.60
Ag					208.00

SER/SC

PB28-12

PB28-7

## Major Elements (Wt %)

SiO2	.01	.01
TiO2	0.00	0.00
Al2O3	0.00	0.00
Fe2O3	0.00	0.00
MnO	0.00	0.00
MgO	0.00	0.00
CaO	0.00	0.00
Na2O	0.00	0.00
K2O	0.00	0.00
P2O5	0.00	0.00
LOI	0.00	0.00

TOTAL

## Trace Elements (ppm)

Pb	5731.00	2364.00
Th	12.00	10.00
U	0.00	8.00
Rb	104.00	75.00
Sr	146.00	86.00
Y	61.00	99.00
Zr	281.00	370.00
Nb	13.00	23.00
Zn	154.00	1209.00
Cu	2407.00	880.00
Ni	5.00	0.00
La	34.00	48.00
Ba	446.00	450.00
V	81.00	45.00
Ce	68.00	90.00
Cr	29.00	4.00
Ga	112.00	68.00
As	80.00	72.00

## S &amp; CO2 (WT %)

S	.58	.61
CO2	.92	.57

## Precious Metals (ppb)

Au  
Ag

## Chlorite/Biotite Schist (CL/BIO)

79-141

PB51-1

38-13

79.83

80-215

## Major Elements (Wt %)

SiO2	66.40	.01	.01	75.00	65.50
TiO2	.83	0.00	0.00	.40	.58
Al2O3	12.80	0.00	0.00	11.20	13.40
Fe2O3	6.05	0.00	0.00	3.33	7.17
MnO	.07	0.00	0.00	.06	.11
MgO	3.30	0.00	0.00	.69	1.35
CaO	3.07	0.00	0.00	2.00	3.41
Na2O	2.38	0.00	0.00	2.94	4.53
K2O	2.46	0.00	0.00	2.34	1.65
P2O5	.20	0.00	0.00	.06	.03
LOI	1.18	0.00	0.00	1.99	1.60
TOTAL	98.74			100.01	99.33

## Trace Elements (ppm)

Pb	8.00	8.00	129.00	23.00	16.00
Th	7.00	0.00	8.00	16.00	15.00
U	7.00	6.00	7.00	2.00	11.00
Rb	101.00	35.00	62.00	70.00	35.00
Sr	113.00	141.00	50.00	101.00	279.00
Y	39.00	62.00	30.00	36.00	121.00
Zr	208.00	246.00	357.00	149.00	682.00
Nb	14.00	29.00	12.00	15.00	37.00
Zn	75.00	117.00	46.00	40.00	145.00
Cu	10.00	26.00	603.00	40.00	28.00
Ni	53.00	10.00	23.00	24.00	0.00
La	53.00	49.00	54.00	33.00	58.00
Ba	530.00	164.00	7629.00	405.00	488.00
V	113.00	466.00	107.00	85.00	34.00
Ce	79.00	118.00	65.00	51.00	107.00
Cr	132.00	24.00	46.00	69.00	6.00
Ga	16.00	19.00	8.00	10.00	25.00
As	0.00	22.00	83.00	23.00	21.00

## S &amp; CO2 (Wt %)

S	0.00	.09	6.72	0.00	.05
CO2		.87	.37	.08	

## Precious Metals (ppb)

Au	7.50
Ag	71.00

## CL/BIO

80-37

80-37B

PB38-4

PB38-12

79-120

## Major Elements (Wt %)

SiO2	49.50	54.60	.01	.01	69.80
TiO2	.68	.47	0.00	0.00	.70
Al2O3	17.60	16.60	0.00	0.00	13.60
Fe2O3	10.24	7.17	0.00	0.00	5.49
MnO	.15	.12	0.00	0.00	.11
MgO	5.25	3.58	0.00	0.00	1.47
CaO	5.48	5.88	0.00	0.00	1.53
Na2O	4.63	4.80	0.00	0.00	4.00
K2O	1.60	1.05	0.00	0.00	3.11
P2O5	.12	.19	0.00	0.00	.11
LOI	1.98	3.55	0.00	0.00	.91
TOTAL	97.23	98.01			100.83

## Trace Elements (ppm)

Pb	12.00	18.00	11.00	16.00	34.00
Th	5.00	5.00	11.00	18.00	12.00
U	1.00	70.00	3.00	4.00	6.00
Rb	45.00	26.00	44.00	50.00	86.00
Sr	126.00	199.00	194.00	63.00	41.00
Y	55.00	20.00	30.00	45.00	79.00
Zr	272.00	53.00	152.00	184.00	345.00
Nb	14.00	3.00	10.00	19.00	19.00
Zn	74.00	73.00	30.00	87.00	116.00
Cu	31.00	45.00	34.00	121.00	9.00
Ni	17.00	6.00	11.00	60.00	16.00
La	42.00	28.00	27.00	50.00	42.00
Ba	513.00	330.00	701.00	837.00	1192.00
V	167.00	202.00	109.00	137.00	65.00
Ce	93.00	46.00	59.00	101.00	90.00
Cr	82.00	12.00	10.00	82.00	10.00
Ga	15.00	15.00	12.00	18.00	15.00
As	0.00	0.00	0.00	11.00	7.00

## S &amp; CO2 (Wt %)

S	0.00	0.00	.02	1.30	0.00
CO2	.12	.43			.03

## Precious Metals (ppb)

Au	4.00	10.90			
Ag	48.00	55.00			

## Graphite Schist (GAST)

	W-80-38	W-80-40	PB4-5	PB15-2	PB19-7
Major Elements (Wt %)					
SiO <sub>2</sub>	60.30	59.50	66.90	.01	.01
TiO <sub>2</sub>	.77	.98	.59	0.00	0.00
Al <sub>2</sub> O <sub>3</sub>	15.20	17.60	12.40	0.00	0.00
Fe <sub>2</sub> O <sub>3</sub>	9.16	5.84	7.23	0.00	0.00
MnO	.74	.13	.25	0.00	0.00
MgO	2.50	1.73	2.86	0.00	0.00
CaO	.60	1.02	1.62	0.00	0.00
Na <sub>2</sub> O	2.46	1.18	.15	0.00	0.00
K <sub>2</sub> O	2.37	4.33	2.72	0.00	0.00
P <sub>2</sub> O <sub>5</sub>	.17	.19	.09	0.00	0.00
LOI	4.57	5.97	4.39	0.00	0.00
TOTAL	98.84	98.47	99.20		

Trace Elements (ppm)					
Pb	25.00	29.00	5.00	12.00	13.00
Th	8.00	15.00	6.00	20.00	0.00
U	1.00	14.00	2.00	10.00	3.00
Rb	123.00	149.00	97.00	165.00	67.00
Sr	46.00	54.00	47.00	60.00	105.00
Y	32.00	39.00	27.00	41.00	46.00
Zr	116.00	180.00	131.00	147.00	151.00
Nb	16.00	21.00	14.00	19.00	25.00
Zn	120.00	79.00	56.00	95.00	93.00
Cu	90.00	102.00	70.00	59.00	54.00
Ni	24.00	36.00	29.00	39.00	46.00
La	54.00	44.00	30.00	57.00	35.00
Ba	381.00	572.00	461.00	673.00	5356.00
V	171.00	412.00	174.00	333.00	296.00
Ce	108.00	64.00	67.00	95.00	72.00
Cr	70.00	94.00	57.00	111.00	105.00
Ga	22.00	27.00	18.00	29.00	17.00
As	14.00	0.00	2.00	18.00	63.00

S & CO <sub>2</sub> (Wt %)					
S	1.07	.84	0.00	.23	.90
CO <sub>2</sub>	.99	1.39	.69	1.61	

Precious Metals (ppb)					
Au	2.70	11.80	5.60		
Ag	24.00	39.00	7.00		



## GAST

	PB19-10	PB26-2	PB27-22	PB38-25	PB38-29
Major Elements (Wt %)					
SiO <sub>2</sub>	61.90	.01	63.00	.01	53.80
TiO <sub>2</sub>	.51	0.00	.23	0.00	.36
Al <sub>2</sub> O <sub>3</sub>	15.60	0.00	9.80	0.00	13.40
Fe <sub>2</sub> O <sub>3</sub>	8.17	0.00	4.70	0.00	8.76
MnO	.19	0.00	.32	0.00	.18
MgO	3.33	0.00	2.73	0.00	3.76
CaO	.27	0.00	7.35	0.00	.58
Na <sub>2</sub> O	.28	0.00	.14	0.00	.22
K <sub>2</sub> O	3.40	0.00	2.32	0.00	3.18
P <sub>2</sub> O <sub>5</sub>	.10	0.00	.15	0.00	.30
LOI	4.35	0.00	8.36	0.00	8.68
TOTAL	98.10	.01	99.10		93.22

Trace Elements (ppm)					
Pb	13.00	25.00	91.00	26.00	197.00
Th	8.00	2.00	0.00	6.00	18.00
U	2.00	11.00	16.00	13.00	7.00
Rb	128.00	101.00	68.00	69.00	108.00
Sr	38.00	66.00	122.00	49.00	51.00
Y	25.00	31.00	28.00	34.00	41.00
Zr	173.00	93.00	182.00	92.00	126.00
Nb	18.00	10.00	12.00	15.00	14.00
Zn	90.00	64.00	305.00	53.00	181.00
Cu	58.00	59.00	57.00	91.00	262.00
Ni	40.00	54.00	18.00	61.00	108.00
La	49.00	32.00	32.00	28.00	50.00
Ba	593.00	1270.00	215.00	2415.00	527.00
V	287.00	218.00	174.00	152.00	336.00
Ce	97.00	40.00	57.00	56.00	82.00
Cr	102.00	83.00	73.00	53.00	70.00
Ga	26.00	14.00	18.00	6.00	15.00
As	109.00	78.00	37.00	159.00	225.00

S & CO <sub>2</sub> (Wt %)					
S	.06	.85	.19	1.50	3.50
CO <sub>2</sub>	.49	1.95	1.90	1.78	1.19

Precious Metals (ppb)					
Au	4.70		7.60		8.50
Ag	36.00		58.00		127.00

## GAST

	PB38-31	PB38-33	PB38-40	PB38-41	PB38-42
Major Elements (Wt %)					
SiO <sub>2</sub>	.01	.01	.01	56.70	62.30
TiO <sub>2</sub>	0.00	0.00	0.00	.29	.34
Al <sub>2</sub> O <sub>3</sub>	0.00	0.00	0.00	10.90	11.40
Fe <sub>2</sub> O <sub>3</sub>	0.00	0.00	0.00	5.19	3.93
MnO	0.00	0.00	0.00	.20	.06
MgO	0.00	0.00	0.00	2.05	1.77
CaO	0.00	0.00	0.00	10.24	2.38
Na <sub>2</sub> O	0.00	0.00	0.00	.96	.13
K <sub>2</sub> O	0.00	0.00	0.00	2.46	2.96
P <sub>2</sub> O <sub>5</sub>	0.00	0.00	0.00	.09	.66
LOI	0.00	0.00	0.00	10.60	9.83
TOTAL				99.68	95.76

Trace Elements (ppm)					
Pb	27.00	88.00	70.00	8.00	82.00
Th	17.00	17.00	5.00	0.00	15.00
U	9.00	11.00	3.00	3.00	17.00
Rb	138.00	163.00	68.00	61.00	104.00
Sr	78.00	44.00	231.00	249.00	80.00
Y	50.00	46.00	30.00	38.00	55.00
Zr	156.00	152.00	107.00	114.00	116.00
Nb	20.00	20.00	10.00	5.00	15.00
Zn	53.00	131.00	85.00	95.00	469.00
Cu	111.00	100.00	33.00	43.00	195.00
Ni	67.00	71.00	27.00	23.00	119.00
La	41.00	51.00	13.00	24.00	36.00
Ba	592.00	492.00	357.00	373.00	343.00
V	439.00	455.00	96.00	89.00	875.00
Ce	63.00	79.00	32.00	35.00	62.00
Cr	102.00	89.00	26.00	19.00	47.00
Ga	19.00	23.00	10.00	10.00	15.00
As	67.00	90.00	18.00	38.00	138.00

S & CO <sub>2</sub> (Wt %)					
S	1.11	1.33	.07	.07	2.85
CO <sub>2</sub>	.81	2.23	1.69	2.31	4.42

Precious Metals (ppb)					
Au				7.90	1.20
Ag				92.00	74.00

## GAST

PB41-4

PB41-7

PB53-1

PB53-4

## Major Elements (Wt %)

SiO2	58.70	.01	63.20	.01
TiO2	.22	0.00	.40	0.00
Al2O3	17.10	0.00	13.30	0.00
Fe2O3	7.27	0.00	7.28	0.00
MnO	.08	0.00	.15	0.00
MgO	3.02	0.00	2.86	0.00
CaO	1.79	0.00	2.48	0.00
Na2O	.21	0.00	.24	0.00
K2O	4.27	0.00	2.89	0.00
P2O5	.13	0.00	.30	0.00
LOI	5.86	0.00	5.12	0.00
TOTAL	98.65		98.22	

## Trace Elements (ppm)

Pb	12.00	409.00	5.00	41.00
Th	9.00	18.00	7.00	0.00
U	16.00	9.00	8.00	6.00
Rb	155.00	126.00	88.00	77.00
Sr	58.00	126.00	38.00	150.00
Y	34.00	46.00	47.00	34.00
Zr	161.00	157.00	128.00	87.00
Nb	19.00	14.00	16.00	3.00
Zn	44.00	168.00	51.00	100.00
Cu	101.00	113.00	92.00	69.00
Ni	54.00	35.00	37.00	26.00
La	49.00	39.00	52.00	24.00
Ba	508.00	398.00	508.00	334.00
V	479.00	406.00	307.00	375.00
Ce	91.00	67.00	90.00	49.00
Cr	106.00	84.00	94.00	93.00
Ga	26.00	32.00	20.00	16.00
As	38.00	417.00	78.00	63.00

## S &amp; CO2 (Wt %)

S	.29	1.12	.19	.16
CO2	1.35	1.80	.62	3.86

## Precious Metals (ppb)

Au	1.60	13.30	13.00	
Ag	17.00	333.00	9.00	

## Port aux Basques Gneiss (PAB/GN)

79-71

79-77

79-150

79-170S

80-47G

## Major Elements (Wt %)

SiO <sub>2</sub>	67.10	56.80	54.00	80.60	66.90
TiO <sub>2</sub>	.29	.68	.80	.73	.57
Al <sub>2</sub> O <sub>3</sub>	14.10	20.40	18.00	8.45	12.80
Fe <sub>2</sub> O <sub>3</sub>	4.20	7.80	9.26	2.76	7.32
MnO	.07	.09	.15	.09	.15
MgO	2.71	2.58	5.46	1.01	3.57
CaO	1.82	.17	4.34	1.75	5.15
Na <sub>2</sub> O	3.97	.45	5.29	2.37	2.94
K <sub>2</sub> O	1.32	5.52	.64	.68	.24
P <sub>2</sub> O <sub>5</sub>	.07	.15	.26	.09	.27
LOI	2.36	4.57	2.98	.22	.35
TOTAL	98.01	99.21	101.18	98.75	100.26

## Trace Elements (ppm)

Pb	36.00	12.00	10.00	7.00	10.00
Th	9.00	26.00	4.00	11.00	5.00
U	0.00	0.00	0.00	4.00	1.00
Rb	30.00	207.00	13.00	30.00	9.00
Sr	247.00	22.00	367.00	227.00	128.00
Y	20.00	50.00	25.00	35.00	39.00
Zr	123.00	193.00	135.00	516.00	90.00
Nb	4.00	19.00	6.00	12.00	4.00
Zn	75.00	48.00	85.00	31.00	59.00
Cu	101.00	35.00	189.00	76.00	34.00
Ni	11.00	20.00	1.00	14.00	7.00
La	20.00	66.00	28.00	31.00	20.00
Ba	1268.00	1275.00	441.00	833.00	171.00
V	159.00	181.00	287.00	67.00	290.00
Ce	49.00	118.00	39.00	77.00	45.00
Cr	16.00	96.00	11.00	74.00	32.00
Ga	16.00	34.00	16.00	4.00	23.00
As	0.00	3.00	0.00	21.00	0.00

S & CO<sub>2</sub> (Wt %)

S	.43	.42	.02	.04	.02
CO <sub>2</sub>	.37	.22		0.00	.06

## Precious Metals (ppb)

Au	3.80	0.00		11.40	3.40
Ag	14813.00	35.00		113.00	30.00

PAB/GN

80-53

80-105

## Major Elements (Wt %)

SiO2	77.60	67.60
TiO2	.18	.92
Al2O3	12.70	15.20
Fe2O3	1.46	7.14
MnO	.04	.19
MgO	1.41	1.48
CaO	.72	.29
Na2O	5.04	.81
K2O	.73	3.93
P2O5	.07	.12
LOI	1.95	1.90
TOTAL	101.90	99.58

## Trace Elements (ppm)

Pb	15.00	10.00
Th	0.00	9.00
U	0.00	5.00
Rb	10.00	163.00
Sr	120.00	45.00
Y	26.00	41.00
Zr	196.00	237.00
Nb	8.00	17.00
Zn	41.00	59.00
Cu	11.00	17.00
Ni	0.00	17.00
La	31.00	43.00
Ba	1826.00	763.00
V	47.00	162.00
Ce	61.00	86.00
Cr	17.00	88.00
Ga	12.00	23.00
As	0.00	74.00

## S &amp; CO2 (Wt %)

S	.13	0.00
CO2		

## Precious Metals (ppb)

Au	0.00
Ag	10.00

## Contact Zone Windsor Point Group (WPGQ)

W-79-64

W-79-122

W-79-110

W-79-111

W-79-116

## Major Elements (Wt %)

SiO2	71.90	50.00	48.30	47.20	59.00
TiO2	.36	2.56	1.80	1.45	1.03
Al2O3	14.20	14.80	14.10	17.00	16.40
Fe2O3	3.29	14.72	12.13	10.66	8.12
MnO	.03	.26	.19	.15	.50
MgO	1.63	4.90	7.37	8.63	3.90
CaO	.51	7.72	12.71	8.55	2.83
Na2O	6.38	3.66	2.73	3.54	1.33
K2O	1.06	1.00	.56	.32	3.29
P2O5	.13	.27	.19	.15	.20
LOI	.77	.91	.67	1.77	3.02
TOTAL	100.26	100.80	100.75	99.42	99.62

## Trace Elements (ppm)

Pb	21.00	17.00	6.00	3.00	10.00
Th	11.00	7.00	0.00	0.00	13.00
U	3.00	3.00	4.00	3.00	10.00
Rb	25.00	38.00	28.00	15.00	102.00
Sr	84.00	145.00	203.00	191.00	97.00
Y	11.00	59.00	32.00	35.00	40.00
Zr	192.00	192.00	121.00	102.00	152.00
Nb	8.00	16.00	9.00	8.00	15.00
Zn	60.00	130.00	115.00	90.00	154.00
Cu	23.00	15.00	9.00	40.00	63.00
Ni	0.00	0.00	45.00	109.00	42.00
La	12.00	38.00	25.00	24.00	34.00
Ba	1203.00	193.00	65.00	115.00	545.00
V	66.00	330.00	268.00	245.00	292.00
Ce	23.00	83.00	41.00	42.00	71.00
Cr	3.00	18.00	190.00	265.00	113.00
Ga	16.00	21.00	18.00	19.00	23.00
As	0.00	21.00	16.00	4.00	15.00

## S &amp; CO2 (Wt %)

S	.06	.06	0.00	0.00	0.53
CO2	.02			.05	0.31

## Precious Metals (ppb)

Au	2.50	49.00	0.00	6.10	0.00
Ag	5.00	26.00	112.00	44.00	34.00

## Retrogressed Port aux Basques Gneiss (PABQ)

79-72      79-151      79-152      79-158

## Major Elements (Wt %)

SiO <sub>2</sub>	61.60	49.90	47.60	69.10
TiO <sub>2</sub>	.57	.38	.35	.45
Al <sub>2</sub> O <sub>3</sub>	10.60	16.30	17.40	13.80
Fe <sub>2</sub> O <sub>3</sub>	12.44	11.08	7.58	4.27
MnO	.23	.14	.23	.08
MgO	4.39	7.40	9.11	2.02
CaO	1.63	2.31	3.95	2.10
Na <sub>2</sub> O	2.62	5.93	4.92	4.83
K <sub>2</sub> O	.19	.78	1.43	2.00
P <sub>2</sub> O <sub>5</sub>	.10	0.00	0.00	.08
LOI	4.53	6.26	6.96	1.60
TOTAL	98.90	100.48	99.53	100.33

## Trace Elements (ppm)

Pb	12.00	19.00	37.00	16.00
Th	0.00	2.00	0.00	16.00
U	0.00	2.00	0.00	4.00
Rb	7.00	23.00	48.00	45.00
Sr	61.00	223.00	254.00	133.00
Y	37.00	18.00	21.00	29.00
Zr	155.00	47.00	53.00	141.00
Nb	12.00	3.00	2.00	8.00
Zn	96.00	67.00	85.00	41.00
Cu	1279.00	26.00	14.00	15.00
Ni	14.00	29.00	39.00	0.00
La	32.00	11.00	17.00	18.00
Ba	56.00	519.00	400.00	847.00
V	199.00	357.00	96.00	114.00
Ce	59.00	15.00	30.00	47.00
Cr	55.00	106.00	366.00	4.00
Ga	11.00	12.00	21.00	14.00
As	27.00	24.00	30.00	0.00

S & CO<sub>2</sub> (Wt %)

S	1.38	3.37	1.80	.01
CO <sub>2</sub>	.32	.09		

## Precious Metals (ppb)

Au	3.00	9.90	13.80	
Ag	40.00	15.00	111.00	

Wall Rocks to Main Shear Showing (WAL/RX)

570

W-80-61A

W-80-61H

W-80-61L

W-80-61L

W-80-64

Major Elements (Wt %)

SiO2	68.80	48.20	48.50	47.40	48.20
TiO2	.51	2.04	.71	.49	2.95
Al2O3	11.60	12.40	18.30	13.60	12.70
Fe2O3	6.45	11.78	10.85	10.78	16.60
MnO	.16	.52	.10	.48	.33
MgO	2.27	3.48	1.57	2.16	3.04
CaO	2.23	6.12	1.20	9.13	6.64
Na2O	.10	.12	.15	1.65	2.77
K2O	2.81	2.99	5.08	2.06	1.54
P2O5	.14	.48	.97	.23	.85
LOI	4.64	10.85	12.37	10.16	2.97
TOTAL	99.71	98.98	99.80	98.14	98.59

Trace Elements (ppm)

Pb	28.00	71.00	542.00	24.00	5.00
Th	19.00	0.00	21.00	1.00	0.00
U	6.00	0.00	74.00	1.00	4.00
Rb	83.00	77.00	153.00	61.00	55.00
Sr	35.00	105.00	57.00	98.00	199.00
Y	56.00	54.00	100.00	47.00	96.00
Zr	317.00	201.00	194.00	162.00	299.00
Nb	17.00	24.00	24.00	13.00	30.00
Zn	80.00	292.00	197.00	88.00	129.00
Cu	24.00	95.00	206.00	41.00	8.00
Ni	19.00	4.00	51.00	0.00	0.00
La	55.00	52.00	70.00	30.00	58.00
Ba	368.00	225.00	801.00	301.00	241.00
V	142.00	505.00	4103.00	305.00	140.00
Ce	103.00	92.00	120.00	80.00	112.00
Cr	72.00	7.00	284.00	26.00	0.00
Ga	18.00	28.00	49.00	20.00	24.00
As	39.00	38.00	221.00	36.00	27.00

S & CO2 (Wt %)

S	0.00	.16	.15	.07	.19
CO2	.59	2.23	5.02	2.63	

Precious Metals (ppb)

Au	5.70	6.60	2.00	3.00	
Ag	126.00	52.00	7100.00	7.00	



W-80-65C

W-80-66A

W-80-182

PB38-5B

PB38-3B

## Major Elements (Wt.%)

SiO2	63.50	48.20	57.20	0.00	0.00
TiO2	.34	.37	1.36	0.00	0.00
Al2O3	16.20	14.40	16.70	0.00	0.00
Fe2O3	7.36	11.90	11.13	0.00	0.00
MnO	.10	.25	.11	.01	0.00
MgO	2.78	3.65	2.74	0.00	0.00
CaO	.40	6.99	.94	0.00	1.00
Na2O	.21	.16	2.62	0.00	0.00
K2O	3.69	2.69	2.50	0.00	0.00
P2O5	.27	.18	.75	0.00	0.00
LOI	5.01	9.66	3.73	.01	0.00
TOTAL	99.86	98.45	99.78		

## Trace Elements (ppm)

Pb	170.00	9.00	14.00	483.00	5.00
Th	17.00	7.00	6.00	16.00	0.00
U	6.00	5.00	3.00	2.00	0.00
Rb	118.00	68.00	100.00	145.00	54.00
Sr	19.00	158.00	72.00	25.00	116.00
Y	65.00	37.00	90.00	29.00	39.00
Zr	149.00	75.00	384.00	148.00	91.00
Nb	14.00	2.00	24.00	9.00	3.00
Zn	141.00	95.00	157.00	107.00	54.00
Cu	59.00	118.00	3.00	293.00	7.00
Ni	29.00	3.00	0.00	6.00	0.00
La	53.00	24.00	79.00	30.00	12.00
Ba	497.00	254.00	445.00	777.00	146.00
V	222.00	468.00	88.00	100.00	135.00
Ce	84.00	37.00	106.00	54.00	26.00
Cr	77.00	39.00	0.00	3.00	0.00
Ga	27.00	19.00	34.00	11.00	17.00
As	70.00	32.00	1.00	52.00	3.00

## S &amp; CO2 (Wt. %)

S	0.00	.21	.01	.74	0.00
CO2	.67	1.40		.05	.54

## Precious Metals (ppb)

Au	9.10	16.60
Ag	127.00	202.00

PB63-6

PB63-8

PB28-13

PB38-36

PB38-20

## Major Elements (Wt %)

SiO2	1.00	57.10	66.80	45.10	.01
TiO2	0.00	.38	.91	.51	0.00
Al2O3	0.00	16.40	12.10	14.10	0.00
Fe2O3	0.00	6.27	5.78	11.52	0.00
MnO	0.00	.27	.11	.25	0.00
MgO	0.00	2.56	1.90	5.41	0.00
CaO	0.00	3.29	3.28	8.06	0.00
Na2O	0.00	.17	1.70	.10	0.00
K2O	0.00	4.60	2.51	2.76	0.00
P2O5	0.00	.13	.16	.05	0.00
LOI	0.00	7.08	4.55	10.57	0.00
TOTAL		98.25	99.80	98.43	

## Trace Elements (ppm)

Pb	64.00	60.00	6.00	57.00	11.00
Th	0.00	14.00	6.00	0.00	6.00
U	3.00	12.00	2.00	3.00	1.00
Rb	58.00	154.00	98.00	75.00	90.00
Sr	68.00	98.00	90.00	203.00	97.00
Y	28.00	46.00	55.00	29.00	50.00
Zr	83.00	152.00	311.00	72.00	155.00
Nb	3.00	16.00	17.00	5.00	10.00
Zn	110.00	113.00	92.00	179.00	40.00
Cu	65.00	85.00	16.00	23.00	48.00
Ni	3.00	40.00	14.00	2.00	21.00
La	15.00	48.00	48.00	9.00	21.00
Ba	296.00	656.00	515.00	328.00	789.00
V	298.00	268.00	104.00	297.00	393.00
Ce	36.00	77.00	77.00	27.00	26.00
Cr	0.00	100.00	59.00	30.00	0.00
Ga	22.00	25.00	19.00	20.00	12.00
As	38.00	107.00	4.00	19.00	35.00

## S &amp; CO2 (Wt %)

S	.10	.35	.01	.01	.12
CO2		2.07	0.00	.89	

## Precious Metals (ppb)

Au	5.30	1.90	1.30	9.50
Ag	32.00	16.00	11.00	120.00

Long Range Mafic/Ultramafic Complex (LRM/UM)

573

W-80-78

W-80-113

W-80-115

W-80-116

W-80-127

Major Elements (Wt %)

SiO2	46.50	47.50	50.30	44.60	.01
TiO2	.48	.30	.25	.17	0.00
Al2O3	13.20	15.30	7.37	26.50	0.00
Fe2O3	10.12	9.09	12.00	4.86	0.00
MnO	.17	.23	.23	.07	0.00
MgO	11.33	11.00	18.70	3.56	0.00
CaO	12.03	12.17	7.66	13.79	0.00
Na2O	.77	.79	.19	1.35	0.00
K2O	1.30	1.74	.04	1.66	0.00
P2O5	.07	.10	.08	.03	0.00
LOI	2.56	3.95	3.95	3.12	0.00
TOTAL	98.53	102.17	100.77	99.71	

Trace Elements (ppm)

Pb	20.00	16.00	6.00	12.00	10.00
Th	7.00	8.00	2.00	0.00	0.00
U	10.00	2.00	4.00	0.00	0.00
Rb	37.00	55.00	3.00	64.00	61.00
Sr	258.00	270.00	0.00	818.00	173.00
Y	21.00	12.00	7.00	3.00	3.00
Zr	36.00	33.00	56.00	15.00	19.00
Nb	3.00	3.00	2.00	3.00	3.00
Zn	98.00	75.00	95.00	42.00	87.00
Cu	137.00	32.00	16.00	21.00	17.00
Ni	73.00	91.00	241.00	29.00	299.00
La	35.00	22.00	19.00	13.00	22.00
Ba	966.00	644.00	6.00	751.00	93.00
V	272.00	166.00	115.00	74.00	77.00
Ce	45.00	20.00	17.00	14.00	25.00
Cr	240.00	90.00	574.00	43.00	723.00
Ga	13.00	14.00	9.00	15.00	11.00
As	0.00	14.00	3.00	0.00	0.00

S & CO2 (Wt %)

S	.04	.01	.01	0.00	.02
CO2					

Precious Metals (ppb)

Au	15.40		2.30	0.00	
Ag	39.00		25.00	5.00	

LRM/UM

W-80-142

W-79-101

## Major Elements (Wt %)

SiO2	48.60	48.60
TiO2	.20	.24
Al2O3	18.40	12.30
Fe2O3	7.33	8.81
MnO	.12	.16
MgO	9.33	13.24
CaO	8.73	12.75
Na2O	1.12	.56
K2O	1.64	.52
P2O5	.13	.03
LOI	3.61	2.61
TOTAL	99.21	99.82

## Trace Elements (ppm)

Pb	9.00	6.00
Th	0.00	0.00
U	1.00	0.00
Rb	64.00	13.00
Sr	528.00	341.00
Y	6.00	14.00
Zr	28.00	30.00
Nb	2.00	3.00
Zn	76.00	74.00
Cu	12.00	8.00
Ni	138.00	35.00
La	21.00	14.00
Ba	464.00	212.00
V	81.00	122.00
Ce	26.00	17.00
Cr	263.00	52.00
Ga	13.00	6.00
As	0.00	23.00

## S &amp; CO2 (Wt %)

S	0.00	.01
CO2		

## Precious Metals (ppb)

Au	6.10
Ag	31.00

Gabbros South of Windowglass Hill Granite (GABWG)

575

W-79-129

W-79-131

W-79-136

W-79-139

W-80-109

Major Elements (Wt %)

	W-79-129	W-79-131	W-79-136	W-79-139	W-80-109
SiO <sub>2</sub>	48.60	48.40	49.00	49.20	45.20
TiO <sub>2</sub>	2.40	2.02	1.45	1.69	.23
Al <sub>2</sub> O <sub>3</sub>	15.10	14.50	17.70	14.90	11.60
Fe <sub>2</sub> O <sub>3</sub>	13.76	12.00	9.85	11.10	10.07
MnO	.26	.18	.24	.19	.19
MgO	6.00	8.30	7.85	7.70	16.00
CaO	10.00	10.17	7.69	9.38	10.84
Na <sub>2</sub> O	3.60	2.43	4.11	2.61	1.49
K <sub>2</sub> O	.41	.21	.40	.46	.05
P <sub>2</sub> O <sub>5</sub>	.21	.23	.18	.19	0.00
LOI	.55	.73	2.00	2.85	2.72
TOTAL	100.89	99.17	100.47	100.27	98.39

Trace Element (ppm)

	W-79-129	W-79-131	W-79-136	W-79-139	W-80-109
Pb	6.00	9.00	9.00	8.00	6.00
Th	0.00	7.00	4.00	0.00	2.00
U	0.00	3.00	1.00	14.00	3.00
Rb	9.00	5.00	14.00	19.00	3.00
Sr	215.00	271.00	311.00	268.00	117.00
Y	38.00	36.00	26.00	45.00	9.00
Zr	137.00	139.00	83.00	136.00	7.00
Nb	12.00	16.00	5.00	4.00	2.00
Zn	132.00	85.00	62.00	97.00	65.00
Cu	8.00	56.00	41.00	28.00	40.00
Ni	19.00	80.00	41.00	41.00	104.00
La	43.00	11.00	8.00	26.00	7.00
Ba	89.00	55.00	94.00	178.00	28.00
V	326.00	318.00	266.00	282.00	207.00
Ce	56.00	19.00	10.00	46.00	10.00
Cr	88.00	201.00	182.00	96.00	424.00
Ga	23.00	14.00	10.00	19.00	9.00
As	12.00	18.00	0.00	31.00	0.00

S & CO<sub>2</sub> (Wt %)

	W-79-129	W-79-131	W-79-136	W-79-139	W-80-109
S	.01	.04	0.00	0.00	0.00
CO <sub>2</sub>		.02			

Precious Metals (ppb)

	W-79-129	W-79-131	W-79-136	W-79-139	W-80-109
Au			.50		
Ag			124.00		

## GABWG

576

W-79-132

W-79-105

W-79-123

W79-123A

W-79-125

## Major Elements (Wt %)

SiO2	48.00	49.00	46.30	46.80	49.50
TiO2	2.54	1.48	1.92	1.81	2.19
Al2O3	14.70	14.10	14.20	15.00	13.10
Fe2O3	15.74	12.55	13.48	12.32	15.00
MnO	.18	.20	.20	.18	.25
MgO	3.50	8.73	9.41	7.66	6.10
CaO	11.30	9.79	10.48	10.14	6.55
Na2O	3.76	2.77	2.38	3.26	3.86
K2O	.52	.29	.40	2.79	1.04
P2O5	.32	.10	.28	.21	.18
LOI	.43	1.40	1.10	1.00	1.45
TOTAL	100.99	100.41	100.15	101.17	99.22

## Trace Element (ppm)

Pb	3.00	0.00	6.00	7.00	13.00
Th	5.00	0.00	0.00	4.00	3.00
U	4.00	0.00	0.00	1.00	2.00
Rb	23.00	9.00	18.00	18.00	53.00
Sr	166.00	209.00	202.00	266.00	203.00
Y	50.00	30.00	48.00	41.00	60.00
Zr	177.00	39.00	154.00	127.00	191.00
Nb	15.00	3.00	11.00	7.00	5.00
Zn	121.00	90.00	95.00	69.00	127.00
Cu	111.00	21.00	110.00	50.00	22.00
Ni	78.00	38.00	71.00	43.00	34.00
La	34.00	28.00	27.00	8.00	29.00
Ba	138.00	76.00	69.00	78.00	169.00
V	50.00	316.00	350.00	350.00	571.00
Ce	65.00	36.00	54.00	13.00	66.00
Cr	96.00	291.00	71.00	185.00	26.00
Ga	18.00	16.00	18.00	13.00	14.00
As	21.00	0.00	15.00	21.00	26.00

## S &amp; CO2 (Wt %)

S	.10	0.00	.40	.01	.11
CO2		.09			

## Precious Metals (ppb)

Au	.80	10.60	2.60		13.00
Ag	55.00	57.00	12.00		51.00

## Gabbro (GABB)

W80-132A

W80-132B

W80-132C

W80-132D

W80-132E

## Major Elements (Wt %)

SiO2	52.20	50.40	55.00	52.60	52.60
TiO2	1.88	1.33	1.45	1.25	2.30
Al2O3	14.30	12.40	13.50	15.00	14.60
Fe2O3	12.34	10.36	9.85	10.23	14.11
MnO	.22	.20	.18	.18	.23
MgO	4.15	5.22	4.05	7.24	4.50
CaO	3.45	5.70	5.15	5.66	3.63
Na2O	4.96	4.76	4.74	5.38	6.62
K2O	.72	.33	.44	.81	1.01
P2O5	.17	.07	.13	.14	.15
LOI	5.61	9.42	5.62	1.61	.58
TOTAL	100.00	100.19	100.11	100.10	100.33

## Trace Elements (ppm)

Pb	10.00	8.00	11.00	3.00	0.00
Th	8.00	4.00	7.00	0.00	0.00
U	2.00	1.00	4.00	0.00	2.00
Rb	27.00	12.00	19.00	23.00	30.00
Sr	50.00	86.00	104.00	81.00	55.00
Y	60.00	46.00	63.00	41.00	69.00
Zr	194.00	138.00	214.00	110.00	215.00
Nb	13.00	8.00	13.00	7.00	13.00
Zn	99.00	91.00	85.00	89.00	112.00
Cu	34.00	47.00	43.00	60.00	23.00
Ni	0.00	5.00	0.00	42.00	0.00
La	41.00	30.00	32.00	18.00	45.00
Ba	284.00	141.00	209.00	223.00	450.00
V	405.00	350.00	326.00	276.00	445.00
Ce	69.00	42.00	61.00	38.00	80.00
Cr	0.00	7.00	0.00	302.00	2.00
Ga	18.00	18.00	20.00	18.00	21.00
As	0.00	0.00	0.00	0.00	9.00

## S &amp; CO2 (Wt %)

S	.02	0.00	.01	0.00	0.00
CO2	.84	1.62	.96	.10	.05

## Precious Metals (ppb)

Au	5.90
Ag	14.00

## GABB

	PB51-5	W-79-36	W-79-36A	W-80-21B	PB27-9
Major Elements (Wt %)					
SiO <sub>2</sub>	.01	45.00	48.60	47.20	46.00
TiO <sub>2</sub>	0.00	2.64	2.80	2.08	1.15
Al <sub>2</sub> O <sub>3</sub>	0.00	14.00	13.20	14.40	17.80
Fe <sub>2</sub> O <sub>3</sub>	0.00	18.44	16.52	11.64	9.21
MnO	0.00	.24	.27	.18	.16
MgO	0.00	6.32	4.86	7.49	9.18
CaO	0.00	7.88	7.81	10.41	9.76
Na <sub>2</sub> O	0.00	2.54	3.13	2.83	2.12
K <sub>2</sub> O	0.00	.24	.21	.36	.41
P <sub>2</sub> O <sub>5</sub>	0.00	.20	.25	.28	.07
LOI	0.00	2.84	2.05	2.39	3.96
TOTAL		100.34	99.70	99.26	99.82

Trace Elements (ppm)					
Pb	10.00	4.00	4.00	2.00	9.00
Th	9.00	1.00	0.00	0.00	2.00
U	9.00	2.00	0.00	3.00	0.00
Rb	45.00	0.00	4.00	7.00	12.00
Sr	173.00	163.00	156.00	272.00	241.00
Y	72.00	47.00	71.00	36.00	20.00
Zr	118.00	105.00	209.00	125.00	80.00
Nb	11.00	5.00	4.00	9.00	7.00
Zn	118.00	125.00	118.00	85.00	72.00
Cu	5.00	11.00	22.00	54.00	44.00
Ni	0.00	31.00	19.00	75.00	98.00
La	44.00	22.00	31.00	16.00	11.00
Ba	151.00	251.00	192.00	82.00	77.00
V	191.00	813.00	618.00	286.00	206.00
Ce	95.00	58.00	83.00	45.00	29.00
Cr	9.00	0.00	0.00	313.00	315.00
Ga	21.00	15.00	17.00	18.00	19.00
As	4.00	27.00	19.00	4.00	9.00

S & CO <sub>2</sub> (Wt %)					
S	.08	0.00	.06	.15	.03
CO <sub>2</sub>				.11	

Precious Metals (ppb)					
Au		5.00		4.00	3.50
Ag		22.00		3.00	66.00



## GABB

W-79-55

W-79-65

W-80-47A

W-80-81

PB19-3

## Major Elements (Wt %)

SiO2	50.20	50.50	43.80	.01	.01
TiO2	1.17	1.19	3.00	0.00	0.00
Al2O3	14.40	15.10	16.20	0.00	0.00
Fe2O3	10.17	9.05	15.12	0.00	0.00
MnO	.20	.16	.13	0.00	0.00
MgO	7.56	5.65	4.70	0.00	0.00
CaO	7.54	8.48	4.48	0.00	0.00
Na2O	4.00	3.00	3.35	0.00	0.00
K2O	.82	.68	.76	0.00	0.00
P2O5	.10	.08	1.75	0.00	0.00
LOI	3.57	6.43	5.48	0.00	0.00
TOTAL	99.73	100.32	98.77		

## Trace Elements (ppm)

Pb	7.00	4.00	0.00	10.00	7.00
Th	1.00	0.00	0.00	0.00	6.00
U	1.00	0.00	0.00	0.00	3.00
Rb	22.00	19.00	32.00	71.00	9.00
Sr	163.00	125.00	75.00	142.00	158.00
Y	37.00	32.00	47.00	35.00	78.00
Zr	104.00	80.00	81.00	98.00	255.00
Nb	6.00	5.00	7.00	8.00	20.00
Zn	88.00	75.00	138.00	107.00	93.00
Cu	25.00	14.00	11.00	89.00	31.00
Ni	13.00	0.00	0.00	28.00	1.00
La	23.00	26.00	43.00	23.00	49.00
Ba	213.00	172.00	168.00	752.00	83.00
V	313.00	241.00	317.00	284.00	227.00
Ce	33.00	34.00	79.00	42.00	103.00
Cr	195.00	43.00	10.00	189.00	6.00
Ga	17.00	16.00	22.00	15.00	21.00
As	0.00	0.00	26.00	51.00	2.00

## S &amp; CO2 (Wt %)

S	0.00	0.00	.07	0.00	.04
CO2		.55			

## Precious Metals (ppb)

Au	2.60	1.80			
Ag	15.00	132.00			

## GABB

PB19-17

PB41-1

PB63-3

## Major Elements (Wt %)

SiO2	.01	0.00	.01
TiO2	0.00	0.00	0.00
Al2O3	0.00	0.00	0.00
Fe2O3	0.00	0.00	0.00
MnO	0.00	0.00	0.00
MgO	0.00	0.00	0.00
CaO	0.00	.01	0.00
Na2O	0.00	0.00	0.00
K2O	0.00	0.00	0.00
P2O5	0.00	0.00	0.00
LOI	0.00	0.00	0.00

TOTAL

## Trace Elements (ppm)

Pb	5.00	85.00	11.00
Th	1.00	3.00	0.00
U	3.00	8.00	4.00
Rb	109.00	74.00	14.00
Sr	105.00	151.00	250.00
Y	17.00	61.00	85.00
Zr	29.00	108.00	145.00
Nb	1.00	10.00	14.00
Zn	82.00	144.00	115.00
Cu	10.00	4.00	8.00
Ni	19.00	0.00	0.00
La	11.00	42.00	56.00
Ba	466.00	255.00	149.00
V	299.00	267.00	184.00
Ce	14.00	73.00	108.00
Cr	116.00	0.00	0.00
Ga	21.00	21.00	22.00
As	0.00	41.00	3.00

## S &amp; CO2 (Wt %)

S	0.00	.04	.05
CO2	.66		

## Precious Metals (ppb)

Au  
Ag

## Port aux Basques Gneiss Amphibolites (PABAM)

W-79-63      W79-170A      W-80-55      W-80-52      W-80-57

## Major Elements (Wt %)

SiO <sub>2</sub>	48.60	51.40	40.90	41.80	50.20
TiO <sub>2</sub>	1.50	.48	.83	.50	.75
Al <sub>2</sub> O <sub>3</sub>	15.40	15.80	16.90	19.20	16.90
Fe <sub>2</sub> O <sub>3</sub>	11.59	9.07	14.58	13.40	12.36
MnO	.29	.17	.49	.45	.41
MgO	8.00	6.63	6.18	7.96	5.64
CaO	7.58	9.89	18.28	11.16	8.46
Na <sub>2</sub> O	3.80	2.47	.22	1.73	2.45
K <sub>2</sub> O	.45	.32	.03	.34	.34
P <sub>2</sub> O <sub>5</sub>	.19	.15	.26	.27	.23
LOI	1.65	.73	1.64	1.95	.61
TOTAL	99.05	97.11	100.31	98.76	98.35

## Trace Element (ppm)

Pb	22.00	8.00	32.00	33.00	17.00
Th	0.00	0.00	0.00	0.00	1.00
U	2.00	6.00	0.00	0.00	4.00
Rb	10.00	6.00	0.00	6.00	7.00
Sr	177.00	310.00	644.00	469.00	162.00
Y	43.00	42.00	15.00	24.00	22.00
Zr	120.00	111.00	123.00	145.00	111.00
Nb	6.00	10.00	4.00	6.00	3.00
Zn	100.00	80.00	130.00	134.00	103.00
Cu	27.00	4.00	39.00	139.00	44.00
Ni	44.00	56.00	111.00	92.00	19.00
La	23.00	15.00	16.00	29.00	27.00
Ba	180.00	84.00	24.00	266.00	196.00
V	278.00	309.00	285.00	362.00	334.00
Ce	57.00	42.00	37.00	44.00	48.00
Cr	243.00	138.00	292.00	174.00	96.00
Ga	14.00	10.00	21.00	24.00	22.00
As	1.00	14.00	27.00	15.00	8.00

S & CO<sub>2</sub> (Wt %)

S	0.00	.01	.04	.24	0.00
CO <sub>2</sub>	.21	0.00			

## Precious Metals (ppb)

Au	23.60	5.50	8.60		5.40
Ag	65.00	61.00	76.00		15.00

## PABAM

W-80-63

Major Elements (Wt %)	
SiO2	59.20
TiO2	.80
Al2O3	16.70
Fe2O3	7.90
MnO	.24
MgO	4.64
CaO	2.16
Na2O	4.57
K2O	.80
P2O5	.19
LOI	2.19
TOTAL	99.39

Trace Element (ppm)	
Pb	9.00
Th	4.00
U	0.00
Rb	19.00
Sr	196.00
Y	24.00
Zr	152.00
Nb	8.00
Zn	99.00
Cu	74.00
Ni	0.00
La	22.00
Ba	726.00
V	138.00
Ce	48.00
Cr	3.00
Ga	19.00
As	0.00

S & CO2 (Wt %)	
S	.07
CO2	.05

Precious Metals (ppb)	
Au	
Ag	

## Basaltic Dykes (BSC/DK)

W-79-13

W-79-14

Major Elements (Wt %)		
SiO2	47.80	45.00
TiO2	2.66	3.06
Al2O3	13.70	13.20
Fe2O3	13.89	15.74
MnO	.21	.26
MgO	5.46	6.64
CaO	8.60	9.41
Na2O	2.62	2.87
K2O	1.07	.31
P2O5	.58	.57
LOI	2.80	2.26
TOTAL	99.39	99.32

Trace Elements (ppm)		
Pb	23.00	6.00
Th	4.00	0.00
U	4.00	0.00
Rb	30.00	7.00
Sr	452.00	347.00
Y	54.00	55.00
Zr	220.00	217.00
Nb	13.00	13.00
Zn	124.00	140.00
Cu	23.00	34.00
Ni	39.00	56.00
La	42.00	45.00
Ba	397.00	150.00
V	363.00	434.00
Ce	97.00	91.00
Cr	19.00	48.00
Ga	16.00	23.00
As	24.00	19.00

S & CO2 (Wt %)		
S	.20	.12
CO2		

Precious Metals (ppb)		
Au	2.00	1.50
Ag	12.00	64.00

## Granodiorite (GRANO)

	133-2	PB133-4	PB133-XA	PB133-XB	PB133-XC
Major Elements (Wt %)					
SiO <sub>2</sub>	59.30	54.50	55.60	48.40	52.60
TiO <sub>2</sub>	1.81	1.21	1.39	2.36	1.29
Al <sub>2</sub> O <sub>3</sub>	12.60	13.40	13.40	13.70	13.00
Fe <sub>2</sub> O <sub>3</sub>	12.13	12.86	9.45	14.18	12.90
MnO	.24	.14	.15	.13	.20
MgO	3.30	2.44	2.56	2.84	1.37
CaO	3.29	1.76	6.25	5.46	12.40
Na <sub>2</sub> O	2.83	5.74	4.29	3.32	.84
K <sub>2</sub> O	.42	.34	.43	1.43	.17
P <sub>2</sub> O <sub>5</sub>	.57	.61	.61	1.16	.70
LOI	3.14	5.57	4.61	6.20	2.72
TOTAL	99.63	98.57	98.74	99.18	98.19
Trace Elements (ppm)					
Pb	10.00	63.00	19.00	28.00	32.00
Th	5.00	6.00	8.00	6.00	1.00
U	4.00	6.00	6.00	0.00	0.00
Rb	19.00	16.00	19.00	62.00	6.00
Sr	239.00	121.00	263.00	125.00	862.00
Y	82.00	95.00	90.00	91.00	0.00
Zr	250.00	360.00	259.00	316.00	240.00
Nb	18.00	31.00	17.00	22.00	22.00
Zn	164.00	209.00	73.00	67.00	55.00
Cu	13.00	45.00	6.00	9.00	3.00
Ni	0.00	0.00	0.00	0.00	0.00
La	58.00	62.00	39.00	52.00	35.00
Ba	226.00	182.00	146.00	387.00	64.00
V	236.00	106.00	129.00	201.00	114.00
Ce	106.00	126.00	86.00	119.00	98.00
Cr	0.00	0.00	2.00	0.00	8.00
Ga	23.00	27.00	23.00	27.00	31.00
As	19.00	163.00	13.00	51.00	81.00
S & CO <sub>2</sub> (Wt %)					
S	.08	2.82	.02	2.58	0.00
CO <sub>2</sub>			.86	.88	.33
Precious Metals (ppb)					
Au	.70	10.00	6.60	4.10	22.00
Ag	16.00	157.00	47.00	86.00	7.00

## GRANO

W-80-165

W-80-189

W-80-191

W-79-59L

PB19-9

## Major Elements (Wt %)

SiO2	.01	65.10	.01	67.40	.01
TiO2	0.00	.54	0.00	.43	0.00
Al2O3	0.00	15.00	0.00	15.70	0.00
Fe2O3	0.00	6.39	0.00	1.12	0.00
MnO	0.00	.16	0.00	.07	0.00
MgO	0.00	1.15	0.00	.39	0.00
CaO	0.00	2.40	0.00	2.73	0.00
Na2O	0.00	5.08	0.00	7.18	0.00
K2O	0.00	1.46	0.00	1.29	0.00
P2O5	0.00	.23	0.00	.17	0.00
LOI	0.00	2.38	0.00	2.40	0.00
TOTAL	.01	99.89	.01	98.88	.01

## Trace Elements (ppm)

Pb	9.00	3.00	5.00	32.00	11.00
Th	11.00	4.00	0.00	10.00	6.00
U	3.00	0.00	3.00	6.00	5.00
Rb	64.00	32.00	0.00	40.00	61.00
Sr	332.00	116.00	69.00	138.00	302.00
Y	13.00	79.00	40.00	36.00	24.00
Zr	241.00	157.00	96.00	250.00	241.00
Nb	6.00	5.00	1.00	11.00	6.00
Zn	94.00	59.00	123.00	30.00	81.00
Cu	32.00	12.00	100.00	23.00	33.00
Ni	1.00	0.00	0.00	0.00	2.00
La	31.00	22.00	9.00	30.00	32.00
Ba	475.00	410.00	33.00	661.00	459.00
V	86.00	6.00	351.00	43.00	80.00
Ce	61.00	54.00	40.00	61.00	69.00
Cr	4.00	0.00	3.00	0.00	9.00
Ga	23.00	20.00	20.00	9.00	25.00
As	0.00	0.00	15.00	1.00	0.00

## S &amp; CO2 (Wt %)

S	.01	0.00	0.00	.08	.04
CO2	.38				

## Precious Metals (ppb)

Au  
Ag

## GRAND

PB27-5

PB28-B

## Major Elements (Wt %)

SiO2	66.60	.01
TiO2	.46	0.00
Al2O3	15.50	0.00
Fe2O3	4.80	0.00
MnO	.07	0.00
MgO	1.90	0.00
CaO	2.56	0.00
Na2O	5.23	0.00
K2O	1.86	0.00
P2O5	.09	0.00
LOI	1.45	0.00

TOTAL	100.52	
-------	--------	--

## Trace Elements (ppm)

Pb	9.00	11.00
Th	10.00	4.00
U	0.00	8.00
Rb	48.00	44.00
Sr	200.00	435.00
Y	35.00	88.00
Zr	158.00	320.00
Nb	10.00	21.00
Zn	50.00	88.00
Cu	14.00	14.00
Ni	0.00	0.00
La	24.00	48.00
Ba	856.00	301.00
V	121.00	123.00
Ce	42.00	107.00
Cr	21.00	0.00
Ga	17.00	24.00
As	4.00	15.00

## S &amp; CO2 (Wt %)

S	0.00	.31
CO2		

## Precious Metals (ppb)

Au		
Ag		

## Port aux Basques Granite (PABGRN)

	A-1	A-2	A-3	A-4	A-5
Major Elements (Wt %)					
SiO <sub>2</sub>	72.10	75.00	77.90	76.70	73.80
TiO <sub>2</sub>	.24	.36	.10	.29	.31
Al <sub>2</sub> O <sub>3</sub>	13.80	13.40	11.30	12.80	14.20
Fe <sub>2</sub> O <sub>3</sub>	2.38	2.15	1.02	1.71	2.11
MnO	.05	.06	.01	.04	.06
MgO	.34	.70	.09	.39	.85
CaO	1.20	1.91	.48	1.01	1.73
Na <sub>2</sub> O	4.00	4.88	3.26	5.69	4.71
K <sub>2</sub> O	5.04	1.34	4.87	1.30	2.77
P <sub>2</sub> O <sub>5</sub>	.04	.03	.01	.03	.03
LOI	.12	.67	.16	.20	.44
TOTAL	99.31	100.50	99.20	100.16	101.01

Trace Elements (ppm)					
Pb	13.00	22.00	27.00	7.00	8.00
Th	12.00	23.00	36.00	17.00	6.00
U	2.00	2.00	4.00	1.00	0.00
Rb	135.00	48.00	112.00	35.00	5.00
Sr	79.00	211.00	27.00	169.00	209.00
Y	68.00	78.00	49.00	59.00	13.00
Zr	233.00	233.00	136.00	201.00	180.00
Nb	57.00	29.00	51.00	55.00	6.00
Zn	49.00	38.00	17.00	38.00	32.00
Cu	10.00	7.00	7.00	14.00	28.00
Ni	0.00	0.00	0.00	0.00	0.00
La	65.00	49.00	17.00	52.00	30.00
Ba	568.00	265.00	132.00	190.00	1753.00
V	15.00	31.00	2.00	14.00	55.00
Ce	109.00	97.00	42.00	94.00	55.00
Cr	14.00	25.00	0.00	18.00	0.00
Ga	23.00	17.00	20.00	23.00	17.00
As	13.00	6.00	14.00	14.00	0.00

S & CO <sub>2</sub> (Wt %)					
S	0.00	0.00	0.00	.01	.01
CO <sub>2</sub>					

Precious Metals (ppb)					
Au	3.30		2.80	3.40	
Ag	235.00		67.00	210.00	



## PABGRN.

A-5A

A-6

## Major Elements (Wt %)

SiO2	74.80	73.80
TiO2	.11	.07
Al2O3	13.80	13.80
Fe2O3	.80	1.04
MnO	.02	.01
MgO	.27	.18
CaO	1.59	.38
Na2O	4.73	3.31
K2O	2.83	6.63
P2O5	.06	.07
LOI	.62	.29
TOTAL	99.63	99.58

## Trace Elements (ppm)

Pb	15.00	15.00
Th	10.00	17.00
U	0.00	0.00
Rb	45.00	191.00
Sr	212.00	61.00
Y	4.00	30.00
Zr	33.00	50.00
Nb	3.00	14.00
Zn	16.00	27.00
Cu	21.00	12.00
Ni	0.00	0.00
La	27.00	73.00
Ba	1845.00	433.00
V	25.00	8.00
Ce	44.00	107.00
Cr	28.00	23.00
Ga	16.00	22.00
As	0.00	0.00

## S &amp; CO2 (Wt %)

S	0.00	0.00
CO2		

## Precious Metals (ppb)

Au	2.00
Ag	55.00

## Tonalitic Cape Ray Granite (CRG-TN)

	CRG-7	W-79-9	W-79-25	W-79-26	W-79-27
Major Elements (Wt %)					
SiO <sub>2</sub>	69.10	69.80	71.10	67.70	66.70
TiO <sub>2</sub>	.54	.53	.41	.49	.70
Al <sub>2</sub> O <sub>3</sub>	14.20	13.80	12.90	14.00	14.00
Fe <sub>2</sub> O <sub>3</sub>	4.65	2.92	4.23	2.91	3.57
MnO	.08	.08	.08	.11	.10
MgO	1.56	2.50	1.74	2.05	2.76
CaO	4.35	3.57	3.49	5.71	3.73
Na <sub>2</sub> O	2.95	2.39	2.98	2.67	2.58
K <sub>2</sub> O	1.20	2.07	.67	1.05	1.60
P <sub>2</sub> O <sub>5</sub>	.12	.15	.07	.08	.23
LOI	.76	2.23	2.43	2.13	2.27
TOTAL	99.51	99.84	100.10	98.90	98.24

Trace Elements (ppm)					
Pb	15.00	3.00	8.00	3.00	10.00
Th	4.00	3.00	3.00	0.00	5.00
U	2.00	2.00	0.00	2.00	3.00
Rb	60.00	69.00	19.00	39.00	70.00
Sr	668.00	249.00	202.00	216.00	144.00
Y	6.00	17.00	16.00	21.00	26.00
Zr	76.00	143.00	156.00	151.00	170.00
Nb	3.00	7.00	5.00	5.00	12.00
Zn	35.00	55.00	53.00	63.00	74.00
Cu	20.00	30.00	18.00	12.00	47.00
Ni	4.00	13.00	1.00	2.00	2.00
La	19.00	25.00	21.00	21.00	20.00
Ba	2433.00	610.00	153.00	275.00	405.00
V	53.00	149.00	128.00	169.00	149.00
Ce	26.00	45.00	40.00	29.00	43.00
Cr	0.00	12.00	19.00	16.00	14.00
Ga	19.00	11.00	13.00	14.00	16.00
As	3.00	0.00	0.00	0.00	13.00

S & CO <sub>2</sub> (Wt %)					
S	.02	0.00	0.00	0.00	0.00
CO <sub>2</sub>			.16		

Precious Metals (ppb)					
Au	13.00	.80	.60		6.00
Ag	46.00	16.00	64.00		42.00

## CRG-TN

W-79-68A

W-79-68B

W-79-69

W-79-96A

W-79-96B

## Major Elements (Wt %)

SiO2	63.80	71.70	70.90	69.40	68.40
TiO2	.55	.36	.47	.65	.46
Al2O3	14.20	13.90	13.90	14.40	14.70
Fe2O3	6.58	3.72	4.51	2.58	2.92
MnO	.09	.06	.07	.07	.06
MgO	2.45	1.18	1.38	.59	1.40
CaO	5.05	4.18	4.27	1.08	2.77
Na2O	2.91	2.83	2.93	3.86	4.40
K2O	1.03	1.12	1.44	5.09	3.25
P2O5	.13	.07	.05	.11	.15
LOI	1.91	.57	.94	.60	1.14
TOTAL	98.70	99.69	100.86	98.43	99.65

## Trace Elements (ppm)

Pb	14.00	13.00	8.00	33.00	14.00
Th	0.00	0.00	1.00	14.00	7.00
U	3.00	0.00	3.00	1.00	0.00
Rb	29.00	30.00	46.00	136.00	89.00
Sr	717.00	240.00	504.00	140.00	777.00
Y	16.00	4.00	11.00	74.00	16.00
Zr	152.00	72.00	110.00	313.00	166.00
Nb	5.00	7.00	5.00	23.00	8.00
Zn	58.00	45.00	45.00	63.00	54.00
Cu	33.00	24.00	17.00	31.00	14.00
Ni	0.00	3.00	1.00	16.00	11.00
La	25.00	6.00	12.00	73.00	49.00
Ba	990.00	482.00	525.00	1115.00	1374.00
V	152.00	74.00	82.00	24.00	64.00
Ce	30.00	27.00	42.00	129.00	75.00
Cr	24.00	12.00	1.00	0.00	17.00
Ga	17.00	18.00	15.00	14.00	15.00
As	8.00	0.00	0.00	1.00	0.00

## S &amp; CO2 (Wt %)

S	0.00	0.00	0.00	0.00	0.00
CO2					

## Precious Metals (ppb)

Au	6.60
Ag	88.00

## Megacrystic Cape Ray Granite (CRG-MX)

	CRG-1	CRG-1F	CRG-2	CRG-2F	CRG-3
Major Elements (Wt %)					
SiO <sub>2</sub>	63.20	62.70	60.80	63.80	63.60
TiO <sub>2</sub>	.35	.03	.25	.04	.49
Al <sub>2</sub> O <sub>3</sub>	16.70	17.30	15.50	16.90	15.80
Fe <sub>2</sub> O <sub>3</sub>	4.13	.89	4.94	1.07	4.73
MnO	.10	.09	.08	.08	.06
MgO	1.08	.25	2.02	.43	1.78
CaO	2.27	2.44	3.91	4.45	3.96
Na <sub>2</sub> O	2.80	3.82	3.92	7.90	4.32
K <sub>2</sub> O	6.29	9.94	2.96	1.20	3.30
P <sub>2</sub> O <sub>5</sub>	.20	.02	.22	.07	.26
LOI	3.36	2.70	4.03	4.19	1.68
TOTAL	100.48	100.18	98.63	100.13	99.98

Trace Elements (ppm)					
Pb	49.00	138.00	12.00	30.00	14.00
Th	44.00	0.00	48.00	0.00	34.00
U	1.00	0.00	2.00	2.00	4.00
Rb	195.00	154.00	93.00	21.00	104.00
Sr	682.00	1279.00	689.00	888.00	661.00
Y	22.00	5.00	26.00	11.00	26.00
Zr	324.00	40.00	304.00	62.00	292.00
Nb	16.00	0.00	23.00	1.00	23.00
Zn	101.00	43.00	80.00	18.00	24.00
Cu	16.00	20.00	16.00	24.00	7.00
Ni	13.00	6.00	14.00	0.00	11.00
La	61.00	13.00	86.00	19.00	100.00
Ba	1903.00	4446.00	2277.00	1205.00	1287.00
V	73.00	13.00	85.00	17.00	93.00
Ce	98.00	72.00	140.00	47.00	151.00
Cr	2.00	0.00	8.00	0.00	6.00
Ga	15.00	10.00	14.00	8.00	10.00
As	15.00	25.00	13.00	20.00	18.00

S & CO <sub>2</sub> (Wt %)					
S	0.00	0.00	0.00	0.00	.01
CO <sub>2</sub>					

Precious Metals (ppb)					
Au	2.70	14.80	2.00	26.80	
Ag	670.00	491.00	90.00	1324.00	

## CRG-MX

	CRG-3A	CRG-3AF	CRG-5A	CRG-5B	CRG-6
Major Elements (Wt %)					
SiO <sub>2</sub>	65.60	68.20	67.80	57.00	61.50
TiO <sub>2</sub>	.56	.12	.16	.80	.53
Al <sub>2</sub> O <sub>3</sub>	15.90	17.10	15.70	15.30	16.70
Fe <sub>2</sub> O <sub>3</sub>	4.48	.75	2.07	6.88	4.53
MnO	.06	.03	.04	.16	.05
MgO	1.79	.25	.83	4.16	1.91
CaO	3.87	1.94	1.82	4.89	2.90
Na <sub>2</sub> O	4.70	7.92	4.20	3.43	4.10
K <sub>2</sub> O	2.40	2.49	3.40	3.90	3.78
P <sub>2</sub> O <sub>5</sub>	.27	.07	.12	.54	.23
LOI	1.56	1.57	2.30	2.98	2.60
TOTAL	101.19	100.44	98.44	100.04	98.83

## Trace Elements (ppm)

Pb	9.00	16.00	33.00	32.00	14.00
Th	41.00	7.00	18.00	25.00	5.00
U	8.00	1.00	0.00	5.00	0.00
Rb	90.00	55.00	95.00	116.00	39.00
Sr	640.00	424.00	1463.00	1330.00	187.00
Y	29.00	4.00	14.00	30.00	11.00
Zr	276.00	74.00	320.00	361.00	142.00
Nb	20.00	2.00	14.00	21.00	4.00
Zn	42.00	12.00	65.00	183.00	54.00
Cu	29.00	43.00	23.00	16.00	20.00
Ni	12.00	0.00	16.00	28.00	5.00
La	112.00	24.00	98.00	79.00	10.00
Ba	1033.00	1416.00	2719.00	1305.00	320.00
V	103.00	16.00	68.00	111.00	83.00
Ce	160.00	50.00	139.00	144.00	32.00
Cr	7.00	0.00	8.00	26.00	12.00
Ga	13.00	6.00	18.00	14.00	10.00
As	14.00	15.00	22.00	32.00	0.00

S & CO<sub>2</sub> (Wt %)

S	.02	0.00	.01	.01	0.00
CO <sub>2</sub>					

## Precious Metals (ppb)

Au	3.10	21.30	7.90	10.00	4.80
Ag	49.00	131.00	69.00	6.00	17.00

## Red Rocks Granite (RD-R-G)

	RRG-1	RRG-2	RRG-2A	RRG-3	RRG-4
Major Elements (Wt %)					
SiO <sub>2</sub>	70.60	71.60	71.20	76.10	74.60
TiO <sub>2</sub>	.17	.19	.23	.07	.05
Al <sub>2</sub> O <sub>3</sub>	15.10	14.20	15.40	13.60	13.60
Fe <sub>2</sub> O <sub>3</sub>	1.38	1.95	1.94	.77	.83
MnO	.07	.05	.05	.03	.01
MgO	.54	.69	.67	.17	.19
CaO	2.51	2.51	2.35	1.71	1.14
Na <sub>2</sub> O	5.34	3.88	3.76	3.64	3.62
K <sub>2</sub> O	2.22	3.78	4.00	3.63	4.42
P <sub>2</sub> O <sub>5</sub>	.04	.06	.07	.02	0.00
LOI	.59	.73	.70	.78	.61
TOTAL	98.56	99.64	100.37	100.52	99.07

Trace Elements (ppm)					
Pb	29.00	25.00	24.00	39.00	45.00
Th	0.00	10.00	11.00	1.00	1.00
U	0.00	3.00	0.00	0.00	0.00
Rb	73.00	106.00	110.00	102.00	120.00
Sr	683.00	758.00	754.00	454.00	332.00
Y	7.00	11.00	7.00	8.00	9.00
Zr	85.00	145.00	140.00	65.00	51.00
Nb	10.00	12.00	12.00	7.00	11.00
Zn	34.00	33.00	36.00	18.00	19.00
Cu	9.00	10.00	9.00	12.00	11.00
Ni	0.00	0.00	0.00	0.00	0.00
La	22.00	45.00	62.00	23.00	22.00
Ba	893.00	2099.00	2173.00	2420.00	1970.00
V	20.00	30.00	27.00	8.00	7.00
Ce	31.00	78.00	95.00	41.00	34.00
Cr	8.00	6.00	17.00	14.00	5.00
Ga	19.00	19.00	17.00	14.00	16.00
As	0.00	0.00	0.00	0.00	0.00

S & CO <sub>2</sub> (Wt %)					
S	0.00	0.00	0.00	0.00	0.00
CO <sub>2</sub>	0.05				

Precious Metals (ppb)					
Au	11.00	4.60			0.00
Ag	225.00	168.00			42.00

## RD-R-G

RRG-5

RRG-6

RRG-7

## Major Elements (Wt %)

SiO2	74.60	76.00	75.80
TiO2	.07	0.00	.04
Al2O3	13.50	13.60	13.40
Fe2O3	.52	.40	.46
MnO	.03	.02	.01
MgO	.09	.08	.08
CaO	1.22	.99	1.16
Na2O	4.20	4.08	3.87
K2O	4.29	4.89	4.77
P2O5	0.00	.01	0.00
LOI	.44	.59	.59
TOTAL	98.96	100.66	100.20

## Trace Elements (ppm)

Pb	54.00	46.00	37.00
Th	8.00	2.00	0.00
U	4.00	4.00	5.00
Rb	134.00	140.00	106.00
Sr	135.00	132.00	209.00
Y	11.00	10.00	10.00
Zr	34.00	34.00	43.00
Nb	10.00	11.00	9.00
Zn	19.00	17.00	11.00
Cu	12.00	11.00	13.00
Ni	0.00	0.00	0.00
La	8.00	11.00	10.00
Ba	193.00	178.00	537.00
V	1.00	3.00	5.00
Ce	26.00	23.00	28.00
Cr	4.00	0.00	6.00
Ga	16.00	16.00	14.00
As	0.00	0.00	0.00

## S &amp; CO2 (Wt %)

S	0.00	0.00	0.00
CO2			

## Precious Metals (ppb)

Au	.60
Ag	1728.00

## Windowglass Hill Granite (WGH-GR)

	WGH-1	WGH-2	WGH-3	WGH-4	WGH-SH2B
Major Elements (Wt %)					
SiO <sub>2</sub>	79.10	78.40	77.80	78.20	81.60
TiO <sub>2</sub>	0.00	.11	.12	.11	.10
Al <sub>2</sub> O <sub>3</sub>	10.90	12.40	12.20	12.20	9.74
Fe <sub>2</sub> O <sub>3</sub>	.88	.79	.83	.65	1.72
MnO	.01	.02	.02	.01	.01
MgO	.02	.06	.04	.05	.16
CaO	.87	.99	.71	.81	.05
Na <sub>2</sub> O	5.87	6.49	5.25	5.66	3.83
K <sub>2</sub> O	.49	.39	2.70	1.55	.84
P <sub>2</sub> O <sub>5</sub>	0.00	0.00	0.00	0.00	.06
LOI	1.21	1.07	.94	1.05	.98
TOTAL	99.35	100.72	100.61	100.29	99.09
Trace Elements (ppm)					
Pb	12.00	9.00	70.00	15.00	1999.00
Th	30.00	17.00	23.00	27.00	16.00
U	10.00	5.00	10.00	7.00	0.00
Rb	24.00	11.00	59.00	41.00	36.00
Sr	61.00	83.00	64.00	84.00	26.00
Y	178.00	146.00	149.00	144.00	18.00
Zr	351.00	352.00	279.00	374.00	108.00
Nb	40.00	39.00	39.00	42.00	24.00
Zn	18.00	11.00	13.00	20.00	50.00
Cu	14.00	15.00	14.00	15.00	594.00
Ni	21.00	15.00	16.00	18.00	0.00
La	57.00	68.00	56.00	56.00	2.00
Ba	30.00	32.00	314.00	201.00	142.00
V	3.00	0.00	4.00	1.00	8.00
Ce	106.00	127.00	115.00	130.00	3.00
Cr	0.00	7.00	0.00	0.00	9.00
Ga	14.00	18.00	14.00	20.00	63.00
As	10.00	12.00	18.00	15.00	13.00
S & CO <sub>2</sub> (Wt %)					
S	0.00	0.00	.01	0.00	.11
CO <sub>2</sub>	.13	.24			
Precious Metals (ppb)					
Au	10.50	6.50	19.40	2.20	3419.00
Ag	707.00	354.00	230.00	1624.00	7500.00



WGH-BR

WGH-SH3

W-79-74

W-79-78B

W-79-112

W79-112A

## Major Elements (Wt %)

SiO2	80.00	74.70	77.20	76.60	78.60
TiO2	.10	.09	0.00	.16	0.00
Al2O3	11.30	13.30	11.90	11.80	12.00
Fe2O3	.32	1.76	1.80	1.44	.96
MnO	.01	.03	.03	.02	.01
MgO	.01	.40	.06	.03	0.00
CaO	.44	.65	.03	.62	.08
Na2O	6.66	1.55	6.32	4.12	6.56
K2O	.19	3.58	.55	3.51	.28
P2O5	.04	.02	0.00	.06	.01
LOI	.59	2.62	1.44	.85	.39
TOTAL	99.66	98.70	99.33	99.21	98.89

## Trace Elements (ppm)

Pb	692.00	1939.00	176.00	8.00	14.00
Th	25.00	28.00	18.00	19.00	27.00
U	3.00	7.00	3.00	5.00	5.00
Rb	6.00	104.00	0.00	117.00	8.00
Sr	55.00	10.00	150.00	38.00	29.00
Y	99.00	118.00	92.00	161.00	100.00
Zr	381.00	305.00	261.00	266.00	326.00
Nb	47.00	31.00	22.00	38.00	43.00
Zn	30.00	455.00	59.00	23.00	21.00
Cu	79.00	26.00	27.00	9.00	12.00
Ni	1.00	23.00	15.00	29.00	7.00
La	37.00	52.00	23.00	104.00	1.00
Ba	54.00	385.00	59.00	329.00	30.00
V	52.00	3.00	12.00	0.00	3.00
Ce	66.00	99.00	66.00	116.00	3.00
Cr	10.00	0.00	0.00	0.00	0.00
Ga	36.00	30.00	13.00	21.00	17.00
As	12.00	34.00	6.00	2.00	21.00

## S &amp; CO2 (Wt %)

S	.15	.40	.38	0.00	0.00
CO2			.17		

## Precious Metals (ppb)

Au	329.40	7.00	5.80	1.80	12.00
Ag	14818.00	244.00	156.00	63.00	22.00

## WGH-GR

W79=112B

W-79-126

W-79-140

W-80-148

W-80-186

## Major Elements (Wt %)

SiO2	78.00	77.20	77.20	74.00	79.40
TiO2	0.00	.28	.18	.10	.07
Al2O3	12.00	13.00	10.80	14.60	12.40
Fe2O3	.34	1.69	.44	.98	.44
MnO	.01	.02	.01	.02	0.00
MgO	.01	.20	.16	.20	.07
CaO	.50	.17	.61	.81	.18
Na2O	6.68	3.82	1.38	4.03	6.92
K2O	.20	4.30	7.40	2.55	.24
P2O5	.05	.03	.03	0.00	.01
LOI	.70	.82	1.00	2.15	.39
TOTAL	98.49	101.53	99.21	99.44	100.12

## Trace Elements (ppm)

Pb	37.00	20.00	8.00	166.00	13.00
Th	18.00	27.00	10.00	24.00	22.00
U	0.00	4.00	0.00	6.00	0.00
Rb	5.00	163.00	121.00	79.00	6.00
Sr	85.00	26.00	28.00	64.00	93.00
Y	133.00	143.00	69.00	140.00	47.00
Zr	314.00	242.00	177.00	328.00	280.00
Nb	38.00	31.00	16.00	31.00	34.00
Zn	18.00	36.00	15.00	77.00	21.00
Cu	12.00	13.00	14.00	38.00	28.00
Ni	14.00	26.00	9.00	3.00	0.00
La	48.00	107.00	19.00	64.00	1.00
Ba	27.00	327.00	750.00	662.00	83.00
V	0.00	4.00	25.00	7.00	7.00
Ce	104.00	278.00	38.00	103.00	17.00
Cr	0.00	0.00	0.00	0.00	8.00
Ga	21.00	15.00	6.00	27.00	25.00
As	17.00	30.00	31.00	0.00	23.00

## S &amp; CO2 (Wt %)

S	0.00	0.00	0.00	.11	.05
CO2					

## Precious Metals (ppb)

Au	12.80	10.00		14.80	.60
Ag	189.00	33.00		107.00	72.00

## WGH-GR

	W-80-164	PB7-10	PB19-25	PB38-2A	PB38-2B
Major Elements (Wt %)					
SiO2	77.00	75.60	76.20	66.70	0.00
TiO2	0.00	.12	.10	.24	0.00
Al2O3	14.00	12.80	13.60	17.00	0.00
Fe2O3	.54	.98	.30	2.29	0.00
MnO	.01	.03	.01	.03	0.00
MgO	0.00	.19	.05	1.12	0.00
CaO	.10	.93	.78	3.72	.01
Na2O	4.68	4.15	7.80	5.27	0.00
K2O	3.97	1.74	.13	1.02	0.00
P2O5	0.00	.02	0.00	.02	0.00
LOI	.42	1.74	.69	2.24	0.00
TOTAL	100.72	98.30	99.66	99.65	

Trace Elements (ppm)					
Pb	67.00	105.00	16.00	11.00	15.00
Th	42.00	19.00	20.00	2.00	0.00
U	11.00	9.00	2.00	0.00	0.00
Rb	273.00	62.00	1.00	24.00	20.00
Sr	31.00	64.00	260.00	553.00	518.00
Y	58.00	111.00	64.00	6.00	8.00
Zr	64.00	295.00	328.00	98.00	107.00
Nb	48.00	28.00	24.00	2.00	1.00
Zn	35.00	347.00	36.00	50.00	29.00
Cu	15.00	39.00	23.00	27.00	22.00
Ni	0.00	0.00	0.00	0.00	6.00
La	2.00	45.00	4.00	7.00	13.00
Ba	89.00	664.00	69.00	416.00	441.00
V	0.00	4.00	6.00	60.00	60.00
Ce	2.00	76.00	23.00	25.00	23.00
Cr	0.00	0.00	1.00	2.00	2.00
Ga	29.00	27.00	17.00	15.00	15.00
As	0.00	12.00	15.00	0.00	21.00

S & CO2 (Wt %)					
S	0.00	.16	0.00	0.00	2.95
CO2		.41	.26	.27	.55

Precious Metals (ppb)					
Au		22.80	1.00	2.00	5.60
Ag		92.00	16.00	3.00	870.00

## WGH-GR

PB38-14

PB133-5

PB133-7

PB133-8

## Major Elements (Wt %)

SiO2	65.70	72.60	.01	.01
TiO2	.23	.18	0.00	0.00
Al2O3	19.00	13.60	0.00	0.00
Fe2O3	.30	2.17	0.00	0.00
MnO	.03	.01	0.00	0.00
MgO	.41	.09	0.00	0.00
CaO	1.42	.19	0.00	0.00
Na2O	10.80	8.10	0.00	0.00
K2O	.13	.11	0.00	0.00
P2O5	.07	0.00	0.00	0.00
LOI	1.27	1.09	0.00	0.00
TOTAL	99.36	98.14		

## Trace Elements (ppm)

Pb	19.00	116.00	1184.00	4136.00
Th	2.00	27.00	28.00	27.00
U	1.00	7.00	3.00	3.00
Rb	1.00	4.00	6.00	3.00
Sr	227.00	117.00	94.00	78.00
Y	21.00	98.00	125.00	170.00
Zr	266.00	269.00	278.00	342.00
Nb	12.00	28.00	27.00	42.00
Zn	12.00	22.00	4071.00	46.00
Cu	20.00	30.00	1808.00	1015.00
Ni	0.00	0.00	0.00	0.00
La	0.00	52.00	50.00	46.00
Ba	57.00	79.00	68.00	61.00
V	42.00	10.00	6.00	4.00
Ce	25.00	100.00	102.00	73.00
Cr	0.00	10.00	9.00	11.00
Ga	6.00	29.00	30.00	93.00
As	17.00	60.00	56.00	95.00

## S &amp; CO2 (Wt %)

S	0.00	1.02	1.73	1.71
CO2				

## Precious Metals (ppb)

Au	5.40	3.50	.40	5.00
Ag	28.00	2959.00	107.00	22189.00

Strawberry Granite (STG)

	STG-1	STG-1B	STG-2	STG-3	STG-4
Major Elements (Wt %)					
SiO <sub>2</sub>	74.60	75.00	71.30	72.40	76.30
TiO <sub>2</sub>	.21	.28	.26	.21	.10
Al <sub>2</sub> O <sub>3</sub>	13.40	13.30	14.90	14.20	13.60
Fe <sub>2</sub> O <sub>3</sub>	1.02	1.36	1.07	1.45	.46
MnO	.02	.04	.04	.05	.01
MgO	.23	.36	.33	.45	.01
CaO	.86	1.10	.80	1.43	.66
Na <sub>2</sub> O	3.55	3.60	3.49	4.05	4.68
K <sub>2</sub> O	5.22	4.85	6.50	5.30	3.98
P <sub>2</sub> O <sub>5</sub>	.03	.05	.06	.05	0.00
LOI	.45	.56	.59	.72	.28
TOTAL	99.59	100.50	99.34	100.31	100.08

Trace Elements (ppm)					
Pb	37.00	33.00	51.00	40.00	34.00
Th	22.00	35.00	29.00	29.00	15.00
U	2.00	4.00	3.00	6.00	25.00
Rb	255.00	243.00	306.00	256.00	206.00
Sr	166.00	158.00	181.00	187.00	46.00
Y	30.00	34.00	24.00	25.00	89.00
Zr	79.00	131.00	109.00	135.00	43.00
Nb	17.00	18.00	15.00	16.00	50.00
Zn	28.00	49.00	39.00	48.00	28.00
Cu	21.00	23.00	24.00	16.00	23.00
Ni	16.00	13.00	14.00	11.00	62.00
La	32.00	38.00	28.00	47.00	1.00
Ba	445.00	423.00	578.00	549.00	95.00
V	13.00	24.00	16.00	19.00	9.00
Ce	68.00	83.00	55.00	90.00	23.00
Cr	0.00	10.00	8.00	7.00	0.00
Ga	15.00	16.00	14.00	15.00	29.00
As	0.00	0.00	0.00	1.00	0.00

S & CO <sub>2</sub> (Wt %)					
S	0.00	0.00	.02	0.00	0.00
CO <sub>2</sub>					

Precious Metals (ppb)					
Au	9.30	5.60	19.80	4.30	1.20
Ag	134.00	44.00	248.00	363.00	1000.00

## STG

STG-5

W-79-94

W79-101P

W-79-102

W-79-162

## Major Elements (Wt %)

SiO2	76.50	73.30	77.10	75.60	74.20
TiO2	.19	.16	0.00	0.00	.09
Al2O3	13.00	14.00	13.30	14.60	14.30
Fe2O3	1.18	.70	.55	.83	.43
MnO	.04	.01	.01	.01	.02
MgO	.12	.20	.38	.46	.09
CaO	.43	.94	1.83	.72	.29
Na2O	3.76	5.31	4.78	7.02	3.78
K2O	4.77	3.32	.91	.42	6.81
P2O5	.01	.05	.02	.01	.10
LOI	.47	1.25	1.00	.57	.30
TOTAL	100.47	99.24	99.88	100.24	100.41

## Trace Elements (ppm)

Pb	32.00	38.00	39.00	5.00	55.00
Th	52.00	36.00	9.00	2.00	13.00
U	8.00	8.00	3.00	0.00	11.00
Rb	207.00	172.00	28.00	13.00	400.00
Sr	15.00	119.00	270.00	103.00	16.00
Y	65.00	15.00	4.00	0.00	32.00
Zr	163.00	103.00	14.00	6.00	24.00
Nb	24.00	12.00	3.00	0.00	48.00
Zn	37.00	38.00	16.00	18.00	18.00
Cu	17.00	22.00	16.00	16.00	7.00
Ni	17.00	7.00	0.00	0.00	19.00
La	74.00	17.00	14.00	0.00	5.00
Ba	111.00	226.00	382.00	196.00	65.00
V	7.00	11.00	11.00	29.00	3.00
Ce	144.00	30.00	37.00	13.00	6.00
Cr	13.00	5.00	11.00	13.00	0.00
Ga	15.00	21.00	1.00	5.00	20.00
As	0.00	2.00	0.00	0.00	2.00

## S &amp; CO2 (Wt %)

S	0.00	.84	0.00	0.00	0.00
CO2					

## Precious Metals (ppb)

Au	16.70	2.10	3.90		
Ag	126.00	263.00	148.00		

STG

W-79-163

W-80-12

## Major Elements (Wt %)

SiO2	74.60	74.90
TiO2	0.00	.24
Al2O3	13.80	12.40
Fe2O3	.16	1.41
MnO	.01	.05
MgO	.06	.41
CaO	.24	1.03
Na2O	3.62	3.59
K2O	6.56	4.87
P2O5	.04	.06
LOI	.30	.53
TOTAL	99.39	99.51

## Trace Elements (ppm)

Pb	55.00	32.00
Th	15.00	37.00
U	9.00	8.00
Rb	414.00	253.00
Sr	38.00	83.00
Y	13.00	38.00
Zr	33.00	133.00
Nb	16.00	17.00
Zn	17.00	40.00
Cu	9.00	9.00
Ni	17.00	0.00
La	1.00	21.00
Ba	194.00	405.00
V	8.00	21.00
Ce	9.00	50.00
Cr	0.00	3.00
Ga	16.00	19.00
As	0.00	0.00

## S &amp; CO2 (Wt %)

S	0.00	0.00
CO2		

## Precious Metals (ppb)

Au	0.00
Ag	5.00

## Isle aux Morts Brook Granite (IAM/GR)

	IAM1 (CON)	IAM-2	IAM-3	W-79-10B	W-80-86
Major Elements (Wt %)					
SiO <sub>2</sub>	73.40	72.80	74.00	77.50	76.40
TiO <sub>2</sub>	.21	.27	.28	0.00	.13
Al <sub>2</sub> O <sub>3</sub>	14.00	14.00	14.00	12.90	13.10
Fe <sub>2</sub> O <sub>3</sub>	1.46	1.30	1.42	.82	.36
MnO	.05	.06	.04	.02	.03
MgO	.46	.42	.41	.11	0.00
CaO	.93	.97	1.01	.52	.25
Na <sub>2</sub> O	3.84	3.98	3.76	3.95	4.28
K <sub>2</sub> O	4.96	4.56	4.98	4.14	4.80
P <sub>2</sub> O <sub>5</sub>	.06	.07	.06	.01	.09
LOI	.50	.49	.59	.34	.24
TOTAL	99.87	98.92	100.55	100.31	99.68

Trace Elements (ppm)					
Pb	40.00	41.00	39.00	53.00	47.00
Th	37.00	30.00	37.00	29.00	40.00
U	8.00	14.00	11.00	10.00	18.00
Rb	310.00	279.00	282.00	394.00	426.00
Sr	135.00	120.00	125.00	12.00	6.00
Y	28.00	51.00	37.00	58.00	30.00
Zr	148.00	126.00	138.00	71.00	62.00
Nb	21.00	21.00	24.00	40.00	52.00
Zn	43.00	45.00	41.00	27.00	25.00
Cu	29.00	14.00	13.00	11.00	25.00
Ni	0.00	10.00	0.00	70.00	0.00
La	28.00	60.00	47.00	4.00	14.00
Ba	494.00	363.00	442.00	47.00	49.00
V	25.00	21.00	23.00	11.00	6.00
Ce	89.00	78.00	77.00	23.00	24.00
Cr	5.00	17.00	19.00	2.00	0.00
Ga	21.00	23.00	22.00	26.00	28.00
As	3.00	0.00	11.00	0.00	9.00

S & CO<sub>2</sub> (Wt %)

S	0.00	0.00	0.00	0.00	0.00
CO <sub>2</sub>					

## Precious Metals (ppb)

Au	5.50		3.40	1.50	4.40
Ag	109.00		68.00	63.00	16.00



## Grab Samples from the Main Shear Showing (ORE)

	80-61C	80-61D	80-61E	80-61F	80-61G
Trace Elements (ppm)					
Pb	467006.00	417.00	86.00	2299.00	49.00
Th	0.00	5.00	0.00	13.00	0.00
U	0.00	8.00	4.00	4.00	0.00
Rb	0.00	7.00	34.00	9.00	1.00
Sr	0.00	0.00	0.00	0.00	0.00
Y	0.00	5.00	15.00	1.00	1.00
Zr	0.00	20.00	37.00	20.00	0.00
Nb	0.00	3.00	3.00	1.00	0.00
Zn	2984.00	404.00	60.00	332.00	11.00
Cu	42240.00	18112.00	47.00	9796.00	50.00
Ni	130.00	0.00	8.00	0.00	1.00
La	17.00	11.00	11.00	6.00	0.00
Ba	29.00	98.00	253.00	64.00	27.00
V	7.00	72.00	151.00	69.00	17.00
Ce	0.00	18.00	32.00	9.00	17.00
Cr	9.00	32.00	51.00	38.00	29.00
Ga	9999.00	0.00	12.00	0.00	3.00
As	3575.00	350.00	40.00	339.00	23.00
S & CO2 (Wt %)					
S	7.09	4.05	.17	2.32	.01
CO2	.31	.18	.08	.05	.05
Precious Metals (ppb)					
Au	2100.00	3520.00	2.90	2433.00	8.00
Ag	214500.00	46449.00	124.00	39565.00	173.00

## ORE

	80-61J	80-61K	80-65A	80-65B	80-65D
Trace Elements (ppm)					
Pb	2854.00	40043.00	60680.00	94517.00	121963.00
Th	1.00	7.00	2.00	0.00	0.00
U	0.00	16.00	1.00	0.00	0.00
Rb	3.00	11.00	12.00	6.00	0.00
Sr	0.00	12.00	11.00	2.00	0.00
Y	0.00	13.00	8.00	0.00	0.00
Zr	3.00	23.00	39.00	20.00	21.00
Nb	0.00	1.00	1.00	0.00	2.00
Zn	15610.00	12906.00	19873.00	88248.00	46066.00
Cu	1454.00	7974.00	210.00	1535.00	14360.00
Ni	0.00	0.00	0.00	0.00	0.00
La	5.00	11.00	18.00	20.00	22.00
Ba	9.00	29.00	58.00	53.00	51.00
V	10.00	28.00	41.00	28.00	47.00
Ce	4.00	7.00	18.00	8.00	7.00
Cr	7.00	32.00	18.00	37.00	60.00
Ga	68.00	964.00	1517.00	3148.00	3185.00
As	74.00	19666.00	745.00	1023.00	1274.00
S & CO2 (Wt %)					
S	2.26	6.05	2.78	8.59	6.56
CO2	.03	.22	0.00	.18	.18
Precious Metals (ppb)					
Au	590.00	19630.00	7780.00	15500.00	35970.00
Ag	11886.00	50564.00	81000.00	79000.00	37500.00

## ORE

	80-66C	80-66D	4-7	15-5	19-13
Trace Elements (ppm)					
Pb	172.00	3087.00	14940.00	1628.00	839.00
Th	6.00	31.00	16.00	10.00	8.00
U	13.00	3.00	28.00	0.00	7.00
Rb	24.00	2.00	49.00	36.00	83.00
Sr	66.00	0.00	25.00	135.00	21.00
Y	44.00	0.00	29.00	20.00	30.00
Zr	72.00	2.00	55.00	110.00	67.00
Nb	5.00	3.00	5.00	11.00	7.00
Zn	224.00	414.00	14154.00	711.00	435.00
Cu	62.00	6477.00	5555.00	38.00	2452.00
Ni	25.00	6.00	32.00	22.00	26.00
La	22.00	6.00	25.00	24.00	23.00
Ba	126.00	21.00	195.00	209.00	301.00
V	112.00	10.00	225.00	193.00	272.00
Ce	35.00	5.00	52.00	56.00	40.00
Cr	10.00	8.00	50.00	77.00	72.00
Ga	18.00	15.00	290.00	45.00	7.00
As	356.00	1274.00	228.00	19.00	35.00
S & CO <sub>2</sub> (Wt %)					
S	4.91	6.56	2.27	.14	.75
CO <sub>2</sub>	1.70	.18	.95	.59	
Precious Metals (ppb)					
Au	430.00	15500.00	7460.00	190.00	1470.00
Ag	363.00	79000.00	24038.00	6435.00	7843.00

## ORE

	19-14	19-18	26-8	27-33	27-24
Trace Elements (ppm)					
Pb	1542.00	28214.00	83109.00	97.00	105.00
Th	10.00	0.00	0.00	0.00	0.00
U	0.00	17.00	0.00	0.00	6.00
Rb	55.00	27.00	36.00	0.00	0.00
Sr	161.00	28.00	10.00	15.00	0.00
Y	31.00	16.00	23.00	25.00	2.00
Zr	102.00	35.00	77.00	4.00	5.00
Nb	12.00	1.00	11.00	0.00	3.00
Zn	437.00	26869.00	16910.00	331.00	278.00
Cu	98.00	7008.00	2930.00	80.00	1759.00
Ni	36.00	16.00	0.00	0.00	49.00
La	44.00	14.00	19.00	5.00	4.00
Ba	384.00	119.00	132.00	26.00	6.00
V	248.00	76.00	5.00	14.00	5.00
Ce	67.00	21.00	18.00	11.00	7.00
Cr	88.00	52.00	0.00	13.00	60.00
Ga	48.00	630.00	2134.00	2.00	0.00
As	25.00	356.00	928.00	1.00	606.00
S & CO <sub>2</sub> (Wt %)					
S	.09	3.31	3.92	.43	6.20
CO <sub>2</sub>	.47	.41	.01	1.68	.35
Precious Metals (ppb)					
Au	220.00	3450.00	1620.00	490.00	540.00
Ag	5361.00	67000.00	54500.00	148.00	3518.00

## ORE.

	27-25	27-26	27-28	28-5A	28-5B
Trace Elements (ppm)					
Pb	60809.00	3797.00	4312.00	65437.00	18857.00
Th	0.00	5.00	7.00	0.00	5.00
U	12.00	0.00	1.00	6.00	19.00
Rb	21.00	2.00	17.00	62.00	57.00
Sr	12.00	0.00	254.00	62.00	52.00
Y	13.00	0.00	9.00	44.00	47.00
Zr	37.00	4.00	28.00	222.00	206.00
Nb	5.00	0.00	0.00	23.00	17.00
Zn	41827.00	3730.00	1431.00	37613.00	38113.00
Cu	7156.00	49.00	63.00	7014.00	4336.00
Ni	21.00	0.00	0.00	13.00	0.00
La	10.00	0.00	23.00	32.00	28.00
Ba	104.00	1.00	91.00	254.00	399.00
V	111.00	5.00	88.00	21.00	16.00
Ce	5.00	18.00	9.00	39.00	48.00
Cr	55.00	69.00	45.00	2.00	42.00
Ga	1514.00	80.00	86.00	1669.00	522.00
As	692.00	51.00	55.00	711.00	243.00

S & CO<sub>2</sub> (Wt %)

S	4.17	.53	.26	5.54	3.83
CO <sub>2</sub>	.41	.01			

## Precious Metals (ppb)

Au	9640.00	200.00	2500.00	8710.00	450.00
Ag	77199.00	1228.00	2759.00	21000.00	9878.00

## ORE

	28-5C	28-5D	28-14	38-21	38-22
Trace Elements (ppm)					
Pb	821.00	282271.00	116539.00	38.00	9179.00
Th	16.00	0.00	0.00	1.00	0.00
U	2.00	0.00	0.00	2.00	14.00
Rb	123.00	0.00	8.00	22.00	16.00
Sr	76.00	0.00	7.00	42.00	32.00
Y	109.00	0.00	0.00	20.00	15.00
Zr	510.00	0.00	20.00	56.00	38.00
Nb	27.00	0.00	5.00	5.00	0.00
Zn	370.00	14599.00	1787.00	38.00	4348.00
Cu	835.00	1673.00	115775.00	8.00	2979.00
Ni	1.00	311.00	76.00	8.00	113.00
La	48.00	29.00	15.00	8.00	8.00
Ba	741.00	75.00	83.00	473.00	359.00
V	31.00	11.00	9.00	111.00	115.00
Ce	90.00	11.00	4.00	11.00	12.00
Cr	0.00	22.00	7.00	22.00	17.00
Ga	37.00	9999.00	1829.00	3.00	66.00
As	30.00	2513.00	1064.00	63.00	318.00
S & CO2 (Wt %)					
S	.24	11.78	15.18	.73	6.41
CO2		1.02	.76	.68	.68
Precious Metals (ppb)					
Au	220.00	3760.00	570.00	50.00	7730.00
Ag	22433.00	74682.00	91642.00	186.00	45455.00

## ORE

	38-23	38-24	38-32	38-35	38-37
Trace Elements (ppm)					
Pb	163.00	33710.00	21615.00	62050.00	187342.00
Th	0.00	0.00	0.00	0.00	0.00
U	0.00	18.00	14.00	0.00	0.00
Rb	60.00	16.00	5.00	22.00	0.00
Sr	4.00	20.00	13.00	25.00	8.00
Y	13.00	11.00	8.00	7.00	0.00
Zr	75.00	27.00	18.00	32.00	0.00
Nb	9.00	1.00	0.00	0.00	0.00
Zn	75.00	51751.00	26325.00	46784.00	164050.00
Cu	76.00	4680.00	2995.00	6167.00	86476.00
Ni	31.00	95.00	28.00	37.00	108.00
La	23.00	22.00	8.00	16.00	35.00
Ba	6434.00	316.00	42.00	122.00	97.00
V	234.00	162.00	25.00	61.00	22.00
Ce	15.00	13.00	0.00	11.00	6.00
Cr	79.00	25.00	38.00	62.00	5.00
Ga	17.00	386.00	220.00	622.00	2974.00
As	107.00	548.00	262.00	667.00	1580.00
S & CO2 (Wt %)					
S	.66	8.62	3.52	4.01	16.72
CO2	.16	.51	.49	.30	.62
Precious Metals (ppb)					
Au	170.00	1120.00	13850.00	21790.00	24160.00
Ag	242.00	41500.00	20315.00	63000.00	173090.00

## ORE

	41-2	41-6	51-9	52-4	53-2
Trace Elements (ppm)					
Pb	12676.00	26626.00	1748.00	210.00	100910.00
Th	31.00	0.00	4.00	1.00	725.00
U	17.00	19.00	10.00	3.00	0.00
Rb	29.00	41.00	158.00	12.00	59.00
Sr	36.00	42.00	6.00	6.00	45.00
Y	17.00	25.00	39.00	8.00	0.00
Zr	34.00	71.00	78.00	16.00	58.00
Nb	4.00	5.00	11.00	2.00	0.00
Zn	1027.00	35067.00	767.00	199.00	645.00
Cu	12682.00	4191.00	1069.00	93.00	1031.00
Ni	6.00	9.00	34.00	17.00	0.00
La	22.00	26.00	29.00	0.00	14.00
Ba	101.00	242.00	712.00	108.00	136.00
V	60.00	69.00	222.00	69.00	78.00
Ce	22.00	20.00	57.00	21.00	22.00
Cr	17.00	35.00	57.00	31.00	7.00
Ga	162.00	648.00	41.00	0.00	2225.00
As	192.00	334.00	1138.00	333.00	1224.00

S & CO<sub>2</sub> (Wt %)

S	4.12	3.56	3.84	.54	1.55
CO <sub>2</sub>	.64	.51	.23	.48	.43

## Precious Metals (ppb)

Au	16090.00	1790.00	2110.00	5.00	1820.00
Ag	32143.00	47387.00	11133.00	227.00	850000.00



## ORE

53-2

63-5

63-7

## Trace Elements (ppm)

Pb	5909.00	133504.00	305.00
Th	47.00	0.00	9.00
U	18.00	0.00	3.00
Rb	13.00	0.00	19.00
Sr	26.00	9.00	33.00
Y	11.00	0.00	16.00
Zr	16.00	16.00	21.00
Nb	0.00	2.00	3.00
Zn	464.00	122862.00	425.00
Cu	869.00	5902.00	14615.00
Ni	11.00	0.00	20.00
La	10.00	33.00	18.00
Ba	74.00	68.00	169.00
V	45.00	46.00	43.00
Ce	16.00	16.00	15.00
Cr	54.00	64.00	40.00
Ga	117.00	4699.00	0.00
As	154.00	1299.00	39.00

## S &amp; CO2 (wt %)

S	4.33	14.16	4.04
CO2			3.33

## Precious Metals (ppb)

Au	10130.00	24400.00	7770.00
Ag	67353.00	62500.00	22330.00

	38-5A	133-6	133-6A	133-9	WGH SH1
Trace Elements (ppm)					
Pb	41549.00	1113.00	2073.00	5736.00	18139.00
Th	0.00	7.00	3.00	28.00	2.00
U	0.00	17.00	0.00	8.00	7.00
Rb	14.00	8.00	6.00	16.00	5.00
Sr	16.00	13.00	75.00	0.00	5.00
Y	14.00	80.00	48.00	29.00	6.00
Zr	23.00	65.00	151.00	90.00	7.00
Nb	0.00	6.00	14.00	6.00	0.00
In	73.00	62.00	2563.00	224.00	94.00
Cu	1865.00	3318.00	103.00	10779.00	1823.00
Ni	4.00	0.00	0.00	0.00	7.00
La	19.00	2.00	6.00	15.00	3.00
Ba	24.00	58.00	84.00	79.00	5.00
V	1.00	8.00	4.00	9.00	5.00
Ce	15.00	40.00	27.00	33.00	4.00
Cr	0.00	49.00	13.00	29.00	45.00
Ga	317.00	0.00	56.00	30.00	396.00
As	1089.00	27.00	41.00	126.00	237.00

S & CO2 (Wt %)					
S	12.21	1.36	.74	6.26	1.03
CO2	.82	.32	.12	.59	.04

Precious Metals (ppb)					
Au	21470.00	700.00	42.00	16400.00	3220.00
Ag	55500.00	20161.00	29368.00	51000.00	19122.00

GR/ORE

WGH SH2A

-----  
Trace Elements (ppm)

Pb	51405.00
Th	0.00
U	0.00
Rb	4.00
Sr	6.00
Y	2.00
Zr	11.00
Nb	0.00
Zn	692.00
Cu	12238.00
Ni	0.00
La	6.00
Ba	29.00
V	6.00
Ce	1.00
Cr	62.00
Ga	1092.00
As	574.00

-----  
S & CO2 (Wt %)

S	3.74
CO2	.06

-----  
Precious Metals (ppb)

Au	73730.00
Ag	90000.00

## IV.2 Rare Earth Element Analyses

	WGH-1	79-112A	79-112	79-78C	79-74
Rare Earth Elements (ppm)					
La	101.80	3.97	72.15	28.85	52.74
Ce	189.34	7.59	123.84	63.04	115.93
Pr	28.19	.31	20.50	7.69	13.02
Nd	125.71	5.82	83.24	31.73	54.30
Sm	29.37	2.98	19.00	6.40	11.79
Eu	5.86	.81	3.59	2.05	2.84
Gd	36.39	7.35	23.80	5.82	8.81
Tb	5.04	2.62	3.59	1.16	1.91
Dy	29.88	14.79	20.83	4.03	5.71
Ho	4.84	4.08	2.91	.79	1.48
Er	17.29	12.27	10.47	2.58	3.51
Yb	18.08	16.17	11.15	3.20	3.90
Lu	4.55	9.17	2.60	2.36	2.29
	38-36	80-61H	80-61I	80-65C	80-66A

Rare Earth Elements (ppm)					
La	3.76	13.36	12.76	13.28	4.58
Ce	6.92	32.62	28.46	31.18	11.80
Pr	1.30	4.77	4.85	4.30	2.25
Nd	7.68	24.21	23.95	18.04	10.87
Sm	2.19	6.39	7.45	4.41	3.90
Eu	1.05	1.81	2.68	1.87	1.67
Gd	4.84	6.74	9.63	6.37	4.38
Tb	.96	.93	2.55	2.73	1.83
Dy	6.24	4.95	9.71	8.68	8.24
Ho	1.36	.49	1.63	1.51	1.60
Er	3.70	2.20	5.47	5.71	4.21
Yb	5.10	1.70	6.13	5.62	4.41
Lu	4.09	.50	3.73	4.29	3.73
	WGH 9H2B	IAM1	IAM3	RRB-2A	RRB-3

Rare Earth Elements (ppm)					
La	0.00	18.12	36.95	36.97	1.13
Ce	0.00	62.83	77.69	74.42	3.71
Pr	.40	5.00	9.55	8.64	.42
Nd	.88	18.71	37.77	30.72	2.17
Sm	1.02	5.28	8.84	4.97	.69
Eu	.65	1.88	2.37	2.01	.47
Gd	1.10	4.78	8.23	4.01	1.00
Tb	.75	2.10	2.05	1.12	.59
Dy	1.95	5.64	7.03	3.49	1.87
Ho	.91	1.12	1.65	.29	.49
Er	1.56	4.82	4.63	2.37	1.88
Yb	2.08	6.22	5.29	2.42	2.10
Lu	.90	4.08	3.01	1.46	1.22

	RRG-5	A-3	A-5A	A-6	CRG-2
Rare Earth Elements (ppm)					
La	10.27	33.91	7.88	45.13	58.42
Ce	18.63	73.07	10.20	97.01	130.77
Pr	2.84	7.88	1.48	10.32	16.47
Nd	8.62	28.31	7.76	38.90	64.86
Sm	2.29	6.75	1.94	7.60	10.96
Eu	.94	1.65	.90	1.87	4.12
Gd	3.00	6.40	2.18	7.01	9.51
Tb	1.16	1.00	.18	1.55	2.59
Dy	2.21	6.56	.80	6.78	6.04
Ho	.43	.87	0.00	1.10	1.08
Er	1.77	4.27	1.80	4.12	3.94
Yb	2.66	5.58	1.52	2.80	4.25
Lu	1.79	1.39	1.47	1.99	4.16
	CRG-5A	CRG-6	CRG-7	STG-3	STG-4

Rare Earth Elements (ppm)					
La	6.62	79.84	15.40	16.29	4.25
Ce	10.03	182.82	26.22	41.57	10.42
Pr	1.57	21.13	3.94	5.26	1.20
Nd	7.81	82.61	13.96	20.68	8.25
Sm	2.35	12.83	3.70	4.75	4.32
Eu	.82	4.69	1.80	1.82	.84
Gd	2.19	7.83	3.51	5.23	6.29
Tb	1.55	1.52	1.93	1.50	2.21
Dy	3.76	4.86	3.52	4.90	8.29
Ho	.44	1.17	1.06	1.84	2.52
Er	2.48	2.10	2.92	4.32	7.75
Yb	3.26	1.97	2.84	6.63	11.75
Lu	3.43	2.19	3.17	4.65	6.70
	STG-5	WPB-4	38-42	79-15	79-27

Rare Earth Elements (ppm)					
La	31.09	99.86	18.27	13.93	9.79
Ce	81.43	206.58	44.12	30.77	19.06
Pr	10.75	25.22	5.83	3.93	3.52
Nd	39.17	95.07	24.82	14.50	12.99
Sm	8.57	17.37	5.96	2.92	4.05
Eu	2.21	5.66	1.69	.80	1.86
Gd	8.98	14.11	7.49	2.09	4.98
Tb	2.41	2.80	1.51	.32	3.13
Dy	8.07	8.54	6.05	1.79	9.35
Ho	1.93	2.18	1.70	.15	1.57
Er	5.93	5.56	4.36	1.08	4.56
Yb	7.34	8.12	6.35	1.22	3.77
Lu	4.99	5.27	4.85	1.25	2.97

	79-68B	79-10B	79-170A	79-170S	80-38
Rare Earth Elements (ppm)					
La	9.84	7.89	13.54	24.67	25.65
Ce	15.77	17.99	28.01	59.80	69.34
Pr	1.87	2.33	3.42	6.17	6.31
Nd	8.79	11.10	17.77	28.86	28.86
Sm	2.10	4.43	4.85	5.89	7.53
Eu	1.18	1.28	2.12	1.74	3.09
Gd	2.02	4.53	7.69	5.45	8.51
Tb	.26	1.87	1.07	1.01	2.75
Dy	2.43	5.33	6.97	5.19	15.01
Ho	0.00	1.28	1.29	.77	2.35
Er	1.10	4.18	3.87	3.27	5.65
Yb	.58	5.13	5.11	4.25	5.13
Lu	.35	3.38	3.27	1.58	3.41
	80-476	80-57			

Rare Earth Elements (ppm)		
La	11.99	24.96
Ce	41.15	50.07
Pr	3.08	6.09
Nd	16.41	24.99
Sm	4.24	5.09
Eu	1.44	2.19
Gd	5.33	4.99
Tb	.44	.84
Dy	6.54	4.44
Ho	1.25	.80
Er	3.79	2.69
Yb	2.76	2.59
Lu	1.22	1.68

# REFERENCES CITED IN APPENDICES

- Abbey, S., 1975. Studies in "Standard Samples". G.S.C. Pap. 74-41, 10p.
- Abbey, S., 1976. SY-2, SY-3 and MRG-1. E.M.R. Canmet Rept. 76-36, 3p.
- Brooks, C., Hart, S.R., and Wendt, I., 1972. Realistic use of two-error regression treatments as applied to rubidium-strontium data. Rev. Geophy. and Space Phy., v.10, pp. 551-577.
- Fryer, B.J., 1977. Rare earth evidence in iron formation for changing oxidation states. Geochim. Cosmo. Acta, v. 41, pp. 361-367.
- Fryer, B.J., and Kerrich, R., 1978. Determination of precious metals at ppb levels in rocks by a combined wet chemical and flameless atomic absorption method. At. Absorp. Newsletter, v. 17, pp. 4-6.
- Flanagan, F.J., 1970. Sources of geochemical standards -II. Geochim. Cosmo. Acta, v.34, pp. 121-125.
- Flanagan, F.J., 1973. 1972 values for internal geochemical reference standards. Geochim. Cosmo. Acta, v.37, pp. 1189-1200.
- Huffman, C., Mensik, J.D., and Rader, L.F., 1966. Determination of silver in mineralized rocks by atomic absorption spectrometry. U.S. Geol. Surv. Prof. Pap. 550-B, pp. 189-191.
- Langmeyer, F.J., and Paus, P.E., 1968. The analysis of inorganic siliceous materials by atomic absorption spectrophotometry and the hydrofluoric acid decomposition technique. Pt. I. The analysis of silicate rocks. Anal. Chimica Acta, v. 43, pp. 397-408.
- Shapiro, L. and Brannock, W.W., 1962. Rapid analysis of silicate, carbonate and phosphate rocks. U. S. Geol. Surv. Bull. 1144A, pp. 31-3.
- Steele, T.W., Wilson, A., Goudvis, R., Ellis, P.J., and Radford, A.J., 1978. Trace element data (1966-1977) for the six "NIMROC" reference samples. Geostds. Newsletter, v. II, pp.71-106.
- Steiger, R.H., and Jager, E., 1977. Subcommission on geochronology: convention on the use of decay constants in geo- and cosmochemistry. Earth Plan.

Sci. Lett., v. 36, pp. 359-362.

Taylor, R.P., and Fryer, B.J., 1983. Strontium isotope geochemistry of the Santa Rita porphyry copper deposits, New Mexico. in press, Econ. Geol.

York, D., 1969. Least squares fitting of a straight line with correlated errors. Earth Plan. Sci. Lett., v. 5, pp. 320-324.







